

Woods Hole Oceanographic Institution Massachusetts Institute of Technology

AD-A231 738



Joint Program
in Oceanography
and
Oceanographic Engineering



DOCTORAL DISSERTATION

Comparative Design, Modeling, and Control Analysis of Robotic Transmissions

by

Hagen Schempf

August 1990

DTIC
S ELECTE D
B FEB 20 1991

DISTRIBUTION STATEMENT A

Approved for public release
Distribution Unlimited

91 2 14 002

WHOI-90-43

**Comparative Design, Modeling, and Control Analysis
of Robotic Transmissions**

by

Hagen Schempf

Woods Hole Oceanographic Institution
Woods Hole, Massachusetts 02543

and

The Massachusetts Institute of Technology
Cambridge, Massachusetts 02139

August 1990

Doctoral Dissertation

Funding was provided by the Office of Naval Research through
Grant N00014-86-C-0038 and NRL through Grant N00014-88-K-2022.

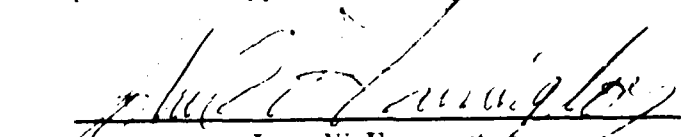
Reproduction in whole or in part is permitted for any purpose of the
United States Government. This thesis should be cited as:
Hagen Schempf, 1990. Comparative Design, Modeling, and Control Analysis of
Robotic Transmissions. Ph.D. Thesis. MIT/WHOI, WHOI-90-43.

Approved for publication; distribution unlimited.

Approved for Distribution:



Albert J. Williams 3rd, Chairman
Department of Applied Ocean Physics and Engineering


John W. Farrington
Dean of Graduate Studies

Dist	Special
A-1	

COMPARATIVE DESIGN, MODELING, AND CONTROL ANALYSIS OF ROBOTIC TRANSMISSIONS

by

Hagen Schempf

Submitted in partial fulfillment of the requirements for the degree of Doctor of Philosophy
at the Massachusetts Institute of Technology and the Woods Hole Oceanographic
Institution in August of 1990.

ABSTRACT

Transmission dynamics are shown to dominate the stability and performance of impedance- and torque controlled rotary electro-mechanical systems. The experimental analysis focuses on planetary, cycloidal, harmonic and cable reducers, but excludes direct-drive, pneumatic, hydraulic and friction drives. Neither sensors nor actuators with better resolution nor increased dynamic range can circumvent reduced stability and performance limitations unless certain hardware criteria can be met. Simple transmission models are proposed to model such effects as (1) transmission stiffness, (2) soft-zones and wind-up, (3) backlash and lost motion, and (4) stiction, friction and viscous losses. These models are experimentally verified using six different transmission types most commonly used in robot designs. Simple lumped-parameter linear/nonlinear models are shown to predict stability margins and bandwidths at these margins fairly closely. Simple nonlinear lumped- and fixed-parameter models were unable to properly predict time responses when the torque signals were of low-frequency and amplitude, underscoring the complexity in modeling the transmission-internal stick-slip phenomena.

The clear distinction between speed reducers and torque multipliers is theoretically and experimentally explored. The issue of actuator and sensor colocation is shown to be extremely important in predicting the reduced bandwidth and stability of torque-controlled actuator-transmission-load systems. Stiffening transmission behaviors are shown to be of a conditionally stabilizing nature, while also reducing the dynamic range of impedance- and torque-servoed systems. System damping, whether active or passive, as well as low-pass filtering motor-controller signals, are shown to dramatically increase stability without having any effect on increasing system bandwidth. Transmission soft-zones are proven to reduce the stability margins of colocated impedance controlled electro-mechanical systems. None of the standard controller structures explored here were able to noticeably increase the system bandwidth of the open-loop system, without reducing the overall system performance.

The different transmissions are tested for system nonidealities and generalizations drawn on the stability and performance margins of impedance and torque-servoed geared, cycloidal, planetary, and cable reducers in hard contact with the environment. Experimental results are furnished which underscore the validity and limitations of the theoretical modeling approach and comparative transmission analysis, while highlighting the importance of different physical system parameters necessary for proper transmission design.

Thesis Supervisor : Dr. Dana Yoerger
Title : Associate Scientist, Woods Hole Oceanographic Institution.

ACKNOWLEDGEMENTS

This labour of 99% perspiration and 1% inspiration would not have been possible without many people's comments, support and dedication. I hope I do not forget anybody, but forgive me if I do - you know who you are and you know that I will not forget you.

- Being a thesis supervisor, **Dana Yoerger** showed more patience and delivered enough support to prop up any failing government. Without his many stories about baseball and camping trips, my arduous lab hours would have been hell. I always enjoyed his fresh and practical view about academic theory and real world realities.

- My **committee members** who spent countless hours directing my efforts and making me see things I never saw, and forcing me to properly formulate my ideas and conclusions. It is tough to be an advisor, but someone has got to do it !!

- How could I have done all of this work without being born I ask myself. Without my parents this 6 year odyssey would never have happened and people would never think of me as an intellectual. Thank you mom and dad, **Christa** and **Roland**, and never forget I love you. *Jetzt faengt das Leben erst richtig an!!*

- A loving companion a man should never have to do without. **Noellette** is someone I could never find again anywhere. I am not very religious, but I have this feeling that she is a gift to me from above (never to be taken for granted of course, and to always be loved and cherished). I would have left long ago if I had not had her support. Whoever says that a Ph.D. is the effort of a single person, deserves to be laughed out of the room.

- **Peter, Chris, Josh, Zlex, Jean, Juan Salchicha, Lube, Ken**, etc. for making this time in Woods Hole fun, and helping me see this effort for what it really is. No parties can compete with the ones they have thrown, nor will I ever watch any worse sci-fi movies than I have watched with you folks. Good luck in all your endeavors as well.

- **Laela, Carla, Raffa, Martha, Gretch, Diane** (both), **Diana & Charlie**, who were always good friends ready with a helping smile and criminally good food. Socializing during these 4 years would never have been as much fun nor diverse, without your presence in my life. THANK YOU !!!

- All my **office mates**, of which I have had so many. Their respect for my toolbox and their belief that I must know a lot, were satisfying and amusing to me. Some day you too will graduate, so hang in there.

- **Dave D.-P., Bill T., Nathan U.**, etc. with whom I have had very interesting discussions not only about theory but also about life. I have learnt a lot from these talks and I hope we can stay in contact in the future.

- All those engineers and technicians at DSL, who made a respectable sea-going student out of me - Thank you for your harassment and support all along the way. Being placed in such an environment you quickly learn the difference between the lab and the real world. I highly recommend it, especially the part about hanging over the side of the ship

and feeding the fish in a force 10 gale!! **Andy, Martin, Bill, Bob², Jim, Skip, Tom, Steve, Dan, etc.,** thank you !!!!!

- **Anita & Gretchen** (alright, I'll include Bill as well), who were always very helpful in untangling the bureaucratic maze present in the lab. Hang in there and keep smiling.

- **Jake and Anna Maria** for feeding, clothing us, and providing an overall fun time, even if I occasionally broke something in their house. I only did it because I knew that Jake loves to fix things. Noellette also promises to never spill wine on the couch again!

- **Bob Ballard** for giving me the chance to work on the JASON Project and to participate in both cruises in search of the BISMARCK. Experiences that I will never forget and will cherish until my grandchildren get sick of hearing these tales.

- **Charlie, Dan & Mark** for doing such a good job in machining all the necessary hardware throughout these years, and fixing the many design flaws and coping with the inhuman deadlines. Thanks guys !!

- **The Education Dept.** (Abbie in particular) for singling me out as one the worst registrants and other overall support in tackling this monumental thesis task.

- All those other people in **Facilities, Receiving and Purchasing** with whom I have dealt over the years. Your efforts and regards are very much appreciated. How could I ever forget your contributions ?!

- **Guys and Gals in Graphics and Repro** who must have gotten tired of seeing my face around there, always asking for changes, additions, impossibly complicated drawings and outrageous deadlines - I know you must have hated it, but it's all over now - **THANKS!!**

- **WHOI** for providing the funding, and Cape Cod for making it a beautiful area in which to work on one's Ph.D.

TABLE OF CONTENTS

(1) INTRODUCTION.	21
(1.1) Background.	21
(1.1.1) Controller Structure Design and Experiments.	22
(1.1.2) Robot Hardware Design.	28
(1.1.3) Physical System Modelling and Stability Analyses.	31
(1.2) Thesis Motivation and Content Summary.	40
(1.3) Thesis Overview.	43
 (2) TRANSMISSION TYPES.	 47
(2.1) Transmission Listing - Functional Descriptions.	47
(2.1.1) Cable Reduction Transmission (WHOI).	47
(2.1.2) Harmonic Drive Transmission (HARMONIC DRIVE).	52
(2.1.3) Planetary and Cycloidal Reducers.	54
(a) Ball Reducer Transmission (KAMO SEIKO).	56
(b) Cycloidal Servo-Match Disk Reducer (SUMITOMO).	58
(c) Cycloidal Dual Track Cam Reducer (DOJEN).	61
(d) Corbac Planetary/Cycloidal Reducer (REDEX).	63
(2.2) Transmission Parameters - Summary.	66
(2.3) Transmission Applications.	70
 (3) REALISTIC TRANSMISSION MODELLING.	 73
(3.1) Complexity/Sophistication in modelling.	73
(3.1.1) General Analysis.	73
(3.1.2) Rigid-Body Model.	75
(3.1.3) Single Transmission Stiffness.	75
(3.1.4) Transmission Soft-Zone or Wind-Up.	79
(3.1.5) Backlash and Lost Motion.	80
(3.1.6) Dissipative Phenomena (Static/Kinetic/Viscous Friction).	86
(3.2) Transmission-specific Parameters.	87
(3.3) Theoretical Parameter Sensitivity Analysis for performance and stability of position- and force-controlled actuator/transmission/load systems.	 89
(3.3.1) Theory & Analysis Background - 2 DOF Model	89
(a) Inertia Distribution.	93

(b) Damping Distribution.	96
(c) Stiffness Distribution.	100
(d) Alternate Controller Structures and Dynamics.	103
(e) Nonlinearities - Size and Distribution.	117
(3.3.2) Theory & Analysis Background - 3 DOF Systems.	121
(a) Inertia Distribution.	125
(b) Damping Distribution.	127
(c) Stiffness Distribution.	128
(d) Alternate Controller Structures & Added Dynamics.	133
(3.4) Summary and Conclusions.	145
 (4) TRANSMISSION FIDELITY STUDY.	153
(4.1) Introduction.	153
(4.2) Experimental Setup.	154
(4.3) Data Trends and Comparisons.	161
(4.3.1) General Data.	161
(a) Impedance Following (Stiffness).	161
(b) Damping - Stiction, Coulomb-, and Viscous-Friction.	171
(c) Ripple Torque.	176
(d) Transmission Stiffness.	179
(4.3.2) Specific Data.	182
(a) WHOI/MIT - Pulley/Cable Reducer - A closer look.	182
(b) H.D. Harmonic Drive - A closer look.	191
(c) SUMITOMO - Cycloidal Reducers - A closer look.	199
(d) KAMO Ball Reducers - A closer look.	210
(e) DOJEN - Cycloidal Cam Reducer - A closer look.	228
(f) REDEX Cycloidal Gear Reducer - A closer look.	234
(g) Brushless DC Sensorimotors.	239
(4.4) Conclusions	244
(4.4.1) General Overview.	244
(4.4.2) Detailed Conclusions.	249
* Performance	249
(a) Transmission Stiction/Friction Characteristic.	249
(b) Transmission Backlash Characteristic.	253
(c) Transmission Stiffness Characteristic.	254
(d) Ripple Torque Characteristic.	258

(e) Sensor Characteristics.	260
* Stability	261
(a) Limit-Cycle Behaviour.	261
* Compensation Schemes	265
(a) Software Compensation.	265
(b) Hardware Compensation.	267
(4.5) Suggestions and Motivation for further Experiments.	269
(5) FORCE CONTROL TRANSMISSION EXPERIMENTS.	271
(5.1) Experimental Setup.	272
(5.2) Experimental Performance and Stability Analysis of force-controlled actuator/transmission/load systems.	276
(5.2.1) Hardware-Setup Experiments.	276
(5.2.2) Open-Loop Experiments.	281
(5.2.3) Closed-Loop Experiments.	299
(5.3) Summary and Conclusions.	319
(6) CONCLUSIONS AND SUGGESTIONS FOR FURTHER RESEARCH.	323
(6.1) Conclusions.	323
(6.2) Suggestions for further research.	331
(7) APPENDICES.	335
(8) BIBLIOGRAPHY.	339

LIST OF FIGURES

- Figure 1.1 : Logic Branching Diagram of Thesis Research Goal, Analysis Approach and Results.
- Figure 2.1a : WHOI underwater manipulator on test stand.
- Figure 2.1b : JASON remotely operated underwater robot with manipulator arm.
- Figure 2.1c : Basic Cable-Pulley Reducer for 3-stage underwater manipulator joint (30:1).
- Figure 2.2 : Cut-away view of the Cup-Type Harmonic Drive Reducer.
- Figure 2.3 : Front-view of elliptical bearing (wave generator), flexspline, and fixed inner spline (inner ring gear), to illustrate tooth engagement.
- Figure 2.4 : Progression in reducer stage design to outline the similarity between planetary gear reducers and cycloidal reducers.
- Figure 2.5 : Cross-section of KAMO Ball Reducer Transmission.
- Figure 2.6 : Cross-sectional view of Servo-Match Cycloidal Reducer, showing (1) input housing flange, (2) roller bearing retaining ring, (3) roller pins, (4) output cantilevers, (5) load transfer cylinder, (6) input-shaft bearing, (7) input cam-shaft, (8) disk roller bearings, (9) cam-shaft bearing, (10) three epitrochoid disks, (11) cantilever output flange, (12) roller-pin housing.
- Figure 2.7 : Cut-away view of FA Series SUMITOMO Servo-Match Cycloidal Reducers, showing epitrochoid disks, roller pins and output flange.
- Figure 2.8 : Cross-Sectional View of DOJEN Cycloidal Cam Reducer, illustrating all the pertinent reducer components.
- Figure 2.9 : Assembly View of the Cam-type cycloidal reducer from DOJEN. Individual epitrochoid disks are replaced by a single cam-type assembly, which is supported on a centrally located bearing. The cam rides on fixed internal pins.
- Figure 2.10 : Cross-sectional view of CORBAC reducer, showing (1) output shaft-assembly cantilevers, (2) output shaft, (3) two eccentrically located crown-gears, (4) split inner gear rings for indexing and backlash reduction and preloading, (A) set screws to hold index pattern, (B) output housing, (C) indication of inner ring gear indexing displacement.
- Figure 2.11 : Cycloidal Principle in the REDEX CORBAC unit, illustrating the use of crown gears (3) riding on the indexable inner gear (4), while transmitting torque to the output shaft driving pins (1).
- Figure 2.12 : Assembly Drawing of REDEX CORBAC unit, which shows the input shaft, crown gears and eccentrically located bearings, split inner gear, and the cantilevered output shaft which takes the load from the milled holes in the crown gears.
- Figure 2.13 : Collection of all the reducers that were tested.
- Figure 2.14 : Basic test stand showing the jig plate with all added fixtures, the motor, shaft, bellows coupling, motor-controller card and power stage and the JR³ force/torque sensor.
- Figure 3.1.1 : Rigid-Body Actuator-Transmission-Load Model

Figure 3.1.2 : Lumped Parameter Simple Stiffness Transmission Model.

Figure 3.1.3 : Variable Transmission Stiffness as a function of transmitted load (torque)

Figure 3.1.4 : Varying relations for transmission stiffness for (a) the model of Figure 3.1.2, (b) the model of Figure 3.1.3, (c) the model of Figure 3.1.5 and 3.1.6, and (d) the model of Figure 3.1.7.

Figure 3.1.5 : Piecewise-linear single-knee transmission stiffness model.

Figure 3.1.6 : Noncolocated variable transmission stiffness zones, reflecting improper spatial load distribution.

Figure 3.1.7 : Complex Actuator-Transmission-Load Model including soft-zone ($\Delta\gamma$) and backlash ($\Delta\phi$).

Figure 3.1.8 : Root-Locus for two-pole system : (a) Instability in the presence of first-order dynamics, (b) Underdamped Response in the presence of Lag-Compensator, (c) Improved Performance for Lead-Compensation, (d) Improper Lead-Compensation, (e) Preserved Stability and Performance for PD Compensation.

Figure 3.1.8(f) : PD Controller Comparison between design locus based on rigid-body model (left plot), and the actual locus for operation in the backlash-zone (right plot).

Figure 3.1.9 : Added damping in the backlash-zone, due to seals, viscous lubricants, etc.

Figure 3.3.1 : 2 DOF actuator/transmission/load model.

Figure 3.3.2 : 2 DOF force-control actuator/transmission/load/environment model representation.

Figure 3.3.3 : Variation in (I_1) Input- (left plot) and (I_2) Output-Inertia (right plot) and the effects on noncolocated PD position control stability.

Figure 3.3.4 : Variation in (I_1) Input- (left plot) and (I_2) Output-Inertia (right plot) and the effects on noncolocated PD force control stability.

Figure 3.3.5 : Stability regimes for PD force-controlled system for (a) varying input damping B_1 and (b) varying output damping B_2 .

Figure 3.3.6 : Stability regimes for PD force-controlled system with added input-damping term - $B_1 \dot{e}(x_1) dt$.

Figure 3.3.7 : Closed-loop bandwidth and damping ratio for PD force-controlled system with added input-damping term - $B_1 \dot{e}(x_1) / dt$.

Figure 3.3.8 : PD Position-Control Stability (a), and (b) PD force-control stability trends, pointing out that stiffening springs can result in instability for a PD controller-structure.

Figure 3.3.9 : System Stability for varying force-sensor/transmission-stiffness ratios : (a) $K_f/K_T=50$, (b) $K_f/K_T=20$, (c) $K_f/K_T=1$, (d) $K_f/K_T=1/50$, and (f) $K_f/K_T=1/100$.

Figure 3.3.10 : Reduction in stability regime by increasing the force-sensor stiffness in the case of a PD force-controller.

Figure 3.3.11 : Stability reduction with increasing force-sensor stiffness for force-error and output velocity PD force-controller.

Figure 3.3.12 : Closed-Loop Bandwidth (a) and corresponding damping ratios (b) as a function of varying sensor stiffness K_f .

Figure 3.3.13 : Regions of damping larger than $\zeta=0.5$ (A) and regions of damping smaller than $\zeta=0.5$ (B).

Figure 3.3.14 : Stability Regimes (plot a) and associated bandwidths and damping ratios (plot b) for a desired $\zeta=0.5$ damping ratio response for noncollocated and colocated velocity damping.

Figure 3.3.15 : Stability decrease for increasing values of integral force-error gain K_I in a pure PID force-controller, accompanied with marginally increased bandwidths but much reduced damping ratios.

Figure 3.3.16 : Decreased Stability for PI force- and D input-velocity controller for increasing values of K_I .

Figure 3.3.17 : (a) Noncollocated and (b) colocated impedance control stability regions as a function of force-feedback gain K_m .

Figure 3.3.18 : Closed-Loop dominant damping Ratio ζ , for (a) colocated and (b) noncollocated impedance control as a function of torque-feedback gain K_m .

Figure 3.3.19 : Stability regions' conditional stability by varying time-constant $1/a$ of first-order actuator/sensor dynamics.

Figure 3.3.20 : Discrete Controller Diagram for reduced backlash dynamics, showing the PD position-controller, and the sampling gates with the zero-order sample-and-hold for the actuator signal.

Figure 3.3.21 (a thru c): Stability Margins for discrete control in backlash zone. Stability margin increase with (a) increasing backlash inertia, as well as (b) increasing passive backlash damping, and reduced stability with (c) reduced sampling rates.

Figure 3.3.22: Physical System representation for noncollocated transmission compliance elements (proximal stiffness K_s and distal stiffness K_T).

Figure 3.3.23 : 3 DOF actuator/transmission/load/environment system to analyze force-control stability and -performance.

Figure 3.3.24 : Conditional Position Controller Stability for varying inertia values: (a) I_1 , (b) I_2 , and (c) I_3 .

Figure 3.3.25 : Force Control stability boundary behavior for increasing (a) I_1 , (b) I_2 , and (c) I_3 .

Figure 3.3.26 : Noncollocated position control stability regimes for varying values of (a) B_1 , (b) B_2 , and (c) B_3 .

Figure 3.3.27 : Noncollocated Force Control stability regions for variations in (a) B_1 , (b) B_2 , and (c) B_3 .

Figure 3.3.28 : Noncollocated PD position control stability boundaries for varying values for (a) K_s , and (b) K_T .

Figure 3.3.29 : Noncollocated force-control stability regimes for variations in (a) K_s , and (b) K_T .

Figure 3.3.30 : Noncollocated Force control stability regions vary with increasing force-sensor stiffness K_f .

Figure 3.3.31 : Noncollocated Force Control stability margins, with B_e as electronic output velocity damping term, replacing the force-rate damping term used in all the previous analyses.

Figure 3.3.32 : Noncolocated Force control with electronic input damping for increasing values of sensor stiffness : (a) stability regimes, (b) dominant closed-loop bandwidth, and (c) dominant closed-loop damping ratios.

Figure 3.3.33 : Noncolocated Force Control with added input velocity damping: (a) Stability regimes and (b) dominant bandwidths for increasing values of proximal stiffness K_g .

Figure 3.3.34 : Noncolocated Force Control with added input velocity damping: (a) Stability regimes and (b) dominant bandwidths for increasing values of distal stiffness K_T .

Figure 3.3.35 : Stability and Bandwidths for varying amounts of (a) passive damping B_1 , and (b) passive damping in B_2 , in noncolocated force control with input velocity damping.

Figure 3.3.36 : Stability and Bandwidths for varying amounts of (a) input inertia I_1 , and (b) intermediate inertia I_2 , in noncolocated force control with input velocity damping.

Figure 3.3.37 : (a) Stability and (b) Closed-Loop Bandwidth trends for increased levels of integral force-error-gain K_I in a pure PID noncolocated force controller.

Figure 3.3.38(a thru c) : (a) Stability Regimes , (b) dominant closed-loop bandwidths, and (c) associated damping ratios for noncolocated force control with input velocity damping, for varying levels of integral force-error gain K_I .

Figure 3.3.39 : System Diagram depicting the placement of first-order unmodelled dynamics in the actuator effort-path. Notice that this unmodelled filter-mode could also have been placed in the feedback loop, resulting in the same system response.

Figure 3.3.40 : (a) Stability and (b) dominant bandwidths for decreasing levels of first-order time-constant $1/a$, for a noncolocated pure PID force-controller.

Figure 4.1a : Plan View of Transmission Test Stand.

Figure 4.1b : Test Stand with mounted harmonic reducer, output torque sensor and the operator crank as well as the motor-controller card and power section.

Figure 4.2 : View of Cable Reduction and Test Setup for experiments.

Figure 4.3 : Manipulator on Test-Stand during Laboratory experiments with IBC computer, Supervisory and Control Computer controlled via the operator handbox and rate-input joystick.

Figure 4.4 : Manipulator Computer Chassis with its separate sections of this 6" OD oceanographic's standard computer hardware.

Figure 4.5 : Typical Stiffness Behaviors for real transmissions.

Figure 4.6 : Stick-Slip Behavior in the 30:1 Cable Reduction of the Underwater Manipulator.

Figure 4.7(a thru f) : Low Level of desired (0.21 N-m/deg) and actual output stiffness for the WHOI Cable Reducer, HARMONIC DRIVE reducer, the REDEX Corbac Geared Cycloidal Reducer, the KAMO Ball Reducer, SUMITOMO Cycloidal Servo-Match Reducer, and the DOJEN Cycloidal Cam Reducer.

- Figure 4.8 : Low and Medium Stiffness Traces for the Cable Reducer to show that energy loss is constant and not dependent on stiffness level.
- Figure 4.9 : Error in achieved stiffness is related to level of desired stiffness - Error decreases with increasing stiffness.
- Figure 4.10 : Realistic Natural Frictional/Viscous Loss Behavior in Transmissions: (a) Saturating Viscous Loss with different levels of Stiction/Friction/Viscous Damping and (b) Linear Viscous Losses with different levels of Stiction/Friction/Viscous Damping.
- Figure 4.11 : Desired and Actual Damping Behavior for (a) Ball Reducer, (b) Cable Reducer, (c) Cycloidal Reducer and (d) Harmonic Drive.
- Figure 4.12(a & b) : Natural Frictional Losses for two different transmissions - (1) WHOI Cable Reducer, (2) KAMO Ball Reducer, (3) REDEX Corbac Geared-Cycloidal Reducer, and (4) the DOJEN Cycloidal Cam Reducer.
- Figure 4.13 : Natural Frictional Losses for two different transmissions - (1) Harmonic Drive, (2) SUMITOMO Cycloidal Reducer.
- Figure 4.14 : Synthesized Torque-Ripple Behavior for Stiffness Fidelity of Motor and/or Transmission.
- Figure 4.15 : Desired and Actual Stiffness Behaviors for (a) Ball Reducer and (b) Cable Reducer.
- Figure 4.16 : Transmission Stiffness of Cable Reducer from Underwater Manipulator Joint.
- Figure 4.17 : Backdriveability of Underwater Manipulator Cable-Reducer Joint as a fct. of cable pre-tension.
- Figure 4.18 : Simple and most commonly used friction compensation schemes in real applications.
- Figure 4.19 : Velocity-based Friction Compensation scheme applied to cable reducer.
- Figure 4.20 : Impedance Compensation scheme for any Motor/Transmission using Force/Torque Feedback.
- Figure 4.21 : Desired and achieved stiffness behavior for impedance compensated Cable reduction.
- Figure 4.22 : Stiction/Friction Torques present in a Harmonic Drive Transmission.
- Figure 4.23 : Stiction/Friction and Viscous Damping inherent in a Harmonic Drive Transmission.
- Figure 4.24 : Presence of Ripple Torque in Stiffness Fidelity Experiment for the Harmonic Drive.
- Figure 4.25 : Reduction of torque-ripple in Harmonic Drive by careful alignment of fixed spline-ring and wave-spline.
- Figure 4.26 : Velocity-based Coulomb Friction Compensation for Harmonic Drive Transmission.
- Figure 4.27 : Impedance Compensation scheme applied to the Harmonic Drive Transmission.
- Figure 4.28a : Transmission Stiffness trace for the Harmonic Drive Cup (60:1) reducer.
- Figure 4.28b : Transmission Stiffness trace for the HARMONIC DRIVE Cup reducer (60:1), and the WHOI cable reducer (30:1).
- Figure 4.29 : Presence of Backlash in the Cyclo-Reducer, detected via simple stiffness test.
- Figure 4.30 : Presence of Backlash and Stiction/Friction in Cyclo-Reducer.
- Figure 4.31 : Transmission Stiffness Test for the SUMITOMO Servo-Match Cycloidal Reducer.
- Figure 4.32 : Stiffness Fidelity Trace for the Cyclo Reducer (29:1).

Figure 4.33 : Velocity-related Coulomb-Friction Compensation for Cycloidal Reducer only shows small improvements in stiffness fidelity.

Figure 4.34 : Impedance Compensation on Cycloidal Reducer shows great potential for success if certain hardware requirements are met.

Figure 4.35 : Desired and actual output stiffness behaviors for the Servo Match Cycloidal Reducer from SUMITOMO (59:1).

Figure 4.36 : Medium and high levels of actual and desired output stiffness, as measured for the SUMITOMO Servo Match Reducer (59:1).

Figure 4.37 : Natural friction behavior in the SUMITOMO Servo Match Cycloidal reducer (59:1), illustrating the high frictional losses present in this type of transmission.

Figure 4.38 : Backlash present in Low-Preload Ball Reducer Transmission.

Figure 4.39 : Removal of Backlash in Ball Reducer through increased Preload - Notice low apparent transmission stiffness level.

Figure 4.40 : Stiffness Fidelity for Ball Reducer as a function of transmission Preload.

Figure 4.41 : Gain from impedance compensation scheme applied to ball reducer hampered by hardware constraints.

Figure 4.42 : Friction Compensation schemes excite (a) limit-cycle behavior in the case of coulomb-friction compensation (left plot) and (b) instability if impedance compensation is used (instability damped out by hand in right plot).

Figure 4.43 : Typical Transmission Stiffness Behavior includes 'soft-zone' around zero-load point and higher stiffness during torque transmission.

Figure 4.44 : Zones of varying stiffness as a function of preload in the ball reducer.

Figure 4.45 : Stiction/Friction and Torque-Ripple as a function of Transmission Preload in a Ball Reducer.

Figure 4.46 : Stability is a function of transmission preload in the case of the ball reducer - (a) limit cycles for low preload (left plot) and (b) stability for high preload (right plot).

Figure 4.47 : Cycloidal Reducer experiences instability due to soft-zones and backlash, despite higher frictional damping (left plot), while cable reducer is stable at all times (right plot) due to absence of backlash and 'soft-zone'.

Figure 4.48 : Natural frictional losses in the new KAMO ball reducer, showing stiction-, coulomb-, and viscous-friction losses at the output.

Figure 4.49 : Desired and actual stiffness behaviors for a low level (0.21 N-m/deg) of desired output stiffness, for the medium-size KAMO Ball reducer (30:1).

Figure 4.50 : Medium and high levels of desired stiffness and the corresponding hysteretic actual behaviors, for the KAMO Medium Ball reducer (30:1).

Figure 4.51 : Transmission stiffness data for the medium-size KAMO ball reducer transmission (30:1), showing two piece-wise data segments.

Figure 4.52 : Stiction/Friction and Viscous Damping Losses inherent in a DOJEN Cycloidal Cam Reducer.

Figure 4.53 : Low Level of desired and actual stiffness for the DOJEN Cycloidal Cam reducer (33:1).

Figure 4.54 : Stiffness Fidelity for medium (1.1 N-m/deg) and high (7.2 N-m/deg) stiffness levels tested on the DOJEN cycloidal cam reducer (33:1).

Figure 4.55 : Transmission Stiffness Trace for the DOJEN Cycloidal Cam Reducer.

Figure 4.56 : Frictional Torques as a function of output velocity measured while backdriving the CORBAC reducer.

Figure 4.57 : Low level of desired output stiffness, showing the desired ideal stiffness behavior and the actual hysteretic behavior of the REDEX Corbac reducer.

Figure 4.58 : Medium and high level of output stiffness for the REDEX Corbac reducer, showing both the desired and the actual levels of achieved stiffness behavior.

Figure 4.59 : Transmission stiffness and associated variability for the REDEX Corbac reducer (30:1).

Figure 4.60 : SEIBERCO Sensorimotor arrangement, illustrating the mutual permeance principle and the location of sensor windings used for position- and velocity sensing.

Figure 4.61 (a thru f) : Transmission Stiffness Traces for (a) the WHOI Cable/Pulley Reducer (30:1), (b) the H.D. Harmonic Drive Cup Reducer (60:1), (c) the KAMO Cycloidal Ball Reducer, (d) the REDEX Corbac Geared Cycloidal Reducer, (e) the DOJEN Cycloidal Cam Reducer, and (f) the SUMITOMO Cycloidal Disk Reducer.

Figure 4.62 : Representation of Linear 1 DOF Motor/Transmission/Load Dynamic System for controller-gain design purposes.

Figure 4.63 : Reduced Dynamic System during transitions through the backlash zone.

Figure 4.64 : Root-Locus representing the dynamic behavior for different dynamic systems and the transition between the two.

Figure 5.1a : Experimental Force/Torque Control Test Setup.

Figure 5.1b : Experimental Setup for most transmissions. Shown here is the harmonic drive coupled to the motor, the torque sensor, contacting the environment profile with the bearing-follower and the rocker arm.

Figure 5.1c : Experimental Setup for cable reducer. Shown here is the housing of the next joint coupled to the torque sensor, contacting the environment profile with the bearing-follower and the rocker arm.

Figure 5.2 : Experimental Torque Linearity of Brushless DC Motor - Measured vs. Commanded Motor Torque with the rotor locked.

Figure 5.3 : Experimental Torque Linearity of Brushless DC Motor - Measured vs. Commanded Motor Torque with the rotor free to move over a limited range.

Figure 5.4 : Open-Loop Torque Input to the Harmonic Drive Reducer with a simple torque wrench - high frequency input signal.

Figure 5.5 : Open-Loop Torque Input to the Harmonic Drive Reducer with a simple torque wrench - low frequency input signal.

Figure 5.6: Measured Output Torque to Square-Wave Input at 1 Hz and 5-to-10 and 5-to-20 N-m amplitudes for the WHOI cable reducer.

Figure 5.7: Measured Output Torque to Square-Wave Input at 1 Hz and 10-to-20 and 10-to-40 N-m amplitudes for the Harmonic Drive reducer.

Figure 5.8: Measured Output Torque to Square-Wave Input at 1 Hz and 5-to-10 and 5-to-20 N-m amplitudes for the KAMO ball reducer.

Figure 5.9: Measured Output Torque to Square-Wave Input at 1 Hz and 5-to-10 and 5-to-20 N-m amplitudes for the DOJEN cycloidal cam reducer.

Figure 5.10: Measured Output Torque to Square-Wave Input at 1 Hz and 5-to-10 and 5-to-20 N-m amplitudes for the REDEX Corbac reducer.

Figure 5.11: Measured Output Torque to Sine-Wave Inputs at 1 and 0.25 Hz with 5-to-10 and 5-to-20 N-m amplitudes for the WHOI cable reducer.

Figure 5.12: Measured Output Torque to Sine-Wave Inputs at 1 and 0.25 Hz with 10-to-20 and 10-to-40 N-m amplitudes for the HARMONIC DRIVE reducer.

Figure 5.13: Measured Output Torque to Sine-Wave Inputs at 1 and 0.25 Hz with 5-to-10 and 5-to-20 N-m amplitudes for the KAMO ball reducer.

Figure 5.14: Measured Output Torque to Sine-Wave Inputs at 1 and 0.25 Hz with 5-to-10 and 5-to-20 N-m amplitudes for the DOJEN cycloidal cam reducer.

Figure 5.15: Measured Output Torque to Sine-Wave Inputs at 1 and 0.25 Hz with 5-to-10 and 5-to-20 N-m amplitudes for the REDEX Corbac reducer.

Figure 5.16: Measured Output Torque to Square-Wave Inputs at 1 Hz with 5-to-10 and 5-to-20 N-m amplitudes for the WHOI cable reducer.

Figure 5.17: Measured Output Torque to Sine-Wave Inputs at 1 Hz with 5-to-10 and 5-to-20 N-m amplitudes for the WHOI cable reducer.

Figure 5.18: Measured Output Torque to Sine-Wave Inputs at 0.25 Hz with 5-to-10 and 5-to-20 N-m amplitudes for the WHOI cable reducer.

Figure 5.19: Measured Output Torque to Sine-Wave Inputs at 1.0 Hz with 10-to-20 and 10-to-10 N-m amplitudes for the HARMONIC DRIVE reducer.

Figure 5.20: Measured Output Torque to Sine-Wave Inputs at 0.25 Hz with 10-to-20 and 10-to-10 N-m amplitudes for the HARMONIC DRIVE reducer.

Figure 5.21: Closed-Loop Resonance Frequencies at maximum proportional force-error gain K_p , for the HARMONIC DRIVE and the WHOI cable reducers.

Figure 5.22: Theoretical Closed-Loop Stability Margin, associated gains and bandwidth, with experimental data points, for the WHOI cable reducer.

Figure 5.23: Theoretical Closed-Loop Stability Margin, associated gains and bandwidth, with experimental data points, for the HARMONIC DRIVE reducer.

Figure 5.24: Response to Square Wave Input for max. K_p gain ($K_p=0.95$) without and with input-velocity damping for the HARMONIC DRIVE reducer - in contact with surface.

Figure 5.25: Response to Square Wave Input for max. K_p gain ($K_p=0.95$) with input-velocity damping with acquisition of surface contact for the HARMONIC DRIVE reducer.

Figure 5.26: Response to Square Wave Input for max. K_p gain ($K_p=0.95$) without damping, and ($K_p=1.94$) with input-velocity damping illustrating similar bandwidths for the HARMONIC DRIVE reducer.

Figure 5.27: Root-Locus for Input-Velocity damping, illustrating the increase in performance due to increased damping of the proximal mode (with increasing K_d), and the negligible change in bandwidth ($\Delta\omega$) at the edge of the stability margin.

Figure 5.28: Lack of performance increase with added Input-Velocity damping due to sensor-hardware limitations (resolution) in the case of the WHOI cable reducer.

Figure 5.29: Time Responses to a Square Wave Input in desired output torque for (i) a purely proportional controller ($K_p=1.3$) with low-pass filtering ($a=20$ rad/sec), and (ii) a PI-controller ($K_p=1.0$, $K_i=5.0$) with low-pass filtering ($a=95$ rad/sec) implemented on the WHOI cable reducer.

Figure 5.30: Block Diagram of a First-order Lag Filter introduced into the feedforward path of a single-compliance transmission model in hard surface contact, together with PD torque controller and P-Torque & D-Input Velocity Controller Stability Margins.

Figure 5.31: Proportional Gains K_p at the edge of the Stability Margin vs. the first-order filter constant 'a', for the WHOI cable reducer and the HARMONIC DRIVE reducer.

Figure 5.32: Response of WHOI cable reducer and HARMONIC DRIVE reducer to a desired sinusoidal output torque (5 to 10 and 10 to 20 N-m), both running with similarly 'tuned' PI controllers.

Figure 5.33: Response of DOJEN Cycloidal cam reducer and KAMO Ball reducer to a desired sinusoidal output torque (5 to 10 N-m), both running with similarly 'tuned' PI controllers - KAMO trace has been offset by -5N-m to show both traces on a single plot with similar scales.

Figure 5.34: Response of WHOI Cable reducer and HARMONIC DRIVE reducer to square wave input running under PI controllers, to illustrate torque-dependent stability and performance issues.

Figure 7.1 : Open-Loop Transmission-Load-Sensor System.

LIST OF TABLES

Table 2.1 : Published Transmission Parameters for the transmission types studied in this thesis: (\$) - measured at input, (#) - measured at output, (*) - measured at output.

Table 3.1 : Real Physical Parameter Values for the Stability and Performance Analysis of the 2 DOF Model Structure.

Table 3.2 : Real Physical Parameter Values for the Stability and Performance Analysis of the 3 DOF Model Structure.

Table 4.1 : Tabular representation of frictional losses in all the six transmission types tested.

Table 4.2 : Measured and Published minimum and maximum transmission stiffness values for all the six transmissions tested.

CHAPTER 1

(1) INTRODUCTION

This section is intended to introduce the reader to the background information needed to understand the motives and implications of the research performed in this thesis. In order to understand the need and the implications of this research topic, we have to illustrate what research has been done in the area of interaction control using different controllers and hardware configurations, and what the accomplishments and difficulties have been in implementing these approaches. Most of the reported research results have cited many barriers to achieving high bandwidth interaction control (achieving in some way, combined/separate position and/or force control), when a robot interacts with its environment. Many researchers have focussed on computational limits (computational and communication delays), sensor characteristics (type, location, resolution, signal-to-noise ratio for position/force transducers), stable and high performance controller structures, robot hardware design (actuators, transmissions, linkages, etc.), as well as purely mathematical physical system modeling techniques to better understand machine behavior and design issues.

We will also motivate the need for the research done in this thesis, by stressing the important relation between hardware design, physical system modeling and control theory. Reasons for the successful implementations of interactive controllers will be shown to be rooted in the proper combination of system design parameters. We will focus our attention on the area of actuator/transmission design, analysis and control. The following chapters will show that these hardware elements impose limiting stability and performance restrictions on most of the 'stiff' robotic manipulators built for academia and industry, when used in force or position control applications with certain types of sensors and actuators.

(1.1) Background

In order to provide adequate background information concisely, the information presented next will be split into different topic-sections. There may be some crossover, but this structure will facilitate in understanding what the current state of the art is in robot interaction control, where the problems are, what problems have been addressed and how successful researchers have been at solving some of these problems.

(1.1.1) Controller Structure Design and Experiments

In this section we will briefly explore the different controller structures that researchers have used to control robots in different task scenarios. The intent is not to rate nor compare them, but to simply give a review of how successful certain controller structures were at achieving the desired performance levels. It is also interesting to note what limitations certain controllers exhibited and what 'fixes' had to be implemented to insure proper system stability and performance levels.

Position Controlled Manipulators and associated research

In order to control robots that perform purely trajectory-following tasks, where no contact with the environment is expected, a whole variety of linear and nonlinear control algorithms have been proposed that may all differ in terms of performance, stability, and robustness. The notion that complicated nonlinear dynamic systems can be described by a set of linearized equations about different setpoints is still a widely used approach in the control of aircraft and submarines [Humphreys & Watkinson (1982)]. Each operating point yields a separate (optimal) set of control gains which is stored away and then intermediate gains can be computed by simple interpolation - an approach known as gain scheduling. There are some interesting stability properties for such systems as discussed by Shamma & Athans (1987) and Shamma (1988).

But in the case of robotic manipulators, nonlinear inertial models can be obtained using the Lagrangian formulation [Hollerbach (1979, 1980)] by following certain conventions (like the Denavit-Hartenberg convention). Not only the dynamics, but also the forward and inverse kinematics are important in order to extract cartesian positions/velocities from joint positions/velocities, or conversely, joint-positions/velocities from cartesian positions/velocities [Hollerbach (1983), Lin (1987)]. Standard joint servo control has been widely applied to the robot systems currently in use [Paul (1973, 1981), Luh & Walker & Paul (1980)], such as the PUMA 560 [Austin & Fong (1980)]. Most research focussed on controlling joint behavior and placing the closed loop poles which would then result in desired behaviors [Freund (1982)] at the joint/cartesian levels.

For an inertial dynamic robot model, the dynamic forces (gravity coriolis inertial, etc.) can be used to compute torques to be added to the desired joint/endpoint behavior [Luh & Walker & Paul (1980)], in order to replace the natural system dynamics with the desired dynamics - a method known as computed torque. This approach turned out to be

very sensitive to uncertainty in parameter values and thus lacked the stability robustness [Markiewicz (1973)] to be universally applied to a general class of robots [Morris (1984)].

With the becoming of age for sliding control [Itkis (1977), Utkin (1971, 1977)] in the field of robotics [Slotine (1983) Hashimoto et al (1987)], these barriers have been largely removed. A lot of work by Slotine cleared up questions about stability robustness issues [Slotine (1985)], while also delving into the areas of sliding observers [Slotine & Hedrick & Misawa (1986)], and adaptive sliding manipulator control [Slotine (1988), Slotine & Li (1986, 1987)], where a minimum set of unknown parameters (nonlinear combination of physical parameters) could be estimated and result in desired performance levels while guaranteeing system stability. Nonlinearities such as actuator saturation [Slotine & Spong (1984)], as well as flexible structures [Slotine & Hong (1986)], could appropriately be dealt with, with this controller structure. Control of other highly nonlinear systems such as underwater vehicles also benefitted from this control approach [Yoerger & Slotine (1985, 1986)]. Some work has also been done to extend this control methodology into the area of combined vehicle manipulator control [Yoerger & Slotine (1987), Longman et al (1987), Yastrebov (1985), Schempf (1987)], where the notion of supervisory control has found an area of large applications [Sheridan (1986, 1987), Yoerger & Sheridan (1985), Yoerger & Newman (1986), Ferrel & Sheridan (1967)].

Solutions to such issues as time-optimal control of robot manipulators [Kahn & Roth (1971), Rajan (1985), Seeger (1985)], design and control of redundant manipulators [Karlen et al (1987), Chang (1986), Hollerbach (1986), Nakamura & Hanafusa (1984), Yoshikawa (1984, 1985), Luh & Gu (1985)], model-referenced adaptive and self-tuning controllers [Dubowsky & Forges (1979), Donaldson & Leonedes (1963), Aylor (1980), DeKeyser (1983), Landau (1974), Ortega & Spong (1988)], robot parameter identification algorithms [Weiping & Slotine (1987), Khosla & Kanada (1985), Lyung (1981), Astrom & Wittenmark (1986), Olsen & Bekey (1986), An & Hollerbach (1986)], and other combinations of linear/nonlinear controllers [Dwyer et al (1985), Egeland (1987), Pierre (1981, 1982)], have been proposed and tested (experiment or simulation). Control structures such as configuration space control [Horn & Raibert (1977)] began studying the trade off between computational load and memory storage, since torques required to move an arm along a desired trajectory could be computed via coefficient look-up tables indexed by the manipulator configuration. Research performed by Luh, Walker & Paul [(1980)] made this approach unnecessary by replacing it with an online computational scheme.

Another area in the field of trajectory control of robots, termed trajectory planning, also received a large amount of research interest [Atkeson & Hollerbach (1984)].

Researchers were trying to automate the way a computer could help determine desired

joint/endpoint trajectories [Brady (1984), Brooks (1982, 1983), Brooks & Lozano-Perez (1982), Donald (1983, 1984, 1985)] based on a simple task description, by a variety of methods. Some of the path planning methods also incorporated the ability to deal with path planning in the presence of obstacles [Gilbert (1984), Lozano-Perez (1980, 1983)], while others also explored path-planning for active interaction with the environment [Lozano-Perez (1981)], e.g., peg-in-hole tasks, where not only a study of desired positions/orientations but also forces/torques was necessary [Ohwovoriole & Hill & Roth (1977), Buckley (1987)].

But most of these control approaches were unable to deal with a robotic system that should be capable of closely following a desired trajectory in free space and then perform a complex task which would involve substantial interaction with its surrounding environment. Some of the expectations of robots heralded early on, could not always be fulfilled with the hardware and controller structures mentioned above.

Several approaches were taken, starting in the late 50's by Goertz, Vertut in the 60's and Drake in the 70's, who built robots and end-effectors based on completely different hardware and control ideas, followed by other researchers which developed different controller structures that could be implemented on (supposedly any) a robot to achieve a high performance and stable interactive behavior. The contributions made by many researchers in the field of interactive controller design can best be described by outlining the different proposed controller structures and their relative performance, stability bounds, and transparency (ease of use, etc.).

Control of Robots interacting with their environment

Goertz [(1952)] and Vertut [& Marchal (1980), (1983), & Espiau (1984)] would use the concept of master/slave manipulators in order to give an operator the ability to interact with their (in this case hostile) environment. The connection was either completely mechanic or remote by using feedback signals. A lot of work has since been done in the field of bilateral manipulator control [Inoue (1981), Gavrilovic (1973), Bejczy (1984), Bejczy & Salisbury (1980, 1983), Streiff (1984)]. It still remains the most successful implementation of robots performing useful work by interacting with their surrounding (unstructured) environments (radioactive hot-cells, underwater salvage, etc.).

One of the earliest approaches taken to understand robot motions in different reference frames was performed by Whitney [(1969, 1972)], by combining rate and position control. But it proved to be unsuited for many constrained task descriptions, since

all motions were differential approximations. Paul [(1973)] was able to assign different joints to provide compliance for each desired degree, and drive the remaining joints in position-servo mode. Paul and Shimano [(1976)] were able to translate a task description, by furnishing information about compliant (or force controlled) orthogonal degrees of freedom and position controlled degrees of freedom, which was then used to control a robot arm to provide these different behaviors in cartesian/tool space. Simunovic [(1975)] also explored assembly processes from the standpoint of a force-driven positioning task.

An early example of computer-assisted force control was performed by Whitney (1971). Whitney [(1985)] also traces the historical development of interactive control by giving a good chronological overview of this field of research. Wu and Paul [(1980)] propose an approach by which the torque to each joint can be controlled to achieve a compliant endpoint behavior. The joint-torque was controlled by measuring torques at the output of the reducer/transmission (using strain gauges) and closing a torque loop around the entire motor/transmission/load system. They also explore the trade-offs between measuring forces/torques at the wrist and at the joints. Both methods have their pros and cons, as will be seen later. Other early work in compliance control was done by Inoue [(1974)].

Explicit force control, in the early stages at least, was not thought of as a necessary control mode for assembly, but once the need for it became obvious [DeFazio et al (1981)], many people thought it would not only be a necessary but also a sufficient control strategy [Inoue (1974), Ishida (1974)]. In order to make it useful though, it had to be combined with some other form of position control in order to perform useful tasks. Control strategies such as hybrid position/force control [Raibert & Craig (1981), Anderson & Spong (1987), Craig (1986)] are based on the notion that an interactive task can be split into position- and force-controlled degrees of freedom [Paul (1987)]. A control algorithm can be developed that would use this information to achieve force control in one direction (usually normal to the contact surface) and 'stiff' position control in the remaining degrees of freedom [Yoshikawa & Sugie & Tanaka (1987), Merlet (1987)]. Calculation of the necessary selection matrices could most prominently be helped by the task analysis done by Mason [(1979), (1981)], who was actively involved in force and compliance control of robot manipulators [Mason (1981)]. Stiffness Control [Salisbury (1980)] translates desired cartesian stiffness/damping behavior into joint coordinates, so that a joint servo can apply torques based on joint position/velocity errors and the configuration dependent stiffness and damping matrices (which are related to the cartesian equivalent matrices via the jacobian). Selection of the cartesian behavior still remained a hard task, since it was highly task dependent (Mason [(1982)], Ohwovoriole [(1977)] and Whitney [(1982)] have

done some task analysis trying to understand position/force constraints). Damping Control [Whitney (1971)] implemented a six degree of freedom damper in cartesian control, by exerting torques at each joint, computed by converting sensed forces to offsets in the reference velocity trajectory. Other researchers [Slotine & Li (1987), Slotine (1988), Niemeyer & Slotine (1989)] have tried to modify stiff trajectory following algorithms to suit interactive tasks, while insuring stability and desired performance levels. Another more esoteric/binary (and certainly low bandwidth) approach was suggested by Giraud [(1984)], that specifies motions and torques/forces to be applied in the tool frame, by considering an assembly task a control problem, and then performing a set of logic branching (analog and binary) comparisons, until required force and positional requirements are met (which implied proper task completion).

The advent of impedance control [Hogan (1979, 1981, 1982, 1984, 1985, 1986, 1987), Hogan & Cotter (1982), Cotter (1982), Wlassich (1986)] resulted from the need of understanding interactive system dynamics and behavior from a more theoretical viewpoint. Hogan postulated that the correct control structure would generate forces based on the imposed displacement/velocity constraints of a manipulator coupled to an environment. The resulting relation was termed an impedance, which is analogous to an impedance in electrical theory, relating effort (force/torque) to flow (linear-/angular-velocity). The control algorithm is based on a cartesian description of impedance elements (springs, dampers, masses) which result in applied interface forces/torques that are purely dependent on a desired- and interface-trajectory. This method represents a compact way to incorporate position and force control into a single controller structure. Its most powerful attribute is that it can be proven to be stable with a wide class of environments, using some simple arguments of passivity [Colgate (1987), Colgate & Hogan (1987)]. The main differences with stiffness control are not only the inherent stability guarantees, but also the ability to alter the apparent system inertia using scaleable force feedback. Issues of bandwidth limitations for such control structures were treated by Kazerooni et al [(1985)] and Kazerooni, Haupt & Sheridan [(1986)]. Further proof that impedance control could indeed perform interactive tasks well (performance- and stability-wise), was given by Wlassich [(1986)] and Kazerooni [(1987)] by controlling or building different robotic hardware setups to contact or to deburr surfaces, problems which have always received a lot of attention before, since force/compliance control seems perfectly suited for such applications (especially deburring [Plank & Hirzinger (1982)]).

Some moderately useful adaptive versions of impedance control have also been proposed [Kelly et al (1989)]. Asada & Asari [(1988)] have attempted to measure (assumed constant) human impedance parameters for a certain task and then replicated them

with a robot, while showing that this approach does yield better performance but is very sensitive to task scenarios. Learning from human performance [Asada & Yang (1988)] or machine performance [Asada & Izumi (1987)] in order to improve robot performance has received some attention, but not shown itself to be widely applicable. Other researchers have used such concepts as operational space control [Khatib & LeMaitre (1978), Khatib (1983), Khatib (1985)] or impedance control (dynamic potential functions) [Andrews (1983), Andrews & Hogan (1983), Newman & Hogan (1987)] to not only control robots, but to also aid in obstacle avoidance.

Many implementation problems still remained [Williams & Glover (1987)]. The most prominent one was termed 'contact instability' or the inability to make contact with a massive or stiff environment without large impact forces and/or going unstable (surface-bouncing limit-cycle). Wlassich's implementation was limited in inertia reduction by an out of plane bending mode of sensor- and arm-linkage. Other approaches [Khatib & Burdick (1986)] use operational space compliant control, which uses large damping during impact to avoid high frequency control action to avoid exciting unmodelled resonant modes. Their implementation was performed on a PUMA 560. Other people have studied the effect of environment and force-sensor stiffness [Roberts (1984), Roberts & Paul & Hillberry (1985)] on the stability of contact acquisition.

The concept of macro/micro manipulation [Sharon (1984, 1988, 1989)] made high bandwidth stable interface force control possible. It relies on a large envelope, low bandwidth macro robot with a high bandwidth, small envelope micro-robot (50 lbs at 45g) mounted to its end, to perform high bandwidth position/impedance/force control. By matching macro- and micro-robot impedances, this hardware setup has been shown to drastically improve force control bandwidths. Position bandwidths of 28 Hz and force control bandwidths of 60 Hz were achieved which lie well above the first resonant mode of the macro manipulator.

Salisbury & Craig [(1982)] and Salisbury & Roth [(1982)] have studied kinematic and force control issues which govern the design of articulated end effectors. Salisbury did build and test a three-fingered end-effector which was then mounted to a PUMA manipulator to perform dexterous manipulation. Shimano [(1973)] also explored other force control issues related to the kinematic design of manipulators. Vafa & Dubowsky [(1987)] have explored the dynamics and control issues of space-borne manipulators [Lee & Bekey & Bejczy (1985)] by reducing the manipulator from its original complexity to a 'virtual' manipulator representation for ease of modeling and computer-control.

(1.1.2) Robot Hardware Design

With the development of new control algorithms to perform interactive control, came new advances in robot design. The design areas were not only limited to material selection and kinematic layout, but were also concerned with the development of new sensors, actuators and transmissions.

One of the earliest pieces of hardware built, which allowed interactive or assembly tasks with tolerances far below those of the positional accuracy and resolution of conventional industrial robots, was the RCC [Drake (1977)]. The addition of a properly designed RCC-device [Whitney & Nevins (1979), Whitney & Rourke (1986), Nevins & Whitney (1978)] has been responsible for the successful use of assembly robots in industrial settings, performing a variety of tasks (most of the IC assembly today is performed with small, light-weight robots, while IC lithography is done with a simple 1 DOF robot and indexing tables). Other researchers have built new input-devices or generalized force-reflecting masters [Handlykken & Turner (1980)] in order to control existing robots outfitted with some force sensing device in order to perform interactive tasks. Many problems still could not be avoided, especially stability limits due to hard surface contact [Hannaford & Andersen (1987)].

The conventional robots with high-reduction non-backdriveable gear reducers have seen a lot of alternate designs which attempt to circumvent many of the problems associated with earlier prototype manipulators [Youcef-Toumi & Nagano (1986)]. Asada & Youcef-Toumi [(1983)] developed a manipulator that gets rid of transmissions by using direct-drive motors [Kondoh et al (1986)]. This design effort not only resulted in the development of new brushless DC motor technology, but also in a kinematic/dynamic design effort [Asada (1983)] to reduce dynamic cross-coupling by diagonalizing the inertia matrix via proper physical design [Youcef-Toumi & Asada (1985, 1987)]. Asada & Toumi & Lim [(1984)] showed that torque control through analog current servo loops has to take into account some possible nonlinear electronic component behavior. They also explored the impact of placing a strain-gauge torque sensor at different locations between the motor-rotor and the output link in order to retain a stiff motor-link system and obtain the necessary sensitivity for fine torque control. The relative success and encountered problems of force control using direct-drive robots are outlined in Youcef-Toumi & Li [(1987)]. Asada [(1983)] and Asada & Ogawa [(1987)] looked at the impact of effective endpoint inertia on the

performance of interactive tasks, using effective endpoint inertia ellipsoids, effective mass and centroid locations, to plan and execute tasks such as deburring, grinding and chipping [Asada (1987), Asada & Goldfine (1985)]. Solutions such as bracing the manipulator against the workpiece to achieve better performance and stability bounds was also presented as an alternative [West & Asada (1985), Book (1984)].

Research into joint configurations for efficiency and dexterity [Salisbury & Abramowitz (1985)], followed by simple prototyping [Lim (1981), Townsend & Eberman (1986)], led to the design of the MIT WAMS (Whole Arm Manipulation System) manipulator [Salisbury (1987), Salisbury & Townsend & Eberman & DiPietro (1988), Townsend (1988)]. A similar design effort resulted in the development of the WHOI Underwater Manipulator [DiPietro (1988)]. Both designs employ cable transmissions [Vertut & Liegois (1979), Vertut (1980, 1983, 1984)] to increase the fidelity of force control necessary for interactive tasks. Townsend [(1988)] and DiPietro [(1988)] give a very good analysis on relative cable reducer design to improve stiffness and reduce friction in the transmission, including a very thorough study of the relative efficiency of cables as transmission elements [Townsend & Salisbury (1988)], and the importance of mechanical bandwidth in performing interactive tasks [Townsend & Salisbury (1988)].

Other special purpose robots or end-effectors have also been built [Kazerooni & Guo (1987)], which proved that impedance control could be applied to such tasks as robotic deburring [Kazerooni & Bausch & Kramer (1986), Kazerooni (1987)] or high-speed assembly [Asada & Kakumoto (1988)]. Introduction of a (possibly redundant) mechanically compliant joint, has been shown by Andeen & Kornbluh [(1988)] to provide better compliance control, but no clear dynamic performance data was given, which related to real tasks. It was an interesting alternative to adding compliance at the interface (gripper, force sensor, etc.), since it gives one the ability to use a well modelled compliance to control interaction behavior [Van Brussel (1979)].

Another interesting hardware solution to achieve high bandwidth stable position/force control is that of a macro/micro manipulator [Sharon (1988)]. As explained earlier, a low weight, high bandwidth, small work envelope micro-manipulator is mounted to the extremity of a low bandwidth, heavy, large work envelope macro manipulator, resulting in a system that can achieve effective endpoint bandwidths in position/force/impedance control that are at least an order of magnitude larger than the first resonant mode of the macro manipulator.

Wrist and end-effector designs have also been an important area of research. Many design philosophies and associated hardware exist today [Hollerbach (1982), Salisbury (1982), Jacobsen (1984), Ulrich (1990), Chiang (1985), Cutkosky (1982), Tilley (1986)]

and the actual research area of grasping and handling objects or the environment itself, are still areas of active research. Another important area is that of designing wrist and end-effectors to handle large impact loads [Kahng & Amirouche (1987)] without causing the well known contact instabilities.

Several other implementations of different actuator/transmission technologies as well as kinematic layouts have been built and are commercially available. Implementations span the field of redundant (electric) manipulators (using harmonic drives) [ROBOTICS RESEARCH OH. or Karlen & Thompson & Farrell (1987), SPINE Robots], hydraulic and pneumatic master/slave manipulators [SCHILLING CA., SARCOS UT., WESTERN SPACE & MARINE CA.] as well as micro robots with resolutions down to nanometers currently being built in England. Many robot manufacturers use different kinematic arrangements to best suit the task. Whether it be a serial configuration, parallel, cartesian or SCARA, they all have their pros and cons - a topic which is beyond the scope of this thesis, but has been well researched by Toumi [(1984)], Townsend [(1988)], Vertut [(1980)] and DiPietro [(1988)].

A separate but related area of research is that of control of flexible structures [Hanselmann & Moritz (1987), Kissel & Hegg (1986)], vehicles [Gevarter (1970)] and manipulators [Tilley et al (1986)]. A lot of recent work concerns itself with the dynamic models of flexible structures [Book (1976, 1984)], and how to control them [Hastings & Book (1985), Pfeiffer & Gebler (1988)]. Cannon & Schmitz [(1984)], Cannon and Rosenthal [(1985)], and Hollars & Cannon [(1985)] have done much work in understanding the complexities of modeling and control of simple and complex structures and robots. The main thrust of the research focussed on achieving bandwidths comparable and hopefully larger than the lowest resonant mode. The idea behind this research was not to try to push the design and manufacture of robot manipulators, but to understand and better model and control the inevitable compliances present in all mechanisms. Issues relating to vibration control are very closely tied to this field of research as well [Meckl & Seering (1988)].

Motor/Controller design has also been an area of intense research, mostly driven by the need for academic-research manipulators [Asada & Toumi & Lim (1984), Person (1989), Poggio & Rosser (1983)]. With the advent of brushless DC motors [MOOG, INLAND, SEIBERCO, KOLLMORGEN, PS, etc.] came the need to properly control motor torques using analog current loops and reducing mechanical ripple-torque to levels acceptable to the control's engineer [Maloof & Forrester & Albrecht (1987)]. The best figures available today are that ripple torque can be reduced to around 1 to 5% of full rated torque via compensation and mechanical design of stator and rotor [Maloof et al (1987)].

Even better closed-loop torque-following with errors around 0.1% were achieved by Levin [(1990)]. He basically mounted the stator on a cylindrical reaction-torque sensor and closed a high-bandwidth servo around this mechanical arrangement. The advantages are clearly that we are servoing in the mechanical domain, and do not have to rely on a measured torque constant to provide the mapping from the electrical to the mechanical domain.

Sensor technologies are still an area of active research. In the past years [Wang (1978)], the need for high fidelity force sensors has become very apparent, and many different companies make strain-gauge based wrist force sensors [BARRY WRIGHT, LORD, JR3]. Since the sensitivity of these devices is inversely proportional to their stiffness, an interesting compromise is necessary in order to trade off stability and resolution in force control tasks. These sensors could be located at (a) the actuator, (b) transmission output, (c) the wrist and (d) the gripper-tips. The relative location of these torque sensors has a direct effect on the stability of torque servos, depending on the mechanical hardware involved, since we are implicitly assuming that transmission dynamics (linear or nonlinear) and structural dynamics can be compensated for. High bandwidth motor-current servos (analog usually) are possible, but closing a digital torque servo around a motor/transmission assembly, or possibly even the entire manipulator by using wrist- or endpoint force-sensors, does not guarantee equal performance nor overall stability. Other sensors include inductive displacement [Piller (1982)] and rate [Seitz (1989)] sensors, as well as piezo-electric [(1989)] and magnetoelastic [Vranish (1982)] force sensors. Some sophisticated gripper sensors are not only able to tell the magnitude and orientation of the force/torque vector applied to the gripper surface [Brock & Chiu (1985)], but also the relative shape and contact pressures of a grasped object/surface [BONNEVILLE SCIENTIFIC UT.]. Many other types of sensors exist to improve the ability of robots to perform tasks (vision, relative position, tactile arrays, proximity sonar), but will not form part of the theoretical treatise in this thesis.

(1.1.3) Physical System Modeling and Stability Analyses

This section concerns itself with the problems researchers have encountered when implementing different interactive control schemes using different hardware configurations, and what theoretical analysis has been done to explain and circumvent the observed behaviors (and with what degrees of success). The intention here is to become aware of what research areas have received the most attention and where the persisting difficulties lie

in terms of realistic physical system modeling and problematic design issues that have to be resolved, in order to achieve high performance (large bandwidths) stable interaction control.

One of the earliest work that began showing some of the problems in stable force control was done by Ferrell [(1966)] and Ferrel & Sheridan [(1967)], where they studied the implications of delays in the force feedback loop to the operator, with respect to task performance and stability in remote manipulation scenarios. This work was essential in understanding performance and stability issues in force-reflecting master/slave systems. One of the simple suggestions, in order to achieve stability, was to use the move-and-wait strategy. This type of telemanipulation is one of the main areas where computer controlled force interactions are important. But even at high sampling rates (low time delays), behaviors such as contact instabilities (mainly in contact of hard surfaces) play an important role in limiting system performance and stability. Whitney [(1985)] give some concise literature examples of experimental setups plagued by this problem.

Luh, Fisher & Paul [(1983)] used the Stanford Arm to close joint torque loops around a motor/harmonic-drive transmission assembly (adding a strain gauged shaft). They modelled the harmonic drive as a backlash nonlinearity and used SIDFs to analyze limit cycles and eliminate them through (analog) phase lead compensators. A constant time-invariant friction torque was fed forward, but neither stiction nor transmission stiffness were modelled. Good, Sweet & Strobel [(1985)] showed that there was a need to model transmission stiffness (harmonic drives), linkage compliance as well as actuator nonlinearities (saturation) in an ASEA robot. They performed a nonlinear simulation that modelled all the above elements and got a moderately close match between simulated and experimental data. Without the dynamic model, the lowest resonance lies at 9 Hz. No data was presented which showed how better models could increase control bandwidth. They also suggest to use joint/endpoint sensors to reduce inaccuracies due to transmission compliance and motor nonlinearities. No analysis is given as to what stability problems that approach would result in. Another related issue was presented by Stepien et al [(1985)]. This paper dealt with the issues of admittance control and relative stability properties of PID controller structures. Their application was that of deburring. They used a velocity-servoed GE-P50 manipulator, coupled with a wrist force-sensor to give force feedback. The generated force error was used to generate velocity setpoint updates to the local joint servos. Modeling the transmission compliance, again due to the presence of harmonic drives, became a necessity in order to properly design the PID (admittance) compensator to increase the system stability without markedly reducing the stability margin. Their deburring task resulted in RMS force errors of about 10% to 30% (taken

from steady-state data only), depending on the rate of deburring-tool feed speed. Even though transmission compliances were modelled and used in the controller design, no mention was made how good these predicted stable gains actually were. The forces/torques in a deburring task are fairly high-frequency, but of small amplitude in general, and thus represent a useful but not very taxing force control task.

Yabuta & Chona [(1987)], showed the effects of friction/stiction, discrete sampling and latency, on the stability properties of a PI admittance controller (position & velocity), and a PI torque-controller. Their results indicated that the stability of any such controller structure is dependent on the type of local servo controller (position- or velocity-setpoint servo). Furthermore, the presence of stiction and friction showed that proportional gains had to be reduced if integral gains were increased, in order for stability to be preserved. The presence of large time-lags was (as expected) found to impose restrictive limitations on controller gains, for stability sake.

The development of the Massachusetts Institute of Technology Direct-Drive Arm (MIT DDARM) [Asada & Youcef-Toumi (1983)], led to the discovery of certain nonlinearities and unmodelled dynamics [Kondoh & Youcef-Toumi (1986)]. The arm structure was shown to have low mechanical stiffness and a backlash-like nonlinearity which was traced to a deadband in the motor controller circuitry. The use of samarium-cobalt DC brushless motors also introduced an effect of cogging or torque ripple. This ripple could be as much as 10% (or more if not compensated) of the fully rated torque. Different motor designs experience different levels of cogging. Pure electronic (digital or analog) compensation is many times not enough. Arranging the magnets on the rotor has a large effect on ripple torque as well. Reducing the ripple to a 2% to 5% level was possible, according to Youcef-Toumi et al., but levels of 0.1% have been achieved in other motor designs (NOT direct-drive motors though). Torque-ripple can have an extremely destabilizing effect on force control, especially in tasks where small endpoint motions are necessary and one relies on a joint-torque or wrist force sensor to close a force control loop.

Other research [Maples & Becker (1986)] focussed on using a robot with stiff, local, high bandwidth joint controllers with a lower bandwidth outer force control servo which would be used to update joint angle setpoints - in effect implementing an admittance controller. Implementing admittance control, where interface forces are used to change position setpoints, is just the inverse of impedance control, where position errors are used to update joint-torques or cartesian torques/forces. A good comparative study between these two control schemes was done [Chapel & Lawrence (1987)], and it was found that sufficient stability sensitivity to a low bandwidth torque loop existed, which reduced the

performance of a manipulator controlled under admittance control. Lawrence and Stoughton [(1987)] and Lawrence [(1988, 1989)] later showed that time delays and actuator saturation characteristics have a direct impact on achievable performance. Lawrence [(1988, 1989)] showed through a SIDF analysis that actuator saturation limits an impedance controlled manipulator to only achieve low impedances very well, while an admittance controlled manipulator has a hard time achieving high admittances (low impedances). This is simply due to the fact that as nonlinearities (saturation, time delays, transmission stiffness, -stiction/friction) grow, the system behaves more and more along the lines of its natural open loop (intersample) dynamics. The resulting stability limits are much more severe for admittance controlled robots attempting to achieve high admittances (low impedances), than for impedance controlled manipulators attempting to achieve high impedances (low admittances).

An & Hollerbach [(1987)] investigate kinematic and dynamic stability issues in a series of 2 papers. The simple (linearized) kinematic stability analysis reveals that Raibert & Craig's [(1981)] hybrid force/position control algorithm is unstable for any kind of revolute manipulator (since it involves a kinematic coordinate transformation in the feedback path), while Salisbury's [(1980)] stiffness control and other operational space control methods [Khatib (1983)] are stable and independent of the robot structure they are implemented on. In their dynamic stability analysis, they show that in order to achieve stable force control, one is best advised to rely on fast open-loop joint-torque, while low-pass filtering force error signals to achieve the steady state accuracy. They clearly state that both Roberts et al [(1985)] and Whitney [(1985)] have shown that a softened endpoint sensor can increase the stability limits for a force controlled environment, unless one is willing to live with reduced performance by adding excessive damping during the expected contact phase [Khatib & Burdick (1986)]. Their implementation was done on a single link of the MIT DDARM [Asada & Youcef-Toumi & Lim (1984)]. They show that neglecting a simple resonance in the system will result in highly underdamped surface contact, which can only be alleviated by passive endpoint damping. The preferred approach, which did not require modeling of any kind, was to use open-loop torque control with an offset provided by a heavily low-pass filtered integrated force-error signal. Their results in the low-force responses were heavily governed by system nonlinearities (magnetic cogging, dead-zones, etc.).

A more detailed attempt at understanding the effect of unmodelled dynamics, be they linear or nonlinear, was also performed by Yabuta & Chona [(1987)]. Their paper analyzes the stability issues in robot force control, of a 1 DOF lumped mass robot coupled to the environment via a linear spring. Effects such as stiction/friction (and the related

stick/slip behavior), digital sampling rate and environment stiffness are studied to reveal their effect on position-, velocity- and torque-servos. Eppinger & Seering [(1986, 1987)] present a somewhat detailed, yet qualitative, analysis of dynamic models for robot systems and the related force control stability issues. A complete summary of these is given in Eppinger [(1988)]. He gives a fairly complete list of the factors (environment stiffness, sensor dynamics, workpiece dynamics, arm flexibility, actuator bandwidth, sampling rate, actuator saturation, low-pass filtering, impact forces, transmission backlash and -friction) that may contribute to instabilities in robot force control. They analyze a wide majority of them and conclude that there are clear qualitative statements that can be made which can explain the stability limitations researchers have been encountering in their research and implementations. Their analysis also shows, that PI force control has a more destabilizing effect than a PD controller or the addition of a simple lead network into the feedforward path, while low-pass filtering also causes increased instability. The most destabilizing effect is the one resulting from noncollocated actuator and sensors (when in the presence of transmission dynamics for joint-servos or also bending modes when doing endpoint measurement and control like with a wrist force sensor).

Pasch & Seering (1984) explore such issues as optimal transmission ratio selection, based on maximizing system acceleration (how to match a motor to a driven load?), matching actuators to system configurations (given a load and a transmission, what is the best actuator?), and how to decide on actuators and transmission to minimize move times with velocity constraints. Their analysis is important because it stresses the need to match driven loads to motor impedances for optimum power transfer, where the optimal transmission ratio is expressed by the square root of the motor-to-load inertia. The actual analysis is obviously designed for trajectory following systems, but some of their results are of importance for the design of actuator/transmission packages for high performance robots, irrespective of their use. Another interesting application of impedance matching was necessary for the control of macro/micro manipulator systems [Sharon et al (1984, 1987, 1988, 1989)]. It was shown to be necessary to properly structure the controllers for the macro and micro robot to achieve the highest bandwidth possible for positioning and force control tasks.

A more advanced and general actuator/transmission design and performance analysis was performed by Townsend [(1988)] and Townsend & Salisbury [(1987, 1988, 1989)]. Their transmission design focussed on cable reductions, which were used to then build the MIT WAMS (Whole Arm Manipulation System) robot [Salisbury & Townsend & Eberman & DiPietro (1988)]. Townsend performed a thermodynamically motivated efficiency analysis that showed that cable drives have an upper efficiency limit due to cable stretching

and shrinking (cable/pulley slip and/or viscous dissipation in bearings or between strands), which usually lies around 96% to 98%. Close attention to transmission characteristics is important if we want to use the entire arm for pushing, grasping and sensing objects. The first prototypes have been built at MIT [Townsend (1988)] and WHOI [DiPietro (1988)] and are currently undergoing testing. Preliminary results show that the claimed capabilities are indeed achievable (bandwidth, dexterity, stability, etc.). Both of these design prototypes take advantage of some very simple design improvements which boost the open-loop bandwidth of the system, resulting in ease of backdriveability. The placement of the actual reducer element as close as possible to the driven output, can be shown to result in the largest achievable effective output stiffness. Furthermore it was shown that in order to increase the stability margin for force control, transmission stiffnesses can be reduced without seriously affecting the closed loop bandwidth, in order to reduce possible contact instabilities due to excessive contact stiffness [Whitney (1985)].

A lot of work has recently been dealing with the understanding of friction and stiction properties in robot actuator/transmission systems. A very good historical perspective about friction research is given by Armstrong (1988), where he traces the research in friction as far back as Leonardo Da Vinci. More recent work in this century shows that Tustin [(1947)], using vector graphics methods (a precursor to the modern describing function analysis), was able to show the effect of stick-slip induced limit-cycling by studying the effect of stiction and friction. Limit cycles were induced even for a simple PD-controller. Rabinowicz [(1959)] also studied the properties of stick-slip motions in very simple experimental setups and proved that the parasitic energy losses due to friction are directly related to the speed and stiffness of a related transmission element. The models proposed for friction span a very large field, expressing the wide disagreement over such a fundamental matter. Many researchers have proposed various models, which show decreased friction with increasing velocity, increasing friction with increasing velocity, break-away distances of varying length, as well as the presence and absence of static friction components (see Armstrong [(1988)] for a complete review). The most commonly used model is that of direction-dependent coulomb friction with viscous damping, where stiction is omitted [Cannudas et al (1986), Dahl (1977), Craig (1986)]. The presence of stiction was first studied by Tustin, but later research expanded on this phenomenon. Gogoussis et al [(1987, 1988)] have studied the effects of feedforward compensation for purely coulomb friction/viscous friction robot joints, when controlled in trajectory following mode. They have tried to model the stiction/friction transition in order to explain limit-cycle behavior of a transmission (harmonic drive) with coulombic friction. They also studied the problem of resolving frictional torques in multi-jointed robots, but gave only a

conceptual proof without any experimental data. They are the first to study the hysteretical frictional behavior of harmonic drives [Gogoussis & Donath (1988)]. Walrath [(1984)] used an exponential friction model during the transition from stiction to friction and applied it successfully to airborne gyro gimbal assemblies. Kuntze & Jacobash [(1985)] used a simple force-dithering (high frequency low amplitude force disturbances) scheme to keep their manipulator joints out of the stiction zone. Kubo & Anwar & Tomizuka [(1986)] show that the introduction of even the simplest schemes for pure coulomb friction compensation can be successful. The only unquoted requirement is that it be chosen conservatively so as not to excite the unmodelled stiction/friction transition. The compensation scheme uses a velocity deadband and control memory decision algorithm to decide upon the magnitude and sign of the feedforward torque. They still report though, that the performance and stability of their harmonic drive robot was clearly dependent on magnitude and class of input which proves the presence of further (unmodelled) nonlinear elements. Dahl [(1977)] has shown that bearings can have life-dependent frictional and hysteretical behaviors, where new bearings have larger hysteretic losses than worn-in bearings but also a lower ripple torque than older bearings (due to localized areas of preferential wear in the bearing race). All his data showed a natural dependence on bearing preload (thrust or axial bearings).

A few researchers have tried to actively compensate for friction effects. They have obviously limited themselves to the purely coulomb friction [Olsen & Bekey (1986)] or the coulomb-viscous friction models [Canudas & Astrom & Braun (1986)]. In both cases the adaptive identification control algorithm succeeded in improving the performance of the system, but the results are only given in terms of simulations. The question of relative stability improvements is thus still unanswered. It is noteworthy to mention that the presence of stiction and its relation to relative motion, make it an acausal phenomenon that is very hard to model and even predict/identify. Armstrong [(1988, 1989)] has done an open-loop off-line identification of these parameters and then used them in a feedforward manner, which circumvents the inherent stability limits of adaptive closed loop identification schemes. He is another proponent, besides Tustin [(1947)], for negative viscous friction during the transition between stiction and friction. From a physical standpoint it seems hard to understand what physical process would be responsible for such behavior. Furthermore the sensors required to accurately measure and compensate for these behaviors, have really large bandwidth and resolution requirements.

The importance of understanding the interaction of stiction/friction behaviors for the performance and stability of force controlled systems is widely recognized, and a few researchers have looked at this problem - most notably Townsend & Salisbury [(1987)].

They looked at the presence of limit cycles in proportional-integral force control. The conclusion was that even though coulomb friction may extend system stability bounds (especially in the low velocity regime where a viscous damper does little to dampen oscillatory behavior), the system stability becomes highly input-dependent. Since compensating for stiction and coulomb friction is an inexact science, a simulation procedure and a describing function analysis were used to demonstrate extended stability regimes for systems with coulomb friction, while stiction behavior causes limit cycles, where the limit cycle amplitude is dependent on the difference of coulomb to stiction forces. The proper selection of distributed stiffness in a transmission with distributed friction and stiffness, has a direct bearing on the stability of the system.

Other research has focussed on how to distribute compliance throughout the robotic mechanism based on enhancing overall stiffness given a knowledge of expected force loading [Thomas & Chou & Tesar (1985)]. The approach taken was to use a numerical optimization scheme, but the scheme relied on criteria developed for positioning schemes where stiffness is necessary to reduce deflections due to external loadings. Wang [(1986, 1987)] has focussed on the optimization problem relating to actuator gains, -transmissions and actuator impedances. The actuator gain analysis is purely non-contact specific, since the numerical optimization criteria (using linear programming) is expressed in terms of joint speeds (reducing required power input to perform a desired move). The criteria are phrased in order to achieve quick endpoint velocity convergence in an isotropic fashion. It is similar (but less specific and more multi-dimensional) to the analysis performed by Pasch & Seering [(1984)].

The research that is more related to the design of stable interactive controllers, has lately brought some very interesting results [Fasse (1987), Fasse & Hogan (1989), Hogan (1987), Kazerooni (1985, 1987), Sharon, Hogan & Hardt (1989)]. The interesting points to note here, are that researchers have also been trying to deal with such real problems as contact instability by designing new controllers that can be shown to have natural physical properties that can be related to simple energy storage and dissipation. Attempting to design a controller for stable interaction with all environments (or at least a representative subset) was done by Colgate [(1987)] in his thesis and a paper with Hogan [(1987)]. It was interesting to see how different kinds of environments have different effects on the stability of manipulators coupled to them. Kazerooni [(1987)] also came up with some design rules in order to achieve coupled stability. Stable contact acquisition was shown to be possible with a macro/micro manipulator, but only because a properly chosen controller structure was implemented that has as its main attribute coupled stability guarantees [Sharon, Hogan & Hardt (1989)]. The selection of a physically achievable target

impedance, based on available sensing and actuation characteristics, is a necessary step in the design procedure of a realistic controller structure.

Fasse & Hogan [(1989)] have shown how to generate Lyapunov-based functions to analyze the coupled stability properties of a robot coupled to an energy-dissipative environment. They showed that contact instability is not only an impact phenomenon which may excite high order unmodelled dynamics, but can also be present when already in contact with the environment. In their paper they show how stability properties are related to unmodelled system dynamics (electromechanical actuator dynamics, drivetrain compliance, force transducer dynamics). Different types of unmodelled dynamics reveal themselves to have destabilizing effects even in the absence of force feedback (actuator dynamics when coupled to a massive environment). Asking for an effective endpoint stiffness greater than the transmission stiffness is not physically possible, while damping levels are also upper and lower bounded for coupled stability of a robot with transmission compliance. Force transducer dynamics were shown to be especially interesting. The stiffness of the force transducer was shown not to play a role in the coupled stability of the system (it does affect performance though), while the damping inherent in a force transducer is indeed shown to have clear implications on coupled stability. This is contrary to the assumed effect transducer stiffness has on stability of force controlled systems [Roberts & Paul & Hillberry (1985)]. The most interesting contribution of this paper is that the resulting dynamic behaviors of coupled systems can be arbitrarily complex, since the coupled stability can be determined analytically for any energy dissipative environment, even though the developed stability conditions are sufficient (but probably not necessary). It is the first appearance of any research that proposes Lyapunov functions to study coupled system stability.

Other researchers [Wang & Mason (1987), Cai & Roth (1987)] have attempted to understand the dynamics of impacting/contacting bodies, by incorporating friction, elasticity and inertial properties to bound contacting bodies as behaving with dynamics that fall somewhat in between the two extremes of impact dynamics (inertia dominated motion) and quasi-static dynamics (friction dominated).

Some very interesting practical impedance control results were obtained from the research performed by Wlassich [(1986)] and Raju [(1986)]. The former was able to show limiting performance in inertia reduction due to unmodelled out-of-plane sensor and link compliance. Raju on the other hand explored the benefits of adjusting operator and/or slave impedance in order to increase task performance. He concludes that given certain criteria, high-level force-feedback will not result in increased performance of a master/slave system (including operator fatigue, comfort and arm strength). Altering the slave impedance was

clearly a function of the task characteristics. This is not only the case for contact acquisition, but also for tasks that present a widely varying degree of constraints and complexities during successful task completion.

(1.2) Thesis Motivation and Content Summary

Many of the robots used for research purposes in interactive control have displayed many of the limiting performance and stability behaviors mentioned earlier. Many manufacturers and researchers claim that their implementations work better than others, but there seems to be no clear consensus on the causes of variability in the degree of success of certain implementations. Many researchers believe (and have shown experimentally and theoretically) that the undesired behavior can usually be traced to the actuator/transmission elements. Unmodelled bending modes of manipulator links are of importance as well, but in most robots those resonant modes are typically of a higher frequency than transmission resonances/nonlinearities.

Most of the badly understood/hard to model phenomena present in actuators/transmissions, can be grouped into the list below :

- Actuator Characteristics
 - * Saturation
 - * Higher Order Electrical/Mechanical Dynamics
 - * Torque Ripple
- Transmission Characteristics
 - * Backlash
 - * Stiction/Friction
 - * Viscous damping
 - * Stiffness characteristics
- Location of actuator and sensor
- Sensor Characteristics

In recent years a lot of research has focussed on the design of purer and higher fidelity transmissions, by removing nonlinearities in the transmission through careful design, increasing stiffness and efficiency by proper material selection and load distribution. Interactive task requirements were impossible to meet with the old notion of a transmission being a pure speed reducer. Bandwidth and performance requirements dictated the need for the design of a transmission to serve as a torque multiplier/divider. It was shown that no amount of control can circumvent some of the unmodelled dynamics or nonlinearities present in the drive-train (and link structure). Once again the need for better

performance (and stability) required the controls engineers to better understand the physical phenomena present, while realizing that certain characteristics could not be compensated for without re-designing a piece of hardware, with the ultimate goal of good 'controllability' in mind.

Since renewed and careful attention is now necessary for the design of a high fidelity transmission, this thesis will analyze the realistic physical characteristics that govern transmission design. Transmission design parameters will be analyzed as to their effect on performance and stability of closed-loop position- and force control. Performance and stability will be measured in the linear sense, by analyzing the envelope of acceptable/stable behaviors and the absolute stability margin, both measured by the locus of dominant closed-loop eigenvalues in the s-plane. This analysis differs from Eppinger [(1988)], in that it will go beyond a purely qualitative presentation, but will deal with the specific transmission design parameters responsible for proper performance and stability.

It becomes necessary to understand the effects of distributed conservative elements (springs and inertias), nonconservative elements (dampers, friction/stiction), and other nonlinear elements (backlash, soft-zones, stiction/friction), throughout the transmission by measuring/predicting the acceptable performance and stability regions of a force/position-controlled robotic transmission. In order to accomplish this task and reducing the number of variables in this analysis, a model of a 1 DOF actuator/transmission with varying degrees of complexities is used purely for analysis purposes. The degrees of complexity in the actuator/transmission model will deal with the presence of backlash, lost motion, transmission stiffness soft-zones or wind-up, varying transmission stiffnesses and their relative distribution, viscous and structural damping as well as the inertia distributions of an actuator driving a load via a transmission.

The effect of different (simple) control algorithms on performance and stability will be analyzed as well. We will show among other things, that adding electronic damping in a non-colocated position/force-controlled joint increases the stability margins without affecting the achievable bandwidth levels, and that low-pass filtering does not always have a destabilizing effect. We will be able to analytically examine the stability margins and stabilizing/destabilizing effects for each of the studied system parameters, using the Routh-Hurwitz stability analysis method and sound engineering judgement.

The experimental apparatus consists of a rotary 1 DOF setup, where different transmissions can be coupled to the same motor, in order to perform identical sets of comparative experiments. Theoretically predicted performance and stability limits are corroborated by experiments performed using this experimental setup. Experiments included open-loop tasks, as well as closed-loop torque-control for hard contact tasks.

The analytical and experimental study performed in this thesis incorporates an almost complete representation of robotic transmissions currently used in industry and academia. The only requirement was that they have (ideally) zero backlash, be extremely backdriveable, and as stiff as possible. The tested set of transmissions consist of:

(a) Cable Reducers	(WHOI/MIT	- 30:1)
(b) Harmonic Drives	(HARMONIC DRIVE	- 60:1)
(c) Cycloidal Disk Reducers	(SUMITOMO	- 59:1)
(d) Cycloidal Cam Reducers	(DOJEN	- 33:1)
(e) Planetary Gear Reducers	(REDEX	- 30:1)
(f) Ball Reducers	(KAMO-SEIKO	- 10:1 & 30:1)

Absent from the above list are hydraulic and pneumatic transmissions, as well as direct drive and friction-drive setups. Direct drive has been excluded since we are mainly concerned with transmission design and understanding the physical parameters governing the performance and stability of generic transmission types. The other missing transmissions were ruled to be too complex to build and test, even though they have a lot of nice properties which will be mentioned but can not be objectively compared, since no experimental setup can be used to generate conclusive data.

The thesis will focus on the performance and stability characteristics of these transmissions with respect to position and force control with colocated and noncolocated sensors and actuators. We motivate and study a fairly complex transmission model which includes linear and nonlinear elements, which attempts describe the respective behaviors of all the transmissions listed above, using lumped parameters. Characteristics such as backlash, friction/stiction, and wind-up or soft-zones, as well as inertia and damping distribution will be shown to have a transmission-type specific effect on the performance and stability of position and torque loops closed locally or around each actuator/transmission system.

The experimental phase includes individual experiments on each transmission in order to get quantitative results for :

- (a) Backdriveability
 - (i) Stiction/Friction
 - (ii) Viscous Damping
- (b) Transmission Stiffness
 - (i) Nonlinear stiffening/softening Spring
- (c) Impedance Following
 - (i) Stiffness
 - (ii) Damping

- (d) Positional Stability
 - (i) Disturbance Rejection
 - (ii) Parameter Sensitivity (Torque, Inertia, ...)
- (e) Force Control
 - (i) Surface Contact
 - (ii) Surface Following

Each experimental setup and procedure will be explained in detail in each of the respective chapters/sections. The thesis will also detail specific results obtained for different transmission types, which were deemed interesting and noteworthy. The conclusions that will be drawn will also highlight the areas where further research will be necessary.

(1.3) Thesis Overview

The goal of this thesis research will be to shed more light on the importance of transmission dynamics in torque- and impedance-controlled actuator systems. The study of different transmission types in terms of their dominant characteristics, will be useful in guiding controller design as well as compensation techniques (if possible) and highlight those areas important in transmission design. Figure 1.1 gives an idea of the logic branching which forms the underlying structure of this thesis.

In order to understand and prove the hypothesis that transmissions dynamics can dominate closed-loop performance, stability and bandwidths, one has to first understand the theoretically derivable trends. The first step is to perform a modeling analysis in which simple linear and nonlinear models are proposed as candidates which should capture the main (dominant) characteristics describing each separate transmission. These models can then be studied in terms of their open- and closed-loop behavior, when subjected to different controllers and performing in different task scenarios. Some of the theoretical conclusions can then be compared via experimentation.

The experimental phase of the thesis research can be split into several distinct parts. In order to provide the modeling process, applied to each specific transmission, with the appropriate parameter values, several different types of experiments had to be performed. One of the net results is thus also a good comparative set of transmission descriptors which can be used as a first-cut design approach, even if the descriptors are lumped-parameter fixed coefficients describing such behavior as stiction/friction, inertia, stiffness, backlash, etc.. These descriptors can then also be formulated in order to underscore their functional variations with respect to transmitted load (such as stiffening transmissions, variable

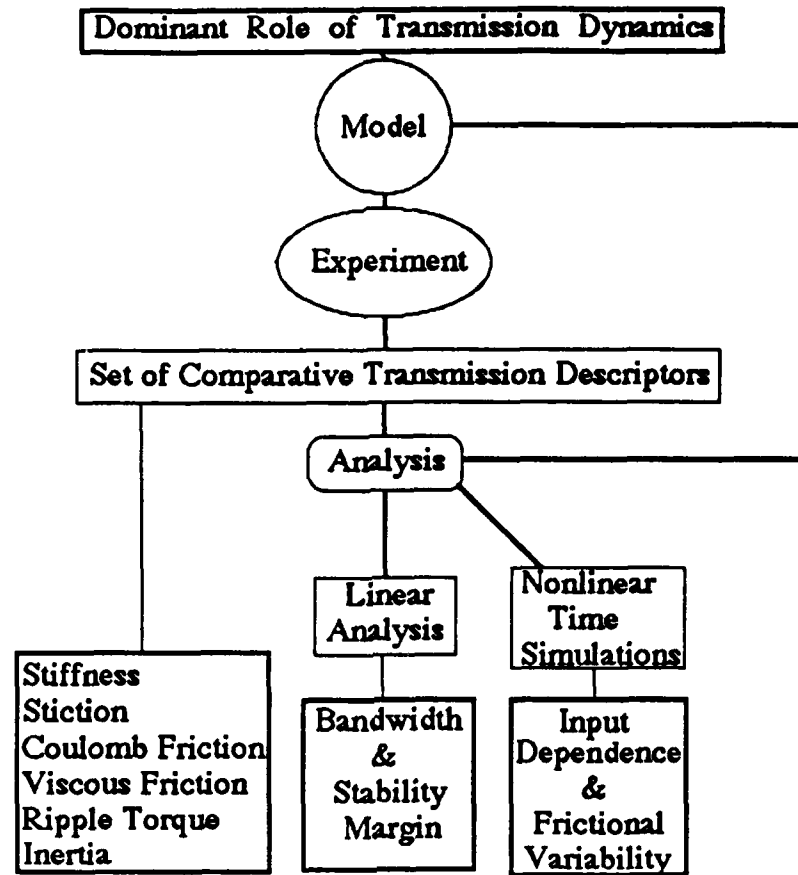


Figure 1.1 : Logic Branching Diagram of Thesis Research Goal, Analysis Approach and Results.

frictional loss), spatial orientation (such as ripple torque dependence on arrangement of reducer components) as well as time (wear-and-tear and thermal properties).

The analysis of the experimental data and the comparison to the model-predictions is performed at three different levels. A linear stability and performance analysis is used to analyze the stability margins and the associated maximum bandwidth levels. Despite the fact that we know that the systems considered here are highly nonlinear, such an analysis will prove fruitful since it may accentuate the more linear-like properties present at larger motion amplitudes, torques, and frequencies. The agreement between theoretically predicted and experimentally determined stability margins for different controller structures can thus be objectively analyzed. Comparing such stability and bandwidth levels for different commonly used controllers, is a further attempt at understanding the limitations imposed on the maximum achievable system performance due to not only the controller structure, but also the transmission dynamics and associated sensor- and actuator-hardware. The nonlinear analysis has at its the core a set of nonlinear time-simulations which employ the previously measured parameter values and attempts to replicate measured

system behavior. This step will allow us to determine the extent to which different transmission characteristics dominate the overall system behavior. Of importance here, are the effects of the highly nonlinear stick-slip phenomenon in each transmission as well as the high dependence of system performance on the type of input signal. Since the dynamics are known to be nonlinear, we expect this dependence to be present, and dominated by different combinations of the identifiable transmission characteristics.

In Chapter 2 we will present in a bit more detail the different transmissions that will be studied. We have made separate sections for each transmission type, and have padded them with hopefully enough diagrams and data so as to provide a good first-glance introduction to their design and work principles. The end of this chapter is mainly made up of a large list of physical variables that describe each unit, such as weight, dimensions, stiffness (published), backlash, etc. This list is not a complete representation of each transmission's behavior, since that is part of the main focus of this thesis, but rather represents the currently published data available from manufacturers/dealers. By the end of the thesis, several other variables used in classifying transmissions will be added for further comparison.

In Chapter 3 we perform most of the theoretical developments in this thesis. We lead the reader through a succession of steps which motivate and justify more and more complex transmission models in order to better understand the dynamic restrictions imposed by certain physical phenomena. We start with a rigid-body actuator/transmission/load model and progressively introduce transmission compliance, soft-zones, lost motion, backlash, etc., into the modeling procedure, to wind up with what we believe to be a more realistic representation of actuator/transmission/load systems. We then perform a whole suite of theoretical position-/force-control stability and performance analyses for each of these models. The analysis focuses mainly on the effect the physical system parameters (inertias, stiffnesses, frictional losses), and different controller structures (PD, PID, Impedance, First-Order Dynamics, etc.), have on the overall output (position/torque/force) stability and performance. Stability will be measured in terms of stable controller gains or parameters, by using the Routh-Hurwitz matrix, as well as numerical and root-locus arguments. Performance is measured based on the bandwidth and damping ratios of the dominant dynamics, which in our case will be shown to be a complex conjugate pole-pair. Conclusions will be made that relate to the stability margins achievable with different controller structures, what physical parameters hold the best promise for stabilizing or increasing system performance. Previously mentioned stability limitations due to force-sensor stiffness, transmission stiffness, inertia-match force gains,

stiffness- and inertia distribution in a transmission, are all topics that will be discussed in this chapter.

In Chapter 4 we have performed a wide array of transmission fidelity studies for each transmission. This chapter presents first a theoretically motivated analysis of expected transmission impedance fidelity, -stiffness, and other related issues. We explain the experimental setup in a bit more detail, as well as the experiments that each transmission was subjected to. Data for each transmission is presented, and all the pertinent physical phenomena in each transmission are studied. This chapter is meant to provide experimental proof for some of the models presented in Chapter 3, especially relating to transmission stiffness, backlash, soft-zones and lost-motion, as well as stiction/friction and torque ripple. An added benefit of this experimental chapter is, that we will be able to generate an additional list of comparative parameters by which to judge different transmissions by. These parameters will differ from those in Chapter 2, by accentuating the different transmission behaviors in real task scenarios, which places an emphasis on where these transmission place between speed reducers and pure torque multipliers.

In Chapter 5 we will present another set of experiments which will further substantiate the modeling procedure in Chapter 3. The additional experiments will consist of a set of open- and closed-loop torque-control tasks, by which we can measure system stability margins and performance levels. The goal of this chapter is to provide a more realistic comparison for each transmission, of the capabilities of each actuator/transmission/load system, when performing a set of more realistic tasks. It will also enable us to study how good a nonlinear lumped- and fixed-parameter transmission model can predict experimentally measured system behavior.

In Chapter 6 we conclude by summarizing all the major results obtained in this thesis. The conclusions will not only focus on the theoretical contributions of this thesis, but will also accentuate the importance of the experimental comparative transmission study. The combination of theoretical analysis and experimental verification for a wide suite of transmission will hopefully prove useful for future transmission design as well as controller design. In another subsection we outline the areas that require further research effort, since they were not covered in this thesis, or were shown to be of importance by this thesis.

Chapter 7 contains some of the information necessary for pursuing this research in more detail. Chapter 8 makes up the bibliography which lists all the references that were researched for this thesis, and that have been included in the discussion contained in the introduction (Chapter 1).

CHAPTER 2

(2) TRANSMISSION TYPES

This chapter will briefly present each of the transmissions studied in this thesis. The transmissions' operation will be explained in each case, supported by sketches and diagrams. Due to certain space restrictions, the individual operating principles could not be explained in as much detail as we would like, but the information given, should suffice to at least demonstrate the differences among each of the units. The last section will present a summarizing list of all the (published) physical parameters for each transmission.

(2.1) Transmission Listing - Functional Descriptions

(2.1.1) Cable Reduction Transmission (WHOI)

A generic cable reduction consists of cables anchored in pulley faces and running from one small diameter pulley onto a larger diameter pulley, where it may be anchored as well. These basic stages can be repeated to achieve the desired reduction ratios. As can be seen from Figure 2.1, the conceptual arrangement of the cable reduction is that of two identical cable loops running on opposite sides of the transmission, which are separately anchored on each split-pulley arrangement, as well as on the output torque-tube. By then counter-torquing the split input shaft, the entire cable transmission could be pre-tensioned to increase stiffness and avoid cable-miswrap. Once pretensioned, a double counternut arrangement would lock the split hub in position, and the transmission acted as a single cable-loop. The design was layed out to have as short an unsupported length of cable as possible in order to further increase stiffness (since that is where the tensile forces cause the largest strain - especially in the high-tension ends). In order to increase stiffness in the high-tension portion of the transmission, the cable diameter was increased in order to keep the cable stress uniform throughout the transmission. Additional wraps were present on each pulley, before the termination was reached, in order to take advantage of the pulley/cable frictional forces to reduce the strain on the termination. Each pulley diameter was chosen so as to reduce the bending stresses acting on the cable as it wraps on and off the pulley. Grooves in the pulley-faces served to loop cables' around for easier anchoring in the previous pulley. The cable used was of a 7x19 construction and consisted of low-stretch stainless steel filaments. Even though the transmission was originally designed for

uncoated cable, testing revealed that the use of nylon-coated cable increases cable life substantially. The penalties were, that the transmission stiffness was reduced by about 4% (due to nylon compression between cable and pulley-face under tension), and the cable/pulley friction was increased by about 30% (based on steel-on-steel and nylon-on-steel friction coefficients).

Even though there is some cable/pulley friction during wrap-off and wrap-on, most of the friction comes from the bearings supporting the shafts that the pulleys ride on. The entire assembly was housed so as to be bathed in mineral oil, which was meant not only for lubrication-, but also pressure-compensation purposes. This step necessitated the use of a shaft-seal at the output end. The final design incorporates a CRANE Ceramic-on-Ceramic spring-loaded rotary face seal, which was especially designed for this application (uniform break-away and frictional torque). The output torque-tube has a tapered portion where the next transmission stage can be attached to, while the cables can be routed through the hollow torque-tube.

The cable reducer that was tested, was one of the joints that actuate the manipulator built for the ARGO/JASON project (DiPietro, 1988). It formed part of a prototype development and was a joint effort between MIT and WHOI, funded as part of the ARGO/JASON Project.

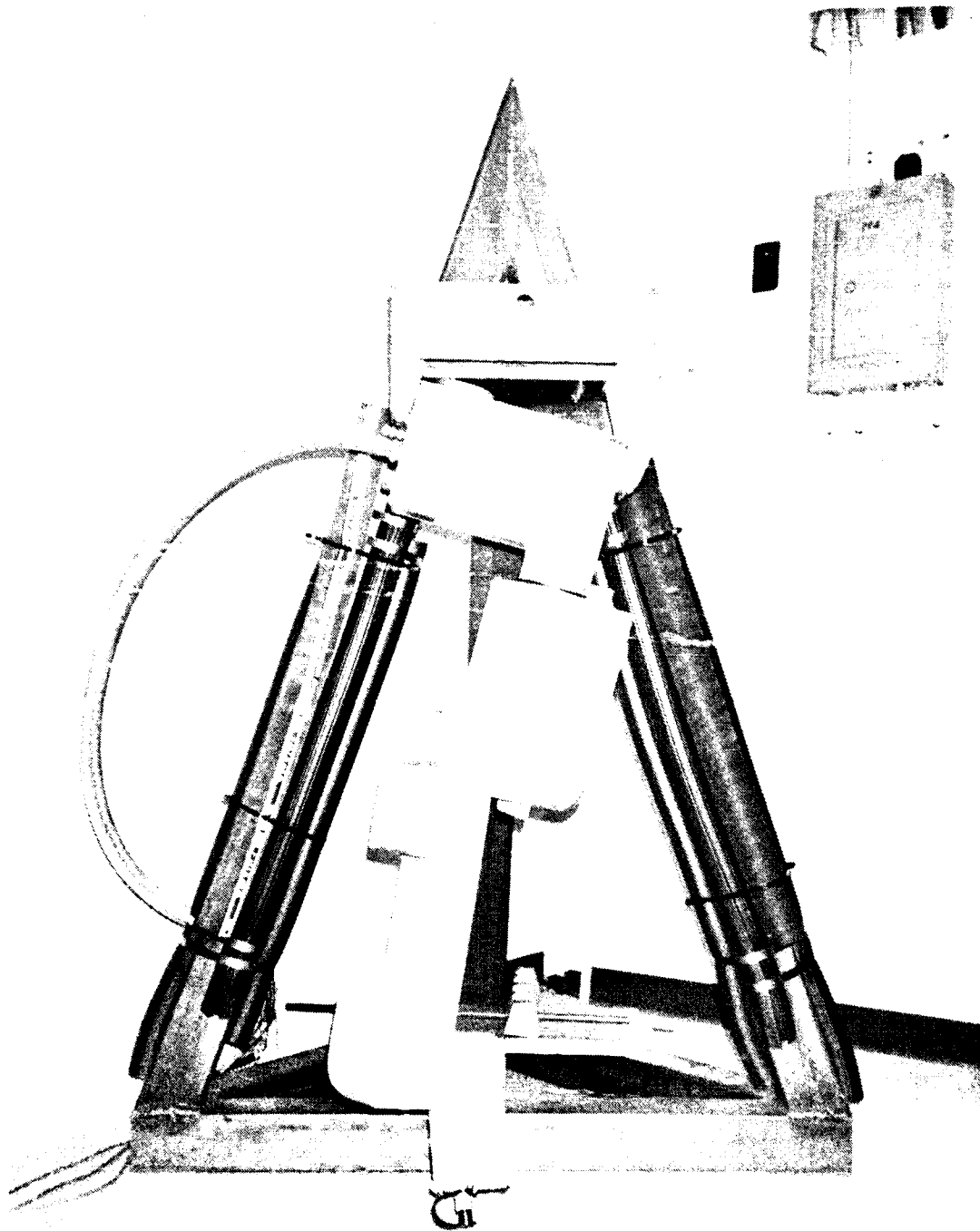


Figure 2.1a : WHOI underwater manipulator on test stand.

Remotely Operated Vehicle JASON

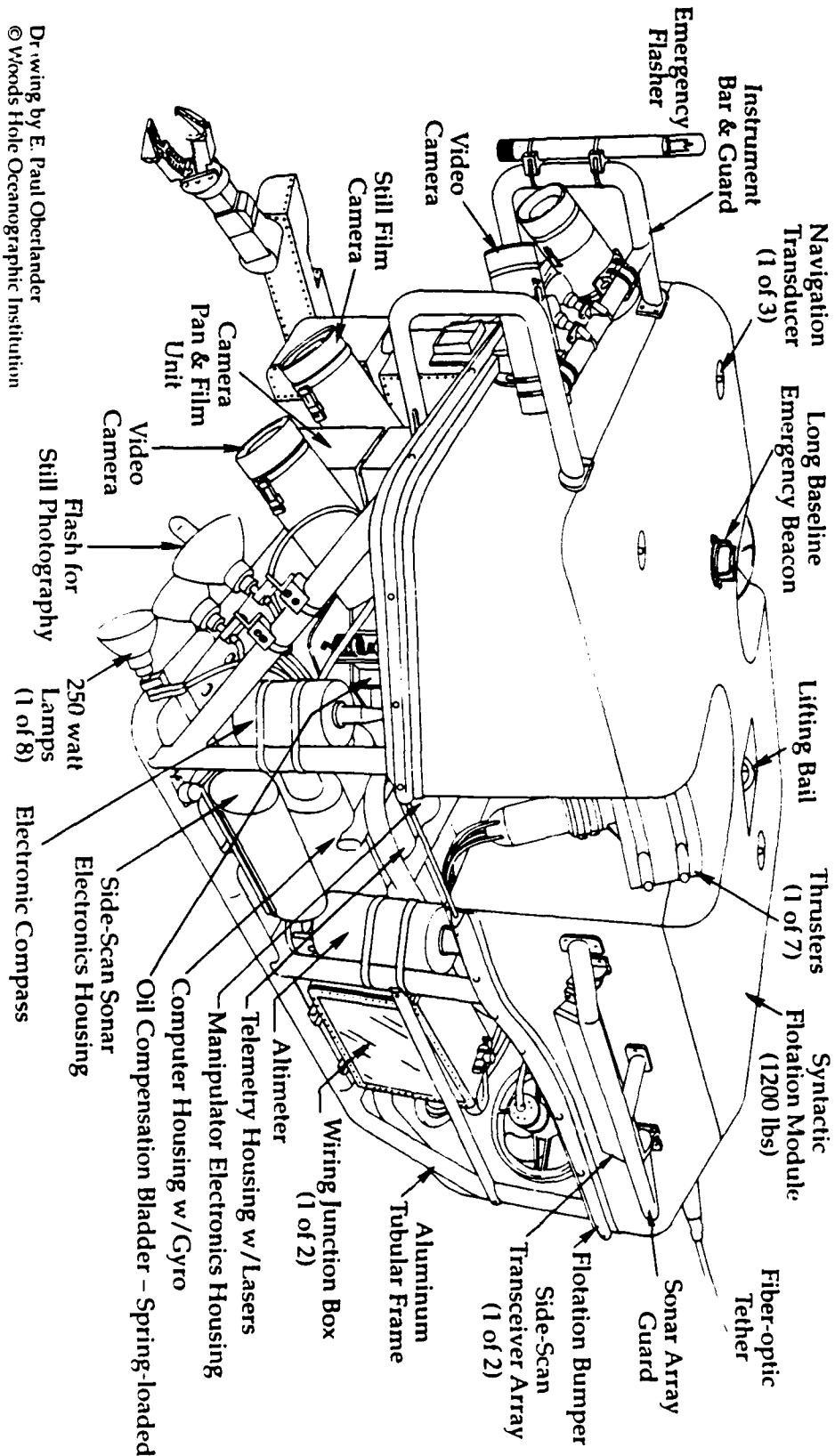


Figure 2.1b : JASON remotely operated underwater robot with manipulator arm.

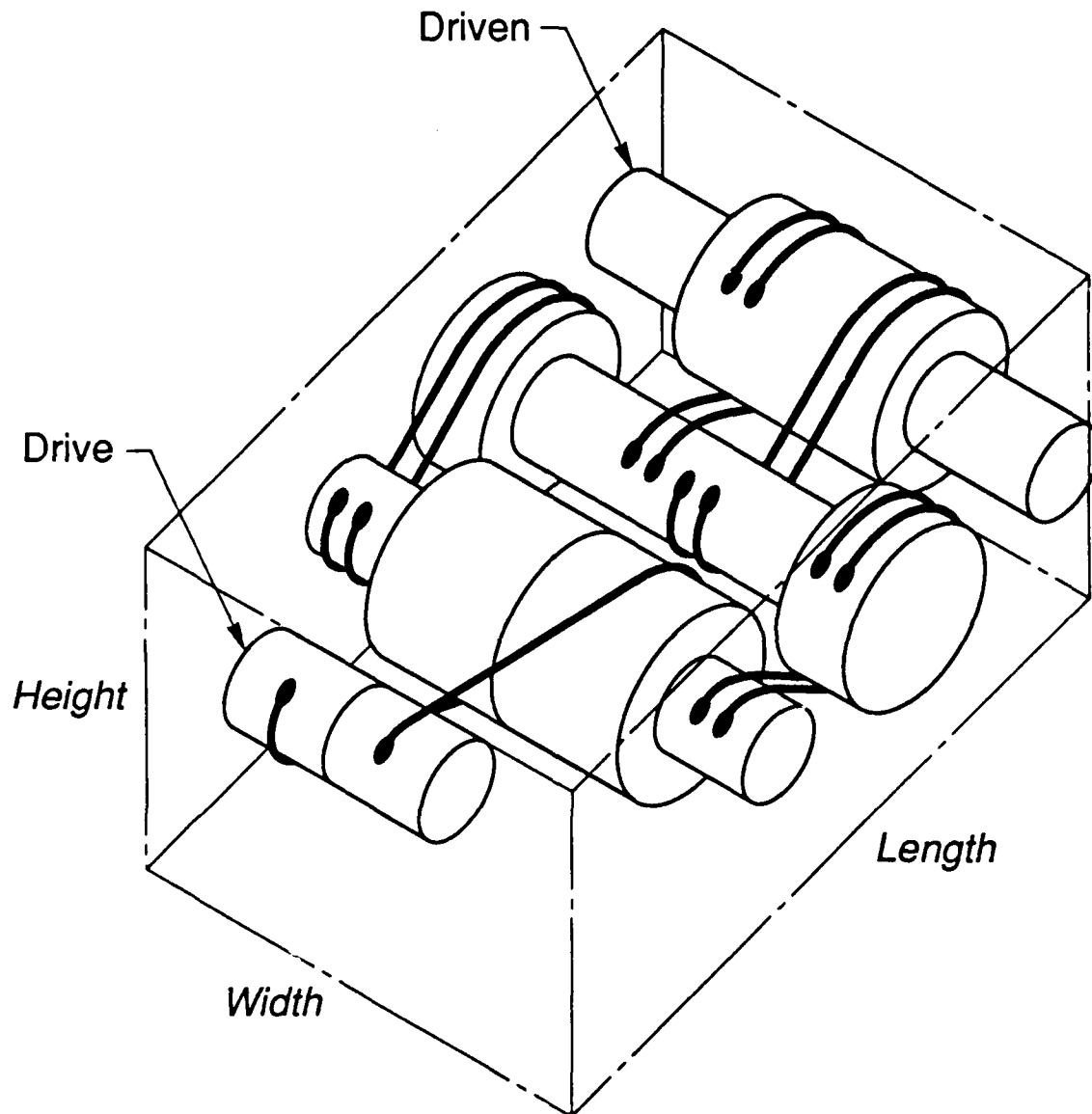


Figure 2.1c : Basic Cable-Pulley Reducer for 3-stage underwater manipulator joint (30:1).

(2.1.2) Harmonic Drive Transmission (HARMONIC DRIVE)

This differential transmission type consists of three parts. The Circular Spline, the wave generator and the cup-shaped flexspline, as seen in Figure 2.2. Normally the input is through the wave generator and the output through the flexspline. That is the arrangement used in the tests described within this thesis.

The circular spline is held fixed, and as the wave generator rotates, it imparts its elliptical shape to the flexspline, which causes successive tooth engagement between the two splines at two points 180 deg apart on the major diameter of the elliptical bearing race of the wave-generator. The flexspline has two teeth less than the circular spline, and thus a full clockwise revolution of the wave generator, causes a two tooth counterclockwise rotation of the flexspline. Hence the reduction ratio is the number of teeth on the flexspline divided by two. The tooth engagement pattern is shown in Figure 2.3. Since the flexspline is forced into elliptical shape, the tooth engagement can no longer be along the entire length of the tooth (despite the supposed modified tooth cross-section). This causes points of high stress concentration, resulting in large frictional losses, perceptible as ripple torque on the output. Re-shaping of the teeth can reduce this phenomenon, but not eliminate it - especially in the high torque regime. The re-shaping of the teeth is necessary to insure zero backlash. Mis-alignment between the input and the output are critical, since they can cause a large increase in (load dependent) frictional losses, due to improper tooth-engagement. The coupling is mostly performed using an Oldham-Coupling at the input to accommodate for such misalignments, which carries with it a backlash penalty (about 20 arc-min), which needs to be avoided in robotic designs.

This transmission is claimed to have zero backlash (due to forced, multiple tooth engagement), efficiencies as high as 90%, high torque-to-weight ratios as well as being fairly affordable. The range of transmission ratios varies from 40:1 (custom model with reduced MTBF) all the way to 200:1 in discrete steps (40, 60, 72, 80, 100, 120, 140, 160, 180, 200). Figures on MTBF vary, but the claimed properties of the drive deteriorate with frequency of usage (mostly tooth wear or outer bearing race metal fatigue), despite proper lubrication.

The harmonic drive tested was their top-of-the-line model in terms of rigidity, backlash and torque-ripple, and is labelled the HDC-1M-060-02A with a 60:1 reduction and a nominal cost of \$474.00.

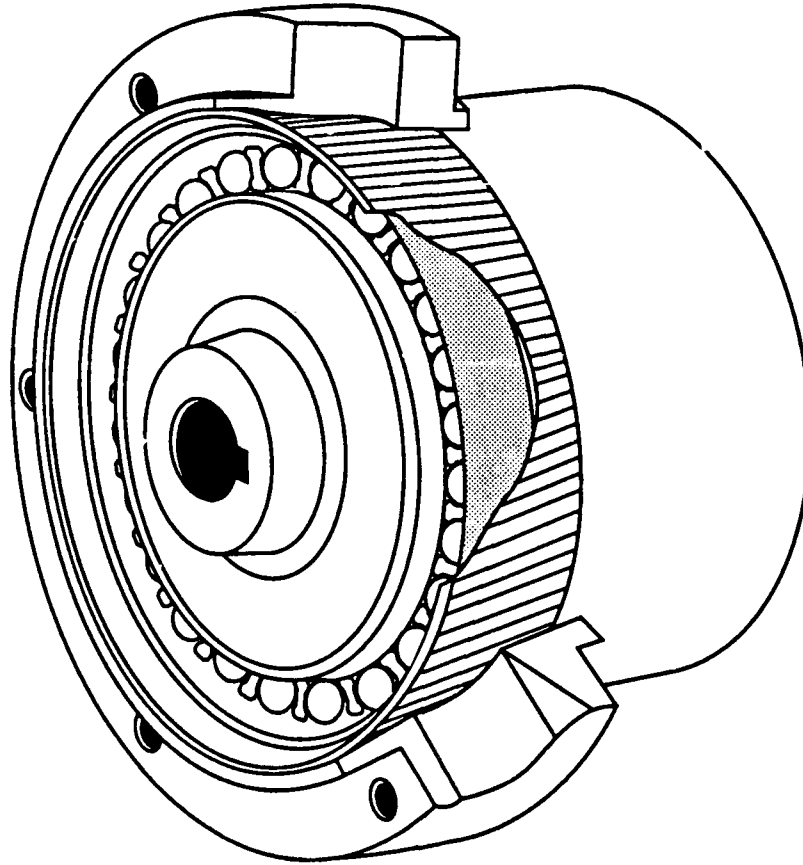


Figure 2.2 : Cut-away view of the Cup-Type Harmonic Drive Reducer.

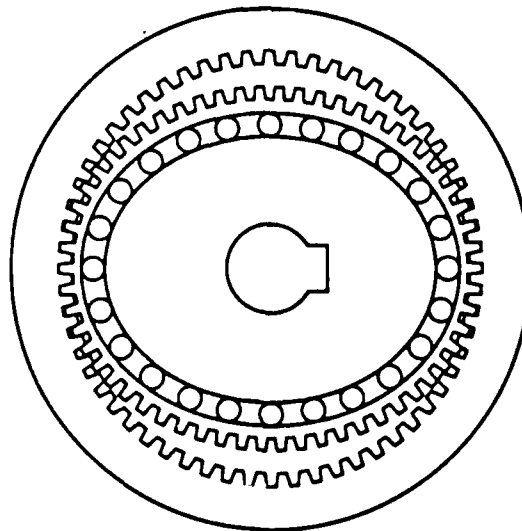


Figure 2.3 : Front-view of elliptical bearing (wave generator), flex-spline, and fixed inner spline (inner ring gear), to illustrate tooth engagement.

(2.1.3) Planetary and Cycloidal Reducers

The types of reducers that were analyzed next, represent a good mix between the common cycloidal and planetary reducers. One of the reducers is actually a hybrid, in that it uses gears in a cycloidal arrangement, which lets us study the combined effects of geared cycloidal reducers, since we are able to physically adjust the backlash and thus the preload in the unit. We have explained below some of the similarities between these types of reducers. The rest of this section presents the different reducer types tested in this study.

The similarities between planetary and cycloidal reducers is illustrated using Figure 2.4. The basic planetary single-stage reduction is shown in the upper left diagram. We can easily think of the sun-gear replaced by a crank that is attached to a single enlarged planetary gear riding on the inside of inner gear (diagram in the upper right hand corner). The trace of the planetary gear can be reproduced by using non-geared components which are in purely rolling contact. The teeth of the inner gear are replaced with stationary circular teeth, which an epitrochoidally shaped disk rides on (shown in the third figure from the bottom). The output is clearly the planetary disk, but the output motion is not yet purely concentric with the input shaft.

Concentricity can be gained by milling holes into the planetary disk, in which the slow-speed shaft pins (connected to the output shaft/flange) can ride in. The holes and the slow-speed pins have to be sized according to the original eccentricity of the planetary epitrochoid disk (shown in the picture second from the bottom).

The last diagram shows how the epitrochoid planetary disk and the fixed ring-gear pins can be combined with the output roller pins to generate a single-stage cycloidal reduction. This basic unit can be combined in series to create higher reduction ratios. The slow speed pins are circular cantilever beams which are connected to an output flange/shaft. In order to reduce bending deflections of these pins under load, and in order to better distribute loads, several (2 to 3) epitrochoid planetary disks can be used (slightly phase-shifted) to transfer loads from the eccentrically located input shaft to the output roller pins/flange/shaft.

Whether cantilever pins, gears, or steel balls are used to transfer torque, the reducers listed next, all fall under the planetary/cycloidal categories.

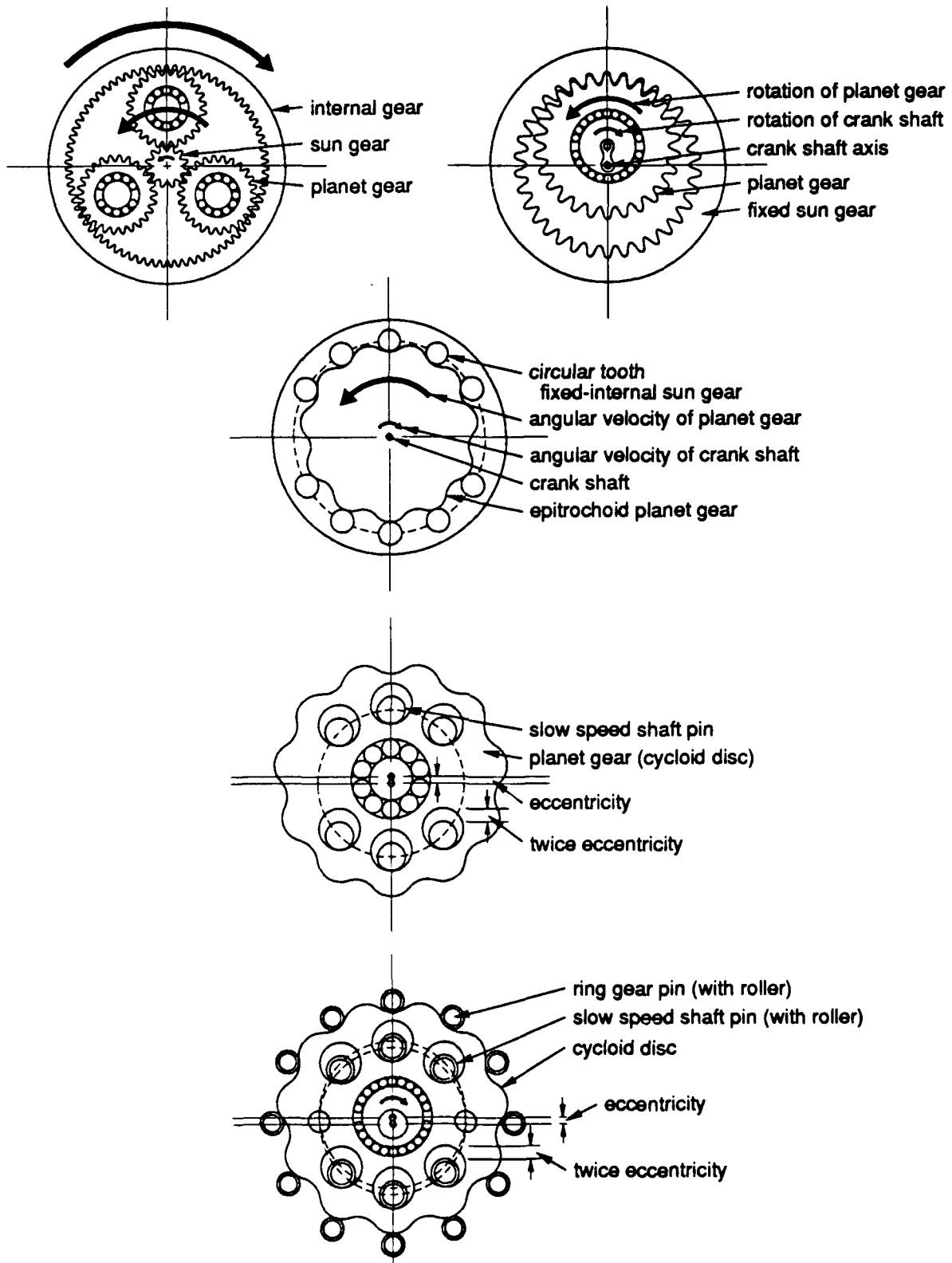


Figure 2.4 : Progression in reducer stage design to outline the similarity between planetary gear reducers and cycloidal reducers.

(a) *Ball Reducer Transmission (KAMO SEIKO)*

The ball reducer is based on a principle of two (or more) disks riding on top of each other, separated by steel balls riding in special grooves milled into opposing faces of these plates. The main torques are transmitted via the contact points of the steel balls, which are always in rolling contact and thus reduce the frictional losses in the drive. As can be seen from Figure 2.5, the input and output shaft are concentric, with the grooved plates riding on separate bearings, separated by balls that run in specially milled grooves.

The two groove profiles milled on opposing faces of these two disks, trace an epicycloid curve on one disk (gotten by rotating a small disk with a certain diameter on the outside of a circle and tracing the path of a fixed point on the outside of this smaller disk) and a hypocycloid curve on the other disk (gotten by rotating a small disk with a certain diameter on the inside of a circle and tracing the path of a fixed point on the outside of this smaller disk). Once the two disks are assembled and relative motion occurs, the balls move partly in the groove of one face and then in the groove of the other face. The net trace of the balls is gotten by superimposing the separate groove traces (it looks very similar to a sinusoid, but it is not). The cross-section of the groove is usually gothic-arc, in order to obtain 4-point contact (better load distribution with higher associated rigidity and lower friction than in a circular-arc cross-section). In order to be able to transmit large torques, the two disks are preloaded, in order to avoid the balls from jumping the grooves. This also has the effect of reducing any backlash present in the system.

The different reduction ratios are obtained from dimensioning the pitch circle diameter of the two groove patterns, and the eccentricity of the separate preloaded disks. The two have to be sized to give an integral epi- and hypocycloid pattern, by which the reduction ratio can be computed. Since the number of hypocycloid lobes is larger than that of the epicycloid lobes by two, the net reduction ratio can be shown to be half the number of integral hypocycloid lobes. Reduction ratios usually come as 5:1, 10:1, 18:1, 20:1, 30:1, 40:1 and 50:1. Size and weight of a unit depend largely on the reduction ratio, since the strength of the material and the diameter of the pitch circle are responsible for the torque-rating/stiffness and the overall dimension of the unit.

The manufacturer claims zero backlash due to constant rolling contact, which in high torque applications is insured by preloading the plates together. Furthermore the efficiency is also claimed to be as high as 90%. The transmission ratio displays a stepwise stiffening behaviour, but the manufacturer only lists values for the stiffer portion. It seems natural to speculate at this point, that frictional losses (coupled to efficiency) as well as the relative

accuracy in transmission stiffness values is a function of the transmission preload. Tolerances in milling the grooves, sizing of the steel balls as well as bearing alignment play a large role in the low-torque transmission stiffness as well as the perceived ripple torque at the output (often perceived as vibration in high-speed applications).

After testing several models, the chosen transmission had a transmission ratio of 30:1 with a torque rating compatible with the cable reduction (max. output stall torque of 1250 in-lbf), with the model # BR100-SS-30, with a nominal cost of \$1200.00.

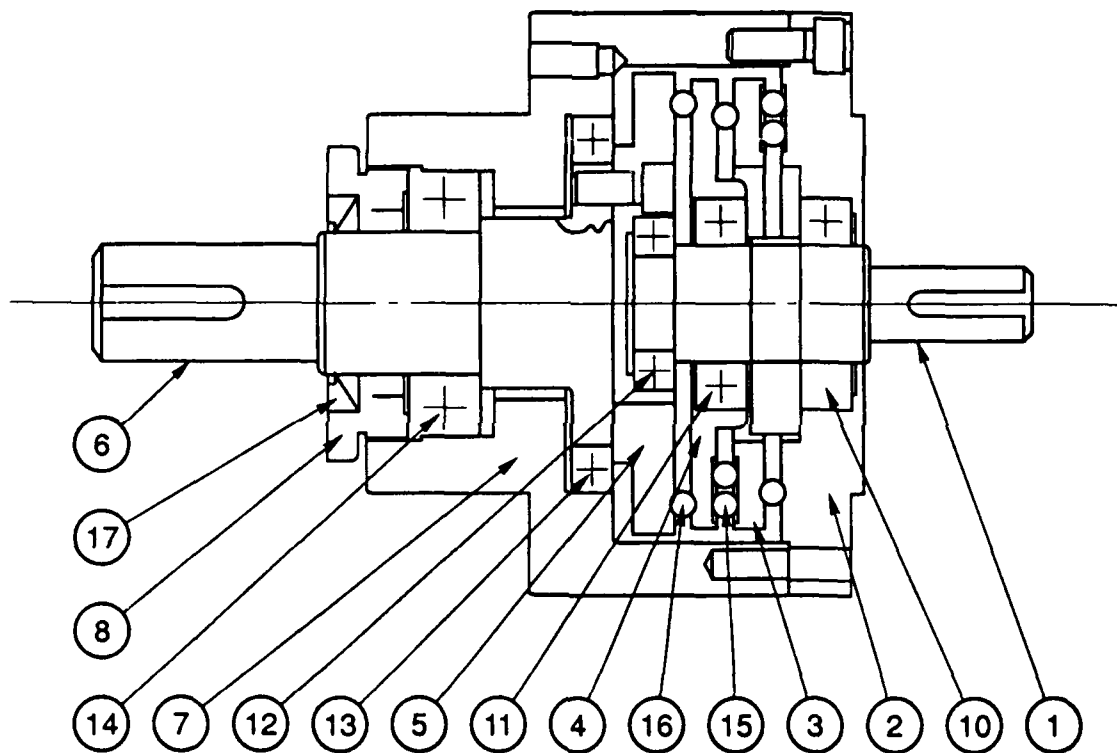


Figure 2.5 : Cross-section of KAMO Ball Reducer Transmission.

- | | |
|--------------------------------------|--------------------------------|
| 1 : Input Shaft | 9 : Ball Bearing |
| 2 : Fixed Disk | 10 Input Shaft Bearing |
| 3 : Oldham Coupling | 11:Plate Bearing |
| 4 : Eccentricity Disk | 12 Shaft Bearing |
| 5 : Output Disk | 13:Output Shaft Thrust Bearing |
| 6 : Output Shaft | 14: Output Bearing |
| 7 : Output Bearing & Preload Housing | 15: Oldham Coupling Balls |
| 8 : Preload Nut | 16: Speed Reducer Balls |
| | 17: Oil Seal |

(b) Cycloidal Servo-Match Reducer (SUMITOMO)

The cycloidal-type reducers are a derivation of planetary gear transmissions, which have replaced meshing teeth with rolling contact parts. As can be seen from Figure 2.6, the fixed internal gear has been replaced by ring gear pins with a bushing-type roller, while the planetary gear has become a disc with cycloidal shape (epitrochoid tooth profile), which rides on the ring gear pins, while being driven by an eccentrically located round input shaft. The input shaft replaces the sun gear with needle bearings transmitting torque to the cycloidal disk, which has holes milled into it, which drive yet another planetary gear consisting of sleeved ring pins. This set of ring pins makes up the output side of the transmission.

As seen in Figure 2.7, the final package can consist of several disks which act on the slow speed ring pins, which are basically cantilever sleeve beams attached to the output shaft/flange. The backlash in these units is a clear function of machining and assembly tolerances. The transmission stiffness is not only a function of the load distribution over the output cantilever beams, but also of the tolerancing that insures equal load distribution over all the beams at the same time. The units built for robotic applications have quoted output backlash of 3 arc-min (or N-times that at the input, which can thus range from 3 deg to 4.5 deg to 6 deg for available transmission ratios), and a very stepwise stiffening spring transmission-stiffness behaviour. The manufacturer quotes all the different regions of stiffness and follows the unwritten convention that lost motion represents the total deflection at $\pm 3\%$ of rated output torque, with an associated stiffness value which is much lower than in the high-torque regime. Notice that no provisions are made to insure that the $\pm 3\%$ torque value exceed the inherent break-away torque of the transmission.

Reduction ratios (for robotic applications) lie in the discrete range of 59:1, 89:1 and 119:1. The reduction ratio is easily computed based on planetary-gear conventions, where the reduction is expressed as the ratio between the number of teeth on the planetary gear and the difference of teeth between the internal gear and the planetary gear-disk. In the case of the cycloidal reducers, the internal gear is replaced by ring gear pins which are one more than the cycloidal lobes on the planetary gear. Thus the ratio is simply dependent on the number of cycloidal lobes on the cycloidal disk. These transmission types have proven themselves to be extremely rugged with large values of MTBF. They also have a large shock-load rating of at least 500%, since unlike gear trains where the loads are usually borne by one tooth (depending on the gear type), here the load is distributed over several

'lobes' (analogous to teeth). The units are moderately priced, have a fairly large weight and are dimensionally quite sizeable.

The unit that was tested is part of the robotic line of transmissions of SUMITOMO, with a transmission ratio of 59:1 (their smallest ratio) and an output stall torque rating of 1250 in-lbf, with the model # F15-59, and a nominal cost of \$761.00.

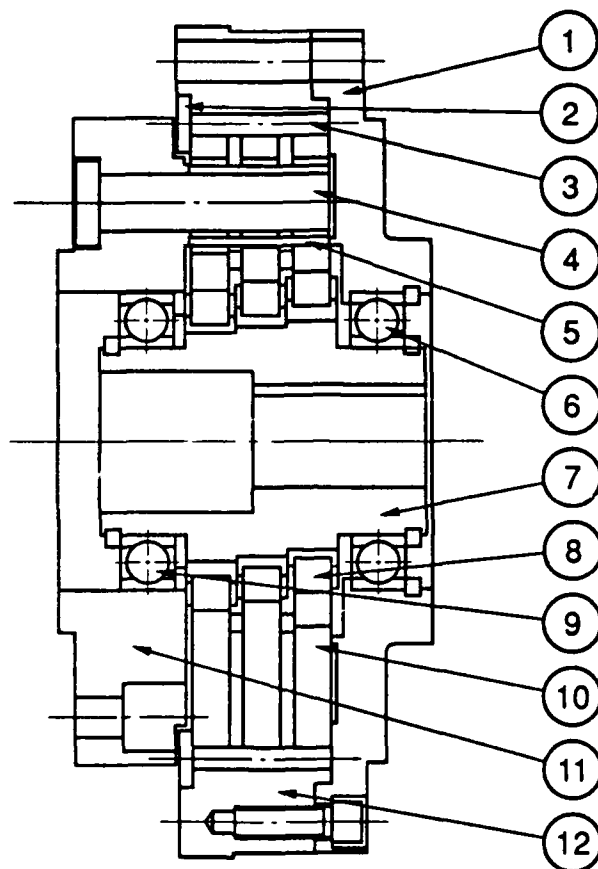


Figure 2.6 : Cross-sectional view of Servo-Match Cycloidal Reducer, showing (1) input housing flange, (2) roller bearing retaining ring, (3) roller pins, (4) output cantilevers, (5) load transfer cylinder, (6) input-shaft bearing, (7) input cam-shaft, (8) disk roller bearings, (9) cam-shaft bearing, (10) three epitrochoid disks, (11) cantilever output flange, (12) roller-pin housing.

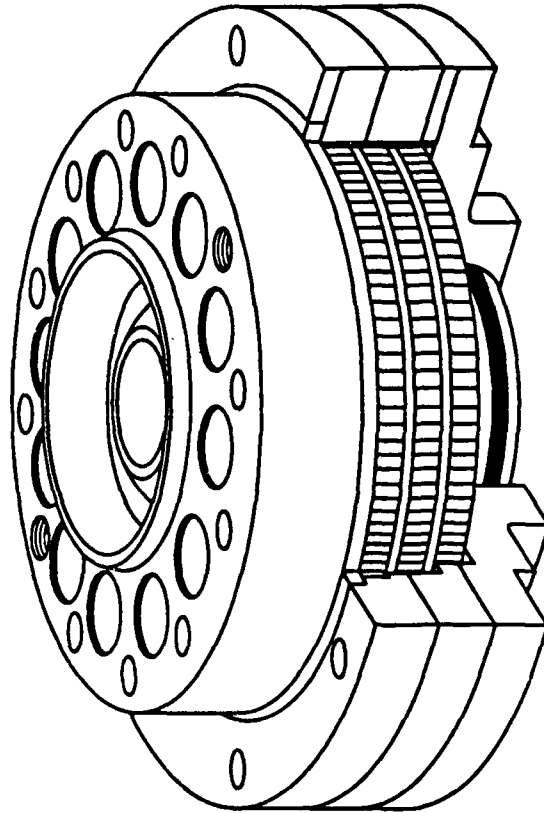


Figure 2.7 : Cut-away view of FA Series SUMITOMO Servo-Match Cycloidal Reducers, showing epitrochoid disks, roller pins and output flange.

(c) Cycloidal Dual Track Cam Reducer (DOJEN)

These reducers are also a type of cycloidal reducer, similar to the SUMITOMO reducers. But they rely on a slightly different mechanical principle (see Figure 2.8). The cycloidal disks are replaced by a single trochoid-shaped cam, which serves as the 'planetary gear', while its lobes ride on a set of fairly short fixed roller pins attached to the input- and output-housing. Input motions are transmitted to the concentrically mounted cam, whose surfaces start rolling on the pins of the input housing. The rollers attached to the output housing roll on the second cam surface, thus imparting a motion to the output flange, which is dependent on the pitch-diameter of the pin-locations, as well as the number of pin-rollers. Shaping of the cam surfaces is crucial, while assembly can also be a crucial factor in terms of proper load distribution, stiffness, and torque-ripple (see Figure 2.9).

The unit is machined with tolerances that preload the mating surfaces in order to eliminate backlash. These units have lower backlash figures than the SUMITOMO units, since they have fewer mating parts. The mating parts create an overall surface area over which the loads are transmitted which results in better load distribution and thus causes a more 'linear' transmission stiffness trace, where the soft-zone or zone of wind-up is reduced if not even eliminated. Dimensional preloading insures that the unit will not have to be tuned throughout its lifetime, since rolling contact causes the least amount of dimensional change under extended periods of high load. Dimensional preloading can be set during assembly (due to offset needle-bearing surfaces for the cantilever pins), and affects system efficiency.

Just like the SUMITOMO reducer, the claimed features of this drive are high torque overload capacity, compact design and a wide range of reduction ratios and torque ratings. DOJEN has by far the largest assortment of ratios and sizes, due to their peculiar transmission design, consisting of variable pin arrangements and cam-shapes/-sizes. Similar to most of the approaches taken by transmission manufacturers, the units are grease lubricated, not only for life-time lubrication purposes, but for damping out internal structural resonant modes. The manufacturer claims this to result in shorter cycle times and increased productivity in the factory environment. Efficiencies between 70% and 80% underscore the frictional losses in these units, which are slightly heavier and larger than the SUMITOMO cycloidal reducers.

The transmission model that was tested had a 33:1 reduction ratio with a 1500 in-lbf output stall torque rating - Model # 03-33-S75-F-BO and a nominal cost of \$1500.00.

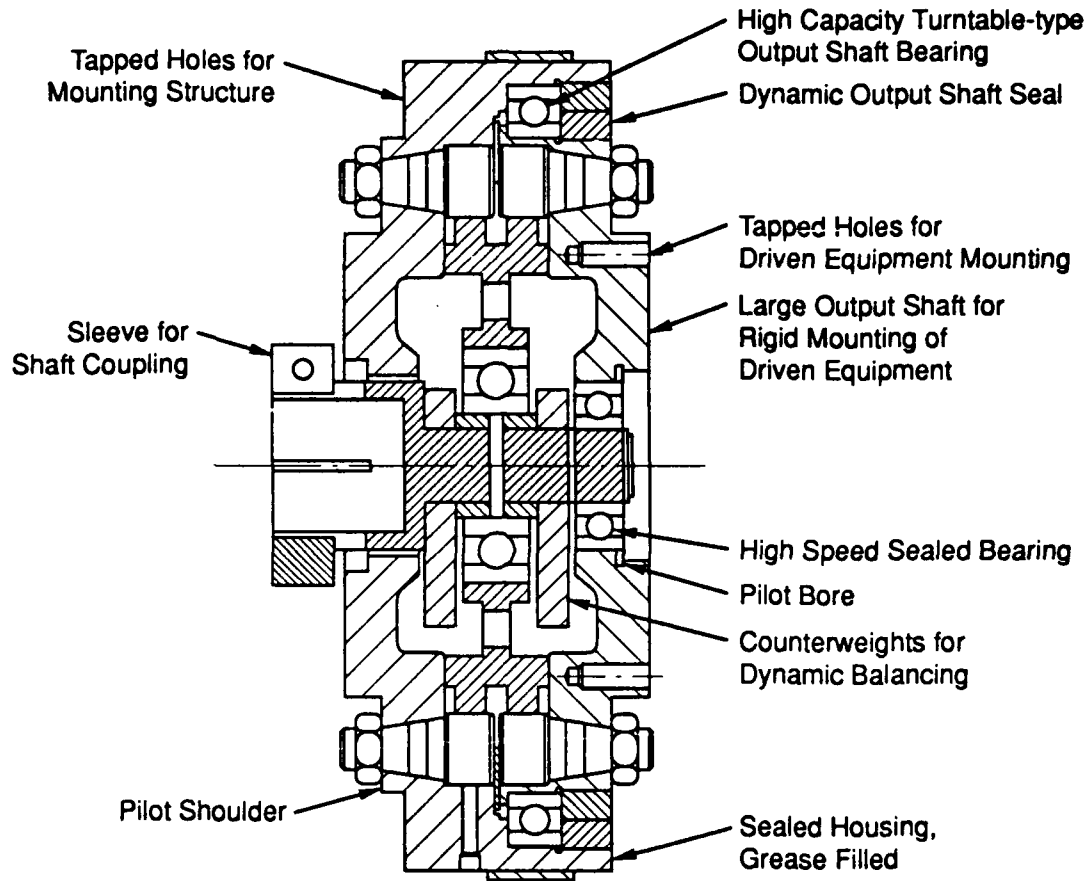


Figure 2.8 : Cross-Sectional View of DOJEN Cycloidal Cam Reducer, illustrating all the pertinent reducer components.

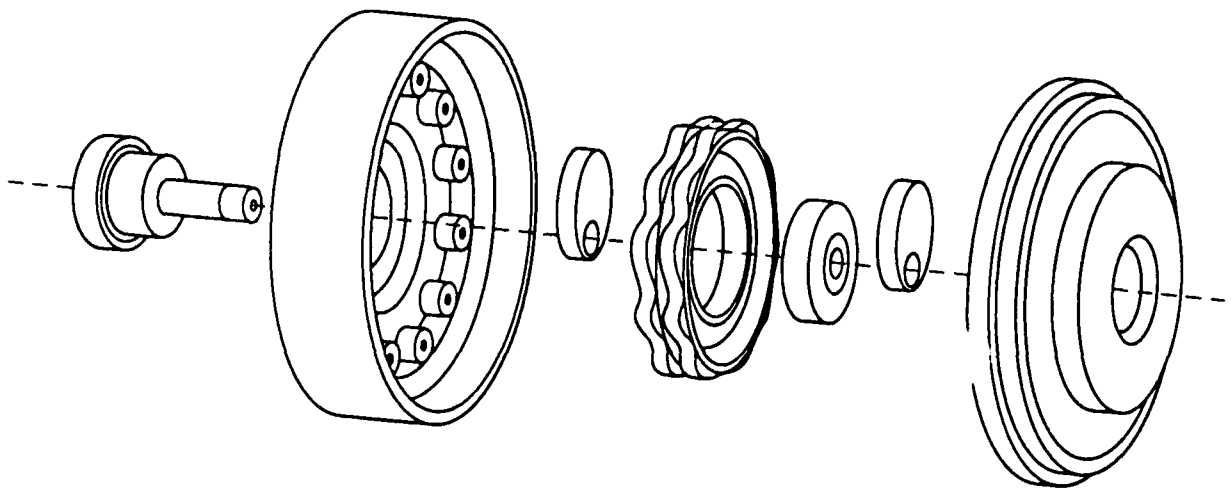


Figure 2.9 : Assembly View of the Cam-type cycloidal reducer from DOJEN. Individual epitrochoid disks are replaced by a single cam-type assembly, which is supported on a centrally located bearing. The cam rides on fixed internal pins.

(d) Correctable Backlash Planetary/Cycloidal Reducer (REDEX)

As seen in Figure 2.10, the input shaft (1) has a double eccentric bearing surface milled into it, with the two cams opposed by 180 deg. These cams drive two crown (or planetary) gears (3) through a set of roller bearings. The two crown gears mesh with a set of fixed internal ring gears. The motion is analogous to a planetary gear arrangement, where the planet gear is increased in diameter, and the eccentricity is decreased. In this reducer the eccentricity is implemented via the two cam surfaces. The rotation of the crown gears is transmitted to the output shaft (2) by a set of pins (7 or 9, depending on the unit), which engage holes in both crown gears simultaneously (see Figure 2.11). An assembly drawing of the entire reducer is shown in Figure 2.12.

The interesting part of this reducer is, that while being a cycloidal reducer, it employs gearing to transmit torque. Since gears may have backlash, this unit has a split ring gear, with each part of the ring gear engaging one of the crown gears. In order to remove the backlash in the unit, the two ring gears can be rotated with respect to each other, thus in effect pre-loading the two crown gears. By re-tightening the ring gear holding screws, this preload can be maintained at all times. This adjustment can be made externally without removing the unit nor stopping the motor. Usually the adjustment is made while monitoring the motor current and looking for a slight increase in motor current (or a reduction in speed), at which point the tolerances have been removed, and any further tightening would only introduce larger frictional losses into the unit.

The manufacturer claims that the unit has at most 1.0 arc-min of backlash at the output, which can be maintained by adjusting the circumferential displacement of the split ring gears (adjustment not only removes clearances between the mating teeth, but also between the crown gear bores and the output pins). The manufacturer supplies a single number for the maximum stiffness of the transmission, which seems to overlook the possibility of soft-zones or wind-up. Nonetheless, this maximum stiffness value is around the same value for the SUMITOMO cycloidal reducer, as well as the DOJEN Cycloidal cam reducer. Impact loads can also be rather large, due to the large surface area transmitting loads at all times. The frictional losses in this unit can be traded off against the size of the backlash in the unit. Values of zero backlash are possible, by preloading of the crown- vs. the ring gear, which in turn controls the amount of friction present in the transmission.

The unit that was tested had a transmission ratio of 30:1 and a 2000 in-lbf output stall torque rating and the model # 2SRSS-O-LM1-30-AA-CORBAC and a nominal cost of \$3096.00.

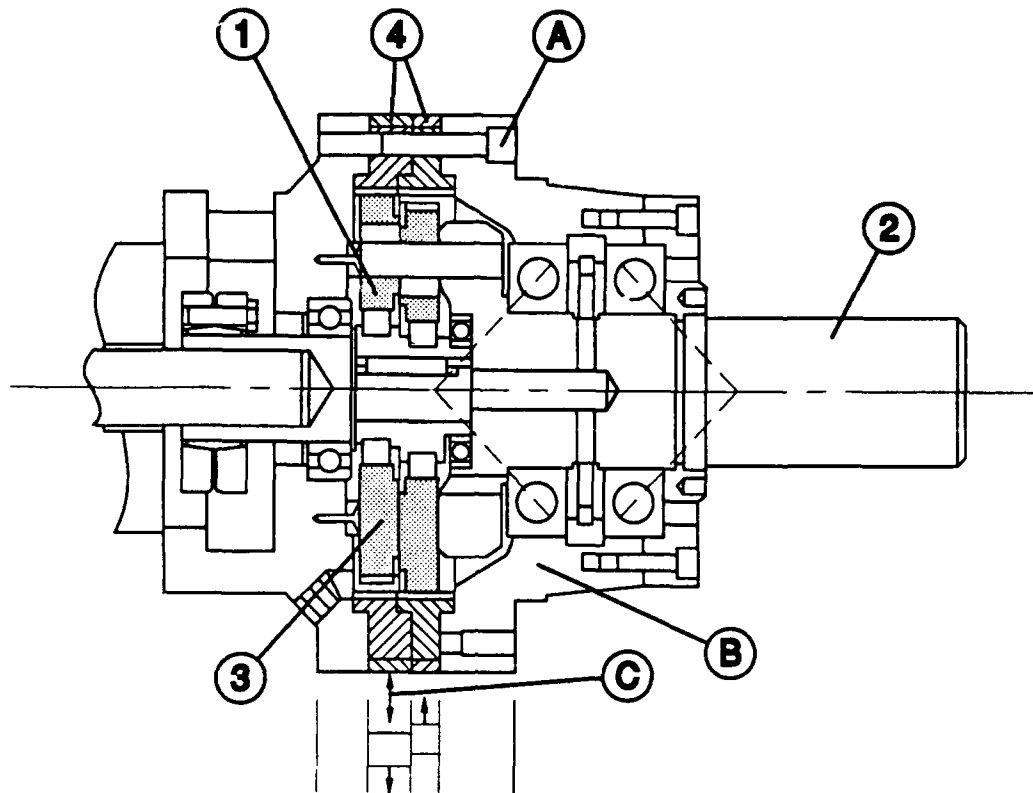


Figure 2.10 : Cross-sectional view of CORBAC reducer, showing (1) output shaft-assembly cantilevers, (2) output shaft, (3) two eccentrically located crown-gears, (4) split inner gear rings for indexing and backlash reduction and preloading, (A) set screws to hold index pattern, (B) output housing, (C) indication of inner ring gear indexing displacement.

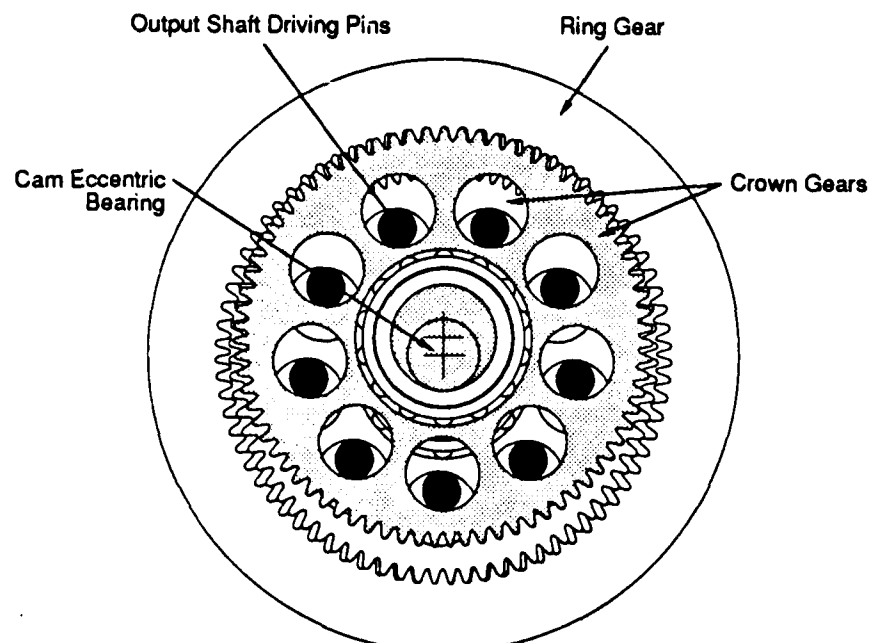


Figure 2.11 : Cycloidal Principle in the REDEX CORBAC unit, illustrating the use of crown gears (3) riding on the indexable inner gear (4), while transmitting torque to the output shaft driving pins (1).

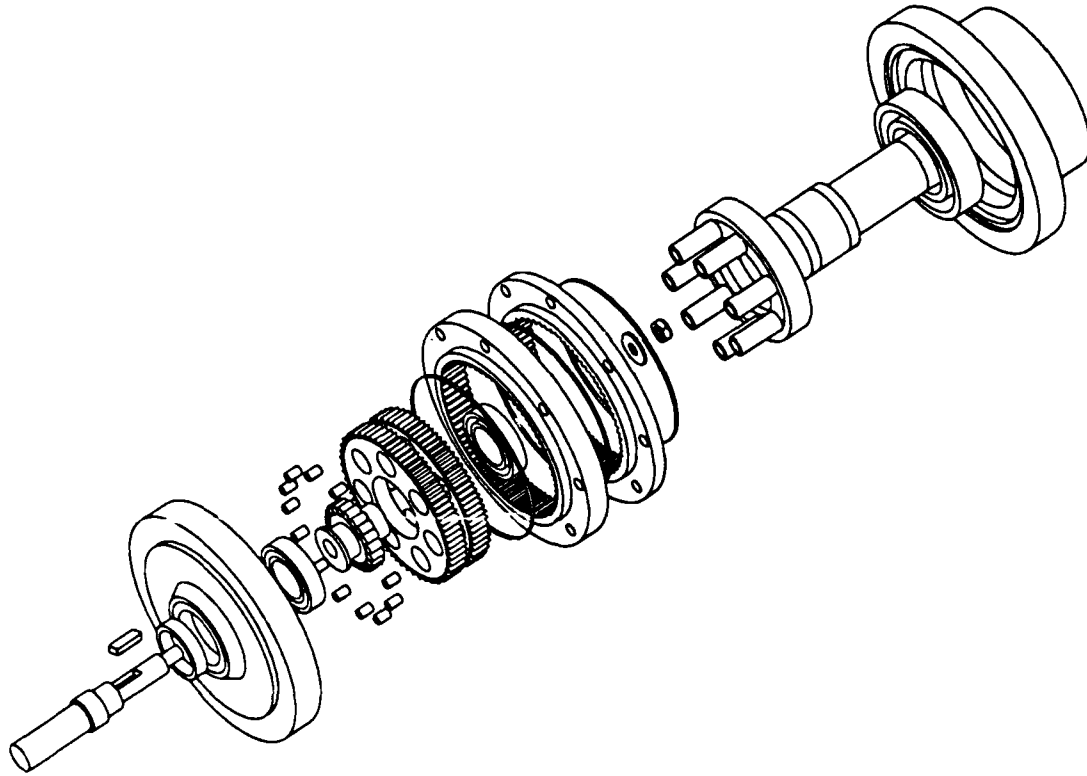


Figure 2.12 : Assembly Drawing of REDEX CORBAC unit, which shows the input shaft, crown gears and eccentrically located bearings, split inner gear, and the cantilevered output shaft which takes the load from the milled holes in the crown gears.

(2.2) Transmission Parameters - Summary

In Table 2.1, we have supplied important information that is readily available from manufacturers/dealers catalogs, as well as measurements taken from the units themselves.

	N	Output τ_{\max} Nm	Input ω_{\max} RPM	Power Watts	Effic. η %	Inertia $I^{\$}$ $\times 10^3$ kgm ²	Back- lash [#] arc-sec	Stiff- ness* K Nm/rad	Weight kg	Length m	Dia. m
WHOI Cable Reducer	30	130	3,000	1,350	>85% and <95%	0.23	NONE	4,000	10	0.39	Width* Height 0.12* 0.15
KAMO Ball Reducer	10 and 30	39 and 113	3,000	1,200	>80% and <90%	0.144 and 0.35	45	6,000 and 25,000	0.8 and 5.0	0.11 and 0.19	0.07 and 0.1
REDEX Geared Cycloidal Reducer	30	200	4,000	2,800	>70% and <90%	0.5	60	40,000	5.0	0.18	0.12
DOJEN Cycloidal Cam Reducer	33	250	6,000	2,400	>70% and <85%	0.66	NONE	15,000	4.0	0.08	0.13
H.D. Harmonic Drive Reducer	60	130	3,500	1,000	>60% and <80%	0.179	NONE	>5,000 and <26000	1.0	0.08	0.11
SUMI TOMO Cycloidal Reducer	59	175	4,000	1,000	>70% and <80%	2.3	180	>2,500 and <30000	3.75	0.055	0.12

Table 2.1 : Published Transmission Parameters for the transmission types studied in this thesis:

(\$)-measured at input, (#)-measured at output, (*)-measured at output.

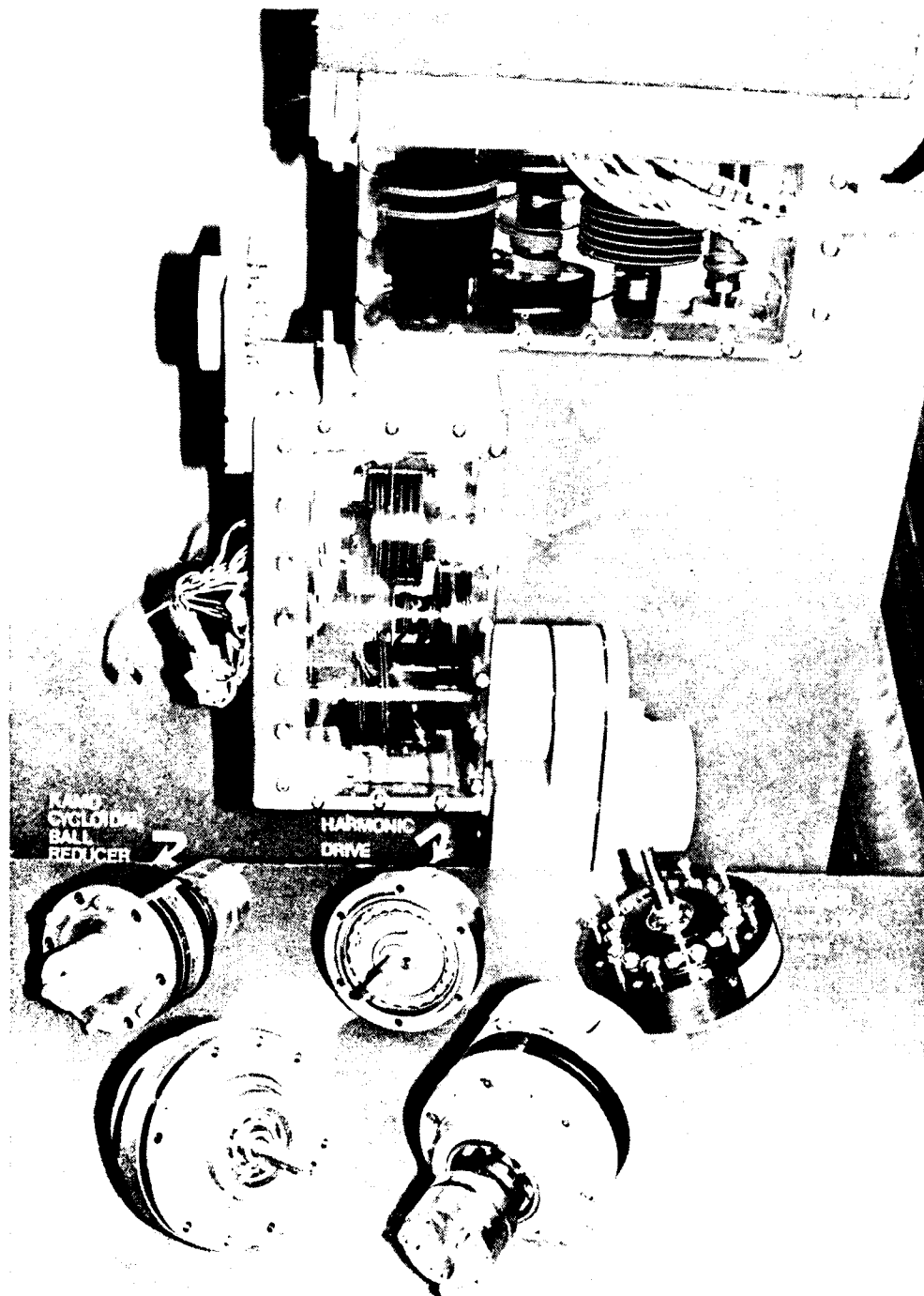


Figure 2.13 : Collection of all the reducers that were tested.

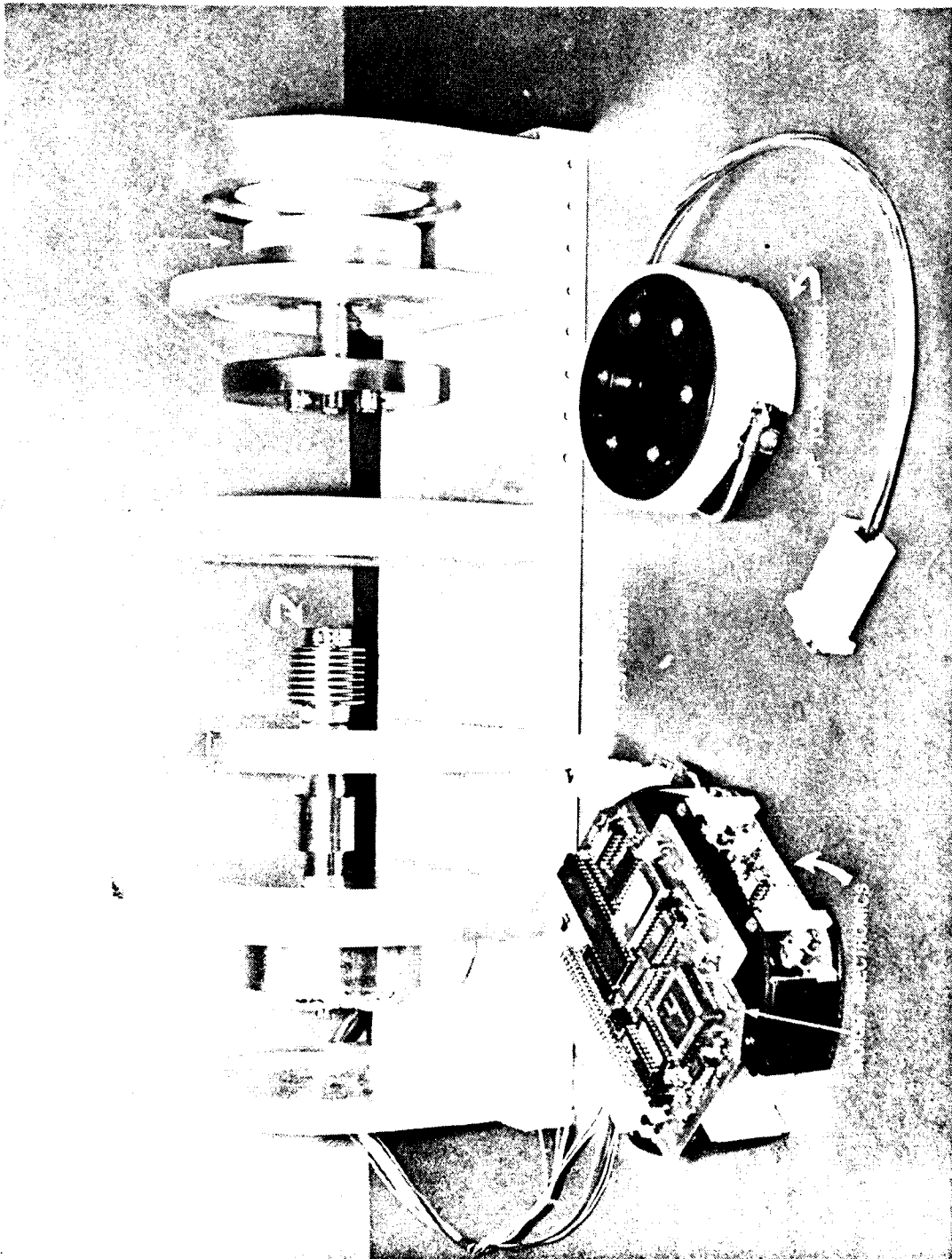


Figure 2.14 : Basic test stand showing the jig plate with all added fixtures, the motor, shaft, bellows coupling, motor-controller card and power stage and the JR³ force/torque sensor.

Figure 2.13 shows a picture of all the reducers that were tested in this thesis. For scaling purposes, the length of the three-stage cable reduction at the top is around 12 inches. All these transmissions, except for the cable reducer, were tested on the same experimental setup, shown in Figure 2.14. The motor and -shaft are located on the left end of the jig-plate, while all the other necessary plates and adapters are spaced along the plate itself. The motor shaft is connected to the transmission via a steel bellows, while the force sensor is attached to the output of the transmission using an adapter plate. The experimental setup is explained in more detail in Chapter 4.

Terminology :

A 'soft-zone' in the transmission stiffness curve, is a zone of reduced stiffness, where for the low torque levels, the transmission stiffness is small compared to the region of larger transmitted torques. Such a behaviour is usually an indication that the transmitted load is not shared by all the load bearing members inside the transmission, and that a certain amount of deformation is necessary, before the load is shared by more internal components. Once the load is properly shared, the load per unit member is reduced, and subsequent increases in load result in smaller amounts of deformation. The subsequent region of suddenly increased transmission stiffness is called torque wind-up zone. For identical deformations as in the soft-zone, the required input/output torque has to 'wind up' or increase much more than was necessary in the soft zone.

A region of 'lost motion' is similar to a zone of backlash, only that it has been defined by industry as the measured deflection when 3% of maximum rated torque (torque rating usually around 1500 RPM) is applied to the transmission. This torque level is assumed to remove all the tolerance fits, yet requires thus that the internal friction levels be below this number. It is in essence a cousin to backlash, but represents a more conservative estimate. It is important to note that this figure is very important as it disguises a zone of extremely low stiffness around the no-load point, which can have important stability and performance implications as will be shown later.

(2.3) Transmission applications

The application regime of the above transmissions is fairly large. Several companies in Japan, the US and Europe are using the cycloidal-type reducers on industrial robots because of their reliability and ruggedness. Other commercial companies in the US have built manipulator assemblies that employ Harmonic Drives - most notably those built by ROBOTICS RESEARCH and MARTIN MARIETTA (buying actuator packages from SCHAEFFER MAGNETICS to build the NASA sponsored Flight Telerobotic Servicer - FTS). European robot manufacturers like ASEA and other research manipulators (like the Stanford arm) also employ harmonic drives. Ball Reducers have so far only been used in Japan, where a new line of SEIKO robots have been built using this technology. Cable reductions have been widely used by the laboratories of the French Atomic Energy Commission (CEA) and other atomic research laboratories in the US, in handling radioactive materials using cabled master/slave systems. Only a few newer cable designs exist in the research community today - at MIT and WHOI. Standard gear transmissions still find wide areas of application in the PUMA line of robots.

Overall these transmission types have found widely different areas of applications that seem to be suited to their respective operational characteristics. Harmonic Drives, by virtue of their zero backlash and comparatively low friction have found wide application in short duty-cycle or indexing applications for space applications (high torque-to-weight ratios). Attempts have been under way to build robot manipulators with them, but there are reports of varying success in implementing such systems. It is interesting to note that most published papers dealing with limiting transmission dynamics all dealt with the harmonic drive. Cycloidal reducers (whether they be a geared, epitrochoid or cam-type) are most certainly the most widely used transmission in industrial robotics besides the standard gear transmissions, where reliability and ruggedness are very important performance criteria. Special designs are available where the backlash can be reduced to a (non-zero) minimum. Cable reductions will be shown to result in devices with as near to ideal a transmission behaviour as is possible today. They have been mostly used in master/slave environments where human presence was too dangerous or impossible (hostile environments such as radiation, underwater, etc.). Latest design efforts at MIT and WHOI have extended the design expertise for these transmissions from the late 1970's to include some interesting conclusions as to bandwidth and stiffness of such drives. Prototypes of such manipulators are currently being tested and evaluated. Ball Reducers are fairly new on the market and

represent an interesting transmission which warrants careful study, since they are meant as a direct competitor to all other cycloidal transmissions.

CHAPTER 3

(3) REALISTIC TRANSMISSION MODELING

(3.1) Complexity/Sophistication in Modeling

Given the premise that we want to design transmissions that are pure torque-multipliers, it becomes important to understand what physical limitations have to be dealt with. Only perfectly massless, frictionless and rigid elements could represent the ideal mechanical transformer - a physical impossibility as we know. All the transmissions analyzed in this thesis have physical parameters that can be used to describe their non-ideality with respect to torque-multiplication. In the world of mechanics, such inherent transmission dynamics can not always be disregarded, since they can be shown to have a limiting effect on the performance and stability of the system they are present in.

Transmission dynamics are most often represented by a combination of mechanical elements, such as inertias, springs and dampers, which can be coupled in a linear fashion so as to make the resulting physical system easy to analyze. Since the analysis is based on linear system theory, we will look at the effect of different linear transmission models shown to be applicable to real systems. These models will increase in complexity, and illustrate the problems in designing a transmission. The addition of nonlinearities such as backlash, stiction/friction, and transmission stiffness with soft-zones will also be studied. The following sections will study the different transmissions and their corresponding models which best represent the physical design and layout. The intent is to understand the performance and stability limitations of each transmission model/type and thus motivate and focus on relevant design issues which are critical in transmission design. Experimentally measured data will be compared to model-predicted data, in order to establish the validity of the proposed model structures.

The analysis will mostly be guided by closed loop performance and stability criteria and is also meant to extend the theoretical and practical design criteria drawn up by Salisbury et al [(1988)] and Townsend [(1988), et al (1989)].

(3.1.1) General Analysis

In order to better understand the analysis to follow, we first have to understand why there is a need to model transmission behavior. Most robotic applications (or any other control applications for that matter) or control algorithms require that joint-torques be

applied by a motor through a transmission assembly to the output of each joint. Most control algorithms neglect the presence of actuator dynamics. Usually simple first-order models are not sufficient to explain nor compensate for performance and stability limitations. But since the ultimate goal behind a physical system model is to use such knowledge to improve the controller performance, we still need to be able to determine which physical system model best approximates the physical device, the regime of validity of the model, and if the use of such a model in controller design can indeed increase closed-loop performance.

Transmission dynamics are usually of high order and can thus increase the complexity of the controller model by several orders. Using such models for control purposes, makes a controller highly sensitive to errors in parameter modeling. The following paragraphs should be seen as a qualitative representation of what we believe to be the most accurate representation of complexities in transmission modeling. The notation to be used can best be summarized in the table below :

I_{rs}	: Rotor & Shaft Inertia
I_t	: Transmission Inertia
I_l	: Load Inertia
N	: Transmission ratio
B_s	: Shaft Viscous Losses
B_t	: Transmission Viscous Losses
B_e^m	: Electronic Motor Damping Coefficient
K_t	: Distal (variable) Transmission Stiffness
K_{sz}	: Proximal Transmission Stiffness
K_e^m	: Electronic Motor Stiffness
τ_{act}	: Actuator Torque
τ_{env}	: Environment Torque
$\Delta\phi$: Angle of Backlash
$\Delta\gamma$: Angle of Soft-Zone or Torque Wind-up

Please note that we have used the approach of reflecting inertias, and all forces and coefficients to the actuator, since it will improve the clarity of the following analysis. Thus in all cases, we can think of all parameters as being reflected/expressed with respect to the actuator or input side. This is an important distinction when one analyzes the stability and performance data presented later.

(3.1.2) Rigid Body Model

The most common approach in controller design is to assume that the transmission is purely an inertial load with added frictional losses, as seen in Figure 3.1.1:

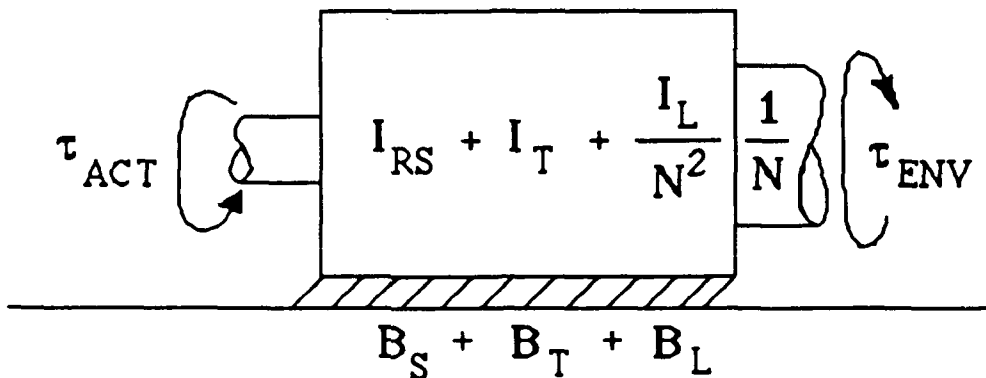


Figure 3.1.1 : Rigid-Body Actuator-Transmission-Load Model

The simplest assumptions are then to lump all inertias (manufacturers usually provide relatively accurate figures for transmission inertias) and viscous losses into single entities and then perform the choice of controller gains (and -structure). The most involved controller design will then also attempt to compensate for directionally (sometimes even temporally) dependent coulomb friction and viscous friction. Many of the attempts at force control have shown that the measured performance and stability limits can not be explained with such a model. Most researchers have tried to explain instabilities with the (unmodelled) presence of transmission/structural compliance (which the above model assumes to be zero) - a scenario studied next.

(3.1.3) Single Transmission Stiffness

The most common increase in system complexity, is to assume the presence of some transmission compliance, usually modelled with a spring. The compliance model is used to represent the rigidity of the load bearing elements of a transmission. Depending on where it is measured, by either locking the input or the output and applying the fully rated torque, it can be represented by the model of Figure 3.1.2 :

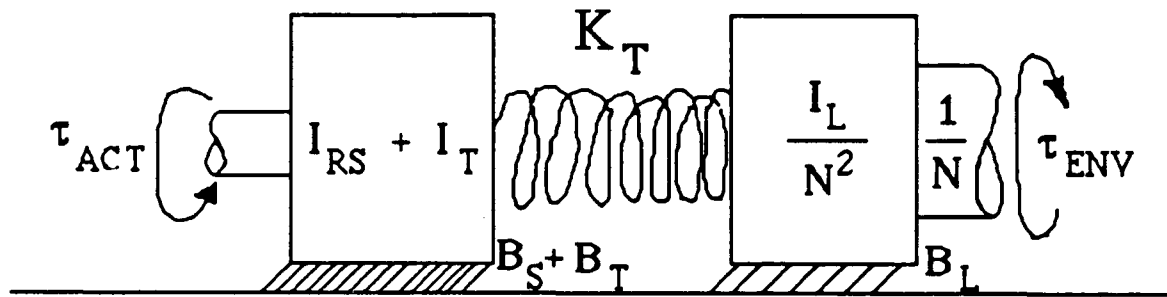


Figure 3.1.2 : Lumped Parameter Simple Stiffness Transmission Model.

Most of the manufacturers of robotic transmissions supply figures for transmission stiffness. The interesting fact that emerges after extensive literature search and phone calls to engineering representatives (circumventing glossy brochures and ignorant salesmen), is that all transmission behaviors can not be represented by a single spring with a given fixed stiffness coefficient (spring-constant). One should always be wary of a manufacturer that supplies a simple number to represent a reducer's stiffness. Most manufacturers represent their transmission's stiffness by tabular or graphical form. These tables and graphs usually give the deflections associated with the applied torque (all static experiments). Thus a more accurate representation would be that of a variable spring stiffness as shown in Figure 3.1.3,

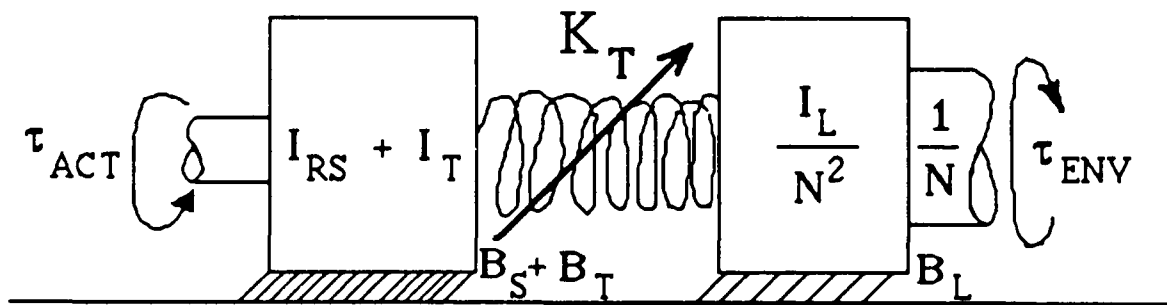


Figure 3.1.3 : Variable Transmission Stiffness as a function of transmitted load (torque).

where we are allowing for the possibility that the spring stiffness may change as a function of relative displacement, which is analogous to transmitted load. This physical phenomenon can very easily be explained, and will later be shown to be of extreme

importance in stability and performance analyses. A simplified plot of the different torque-to-angle relations for the above models can be seen in Figure 3.1.4, where the linear and nonlinear stiffness behaviors are depicted:

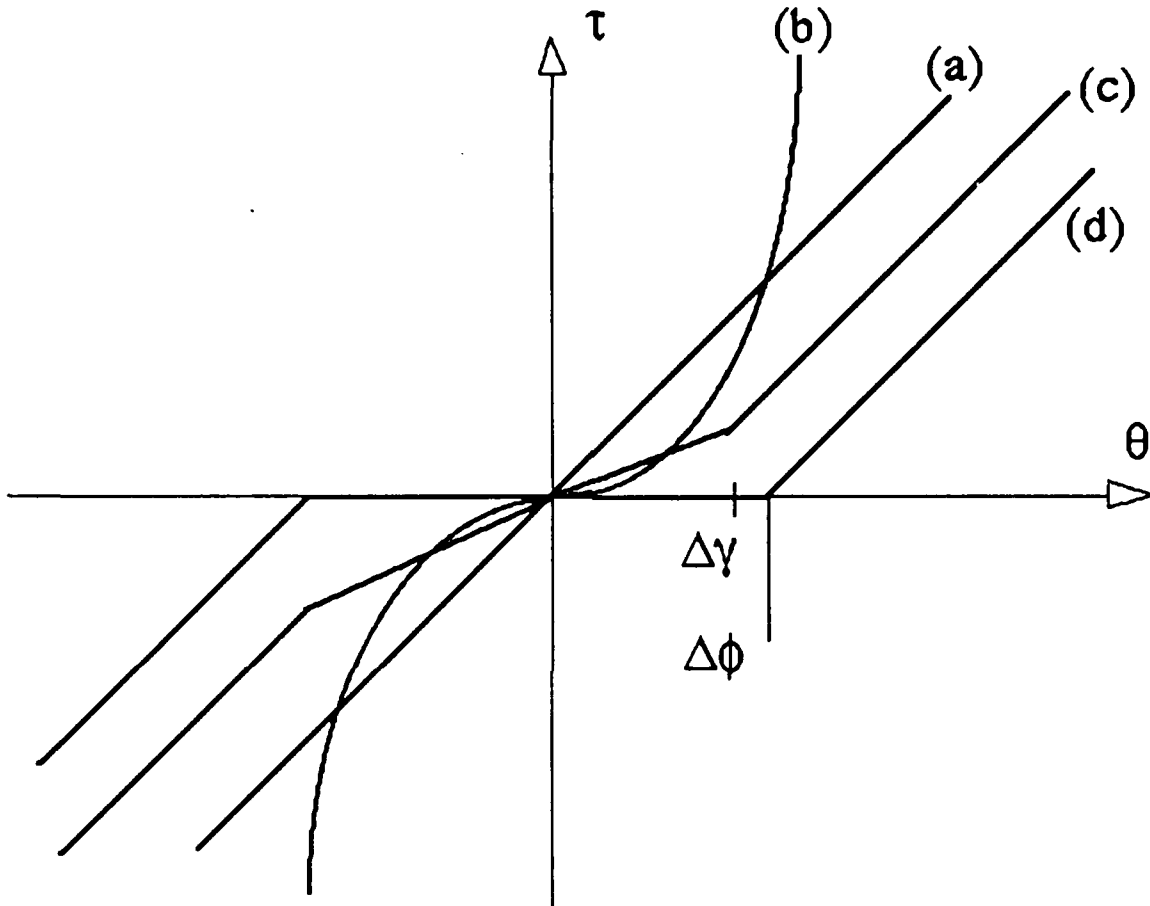


Figure 3.1.4 : Varying relations for transmission stiffness for (a) the model of Figure 3.1.2, (b) the model of Figure 3.1.3, (c) the model of Figure 3.1.5 and 3.1.6, and (d) the model of Figure 3.1.7.

Figure 3.1.4 illustrates the increased levels of sophistication in transmission stiffness modeling. The simple fully linear models differ widely from the piecewise linear to the fully nonlinear behaviors some researchers have used to model transmissions. The variable transmission stiffness has been mostly modelled as a cubic nonlinearity, which has certain properties which make it a suitable candidate for certain frequency domain stability studies (Sinusoidal Input Describing Function Analysis). On the other hand, such a model is not borne out by the data supplied by the manufacturer, nor the experimental data presented in this thesis. A third order polynomial representation may approximate the phenomenon

quite well, but a more piece-wise linear representation represents a more physically motivated stiffening behavior.

Such stiffening behavior is best explained with some very simple mechanical principles. Every unit that has several moving parts can not be made with perfectly mating parts. For ease of assembly, tolerances are usually kept under the nominally specified values. The lower the tolerances, the smaller the slop, or in our case backlash, the system will have. Tolerance fits are usually distributed throughout the transmission. Thus when a transmission is locked at either end, and increasing levels of torque are applied, these tolerances are first removed (a physical phenomenon usually labelled backlash) and components bearing any loads begin to deflect. The amount of torque wind-up or soft zone is dependent on how well the unit was designed and manufactured so as to evenly distribute loads over all the (by design) load-bearing surfaces. Thus a transmission soft-zone is indicative of a transmission with (a) load bearing member(s) that due to tolerancing and assembly bear(s) all the load, until its own deflection causes the remaining load-bearing components to share the load, thus distributing it properly. Hence the type and design of these load-bearing components is critical. Oversizing certain components to achieve interference fits (so-called 'dimensional preloading') can reduce such behaviors, but it also incurs the price of higher frictional losses (reduced transmission efficiency and increased stiction/friction behavior). A rather simple stiffness model with a single 'knee' could be represented by Figure 3.1.5,

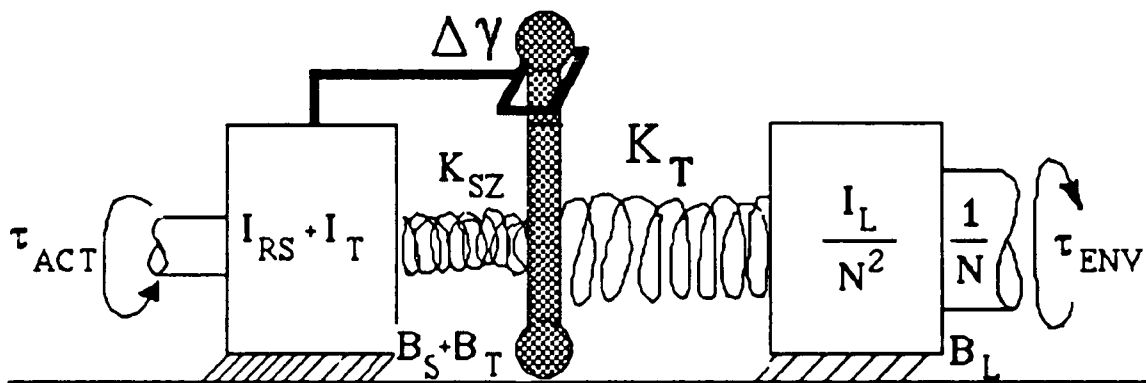


Figure 3.1.5 : Piecewise-linear single-knee transmission stiffness model.

where the soft-zone (K_{SZ}) and stiff zone (K_T) are represented by two springs in series. The net effective stiffness depends on the amount of transmitted torque and is represented by a deflection-modulated nonlinearity ($\Delta\gamma$). Such wind-up zones can be large, and represent an excessive amount of material compliance before even load distribution decreases the level

of incremental compliance (or deflection). Such stiffening behavior is thus not only transmission-type dependent, but will also depend on operating conditions and differ from unit to unit. Controlling this physical phenomenon and reducing the inter-unit variability are thus also very important.

(3.1.4) Transmission Soft-Zone or Wind-up

An inherent assumption in the above discussion was, that the soft-zone and the ultimate stiffening zones were all co-located inside the transmission. The resulting stiffness behavior is thus localized to a single location in the transmission. On the other hand, other transmissions can have distinct areas of distributed stiffness, with different localized areas of compliance.

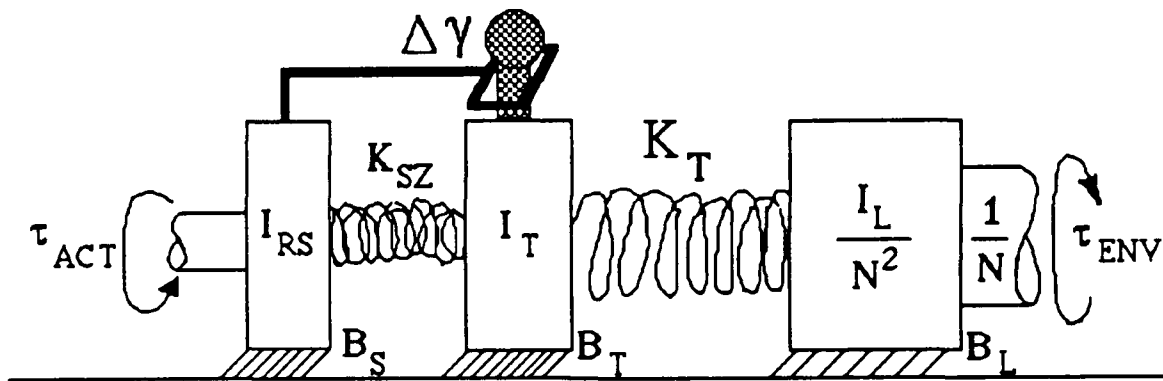


Figure 3.1.6 : Non-co-located variable transmission stiffness zones, reflecting improper spatial load distribution.

This is especially troublesome, when as in Figure 3.1.6, the soft-zone of the transmission is not co-located with the true load-bearing members of the transmission. The effective stiffness in the soft-zone K_{SZ} , as well as the region over which it is present ($\Delta\gamma$), are dependent on the type of transmission. The load-dependent effective stiffness is represented by a relative displacement $\Delta\gamma$, which corresponds to a net transmitted torque before all load bearing surfaces share equal (design) loads. The reason why the distinction between this model and the one with localized variable spring stiffness is so important, is because we have introduced an indirectly controlled oscillatory system which may result in more severe closed-loop performance and stability constraints than expected. Another level of sophistication may be to attribute a variable spring stiffness to K_{SZ} , in order to reflect the

highly nonlinear behaviors in the low-torque end. For the moment this effect will be neglected, albeit the near certainty that it is probably present in most transmissions.

(3.1.5) Backlash and Lost Motion

A transmission may many times also exhibit some sort of backlash. This backlash is due to loose fits among parts due to loose tolerancing and improper assembly. The purest definition of backlash is the angular displacement necessary to get all the mating parts to contact each other as specified in the design (in the absence of any friction), so that torque is transmitted through the transmission. Notice the absence of any specific applied torque values and any mention of where to measure and apply torque. The physical representation of backlash, shown in Figure 3.1.7 (with all the previous dynamics as well),

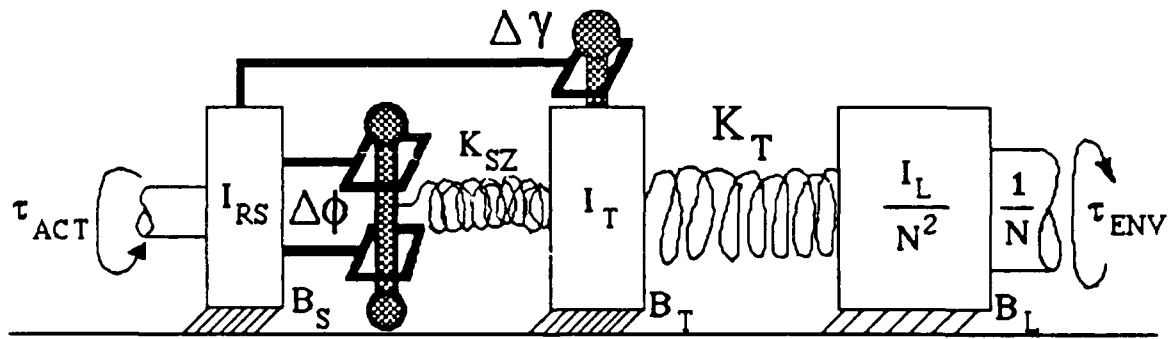


Figure 3.1.7 : Complex Actuator-Transmission-Load Model including soft-zone ($\Delta\gamma$) and backlash ($\Delta\phi$).

shows the backlash expressed as a relative displacement ($\Delta\phi$) measured at (or reflected to) the input shaft.

The actual value of backlash can be determined in a variety of ways. Reading a manufacturer spec sheet is not always enough, due to the specsmanship manufacturers usually use. Most of them spec their backlash at the output, since they are concerned with tasks requiring high positioning accuracy such as in NC machines, IC assembly, etc.. The associated test thus should involve measuring output displacement without any input displacements. This is however not how most manufacturers measure backlash. The correlation between backlash at the input and the output is usually quite well approximated by the reduction ratio, N (assuming even distribution of backlash throughout the

transmission). This figure is very important in robotic systems, since we have bidirectional high bandwidth control action present, irrespective of transmitted loads.

Most of the manufacturers perform a much different test which is easier to perform, many times flawed, and does not provide the same information. They lock the input shaft and apply a given tare torque (usually $\pm 3\%$ of the fully rated torque at a given RPM) at the output and measure the associated deflection (usually with a high resolution optical encoder). The associated displacement is then called lost motion. The reason for this convention is quite simple to understand. Not every transmission has a discrete value of backlash lumped at the output, but a certain (lumped) distribution throughout the transmission. Since frictional torques are also distributed throughout the transmission, simply applying very small torques at the output and calling the measured displacement backlash, would be incorrect. The reason is that not all tolerance fits would be brought into contact since transmitted torques decrease as they go through the transmission by the localized value of the transmission ratio. Thus if this transmitted load decreases below the level of local frictional torques, any tolerances downstream would not be removed. The (undocumented) convention of $\pm 3\%$ torque levels for a lost motion measurement would thus seem very inappropriate. But on the other hand this can only be a valid experiment if the $\pm 3\%$ level is above that of the total frictional torques inside the transmission. In other words, measuring the lost motion on a transmission with a 20/10 N-m stiction/coulomb frictional behavior, by applying a ± 4 N-m torque at the output, will not result in a reliable value for backlash or even lost motion. To be fair, one would at least require to perform this test at a ± 10 N-m level - the value for coulomb frictional torques in the transmission. Ignoring this simple requirement can yield seemingly complicated transmission stiffness curves with several 'knees' or linear regions with increasing stiffness, as in the case of the epitrochoid cycloidal disk reducer from SUMITOMO.

For systems which have a backlash-zone, and can thus be represented by a model as in Figure 3.1.7, performance and stability margins are much different from those of a system which has no real appreciable backlash. If a controller is designed based on the assumption of dealing with a system as in Figure 3.1.1, the controller structure and gains can easily be shown to be of a destabilizing nature or at least result in a highly underdamped system behavior, for a system operating within its backlash zone.

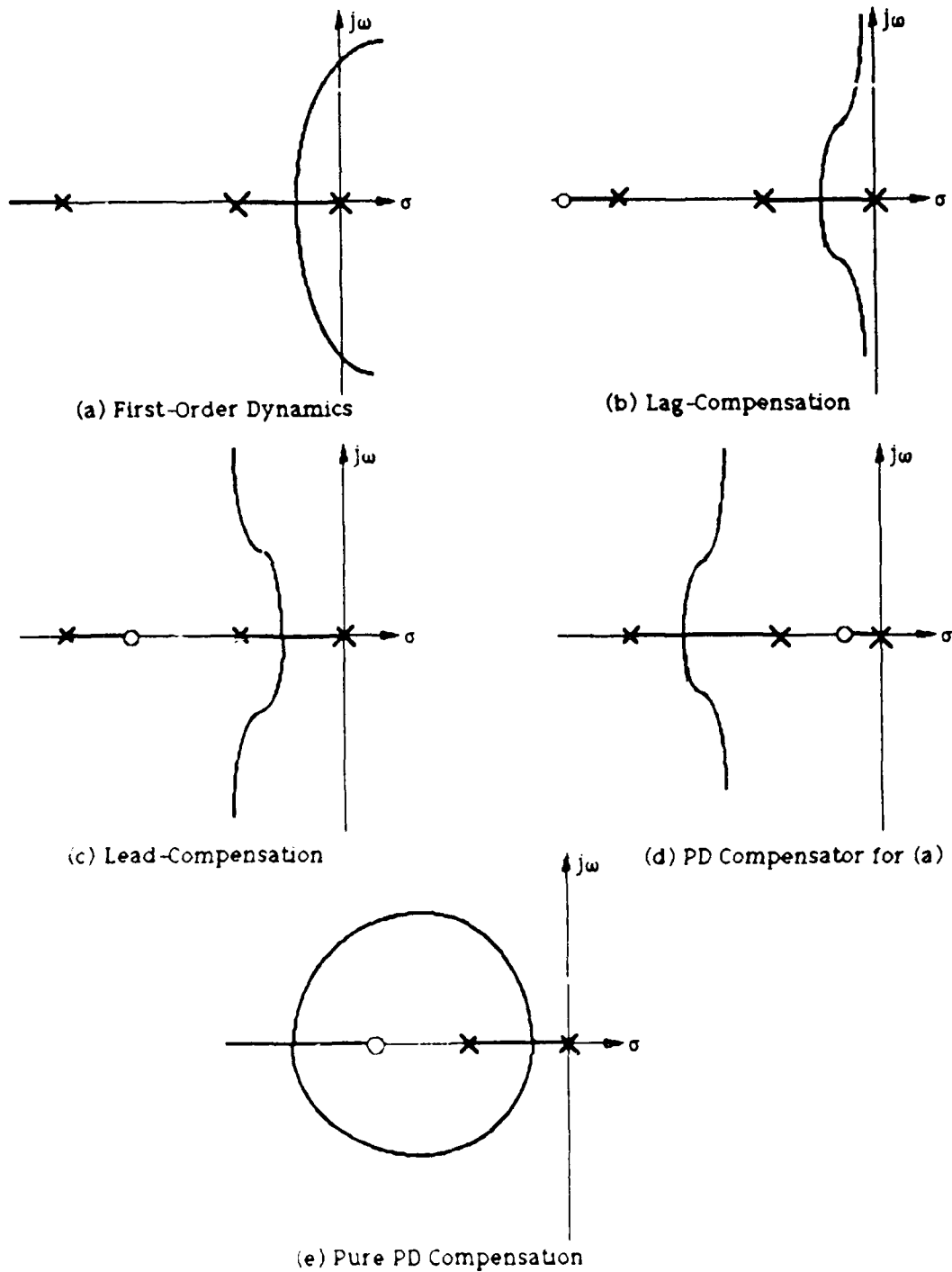


Figure 3.1.8 Root-Locus for two-pole system : (a) Instability in the presence of first-order dynamics, (b) Underdamped Response in the presence of Lag-Compensator, (c) Improved Performance for Lead-Compensation, (d) Improper Lead-Compensation, (e) Preserved Stability and Performance for PD Compensation

Take the very simple diagram of Figure 3.1.8 (a thru e), where we have shown the influence of adding different controllers and dynamics to a two-pole system. This two-pole system represents a model of the true dynamics apparent to the actuator, for a system that operates within its backlash zone. The inertia would be purely that of the shaft/rotor, and the damping due to bearing losses. In Figure 3.1.8(a), we can easily see that the addition of first-order dynamics in the feedforward path (actuator dynamics, filtering, etc.) will result in unstable dynamics if not properly compensated for. If the original pole pair is taken to represent the dynamics in the backlash-zone, the region of stability is drastically reduced. Adding a lag compensator, as shown in Figure 3.1.8(b), can result in bounded stability regions and increasingly underdamped response. For a given location of the lag-compensator pole-zero pair, the response may not only become underdamped very fast, but will also result in instability if a discrete-time stability analysis is performed. Figure 3.1.8(d) shows how choosing a lead network has a direct effect on the stability and effective damping of the closed-loop system. If a properly chosen lead network compensator is used (Figure 3.1.8(c)), system stability may be improved, but with the price of highly underdamped response while operating within the backlash zone.

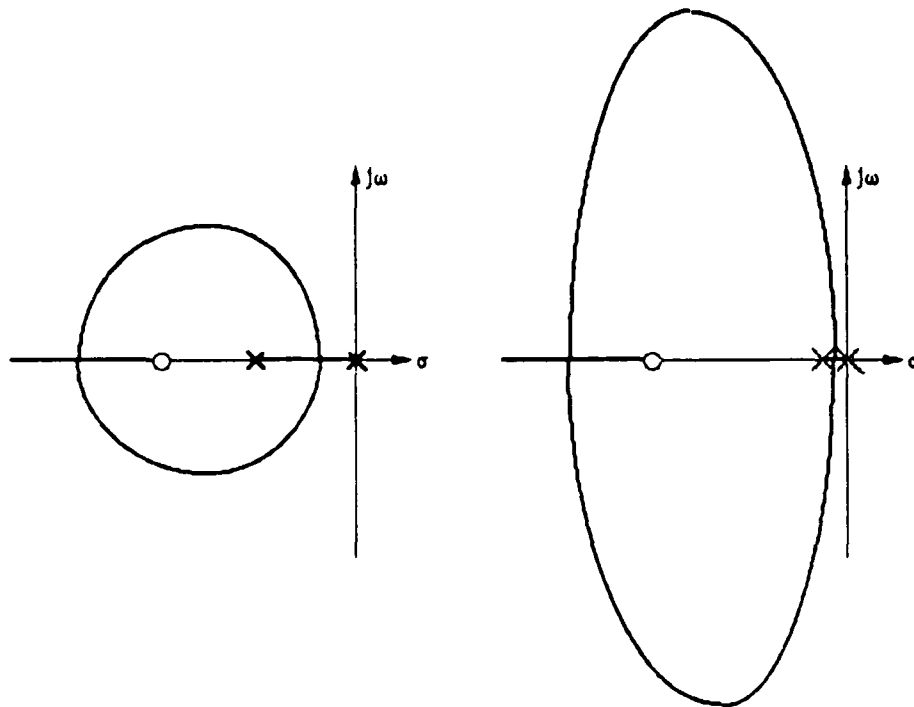


Figure 3.1.8(f) : PD Controller Comparison between design locus based on rigid-body model (left plot), and the locus for operation in the backlash-zone (right plot).

Using a simple PD controller structure for a rigid-body model with reflected inertias and effective system damping, as shown in Figure 3.1.8(e), would seem to guarantee stability, but will again result in underdamped responses for systems with reduced inertias and viscous damping losses (i.e. systems operating within their backlash zones). That this is true can be seen for the case of an identical controller operating on a system with reduced inertia and/or reduced damping when operating in the backlash-zone as illustrated in Figure 3.1.8(f). The relationships between the effective bandwidth

$$\frac{\omega_n^{(\text{backlash})}}{\omega_n^{(\text{rigid-body})}} = \sqrt{1 + \frac{I_T}{I_{RS}} + \frac{I_L/N^2}{I_{RS}}} \quad (\text{Eqn. 3.1.a})$$

of the backlash dynamics and the rigid-body dynamics is shown to be highly dependent on the inertia distribution in the transmission (see Equation 3.1.a. above). The effective damping ratio clearly illustrates the underdamped high-frequency nature of backlash dynamics (see Equation 3.1.b.).

$$\frac{\zeta^{(\text{rigid-body})}}{\zeta^{(\text{backlash})}} = \frac{\omega_n^{(\text{backlash})}}{\omega_n^{(\text{rigid-body})}} \left\{ 1 + \frac{B_T + B_L/N}{B_{RS} + B_e^M} \right\} \quad (\text{Eqn. 3.1.b})$$

It is clear from the above equations, that the effective damping ratio is proportional not only to the electronically supplied damping, but also to the damping present at the input and the damping distributed throughout the transmission.

Thus for certain controller structures and gains, the closed-loop dynamic behavior of a system within the backlash-zone may be unstable or highly underdamped. Once the backlash is removed, the root locus becomes increasingly damped again, but we now have the certain possibility of (stable) limit-cycle behavior. Magnitude and frequency of the limit-cycle depend mainly on the actual physical system parameters, controller structure and -gains, sampling and controller bandwidth, etc.. In some cases, the resulting closed-loop frequency of the backlash dynamics may be higher than the theoretical Nyquist criterion allows (which even then is the absolute limit - a factor of 10 to 20 for the ratio of sampling-to controller-bandwidth is the usual rule of thumb). Violating or reducing this safety margin, only increases oscillatory tendencies, which can not be proven to exist via a simple continuous-time root-locus analysis. On the other hand, if the continuous-time system is mapped into the discrete-domain, to study the effect that finite sampling has on overall stability, the possibility of instabilities can easily be shown to exist. Thus a simple rigid-

body system with viscous damping may only be stable for certain ranges of inertia, damping and sampling rate.

A point worth mentioning is what can be done (intentionally or unknowingly) to minimize backlash and thus the onset of limit-cycles. The most involved method has been termed dimensional preloading, which simply means that all parts are dimensioned so as to force parts to contact at all times (basically an interference fit assembly). The disadvantage of such approaches is the increase in frictional losses and the undisputable increase in static and kinetic friction because of increased normal forces. Forcing load sharing in this fashion also has thermal implications, since as the unit operates it will warm up and thermal expansion can drastically alter system behavior. This physical phenomenon can be shown to be detrimental to control performance (hard if not impossible to compensate for stiction) and stability (onset of limit-cycle behavior). A more simple and effective way to reduce unwanted behaviour in the backlash-zone or the soft-zone, is to introduce larger damping into the transmission (passive or electronic), as shown in Figure 3.1.9 below.

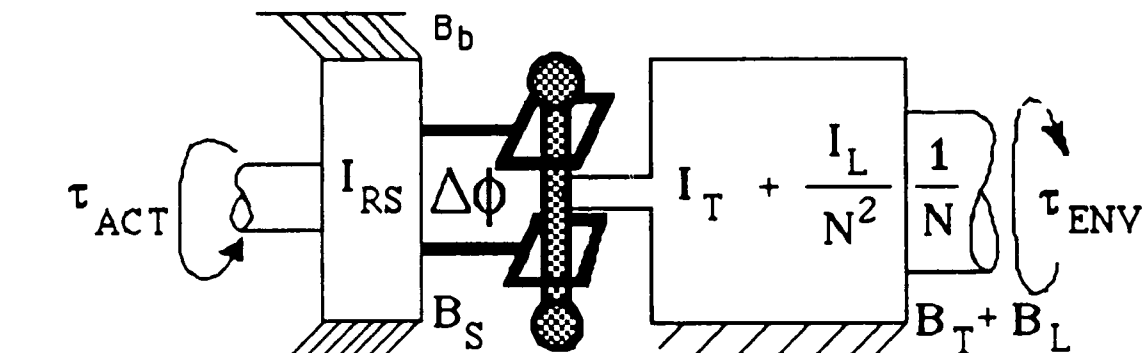


Figure 3.1.9 : Added damping in the backlash-zone, due to seals, viscous lubricants, etc.

The necessity to lubricate a transmission is obvious since it reduces wear and thus increases life while reducing frictional losses between contacting surfaces. The choice of lubricant though, is a completely different story. It is well known in tribology, that surfaces at rest have a very thin film of lubricant separating contacting surfaces, besides the surfaces asperities that are in solid contact resulting in plastic and elastic deformation (Dahl Effect). This phenomenon is called boundary lubrication, and makes break-away measurements non-repeatable. When relative motion sets in, the fluids' viscosity and other factors force a region of lubricant to remain between the contacting surfaces thus reducing the overall friction effects due to reduced metal-to-metal contact - a physical process called full fluid lubrication. Viscous friction effects which are proportional to velocity are a clear

indication of hydrodynamic lubrication. The choice of a medium viscosity lubricant would usually necessitate the use of some sort of shaft seal on robotic transmissions. Most manufacturers though use the much higher viscosity greases (like Beacon 325), which have much higher viscous losses than lower viscosity fluids, and thus have a much more stabilizing effect on overall transmission dynamics. This could easily be shown to be the case for a root locus in the backlash-zone with increased viscous damping. This increased damping will later be shown to also be of extreme importance in damping structural resonances inside the transmission itself.

(3.1.6) Dissipative Phenomena (Static/Kinetic/Viscous Friction)

The distribution of viscous dampers in the transmission is also lumped together in the lumped-parameter model of the transmission- and load-inertias shown earlier. This represents a simple and linear model which lends itself well to control performance analysis. On the other hand, one should clearly be aware that the true dissipative phenomena are also of a stick/slip nature, implying the presence of stiction and friction. The degree of difference between these two physical phenomena varies greatly among transmissions. In gear transmissions without any preloading, the tolerance fits are intended to allow better lubrication and material expansion due to heating. Once preloaded, more teeth are in contact (disregard spur and bevel gears, where the entire load is borne by ~ 1 tooth) like in a planetary gear train, and this increased contact area with increased normal forces results in larger stiction/friction magnitudes. The problem of material expansion due to heating is a big problem in reducer design - especially for those high-reduction reducers which run at high speeds and have large preloads or transmit large torques. Such a phenomenon is hard to model, yet it affects most of these types of reducers. One of the reducers that was not tested, was a preloaded planetary gear-head, whose outside diameter was covered by custom-made cooling fins !!! Most manufacturers thus rate their reducers to run at a certain speed for only a certain period of time (or in terms of a duty-cycle). Such effects, albeit important, are not covered within this thesis.

Bearings and lubrication-type and -amount can also account for a substantial amount of dissipative losses in a transmission. Another design element is that of seals. Some of the commercially available transmissions can only be had with some combination of hollow/solid input/output shaft, with internal bearings already installed, as well as input and output shaft seals. The seal type depends not only on the application environment but also on the type of lubricant used. The more viscous the lubricant (grease vs. synthetic or

mineral oil), the less critical the sealing of the shaft seal becomes. The cable reduction designed at WHOI is a good example, where a lot of thought has gone into the design of a low-friction/stiction seal. Since it was placed at the output and served as an oil-reservoir retaining seal, its low-speed properties (break-away, etc.) were very important, since researchers [Townsend & Salisbury (1988)] have shown that stick/slip is a destabilizing phenomena in robot force control. Not only was it important to reduce the absolute frictional torque, but the design of the carbon-on-ceramic seal faces reduced the difference between running- and break-away-torque, to a point where the ratio was about 1.2. The absolute break-away torque lies at around 1.25 to 1.5 N-m. The newer generation of seals come with silicon-carbide on silicon-carbide faces, with break-away torques reduced by an order of magnitude!! It is an interesting and important design question as to where to place such a seal if one has the choice. Such questions will be answered later on in the thesis in a more experimentally motivated setting. We will give a guide for seal placement based purely on stability arguments later in this chapter. On the other hand, the stability analysis will not deal with describing-function equivalents, since it will generate all its stability criteria based on time-domain analysis techniques. Thus such phenomena as friction/stiction and backlash will be dealt with in a more qualitative sense. Theoretical arguments and experimental data will be used to justify claims about their relative size, location and importance in performance- and stability criteria for robot transmissions.

(3.2) Transmission-specific Parameters

The theoretical analysis to follow in the next section will require that certain parameters be assigned realistic numeric values. For that purpose, we will present in this section a collection of those parameters needed in the analysis. The different parameter values were either taken from manufacturer data sheets (inertias), measured off the real hardware, and determined through careful off-line examination of experimental data. We will present the results in a simple table that lists the different parameter values, after which we will discuss the physically realizable variation in the different parameters which we intend to study.

The different parameter values, given here in terms of their variable names are split into the different modeling groups we used. Notice that at this point we have made a decision as to how different transmissions can be represented by certain models. This decision was reached after careful study of the data presented in Chapter 4.

2 DOF Model

	H.D. Harmonic Drive	DOJEN Cycloidal Cam	KAMO Cycloidal Ball	SUMITOMO Cycloidal Disk	REDEX Geared Cycloid
I₁ kg-m ²	1.8x10 ⁻³	7.1x10 ⁻³	8.6x10 ⁻³	28.1x10 ⁻³	1.1x10 ⁻²
I₂ kg-m ²	1.79x10 ⁻⁴	6.6x10 ⁻⁴	7.5x10 ⁻⁴	2.3x10 ⁻³	5.0x10 ⁻⁴
B₁ N-m/rad/sec	0.0043	0.0025	0.0011	0.006	0.002
B₂ N-m/rad/sec	0.002	0.008	0.005	0.08	0.004
K_T min N-m/rad	0.638	5.8	4.8	1.73	7.7
K_T max N-m/rad	6.50	13.8	12.0	7.5	44.4
K_f N-m/rad	140	459	556	143	565

Table 3.1 : Real Physical Parameter Values for the Stability and Performance Analysis of the 2 DOF Model Structure.

3 DOF Model
(WHOI Cable/Pulley Reducer)

I₁ kg-m ²	I₂ kg-m ²	I₃ kg-m ²	B₁ N-m/rad/sec	B₂ N-m/rad/sec	B₃ N-m/rad/sec
2.3x10 ⁻³	1.7x10 ⁻⁴	9.9x10 ⁻⁴	0.0013	0.001	0.004
K_s N-m/rad			K_T N-m/rad	K_f N-m/rad	
3.2			2.2 to 4.8	556	

Table 3.2 : Real Physical Parameter Values for the Stability and Performance Analysis of the 3 DOF Model Structure.

Notice that the range of stiffnesses can easily vary by a factor of 50 amongst transmissions, as can the ratio of inertias. The output of the transmissions were not really loaded up with any excessive inertial loadings (as would be the case in a multi-jointed robot), and thus a variation in output to input inertia by a factor of 100 is certainly feasible. The values for the damping coefficients at the output (B_2) are also variable by an order of magnitude among the units. The variations in each of these parameters was used to determine the system stability and performance criteria in the section to follow. Variations were programmed to run from the smallest to the largest values in the above table.

(3.3) Theoretical Parameter Sensitivity Analysis for performance and stability of position- and force-controlled actuator/transmission/load systems

The multi-lumped-body dynamic systems proposed earlier were only a theoretical approach to understanding transmission dynamics. Some of the transmissions studied, were fit to the more simple model, while others were fit to the more complex one. It now becomes important to move ahead into the qualitative stage, and analyze the effect that certain model parameters have on overall system performance and stability. At this point, the analysis will still be of a somewhat qualitative nature, but the analysis will include physical interpretations to match numerical representations of parameters, representative of the transmissions being analyzed.

The analysis will deal with performance and stability regions for closed-loop position- and force-controlled actuator/transmission/load systems. We will be looking at the issues of colocated and noncolocated position and force-control. Experimental data will only be presented for the colocated position-control and non-colocated force control scenarios. Each model structure will be dealt with separately, and equations will be presented which will then be used to generate the stability and performance regions shown on the plots.

(3.3.1) Theory & Analysis Background - 2 DOF Models

The analysis will simply deal with fourth- through sixth-order models to represent actuator dynamics. The most simple model used, is similar to Figure 3.1.2, repeated here for notational purposes:

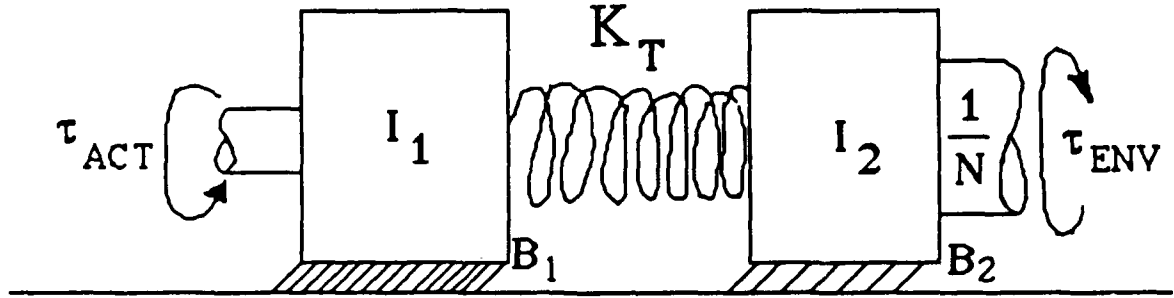


Figure 3.3.1 : 2 DOF actuator/transmission/load model.

The parameters are clearly indicated as representing inertias, spring constants, viscous damping elements, and pure effort sources - one due to the motor (τ_{act}) and the other due to torques applied by the environment (τ_{env}). The simple linear model representation is :

$$\begin{bmatrix} \dot{X}_1 \\ \ddot{X}_1 \\ \dot{X}_2 \\ \ddot{X}_2 \end{bmatrix} = \begin{bmatrix} 0 & 1 & 0 & 0 \\ -\frac{K_T}{I_1} & -\frac{B_1}{I_1} & \frac{K_T}{I_1} & 0 \\ 0 & 0 & 0 & 1 \\ -\frac{K_T}{I_2} & 0 & -\frac{K_T}{I_2} & -\frac{B_2}{I_2} \end{bmatrix} \begin{bmatrix} X_1 \\ \dot{X}_1 \\ X_2 \\ \dot{X}_2 \end{bmatrix} + \begin{bmatrix} 0 & 0 \\ \frac{1}{I_1} & 0 \\ 0 & 0 \\ 0 & -\frac{1}{I_2} \end{bmatrix} \begin{bmatrix} \tau_{act} \\ \tau_{env} \end{bmatrix} \quad (\text{Eqn. 3.3.1})$$

In the case of position control, we can distinguish between using the feedback from the input stage or from the output stage, for control purposes (x_1 vs. x_2). For the moment we will assume that we only deal with proportional-plus-derivative controllers, which in the co-located and non-co-located position-control case yield the control laws:

$$\text{Co - Located} : \tau_{act} = K_e(x_D - x_1) - B_e \dot{x}_1 \quad (\text{Eqn. 3.3.2})$$

$$\text{Non - CoLocated} : \tau_{act} = K_e(x_D - x_2) - B_e \dot{x}_2 \quad (\text{Eqn. 3.3.3})$$

The closed-loop system dynamics are then governed by the roots of the characteristic equations, which can be determined by obtaining the determinant of the closed-loop system matrix ($|sI - A_{cl}|$). The general structure is of the form

$$X_2/X_d|_{c.e.} = As^4 + Bs^3 + Cs^2 + Ds + E, \quad (\text{Eqn. 3.3.4})$$

where

COLOCATED CASE

$$A = I_1 I_2$$

$$B = I_1 B_e + (B_1 + B_e) I_2$$

$$C = B_2 (B_1 + B_e) + I_1 K_T + I_2 (K_e + K_T)$$

$$D = K_T (B_1 + B_2) + K_T B_e + B_2 K_e$$

$$E = K_e K_T$$

NONCLOCATED CASE

$$A = I_1 I_2$$

$$B = I_2 B_1 + B_2 I_1$$

$$C = K_T (I_1 + I_2) + B_1 B_2$$

$$D = K_T (B_1 + B_2 + B_e)$$

$$E = K_e K_T$$

(Eqn. 3.3.5)

In the case of force control, we will assume that we are connected to a stationary environment, via a force sensor which will give us information about the interface force we are trying to control. We do not have to choose impact scenarios or simulations, to show that this scenario can equally well be proven to have important stability limitations (Fasse & Hogan [1989]).

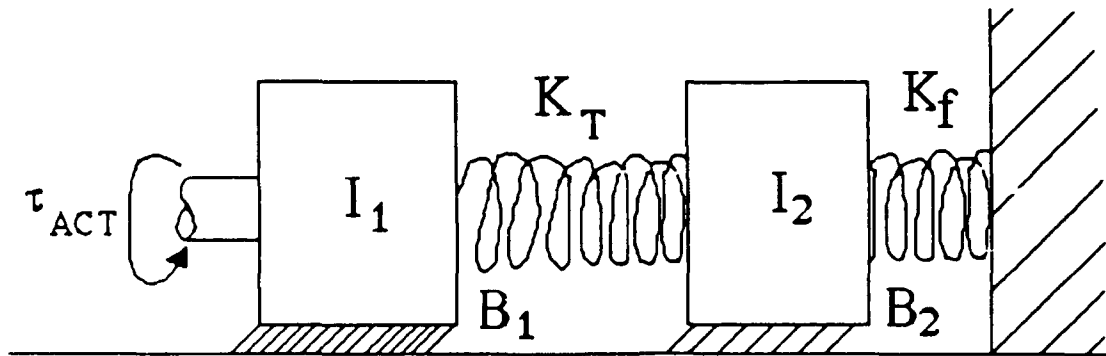


Figure 3.3.2 : 2 DOF force-control actuator/transmission/load/environment model representation.

Figure 3.3.2 above illustrates the actual physical system used for control and analysis purposes. It is now clear that the implementation of force-control falls in the regime of non-colocated sensing and actuation, since in our analysis we are dealing with the fidelity and stability of closing torque-loops around transmissions with significant dynamics. The formulation for the non-colocated control law for force-control of such a system can be chosen to be

$$\text{Non - CoLocated : } \tau_{act} = K_e (\tau_D - \tau_{env}) - B_e \dot{\tau}_{env} = K_e (\tau_D - K_f x_2) - B_e K_f \dot{x}_2, \quad (\text{Eqn. 3.3.6})$$

resulting in a closed-loop dynamic system with a characteristic equation of the form

$$\tau_{env}/\tau_{d|c.e.} = As^4 + Bs^3 + Cs^2 + Ds + E, \quad (\text{Eqn. 3.3.7})$$

where

NONCLOCATED CASE :

$$A = I_1 I_2$$

$$B = B_1 I_2 + B_2 I_1$$

$$C = (K_T + K_f) I_1 + K_T I_2 + B_1 B_2$$

$$D = B_1 (K_T + K_f) + K_T B_2 + B_e K_f K_T$$

$$E = K_T K_f (1 + K_e)$$

(Eqn. 3.3.8(a))

Note the difference in how the controller parameters show up in different coefficients for the parameters of the non-collocated characteristic equation. This will be seen to be of importance later on in the analysis.

A stability (and thus also a performance) analysis can now be performed on these coefficients, following the Routh-Hurwitz stability criteria. As explained by Ogata [(1977)], it is necessary but not sufficient that the signs of all coefficients in the characteristic equation be identical. By inspection, one can see that if we limit ourselves to positive real values for all parameters, this will always be the case. The necessary and sufficient requirement for stability can be formulated by building up the upper-left diagonal Routh-Hurwitz matrix based on the coefficients and some simple mathematical rules (Ogata [1977]). The stability analysis can then be performed by requiring a strict uniformity in the signs of the following computed coefficients of the column vector,

$$[A \ B \ C-AD/B \ D-BBE/(BC-AD) \ E]^T \quad (\text{Eqn. 3.3.8(b)})$$

which represent the four elements in the first column of the Routh-Hurwitz matrix. Sign changes in any of the elements of this column matrix indicate the presence of one (or more) unstable eigenvalues in the characteristic equation and thus result in an unstable system behavior. This procedure can be automated via computer and result in a simple way of performing qualitative stability studies in the multi-parameter space of this model.

Analyzing performance regions is a bit more involved, but can also be automated. At every step in the multi-parameter scheme, one can compute the system's eigenvalues and then compare to see if the dominant poles have characteristics (expressed here in terms of

bandwidth and damping ratio) that are within the desired limits. Performing such iterative schemes, can then also result in establishing a performance region based on any time-domain performance specification.

The parameter-space analysis uses physical values which were measured/computed for the harmonic-drive reduction (inertia at the input, damping losses and transmission stiffness). We will now look at the effect on stability and performance of varying each parameter within physically reasonable values. The corresponding physical scenarios will accompany the qualitative analyses in order to keep the connection to the real world.

Since we will be dealing with PD control algorithms at the beginning, we will assume a range of controller gains that are physically achievable with the motor-setup we used for the experiments. Physically achievable actuator stiffnesses (barring saturation characteristics of course) which can be (theoretically) achieved by the motor-hardware we are using, are

$$\begin{aligned} 7 \times 10^{-3} < K_e < 7 \times 10^3 & \quad [\text{N-m/rad}] \\ \text{and} \\ 7 \times 10^{-3} < B_e < 1.2 \times 10^2 & \quad [\text{N-m-sec/rad}]. \end{aligned} \quad (\text{Eqn. 3.3.9})$$

We will present stability and performance regions by showing a trace of combined K_e & B_e values, for which the system is just barely stable. Traces will be given in the K_e - B_e plane as lines of constant but varying physical parameters being analyzed.

(a) Inertia Distribution

There are a total of two inertias distributed in this model. I_1 represents the inertia of the motor-rotor, shaft and coupling as well as the transmission input-inertia. I_2 represents all the load inertias and the transmission output-inertia, which are reflected to the input via a division by the square of the transmission ratio N . This is an extremely good approximation in the case of the harmonic drive, where 99% of the transmission inertia is represented by the elliptical wave generator. Notice also that output damping coefficients are scaled by the square of the transmission ratio. The rotor-, shaft-, and transmission inertia were also measured and included in the analysis. By varying the values for I_1 by a factor of 50, and the values for I_2 by a factor of 50, we can not only cover most of the realistic designs physically feasible, but also most of the robot scenarios where the effective inertia seen by a robot joint may vary depending on the link configurations.

The two plots in Figure 3.3.3 depict the stability regime for a harmonic drive transmission driving a load in a non-located position-control mode:

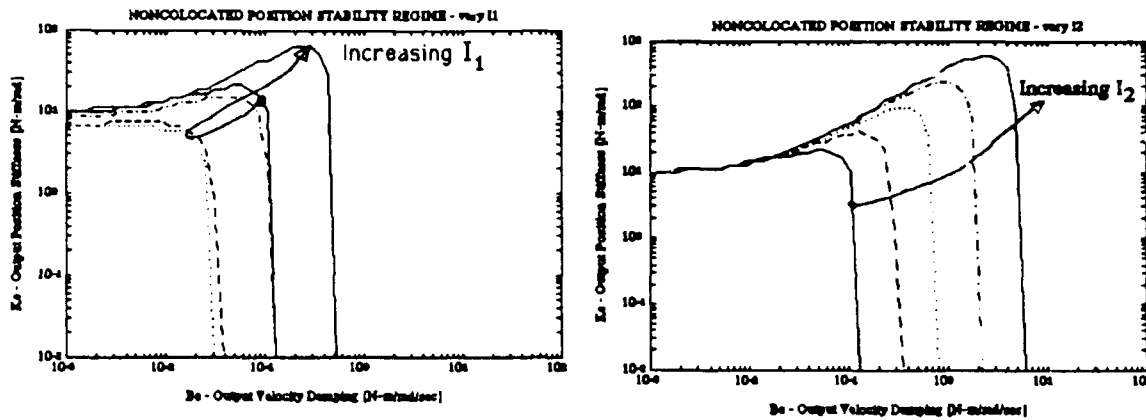


Figure 3.3.3 : Variation in (I_1) Input- (left plot) and (I_2) Output-Inertia (right plot) and the effects on noncollocated PD position control stability.

The plot on the left shows how the variation of the rotor/motor-shaft inertia (and other lumped transmission-input inertia) affects the stability regime for a non-located PD position controller. A multi-fold increase in input inertia has a marked effect on the system stability regimes. As indicated by the trend-arrow, the system's stability range is reduced to a point after which it recovers and actually result in an increasing stability regime. The lowest stability boundary seemed to be present for a system in which the input and reflected output inertias were identical. This would be a rather surprising result, since it indicates that a system which was designed based on impedance-matching criteria, where $I_1 = I_2/N^2$, has the lowest stability regime than any other possible ratio of I_1/I_2 . This phenomenon is independent of transmission stiffness, and adds a new twist to the basic principle behind impedance matching, which states that maximum power transfer is the most desirable transmission quality, but can also result in the worst stability if transmission dynamics are neglected in a noncollocated position-control mode. Even though only stability regimes are shown, the regime for a desired damping ratio and natural frequency for the dominant closed-loop pole-pair are similar in shape but enclose a smaller area than the stability boundaries shown on the above plots. The bandwidth of the system with ratios of I_1/I_2 smaller than unity, is reduced with increasing values of output inertia I_2 , and is also a strong function of electronic motor-damping (based on output-velocity feedback).

The increase in output inertia (right plot) by any factor results in an interesting tendency for the stability regime. The stability will monotonically increase with increasing output inertia, with increased stability regions for certain electronic output velocity damping

values. Thus a system which has its controller coefficients based on the lowest expected inertial loads, will have increased stability guarantees for increased load inertias. This is an important guarantee for manipulators where inertial loads are configuration-dependent or a function of the load handled at the endeffector. The physical equivalence could be sought by imagining a robot endpoint at a point in the workspace (NOT at a singularity obviously), where the effective endpoint inertia is a minimum, and then traversing a trajectory that leads the endpoint to a location at the boundary of the workspace, where the effective endpoint inertia may be drastically increased.

The behavior is quite similar for a force-controlled task scenario. In Figure 3.3.4, we have shown the stability regimes for a force-controlled system, using a PD force-error gain structure, for a non-colocated force-control scheme.

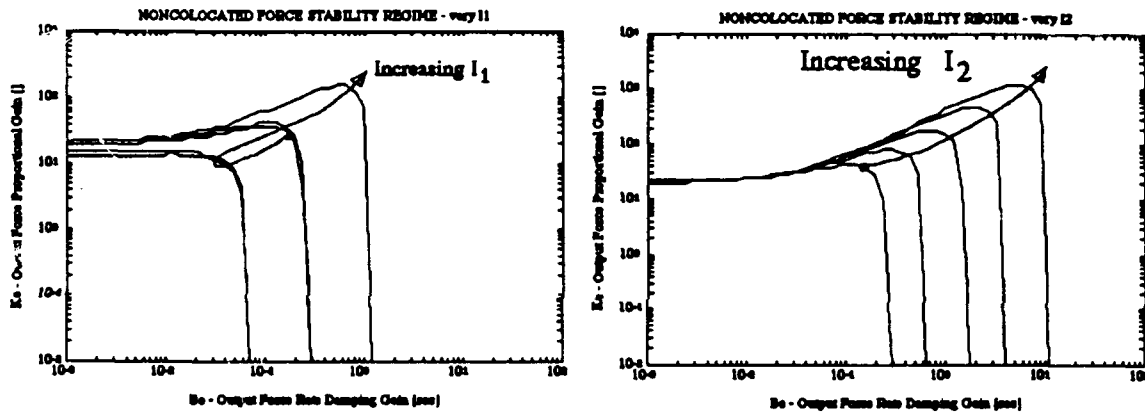


Figure 3.3.4 : Variation in (I_1) Input- (left plot) and (I_2) Output-Inertia (right plot) and the effects on noncolocated PD force control stability.

Similar to the position-control task, increasing input inertia affects the stability and performance regime in a way that depends on the ratio of input-to-output inertia. The increase in stability with increasing output inertia is also an evident trend. The increase in system stability is also accompanied with a reduction in effective dominant closed-loop bandwidth. In order to get any increase in force-control stability, through an increase in input inertia I_1 , it would seem that we have to increase the inertia ratio

$$i = I_1/I_2 \quad (\text{Eqn. 3.3.10})$$

to the point where the new input inertia (I_1^s) should be at least $(1/i)^2$ -times bigger, resulting in a stabilizing inertia effect for I_1^s :

$$I_1^s = (1/i)^2 I_1 \quad (\text{Eqn. 3.3.11})$$

The proof for the above statements would have to be sought numerically, since we would have to formulate the requirement, that

$$D - (B^2 E) / (BC - AD) > 0 \quad (\text{Eqn. 3.3.11a})$$

which makes a closed-form solution rather messy. It is obvious from the above formulation of Eqn. 3.3.11a, that all the system parameters affect the stability margin, but the tendencies present by varying the inertia ratio can be shown numerically as well as with the Routh-Hurwitz stability margins earlier. Any further analysis will not be provided by this thesis, but the above stated tendencies can be numerically substantiated for the physical systems that we are analyzing here. Further research into this area is certainly warranted.

Increasing effective endpoint inertia in order to increase the regime of stable force-control gains may seem like a viable solution, but it will also increase the forces present during environment contact, where impact forces can be significant. It is thus clear that since we always try to design lightweight robots for high-performance control, a trade-off has to be made in terms of stability and effective inertia. Designing a system with large output inertia may result in guaranteeing larger stability regimes for systems already in hard contact with the environment, while acquiring contact with high effective output inertia will result in larger impact forces and reduced effective endpoint bandwidth.

Thus the reduction of input inertia has a positive effect on system stability for non-colocated position- and force-controlled devices, when the effective inertia ratio I_1/I_2 is much different from unity. Using motors with reduced rotor inertia (which is usually the largest contributor to input inertia), increases stability margins for force-controlled systems, with sensitivity to this design parameter being as strong as the sensitivity to changes in output inertia. Increasing output inertia on non-colocated position- and force-controlled systems drastically increases regimes of guaranteed stability at the expense of reduced system bandwidth, and increased impact forces and response-times in systems performing tasks such as hard contact acquisition of surfaces in the environment.

(b) Damping Distribution

The use of viscous damper models are an attempt at modeling the dissipative (assumed to be linear for modeling purposes) behaviors in an actuator/transmission system.

If we control a system in position- or force-control, one of the interesting questions is what kinds of shaft-/flange-seals to use, and where to place them, or where to avoid/introduce excessive frictional losses. The relative stability and performance benefits for different scenarios can be studied by considering the non-colocated PD force-control data shown in Figure 3.3.5. We have chosen the range of damping losses to vary by a factor of 50. The actual physical values measured for all the transmissions, are midway between these two extremes. This variation in viscous losses represents the difference between simple mineral-oil film-lubrication and grease lubrication for shafts/bearings, which was measured during the experiments that were performed.

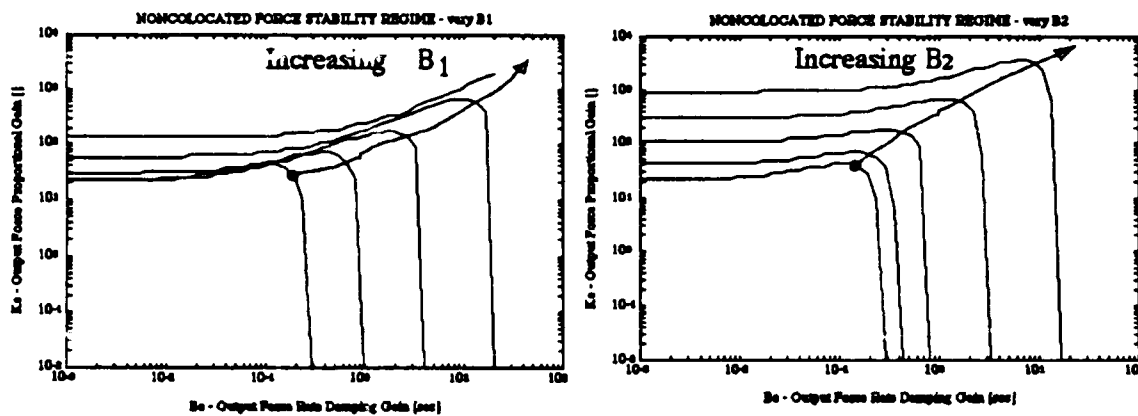


Figure 3.3.5 : Stability regimes for PD force-controlled system for (a) varying input damping B_1 and (b) varying output damping B_2 .

Figure 3.3.5(a) shows the sensitivity of the stability regime (and similarly also the performance regime) to changes in viscous input damping coefficient. A similar behavior is observed in Figure 3.3.5(b), where the sensitivity to changes in viscous output damping is shown.

Comparing the two plots, one will detect that the stability margins are drastically increased in the presence of increased physical damping. Equal increases in output and input damping illustrate the difference between the effects these two design parameters have on system stability. Increasing the viscous input damping levels is mostly beneficial only in a small range of electronic force damping. The difference between the two separate stability regions though is not very big (about 10%). A simple numerical comparison of viscous damping elements is not a correct indication of relative stability, since the effective viscous output damping has been reflected through the transmission ratio. Thus the actual range of realistic output viscous damping coefficients is really N^2 times larger. Placing the identical viscous damping element at the input vs. the output, thus has a drastically different

effect. The correct way to compare the effect of viscous damping losses on system stability and performance, is to observe the difference between an increase in B_1 by a certain amount and then compare it to a $1/N^2$ increase in B_2 . Such a physically motivated comparison then illustrates the stability benefits of adding viscous damping to the input of the transmission, since the relative increase in stability is much larger than attempting to damp the output behavior.

In order to achieve similar increases in stability and performance, the placement of a large and heavy viscous damper at the output-end of the transmission is not only unrealistic but can be achieved much easier by damping the input to the transmission. The need for differently sized dampers is thus obvious, but not necessarily easily available in the commercial sector. The reason for stability is simply due to the fact that the damping forces are independent of the non-colocated feedback signals, and thus provide 'phase-independent' viscous damping torques. Furthermore, the vibrational mode that goes unstable is due to the inertia at the input (I_1), termed the proximal vibratory mode. A similar behavior could also be achieved if the control law were expanded to include a dissipative term,

$$\text{Non - CoLocated : } \tau_{act} = K_e(\tau_D - K_f x_2) - B_e K_f \dot{x}_2 - B_{e1} \dot{x}_1 \quad (\text{Eqn. 3.3.12})$$

which reflects the equivalent electronic damping at the input shaft. Such a practice is a quite common fix to stability problems with non-colocated force-control systems. The advantage is that stability is extended, but at the price of reducing the damping ratio of the closed-loop system at large force-rate damping gains.

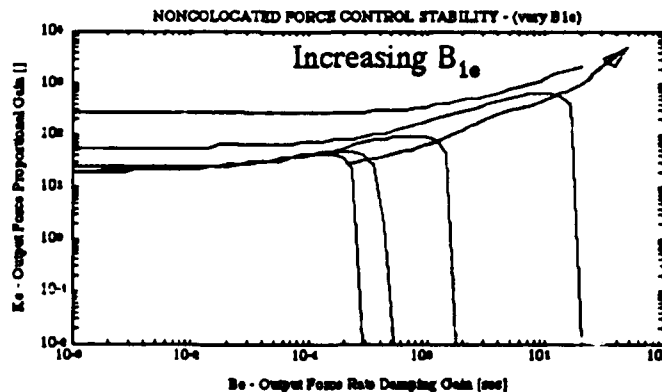


Figure 3.3.6 : Stability regimes for PD force-controlled system with added input-damping term $B_{1e}d(x_1)dt$.

Figure 3.3.6 illustrates the increase in stability, while Figure 3.3.7 demonstrates that the system does indeed experience a somewhat increased bandwidth with added input damping, but again only for large values of electronic force-rate damping and then only with reduced damping ratios:

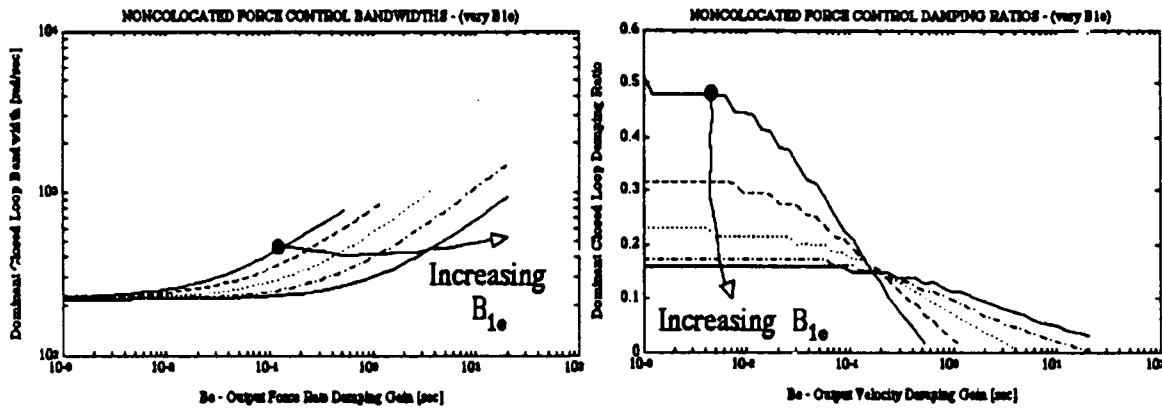


Figure 3.3.7 : Closed-loop bandwidth and damping ratio for PD force-controlled system with added input-damping term $-B_{1e}d(x_1)/dt$.

On the other hand though, increased bandwidths are only achievable at a reduced damping ratio. The effective damping can not be affected by either increasing B_{1e} , nor any force-rate damping B_e . It should be noted here, that adding output velocity damping has very little effect as well, since it could be added to the original control-term in B_e , and thus still result in a limited stability regime (which was outlined earlier). It is important to note here, that for little or no force-rate damping, the system bandwidths at the stability margin vary little if at all. Beyond certain electronic gain values, damping ratios above a certain value are no longer possible, indicating that the closed-loop roots are moving to the $j\omega$ -axis and are thus destabilizing the system.

It was mentioned by Fasse & Hogan [(1988)], that damping in the force sensor was more important to stability than sensor stiffness. From the above analysis, one can conclude that such a remark is quite true, but that it also has to be seen in the light of how much easier it is to achieve overall system stability with added input damping. The penalty one pays is in the actual endpoint force-control performance (excessive overshoots/transients and oscillations and reduced bandwidths if certain damping ratios are desired).

(c) Stiffness Distribution

The importance of the transmission- and sensor-stiffness in this stability and performance analysis is obviously at the center of this study. The range of transmission stiffnesses that was used in the analysis to follow, reflects the range of stiffnesses present in the harmonic drive. The lowest value was chosen to be that of its soft-zone (2500 N-m/rad), while the upper value is 20 times larger and represents the stiffest transmission tested in the entire analysis (geared cycloidal transmission). The force sensor stiffness was about 15 times larger than the stiffest transmission we tested ($\sim 7.75 \times 10^5$ N-m/rad).

The two plots of Figure 3.3.8 illustrate the effects of increasing the transmission stiffness for a non-colocated position- and force-controlled actuator/transmission/load system:

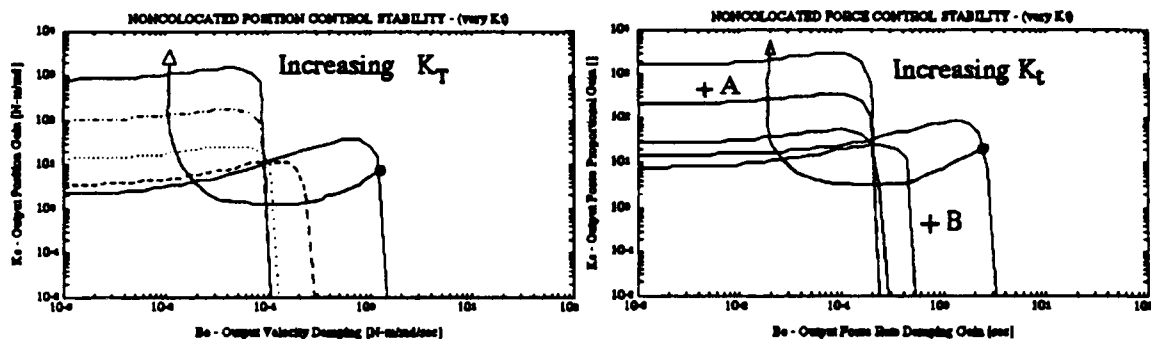


Figure 3.3.8 : PD Position-Control Stability (a), and (b) PD force-control stability trends, pointing out that stiffening springs can result in instability for a PD controller-structure.

The two graphs look fairly similar, and point out two important distinctions which have important implications on system stability. In both control scenarios, the increase in transmission stiffness is clearly accompanied by a conditional increase of the stability regime, dependent on the added electronic damping. In the case of position control, the feedback signals are output position and velocity. In the case of non-colocated force-control, the stability constraints are also very interesting, with the proportional and derivative gains acting on output force-error and output force-rate feedback signals. The profiles of the stability regimes as a function of increasing transmission stiffness indicate that there are two clear stability constraints on controller gains, illustrated in Figure 3.3.8(a & b) above. If a set of PD gains is selected to lie at location A (see Figure 3.3.8(b) above),

the system will be unstable for transmissions with reduced stiffness, resulting in a stability regime upper-bounded by A. The stability is thus only jeopardized by controlling a transmission with softening-spring behavior. On the other hand, if a set of gains is selected to lie at location B (based on an argument of stability for reduced stiffness systems), an increase in transmission stiffness can cause the system to go unstable. The clear difference between the two scenarios is, that operating point A will result in unstable behavior for hard contact tasks with softening stiffness behaviors, while operating around B results in an unstable system during contact, when a stiffening-spring behavior is present (which is mostly the case). Force-rate damping thus experiences conditional stability regimes depending on the transmission stiffness - a tendency which may not make it a very appealing controller structure. Furthermore, the actual implementation of large force-rate damping gains presents a serious implementation challenge. In order to get a clean estimate of force-rate, we require low noise-levels and latency in the measurement. Any noise- or discretization levels are amplified at large gains, resulting in destabilizing tendencies, which force-rate-signal low-pass filtering only worsens, since it introduces phase-lag into the system. Our digital force-rate implementation suffered greatly from these problems, and we were thus only able to achieve fairly small values of electronic force-rate damping. We were never able to observe the conditional stability regime outlined above.

The operational regime which may result in catastrophic system instability should at all costs be avoided. This in turn limits the performance of the system, since only a limiting amount of electronic damping (acting on the rate of force change) can be added to the system to increase the bandwidth of the dominant closed-loop pole-pair. Since stiffening-spring behaviors are almost always present in the most common robotic transmissions, this becomes an absolutely critical point. The above analysis also shows, that catastrophic instability can be avoided by having a relative force sensor-to-transmission stiffness ratio (K_F/K_T) of at least 20. The effects of varying this ratio is shown in Figure 3.3.9,

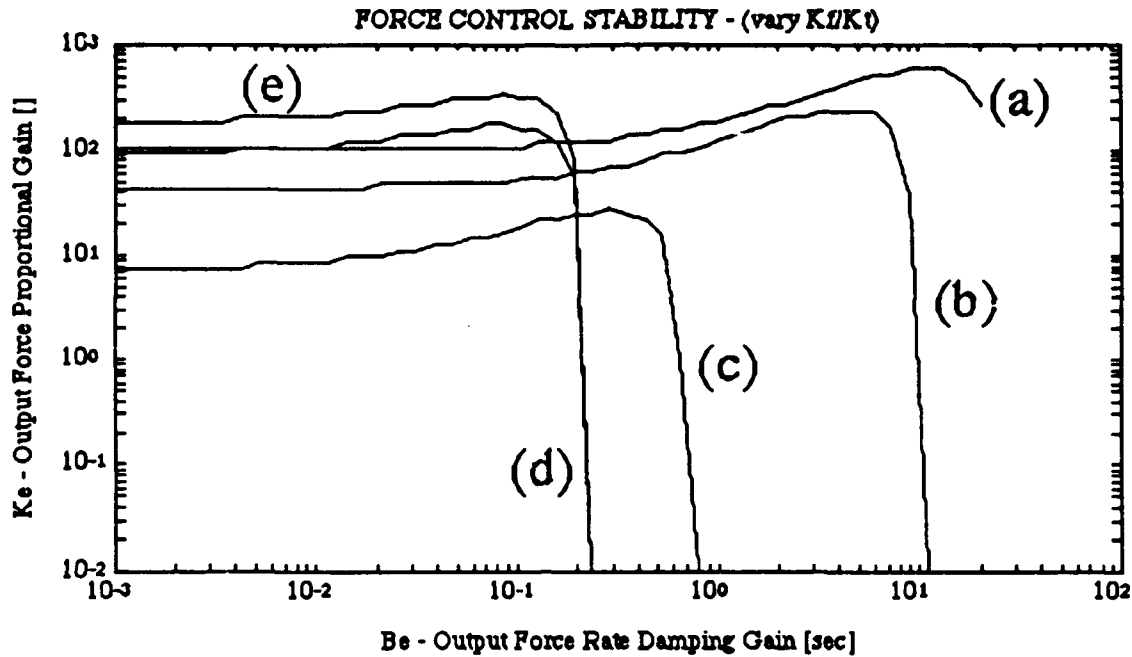


Figure 3.3.9 : System Stability for varying force-sensor/transmission-stiffness ratios : (a) $K_f/K_T=50$, (b) $K_f/K_T=20$, (c) $K_f/K_T=1$, (d) $K_f/K_T=1/50$, and (e) $K_f/K_T=1/100$.

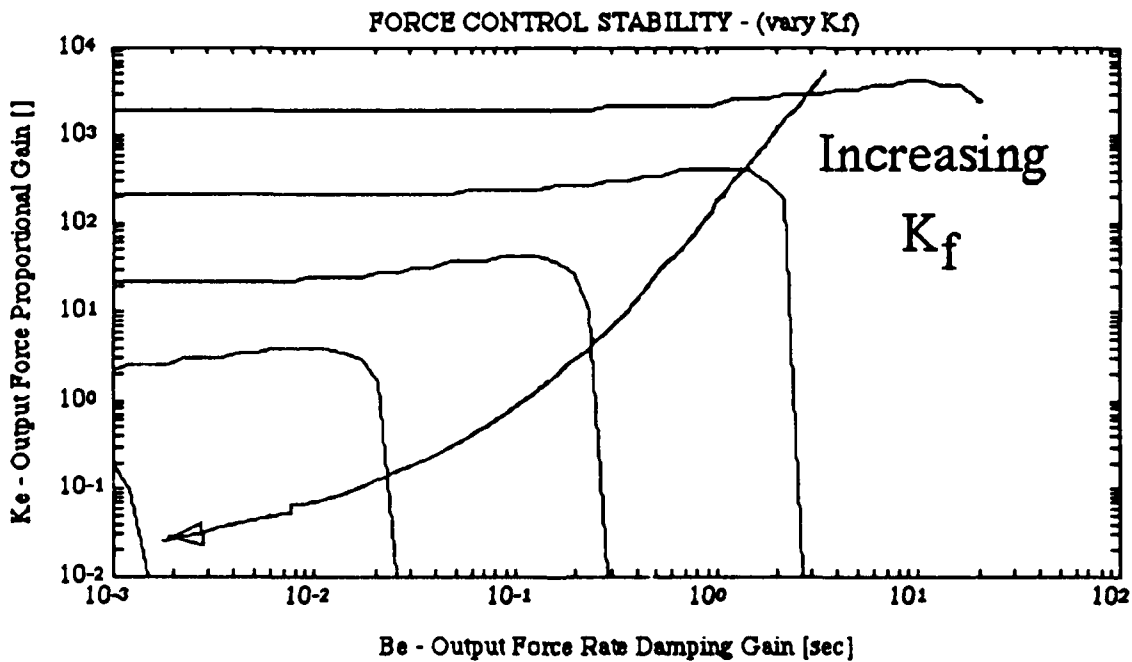


Figure 3.3.10 : Reduction in stability regime by increasing the force-sensor stiffness in the case of a PD force-controller.

where we have shown the stability regimes for various ratios of K_f/K_T for the PD force-controller. We have selected the ratio of K_f/K_T to lie at 50, 20, 1, 1/50, and 1/100, by

varying the transmission stiffness K_T . Increasing stiffness ratios also imply increased closed-loop bandwidths. The sensitivity of stability and performance regimes to parameter changes in force-sensor stiffness is also an important component of a systems' characteristics. Figure 3.3.10 illustrates how the increase in torque sensor stiffness reduces the range of stable controller gains in the case of PD force control. The values for the sensor stiffness were taken from the actual transmission stiffness value, and then spanned all the way to the stiffest sensors available commercially. The argument that has been given over and over again over the last few years in the robotic community, which stipulated and showed that sensor stiffness does reduce system stability, is also shown to be true in this instance. Besides the addition of system damping, the variation in force-sensor stiffness has proven to be highly sensitive in determining system stability and performance. In real physical terms, variation (decrease in this case) of the sensor stiffness brings with it the largest percent increase in system stability than any other design parameter considered in this transmission modeling procedure.

(d) Alternate Controller Structures and Dynamics

The previous analysis assumed a PD controller structure in either position- or force-error. There are obviously other controller structures which could result in better performance and stability margins. Typically, the modeling procedure (without including the model in the controller structure) is a step used to decide on proper controller (compensator) design. A good example for such a procedure was given for a PID admittance controller to achieve stable endpoint force control in view of substantial transmission dynamics, by Stepien et al [(1985)]. Stability was extended, yet not considerably.

Other controller structures which may be beneficial after viewing the previous analysis, as well as other commonly used linear controller structures will be dealt with in this section. Differences between them will illustrate the limitations of certain schemes, and some of the misconceptions certain physical/controller phenomena have attached to them.

P in Force & D in output/input damping

The most obvious approach, based on the parameter sensitivity analysis presented earlier, deals with the introduction of dissipative forces into the transmission dynamics.

The clear advantage of input viscous damping was shown to result in the largest relative increase in system stability. Such viscous damping could be reproduced not only mechanically, but also electronically. The change in control law, could represent two different structures, which, instead of electronic force damping, provide electronic velocity damping. This damping could be either based on output velocity, or input velocity. Both of these laws are listed below :

$$\begin{aligned}\text{OUTPUT DAMPING} &: \tau_m = K_e(\tau_d - \tau_{env}) - B_e d(x_2)/dt \\ \text{INPUT DAMPING} &: \tau_m = K_e(\tau_d - \tau_{env}) - B_e d(x_1)/dt\end{aligned}\quad (\text{Eqns. 3.3.13})$$

The use of output electronic damping is not going to change the system behavior at all, since the effect of this damping parameter only shows up in the next-to-last term of the Routh coefficients. Thus the only difference in the closed-loop stability analysis would be based on two different expressions for the s^1 -term:

$$\begin{aligned}\text{FORCE DAMPING} &: D = B_1(K_T + K_f) + B_2 K_T + B_e K_f K_T \\ \text{VELOCITY DAMPING} &: D = B_1(K_T + K_f) + B_2 K_T + B_e K_T\end{aligned}\quad (\text{Eqns. 3.3.14})$$

The only difference is between the damping terms, which in effect is nothing else than a scaling factor, since we can replace these two terms with an equivalency, stating that the relation between electronic output-velocity damping and force-rate damping is :

$$B_e^* = B_e K_f. \quad (\text{Eqns. 3.3.15})$$

The equivalency is applicable in all cases, except for the case of stability changes due to variations in force-sensor stiffness. Figure 3.3.11 should be compared to the same plot generated earlier for force damping.

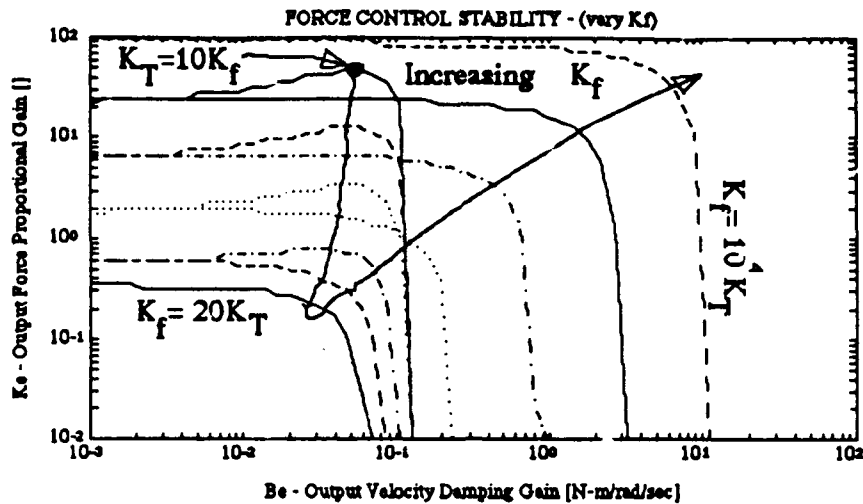


Figure 3.3.11 : Stability reduction with increasing force-sensor stiffness for force-error and output velocity D force-controller.

It is important to note that even through addition of noncolocated velocity damping, the system still exhibits a clearly bounded stability behavior for certain values of K_f/K_T . When the sensor stiffness is much larger (in this case by a factor of 20) than the transmission stiffness, the stability region increases again. Increased sensor stiffnesses also reduce the maximum amount of damping possible before the onset of unstable behavior. Performance in terms of dominant closed-loop bandwidth and damping ratios barely changes, and is shown in Figure 3.3.12 for the same range of sensor stiffness used in generating Figure 3.3.11.

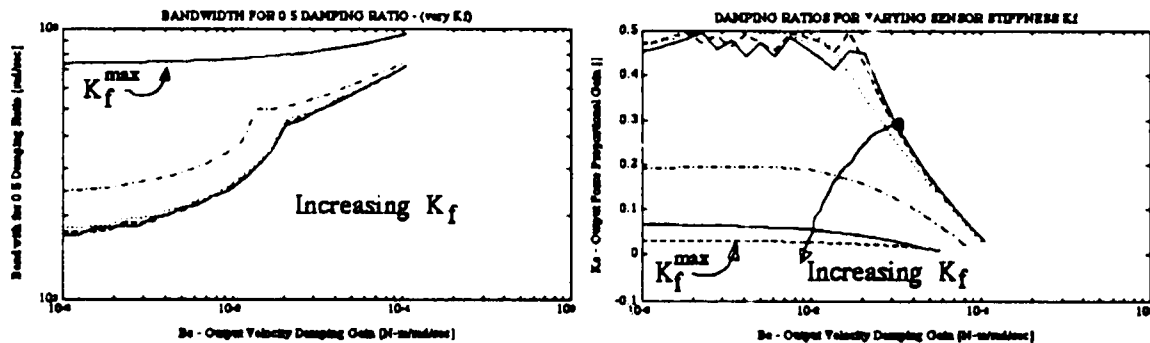


Figure 3.3.12 : Closed-Loop Bandwidth (a) and corresponding damping ratios (b) as a function of varying sensor stiffness K_f .

Figure 3.3.12 illustrates some of the more interesting points of closed-loop performance with varying sensor stiffness. Assume that we want to retain a closed-loop damping ratio that is no smaller than 0.5. Figure 3.3.12 (b) illustrates that this damping

ratio can be achieved for most of the increasing values of sensor stiffness. The associated closed-loop bandwidths do not vary significantly (see Figure 3.3.12 (a)). On the other hand, when the sensor stiffness is increased substantially, the lowest damping ratio that can be achieved is far below the $\zeta=0.5$ value specified earlier. The reason for that is that the closed-loop dominant conjugate complex pole pair (proximal vibratory poles) has transitioned from inside the damping cone (region A in Figure 3.3.13), to a region where the effective damping is already smaller than 0.5 (region B in Figure 3.3.13).

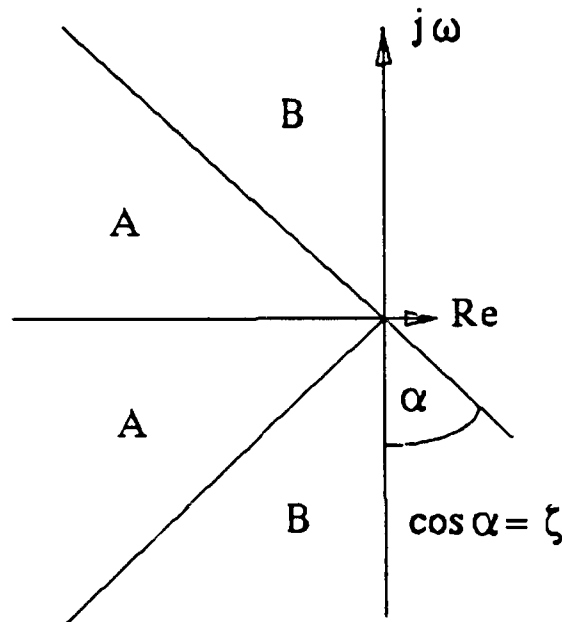


Figure 3.3.13 : Regions of damping larger than $\zeta=0.5$ (A) and regions of damping smaller than $\zeta=0.5$ (B).

No amount of electronic output velocity damping can cause the root-locus to achieve larger damping ratios if this PD controller structure is used. Note further that for increased levels of electronic output velocity damping, the closed-loop bandwidth increases, but at the price of reduced damping ratios, to the point where we have zero damping and we are approaching unstable behavior.

The main difference between these two approaches (electronic damping using either force-rate or output-velocity measurements) has to also be analyzed from a more physical standpoint. Measurements of force-rate are usually extremely noisy (unless filtered which introduces phase-lag), and have to be generated by some sort of digital filtering process. The controls engineer will realize that phase lag and bandwidth issues in such a filtering procedure have to be traded off with signal fidelity. It is generally accepted, that such a procedure is not without its faults, and thus requires a fair amount of design effort for

meaningful overall performance improvements. Relying on sensor damping is not very meaningful, since most sensors have very little (structural) damping. Adding passive sensor damping is helpful, but masks the true endpoint force measurements. Using velocity damping instead, is inherently a lower-frequency approach, which can not be harnessed in the case shown above. The signal to noise ratio for even a good optical encoder (at the output), is important in this analysis, since we are dealing with low-amplitude motions of the output, due to rigid coupling to a stiff environment. Thus in order to generate any meaningful damping forces, a large velocity gain may itself introduce broad-frequency energy into the system - especially if we use differentiated position measurements (even with a high-resolution optical encoder) without using a tachometer (which may itself not have the necessary resolution). The above methods are in general very hard to implement successfully in practice.

Another approach would be to add electronic damping at the input, thus implementing the control-law :

$$\text{INPUT DAMPING} \quad : \tau_m = K_e(\tau_d - \tau_{env}) - B_e d/dt(x_1). \quad (\text{Eqn. 3.3.16})$$

The resulting coefficients of the closed-loop characteristic equation, reflect the presence of this damping term. Using the same convention as before, we get :

$$\tau_{env}/\tau_d|_{c.e.} = As^4 + Bs^3 + Cs^2 + Ds + E \quad (\text{Eqn. 3.3.17})$$

where

NONCLOCATED CASE

$$A = I_1 I_2.$$

$$B = B_1 I_2 + B_2 I_1 + B_e I_2.$$

$$C = K_T(I_1 + I_2) + K_f I_1 + B_2(B_1 + B_e).$$

$$D = (K_T + K_f)(B_1 + B_e) + K_T B_2.$$

$$E = K_T K_f (1 + K_e).$$

(Eqn. 3.3.18)

As seen earlier in the colocated measurement and actuation examples, the distribution of any of the controller parameters beyond the last two coefficients (s^0 - and s^1 -terms) implies increased stability boundaries. That this is indeed the case can be shown by comparing the stability boundaries for the output- vs. the input-damping case for a fixed set

of actuator/transmission/load parameters (as given by the harmonic drive system) in Figure 3.3.14:

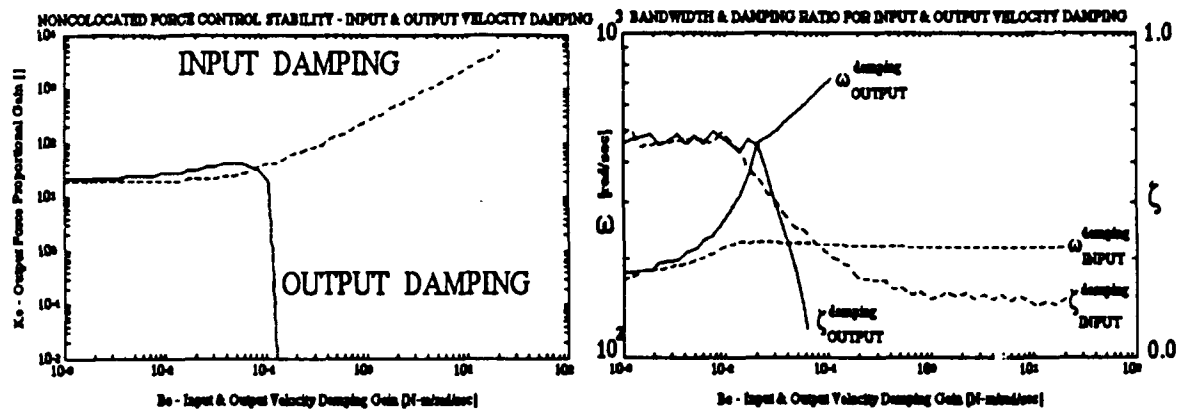


Figure 3.3.14 : Stability Regimes (plot a) and associated bandwidths and damping ratios (plot b) for a desired $\zeta=0.5$ damping ratio response for noncollocated and colocated velocity damping.

The input velocity damping case also illustrates that bandwidths will not be as high as in the output velocity damping case, but the damping ratios can at least be guaranteed to be higher over a much larger region, including an unconditional stability guarantee. Thus stability margins are much larger in the case of input velocity damping, but larger bandwidths may be possible with output velocity damping, at an increased risk of instability due to a reduced stability margin. The extended stability region for input-damping using analogous design-parameter sets, clearly illustrates this claim. This approach, though it may be lower-frequency than endpoint force-rate damping, and involve larger signal-to-noise ratios, still suffers under the laws of physical realities. The sensor (tachometer) supplied may not have the required resolution to give fine torque levels/increments. Compounding the problem is the presence of certain electronic breakaway torques required to start the rotor, thus creating a deadband which affects stability by not delivering any damping at low velocities (which is the actual operational mode of the two-mass model presented at the beginning). In essence, using electronic damping may be much more beneficial in large displacement tasks, but it can not beat the advantages of a passive damping approach, even if it means using a damper with fixed coefficients. Furthermore, damping a signal that has frequency content of the order of the unmodelled transmission dynamics, using an actuator whose frequency response is (or has to be) much lower than these levels, holds little promise of real success. The ideal situation would be to have an adjustable passive damper, which could be sized according to the

application requirements. The design of such a physical entity would be a worthwhile, yet challenging endeavor.

PI in Force & D in output/input damping

One of the more commonly applied control algorithms in force-control is that of an added integral term to reduce steady-state force errors. In this section we will compare the stability properties for three different controllers:

- (i) Proportional Force Error Control
 - with Derivative Force Error Control
 - with Integral Force Error Control
- (ii) Proportional Force Error Control
 - with Derivative Output Velocity Damping Control
 - with Integral Force Error Control
- (iii) Proportional Force Error Control
 - with Derivative Input Velocity Damping Control
 - with Integral Force Error Control

The first two controllers have previously been shown to result in closed-loop systems that are almost identical except for a simple scaling effect in the damping term. In other words, the stability properties are identical, but the realistic success of either of those methods depends on sensor quality, resolution, actuator bandwidth, etc. The stability regimes shown in Figure 3.3.15,

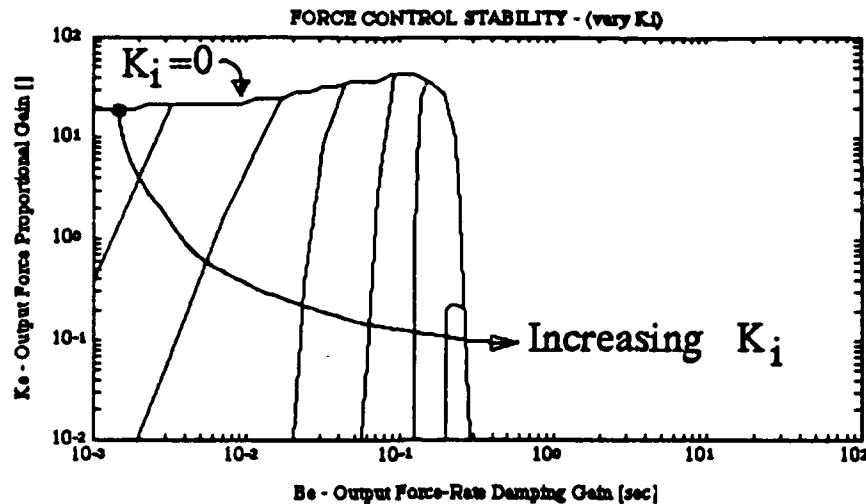


Figure 3.3.15 : Stability decrease for increasing values of integral force-error gain K_i in a pure PID force-controller, accompanied with marginally increased bandwidths but much reduced damping ratios.

show that for a given (and fixed) set of parameters (Harmonic Drive), the increase in Integral Force Error-Gain reduces the stability regime in a very interesting way. The stability of a system for increased values of integral gain, can only be achieved by reducing the proportional gain and increasing the derivative gain. This requirement is also supported by physical intuition, since increased integral gains result in oscillatory systems of larger frequency and lower damping ratios, whose oscillations need to be reduced through larger damping and/or reduced proportional gains.

If we were to replace the force-rate damping term with output velocity damping, the stability picture would not be different. The reason here is that we have assumed the interface forces to be dependent on the output motion and velocity. Thus adding output velocity damping is no more than a scaling of the force-rate damping approach used earlier. Performance in terms of closed-loop bandwidth is also unaffected by this change and differences in performance are thus extremely small and negligible.

Replacing force-damping with input-velocity damping, changes stability properties quite remarkably, as shown in Figure 3.3.16:

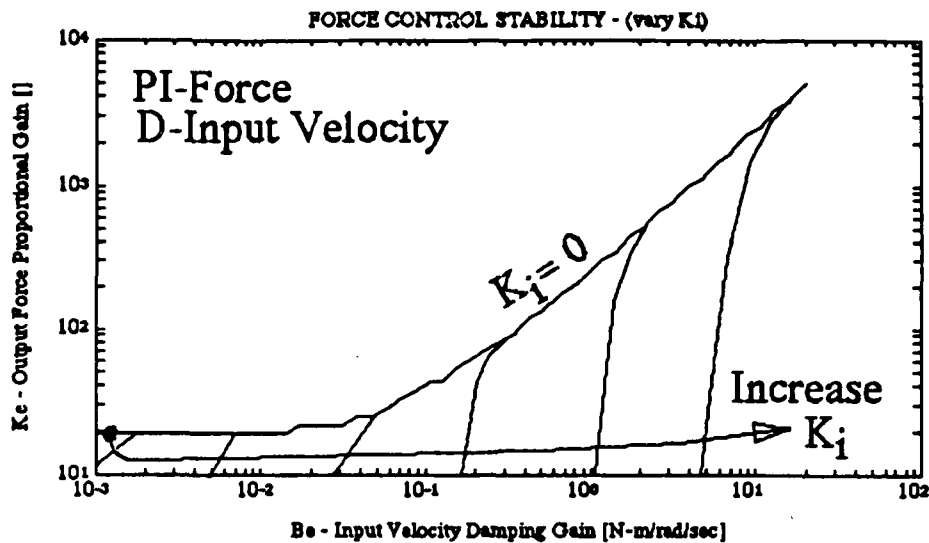


Figure 3.3.16 : Decreased Stability for PI force- and D input-velocity controller for increasing values of K_i .

For increased values of integral gain, the addition of (theoretically available infinite amount of) electronic damping can stabilize a system. It is also noteworthy to point out, that no longer is there a hard limit on electronic damping beyond which stability can no longer be guaranteed. On the contrary, one could stipulate, that the addition of electronic velocity damping would always result in a closed-loop stable system.

There are of course serious physical limitations to the implementation of such high-damping schemes (actuator- and sensor-accuracy, -resolution, and dynamic range). One should never confuse the benefits of passive viscous damping, with those of an electronically emulated viscous damping behavior. The ideal case, and a winner in such a scenario, would be to have at one's disposal an electronically tunable passive viscous damping element (analogous to an eddy-current brake, which would reside at the input-shaft, since its efficiency decreases with reduced speeds).

Impedance Controller

The importance of studying the impedance control structure, lies in the fact that one can not necessarily get away from the stability problems associated with noncollocated feedback, since this controller structure uses an additional term which permits the user to set the level of apparent output inertia. This is accomplished by feeding back output torques, which are then scaled by a specific gain, and fed into the actuator effort

commanded to the motor. Barring any inherent dynamics which have to be compensated for, the actuator effort thus consists of a tunable position-error gain, as well as an electronic damping gain, and a scaled value of measured output torque.

The stability and performance characteristics of an impedance controller can also be studied using the above methods. Two ways that an impedance controller could be formulated are used in this analysis, but in no way represent the state of the art in impedance control. Colgate & Hogan [(1988)] have shown that there are different and better ways to design impedance controllers if rigid-body dynamics are not present. In essence the study of the theory behind the design of appropriate impedance controllers has only just begun, and the book is far from closed on this topic. The two impedance control schemes that we employ here are a more 'naive' approach to system control. The actuator control law could (1) base its actuator effort completely on output measurements such as position and velocity, or (2) simply use input measurements of position and velocity to generate a part of the actuator effort. Assuming for the moment that there are no inverse dynamics to contend with, the controller also weighs the measured interface force with an inertia-dependent gain. Thus the two simple controller laws can be summarized as :

$$\text{Non - CoLocated : } \tau_{act} = K_e(x_D - x_2) - B_e \dot{x}_2 + \left(1 - \frac{I_a}{I_d}\right) \tau_{env} = K_e(x_D - x_2) - B_e \dot{x}_2 + K_m \tau_{env}$$

and

$$\text{Co - Located : } \tau_{act} = K_e(x_D - x_1) - B_e \dot{x}_1 + \left(1 - \frac{I_a}{I_d}\right) \tau_{env} = K_e(x_D - x_1) - B_e \dot{x}_1 + K_m \tau_{env}$$

(Eqns. 3.3.19)

Notice that we have introduced a new gain factor $K_m = (1 + I_a/I_d)$, which represents a force gain whose sign and magnitude depends on whether we want to increase or reduce the desired output inertia (I_d) as compared to the actual inertia (I_a). The only difference from a purely position-controlled system, is that we have the added weighted output torque term. If we perform the math to obtain the basic stability relations, the coefficients of the characteristic equation can be shown to be :

COLOCATED CONTROL

$$s^4 : I_1 I_2.$$

$$s^3 : B_2 I_1 + (B_1 + B_e) I_2.$$

$$s^2 : K_T(I_1 + I_2) + K_f I_1 + B_2(B_1 + B_e).$$

$$s^1 : (B_1 + B_e)(K_T + K_f) + B_2(K_T + K_e).$$

$$s^0 : K_e(K_T + K_f) + K_T K_f(1 - K_m).$$

NONCOLOCATED CONTROL

$$s^4 : I_1 I_2.$$

$$s^3 : B_2 I_1 + B_1 I_2.$$

$$s^2 : K_T(I_1 + I_2) + K_f I_1 + K_e I_2 + B_1 B_2.$$

$$s^1 : K_T(B_1 + B_2 + B_e) + B_1 K_f.$$

$$s^0 : K_e K_T + K_T K_f(1 - K_m).$$

(Eqns. 3.3.20)

Notice, how compared to the simple position-control analysis performed earlier in this section, we have additional terms in the s^0 -coefficient, which will affect system stability. The effects on system stability can be easily studied, by analyzing how K_m has affected the regime of stable K_e - and B_e -gains. An important point to remember in this analysis, is that the gain K_m is dependent on the ratio of actual vs. desired output inertias. the simple relation between K_m , I_a (actual inertia) and I_d (desired output inertia), can be simply stated in the inequality below :

$$\begin{aligned} -\infty < K_m < 1 \\ \text{or} \\ I_d \rightarrow 0 < \frac{I_a}{I_d} < I_d \rightarrow \infty \end{aligned} \quad (\text{Eqns. 3.3.21})$$

If we thus begin to vary the value of K_m from some finite negative value, and asymptotically approach unity, the stability boundaries of the system can be theoretically predicted. In Figure 3.3.17, we have shown the stability regimes for colocated (using input position and velocity feedback) and noncolocated (using output position and velocity feedback) impedance control as a function of K_m . A very interesting stability trend can be observed, which is independent of the state feedback used in the position- and velocity-gains.

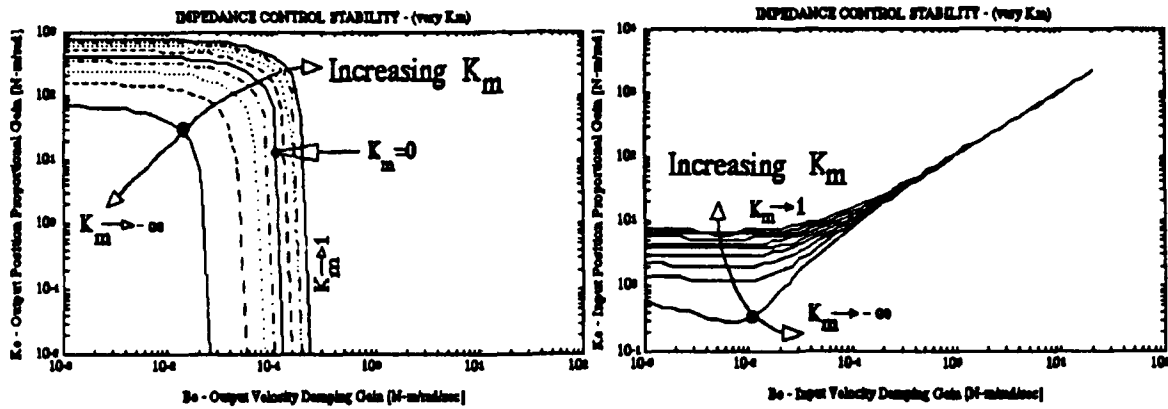


Figure 3.3.17 : (a) Noncolocated and (b) colocated impedance control stability regions as a function of force-feedback gain K_m .

For very large values of desired output inertia I_d (K_m approaches 1), the system reaches an asymptotic stability boundary, which is slightly larger than for the case where no force feedback is used to alter output inertia ($K_m = 0$). The sensitivity of the stability regime to increases in K_m is extremely small. On the other hand, when we attempt to achieve inertia levels below the physically present levels (K_m tends towards negative Infinity), the stability regime is progressively reduced, with an increasing sensitivity to changes in K_m . In other words, a stability increase for increased levels of desired output inertia ($I_a/I_d \ll 1$) is possible yet incrementally small, while incrementally larger reductions in stability are present for reduced levels of desired output inertia ($I_a/I_d \gg 1$). This is a phenomenon that was discovered to be present in the experimental setup used by Wlassich [(1986)] (out-of-plane bending mode of the force-sensor arrangement), where the system experienced contact instabilities when desired output inertia levels fell below a certain value. A simple sensitivity analysis (expression for $[(1/K_m) * \delta/\delta K_m]$) of the governing coefficient in the Routh array can furnish the necessary stability-margin for a given K_e and B_e value. Notice that the stability margin may be linear in K_m , which implies that it is inversely proportional to $1/I_d$.

If the performance of the system is analyzed in terms of a (fixed) desired dominant damping ratio, the bandwidth of the dominant closed-loop behavior is seen to vary insignificantly and can thus be termed invariant. None of the two feedback impedance controllers had any change in the achievable system bandwidth, as the value of K_m was varied. The effect on the dominant damping ratio was found to be most dramatic in the low-damping range for B_e , with increased values of ζ as K_m approached unity (or I_d tended to infinity). Thus asking for a reduced level of output inertia not only reduces stability regimes, but is also accompanied by a reduction in damped system response. This

trend can be observed in Figure 3.3.18, where we have shown the tendencies of the closed-loop dominant damping ratios as a function of the gain K_m , for the cases of the colocated (left picture), and the noncolocated (left picture) impedance controllers (this distinction only applies to the position- and velocity-feedback). Notice how only colocated impedance control (picture (a) on the left) is capable of avoiding a completely undamped oscillatory system response, while noncolocated impedance control unavoidably results in an increasingly oscillatory system. The asymptotic damping ratio is due to the distal vibratory mode, which is mainly governed by the values of the output inertia and the force/torque sensor stiffness (as well as the local damping levels).

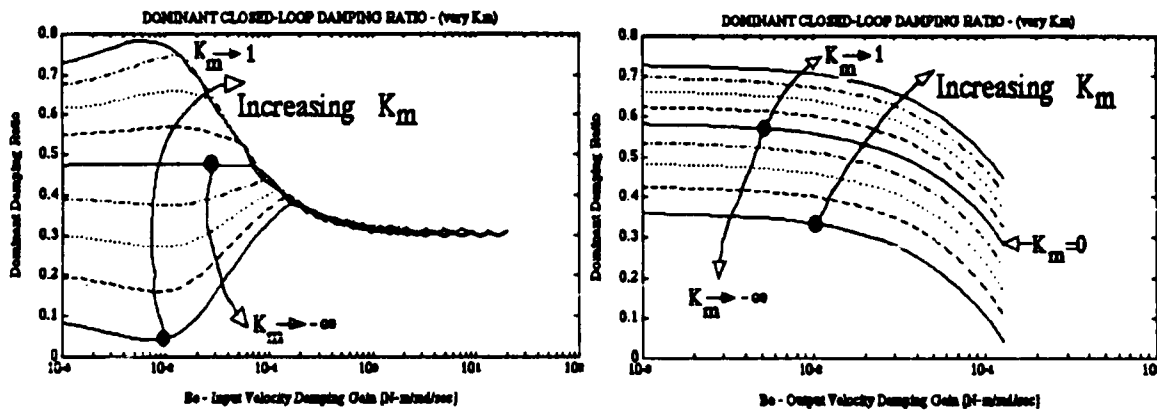


Figure 3.3.18 : Closed-Loop dominant damping Ratio ζ , for (a) colocated and (b) noncolocated impedance control as a function of torque-feedback gain K_m .

First Order Actuator/Sensor Dynamics

Eppinger & Seering [(1987)] explored the issue of low-pass filters in the feedforward path (thus filtering torque-inputs to the dynamic system), and concluded that first-order lag filters result in closed-loop systems with conditional and reduced stability. An & Hollerbach [(1987)] were strong proponents of low-pass filtering for stability purposes. They simply used open-loop torque-control, with low-pass filtered integral force-feedback errors to retain steady-state accuracy. They thus differ from the Eppinger & Seering's analysis in that they only partially filter the input actuator effort (by filtering the force-error signals only), and did not observe the predicted instability as proposed by Eppinger & Seering.

This analysis will show that their conclusion is only partially valid, revealing an increase in overall stability for very large first-order time-constants (sluggish response and also atrociously poor performance), and then a decrease in stability with increasing time-constant. The stability 'margin' can be reduced to a level below that of the infinitely-fast time-constant, but it reaches a minimum level, before recovering and increasing again and approximating the stability boundary for a system with infinitely fast first-order dynamics (or a system without any such dynamics at all). The relative extent of stability loss is clearly dependent on every physical system parameter. The important trend remains though, where the reduction in stability is only present for a certain range of time-constants with a certain value for the time-constant resulting in an absolute minimum stability margin, before the stability region increases again (and asymptotically approaches the infinitely fast first-order dynamic case). The difference in stability margin between infinitely fast first-order dynamics and those resulting in a minimum stability margin, are not of any appreciable size though, as seen in the figures to follow.

The introduction of first-order dynamics into the dynamics of a non-colocated force-control actuator/transmission/load system, assuming that τ_{act} is the desired motor torque, and τ_m the actually commanded motor torque, uses a control law of the form

$$\tau_{act} = K_e(\tau_D - \tau_{env}) - B_e \dot{\tau}_{env} = K_e(\tau_D - K_f x_2) - B_e K_f \dot{x}_2$$

and

$$\dot{\tau}_m = -a\tau_m + a\tau_{act},$$

(Eqns. 3.3.22)

if we assume that $\tau_{env} = K_f x_2$, resulting in

$$\tau_{env}/\tau_{dlc.e.} = As^5 + Bs^4 + Cs^3 + Ds^2 + Es + F,$$

where

NONCLOCATED CASE

$$A = I_1 I_2.$$

$$B = B_1 I_2 + B_2 I_1 + a I_1 I_2.$$

$$C = K_T(I_1 + I_2) + K_f I_1 + B_1 B_2 + a(B_1 I_2 + B_2 I_1).$$

$$D = B_1(K_T + K_f) + K_T B_2 + a(B_1 B_2 + K_T(I_1 + I_2) + K_f I_1).$$

$$E = K_T K_f(1 + a B_e) + a(K_T(B_1 + B_2) + B_1 K_f).$$

$$F = a K_T K_f(1 + K_e),$$

(Eqns.3.3.23)

clearly indicating the increase in system order as expected. A simple stability analysis, using the previously determined harmonic-drive parameters can be performed, by varying the time constant $1/a$ of the filter dynamics. Figure 3.3.19 below,

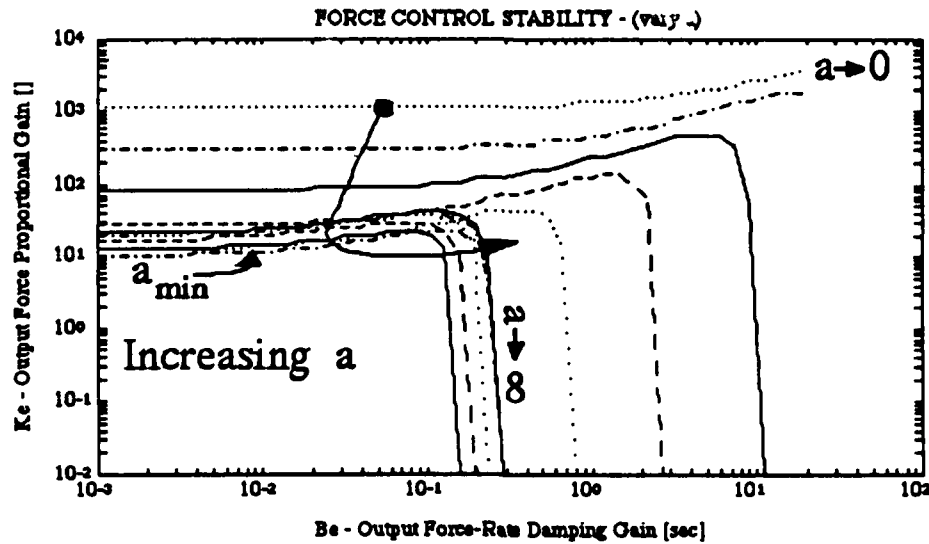


Figure 3.3.19 : Stability regions' conditional stability by varying time-constant $1/a$ of first-order actuator/sensor dynamics.

illustrates the previously indicated behavior of a conditional stability with a clear minimum for a certain level of low-pass filtering time-constant. This behavior can be shown to be present no matter what the chosen design parameters may be. This controller, its performance together with experimental data will be demonstrated in Chapter 5. The above trends will be shown to be present in real transmissions, and the relative stability margin increases and the associated performance, will be shown to be predictable to within small error margins (less than 20%).

(e) Nonlinearities - Size & Distribution

Any real transmission will have other nonlinearities, which can not be fully incorporated into any linear model, without a certain amount of approximations. This analysis, despite using frequency-domain tools to determine stability properties, will try to rely on a more time-domain based and physically motivated approach. This approach will become clear when we study different nonlinearities and try to understand them as a

discrete number of discontinuous dynamic systems, to which we can apply linear time-domain analysis tools.

Backlash

The presence of backlash can be best understood, by referring back to the original system diagram, where we attempted to model backlash as a load- and positionally dependent phenomenon, which in the simplest case can be thought of as different systems of rigid-body models. When the system is in a state where it is operating in (or transitioning through) the backlash zone, we are dealing with a reduced-order dynamic system with reduced inertia and damping. Thus a controller designed for the entire system dynamics, will result in a closed-loop dynamic system of higher bandwidth and reduced damping. Analysis in the continuous-time domain has shown this to be the case. On the other hand, one can show that such a system under discrete control, can also exhibit unstable behavior, which continuous-time analysis tools can not predict.

If we assume the simplest of rigid-body models using an inertia and damping term, controlled via a sampled PD position-control law and through a zero-order hold,

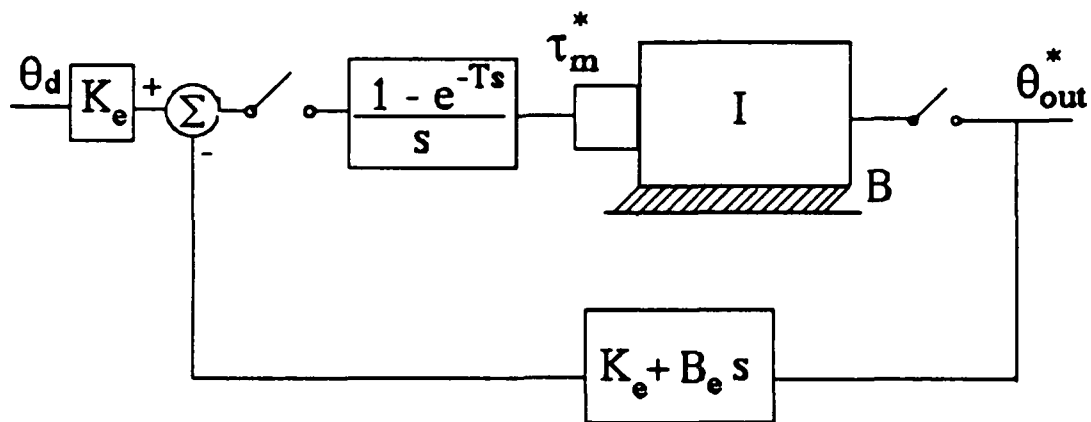


Figure 3.3.20 : Discrete Controller Diagram for reduced backlash dynamics, showing the PD position-controller, and the sampling gates with the zero-order sample-and-hold for the actuator signal.

we can show the controlled system in Figure 3.3.20, which is then used to generate the characteristic equation of the closed-loop system in the z-domain:

$$A'z^3 + B'z^2 + C'z + D,'$$

where $a = B/I$, $\alpha = 1/I$, and

$$A' = K_e \alpha a T (1 - e^{-aT}).$$

$$B' = 2a^2(1 - e^{-aT}) + \alpha \{ (K_e + 2B_e/T)(aT - 1 + e^{-aT}) - (K_e - 2B_e/T)(1 - e^{-aT}(1 + aT)) \}.$$

$$C' = 4a^2 - \alpha \{ (K_e + 4B_e/T)(1 - e^{-aT}(1 + aT)) + K_e(aT - 1 + e^{-aT}) \}.$$

$$D' = 2a^2(1 + e^{-aT}) + \alpha \{ (K_e + B_e/T)(2(1 - e^{-aT}) - aT(1 + e^{-aT})) \}.$$

(Eqns. 3.3.24)

Using a simple mapping relation, where

$$z = (r+1)/(r-1), \quad (\text{Eqn. 3.3.25})$$

we can again apply the Routh-Hurwitz matrix stability analysis to study stability properties of this sampled-data system, in terms of physical system parameters.

It is not surprising to find that only a discrete-domain analysis can show that even a rigid-body system can go unstable - a fact that could not be shown using continuous-domain techniques. The most one could predict was reduced damping ratios coupled with higher bandwidths. Besides the two controller parameters (Proportional Gain K_e & Derivative Gain B_e), the only parameters of interest are the effective input inertia I seen by the actuator, the passive damping coefficient B acting at the motor, and the sampling rate T of the controller.

The results for one of the cycloidal transmissions tested, where input inertia and damping were known, are shown in the three plots of Figure 3.3.21 (a thru c):

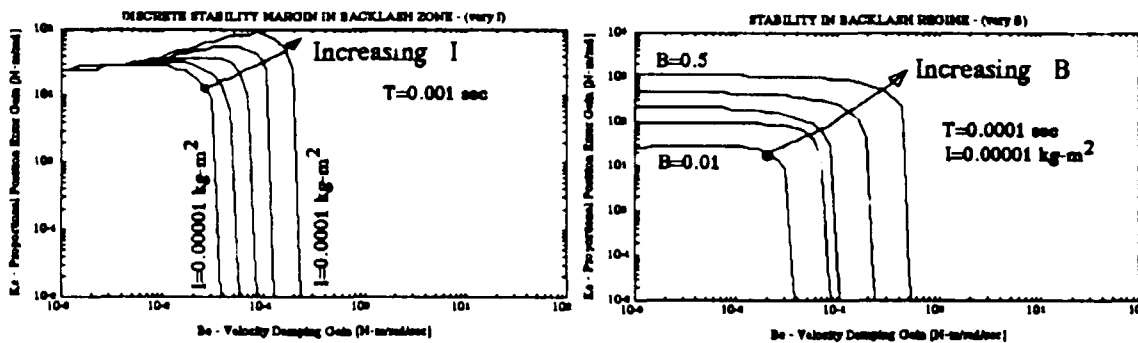


Figure 3.3.21(a, b) : Stability Margins for discrete control in backlash zone. Stability margin increase with (a) increasing backlash inertia, as well as (b) increasing passive backlash damping.

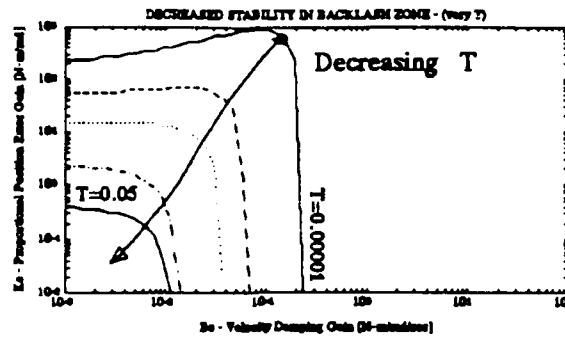


Figure 3.3.21 (c): Stability Margins for discrete control in backlash zone. Stability margins are reduced with (c) reduced sampling rates.

As predicted, the transition from a system with low inertia, to a system with higher inertia (an order of magnitude in our case) is shown to be a stabilizing phenomenon in plot (a). The converse is not true, since a system with reduced inertia will exhibit instabilities for a certain range of gains. A similar tendency can be observed if we analyze the stability regime for varying amounts of damping coefficients (plot (b)). It is worth mentioning that the unit we tested showed a much larger stability regime when the unit was tested with the factory-applied heavy grease, than when we tested it after removing seals and internal grease (replaced by mineral oil) to reduce frictional effects and increase backdriveability. It is then also no surprise, that the reduction in sampling rate (increase in T - plot (c)), will also result in a seriously diminished stability regime. This phenomenon alone underscores the necessity for high and uniform communication and control bandwidth. Introducing excessive integral gain into the controller will also reduce the stability regions in a manner similar to the continuous-time scenario presented earlier. Thus reducing and avoiding backlash all together is a very important requirement in transmission design. The possibility of instabilities within the backlash zone also explains the presence of sustained limit-cycles, their amplitude highly dependent on the width of the backlash-zone. The frequency of the limit-cycles depends on controller gains, inertia and sampling rate.

The reason why there is no treatment of the so-called lost-motion phenomenon one reads about in all the manufacturer-supplied data, is that we have decided to lump such phenomena into the variable transmission stiffness behavior. The reason is that lost motion involves torque transmission and thus component deflection, but is due to improper load distribution, high contact friction and displacement of excessive lubricant from in between the load-transmitting members. It is thus not really a backlash phenomenon by definition.

(3.3.2) Theory & Background - 3 DOF Systems

This part of the analysis will deal with sixth-order systems to represent actuator/transmission/load dynamics. The most simple model used, is similar to Figure 3.1.5, repeated here for notational purposes in Figure 3.3.22:

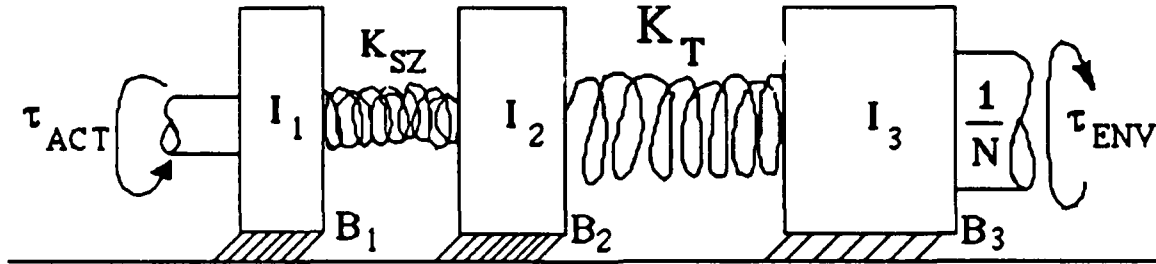


Figure 3.3.22: Physical System representation for noncolocated transmission compliance elements (proximal stiffness K_s and distal stiffness K_T).

The parameters are clearly indicated as representing inertias, spring constants, viscous damping elements, and pure effort sources - one due to the motor (τ_m) and the other due to torques applied by the environment (τ_{env}). Notice that we have introduced another vibratory mode into the transmission, trying to model multi-stage transmissions, or those transmissions that may have a soft-zone that is not co-located with the actual (or primary) load-bearing stiffening members. The simple linear model representation is :

$$\begin{bmatrix} \dot{x}_1 \\ \ddot{x}_1 \\ \dot{x}_2 \\ \ddot{x}_2 \\ \dot{x}_3 \\ \ddot{x}_3 \end{bmatrix} = \begin{bmatrix} 0 & 1 & 0 & 0 & 0 & 0 \\ -\frac{K_s}{I_1} & -\frac{B_1}{I_1} & \frac{K_s}{I_1} & 0 & 0 & 0 \\ 0 & 0 & 0 & 1 & 0 & 0 \\ \frac{K_s}{I_2} & 0 & -\frac{K_s + K_T}{I_2} & -\frac{B_2}{I_2} & \frac{K_T}{I_2} & 0 \\ 0 & 0 & 0 & 0 & 0 & 1 \\ 0 & 0 & \frac{K_T}{I_3} & 0 & -\frac{K_T + K_f}{I_3} & -\frac{B_3}{I_3} \end{bmatrix} \begin{bmatrix} x_1 \\ \dot{x}_1 \\ x_2 \\ \dot{x}_2 \\ x_3 \\ \dot{x}_3 \end{bmatrix} + \begin{bmatrix} 0 & 0 \\ \frac{1}{I_1} & 0 \\ 0 & 0 \\ 0 & 0 \\ 0 & 0 \\ 0 & -\frac{1}{I_3} \end{bmatrix} \begin{bmatrix} \tau_{act} \\ \tau_{env} \end{bmatrix} \quad (\text{Eqn. 3.3.26})$$

For position control, we can employ local feedback as measured at the motor-end (x_1), or use an external position sensor, like a high-resolution optical encoder at the transmission output (x_3), for control purposes (x_1 vs. x_3). Once again, we will only deal

with proportional-plus-derivative controllers at this point, which in the co-located and non-colocated position-control case yield the control laws:

$$\begin{aligned}\text{Co - Located} & : \tau_{act} = K_e(x_D - x_1) - B_e \dot{x}_1 \\ \text{Non - CoLocated} & : \tau_{act} = K_e(x_D - x_3) - B_e \dot{x}_3\end{aligned}$$

(Eqns. 3.3.27)

The closed-loop system dynamics are then governed by the roots of the characteristic equations, which can be determined by obtaining the determinant of the closed-loop system matrix ($|sI - A_{cl}|$). The general structure is of the form

$$\tau_{env}/\tau_{dlc.e.} = As^6 + Bs^5 + Cs^4 + Ds^3 + Es^2 + Fs + G,$$

where

COLOCATED CASE :

$$A = I_1 I_2 I_3$$

$$B = I_1(B_2 I_3 + B_3 I_2) + I_2 I_3(B_1 + B_e)$$

$$C = I_1(K_T I_2 + B_2 B_3) + I_2 I_3(K_s + K_e) + I_1 I_3(K_s + K_T) + (B_1 + B_e)(B_2 I_3 + B_3 I_2)$$

$$D = I_1 B_2 K_T + (B_1 + B_e)(K_T I_2 + B_2 B_3) + B_3 I_1(K_s + K_T) + I_3(B_1 + B_e)(K_s + K_T) + (K_s + K_e)(B_2 I_3 + B_3 I_2)$$

$$E = B_2(B_1 + B_e)K_T + I_1 K_s K_T + B_3(B_1 + B_e)(K_s + K_T) + (K_s + K_e)(B_2 B_3 + I_2 K_T) + I_3 K_s(K_e + K_T) + I_3 K_e K_T$$

$$F = K_s K_T(B_1 + B_e) + K_T B_2(K_s + K_e) + K_s B_3(K_e + K_T) + K_e K_T B_3$$

$$G = K_s K_T K_e$$

(Eqns. 3.3.28)

NONCLOCATED CASE :

$$A = I_1 I_2 I_3$$

$$B = I_1(B_2 I_3 + B_3 I_2) + I_2 I_3 B_1$$

$$C = I_1(K_T I_2 + B_2 B_3) + I_2 I_3 K_s + I_1 I_3(K_s + K_T) + B_1(B_2 I_3 + B_3 I_2)$$

$$D = I_1 B_2 K_T + B_1(K_T I_2 + B_2 B_3) + B_3 I_1(K_s + K_T) + I_3 B_1(K_s + K_T) + K_s(I_2 B_3 + B_2 I_3)$$

$$E = B_2 B_1 K_T + I_1 K_s K_T + B_3 B_1(K_s + K_T) + K_s(B_2 B_3 + K_T(I_3 + I_2))$$

$$F = K_s K_T(B_1 + B_2 + B_3 + B_e)$$

$$G = K_s K_T K_e$$

(Eqns. 3.3.29)

In the case of force control, we are again connected to a stationary environment via a force sensor, to give us information about the interface force, which we will be trying to actively control (see Figure 3.3.23).

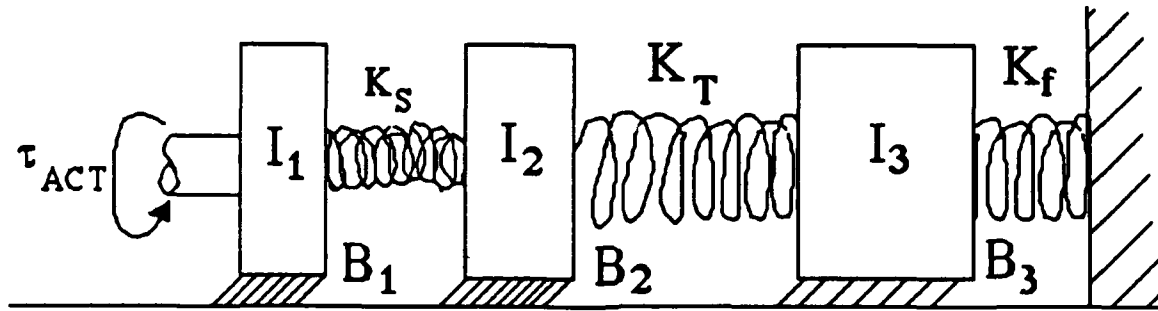


Figure 3.3.23 : 3 DOF actuator/transmission/load/environment system to analyze force-control stability and -performance.

The force-controlled actuator-transmission system is inherently a noncollocated control problem, and thus brings with it some interesting stability problems. The control law is again a PD controller on force error and rate of force change, and can be expressed as

$$\text{Non - CoLocated : } \tau_{act} = K_e(\tau_D - \tau_{env}) - B_e \dot{\tau}_{env} = K_e(\tau_D - K_f x_3) - B_e K_f \dot{x}_3, \quad (\text{Eqn. 3.3.30})$$

resulting in a closed-loop dynamic system with a characteristic equation of the form

$$\tau_{env}/\tau_d|_{c.e.} = As^6 + Bs^5 + Cs^4 + Ds^3 + Es^2 + Fs + G, \quad \text{where}$$

NONCLOCATED CASE :

$$A = I_1 I_2 I_3$$

$$B = I_1 I_2 B_3 + I_3 (B_1 I_2 + B_2 I_1)$$

$$C = K_S I_3 (I_1 + I_2) + K_T I_1 (I_2 + I_3) + K_f I_1 I_2 + B_1 B_2 I_3 + B_3 (B_1 I_2 + B_2 I_1)$$

$$D = (K_T + K_f) (B_1 I_2 + B_2 I_1) + (K_S + K_T) (B_3 I_1 + B_1 I_3) + K_S (B_2 I_3 + B_3 I_2) + B_1 B_2 B_3$$

$$E = B_1 B_2 (K_T + K_f) + K_T (B_1 B_3 + I_1 K_f) + K_S (B_3 (B_1 + B_2) + K_T (I_1 + I_2 + I_3) + K_f (I_1 + I_2))$$

$$F = K_S (K_T + K_f) (B_1 + B_2) + K_T (K_f (B_1 + B_e K_e) + K_S B_3)$$

$$G = K_S K_T K_f (1 + K_e)$$

(Eqns. 3.3.31)

A similar Routh-Hurwitz stability analysis can now be performed on the first column of the Routh-array, yielding similar results for stability and performance, as explained in the earlier sections. The only difference is that now the Routh-array column of interest is composed of the coefficients

$$[a \ b \ c \ d \ e \ f \ g]^T$$

where :

$$a = A$$

$$b = B$$

$$c = C - AD/B$$

$$d = D - B(BE - AF)/(BC - AD)$$

$$d1 = F - BBG/(BC - AD)$$

$$e = (EB - AF)/B - c \cdot d1/d$$

$$f = d1 - dG/e$$

$$g = G,$$

(Eqns. 3.3.32)

which represents the six first-column elements of the Routh-Hurwitz matrix. Sign changes in any of the elements of this column matrix indicate the presence of at least one unstable eigenvalue (or more) in the characteristic equation and thus indicates unstable system behavior.

The specific parameter values used in the analysis, are physical values which were measured for the two-stage cable-drive reduction (inertia at the input, center, and output, damping losses and transmission stiffnesses, etc.). Once again we will motivate the parameter sensitivity analysis with real physical scenarios and conclusions. The controller gains are also chosen based on physically achievable motor behaviors, and can thus be used in the real experiments.

As will be seen in the different analysis sections, the range of stable force control PD gains is reduced by as much as an order of magnitude, resulting in an effective reduced endpoint force-control bandwidth which is about a factor of 3 lower than in the case of the 2 DOF actuator/transmission/load model (depending of course on the parameters of the 2 DOF model). This phenomenon holds true no matter which parameter sensitivity analysis is selected for comparison. It is thus important to understand which type of model is most representative of a certain transmission type.

(a) Inertia Distribution

Analyzing the stability and performance sensitivity to inertia size and distribution is a bit more complicated than for the previous two-mass model. As previously mentioned, the physical starting parameters were taken from the two-stage cable reduction, and their variation by a factor of 10 in each case represents a physically realistic scenario. In Figure 3.3.24 below,

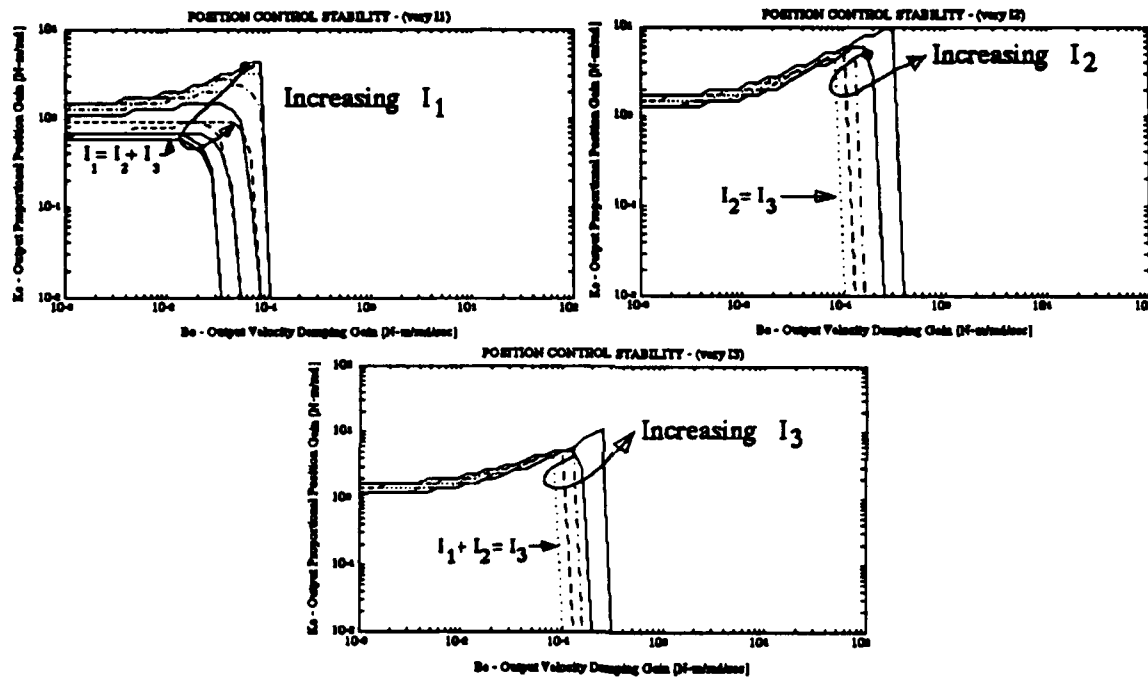


Figure 3.3.24 : Conditional Position Controller Stability for varying inertia values: (a) I_1 , (b) I_2 , and (c) I_3 .

we can see the parameter sensitivity analysis for all three system inertias w.r.t. system stability bounds for the case of non-colocated position control. Notice again, how stability margins can decrease to a minimum level, beyond which an increase in inertia results in increased stability boundaries. The limiting values for the stability bounds can numerically be determined to lie very close to the effective (reflected) sum of all the connected inertias. This behavior is similar to the one in the 2 DOF situation, with increased levels of inertial loading. These tendencies once again point at the clear possibility of configuration-dependent stability regimes for multi-jointed manipulator systems, as explained in the section on 2 DOF actuator/transmission/load models, where reduced joint-inertial loadings may create stability problems, while increased inertias have a stabilizing effect on

noncolocated position control (irrespective of joint-space or cartesian control). Bandwidths can be shown to be continuously reduced for any kind of increased inertial parameters.

The tendencies in the stability regions for non-colocated force controlled systems are exactly analogous to the differences found in the previous section, as shown in Figure 3.3.25:

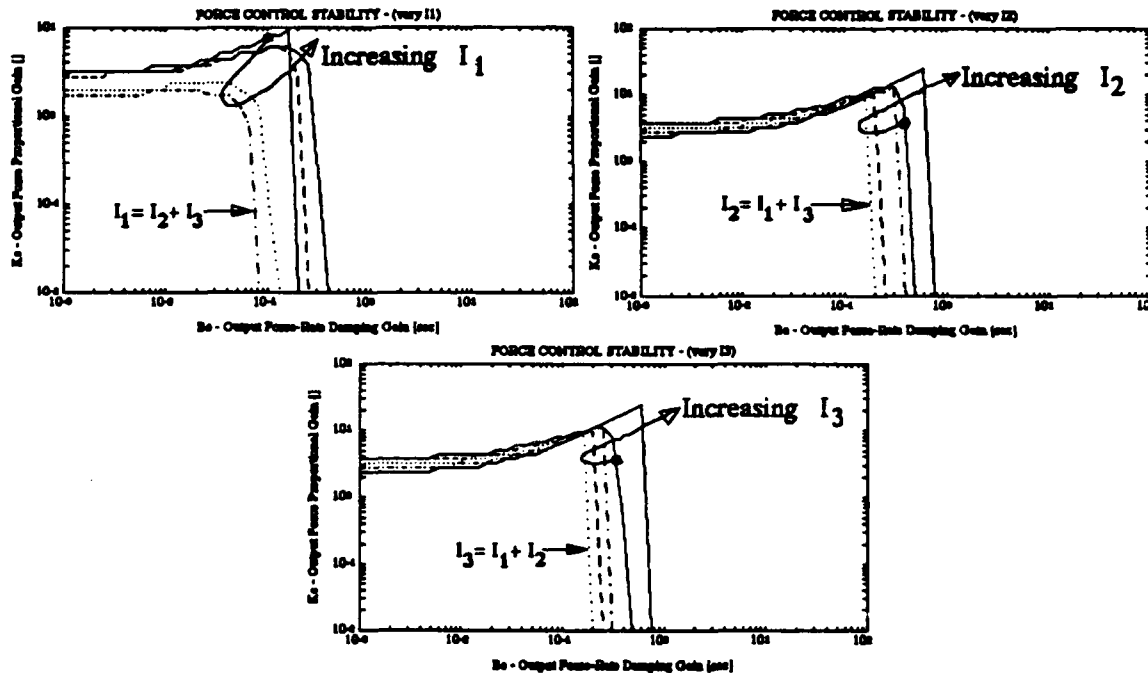


Figure 3.3.25 : Force Control stability boundary behavior for increasing (a) I_1 , (b) I_2 , and (c) I_3 .

The conditional decrease/increase in stability regimes for increases in I_1 , I_2 and I_3 , is analogous to the noncolocated position control scenario illustrated earlier. The performance levels in terms of closed-loop bandwidth continually decrease, irrespective of the stability properties, when any system inertia is increased. Adding electronic damping can also be used to achieve a certain performance level, measured by the damping ratio of the dominant closed-loop conjugate pole-pair, yet the increase in bandwidth will always be accompanied by a decrease in damping ratio in the case of force-rate or output-velocity damping.

Summarizing one can say, that increasing system inertias in noncolocated position- or force-controlled systems, conditionally decreases/increases system stability and reduces available closed-loop bandwidth. Added noncolocated electronic damping (output force-rate or -velocity) only reduces the damping ratio and increases bandwidth of the dominant closed-loop dominant conjugate pole-pair. This results in a progressively higher frequency underdamped oscillatory system response.

(b) Damping Distribution

The three-mass model has three discretely modelled viscous dampers, whose relative effects on stability are interesting to analyze. In Figure 3.3.26, we show the sensitivity

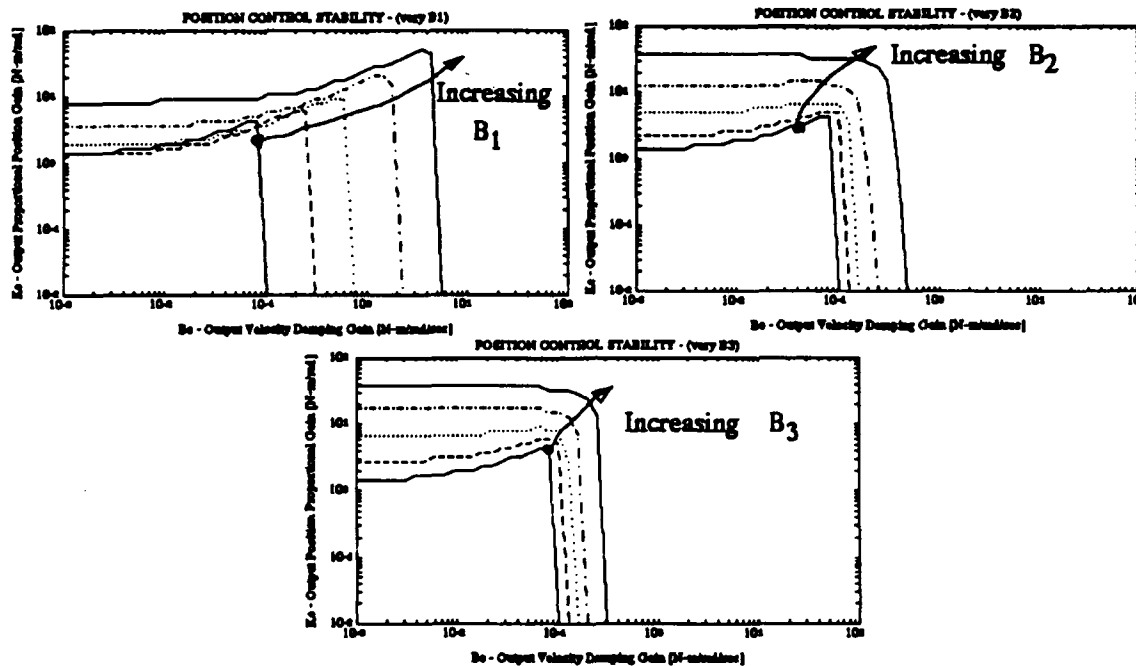


Figure 3.3.26 : Noncolocated position control stability regimes for varying values of (a) B_1 , (b) B_2 , and (c) B_3 .

of relative stability regimes to a variation in the three different viscous damping coefficients for non-colocated position control. The variation in the coefficients of viscous damping was by a factor of 20. It is clear from the above results, that the relative stability can be mostly affected by increasing the damping losses at the output stage. But as before, the numerics are misleading, due to the N^2 mapping of output coefficients to the input stage. Variations in B_1 and B_2 are much more realistic, but even then can only increase system stability by a marginal amount.

In the case of non-colocated force-control, the stability regimes are similar, as shown in Figure 3.3.27, but they differ in a very important point. Increases in the viscous damping losses at the input shaft have a proportionally larger effect on stability than in the position-control case. That in itself does not mean much, unless we compare it to relative increases in stability regimes when increasing B_2 .

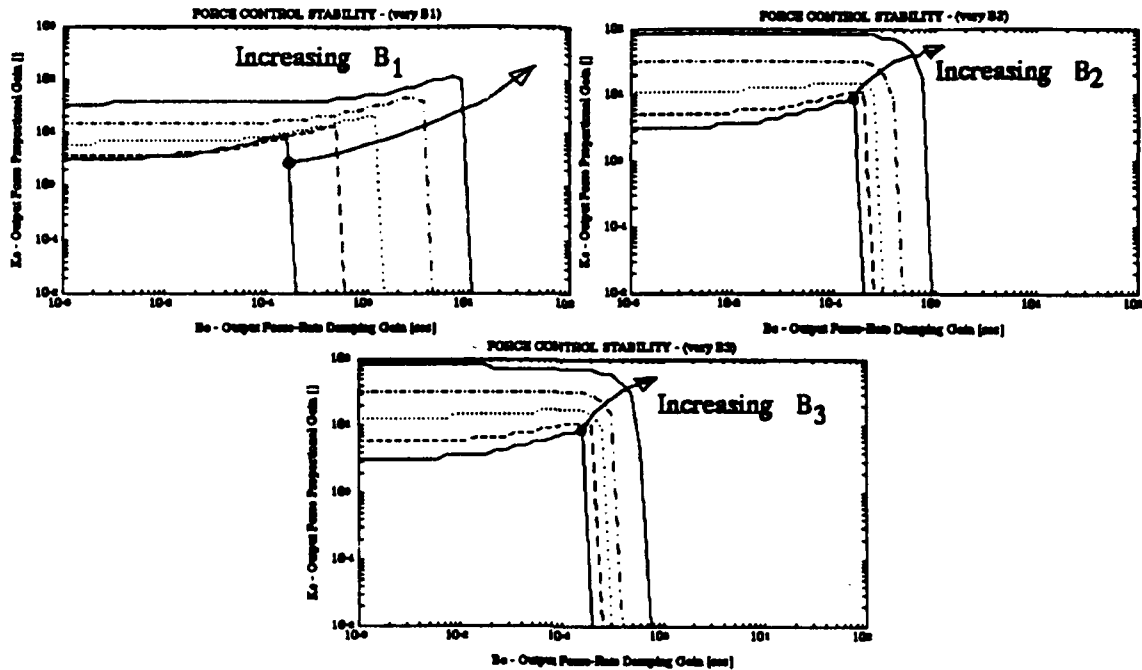


Figure 3.3.27 : Noncollocated Force Control stability regions for variations in (a) B_1 , (b) B_2 , and (c) B_3 .

The plots clearly show, if physically realizable behaviors are considered, that the most appropriate place to damp system instabilities, is at the input. The next most appropriate place would be located at the lumped location of B_2 . In certain instances, such a procedure may be hard to accomplish, unless it was performed at the design stage, since getting inside a transmission, may not be possible if one wanted to add increased damping. Even then, adding controllable damping is not always easy to implement! One simple solution many manufacturers use, is to lubricate transmissions with an overly viscous grease. Their intent is many times to lubricate the unit for life, by using an overly viscous lubricant to avoid any fancy shaft/face seals. Highly viscous lubricants also bring with them the benefit of damping oscillatory modes in a completely passive fashion. Designing a purely viscous dissipative (actively controllable) element which should be small and lightweight, is not a trivial endeavor, but may be worthwhile if such a principle as eddy-breaking can be harnessed and prove itself to be physically feasible, efficient, and deliver well controllable viscous behaviors over a wide dynamic range.

(c) Stiffness Distribution

The three-mass model represents a lumped-parameter multi-stage transmission, like in the case of the two-stage cable reduction designed and built at WHOI, forming part of

the 5 DOF underwater manipulator. This model may also be appropriate for describing the transmission designed for the MIT/WAMS manipulator [Salisbury (1988)], which uses discretely separated reducer stages, connected via cables. This model not only lets us explore such transmission designs, but also offers the possibilities to analyze multi-stage transmissions, where soft-zones and stiffening load-bearing members may not be located at the same physical location inside a transmission. This analysis could also help in determining how different cable-sizes should be chosen in order to distribute stiffnesses in order to maximize stability and performance in the eventual task setting.

I we look first at the variation in transmission stiffnesses K_S and K_T in Figure 3.3.28,

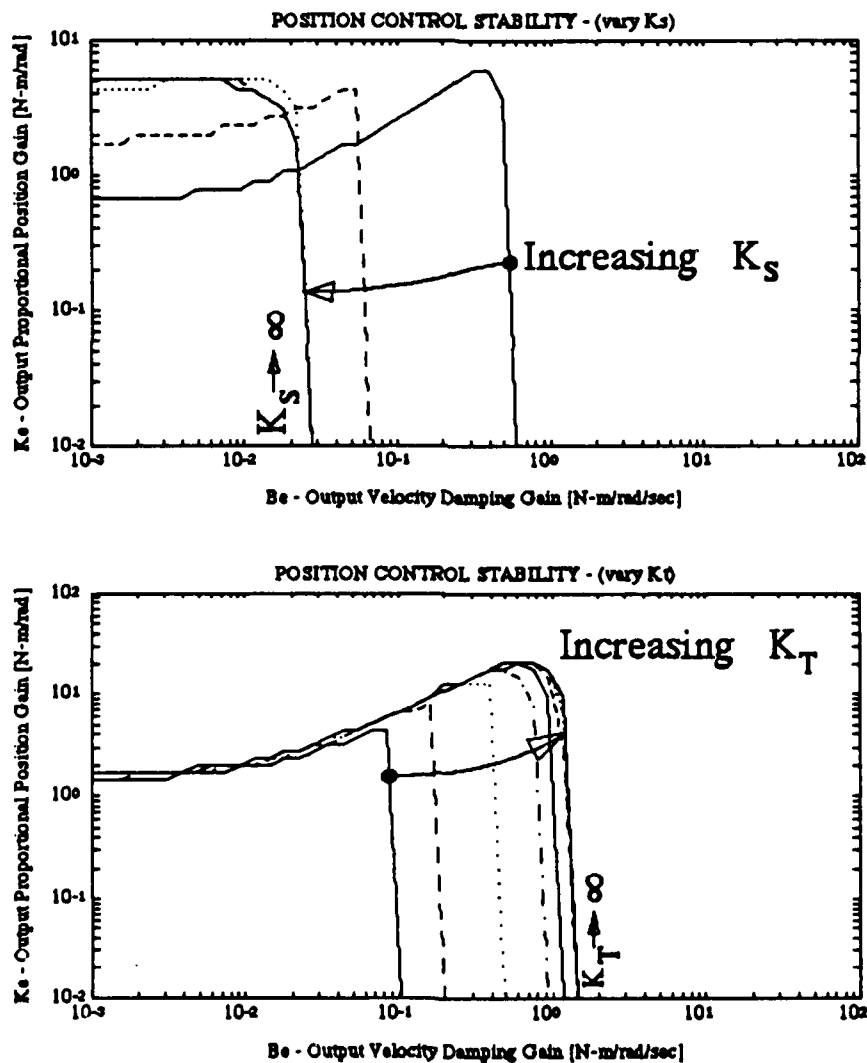


Figure 3.3.28 : Noncollocated PD position control stability boundaries for varying values for (a) K_S , and (b) K_T .

where we deal with PD position-controlled non-colocated systems, a few interesting tendencies emerge. Increase of stiffness in the truly 'stiff' load bearing members above and beyond the actual soft-zone stiffness, has very little effect on overall stability regime increases. The first plot shows, how for a value of K_T/K_s of 1 and smaller (with a fixed value for K_T), only small increases in stability region are observed (here we increased K_T to get a ratio $50 < K_T/K_s < 1/50$). This behavior can be expected though, since the analogy of a chain being as strong (stable) as its weakest link, could be applied here as well. In other words, as the soft-spring is stiffened beyond a certain value, the stability properties of the system are governed by the remaining compliant elements in the system (K_T in this case). It is also important to note that the act of stiffening up the 'soft-zone' does not reduce the effective endpoint bandwidth, but it does reduce the damping ratio. While the bandwidth levels remain unchanged, the damping ratio approaches asymptotically the value corresponding to a system where K_s goes to infinity, which brings us back to a system with the stability properties of a 2-mass model (which we analyzed earlier), whose stability and performance is mainly governed by K_T and connected inertias.

One interesting tendency to point out, is that for transmission stiffness ratios K_T/K_s smaller or equal to unity, the stability region grows only by a minuscule amount. Since soft-zones usually also have a stiffening behavior associated with them, certain selected controller gains could result in unstable behavior, even for stiffening springs. Thus stiffening spring behavior's stabilizing effects are highly dependent on the controller type and the actual physical location of said spring. Furthermore, this analysis shows how important it is to maximize and properly scale transmission stiffnesses in discrete, multi-stage transmissions. Data for the cable-driven underwater manipulator designed by DiPietro [(1988)], reflect this important design step, by implementing a ratio equal to approximately $K_T/K_s \approx 1.8$. This value clearly avoids a possible limit-cycle or even plain instability, because the changes in stability boundaries become negligible. The fact that cable-pulley transmissions do not seem to exhibit any marked stiffening behavior is also an important stabilizing attribute (see the data sections in Chapter 4).

The implications for a non-colocated force-control implementation are almost analogous. Figure 3.3.29 shows the stability regimes for a variation in K_s and K_T :

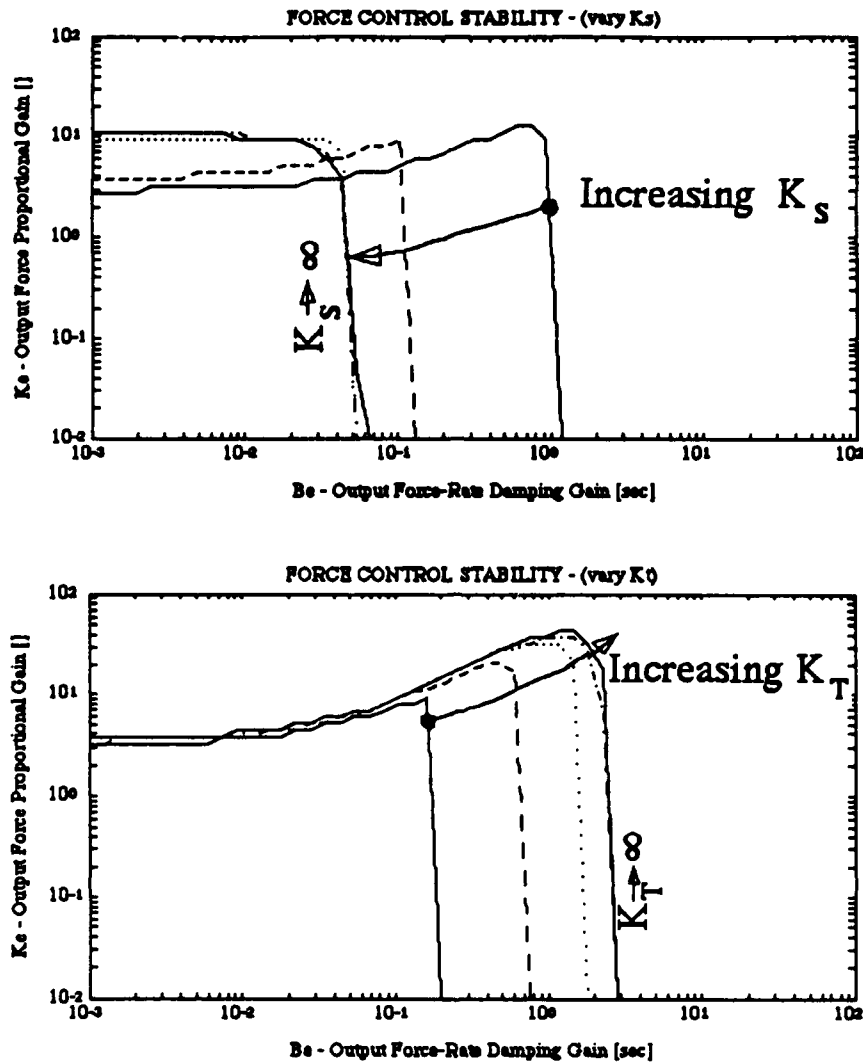


Figure 3.3.29 : Noncollocated force-control stability regimes for variations in (a) K_S , and (b) K_T .

Increasing the proximal transmission stiffness K_S above equal (reflected) values, s.t. the ratio of K_S/K_T lies above unity, results in reduced stability regions and slightly increased performance, while reducing the danger of instability due to a stiffening transmission behavior. The increase in performance is minimal, and manifests itself mostly in unchanged bandwidths at slightly increased damping ratios. Stiffening the distal transmission stiffness K_T , results in an asymptotically increased stability regime, with increased closed-loop bandwidth, but at reduced damping ratios. The increased stability regime is only possible at larger values of electronic force rate damping, which we know is a region of highly underdamped response. The addition of electronic force-rate damping

has no effect on raising the damping of the dominant complex conjugate pole-pair (on the contrary - it reduces it !!).

The effects of increasing the force-sensor stiffness are quite different to the two-mass actuator/transmission/load model presented earlier. In Figure 3.3.30,

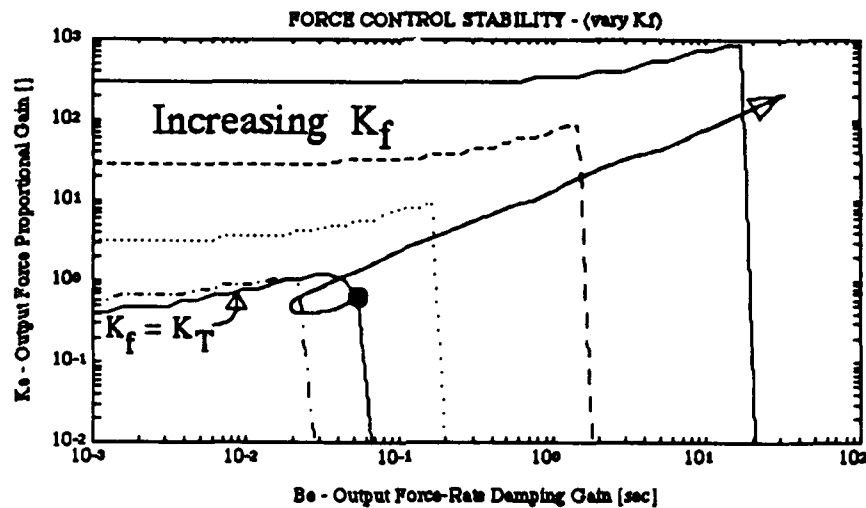


Figure 3.3.30 : Noncollocated Force control stability regions vary with increasing force-sensor stiffness K_f .

we see that the effects of force transducer stiffness is one of the main variables which results in the largest sensitivity in overall stability and performance of the closed-loop system. Notice that the sensor-stiffness was chosen to start at a value equal to the distal transmission stiffness K_T , and increase to a value which represents the stiffness of the torque sensor used in the experiments (which is at least two orders of magnitude stiffer than K_T). The lowest stability bound was generated for a K_f/K_T ratio of about 10, after which the size of the stable regions would monotonically increase. Such a phenomenon also illustrates the presence of conditional stability, which depends on several of the physical system parameters. Comparing the conditionally stabilizing behavior of force-sensor stiffness in this 3 DOF model to the unconditional reduction in stability for the 2 DOF model, it becomes obvious that these two tendencies are complete opposites, which may seem rather counterintuitive at this point. The price is paid in terms of reduced bandwidths & damping ratios. The reason is that now the internal resonant modes became more and more pronounced, and they tend towards reduced resonance levels, at reduced frequency levels.

The performance of the 3 DOF noncollocated force-controlled system is also directly slaved to the sensor stiffness. Bandwidths are monotonically reduced with increasing sensor stiffness, while the actual damping ratio may be maintained at a constant level. No level of electronic force-rate damping can increase this damping value above the open-loop value, nor can the destabilizing effect of increased electronic damping be avoided. Thus the main effect on system damping can only be achieved through passive damping, which will be proven in one of the alternate controller structures presented next.

(d) Alternate Controller Structures & Added Dynamics

P in Force & D in output/input damping

The stability margins for a Proportional force-error gain and derivative output-velocity gain are completely analogous to the PD-force controller margins presented earlier. The reason is that the coefficients of the closed-loop characteristic equation are identical, except that the s^1 -term coefficient $B_e K_f K_s K_T$ is replaced with $B_e K_s K_T$, with B_e now representing a velocity damping coefficient. The only difference here is a simple scaling process, which leaves the stability and performance characteristics unchanged, except for the effects of varying sensor stiffness. Thus if we analyze the stability boundaries for varying values of force-sensor stiffness K_f ,

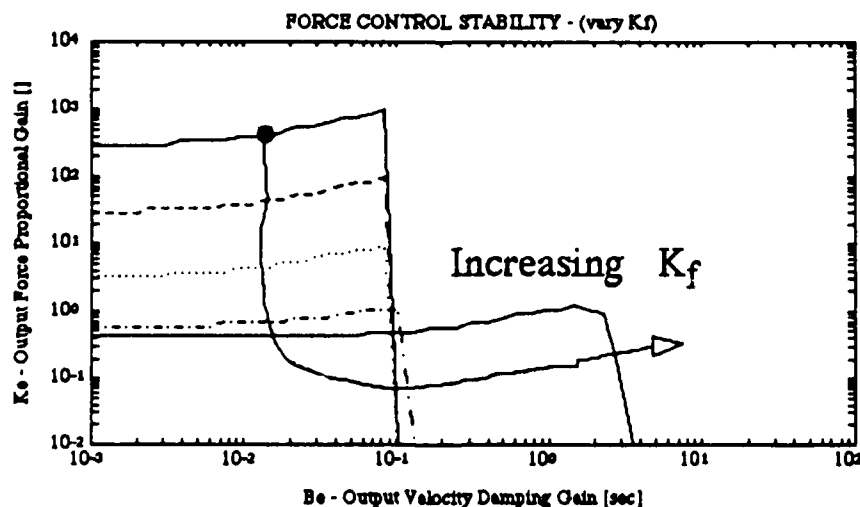


Figure 3.331 : Noncollocated Force Control stability margins, with B_e as electronic output velocity damping term, replacing the force-rate damping term used in all the previous analyses.

we get the curves in Figure 3.3.31. Stability is reduced, without largely affecting system bandwidth nor altering the system's natural damped response. In other words, the added electronic output velocity damping has no effect on the damping of the response, while only reducing bandwidth by very small amounts.

Replacing force-rate damping with input velocity damping, changes the stability and performance properties drastically. The associated control law and characteristic equation become :

$$\tau_{env}/\tau_{dlc.e} = A s^6 + B s^5 + C s^4 + D s^3 + E s^2 + F s + G$$

where

$$A = I_1 I_2 I_3.$$

$$B = I_1 I_2 B_3 + I_3 (B_2 I_1 + (B_1 + B_e) I_2).$$

$$C = K_s I_3 (I_1 + I_2) + K_T I_1 (I_2 + I_3) + K_f I_1 I_2 + (B_1 + B_e) B_2 I_3 + B_3 ((B_1 + B_e) I_2 + B_2 I_1)$$

$$D = (K_T + K_f) ((B_1 + B_e) I_2 + B_2 I_1) + (K_s + K_T) (B_3 I_1 + (B_1 + B_e) I_3) + K_s (B_2 I_3 + B_3 I_2) + (B_1 + B_e) B_2 B_3.$$

$$E = (B_1 + B_e) B_2 (K_T + K_f) + K_T ((B_1 + B_e) B_3 + I_1 K_f) + K_s \{ B_3 (B_1 + B_e + B_2) + K_T (I_1 + I_2 + I_3) + K_f (I_1 + I_2) \}.$$

$$F = K_s (K_T + K_f) (B_1 + B_e + B_2) + K_T (K_f (B_1 + B_e) + K_s B_3).$$

$$G = K_s K_T K_f (1 + K_e).$$

(Eqns. 3.3.33)

Once again, the presence of the controller parameter B_e in more than the coefficient of the s^1 -term (F), indicates that the stability regime will not be upper-limited by a certain value of electronic damping. On the contrary, under the assumption of infinite resolution and actuator effort, this system can always be stabilized for a given proportional gain, through the addition of damping

The above tendency can be clearly observed in Figure 3.3.32, where we study the influence of force-sensor stiffness on the overall system stability regime for noncolocated force control using proportional force-error gain K_e , and input-velocity damping gain B_e :

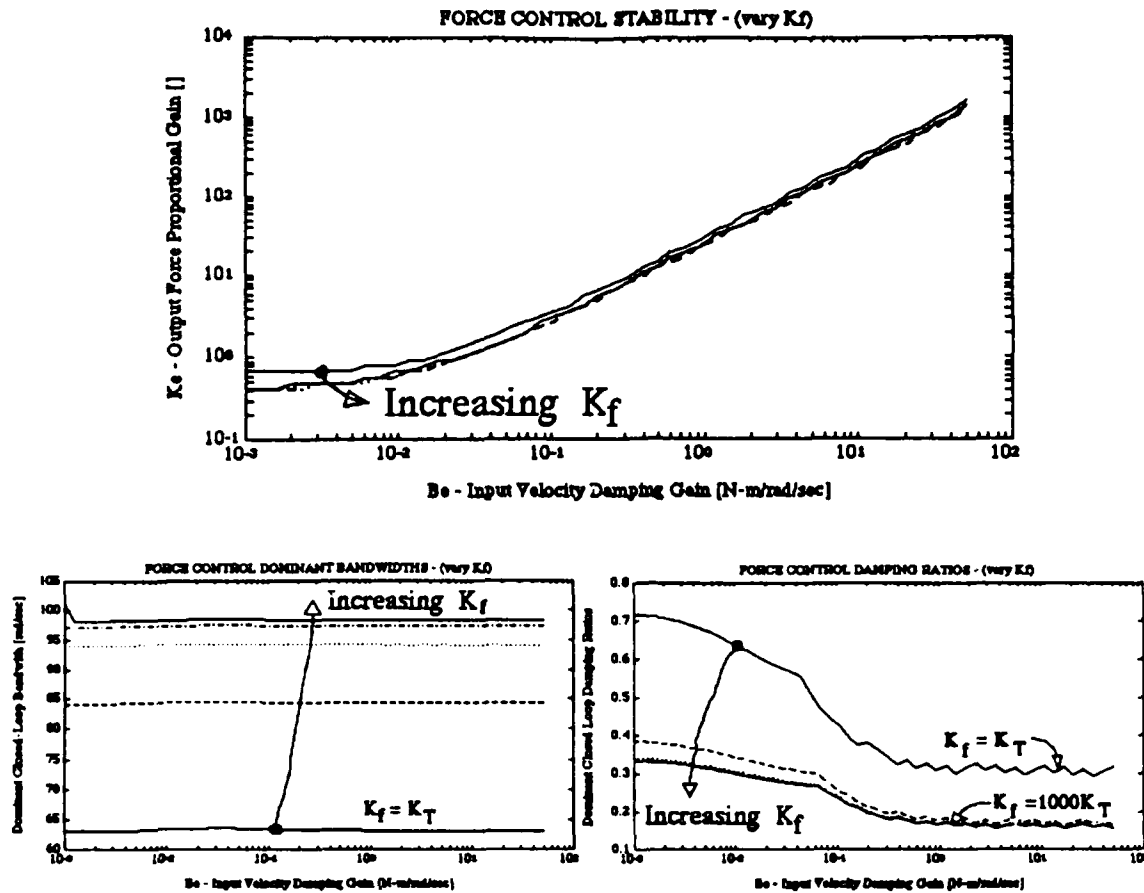


Figure 3.3.32 : Noncollocated Force control with electronic input damping for increasing values of sensor stiffness : (a) stability regimes, (b) dominant closed-loop bandwidth, and (c) dominant closed-loop damping ratios.

The tendency of reduced stability with increasing sensor stiffness is not really present in the above plot, as is the case in all other previous controller implementations. It is important to note that the relative increase in closed-loop bandwidth with increasing sensor stiffness, is not dependent on how much electronic damping is added to the system. The addition of increased electronic damping at the input can stabilize such a system for any proportional gain. In each case, for a minimum performance level, the level of added damping has no effect on system bandwidth, but increasing the sensor stiffness results in a system with reduced damping ratio, and thus more oscillatory behavior. Increasing the sensor stiffness actually increases the overall system bandwidth, but also decreases/increases system damping/oscillatory behavior. The relative increase in bandwidth is small, and does not exceed a factor of 2 in our application. Thus adding input velocity damping may result in an overall stable system, but it can not improve the closed-loop damping ratio above that of its open-loop response.

Two of the more interesting trends, relate to the variation in the two distributed (proximal & distal) stiffnesses, K_S and K_T . If we vary K_T by a factor of 100 (typical for the harmonic-drive for instance), and K_S by a factor of 50 (also possible with the WHOI cabled manipulator), the resulting stability and frequency plots in Figure 3.3.33 and 3.3.34 show an interesting tendency:

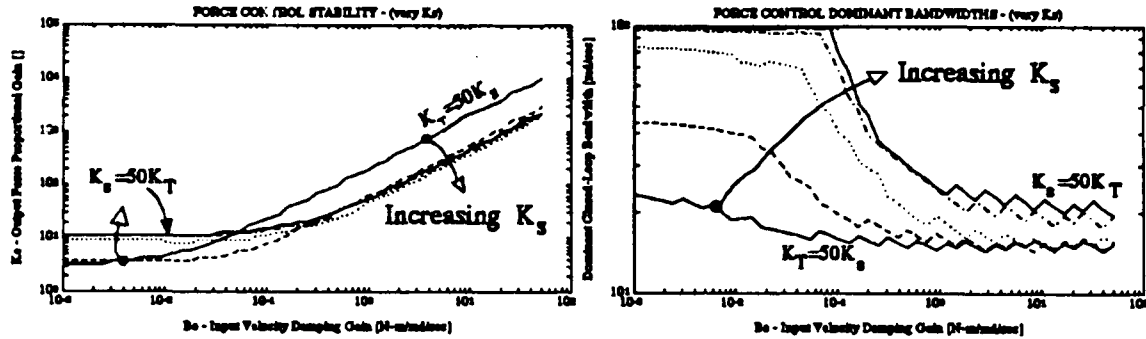


Figure 3.3.33 : Noncollocated Force Control with added input velocity damping: (a) Stability regimes and (b) dominant bandwidths for increasing values of proximal stiffness K_S .

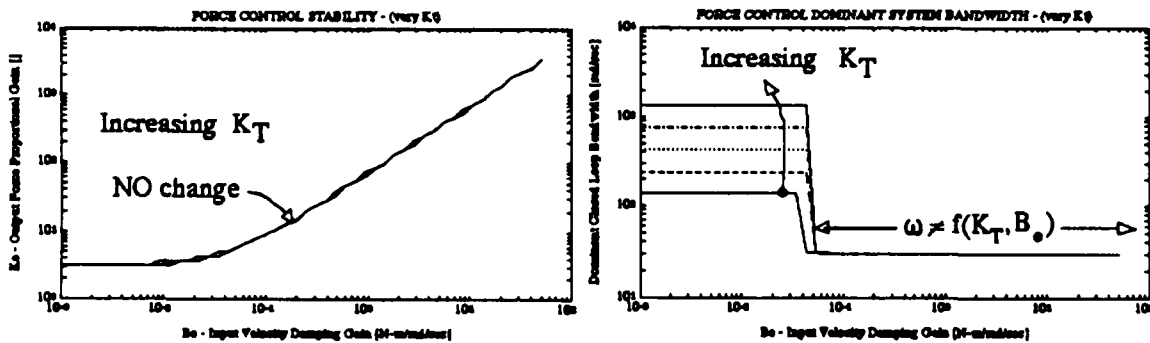


Figure 3.3.34 : Noncollocated Force Control with added input velocity damping: (a) Stability regimes and (b) dominant bandwidths for increasing values of distal stiffness K_T .

The system stability is not affected by changes in the distal stiffness K_T , whereas an increase in K_S results in some conditional increases in system stability. The bandwidths for each value of distal/proximal transmission stiffness were computed based on maintaining a certain minimum performance level measured in terms of settling-time and thus a fixed/desired damping ratio (for the dominant second-order behavior, selected to be $\zeta \geq 0.6$). As expected, both cases show a decrease in bandwidth with increasing input velocity damping, which asymptotically approaches similar values for both cases. A dramatic increase in bandwidth can be accomplished only for low values of electronic input damping. Thus if larger values of K_e are selected to increase the desired force-control

bandwidth, the system may go unstable and can only be stabilized with increased input damping, which in turn results in decreased bandwidth levels - just the opposite of what we wanted to achieve (but at least we can guarantee stability). In terms of mechanical design, the system stability is not greatly affected by the selection of K_S nor K_T . Slight stability improvements for low input damping can mostly be affected by increasing the proximal stiffness K_S , to levels where the ratio of K_S/K_T is greater or equal to unity. System bandwidths can be drastically improved (once again only at low levels of input damping), by increasing the distal stiffness K_T , which has a more pronounced effect than increasing the proximal stiffness K_S . Given such a design freedom, like in the two-stage cable-reducer at WHOI, this effect may be achieved by performing most of the reduction in the proximal stage (using a long-travel small-diameter cable), and the rest in the distal stage (using short-travel larger-diameter cables), and matching cable diameters and running lengths to achieve proper ratios of K_S/K_T .

Increasing levels of damping throughout the transmission has the anticipated effect of increasing stability regimes, while reducing closed-loop bandwidth to some extent. The difference is again that the largest (physically achievable) increase can be obtained by tuning the input viscous damping coefficient B_1 . The interesting point worth mentioning here, is that even though increasing B_2 or B_3 may be harder to physically achieve, it will result in increased closed-loop system stability and bandwidth for small levels of electronic input damping. This is obvious from the plots of Figure 3.3.35 below,

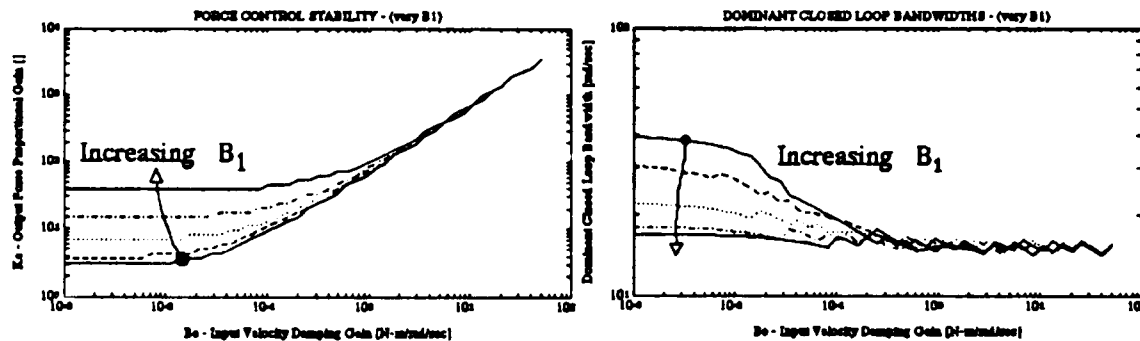


Figure 3.3.35(a) : Stability and Bandwidths for varying amounts of passive damping B_1 in noncollocated force control with input velocity damping.

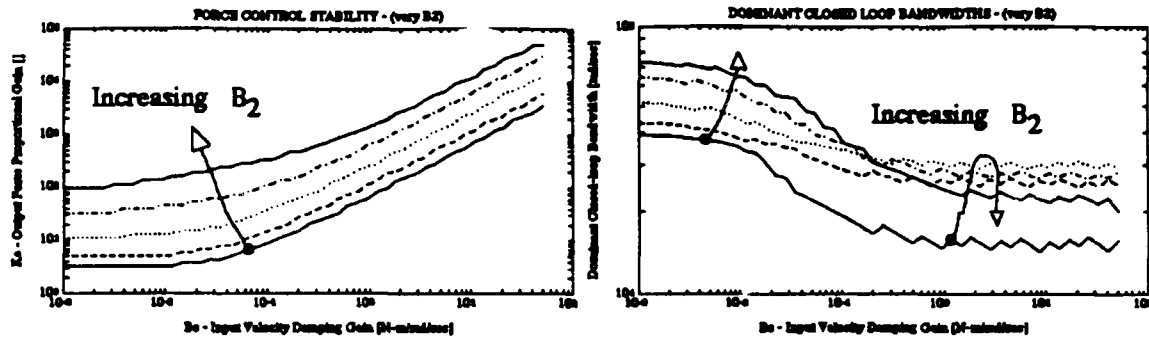


Figure 3.35(b) : Stability and Bandwidths for varying amounts of passive damping B_2 in noncollocated force control with input velocity damping.

where the system stability is monotonically increasing for increasing damping levels in B_2 , with the system bandwidth increasing for up to certain input damping levels B_e . On the other hand, adding passive input damping levels (B_1) to the system, decreases available bandwidth, while increasing stability regimes. This is no surprise, since B_1 and B_e are in the ideal (and continuous domain) no different, and their respective effects on stability and performance should be, and are, identical. The important difference between the two approaches is that system bandwidth can be slightly increased if passive distal damping is introduced into noncollocated force-controlled systems. The behaviors for B_2 and B_3 are almost identical, but only data for B_2 is shown, because it would be physically easier to introduce damping at the x_2 -node, due to reduced transmission ratios (and thus higher speeds) as compared to the output-node, since all these parameters scale as $1/N^2$.

The effects of increasing system inertias are very different for the proportional force-error and input velocity damping controller. The two sets of plots in Figure 3.3.36 below,

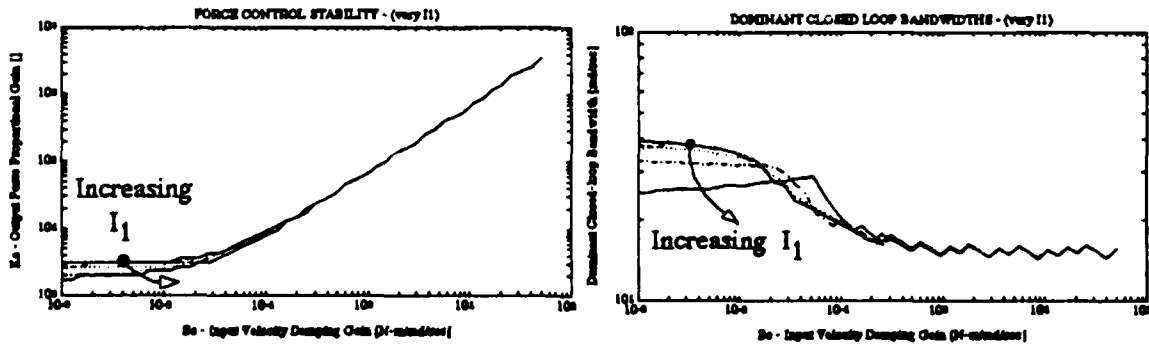


Figure 3.3.36(a) : Stability and Dominant Bandwidth for varying levels of I_1 for noncollocated force control with added input velocity damping.

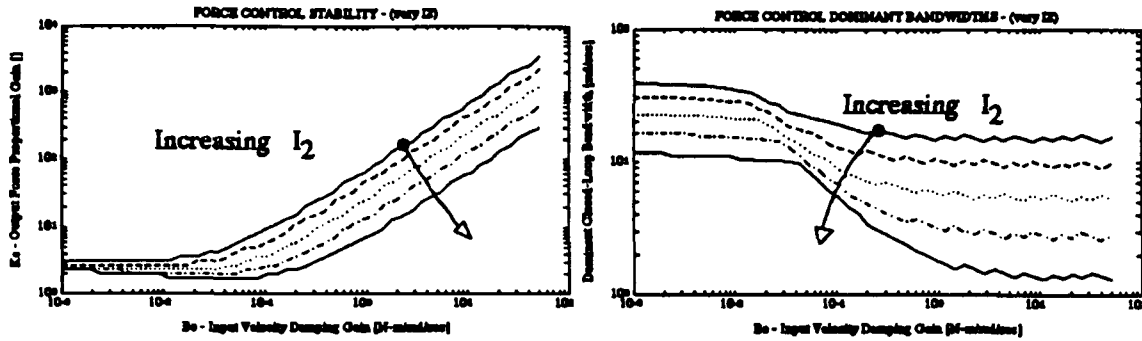


Figure 3.3.36(b) : Stability and Dominant Bandwidth for varying levels of I_2 for noncollocated force control with added input velocity damping.

illustrate that increasing any (trends for I_3 not shown, but are identical to I_2 -trends) of the system inertias reduces not only stability margins but also closed-loop system bandwidth. Decreasing input inertia I_1 has the largest effect on increasing stability in the low-damping region, while the opposite is true for increasing levels of I_2 (and I_3) at higher damping levels. Increasing distal inertias like I_3 , results in clear bandwidth reductions, which are accentuated further by increasing the level of input velocity damping. Thus in a system like a multi-DOF manipulator with configuration-dependent inertia matrices, bandwidth and stability may be easily reduced/increased, depending on the effective inertia reflected to the motor input-stage, as well as the inertia of the rotor/shaft/transmission-input assembly.

PI in Force-Error & D in force-rate/input-velocity damping

Similarities in system stability and -bandwidth can be observed for the two- and three-mass PID-force controllers. From Figure 3.3.37 below,

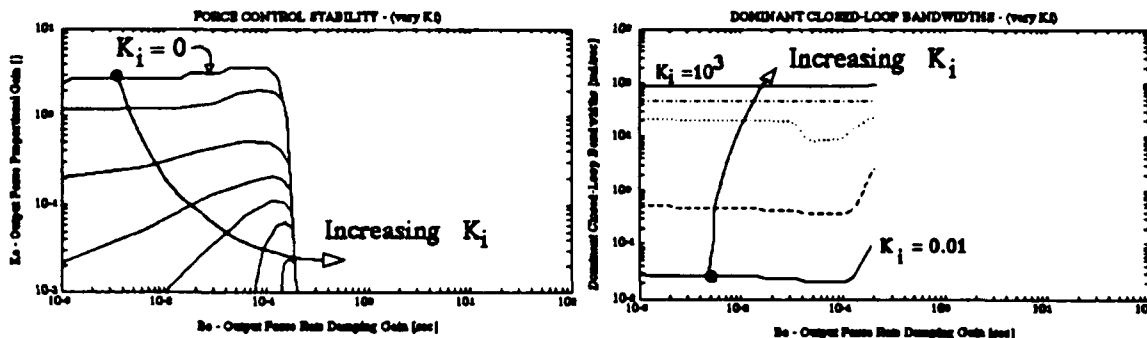


Figure 3.3.37 : (a) Stability and (b) Closed-Loop Bandwidth trends for increased levels of integral force-error-gain K_i in a pure PID noncollocated force controller.

it is obvious that for increased levels of K_i , the stability margin in terms of K_e and B_e is reduced to small levels, while bandwidth seemingly increases. This would actually seem to be the ideal solution, but we have not explored what happens to the actual damping ratios for a given system bandwidth. We know from more simple implementations that integral control increases overshoot and settling times, which we should be able to measure in terms of the damping ratio at a given closed-loop frequency. Requiring a certain minimum damping ratio in a controller with integral control, requires a certain level of integral gain, which may drastically reduce stability limits. In order to achieve a certain bandwidth, performance has to be sacrificed, since the increased frequency content of the control system will result in highly underdamped system responses and highly oscillatory force response. Such high-frequency oscillations can prove especially destabilizing if the above controller is implemented digitally.

Changing over from force-error rate damping to output velocity damping, has no effect on system stability nor performance, and this section is thus omitted since the results are the same for a pure PID force-controller. We have shown earlier that this claim is indeed correct, since the effect is only that of scaling one of the terms in the s^1 -coefficient for the closed-loop characteristic equation.

If we replace the force-damping term with an input-damping term, we can again plot stability and bandwidth traces for varying integral force gains. Shown below in Figure 3.3.38,

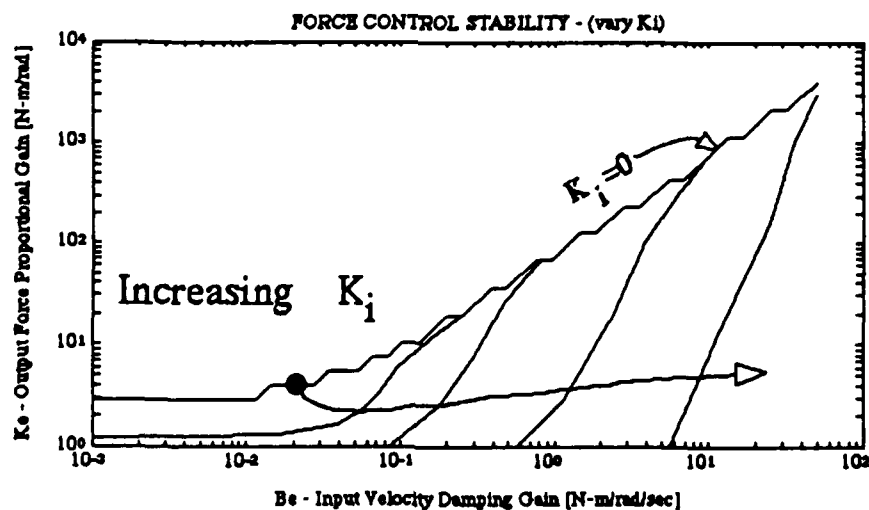


Figure 3.3.38(a) : Stability Regimes for noncollocated force control with input velocity damping, for varying levels of integral force-error gain K_i .

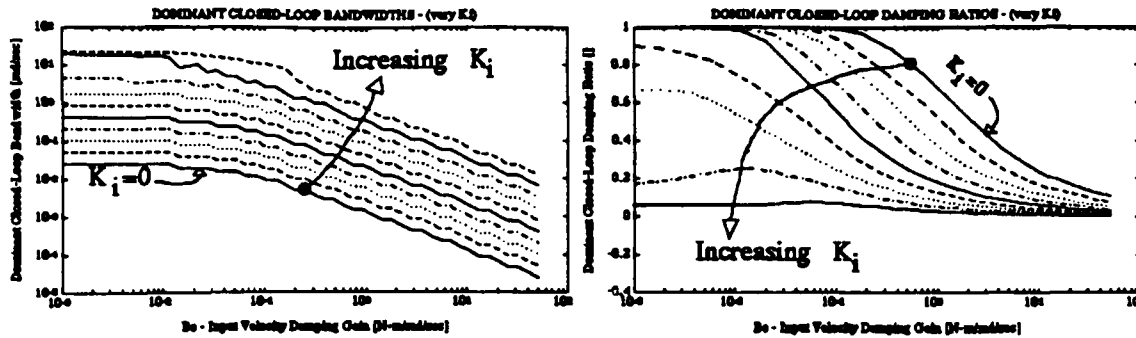


Figure 3.3.38(b & c) : Dominant closed-loop bandwidth, and dominant closed-loop damping ratios for noncollocated force control with input velocity damping, for varying levels of integral force-error gain K_i .

are the stability, bandwidth, and damping ratio traces for increased levels of integral force-error gain K_i . Notice again how integral gains reduce system stability, and only added input damping can stabilize a system for a given proportional gain. Another interesting trend that can be observed, is that increased levels of input damping will reduce the bandwidth of the system, as well as the damping ratios, resulting in increasingly oscillatory systems. Thus input damping for excessive levels of integral gain can not always guarantee a good performance level, despite the guarantee for stability. Trying to compensate for gravity- and stiction-errors through integral gain is a fairly common approach, but will not necessarily result in a higher bandwidth system, nor will performance be optimal, and it may even induce unstable system response. Nonlinear effects such as limit-cycles due to integral gain on 'sticky' systems are an even tougher behavior to control/stabilize or even avoid. We will perform experiments in the next two chapters to highlight some of these issues.

First Order Actuator/Sensor Dynamics

It does become important to look at the effect of first-order actuator/sensor characteristics in a 3 DOF model, because the conclusions differ from the 2 DOF model in certain respects. Introducing first-order sensor/actuator dynamics, increases the system order from six to seven, with the pure PID force-control law, system representation, and characteristic equation being :

$$\text{Non-Collocated : } \tau_{act} = K_e(\tau_D - \tau_{env}) - B_e \dot{\tau}_{env} + K_i \int_0^t (\tau_D - \tau_{env}) dt$$

and

$$\dot{\tau}_m = -a\tau_m + a\tau_{act} \quad (\text{Eqns. 3.3.34})$$

and the characteristic equation

$$\tau_{env}/\tau_d|_{c.e.} = A s^7 + B s^6 + C s^5 + D s^4 + E s^3 + F s^2 + G s + H$$

where

$$A = I_1 I_2 I_3.$$

$$B = I_3(B_1 I_2 + B_2 I_1) + I_1 I_2(a I_3 + B_3).$$

$$C = a I_1 I_2 B_3 + B_1 B_2 I_3 + (a I_3 + B_3)(B_1 I_2 + B_2 I_1) + I_1 I_2(K_T + K_f) + I_1 I_3(K_s + K_T) + I_2 I_3 K_s.$$

$$D = a B_3(B_1 I_2 + B_2 I_1) + B_1 B_2(a I_3 + B_3) + I_1(K_T + K_f)(a I_2 + B_2) + I_2(K_T + K_f)B_1 \\ + (K_s + K_T)(B_1 I_3 + I_1(a I_3 + B_3)) + K_s(I_3 B_2 + I_2(a I_3 + B_3)).$$

$$E = a B_1 B_2 B_3 + (K_T + K_f)(a I_1 B_2 + B_1(a I_2 + B_2)) + (K_s + K_T)(a I_1 B_3 + B_1(a I_3 + B_3)) \\ + K_s I_1(K_T + K_f) + K_f K_T I_1 + K_s(a I_2 B_3 + B_2(a I_3 + B_3)) + K_s I_2(K_T + K_f) + K_s K_T I_3.$$

$$F = a B_1(B_2(K_T + K_f) + B_3(K_s + K_T)) + (a I_1 + B_1)(K_f K_T + K_s(K_T + K_f)) + a K_s B_2 B_3 \\ + K_s(K_T + K_f)(a I_2 + B_2) + K_s K_T(a I_3 + B_3) + K_s I_2(K_T + K_f) + K_s K_T I_3.$$

$$G = a K_T(B_1 K_f + B_3 K_s) + a K_s(K_T + K_f)(B_1 + B_2) + K_s K_T K_f(1 + K_e + a B_e).$$

$$H = a K_s K_T K_f(1 + K_e).$$

(Eqns. 3.3.35)

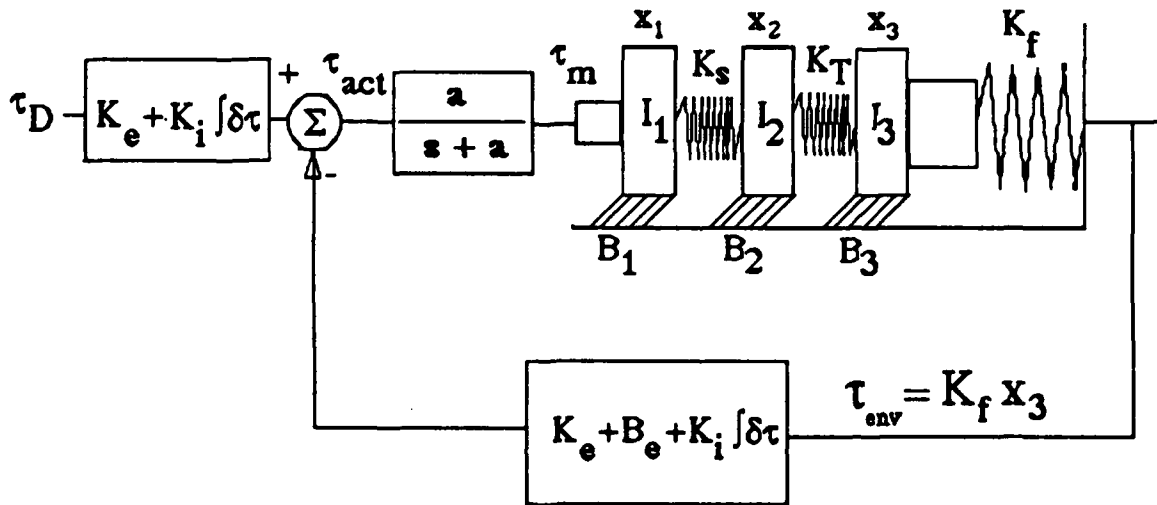


Figure 3.3.39 : System Diagram depicting the placement of first-order unmodelled dynamics in the actuator effort-path. Notice that this unmodelled filter-mode could also have been placed in the feedback loop, resulting in the same system response.

The block diagram of Figure 3.3.39, shows how the low-pass filtering is performed. The same two multiplier blocks in the feedback path as well as in the feedforward path before the summing junction, are the simplest way to insure that the low-pass filter acts on the entire components making up the desired actuator torque (τ_{act}). The commanded torque to the motor τ_m is thus a digitally low-pass filtered version of τ_{act} !

Upon analyzing the stability bounds using the Routh-Hurwitz Stability Criterion, we observe that the variation in stability regime due to variations in the time-constant ' $1/a$ ' of the first-order dynamics is non existent.

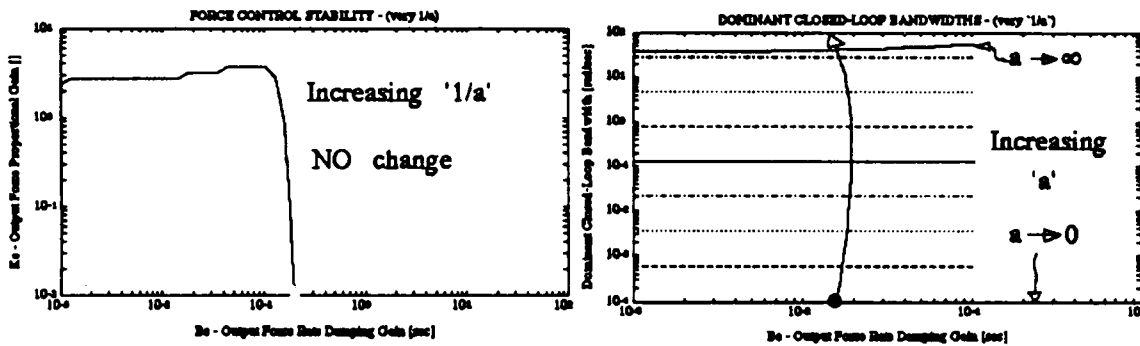


Figure 3.3.40 : (a) Stability and (b) dominant bandwidths for decreasing levels of first-order time-constant $1/a$, for a noncollocated pure PID force-controller.

Figure 3.3.40(a) shows, that the stability bounds remain unchanged for any value of time-constant ' $1/a$ '. On the other hand, Figure 3.3.40(b) also reveals that the closed-loop frequency at which instability sets in (taken from the dominant mode), increases with decreasing time-constant ' $1/a$ ' (increasing values for ' a '). In other words, the PD control gains' effects on stability are negligible, but the introduction of first-order dynamics controls the dominant bandwidth behavior. In the limit as ' $1/a$ ' goes to zero (negligibly fast first-order dynamics), the dominant bandwidth approaches that of the simple PD force-controller presented earlier. Note that the limiting dominant closed-loop natural frequency tends towards an upper limit, which represents such a system with infinitely fast first-order dynamics (in other words they are negligible). It is an interesting phenomenon, since it clearly illustrates that the first-order dynamics reduce the frequency content of the actuator signal, but even then the system still only remains stable for a certain range of PD-gains. Thus not even every system with a PID controller can be stabilized by simply introducing a low-pass filter into the sensor/actuator path.

If a PD controller with proportional force error gain and input (or output) velocity damping, or a PID controller with proportional force error gain, input/output velocity damping and integral force error gain is used, the phenomenon is exactly analogous. First-order dynamics only determine the dominant closed-loop system bandwidth, thus leaving the stability issue dependent on proper selection of P-, I-, and D-gains. This behavior is completely different to the one observed for the 2 DOF system model, where we could achieve larger stability ranges (at reduced bandwidth levels), as well as reduced stability regimes for time-constants ' $1/a$ ' beyond a certain value. Both showed the asymptotic stability and bandwidth trends one would expect as ' a ' tends to infinity and towards zero.

(3.4) Summary and Conclusions

In this chapter we have analyzed the stability and performance characteristics of closed-loop position- and force controlled actuator/transmission/load systems. We have proposed different lumped parameter system models to account for (1) the inertia distribution, (2) stiffness distribution and variability, (3) frictional losses, (4) backlash, and (5) discrete control effects that are present in such systems. The presence of such effects as 'soft-zones', 'wind-up', lost motion, backlash and stiffening/softening stiffnesses was lumped into all of the models studied earlier. An important aspect is to be able to discern not only what model best fits what transmission, but also what the numerical values for the lumped parameters could be. The beginning of this chapter explored these issues and presents the physical parameters that were measured in order to perform the stability/performance analysis. It has become clear, that depending on the model complexity, distribution of physical system parameters as well as the controller structure used, system stability and performance may vary drastically and thus warrant the in-depth study performed in this chapter. Despite the fact that all the results obtained are for purely linear systems, they are very helpful in the design-stage of a reducer, and will also turn out to be reliable predictors for certain operational conditions (see Chapter 5). Hence, despite the fact that real transmissions are highly nonlinear, a linear performance/design analysis offers some useful conclusions and insight.

General Remarks

We were able to measure stability in terms of the Routh-Hurwitz matrix, which yields a necessary and sufficient guarantee for stability, when not only the coefficients of the characteristic equation, but also the signs in the first matrix-column are analyzed. Each of the entries in this column can be determined symbolically, and thus a stability analysis can be performed in terms of system/controller parameters. If we analyze the composition of the first column for the 2 DOF model (Eqn. 3.3.8(b)), we realize that due not only to the closed-loop asymptotes in a root-locus, but also the symbolic expressions, that there will be two sign changes which imply an unstable complex-conjugate pole-pair for systems which may exhibit instability. Thus looking at the next-to-last term in the first column,

$$D-B^2E/(BC-AD),$$

we can show that the stability of the system will be governed by the sign of this term, the stability margin can be given by the value of this term, and that the rate of stability loss is dependent on the expression $B^2E/(BC-AD)$. Using this information, we can construct the symbolic representation of this coefficient, and thus analyze stability margins. A similar analysis can be performed for the 3 DOF model, resulting in the same requirement, with an expression that is a bit more complicated. Obviously the complexity of the above expression increases with the order of the system. The fact that we predict a complex-conjugate pole-pair to go unstable, illustrates the stability properties of the proximal vibratory mode, which is located at the input and is the lowest resonant mode of the actuator/transmission/load system.

Performance was measured in terms of closed-loop bandwidth and damping ratios. We required a minimum damping ratio (for a certain performance level) and then observed at what frequencies we were still able to achieve it, as we varied controller- and system-parameters. This approach requires that the system's eigenvalues be determined at each point in parameter-space. This was done using the numerical values taken from the real transmissions, underscoring the importance for proper and realistic numerical parameter values.

The most simple model that we studied, had a lumped transmission stiffness located between the load/transmission- and rotor/shaft-inertias. The value for the spring constant need not be constant, and does vary significantly for different transmissions. The amount of variation was a good indication of the presence and size of any soft-zones or wind-up. Most of the transmissions that we studied (all except the cable reducer) we believe to be described by the model of Figure 3.1.3. This claim can best be substantiated by not only understanding the physical build-up of the units (see Chapter 2), but also by examining the data in Chapter 4. The more complex model involving a 3 DOF actuator/transmission/load system, was much better suited to the cable reducer, since it had discrete stages of cable-lengths and pulley-inertias. No real hard physical evidence could be found that would substantiate the presence of a non-colocated soft-zone inside a transmission, which would have meant a separate load-dependent oscillatory mode within the transmission. It is generally true, that if a system of fixed system parameters is described by increased numbers of oscillatory modes, the overall system bandwidth and performance is reduced at the same time. Thus the stability and performance analysis for the 3 DOF system compared well to that of the 2 DOF model, but with reduced performance and stability guarantees (these of course depend on the individual system parameters).

We will limit ourselves mainly to the discussion of force/torque control of these systems. Even though we have extended the analysis to colocated and noncolocated position-control, the conclusions will mainly be drawn for the noncolocated force/torque control scenarios of hard environment contact.

Controller Structures

The use of pure PD torque controllers (P on torque-error and D on torque-rate) exhibited clear stability limits not only in terms of proportional force-error gain, but also in terms of derivative gain. This derivative gain could be either acting on rate of output-torque or output velocity - the stability and performance margins were almost identical. The increased addition of such damping into the system drove the system unstable. Instabilities were accompanied with increased frequency oscillations (and of course reduced damping ratios). If we replaced the derivative feedback with input velocity damping, such that the damping would be generated using a colocated velocity measurement, the system was stabilizable at any proportional gain levels. The addition of such damping levels slightly reduced the system bandwidth and resulted in a system with an asymptotically reduced value for the dominant closed-loop damping ratio. In other words, the system could be stabilized, but at the cost of a slight reduction in bandwidth at the stability margin and an asymptotically constant level of increased damping ratios. This behavior can be observed in any of the data sets in the previous sections. This trend is completely independent of the model structure that we analyzed.

Introducing integral gains into the controller drastically reduces the stability margins, creating conditionally stable systems only for certain ranges on proportional and derivative gains (irrespective of the type and location of damping feedback). The system response becomes more oscillatory and increases in overall frequency content, and thus exhibits reduced damping ratios. Once again, adding input-velocity damping to the PI control terms, results in a stabilizable system for certain values of damping above a certain threshold. It becomes important to note though, that the system bandwidth increases for increased integral gains, as does the reduction in damping ratio. The addition of input-velocity damping again only steers the system to an asymptotic damping ratio which can be fairly low, depending on the amount of proportional force-error gain. In other words input velocity damping may not be the solution to all the problems, since in order to achieve a certain dynamic response and steady-state error decay, a certain level of damping becomes necessary. Increased proportional gains are then possible, but the system bandwidth can

not be changed beyond that of an undamped system. Implementation issues may limit the amount of electronic input-velocity damping which is possible. Thus not every system can be stabilized to a certain level of damping ratio by simply adding input-velocity damping.

Use of an impedance controller has the same typical constraints/advantages of noncollocated/collocated position/velocity control present in position-controlled systems (especially for high-gain impedance controllers). We showed via the Routh-Hurwitz stability analysis, that stability may not only be reduced by output feedback but also by the selection of reduced levels of endpoint inertia. Even in the presence of input-position and -velocity feedback, the selection of desired endpoint inertia has a marked effect on system stability and performance. The system shows a much larger sensitivity to reductions in desired inertia, than to increases in desired inertia levels. This phenomenon is independent of damping approach. Once again, using input damping may guarantee stability, but increased gain levels will reduce the damping ratio to a level which may be quite unacceptable. At increased desired levels of output inertia, the system exhibits no changes in closed-loop bandwidth but the achievable damping ratios increase. For reduced levels of desired output inertia, the frequency of the dominant pole pair remains almost constant, but the system exhibits a clear reduction in damping ratio. It is thus obvious, that adding input damping may only result in proper performance for a certain range of desired inertias (despite the stability guarantee) - see Figure 3.3.18.

The addition of first-order actuator/sensor dynamics to any model structure, resulted in reduced levels of achievable closed-loop bandwidth. The stabilizing effect of such first-order dynamics is thus obvious, and is shown to be independent of controller type. Changes in stability regimes were very obvious for the 2 DOF model, where we even experienced a reduction in stability below the levels of no-first-order dynamics. Stability margins could thus only be increased for values of first-order time-constants above a certain threshold. The effect on bandwidth remains independent of model structure though.

The stability and performance properties of systems with backlash are independent of the rest of the system dynamics, since we are primarily concerned with a dynamic system of reduced order. It is fairly obvious that we will decrease the stability margin and increase system oscillatory response (larger frequencies & lower damping ratios) if we increase the system inertia (and proportional gain also). Adding integral gains to the controller only worsens the problem by increasing oscillatory system response. Adding damping to the system which is not collocated has no stabilizing effect. The addition of collocated damping (via input-velocity damping for instance) has by far the largest stabilizing effect, as it increases the natural damping ratio levels. This is an important point, since it may explain why so many transmissions, being lubricated by the

manufacturer for life by adding highly viscous grease, have a limit-cycle instability if lubricated with a mineral oil of reduced viscosity. A good example was the cycloidal reducer which exhibited perfectly proper behavior when grease-lubricated, but had a limit-cycle behavior around the no-load setpoint when lubricated with mineral oil (the change in lubricant was done in order to reduce the stiction/friction behavior and increase the backdriveability of the unit). Another good example is that of the harmonic drive, which could be forced to remain stable at higher levels of controller gains, if the manufacturer-supplied highly viscous grease (BEACON 325) was used for lubrication, instead of pure mineral oil (backlash was not the problem here, but rather a large transmission stiffness soft-zone). The effects of discrete sampling rate are shown to be even more important for such simple systems, with reduced sampling rates reducing the stability margins and performance levels, irrespective of the controller being used. This statement is of course also valid for any of the other model- and controller-structures analyzed throughout this thesis.

Model Structures & Parameter Sensitivity

We have tried to solve some of the more important modeling questions that relate to understanding the true physical description of actuator/transmission/load systems. In the case of the 2 DOF model, the distribution of inertias (in order to represent the presence of an oscillatory mode) raised the question of what effect the inertia distribution had on the system's stability margin and performance level. Increasing the output inertia has the effect of increasing the system stability boundaries. The increase in system performance is only possible for a certain range of electronic damping coefficients, otherwise reducing the closed-loop system bandwidth as well as damping ratios. The increase in input system inertia results in a conditional decrease in stability up to the point where we have nearly matched impedances ($I_1=I_2$). After that point the stability margin increases again, resulting in reduced performance levels. This phenomenon can be seen to also be present in the 3 DOF model representation, indicating the necessity to properly select inertias during the design phase. The reason why increased input inertia is not recommended, is because it clearly reduces system bandwidth, without resulting in any conditional performance regimes, where the overall performance could be increased or at least maintained. The lowest stability regimes are observed for those systems where the reflected inertias are nearly identical. Thus for a 2 DOF model, that would be the case when $I_1=N^2I_2$, or in a 3 DOF model, when $I_1=N_1^2I_2+N_2^2I_3$ (N_1^2 and N_2^2 represent the local discrete ratios in

multi-stage transmissions). This behavior can be shown to be present, if we analyze the dominant stability requirement:

$$\frac{K_T(B_1+B_2+B_e K_f)+B_1 K_f-K_T K_f(1+K_e)(B_1 I_2+B_2 I_1)^2}{\{K_T(B_1 I_2^2+B_2 I_1^2)+B_1 B_2(B_1 I_2+B_2 I_1)+K_f I_1(B_2 I_1-K_T B_e I_2)\}} > 0$$

Plotting the value of the above expression w.r.t values of I_1/I_2 , reveals a minimum near $I_1=I_2$, which, since I_2 is a reflected value, means that the input inertia is equal to the reflected output inertia at that point. This phenomenon may be important in choosing not only motor-rotor inertia, but also the transmission ratio, so as to optimize the stability regime and performance, especially in a system where the effective joint-inertia may be configuration-dependent, such as in a serial-link manipulator. The correct location of the minimum is a function of all the system parameters. The conclusions drawn above, are based on a numerical and graphical analysis only. A more rigorous theoretical approach may be able to shed more light on this issue, but is beyond the scope of this thesis.

The distribution of discrete dampers also plays an important role, since they have an important stabilizing effect on the dominant closed-loop pole pair. This is an important point, since it could answer the question as to where to place such an element as a shaft-seal in order to reap the largest performance and stability benefits from any transmission setup. Whether we are dealing with a 2 DOF or 3 DOF model, the addition of internal system damping always increases system stability boundaries. The drawback though, is that performance suffers, since we are also reducing the effective system bandwidth by increasing the dominant damping ratio. The system's sensitivity (whether in 2 DOF or 3 DOF model structures) to increases in passive system damping was shown to be largest for the situation of distal damping. Thus adding damping at the output was the most efficient way to increase system stability. On the other hand, since the damping values were all reflected by the local transmission ratios, such behaviors could only be achieved through N^2 -times larger damping coefficients. In effect we would be requiring 'mammoth' dampers as close as possible to the output, to achieve the same effect an N^2 -times smaller damper could achieve at the input-end. Adding electronic damping based on a non-colocated feedback measurement (output-velocity or force-rate) does not have stabilizing effects like adding input-velocity damping has (electronic damping based on colocated velocity-feedback for instance). We have shown earlier that stability may be guaranteed, but only at a certain reduced/increased performance level which may still not be suitable for all task scenarios (since it results in an asymptotically constant damping ratio). The use of

a passive damper is always recommended over that of an active electronic damper, since in essence it delivers damping torques which are based on an (ideally analog) signal that is not subject to discretization nor noise-levels. The actual application of such damping torques is then also independent of any torque-discretization or break-away levels present in any real analog current-loop motor-system.

The question of transmission stiffness distribution is probably the most interesting one, and requires that a distinction be made between 2 DOF models and 3 DOF model representations. In the case of 2 DOF models, it was shown that non-colocated position-control can result in unstable behaviors for stiffening spring transmission characteristics if we use a PD torque-controller. The same was found to be true in the case of torque-controlled transmissions. Stability regimes continuously decreased, until the transmission stiffness reached a certain value, beyond which any further increases resulted in increased stability regimes. This was shown to be extremely important, since the selection of controller parameters may result in a stable system only for certain effective transmission stiffness values. Since most transmission stiffnesses increase with increased applied loads, it would seem obvious to imply that a system can go unstable at larger torque-levels than at lower levels of transmitted torque. Thus handling situations of contact acquisition or increased loads during contact, could be termed task-scenarios in which such a stability constraint may result in undesirable behavior (increased oscillatory behavior and possibly instability). This stability constraint was present mostly at large levels of force-rate damping. Such high-gain damping schemes may be very hard to implement, due to the constraints of obtaining an accurate, noise-free, in-phase estimate of force-rate. Such predicted behaviors may thus be hard to observe, due to hardware constraints. The increase in sensor stiffness was also shown to be of a destabilizing nature in any PD torque-controlled 2 DOF system. If output-velocity instead of force-rate is used for damping purposes, the system will exhibit reduced stability until the ratio of K_P/K_T crosses a certain threshold, after which the stability boundaries will (marginally) increase again. The net result of increasing transmission stiffness is that closed-loop bandwidths are can be increased, but at the expense of continuously reduced damping ratios. The system response will thus become more and more oscillatory and underdamped. The addition of input-velocity damping can avoid system instability, by increasing the damping ratio to certain physically achievable levels which may still be too underdamped for certain transmission or task scenarios.

In the case of the 3 DOF model representation, we were able to show, that increasing the distal (K_T) and proximal (K_S) transmission stiffnesses has drastically different effects.

In order to avoid instability problems for a stiffening proximal transmission stiffness K_s , it was found that increasing K_s to the point where the ratio of K_s/K_T lies at or above unity, results in the most conservative and desirable stability guarantees. The benefit of insuring such a threshold can be seen in increased system bandwidths, irrespective of the controller type used. The design of the WHOI cable reducer has an actual K_s/K_T ratio that lies around 1.8, thus insuring the largest bandwidth possible, while avoiding instabilities due to stiffening spring behaviors. Increasing the distal stiffness K_T always results in an increased stability and performance (bandwidth) regime. The sensitivity of system performance to changes in transmission stiffness is greatest for the distal stiffness K_T . It is important to point out though, that such a step may not necessarily always be beneficial, since in the case of input-velocity damping (with or without integral control terms), the effective system bandwidth will approach a fixed bandwidth for increasing values of electronic damping. The increase in performance can thus only be achieved for certain restrictions on proportional and integral controller gains

It is also worthwhile noting the different behaviors that torque-sensor stiffness has on system stability and performance. For increased levels of sensor stiffness, a reduction in system stability was observed, which resulted in higher frequency oscillatory responses and reduced damping ratios. In the case of input-velocity damping, the stability of the system was only limited by the range of proportional gain (in the case of added integral control action, the integral gain would be important too). Added sensor stiffness would seriously increase system bandwidth, with damping controlling not only the stability of the system but also the asymptotic convergence of the damping ratio to some physically achievable value which would insure stability but possibly unacceptable performance.

CHAPTER 4

(4) TRANSMISSION FIDELITY STUDY

(4.1) INTRODUCTION

This experimental analysis and discussion sheds light on the different transmission behaviors that were observed in the experiments outlined below. The tests were designed to demonstrate the natural (and controlled) system behaviors of each transmission type analyzed and to test the transmission fidelity in terms of achieving desired impedance behaviors. We want to motivate the need for interplay between mechanical design and control analysis, especially as it applies to the area of robotics. Each of the different transmissions studied in this thesis was put through tests in order to measure such characteristics as backlash, stiction/coulomb-/viscous-friction, transmission stiffness, and impedance following fidelity (in terms of achievable stiffnesses only at this point).

The different sections on data analysis are split so as to provide a general overview of the data gathered and what the general implications are. But there are also separate sections on each different transmission type studied and the results that were obtained using the different test methods outlined in each section. We will outline and substantiate, with data presented in the earlier sections, what the general shortcomings and requirements are for, not only the transmissions considered here, but transmissions in general, as they relate to specific task behaviors. In the section on further suggested experiments, we will propose and outline further experiments necessary to fully complete this analysis. Those experiments are performed and discussed in the next chapter. The analysis in this chapter and the next, is to be seen as a comparative study in terms of variables deemed important in characterizing transmission fidelity/behavior for analysis/design and control purposes. The selected sets of comparative variables are also deemed important for issues such as force-control of robot-joints, and how certain factors can degrade/improve robot performance/stability for interactive task behavior. This issue will be experimentally addressed in Chapter 5.

(4.2) EXPERIMENTAL SETUP

Comparison of the different transmissions centered around understanding (1) how well different stiffnesses and dampings could be achieved, (2) what were the physical phenomena responsible for such behavior, and (3) what compensation (if any) was possible and successful in assuring a higher fidelity in impedance following. The idea will be to perform certain experiments that will illustrate how these physical phenomena affect task behavior. The different transmissions that were tested, were:

<u>TRANSMISSION TYPE</u>	<u>REDUCTION</u>
WHOI Cable Reduction	(30:1)
H.D. Harmonic Drive	(60:1)
SUMITOMO Cycloidal Reducer	(29:1 & 59:1)
KAMO Ball Reducer	(10:1 & 30:1)
DOJEN Cycloidal Cam Reducer	(33:1)
REDEX Planetary Cycloidal Gear Reducer	(30:1)

These six transmission types were chosen because they represent the most common and more interesting transmission types currently in use or could be considered potential candidates for robot manipulator transmissions. They were chosen because of their high stiffness, backdriveability or because of innovative design. Excluded from this analysis were hydraulic or pneumatic and friction drives, as well as direct-drive systems.

The cable reduction transmission idea has been revived again at MIT and Woods Hole, and 2 new manipulator prototypes have been built and are currently undergoing testing. The harmonic drive is one of the most widely used transmissions in robotic applications and is the main component of the actuator packages made by SCHAEFFER MAGNETICS that are being delivered to MARTIN-MARIETTA for use as the actuation devices of the FTS (Flight Telerobotic Servicer) for the US Space Station. The cycloidal reducers are some of the more rugged, tried and tested robot transmissions and therefore warrants attention for comparative purposes. There are three types that will be compared in this study. Others may be hybrid cycloidal types, but are listed separately for clarity. The Ball reducer is the latest addition to the family of different transmission candidates for robot manipulators. It has been developed by KAMO/TODEN of Japan and is based on a turn of the century invention in Europe. In addition a few interesting tests were run on the brushless DC motor that was used to test all of these transmissions, in order to understand its behavior and the effect it has on the data.

This entire analysis is meant to illustrate the characteristics of different commercially available transmissions that are currently in use in the field of robotics. The idea is to try and establish how faithfully these different transmissions can reproduce a desired behavior imposed by the motor-controller. These different transmissions can then be catalogued in terms of how well they can reproduce a desired behavior - a new approach that may give a better comparative metric to the designer (in terms of choosing a transmission) and the controls engineer (in terms of deciding if and how to compensate for the expected errors between desired and actual behavior.).

The experimental apparatus used consisted simply of a solid rectangular base with supports to concentrically mount a SEIBERCO brushless DC motor, with a rotor mounted on dual bearing supports and a stiff coupling to attach the different transmission types to the motor shaft. Each transmission had flanges or keyed shafts (special tapered keys were ground to insure an interference fit and zero backlash at the mounting interfaces) that could be interfaced to the motor shaft and the attached force sensor. A JR³ torque-sensor was mounted to the output of each transmission and yielded all the force(torque)-data in this report. The position and velocity data were all obtained from the resolver built into the motor (used for commutation and the motor-controller). Motor-torque was obtained thru measurement of the motor-current - also supplied by the motor-controller (Analog Current Loop).

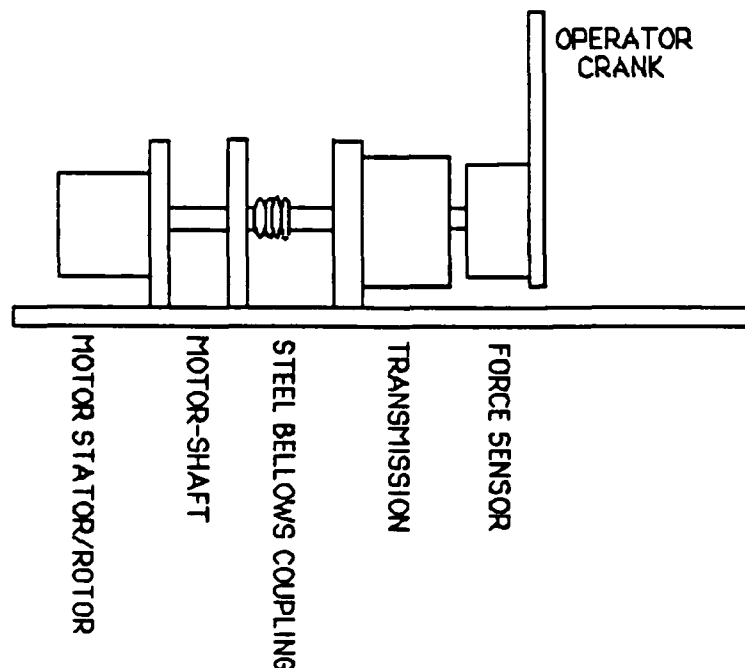


Figure 4.1a : Plan View of Transmission Test Stand.

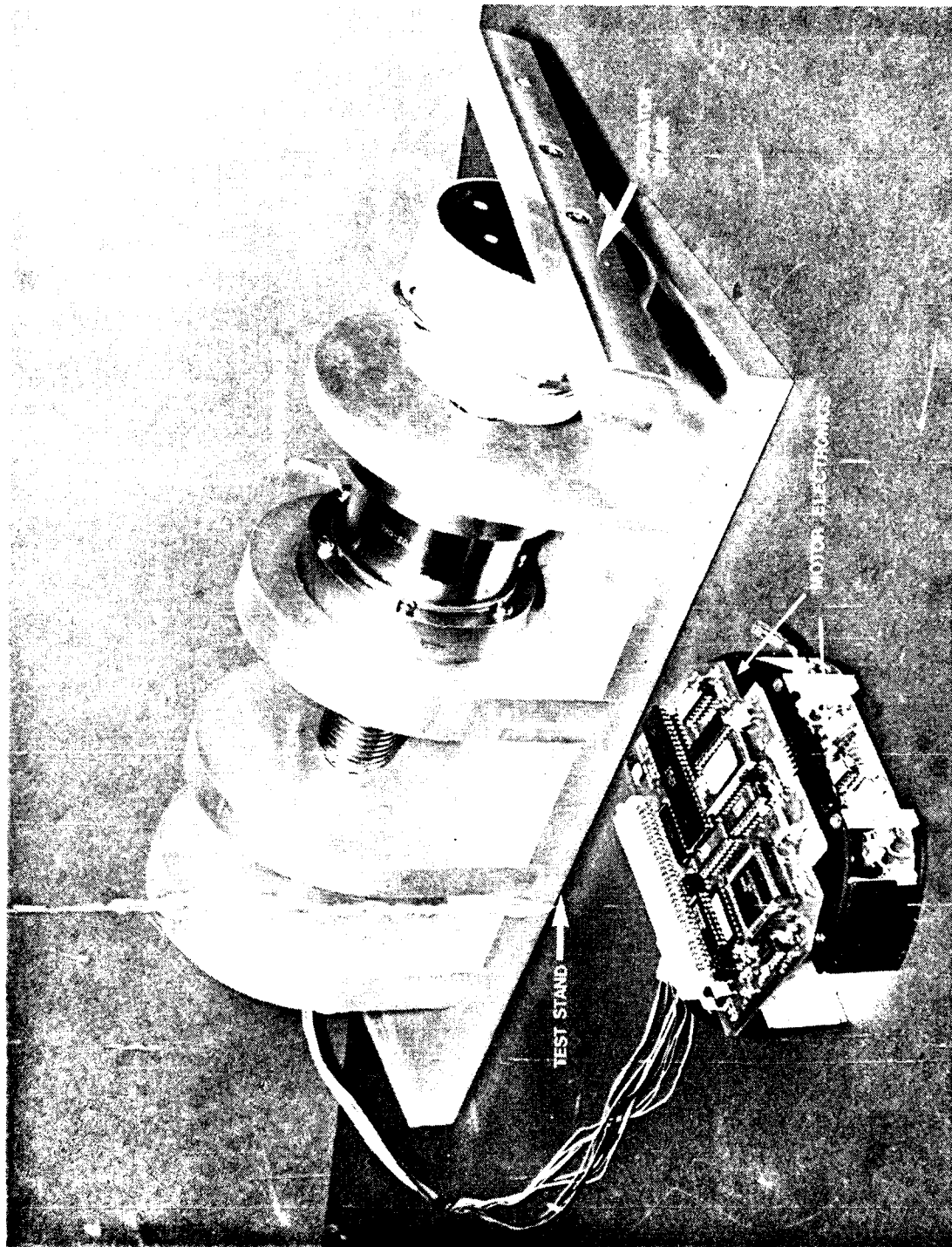


Figure 4.1b : Test Stand with mounted harmonic reducer, output torque sensor and the operator crank as well as the motor-controller card and power section.

A simple plan view in Figure 4.1a illustrates the experimental setup used for the testing of the harmonic drive, ball reducer and cycloidal reducers. Many mechanical details have been omitted for clarity's sake. Figure 4.1b shows a picture of the test stand, with the harmonic drive mounted, and the operator crank hooked up to the output of the torque sensor. This was the setup used for all transmissions for all the backdriving data that was gathered. The measurement of the transmission stiffness was performed by locking the output of each transmission to the support base, and applying torque to the motor shaft.

The entire motor setup was held to very tight tolerances in order to reduce any losses due to bearing-friction or misalignments in the system. The coupling between the motor-shaft and the transmission input was achieved via a steel bellows-coupling in order to compensate for misalignment. The stiffness of the bellows was chosen so as to deflect less than the positional accuracy of the motor under more than twice its full rated torque. The effective bellows-stiffness was chosen to be more than 3 orders of magnitude above the stiffest transmission tested in these experiments.

Delrin washers had to be used between the transmission outputs and the force sensor in order to reduce stray readings due to eddy currents, set up by the magnetic field of the motor (and other EMR sources), creating a ground loop (determining and isolating this phenomenon proved to be a major challenge and time-sink). All transmissions except the harmonic drive had external bearing-supported input and output shafts. The harmonic drive had to have a second bearing support built for it in order to properly align and support the output wavespline. All other transmissions were delivered with support bearings that insured alignment even for overhung loads.

The cable reduction was tested on a joint-by-joint basis, since the manipulator was fully assembled. The approach taken, was to mount the force transducer on the output of the joint #0 (which is the housing of joint #1) in order to be able to exclude gravity from the actual measurements. Vectorial addition was performed in order to compute the exact output torque and the error in the calculations was kept to a minimum by taking dimensions off the blue prints and precise machining of the support base for the sensor. The simple diagram of Figure 4.2 illustrates this setup.

CABLE REDUCTION & TEST SETUP

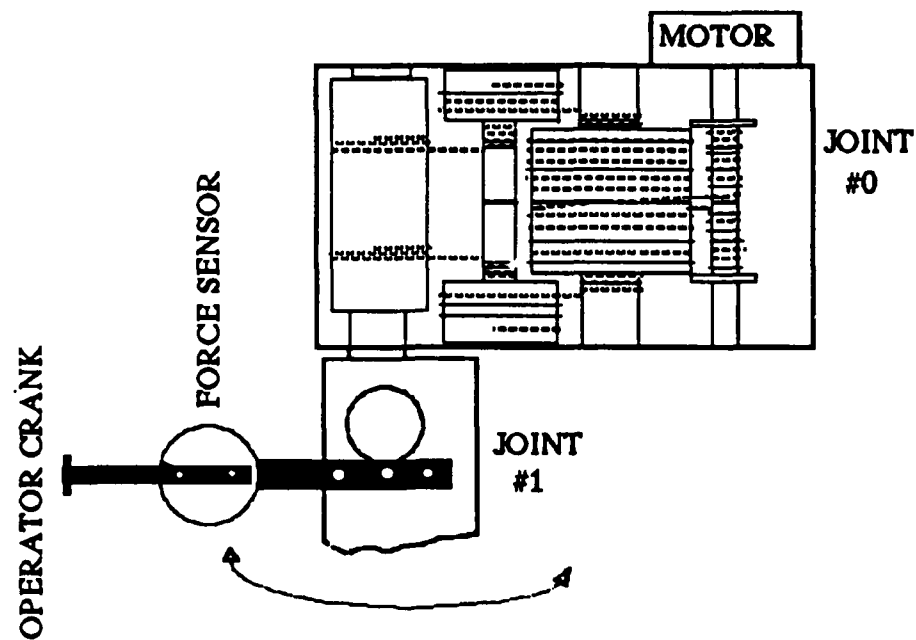


Figure 4.2 : View of Cable Reduction and Test Setup for experiments.

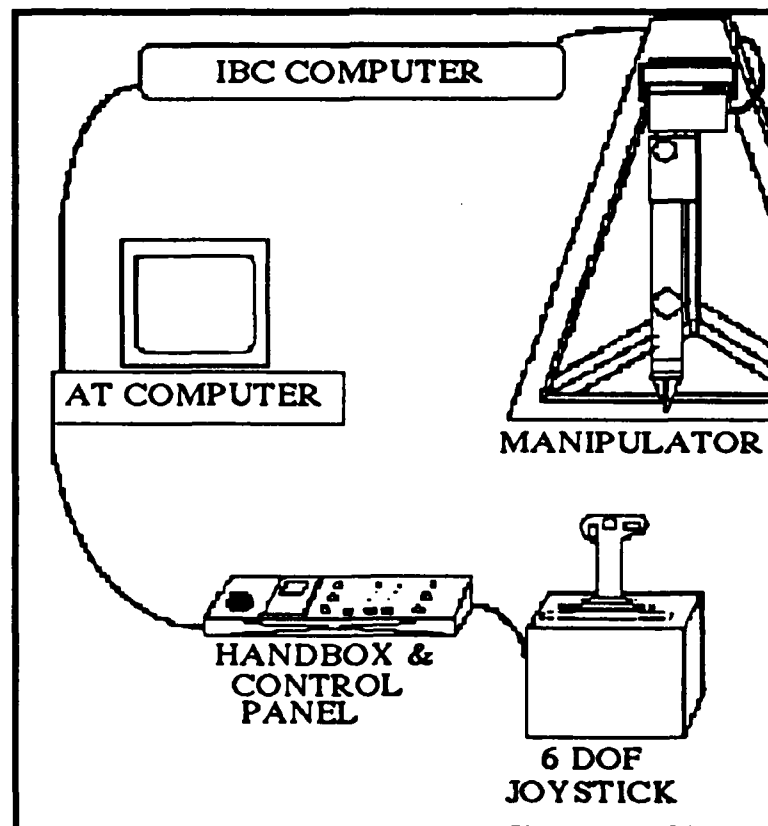


Figure 4.3 : Manipulator on Test-Stand during Laboratory experiments with IBC computer, Supervisory and Control Computer controlled via the operator handbox and rate-input joystick.

The software developed for the manipulator operational scenario as well as the handbox and joystick interface hardware/software were built/written and constantly modified to suit the test being planned. The overall test setup was a laboratory environment reproduction of the system's real world operational setup (the test stand becomes the underwater robot JASON). Figure 4.3 illustrates the components of the test hardware.

The manipulator was mounted on a test stand and the control/sensor cables were routed and interfaced to the bottom-side computer which usually resides in a 6 inch ID titanium pressure housing. Figure 4.4 shows a side view of the physical layout of the computer chassis. There are 5 main sections that can be identified as the blind-mate (male connectors to interface to wiring harness), the power-driver sections for the manipulator joint-motors (analog power-, commutation and sensing electronics for each joint), the actual computer chassis (with the IBC bus on the backplane), the force sensor electronics (for the wrist force/torque transducer) and the power regulation and conditioning section (DC to DC converters and regulators).

IBC COMPUTER CHASSIS

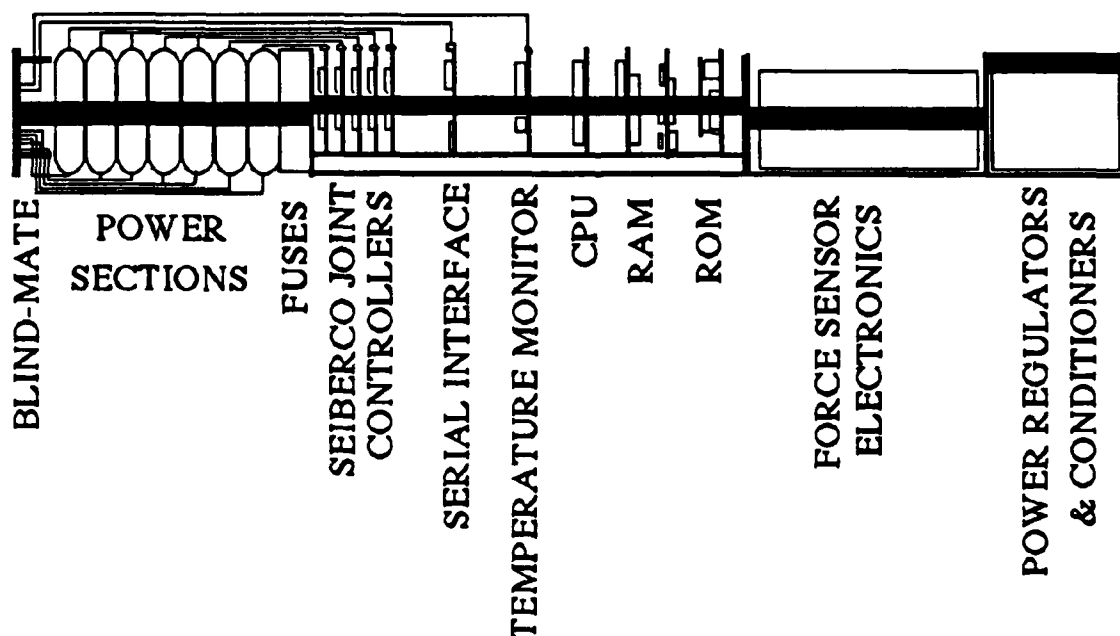


Figure 4.4 : Manipulator Computer Chassis with its separate sections of this 6" OD oceanographic's standard computer hardware.

The manipulator computer chassis (shown above in a simplified plan view) consists of 7 power sections (termed pancakes due to their form factor) and the associated 5 joint-controller cards that were plugged into the computer chassis. The manipulator consists of 3 rotary joints (using a total of 5 power cakes), and a 2-function wrist consisting of continuous wrist-rotate and jaw open-close (2 power cakes, where one drives an electric motor through a piston and displaces hydraulic fluid to operate the powerful multi-fingered claw). These controller cards, manufactured by SEIBERCO, are the bases for the individual CPUs that perform communication, sensing, commutation and control for each joint (or motor) separately. The bottom-side computer chassis is controlled from the IBC (Instrument Bus Computer) hardware that shares the computer bus. It consists of a modified 80C86 CPU (basically a low-power modified IBM XT-architecture suited for oceanographic tasks) that has support-RAM and -ROM, while communicating with the controller boards via shared DPRAM. The internal event clock interrupts the processor at 20 Hz and the on-board program, running under the real-time operating system VERTEX, wakes up and enables/disables certain tasks according to a pre-programmed schedule. The main task of the bottom-side software loop consists of handling the communications between the topside supervisory computer and the bottom-side joint-controllers. It basically gets/places data from/into DPRAM of each controller and decodes/packetizes the data streams coming/going from/to the supervisory program running on the topside computer. A parallel communication scheme was added to increase the overall communication bandwidth to 400 Hz.

The topside computer is an 80386 10MHz based AT clone running under MS-DOS with code developed with MICROSOFT C. The topside software performs a whole variety of tasks necessary to control the manipulator (sequential program with a simple state-machine coordinating tasks at different levels). It interfaces to the custom-built controller handbox and joystick, computes desired joint setpoints depending on whether joint- or cartesian-space control is selected, updates gains, watches temperatures, torques, motion limits, etc. and alerts the operator by displaying all levels of information on different windows/pages of the computer display. Selections as to operational modes of the manipulator are made entirely from the handbox, and the operational mode excludes the keyboard entirely, except that the engineer on duty uses it to page through the display to monitor the 'health' of the system during operations. Setpoints are commanded via the rate-input device - a simple 6 DOF joystick.

(4.3) DATA TRENDS AND COMPARISONS

The purpose of this section is to analyze the data in greater detail by using certain simple concepts. These concepts are based on the fact that different transmissions have different levels of undesirable nonlinearities. The main nonlinearities affecting the individual impedance parameters are analyzed separately and data is presented in each case to support these claims.

The data is presented in 2 sections. The preliminary test data for all the transmissions examined are presented in the first section and demonstrate general trends apparent in the data, which will be explained via linear/nonlinear physical phenomena. The second section will take a more specific look at each transmission and reveal some of the finer details in the testing procedure and the data gathered. This section became necessary not only for documentary purposes but because interesting trends were discovered through the initial analysis which led to further experiments in order to explain unexpected and sometimes unstable behaviors.

(4.3.1) General Data

In this sub-section we will look at overall transmission behavior with respect to the desired impedance parameters (stiffness and damping). The purpose is to understand the difference in system fidelity of the tested transmissions. The outcome is a clear ranking of each transmission with respect to its pros and cons for use in robotic applications. The analysis in this section however is not final, since several hardware and software modifications were tested and proved to highlight problems and advantages inherent in some of the transmissions being analyzed.

(a) IMPEDANCE FOLLOWING - Stiffness

Stiffness behavior was tested with quasi-static experiments, where the output-joint was moved slowly through a full ± 360 degrees of motion, and the force (measured at the output-shaft by a 6 DOF force/torque sensor from JR³) and displacement (measured as the motor displacement from which we inferred the output motion via the transmission ratio N) data were logged. The motor was commanded to behave like a pure spring with constant levels of stiffness using a purely proportional controller. The rate at which the output was

manually moved was slow yet continuous enough to insure continuous motion, once the system broke away from its rest or no-load position. Some reducers had friction characteristics that would sometimes cause stick-slip behavior, and result in spikes in the data. We will comment more on that in the individual data sections. Some very interesting results were found that can be explained fairly well by classic nonlinear stiction/coulomb-friction in the transmission stage.

Shown in Figure 4.5 is a typical behavior for a transmission with (a) pure stiction, (b) pure coulomb-friction and (c) a combination of the two - note that the relative values of F_s and F_k make for quite distinct behaviors.

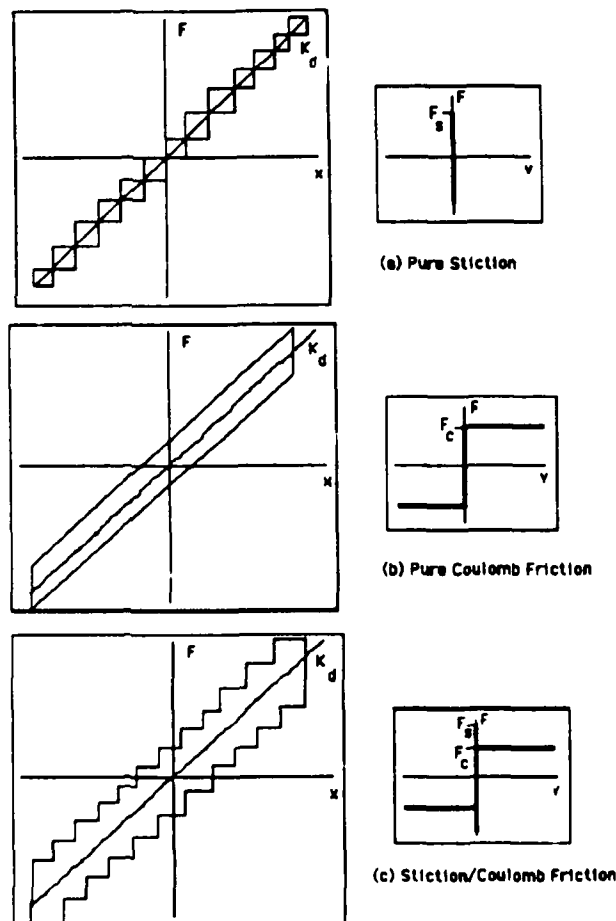


Figure 4.5 : Typical Stiffness Behaviors for real transmissions.

The behaviors synthesized in Figure 4.5 are present in every transmission that was tested. Even the most ideal transmission (cable reducer) displays this behavior, which is independent of system stiffness. This can be shown with data taken for the cable reducer's

stiffness behavior at 3 different levels of stiffness values (see Figure 4.6). The scales are expanded around the zero crossing to show this behavior.

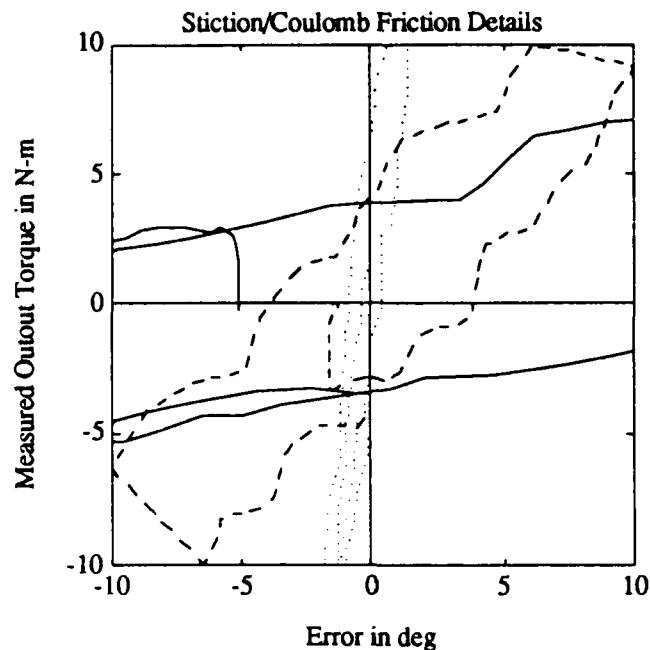


Figure 4.6 : Stick-Slip Behavior in the 30:1 Cable Reduction of the Underwater Manipulator.

The area contained inside each trace represents lost work. The power loss is attributed to the stiction and friction phenomena in a transmission. The theoretical energy-loss can simply be computed from the graphical representation of Figure 4.5(c) if F_s and F_c are known. Once again in every transmission that was tested, F_s and F_c had different values which differed substantially from each other and amongst different transmissions.

Stiction and friction are not the only phenomena that can cause a mismatch in stiffness. The physical layout of each transmission is such that there should always be rolling contact between force-transmitting members. For a geared mechanism, the tooth-profile is involute, causing the teeth to roll when they are engaged - like in the planetary-gear arrangement of the harmonic drive. The cycloidal reducer has a different design in which the inner gear of its planetary gear-arrangement has no teeth but rather a precision-machined profile in order to roll on pins fixed to a disk. Yet another approach is to have two eccentrically located circular plates with 'sinusoidal' machined grooves on their inside faces riding on top of each other, separated by especially hardened steel balls that run in those machined grooves (principle behind the ball reducer). In every case, the rolling members have a spatially dependent ability to perfectly transmit torque. Since there always

is some sort of spatially dependent friction, each transmission will have its own level of so-called torque-ripple. In some transmissions this phenomenon is more pronounced than in others.

The plots in Figure 4.7 show comparative behaviors for a low value of desired stiffness. The six traces shown are those for the KAMO Ball Reducer, the WHOI Cable Reducer, Harmonic Drive, REDEX Corbac Reducer, SUMITOMO Servo-Match Reducer, and the DOJEN Cycloidal Cam Reducer. A few obvious conclusions concerning stiction, friction and torque-ripple can be drawn from the above plot. All these different transmissions behave differently and each of the phenomena evident in this plot will be dealt with separately.

The traces with the largest ripple were generated by the harmonic drive and the SUMITOMO cycloidal reducer. They not only display large ripple as the transmitted torque increases, but also show that the friction and stiction levels are much higher than for any of the other transmissions. In the case of the harmonic drive, the stiction/friction stick-slip behavior is quite strong and the measured spatial distribution of the torque spikes correlates very well with the intertooth spacing on the flexspline (output). Each time a tooth engages and disengages, gives rise to a large torque spike. This phenomenon is typical for the harmonic drive, which despite the presence of involute teeth profiles on the spline ring and cup, has very short teeth which reduce the area over which torque is transmitted. Furthermore, since the tooth-height is specially dimensioned to account for cup-deflection, and since deflections are torque-dependent, tooth contact-area changes with increasing transmitted torque. Having several teeth engaged (forced fit via the wave generator) reduces the backlash to virtually zero, but gives rise to increased friction. As the contact force between teeth rises, the ripple effect becomes more and more pronounced. Any kind of misalignment greatly affects the surface area of meshed teeth and their orientation (remember that the wave spline which is the output is in the shape of a cup and physically deforms into an ellipsoid under load).

The SUMITOMO cycloidal reducer exhibits large stiction and ripple phenomena which are most probably due to the dimensional preload on its components. The achieved reduction in backlash has resulted in an extremely inefficient drive, whose ripple-torque can be traced back to the rolling contact with the rollers on the outer housing. The use of lubricants with different viscosities has a very large effect on the drive's efficiency. We removed most of the excess grease and replaced it with lower viscosity mineral oil. The manufacturer's requirement that the oil bath be as complete as possible was maintained throughout the experimental phase.

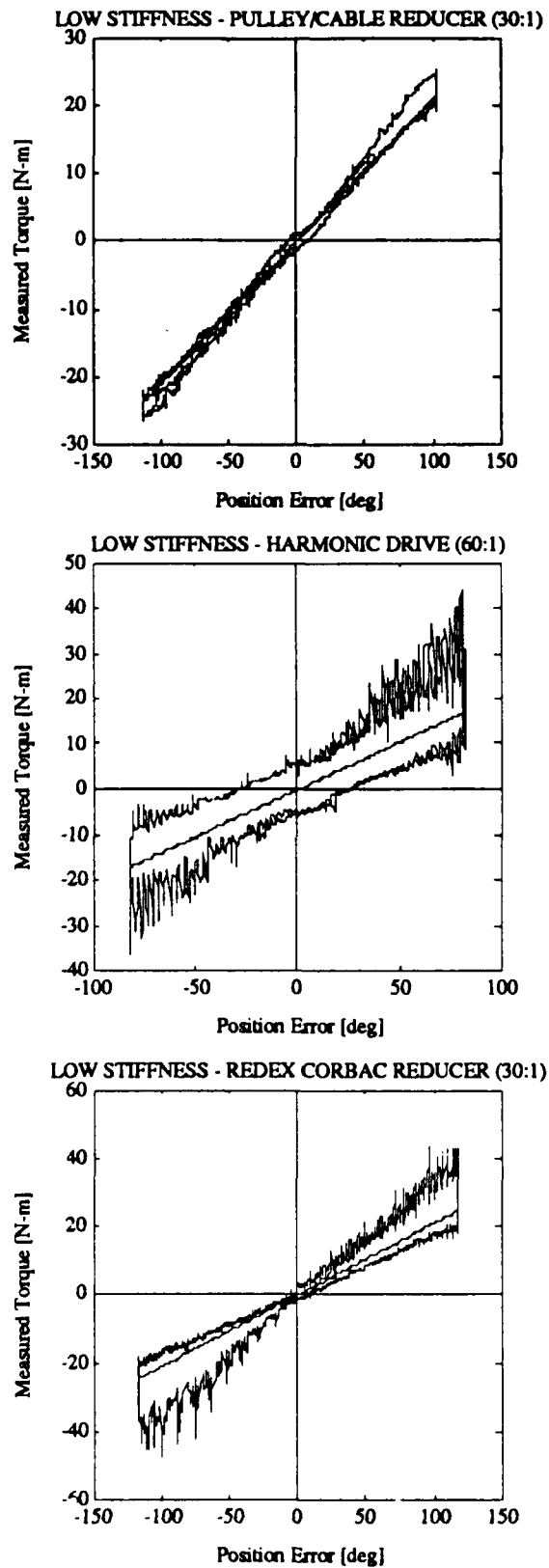


Figure 4.7(a thru c) : Low Level of desired (0.21 N-m/deg) and actual output stiffness for the WHOI Cable Reducer, Harmonic Drive, and the REDUX Corbac Geared Cycloidal Reducer.

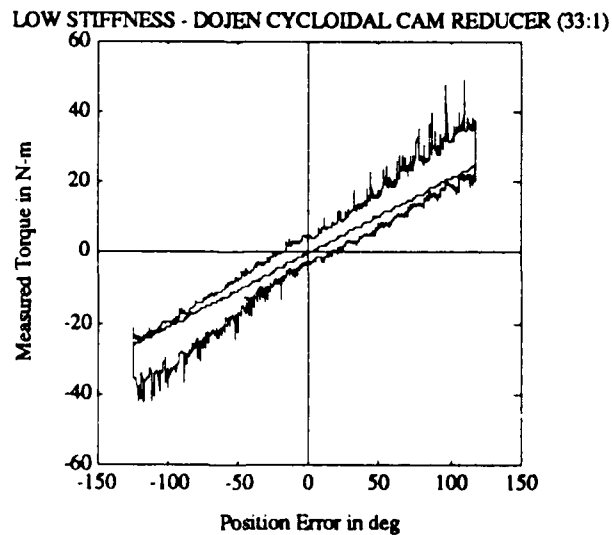
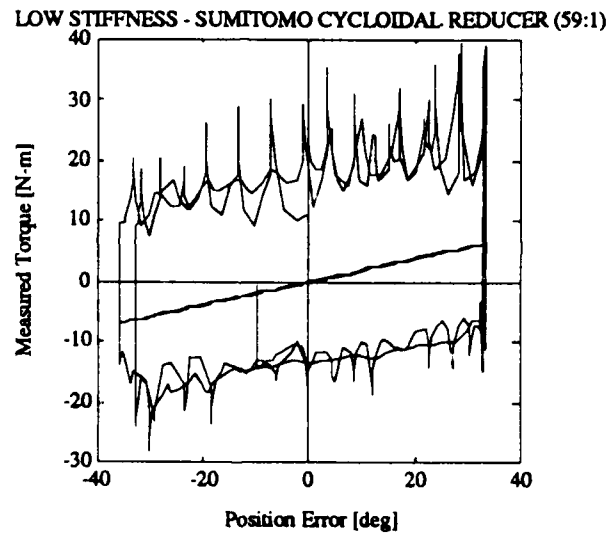
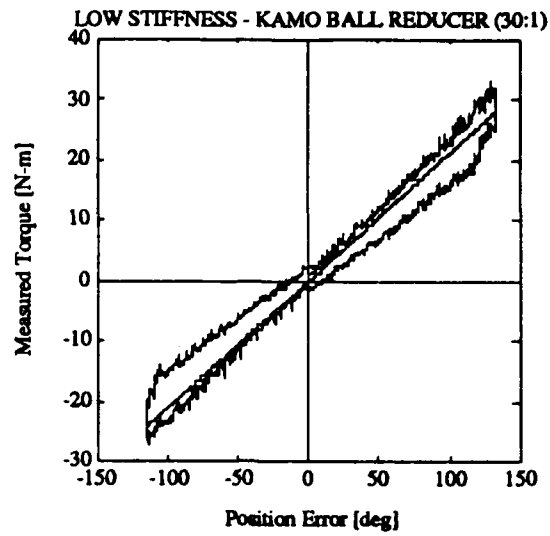


Figure 4.7(d thru f) : Low Level of desired (0.21 N-m/deg) and actual output stiffness for the KAMO Ball Reducer, SUMITOMO Cycloidal Servo-Match Reducer, and the DOJEN Cycloidal Cam Reducer.

Even then the unit still had output break-away torques that amounted to 50% of maximum motor torque. In order to make this a useful drive, the motor would have to be sized according to these figures, and even then closing a torque-loop around such a high-friction transmission would be quite challenging - a claim which will be proven in the next experimental chapter.

The DOJEN cycloidal cam reducer, and the REDEX Corbac geared-cycloidal reducer exhibited similar behaviors. The hysteretic energy losses are almost identical, but they are distributed differently. The REDEX reducer has a lower break-away torque than the DOJEN reducer, with the frictional losses increasing as the transmitted torque increases. This phenomenon is typical of most geared transmission, but becomes more pronounced in preloaded gear assemblies. The flaring-out of the hysteretic stiffness trace for the REDEX reducer is also accompanied by increased levels of ripple torque. These ripples can reach levels of about 10% to 15% of transmitted torque levels. Such high levels of ripple torque are quite possibly due to manufacturing tolerances in the involute tooth profiles, as well as in the assembly and preloading of the crown- and ring-gears. The REDEX reducer has these ripples present over all levels of transmitted torque, and mainly when the unit is backdriven from the output. Forward driving the unit from the input, it becomes hard to detect any appreciable ripple levels - they are present nonetheless. The DOJEN reducer has a similar ripple phenomenon, which may coincide with the passage of cam lobes past the rolling pins. Due to such (almost) pure rolling motion, the ripple is reduced to levels around 5% to 10% of transmitted torque levels.

The two transmissions that followed the desired stiffness behavior most faithfully, were the WHOI cable reducer and the KAMO ball reducer. In the case of the KAMO reducer, the hysteretic behavior clearly indicates larger levels of internal frictional losses, which are only slightly dependent on transmitted torque. The level of torque ripple was well below the 5% level. The data shown here, represents the specially designed 30:1 reducer made by KAMO to our specs. Another commercial unit, with a 10:1 reduction was also tested, and shown to be at least as efficient as the cable drive, except that it had other stiffness- and stability-problems, as well as appreciable ripple, all to be outlined later in this chapter. The 30:1 reduction will now always be used as the representative transmission from this manufacturer.

The trace for the cable reduction shows extremely small levels of hysteretic losses, which translate into low levels of internal friction and thus high efficiency. Frictional losses are almost completely independent of transmitted torque, and ripple torque is almost negligible and then also just slightly dependent on levels of transmitted torque. The actual

friction levels are certainly dominated by bearing friction. This was determined by comparing a pre-tensioned stage, to an untensioned stage. By preloading the transmission, the radial loads on the bearings increase the rolling friction, and thus the losses measured at the output. The break-away torque for this transmission is thus mainly due to the pretensioned cable stages running over pulleys running in bearings, which offer some rolling resistance, which is known to be dependent on radial bearing loading. This trace was obtained by running the transmission completely immersed in oil with a dynamic friction seal on the output shaft. The friction effects of the CRANE seal were very carefully tested and documented, and its effects were removed from the data set. The frictional characteristics of the seal accounted for about 50% of the frictional losses of the transmission (about 1.5 N-m break-away torque, with a running torque of about 1.2 N-m).

Notice that the REDEX, the HARMONIC DRIVE and the KAMO reducers experience a very interesting frictional phenomenon. The HARMONIC Drive has a fairly constant coulomb-like loss which is independent of load and direction of motion. The desired level of stiffness bisects the hysteretic trace almost perfectly. On the other hand, the REDEX reducer experiences a much larger coulomb loss and ripple when the unit is backdriven (the restoring motor-torque and the direction of motion are opposites) than when it is being forward driven (the restoring torque and the direction of motion coincide). The complete opposite behavior can be observed for the KAMO reducer. This directional dependence of frictional losses is very important, as the variation can be quite large. No discrete number of cascaded stiction nodes can emulate this type of behavior accurately, pointing at a more complex mechanism which can at this point not be clearly identified. The high degree of variability makes this behavior highly reducer dependent and thus a study would have to be highly empirical. Resolving this question would nonetheless yield very interesting answers and possibly aid in improving the individual transmission designs.

The energy loss contained within each actual stiffness trace is due to traceable physical phenomena inherent to each of the transmissions studied. If one studies the stiffness traces in the preceding discussion, one will observe that as the desired electronic input stiffness increases, the apparent energy loss is decreased. This is only partially correct, however, as without any compensation for these parasitic losses, the energy loss per unit displacement is the same, regardless of stiffness level. On the other hand, in systems where we are limited by such phenomena as torque-saturation, the energy loss is indeed decreased with increased stiffness. This is clearly shown in Figure 4.8, where two stiffness levels are shown together with real data (taken from the cable transmission for low and medium stiffness, without correcting for dynamic seal friction).

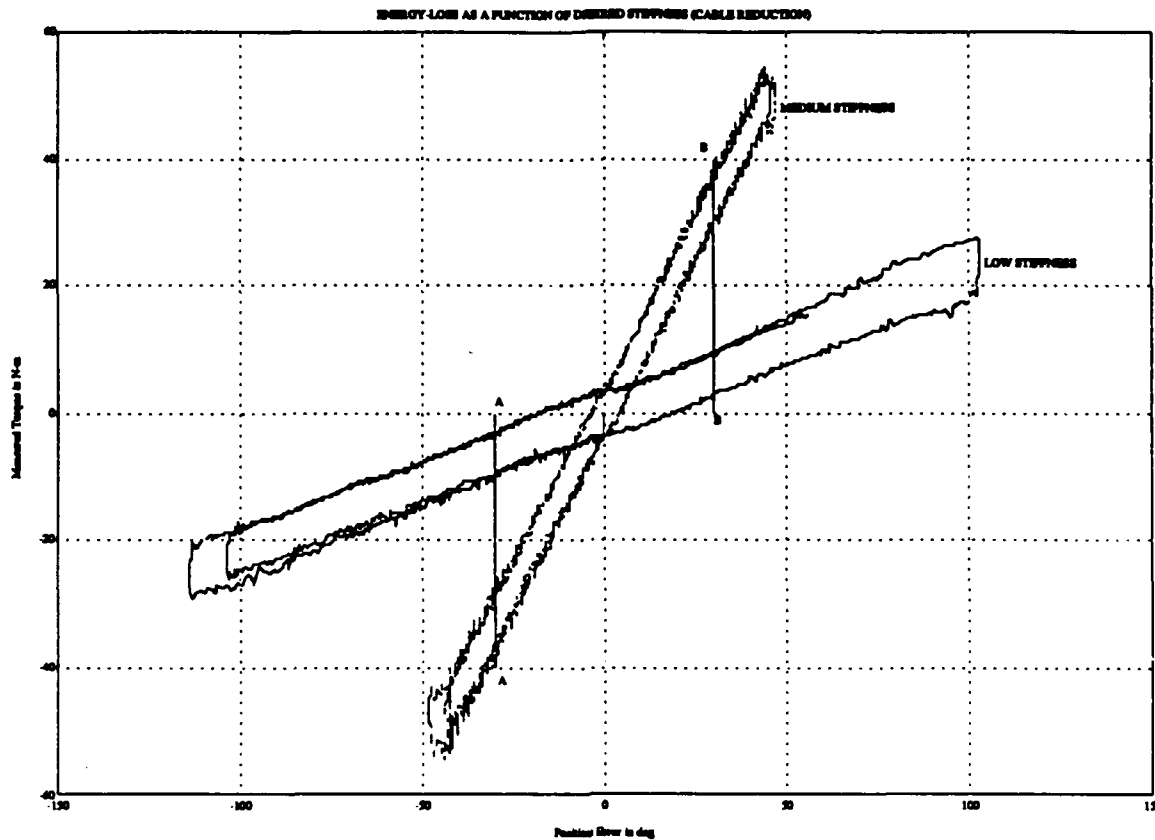


Figure 4.8 : Low and Medium Stiffness Traces for the Cable Reducer to show that energy loss is constant and not dependent on stiffness level.

The areas contained inside of each trace between the lines AA and BB are identical. If we tested this transmission up to the value of the saturation torque and computed the area inside each trace, we would see that it decreases with increasing stiffness levels. Notice how repeatable and constant the break-away and hysteresis behaviors are, and how unaffected they are by the amount of transmitted torque. The ripple in the observed data is very small, and after performing a torque-linearity test on the motor (shown in Chapter 5), it becomes hard to say whether the ripple is introduced by the motor, or whether it is due to rolling friction properties of the bearings. The relative magnitudes of ripple are consistent with both phenomena. This phenomenon thus certainly warrants more careful study.

Not only the energy loss is reduced with increased system stiffness, but also the lack of fidelity in stiffness-following. If for a given error in displacement x_e we implement two different desired stiffness levels K_1 and K_2 (where $K_2 > K_1$), and we have a certain value of force error due to stiction/friction/ripple ΔF , we can represent it in a stiffness diagram as shown in Figure 4.9.

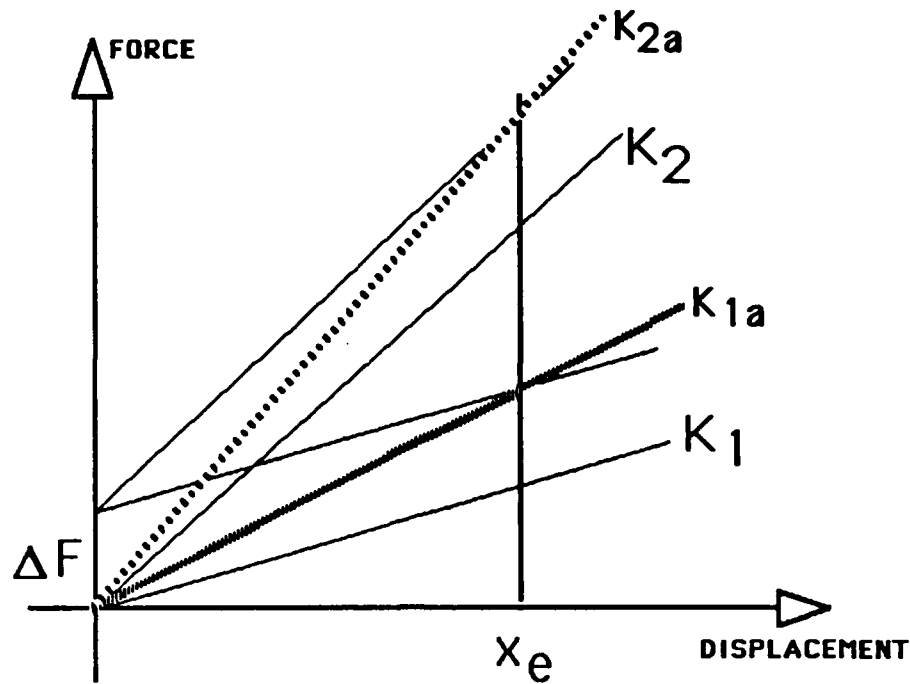


Figure 4.9 : Error in achieved stiffness is related to level of desired stiffness - Error decreases with increasing stiffness.

The ratio of actual stiffness to desired stiffness is in error by

$$|K_{1a}/K_1 - 1| = \Delta F/(K_1 \cdot x_e)$$

and

$$|K_{2a}/K_2 - 1| = \Delta F/(K_2 \cdot x_e)$$

Since $K_2 > K_1$, the ratio of stiffness following errors is simply the ratio of K_1/K_2 (following error is inversely proportional to desired stiffness levels) and we can easily see that the stiffness following error is smaller for the larger desired stiffness level.

Another interesting aspect of achievable stiffness levels is that the trace for any desired stiffness value would also be smaller (reduced energy loss) for increased speeds, up to certain values. This can easily be explained by the fact that we are now mostly dealing with frictional forces that are lower than the stiction torque (break-away torque) in a transmission. This phenomena would only remain present until the viscous and coulomb torques add together beyond certain speeds to yield a larger dissipative torque than the value of the break-away torque. There is no data shown here to support this theory,

because even though present it only represents a marginal effect with respect to stiffness fidelity.

(b) DAMPING - Stiction, Coulomb-, and Viscous-Friction

The test performed for pure damper behavior consisted of implementing a purely viscous motor behavior via proper choice of the discrete motor gains. The experiment involved backdriving the transmission from the output, logging the applied torque at the output, as well as the velocity. The latter was inferred from velocity measurements at the motor-end. The static measurements for stiction and break-away were obtained by slowly increasing the output torque, until break-away was detected by a few successive non-zero velocity measurements. Data for the non-zero portions was obtained by logging only those data points, where the measured velocity was constant (within the noise- and sensor resolution level) over a few samples. This process makes the data gathering a very long and tedious process, if data is to be gotten for (ideally) all positive and negative speeds. This process though, results in data sets which are extremely clean, even if they have a small 'fuzz' band. Using this type of backdriving measurement is better than a forward-driving experiment, since the discretization level of the torque sensor at the output, is much smaller than that of the motor-torque controller. Furthermore we do not have to compensate for any speed characteristics, as would be necessary in the motor case, since the applied torque depends on the speed of the input shaft.

Each transmission has a natural damped behavior that can ideally be described as in Figure 4.10 shown next. The level of stiction in the transmission may vary with direction of motion as well as the level of viscous friction (notice that B_1 need not be equal to B_2). It was generally found that all transmissions exhibited a more or less saturating viscous damping behavior as shown in the two curved traces in the Figure 4.10(a). This natural level of damping in many cases can be very large and account for overly damped system behavior. In most cases the true damped behavior of any transmission could be idealized by the second graph (Fig. 4.10(b)) above. The motor controller is locally implementing a desired damped behavior equal to B_{des} , while in reality the true damped behavior lies on the thickly drawn line with a slope of B_{actual} (once again, even though not shown here, the stiction- and slope-values need not be omni-directional). The different transmission types that were tested had different levels of such a non-ideality. The data gathered did not always fit perfectly on a line, but was very evenly distributed about the (non) -linear damping computed from a simple non-linear regression analysis.

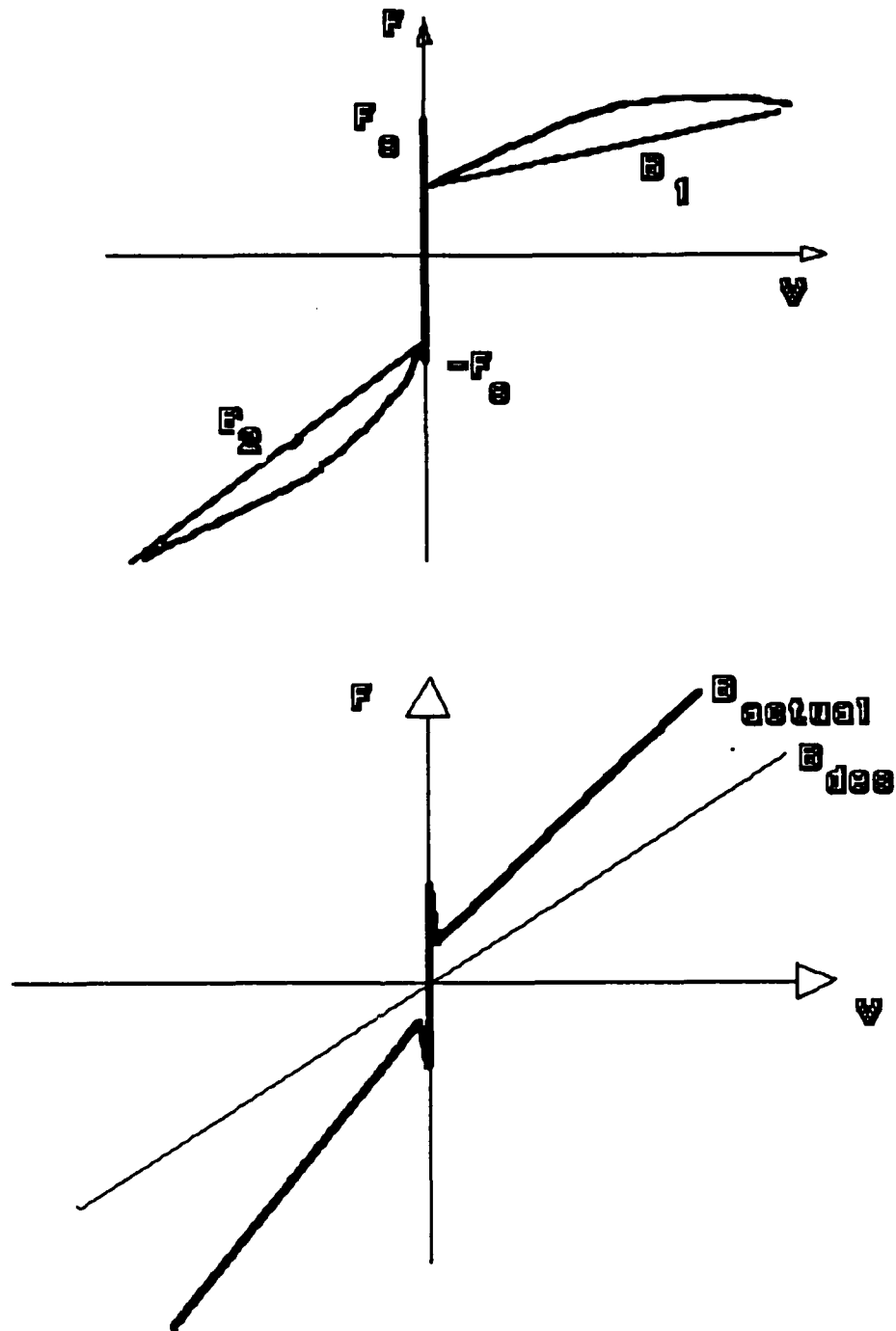


Figure 4.10 : Realistic Natural Frictional/Viscous Loss Behavior in Transmissions: (a) Saturating Viscous Loss with different levels of Stiction/Friction/Viscous Damping and (b) Linear Viscous Losses with different levels of Stiction/Friction/Viscous Damping.

Next we show a plot with a representative data set for four transmissions (Figure 4.11). The selected viscous damping coefficient was chosen so as to prevent actuator saturation at the highest speed that would be needed for the underwater manipulator.

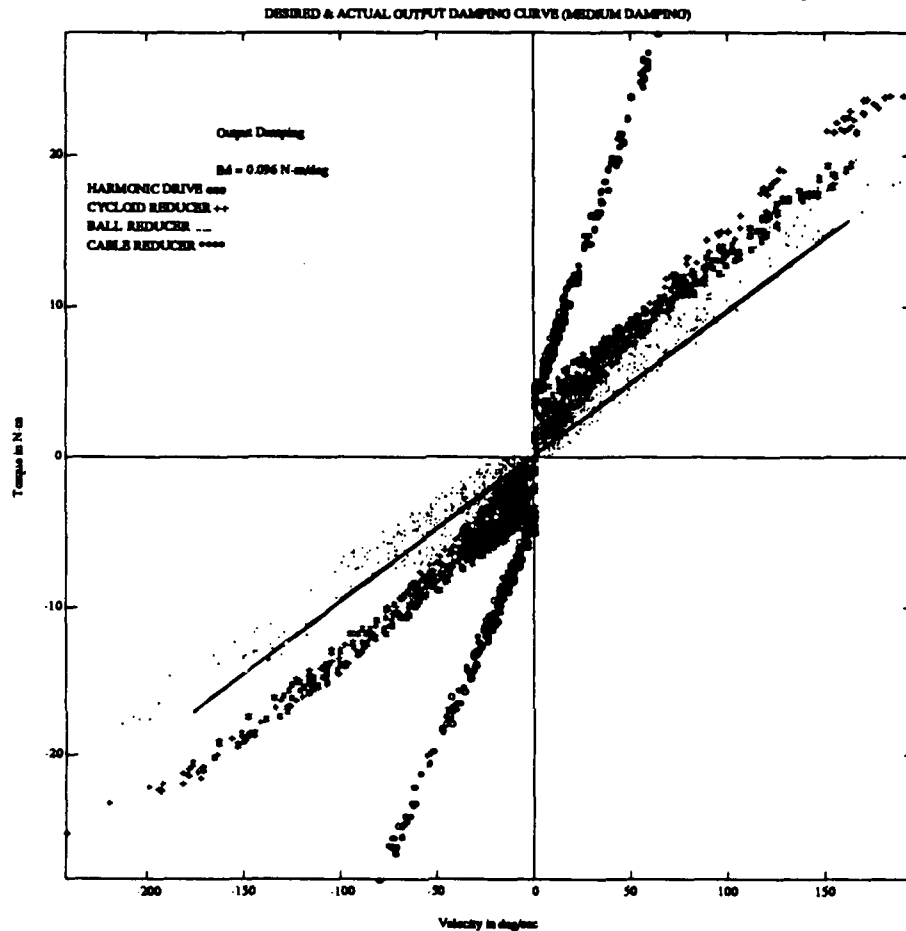


Figure 4.11 : Desired and Actual Damping Behavior for (a) Ball Reducer, (b) Cable Reducer, (c) Cycloidal Reducer and (d) Harmonic Drive.

Each transmission has a different symbol for its data set. Notice also that no effort was made to clean up the data; raw and unaltered data is shown (only corrected for inertial forces by enforcing a multi-sample zero-acceleration behavior). The test was run at different and widely varying speeds and data was collected while minimizing any inaccurate force readings due to inertial loads.

The solid line represents the desired viscous damping. The response of the (10:1) ball reducer (dots) comes closest to the desired behavior (this was the case for all levels of desired damping), while the (30:1) ball reducer (not shown here - see dedicated section) does worse than the cable reduction. The worst fidelity was displayed by the harmonic

drive (little circles) and the SUMITOMO cycloidal reducer (not shown because the necessary plot scaling would dwarf the other reducer responses), whose damped behaviors are clearly following that of their own internal damping plus that of the desired damping, since these forces are additive. The cable reduction performed very well, since the industrial-version cycloidal reducer whose data is presented above, is a commercial version which has excessive backlash and created some serious stability problems (to be shown later). This industrial version of the cycloidal reducer was first bought under the assumption that it would perform according to the specs listed in the brochure. After removal of shaft- and bearing-seals, replacement of heavy grease with mineral oil, the unit's performance drastically changed. Increased backdriveability came at the price of sizeable backlash. This reducer was then replaced by its robotic version - the SUMITOMO F-Series cycloidal reducers, whose performance is tested in all the experiments to follow.

The best way to compare the relative transmission performances, is to compare the natural damping behaviors of the six main transmissions studied. In Figures 4.12(a & b) and 4.13, we can compare the relatively large differences in frictional losses for each transmission. These figures show completely unfiltered data, which has only been corrected for fictitious inertial loads, but is otherwise completely unaltered.

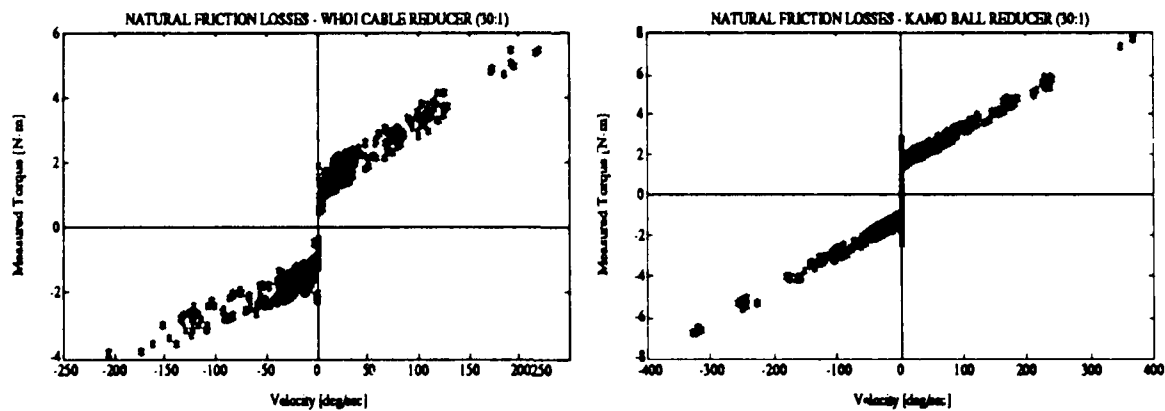


Figure 4.12(a) : Natural Frictional Losses for two different transmissions - (1) WHOI Cable Reducer, (2) KAMO Ball Reducer.

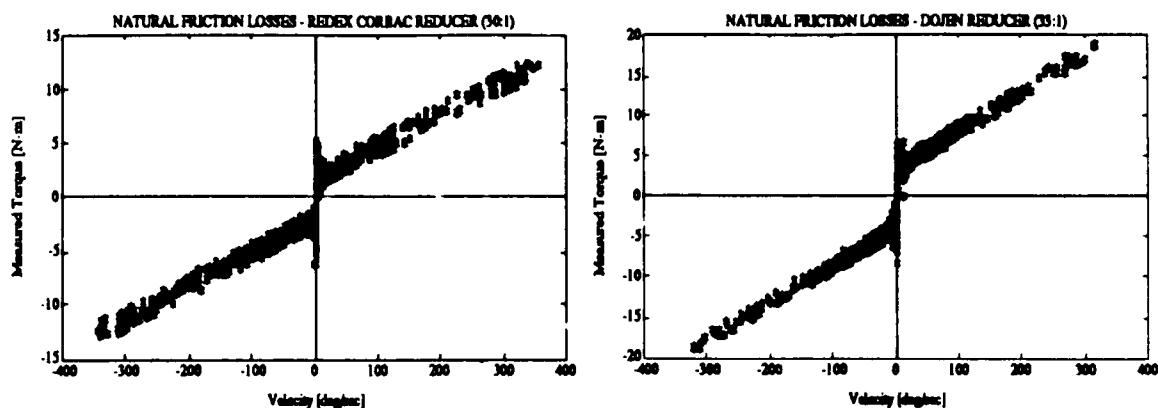


Figure 4.12(b) : Natural Frictional Losses for two different transmissions - (1) REDEX Corbac Geared Cycloidal Reducer , (2) DOJEN Cycloidal Cam Reducer.

The WHOI cable reducer and the KAMO ball reducer have by far the lowest stiction/friction/viscous losses of all the transmissions studied. Notice further that there is no real clear transition between stiction and coulomb friction in the cable drive, as there is in the ball reducer. Numerical values are tabulated in the next section. The REDEX and DOJEN reducers are also quite similar, except that the REDEX reducer is certainly more efficient, as we can see by its lower viscous losses. Its coulomb losses are also lower than in the DOJEN reducer.

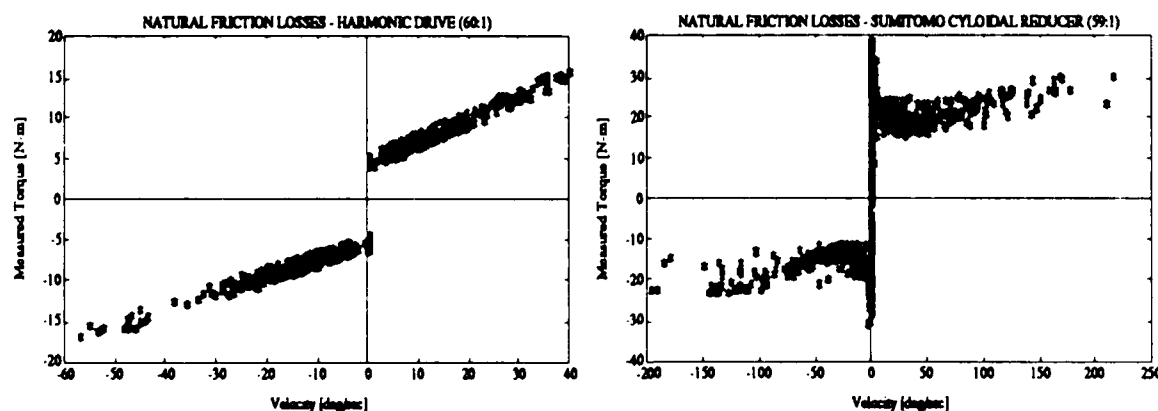


Figure 4.13 : Natural Frictional Losses for two different transmissions - (1) Harmonic Drive , (2) SUMITOMO Cycloidal Reducer.

The Harmonic Drive and the SUMITOMO cycloidal reducers show by far the largest frictional losses, despite their larger reduction ratios. Even if we assume that all the frictional losses in the cable- and ball-reducers are located at the input stage, and we increase the reduction ratio by a factor of two, the harmonic drive still remains less

efficient, and with a larger discrepancy between stiction and coulomb friction. The SUMITOMO reducer is by far the most inefficient and non-backdriveable unit tested in this experiment. Change of lubricant accounted for about 5 to 10% increase in efficiency, but even then these figures do not compare favorably with any of the other transmissions tested.

(c) RIPPLE TORQUE

The ability of a transmission to transmit a torque is not the only critical issue in fine robot control. The motors used on each joint are very critical in the fidelity of the transmission to generate a certain desired dynamic behavior. Many motors in the robotic world today are of the brushless type, and many such designs exist on the market today. Their design and eventual performance of these types of motors has been recently published in several magazines/journals/reports and the reader is referred to those sources for a more in-depth study of motor-design and performance. The issue that will be addressed here is of much concern in motor design and control and is known as ripple torque or detente torque.

Ripple Torque is a deviation from the desired motor-torque and is a function of the rotor position and commutation accuracy. The reasons for ripple torque are plentiful, but the main contributors can be listed as being:

Rotor Magnets (Homogeneity, Placement)

Stator Poles (Number, Shape)

Stator Windings (Discrete Distribution)

During commutation, the magnetic field set up by the sinusoidally varying current, is never homogeneous and will fail to create a constant torque as a magnet on the rotor moves from stator pole to stator pole. Many motor manufacturers try to solve this problem by either using many stator poles (24 in the case of the SEIBERCO motor which compares well to the usual 50 in a stepper motor) and then winding the armature so as to induce a sinusoidal (albeit discrete) magnetic field, while others have a small number of stator poles (usually 4, as in a standard MOOG motor) which requires that the stator poles be shaped separately (and carefully) so as to induce (as close as possible) a sinusoidally varying magnetic field strength. The tolerances in placement and shaping of poles have a big effect on the final shape of the torque vs. position curve for each motor.

The number of magnets and their material is important, yet their placement and the homogeneity of the magnetic material play an even bigger role in inducing torque-ripple. No magnet manufacturer can promise a material consistency that will result in magnetic field strengths that vary less than 1% across the face of each magnet and also from magnet to magnet. If magnets are placed on a rotor, their spacing and orientation is also critical. SEIBERCO motors have a 7° tilt on each magnet, which reduces the efficiency of the motor slightly (maximum torque) but drastically reduces the magnitude of the torque detente. The current magnets in use with our motors (made of samarium cobalt) have all been tested and show a much lower ripple torque value (within the manufacturer's 1% of maximum rated torque spec). Motor detente torque levels are usually given as a percentage of maximum torque capability of the motor. These levels of torque, as they are multiplied by the transmission ratio, could ostensibly be measured at the transmission output. The transmission itself can also introduce a large amount of ripple as was shown earlier for most of the transmissions studied. The theoretical torque ripple generated by the motor in terms of magnitude (at the motor : 0.016 N-m) and frequency (62 Hz at the motor) could not be observed in any transmission except the cable reducer.

The overall effect on (especially) stiffness fidelity can best be represented by a graph showing how by careful design of all previously mentioned aspects of a motor, torque-ripple can be reduced dramatically. In a transmission where the level of stiction and friction is equal to or higher than the level of motor torque-ripple, ripple will not affect the system fidelity at low speeds, since the stiction/friction forces mask this behavior (see Fig. 4.14). The second trace shows a behavior, where the levels of stiction and friction are small compared to the ripple torque and the ripple is thus very evident in the stiffness behavior. If we run the experiment at moderate speeds, the motor-induced ripple-torque will be added to the hysteretic envelope, and would show up as a constant-magnitude high-frequency noisy signal, representing the hysteretic envelope of the transmission. Employing a very simple-minded friction compensation scheme can reduce the level of coulomb friction in the drive, but will do nothing to reduce the high-frequency ripple-torque. A simple method for compensating for such errors is presented later as well as a discussion concerning its usefulness.

If torque-ripple is indeed present, the stiffness trace would look something like that shown in Figure 4.14, where the amount of torque spikes is a function of the spatial frequency of the ripple phenomenon. Figure 4.14 represents synthesized behaviors which are present in real systems. In the next plot (Figure 4.15) we have shown a desired stiffness behavior for the 10:1 ball reducer transmission and the pulley-cable reducer, as well as the actual system behavior.

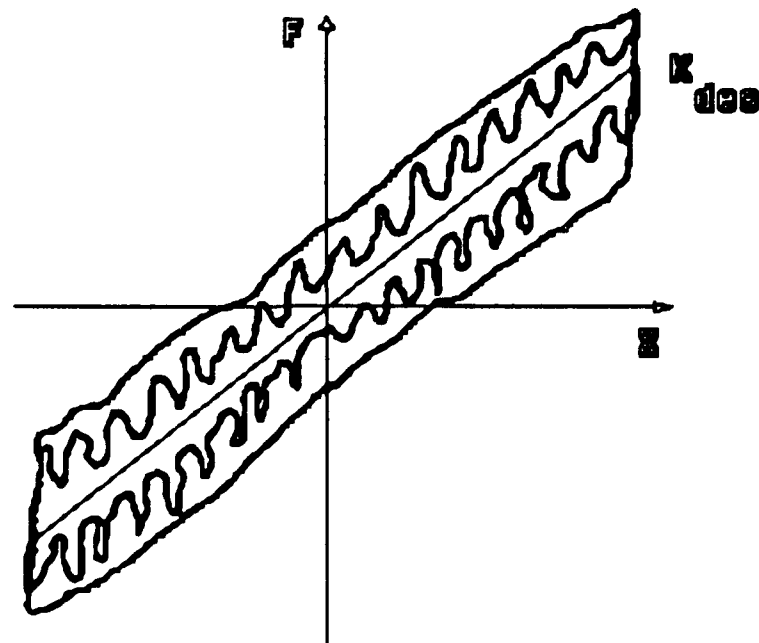


Figure 4.14 : Synthesized Torque-Ripple Behavior for Stiffness Fidelity of Motor and/or Transmission.

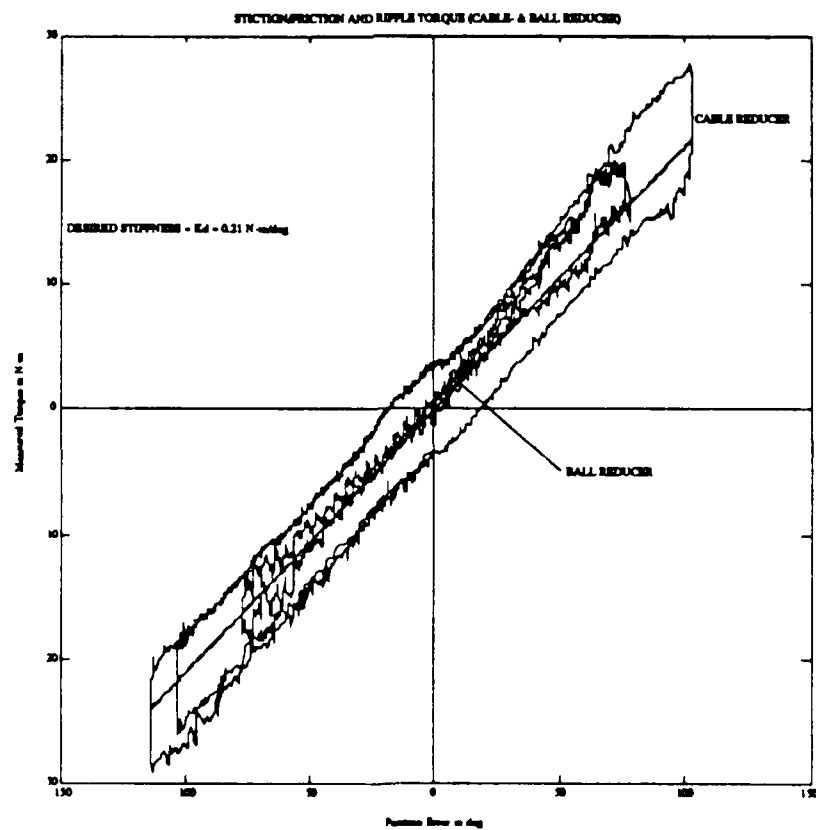


Figure 4.15 : Desired and Actual Stiffness Behaviors for (a) Ball Reducer and (b) Cable Reducer.

As can be seen from Figure 4.15, the theoretical behavior is very well matched by the actual data. In the case of the cable reducer, the motor-induced torque-ripple should be at most 0.5 N-m. Most of the ripple apparent on the hysteresis trace falls well within that region, with about 50% of the remaining ripple introduced by some other transmission-related phenomenon. Yet overall, the dominant ripple contribution in the case of the cable reducer, is the motor-induced detente torque. The story is different for the (10:1) ball reducer. The theoretically (maximum) possible ripple torque is no bigger than 0.2 N-m. As can be seen, motor-induced ripple level is far overshadowed by other ripple phenomena which must reside within the transmission. The ripple is clearly dependent on the amount of transmitted torque and is fairly repeatable. This phenomenon is most probably due to the uneven running of the steel balls within the ground gothic-arch grooves. This phenomenon was also found to be related to the preload of the transmission, which is to be expected, since it controls the internal contact forces of each steel ball in four-point contact with the grooves. The second reducer from this company (30:1) was carefully manufactured to not only maximize stiffness and backdriveability, but to reduce the measured ripple-torque (more about this reducer later).

Torque ripple can be much worse than the levels shown in Figure 4.15. In the section on impedance fidelity, where we tested the stiffness-following properties of all transmissions, data was shown which proved that such phenomena are highly dependent on transmission type and transmitted torque. The detailed discussions for each transmission will be left to the detailed sections which analyze each transmission separately and in more depth.

(d) TRANSMISSION STIFFNESS

A very important comparative factor during the time of transmission selection, is that of transmission stiffness. Manufacturer's data sheets usually provide information about the stiffness of their transmission. Some manufacturers supply a single stiffness figure, some provide a cryptic graphical representation of the linearized stiffness regions, while another may even supply the real data. Those manufacturers which only show a single numeric value for stiffness are usually not being completely up-front about the real behavior. Such a case in point is the REDEX Corbac unit, where the catalog supplies a single number (which was the highest for all the transmissions tested), but upon testing for the real and

complete data set, we discovered a variable transmission stiffness, dependent on the amount of transmitted torque. The highest value is then published. Other companies provide only a graph and/or table of their 'linearized' data sets, without showing any hysteretic behavior during load reversals. Some of these data sets indicate two or three regions of different stiffness. The two-region or single-knee stiffness behavior is usually due to a process of load-sharing, in which at lower loads only a few of the load-bearing members support the load, and thus deflect excessively. Upon deflection, due to machining tolerance and assembly, the rest of the load-bearing members begin to take up more and more of the load, until the entire load is properly distributed (as intended by the design), and the unit becomes stiffer. A transmission with three distinct zones of stiffness, is either badly manufactured and/or assembled, or the unit has a large amount of discretely located friction-contacts, where the contact forces between mating load-bearing parts have to be overcome first, and thus we are faced with a successive stiffening process, as more and more components in the transmissions share the entire load.

The industry seems to have adopted a standard of calling the deflection measured for an applied torque level of 3% of maximum rated torque, the deflection corresponding to wind-up, and they refer to it as 'lost-motion'. In reality, this zone is really a region of extremely low stiffness, as tolerance fits and frictional torques in the unit are removed. It is also important to distinguish whether the $\pm 3\%$ torque-level exceeds the entire break-away torque of the transmission - such oversight usually gives rise to a double-knee transmission stiffness trace.

Furthermore, one has to make a distinction whether the transmission stiffness trace was generated by locking the input and torquing the output while measuring output torque and -deflection, or whether one locked the output and torqued up the input, while measuring input torques and -deflections. All the data in this chapter was obtained via the latter method. Measuring transmission stiffness from the input usually results in lower transmission stiffnesses for the low-torque region. This phenomenon will indeed be shown to be present in our experiments. It can be explained by simply acknowledging the fact that stiction nodes are distributed throughout the transmission, and may create steeper torque-displacement curves before they break away (transition from stiction to friction), if the measurement is done from the output side. In some reducers the differences may be quite severe, since actual torque-bearing components may wedge and result in increased stiction levels which would result in fictitiously high stiffness traces - especially for low to medium torque levels. The forward stiffness measurement was mainly made because of the belief in its usefulness for dynamic modeling, as well as ease of measurement. In order to measure the output stiffness for all reducers, a fairly elaborate experimental setup would

be required in order to properly measure torques and deflections to the desired levels of accuracy and resolution. This type of experiment is still quite important, but its complexity and time- and money-investment make it lie beyond the scope of this thesis. The only important requirements of the forward-stiffness measurement which had to be carefully met, were (1) the locking elements of the output shaft be absolutely rigid and capable of sustaining large torque levels, (2) that these elements be rigid and properly aligned, and that (3) the input-torque and deflection be measured with enough accuracy and low levels of discretization.

No clearer description about this experiment is necessary at this point, since each separate section will be dealing with this topic in more detail, explaining the particular circumstances responsible for the stiffness behavior of each transmission. A concluding summary is given in the conclusions section of this chapter, which will contrast the experimentally obtained data sets.

(4.3.2) Specific Data

This section gives a more detailed view of the data sets that have not been shown previously and sheds light on further aspects and experimental details of each transmission, that are worth mentioning. Each of the data sets presented below is particular to a certain transmission and will highlight some of the more important aspects that are many times glanced over or improperly reported, when it comes to the ranking of transmissions in terms of their merits for different applications/tasks.

(a) **WHOI/MIT - CABLE/PULLEY REDUCER - A closer look**

Transmission Stiffness

One of the main quoted drawbacks of cable-transmissions (besides premature failure through cable fatigue, as compared to geared mechanisms) is their lower inherent stiffness. The experimental setup that was used to test transmission-stiffness, involved locking the output-shaft (by securing the force-sensor to a stationary and rigid support-base), and commanding the input-torque to ramp up and down to full positive and negative saturation-torque while logging the measured output torque and the input motion. The value for the transmission stiffness (or -compliance) should be computed as the ratio of the output-torque to the output-motion (taken as the relative motion of the input w.r.t. the output divided by N , since the output is assumed to be perfectly stationary). An output-stiffness measurement was performed in 1987 and showed that the transmission has a stiffness of about 4700 N-m/rad or 82 N-m/deg (all values are quoted at the output). Since the full reach of the manipulator is about 1 meter, we would get a linear endpoint stiffness of about 4700 N/m. The input-stiffness test performed in 1989, and the resulting data are shown in Figure 4.16. This experiment used cables coated with a hardened nylon jacket. The use of the coating was made necessary to reduce the first failure mode of the cables which was due to adjacent-cable chaffing as well as pulley-wrap chaffing. The data presented here shows the zero-motion behavior of the transmission under a full loading cycle in all directions. Note that the approximate transmission stiffness can be linearized by a value of 4300 N-m/rad or 72 N-m/deg, which in turn translates into a translational stiffness at the outer edge of the manipulator envelope of about 4300 N/m.

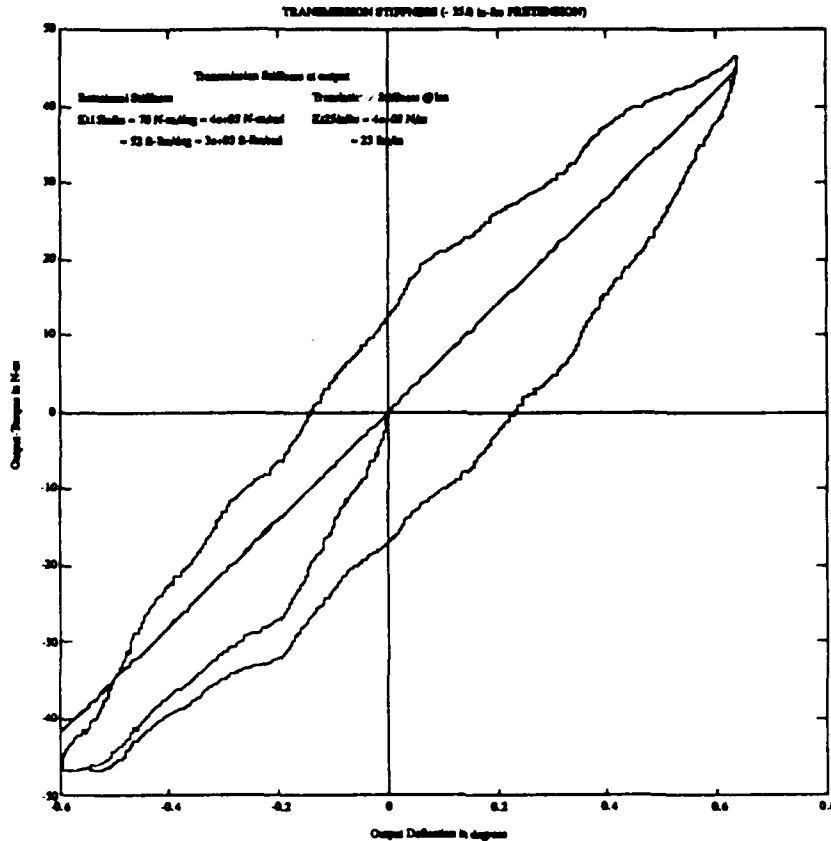


Figure 4.16 : Transmission Stiffness of Cable Reducer from Underwater Manipulator Joint.

Notice also that the resulting transmission stiffness compares very well with that for the output-stiffness measurement. The relative loss (as could be expected) in stiffness (about 10%) is very small and thus the usage of input-stiffness data seems accurate enough for modeling and control purposes. The usage of coated cables probably resulted in slightly lower stiffness values, but this arrangement was worth it in order to increase the life-expectancy of the cables. Remember though, that coating a cable does nothing to reduce cable failure due to bending. Using grooved pulleys would force the cable to retain most of its shape under tension and when it is cycle-wrapped on circular pulleys, and would thus be an interesting alternative to coated cables. This design issue warrants a good deal of further study.

What is noteworthy here is that these figures compare very well with those for standard cable-driven master-slave units that have been mainly developed by the French Atomic Energy Commission (and a splinter company) for their atomic reactor plants (J. Vertut & others since the 60's). On the other hand our experimental value is about 4 times lower than the latest design that the French have undertaken. This new design employs a non-backdriveable gear-transmission that has strain-gauged output-shafts that are used to

close a(n) (open-loop feedforward) torque-loop around the transmission. Their reported stiffness figure lies around 15,000 N/m for the same-size manipulator-workspace with a load-capacity that is 5 times larger than our spec. (25 lbs for us vs 75 kgs for theirs). This comparison may seem a bit far-fetched, but for a cable-driven manipulator with the same load-capacity, we would expect the stiffness compared to a gear transmission, to be about 5 to 10 times lower.

Our cable-reducer design (underwater manipulator) has another characteristic spec. that makes it an interesting competitor to gear-transmissions. The force-resolution of the torque-loop-sensitized gear-transmission manipulator built by the French was brought from 60 kgs (no mistake in units here) to around 800 gms when the torque-loop was active (this is a pure torque feedforward scheme in order to overcome friction - the remainder is the difference between stiction and friction). The measured value for our transmission lies around 125 gms. The value for their dynamic range would thus lie at 95 (75/.8), while ours lies more around 85 (13/.125) for a fully extended arm-reach inside the envelope. The relatively close values of dynamic range clearly illustrate that our design can be expected to perform better in the higher-sensitivity range with a reduced high-end payload rating. The two designs should thus be thought of as having their usefulness defined as a function of the tasks that they can be expected to accomplish (our design being more sensitive yet less powerful while theirs is less sensitive but with a higher load capacity).

Backdriveability

The force-resolution quoted in the previous section is a function of the preload that is applied to the cables to keep them tensioned for all values of input torque (a precaution to insure proper cable-wrapping and maintain higher transmission stiffness). In Figure 4.17 we show a few data-points that were taken from the transmission by pre-loading it from a minimum to a maximum value and measuring the backdriving-force required at the outer limit of the work-envelope (1 meter). Furthermore the tests were run with the stator in place (allowing for 'magnetic drag') as well as the stator removed (to purely measure transmission friction levels). Notice that the 'error' bars represent the uncertainty due to the presence of stiction/coulomb-friction behavior. The tests were performed with a 'wet' transmission (oil volume was drained for easy access to the mechanism and then re-filled) and are thus representative of a real-life scenario. The values represent the mean of several data runs over a large time period in order to allow the oil to penetrate everywhere and the change in preload to work its way evenly through the transmission (remember that stiction

and friction are distributed in a discrete fashion throughout the mechanism, namely the pulley bearings and the shaft seal).

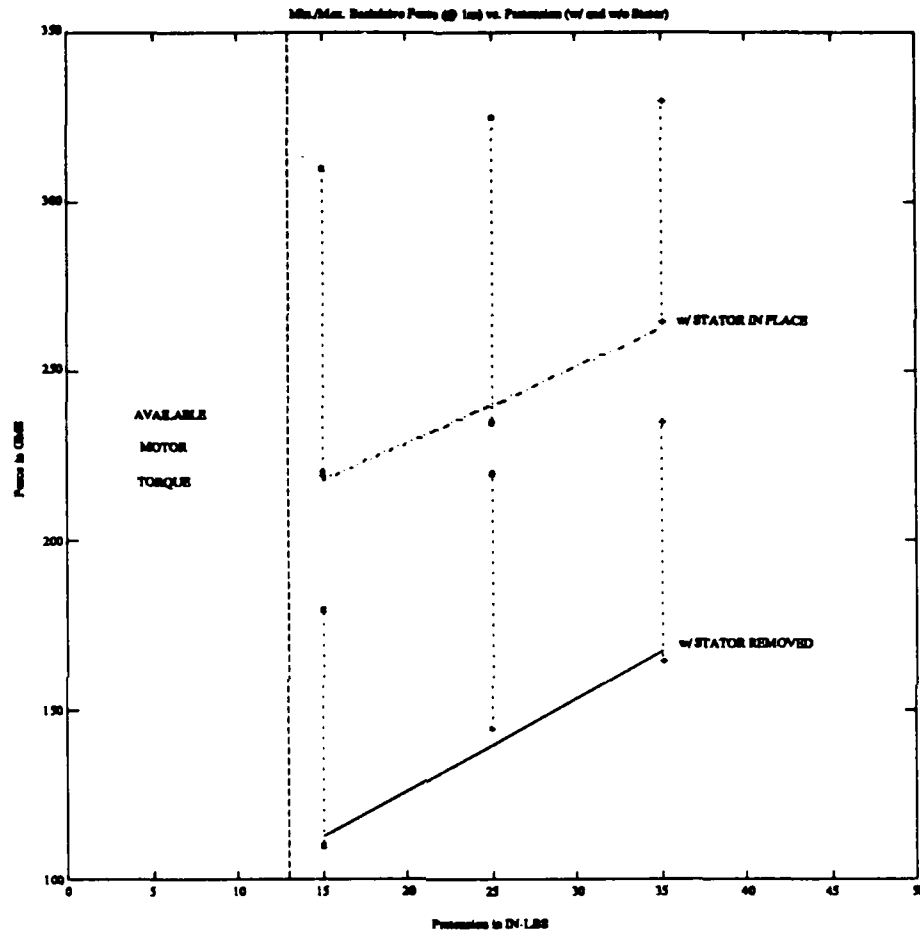


Figure 4.17 : Backdriveability of Underwater Manipulator Cable-Reducer Joint as a fct. of cable pretension.

The data set illustrates clearly the presence of stiction and friction. The vertical line drawn at about 13 in-lbs represents the maximum torque the motor can deliver at the output, and is thus a hard lower limit for the pretension torque. The sloped lines represent a linear fit for the Coulomb friction data of the transmission for different values of the pretension. What is interesting is that the presence of the stator makes quite a large difference (about 100% difference in friction levels) in the measurement of a transmission's ability to be backdriven (we expect such 'magnetic drag' to be present).

Impedance Compensation

This section deals with the possibilities and benefits of using some simple compensation schemes in order to obtain a higher fidelity in impedance following. The two parameters being studied were stiffness and damping fidelity. The desire is to remove much of the energy-loss evident in the stiffness traces shown earlier. Since friction, stiction and torque-ripple are the main reasons for this nonideal behavior we will address how to compensate for these in some open- or closed-loop fashion. The first approach is based on one of the more basic techniques to compensate for transmission friction presented in the literature and used in situations of telescope tracking, disk-drive controllers and also robot control. It consists of feeding forward a velocity-dependent approximation to the natural friction behavior present in a transmission. It consists of a coulomb friction term and possibly even a viscous friction compensation term. The simplified plot of Figure 4.18 below, depicts the nonlinear compensation scheme most widely used.

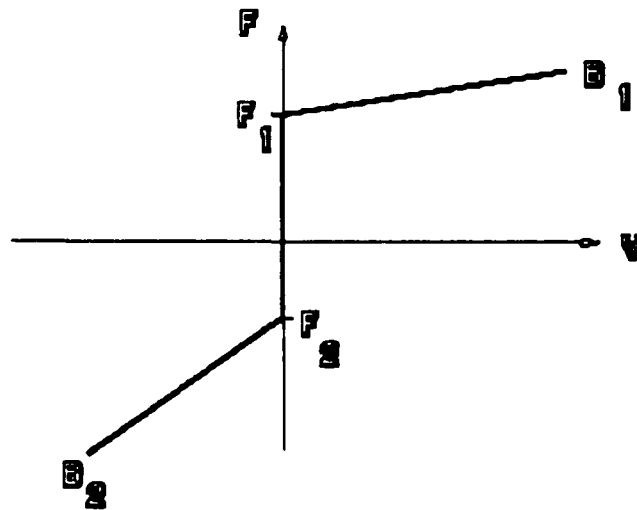


Figure 4.18 : Simple and most commonly used friction compensation schemes in real applications.

In the case of the cable reduction, we have chosen to simply feed forward a coulomb friction compensation term for (a) simplicity sake and (b) stability guarantees. The use of even such a simple compensation term will be shown to have quite an impact on overall impedance fidelity. In the next plot, Figure 4.19, selecting a level of low desired stiffness, we have shown the familiar trace for the cable reducer without any compensation, while the

second trace was generated by simply feeding forward a coulomb friction compensation torque (magnitude directionally dependent and determined experimentally and off-line previous to the experiment).

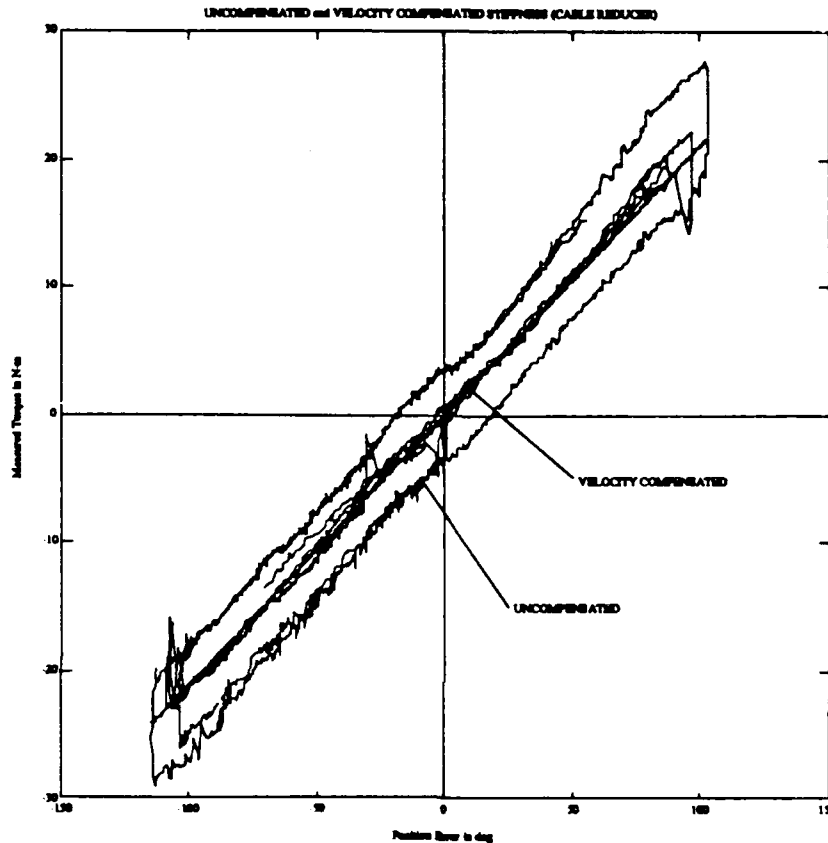


Figure 4.19 : Velocity-based Friction Compensation scheme applied to cable reducer.

As one can see, with this compensation scheme we can reduce the losses dramatically, while ensuring a closer stiffness fidelity. Notice here that the level of ripple-torque mentioned in an earlier section is very small, and dominates the overall behavior. If there was a substantial level of ripple-torque, this technique would be unable to properly compensate for it (a high bandwidth position-dependent compensation loop would be required). The feedforward control loop was closed in the main computer and ran at 10 Hz. It required several velocity measurements of the same sign, before applying a corrective torque. Since the task of deflecting the output was done fairly slowly to get good stiffness data, this condition can be met most of the time. The larger spikes in the compensated trace are proof that the scheme would sometimes have trouble deciding on what torque to apply (especially at extremely slow speeds) and we were thus limited to the behavior that an uncompensated transmission would have. Thus, this technique can clearly

be of no benefit if the task involves very slow motions or motions with rapidly changing directions of motion. The proper way to perform this compensation would be at the motor controller level (running at 1000 Hz), where the faster bandwidth could insure even better performance. If the velocity signal at that level is clean enough (which it must be since it is used for commutation and PD control), this approach can turn out to be quite reliable and will not result in high-frequency chatter of the actuator torque, as long as the feedforward term is chosen to be equal to (physically impossible) or slightly below the actual frictional torque (this insures better system stability as well).

The second approach involves compensation that is based solely on a figure of impedance mismatch - see Figure 4.20 for the following discussion. If we consider that we want to achieve a perfect stiffness behavior, we would want the measured output torque to be linearly dependent on the position error. But as we have seen earlier, stiction/friction and motor/rotor phenomena can create a behavior that is far from ideal. The compensation scheme is a very simple one as explained in the simple graph of Figure 4.20:

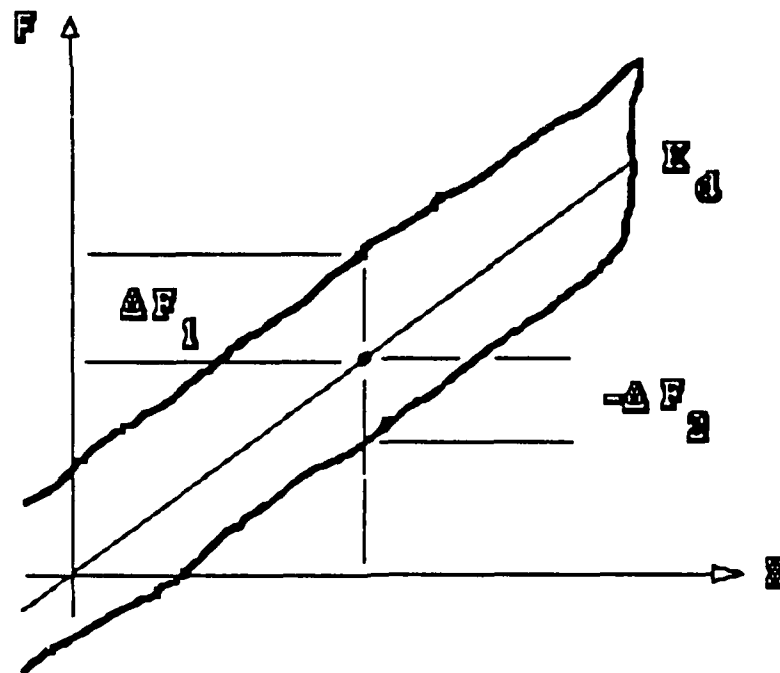


Figure 4.20 : Impedance Compensation scheme for any Motor/Transmission using Force/Torque Feedback.

The torque that is fed forward by the motor controller is basically the difference (ΔF_1 or ΔF_2) between the currently desired output torque ($K_d \cdot \Delta x$), based on the

measurement of position error, and the currently measured output torque (F). In an ideal world, this scheme should be able to compensate for any nonlinearity that could result in nonideal stiffness tracking. But in reality, this approach is dependent on sensor accuracy, noise, drift, as well as the bandwidth at which this control loop could run at. In our setup we were limited to run it at a meager 10 Hz. Even if the task was performed very slowly, there was some excess ripple that was due to the fact that we had a delay of one full sample before the proper control action could be applied in order to match actual and desired stiffness behavior. The results of the experiments are shown in Figure 4.21:

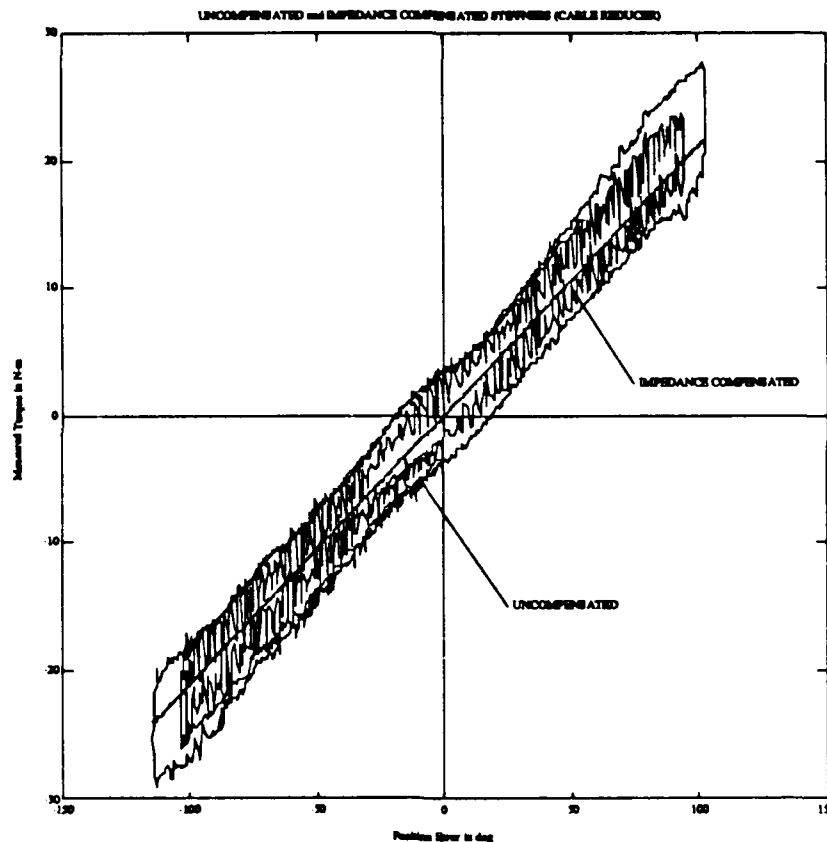


Figure 4.21 : Desired and achieved stiffness behavior for impedance compensated Cable reduction.

This phenomena can clearly be seen to be present in the plot above. In every sample where there was compensation present, the desired and actual stiffness levels are close to being identical. I believe this technique to be useful and would prove to be quite successful if the bandwidth of this controller could be upped by a factor of 20 to 50. This would require some hardware re-design but is physically possible. On the other hand though, such compensation would only be meaningful if dynamic forces are negligible, or if a task is almost quasi-static and an accurate stiffness at the endpoint was crucial.

In concluding this section it should be clear that the main type of nonlinearities that this transmission presents when it comes to stiffness fidelity are mainly due to stiction and friction, as well as ripple torque. The extent to which these are present depends not only on the motor-qualities, but also the transmission-dependent ripple. Some reducers may introduce ripple levels that far overshadow reflected motor-student torques. Such ripple phenomena are usually of fairly high spatial frequency content, which makes any compensation hard to successfully implement. Compensating for (a conservative estimate of) coulomb friction can have a lot of advantages in reducers where coulomb friction is dominant and constant. The presence of ripple torque places a hard limit on the fidelity of the stiffness following behavior. Compensation is tricky, as the presence and magnitude of such ripple phenomena depend on the operating conditions, and are thus quite unrepeatable phenomena. The limits on impedance fidelity due to load-dependent coulomb friction and ripple torque will become more obvious in the following sections that deal with the other reducers we studied.

(b) H.D. - HARMONIC DRIVE - A closer look

The harmonic drive has been available for the last 10 or 15 years and has found wide use in robotics as well as self-contained space applications. The main advantage of this transmission type is that the design results in zero backlash at a 'reasonable' expense in terms of frictional losses, and the stiffness of the transmission itself is moderately to fairly high. Since this is a transmission type similar to a planetary arrangement and involves meshing teeth, the reduction or absence of backlash is always connected with higher frictional losses. The most common failure mode of this transmission is the wear of the teeth on the wavespline and the subsequent stripping of these teeth. The excessive wear of these teeth is due in part by their short height and the inherent preload that they are submitted to. Despite their involute profile, they wear rather quickly and incur backlash as well as large ripple torque (data presented here) at large levels of transmitted torque.

Due to the design and material properties, it is very hard to make a harmonic gear reducer with a reduction of less than 1:60, with the same life expectancy (MTBF) and stiffness. Despite the fact that most of the transmissions tested here had a reduction of around 30:1 and 10:1, we tested this transmission because of its popularity and widespread use in such critical applications as the FTS (Flight Telerobotic Servicer). Using some very simple assumptions, we will be able to directly compare it to the other transmissions analyzed in this chapter.

Backdriveability

As previously mentioned, this drive has a (published) zero backlash figure. They achieve it, as in any other geared mechanism by preloading (multiple) meshed teeth. The comparatively high stiction/friction forces in the mechanism are due to the fact that we have a single reduction with more than one tooth in contact at any one moment. The frictional losses are due to the rolling and sliding friction of the meshed teeth with respect to each other. The relative size of this stiction/frictional loss has become apparent in earlier plots, but a clearer picture will be shown here.

The next figure (4.22) shows the actual stiffness behaviors for a low level of desired stiffness around the no-load operating (setpoint) point of the controller. As one can tell from Figure 4.22, the stiction and frictional losses are present at all times (no surprise there - but it is interesting to note the consistency/repeatability in the data), and there is a large

difference between the stiction and friction forces in the transmission. Another plot which simply shows the force required to backdrive the transmission for different speeds is shown in Figure 4.23.

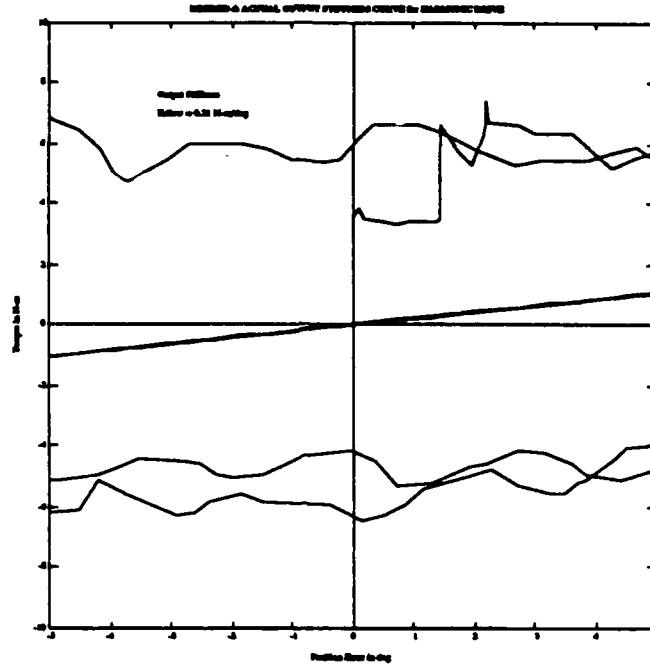


Figure 4.22 : Stiction/Friction Torques present in a Harmonic Drive Transmission.

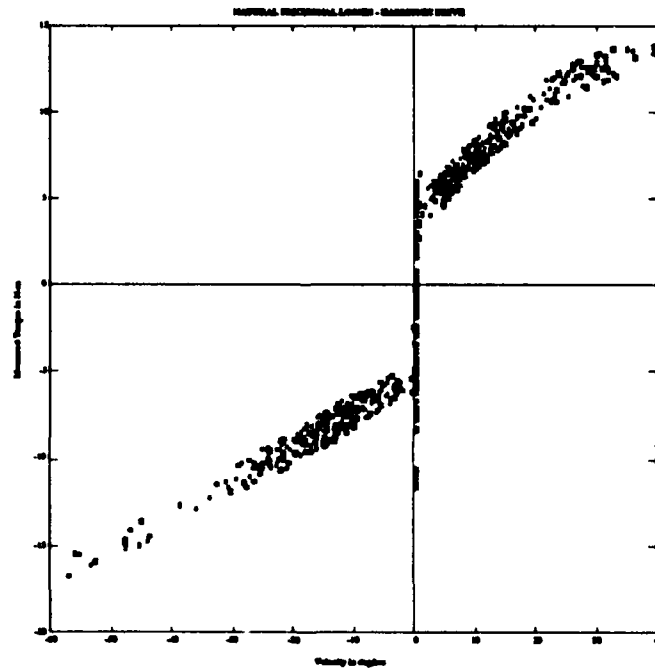


Figure 4.23 : Stiction/Friction and Viscous Damping inherent in a Harmonic Drive Transmission.

The important details to note here are the large difference between stiction and frictional forces (+8N-m/-12N-m vs. +5N-m/-6N-m) in addition to the fairly high viscous frictional losses (a claim made based on the relative viscous losses inherent in the other transmissions tested) which seems to indicate slightly different functional relationships (with respect to speed) depending on the direction of motion (positive speeds have more saturating frictional viscous losses, while negative viscous speed losses seem fairly linear).

Ripple Torque

During the tests performed on this transmission, a very interesting behavior was apparent from the data. During the times of large applied torque, the magnitude of the torque-ripple increased rapidly as can be seen from figure 4.24, where we have shown the stiffness following capability of this drive at a low levels of desired stiffness.

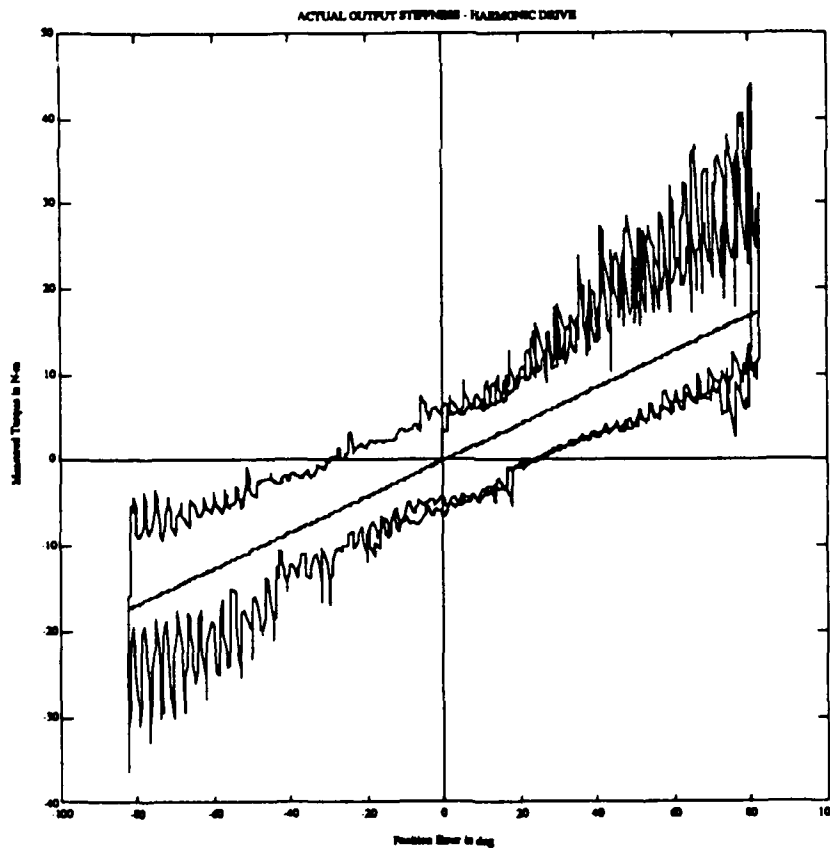


Figure 4.24 : Presence of Ripple Torque in Stiffness Fidelity Experiment for the Harmonic Drive.

The most plausible explanation for this phenomenon, underscores the high probability that this phenomenon may not always be avoidable. The above experiment was performed with the output (spline cup) simply attached to the force sensor. There was thus the possibility of misalignment between the cup and the fixed spline. Once the teeth were not properly meshed, the involute-profile teeth would no longer roll on top of each other but rather slide and would thus increase the frictional forces tremendously, especially during the moments of large torque transmission, due to the higher contact forces.

A new experiment was designed which would force the alignment to be well within 1/1000th of an inch at the input of the cup (about 5/1000th of an inch at the output). This alignment figure (to within 3/10000th - the resolution of our machine tools) is difficult to obtain even with good machine tools (since a new concentric bearing support was made for the wave-spline). The same experiment was repeated and the ripple was somewhat decreased (as can be seen from Figure 4.25).

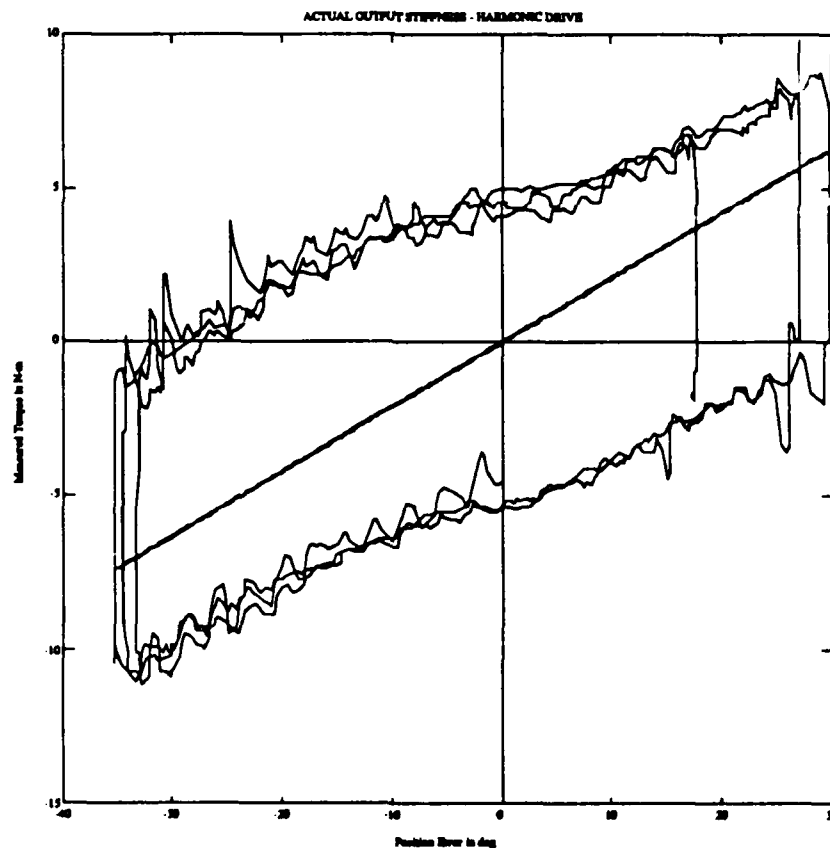


Figure 4.25 : Reduction of torque-ripple in Harmonic Drive by careful alignment of fixed spline-ring and wave-spline.

Since perfect alignment is never possible, we can always expect this transmission to have a large ripple-torque present. The way the meshed teeth are designed (short and stubby involute teeth that despite the preload will never be meshed perfectly especially in the presence of even slight misalignment) and the way that the wave spline transmits torque (while deflecting), seem to be very plausible reasons for the always present ripple. Shaping the teeth to compensate for cup-deflection may help in load-sharing, but will not entirely avoid the above ripple phenomenon.

Impedance Compensation

The harmonic drive became a prime candidate for any compensation scheme, because it exhibited the most frictional losses of all the transmissions studied. The most simple and obvious scheme to try first was that of simple coulomb friction compensation, and the results are shown in Figure 4.26.

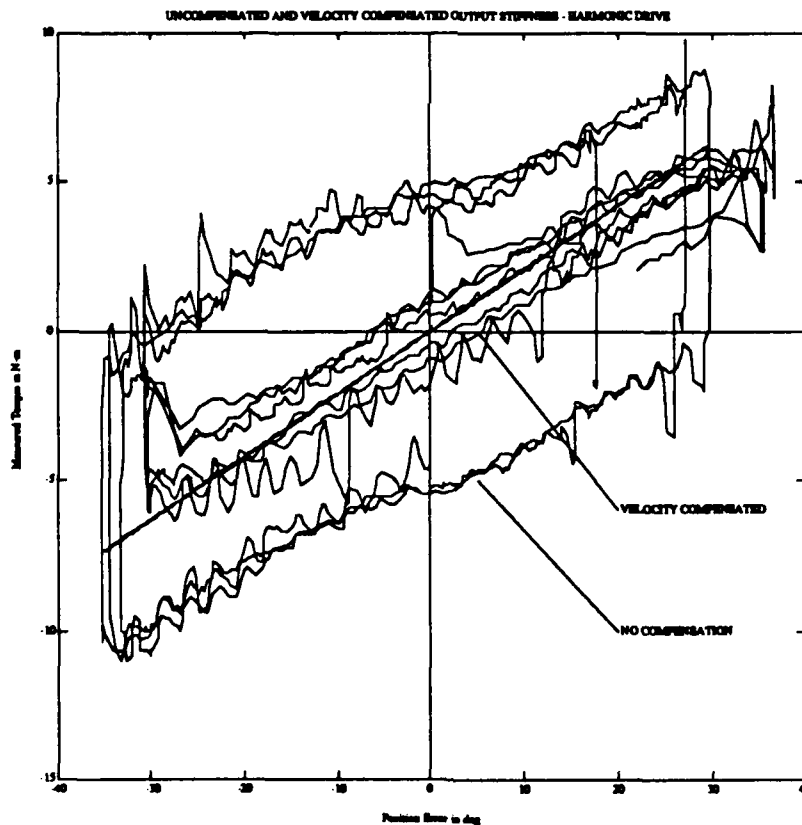


Figure 4.26 : Velocity-based Coulomb Friction Compensation for Harmonic Drive Transmission.

The previous figure clearly illustrates that there is quite a bit to be gained from performing a simple coulomb friction compensation on this transmission. On the other hand it also shows that there is still an appreciable amount of torque ripple that this scheme will not catch, and thus cannot be compensated for with this technique.

The next step is to try the impedance compensation scheme (on stiffness here only). Despite the hardware-related shortcomings of the implementation mentioned earlier, we can show a plot (Figure 4.27) that represents the uncompensated stiffness behavior (outer trace) and the compensated trace (inner trace) for a medium level of desired output stiffness ($K_d = 1.1 \text{ N-m/deg}$).

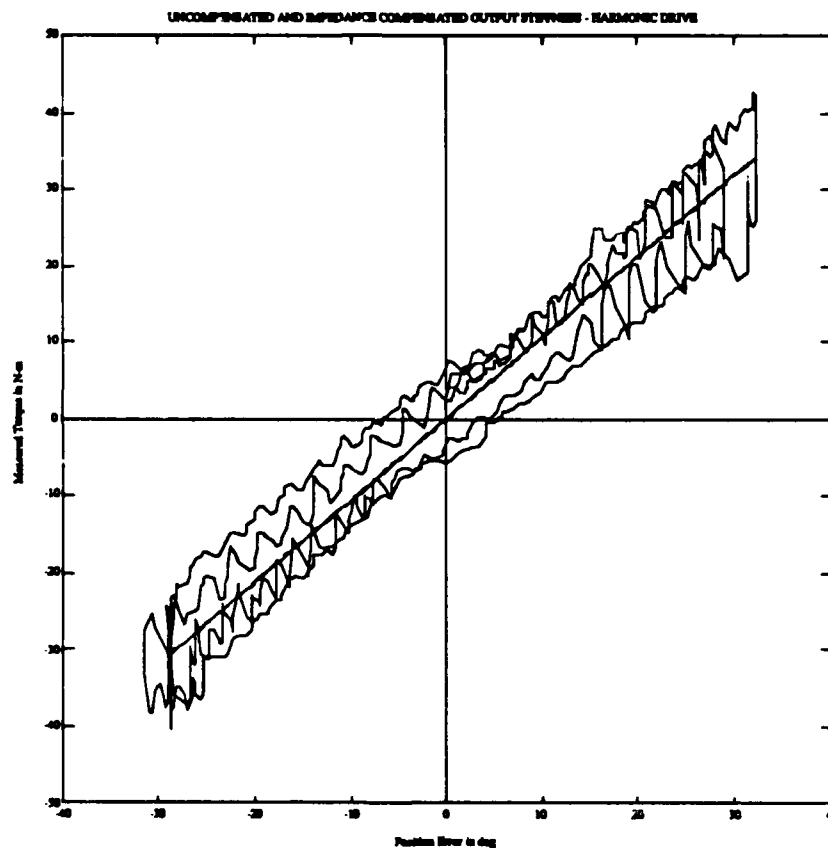


Figure 4.27 : Impedance Compensation scheme applied to the Harmonic Drive Transmission.

The impedance compensation scheme is shown here to be quite useful, except that the bandwidth necessary for smoother behavior is far faster than that which our hardware is capable of delivering. The fact that all spikes of the inner trace do indeed approach the desired stiffness slope is an indication that the scheme could be successful if better implemented (within limits of course). The above plot also points out that there may have to be a combination of coulomb- and ripple-compensation to get even better stiffness

fidelity. If one looks at the data section of the inner trace between 0 and 20 deg of position error, one recognizes that the desired stiffness behavior is not achieved, since the impedance compensation scheme is feeding forward a torque that is smaller than the coulomb friction itself (about 5 N-m) and thus the stiffness following can not be perfectly guaranteed in this operational region. This experiment also proves that once we remove coulomb-friction almost entirely, the behavior will be dominated by transmission-internal ripple phenomena (assuming they overshadow the motor-induced ripple, which they do in this case). The ripple phenomenon can be seen to reach magnitudes between 2 and 8 N-m !

Transmission Stiffness

The harmonic drive has long been a favorite candidate for many robotic transmission applications, due to its large torque-to-weight ratio. Some of its main drawbacks have been claimed to be its inability to withstand shock-loads, retain its zero-backlash properties, and its lack of overall stiffness. The nature of the harmonic drive requires that attention not only be given to its torsional (axial) rigidity, but also its compressive (radial) rigidity. Its transmission stiffness behavior is shown in the trace of Figure 4.28a.

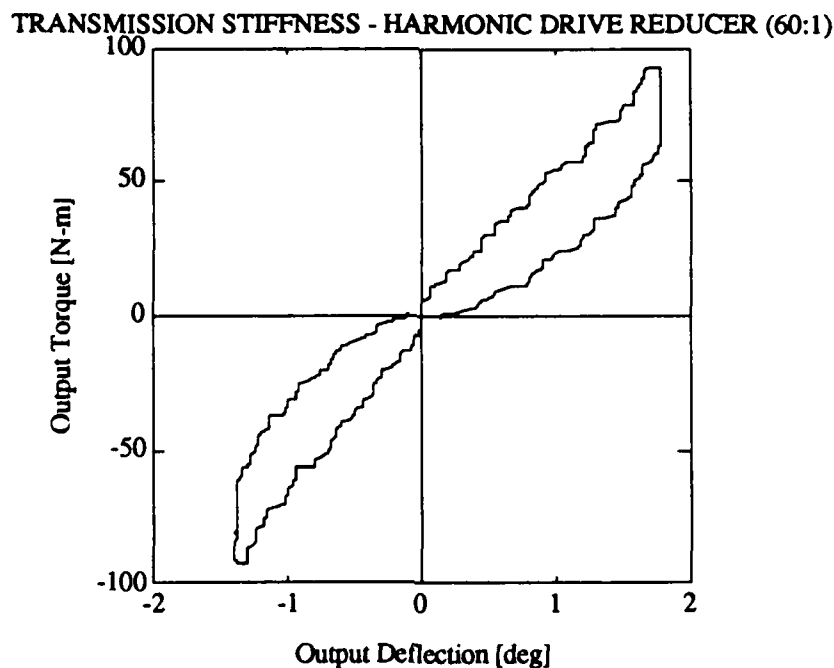


Figure 4.28a : Transmission Stiffness trace for the Harmonic Drive Cup (60:1) reducer.

The initial soft-zone behavior of the harmonic drive is most likely due to the elliptical bearing-race forcing the wavespline's teeth to mesh with the fixed spline. This process allows for relative motion over a certain rotational range, before the teeth can not slide with respect to each other any more. This is especially the case due to the slanted shape of the teeth, which compensate for cup flexure by changing the contact angle. Shown on the above scales, it is important to compare this behavior with that of the cable reducer. This comparison is made in Figure 4.28b. Notice that despite the stiffening transmission behavior, the harmonic drive has a soft-zone which is very large, with a stiffness that is below its maximum achievable value, as well as being lower than that for the cable reducer.

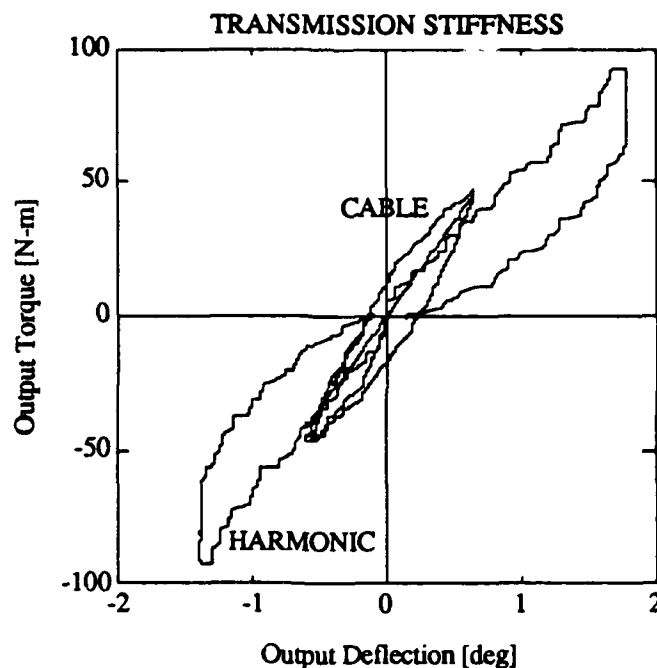


Figure 4.28b : Transmission Stiffness trace for the HARMONIC DRIVE Cup reducer (60:1), and the WHOI cable reducer (30:1).

The recognition of such soft-zones and their extent is very important in determining the overall stability of such reducers in closed-loop torque control scenarios. The ultimate maximum stiffness for the harmonic drive is far above that for the cable reducer, yet the presence of a large 'soft-zone' dominates the system characteristics when a comparison is made with the cable reducer over a mutually achievable torque range. Such a comparison is useful as it outlines the different operational regimes in which certain reducers may perform better than others.

(c) SUMITOMO - CYCLOIDAL REDUCERS - A closer look

The cycloidal reducers made by SUMITOMO can be separated into two classes. The first is a mass produced unit available in a wide variety of sizes (Cyclo-reducer), and a second series, which has been especially designed for indexing, NC machining, and robotic applications in mind. We began the tests with the standard Cyclo-reducer, and realized very soon that this unit had some very severe deficiencies. On the other hand it proved to be a very interesting data set, which resulted in the study of some finer points in transmission design and control, and thus this data set has been presented as well. The robotic version of the cycloidal reducer was also included in the experiments (termed Servo-Match), and its characteristics differed widely from the cyclo-reducer. The principle of operation was identical, only that extra components and tighter tolerances were employed in the assembly of this unit. Its data set is also included and clearly labelled. The Servo-match cycloidal reducer was explained in an earlier section, and will from now on be used for comparative purposes, unless otherwise stated.

The cyclo-reducer purchased from SUMITOMO is a standard industrial model that is known to be extremely rugged. Upon receipt of the unit, all the seals on the input- and output-shaft were removed, in order to make a fair comparison with the other transmissions. Even then the unit was barely backdriveable, so the unit was disassembled and all the excess grease was removed and replaced with lighter and less viscous mineral oil-bath. The unit purchased had tolerances on the inner waveplate and pin bushings that resulted in a fair amount of backlash (about 25° at the input or 1° at the output). The manufacturer would have provided (at a cost) a unit with closer tolerances (if one was willing to wait 3 months), but even then the unit would have had some amount of backlash and an increased level of frictional losses (according to their own engineering literature). The main idea of testing this transmission was that we wanted to learn the effects of fixed backlash systems on impedance fidelity and possibly even system stability. Furthermore, once the system was under unidirectional load this effect would not be present and we would still be able to characterize this transmission with enough accuracy.

The Servo-match unit which was designed for robotic applications was pre-lubricated at the factory, and had to be partially assembled upon receipt. We decided to clean out all the excess grease and replace the bulk of the grease with low viscosity mineral oil. This change had a tremendous impact on how much effort was required to forward-drive the unit. Notice that this unit is also dimensionally preloaded by design, and has to be force-assembled. Tolerancing and oversizing define the efficiency of the unit. The F-

series unit we received has by now been replaced by the FA-series, which basically is about 30% stiffer, but also has increased levels of friction, and is thus also less efficient.

Backlash and Torque Linearity - Cyclo Reducer

The presence of backlash in the cyclo-reducer can clearly be shown by performing a simple transmission-stiffness test (lock the output shaft with the attached force sensor and ramp the motor-torque up and down) and plotting the input deflection vs. the measured output-torque. The theoretical trace should look like the one shown in Figure 4.29:

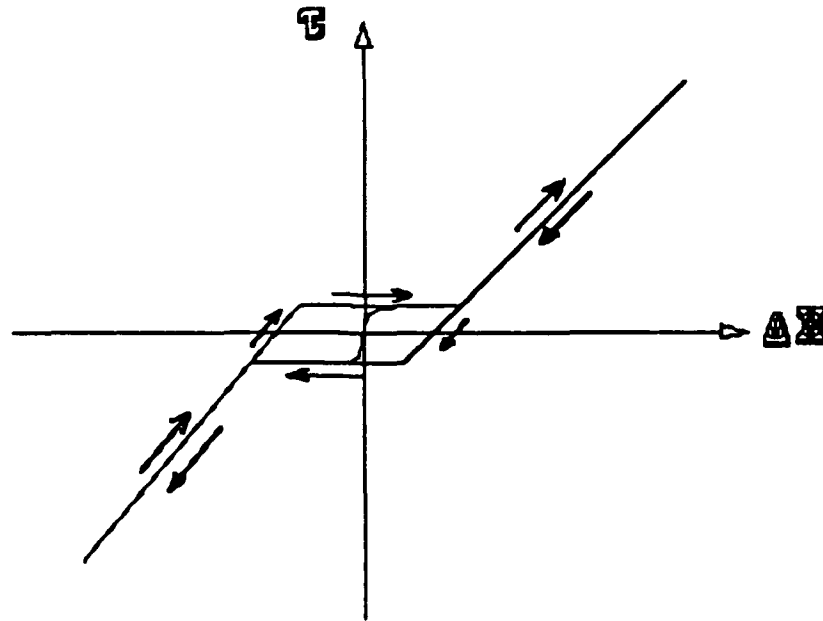


Figure 4.29 : Presence of Backlash in the Cyclo-Reducer, detected via simple stiffness test.

The arrows show the direction of loading and unloading. The variables Δx and τ represent the measured input deflection and measured torque at the output. The reason for the hysteresis loop is due to the frictional torque required to move through the zone of lost motion. Note also that this plot could be shifted along the x-axis, depending on where the system starts out in the dead-zone. The slightly curved traces around the coordinate origin represent the possible start-up from zero torque and deflection. Note also that no indication was made for any further frictional losses as well as the decision to consider all the backlash to be lumped at the input.

The next plot (Figure 4.30) shows the real data set taken using the test explained above, as well as a straight line drawn using a least squares fit to the data in order to determine the 'best-fit' transmission stiffness.

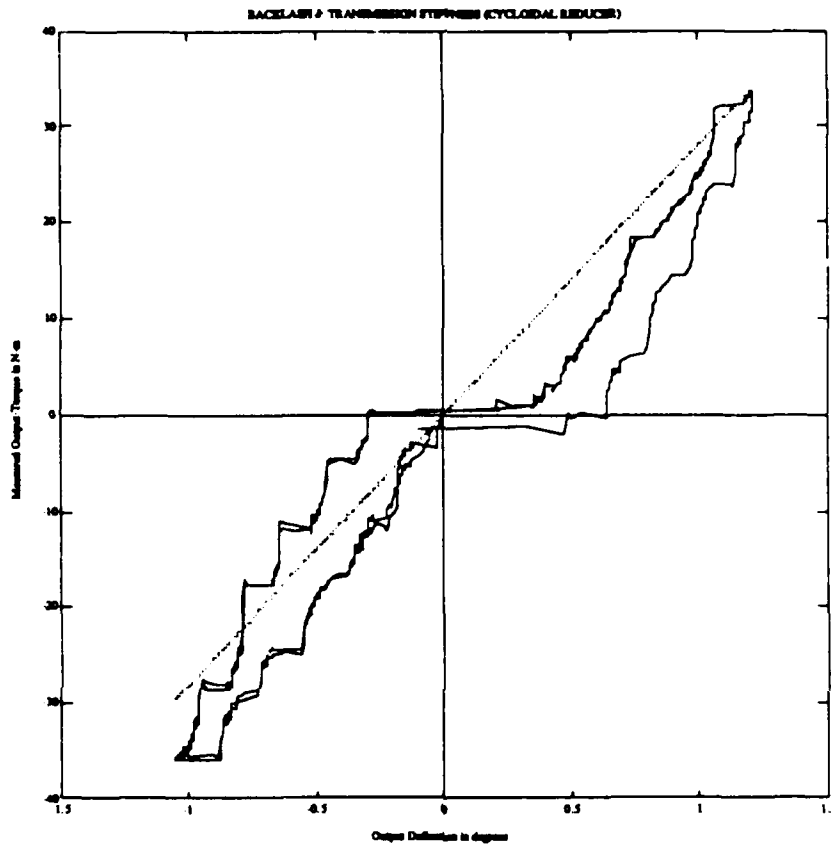


Figure 4.30 : Presence of Backlash and Stiction/Friction in Cyclo-Reducer.

Notice the presence of stiction/friction, creating a 'hysteresis envelope', while the system transmits larger and larger loads and all the backlash is taken out of the transmission. It should be noted that this plot also seems to illustrate the presence of 'distributed' stiction/friction in this unit. This transmission has various stages of moving and torque-transmitting parts, each with their own level of stiction/friction, which will eventually be removed and overcome once under an increasing load. The two previous plots look very much alike and thus prove the presence of backlash. We will see in the next section how this does affect impedance fidelity and transmission stability.

The Servo-Match unit was also tested to analyze the stiffness data provided by the manufacturer. This design, due to 'dimensional preloading', can be shown to exhibit no backlash-behavior, as seen in Figure 4.31 :

TRANSMISSION STIFFNESS - SUMITOMO SERVO MATCH REDUCER (59:1)

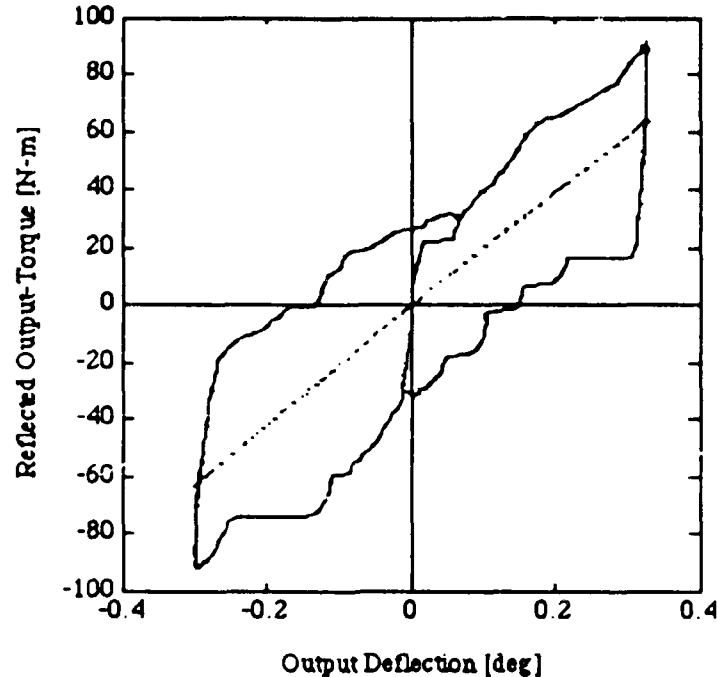


Figure 4.31 : Transmission Stiffness Test for the SUMITOMO Servo-Match Cycloidal Reducer.

On the other hand, the frictional hysteresis losses are very large, accentuated by the step-wise release of internal frictional torque-loads (horizontal line-traces). The measured stiffness can be computed to lie no higher than 200 N-m/deg or 12,000 N-m/rad. This is far from the published value, which is 10 times higher. The torque applied in this experiment only covers about 50% of the torque-rating, but includes all the soft-zones measured by the manufacturer. The manufacturer claims to have two 'knees' in his transmission stiffness data. The fact that there is more than one knee is due to the (arbitrary) convention of calling the $\pm 3\%$ (of full rated) torque level the lost-motion zone, without considering whether this exceeds the internal frictional torques in the unit. In this case it does not, so the unit has not been fully preloaded to the point where the loads are distributed evenly throughout the transmission's load-bearing components. Furthermore, the unit exhibits interesting softening/stiffening steps during load transmission, which is not a very stabilizing phenomenon when it comes to controller stability.

The Servo-Match unit is one of the stiffest transmissions tested, including the perceived stiffnesses in the soft-zones (at around 6000 N-m/rad), but it also displayed large hysteretic losses, due to excessive preload in the unit, which also results in very large stiction/friction torque-loads which are a sure sign of possible limit-cycle behavior for most of the commonly used force-controllers applied to a motor/transmission/load assembly.

Impedance-Fidelity and -Compensation - Cyclo Reducer and Servo Match Units

The ability of the cycloidal reducer to emulate a desired stiffness without any kind of compensation can be illustrated in the figure below (Figure 4.32), for a low level of desired stiffness for the cyclo reducer:

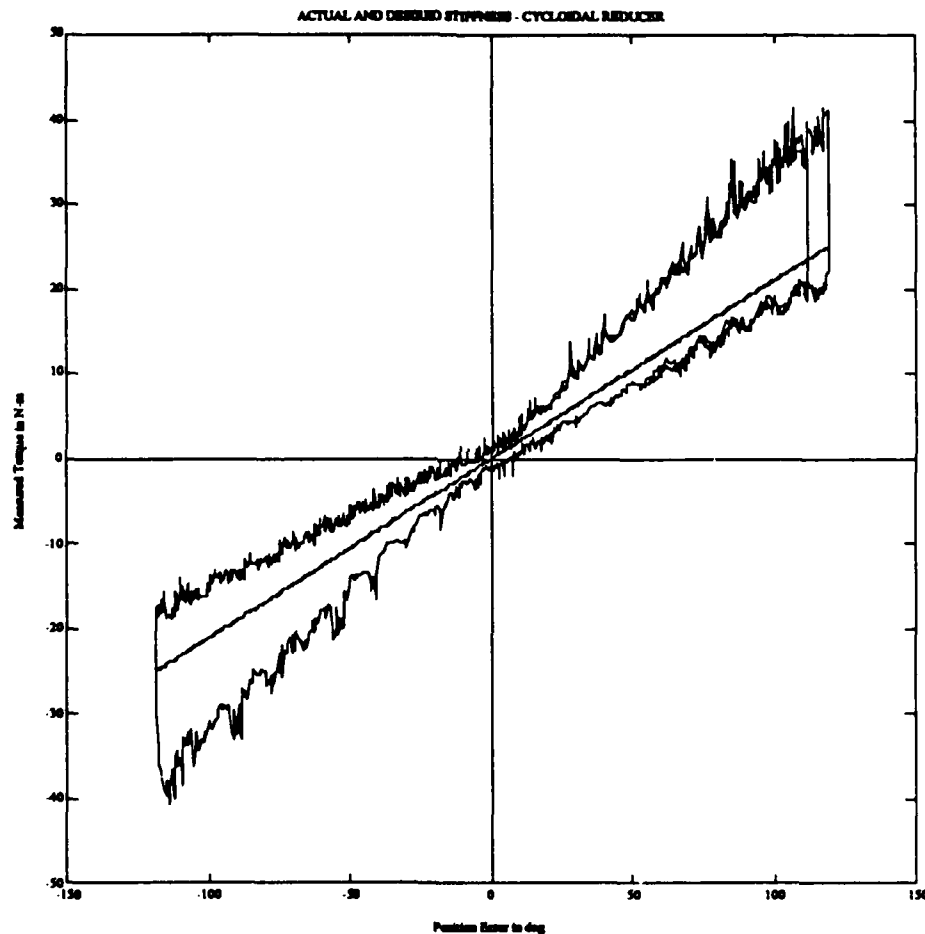


Figure 4.32 : Stiffness Fidelity Trace for the Cyclo Reducer (29:1).

What is interesting to note here is the usual presence of frictional losses, in addition to their increase with rising torque loads. Furthermore there seems to be a fairly high frequency ripple torque (spatially) which can not be explained away as measurement noise (too big), motor torque-detente (also too big) and could very well reside on the input side of the transmission (some sort of undesired shaft eccentricity or improper plate/bearing

eccentricity). The size of the frictional losses are about the same with respect to the cable reducer for low levels of transmitted torque, but that is no longer the case for increasing levels of transmitted torque. The beating-phenomenon in the trace is claimed to be due to the rolling of the epitrochoid 'wave' plate over the fixed rolling pins in the reducer housing.

The simple coulomb-friction compensation scheme applied to the above reducer should thus not be completely successful in removing all levels of undesired stiffness errors, since it is a constant value based on a no-load experiment. The resulting data is shown in Figure 4.33 below:

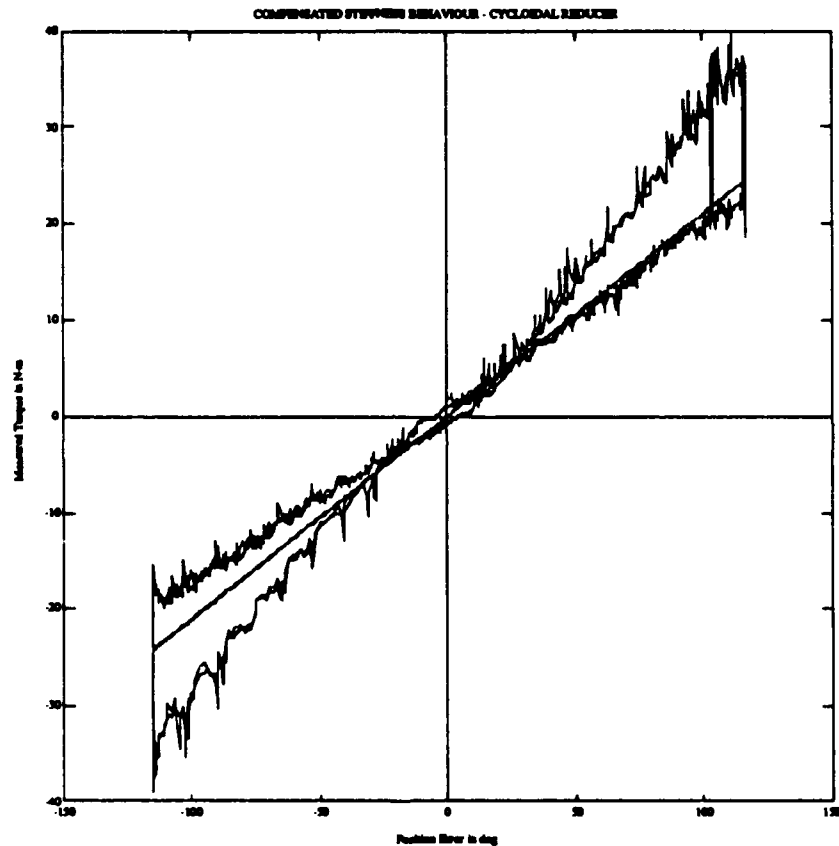


Figure 4.33 : Velocity-related Coulomb-Friction Compensation for Cycloidal Reducer only shows small improvements in stiffness fidelity.

If the original uncompensated behavior was overlaid on the above plot, one would see that the compensation only works well in the area of low torque loads, as was expected (and is obvious from the plot). The earlier proposed impedance compensation scheme though, should be able to deal with this unpredicted phenomenon. The resulting plot is shown in Figure 4.34 :

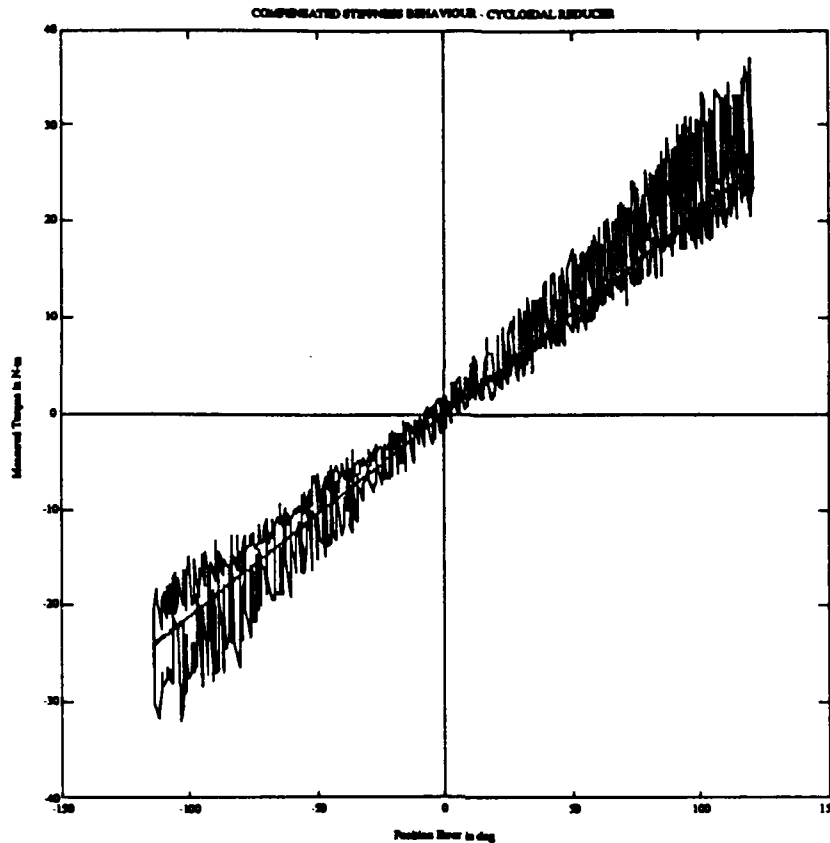


Figure 4.34 : Impedance Compensation on Cycloidal Reducer shows great potential for success if certain hardware requirements are met.

Once again it seems clear that the above scheme could be more successful if the bandwidth of this controller could be increased by a factor of 10 to 50 at least. The uncompensated trace actually exactly envelops the above trace.

A very interesting phenomenon occurred while performing some of these tests. Compensating for coulomb friction or impedance mismatch in a transmission with backlash, while running under a fairly stiff (high-gain) controller induces high frequency limit cycles around the setpoint of the controller under low load conditions. The high frequency and low amplitude oscillations would only die out once the torque being transmitted increased so as to move the motor away from its setpoint. The presence of this limit cycle is clearly due to the presence of a low-friction lost-motion zone (backlash), coupled with a high gain servo controller (only through the addition of extremely large controller damping could this behavior be reduced - a not too realistic approach). Unfortunately in the cycloidal drive there is no way to reduce the backlash in the system (one can only damp it by inserting heavy grease into the mechanism - the way the manufacturer ships these units), but a similar behavior was observed with one of the ball

reducer transmissions (see the section on ball reducer analysis). Although the complete analysis and discussion is thus deferred to that section, it is mentioned here because it represents a very interesting and important behavior that has an effect on the eventual usefulness of such schemes as well as on the question of transmission fidelity, which stands at the core of this whole thesis.

The Servo Match unit was then tested for its fidelity in following desired impedance (stiffness here only) behaviors. We ran several tests at increasingly higher levels of desired output stiffness, and logged the data. Presented below in Figure 4.35, are the desired and actual traces for a low level of desired output stiffness (0.21 N-m/deg):

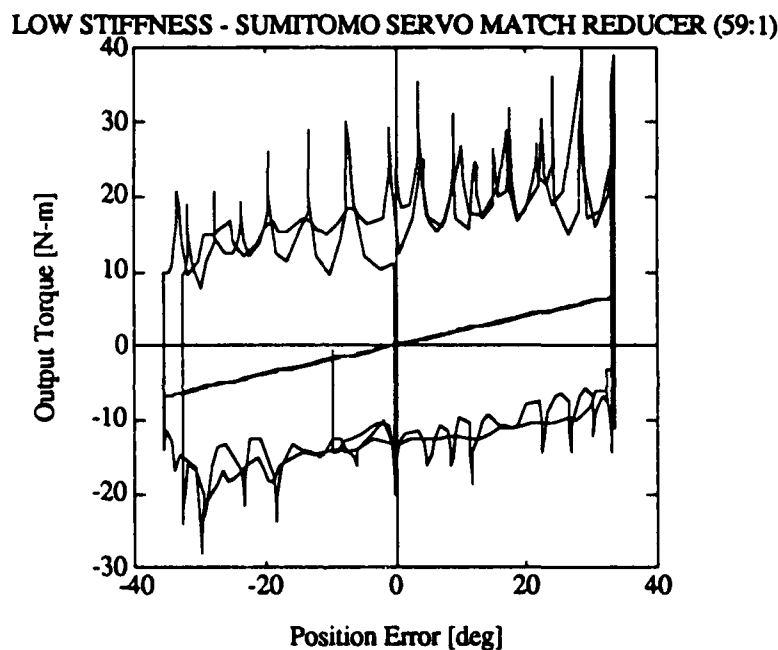


Figure 4.35 : Desired and actual output stiffness behaviors for the Servo Match Cycloidal Reducer from SUMITOMO (59:1).

Notice the large hysteretic losses of $\pm 10/15$ N-m, as well as large torque-spikes which are present at all times and seem independent of transmitted load. This unit has a tremendous amount of 'dimensional interference fits' in order to reduce backlash, and is thus not a recommended candidate for a torque multiplier in colocated control scenarios. The large discrepancy between stiction- and friction-torques will certainly pose problems when we try to close a torque-loop around such a transmission, especially in the presence of such large torque-ripple.

The transitions between stiction and friction behavior can be documented especially well, if we trace the actual hysteretic stiffness behavior for medium and high levels of desired output stiffness. Figure 4.36 shows these two traces:

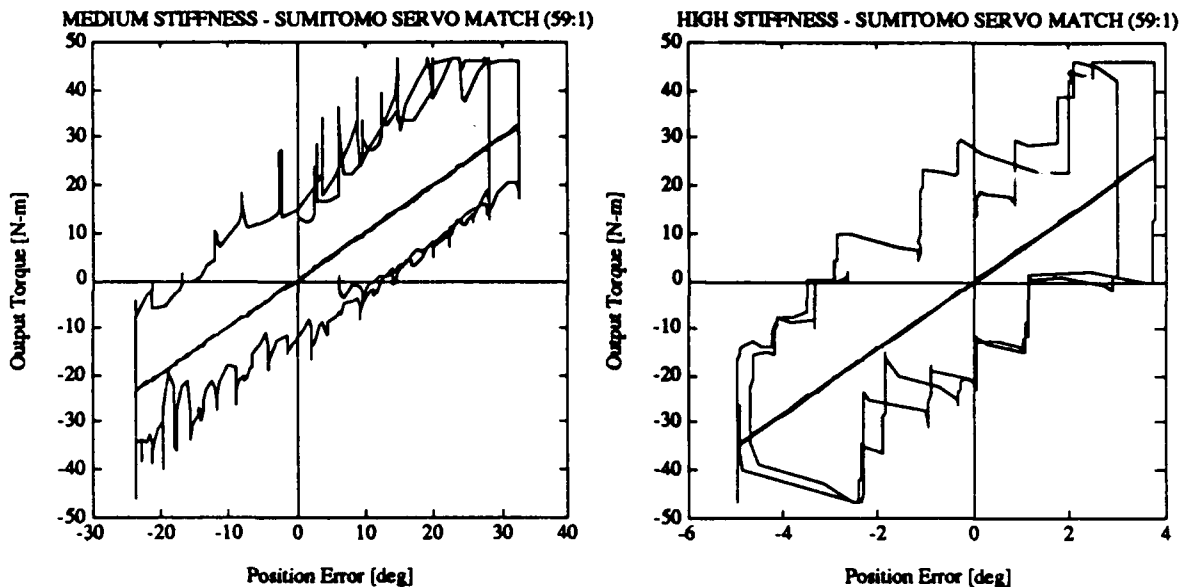


Figure 4.36 : Medium and high levels of actual and desired output stiffness, as measured for the SUMITOMO Servo Match Reducer (59:1).

In the above Figure 4.36, it is obvious how much stiction and friction plays a role in the stiffness fidelity of this transmission. The torque-ripple is most likely spatially correspondent to the epitrochoid gear-disks rolling over the rollers on the inside housing. During the testing period, it was noticed that the transmission output flange had a tendency to 'walk' out of the retaining housing and thus was preloading the support bearing on the output shaft to the point where we were incurring large frictional losses due to rolling bearing friction. The tests were then repeated with the support bearing removed, which resulted in a slight improvement in terms of friction. In a real application though, this bearing would have to be present and be a thrust-bearing, which would deteriorate the transmission's performance even further. The SUMITOMO factory was contacted in Virginia, and made aware of this problem, to which the design engineers simply said that it was a known phenomenon, and that even though it is not mentioned in the catalog, all users have to install a thrust bearing of a certain size to accommodate for this feature.

The natural friction losses are the most important descriptors for the Servo Match unit, since they describe the most important behavior of this unit. In Figure 4.37, we have

shown the torques and associated velocities necessary to backdrive the unit from the output.

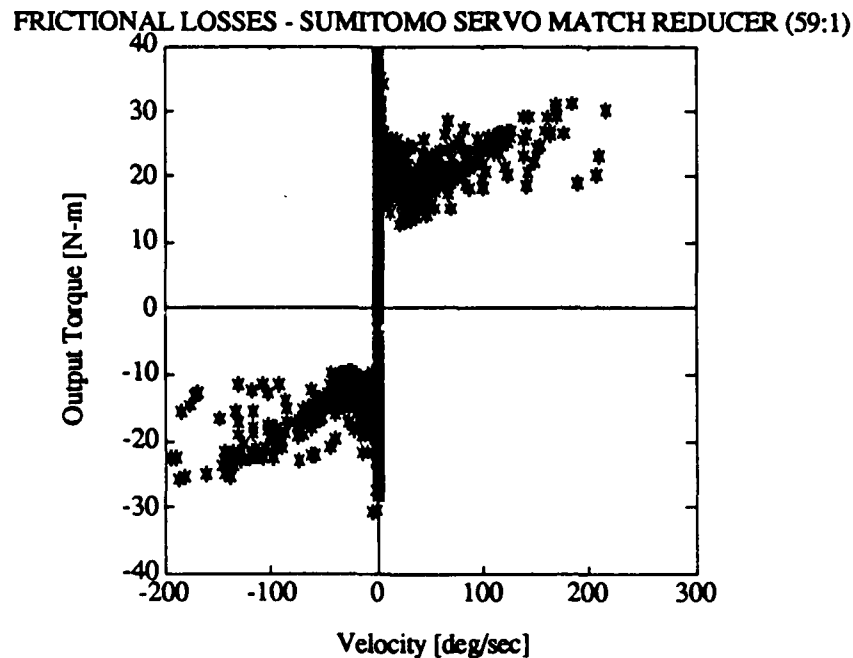


Figure 4.37 : Natural friction behavior in the SUMITOMO Servo Match Cycloidal reducer (59:1), illustrating the high frictional losses present in this type of transmission.

This data set gives a clear indication of the stiction/coulomb/viscous-friction present in a unit of this type. Notice that the stiction- or breakaway-torque is extremely high ($\pm 39/31$ N-m), as is the coulomb torque ($\pm 19.2/15.4$ N-m), which results in extremely large ratios for stiction/friction torque. This ratio could even be much higher, since due to the large data scatter it is very hard to properly determine a coulomb offset (achieving very low speeds at the output was very difficult, due to the high stiction torques in the unit, which had wide spatial variations as well). The typical stiction-to-viscous transition is very obvious from the above data, and results in directionally dependent viscous losses of around $\pm 0.036/0.022$ N-m/deg/sec.

This unit required above 60% of full rated torque of our motor to even break away at the input. Such phenomena underscore the wrong design approach, where one would have to select a motor, based on the break-away criteria of a transmission. Selection of motor horsepower to suit the stiction of a transmission is the wrong design procedure, and even then will not get around the problems of stiction in robot force control. The use of this transmission makes the use of a force-sensor at the output necessary, in order to achieve

some sort of accuracy, but will then also be subject to stability and limit-cycle constraints that seriously degrade task performance. This transmission has the worst performance of all the units tested, and we do not recommend its use in the design of force-controllable robots, unless it is redesigned to address the problems mentioned earlier.

(d) KAMO - BALL REDUCERS - A closer look

The so-called ball reducer is a turn of the century German invention that has been successfully built for the transmission market by the Japanese. The basic design consists of two thick disks, eccentrically rotating, that are separated by many precision ground spheres running in precisely milled grooves that are machined into both opposing faces of these disks. The two grooves are milled in a hypocycloidal and epicycloidal trace with respect to a fixed-radius circle inscribed on both disks. The plates rotate so as to make the balls traverse a quasi-sinusoidal trajectory, while the disks themselves rotate with respect to each other at different speeds; that is how the speed reduction is accomplished. The torque is transmitted by the balls in contact with the grooves. In order to insure full body contact (a newer design involves a four-point contact) between the spheres and the plates at all times, the plates have to be preloaded, which in turn increases the frictional losses in the drive. On the other hand, through careful machining and maintaining tight tolerances, this drive can be made to have virtually zero backlash and also extremely small ripple torque.

We first started by acquiring an off-the-shelf 10:1 ball reducer, which represented their standard model. Most of the data in the first section represents the results obtained for this first unit. We realized that KAMO would have to build a custom unit in order to prove its claims and comply with the specs that we required from an ideal transmission. This second reducer was a 30:1, and was also sized to handle the loads that the manipulator joints were designed for. It proved to have markedly different behavior, as proven in the second section of this chapter.

Small Model (10:1) - Backlash, Impedance Compensation, Torque-Ripple & Transmission Stiffness

When the first unit was purchased under consignment, the pretension was lowered to a point where the frictional losses were very small, and a series of tests was conducted. The results are given below, as well as subsequent changes to the transmission which resulted in an interesting new data set. We were rather surprised at the unbelievable large range of possible behaviors (high-fidelity yet only conditionally stable, and also low-fidelity yet stable) that this transmission exhibited in almost every aspect during the second

set of tests, when we reconfigured the transmission and were able to make some interesting conclusions.

As was previously mentioned, the manufacturer claims virtually zero backlash on his transmission design. For all intents and purposes, upon receipt of the unit, we were unable to measure any backlash with the sensors at our disposal. This behavior was only possible though, by preloading the disks to a point where 40% of the full torque available from the motor was necessary to just brake the stiction torque (a typical figure for industrial robots - especially the PUMA robots which use preloaded gear boxes). This was of course not a useful transmission for our test purposes.

Upon conferring with the technical staff at KAMO SEIKO (the manufacturer), we agreed to reduce the pretension to a lower level. The result was of course a drastic increase in the backlash of the unit (about 10° at the input). As can be seen from the test of transmission stiffness, the backlash is indeed present (Figure 4.38).

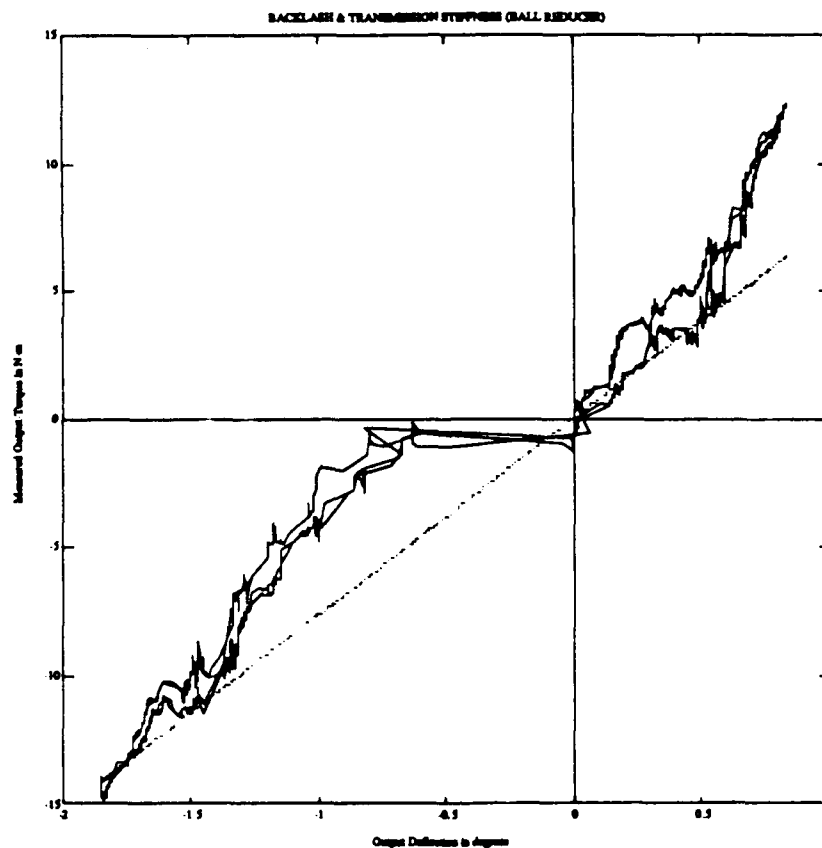


Figure 4.38 : Backlash present in Low-Preload Ball Reducer Transmission.

Once the trace is shifted on the x-axis, the full backlash at the output can be measured to be about 1° . The transmission unit was then 're-tensioned' to the point where

the above behavior could neither be felt by hand (a trained person can feel about 10 arc-min or 1/6 deg) nor measured by the encoder (less than 50 arc-sec). The same test was repeated and the resulting data is shown in Figure 4.39. Notice that there is some level of torque ripple which is due to the transition of the torque transmitting steel spheres transitioning from one milled groove on one disk to another groove on the opposite disk. Stiction and friction are also present in the drive as evidenced by the stepwise changes in the load pattern. Furthermore note that the transmission stiffness does not seem to be very high - this is discussed in more detail later.

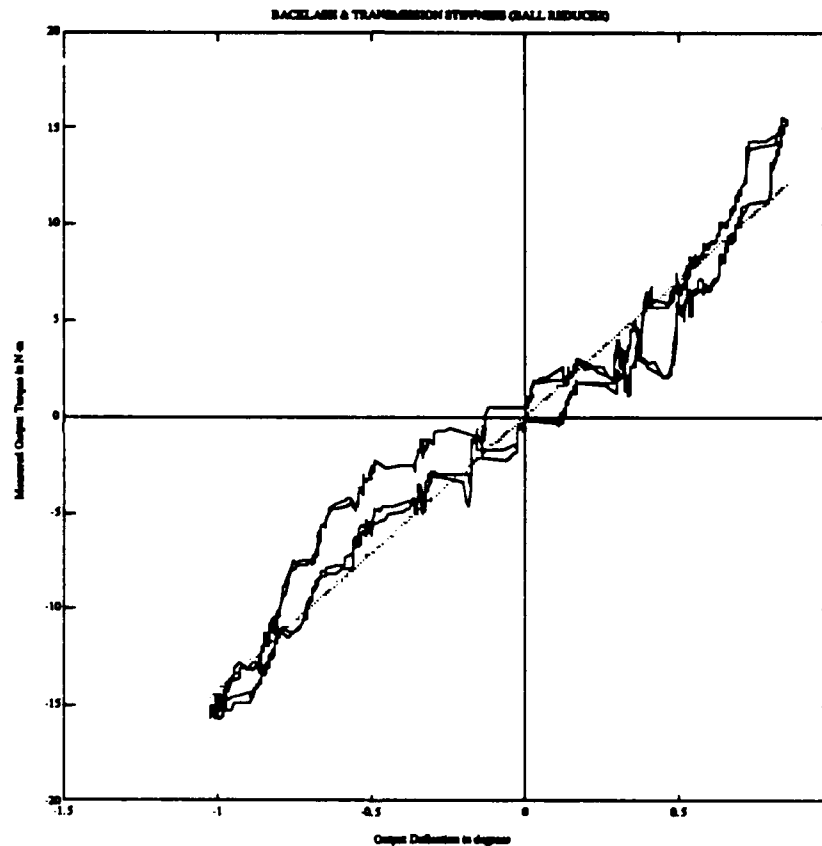


Figure 4.39 : Removal of Backlash in Ball Reducer through increased Preload - Notice low apparent transmission stiffness level.

As was claimed by the manufacturer, the backlash can be reduced to any desired point where the frictional losses are at an 'acceptable' level. The penalty one pays is in the reduced amount of maximum torque the unit can transmit before the torque ripple increases drastically, transmission stiffness is reduced and the unit eventually fails (loss of 4-point contact on each torque-transmitting steel balls and the uneven riding and distribution of

these balls inside the grooves accompanied with possible jamming of the balls or even jumping of the balls out of their grooves).

The ability of the transmission to faithfully implement a desired stiffness was tested next. The desired and actual stiffnesses for the low preload and higher preload transmission scenarios described above, are compared below, and the experimental results are shown in Figure 4.40:

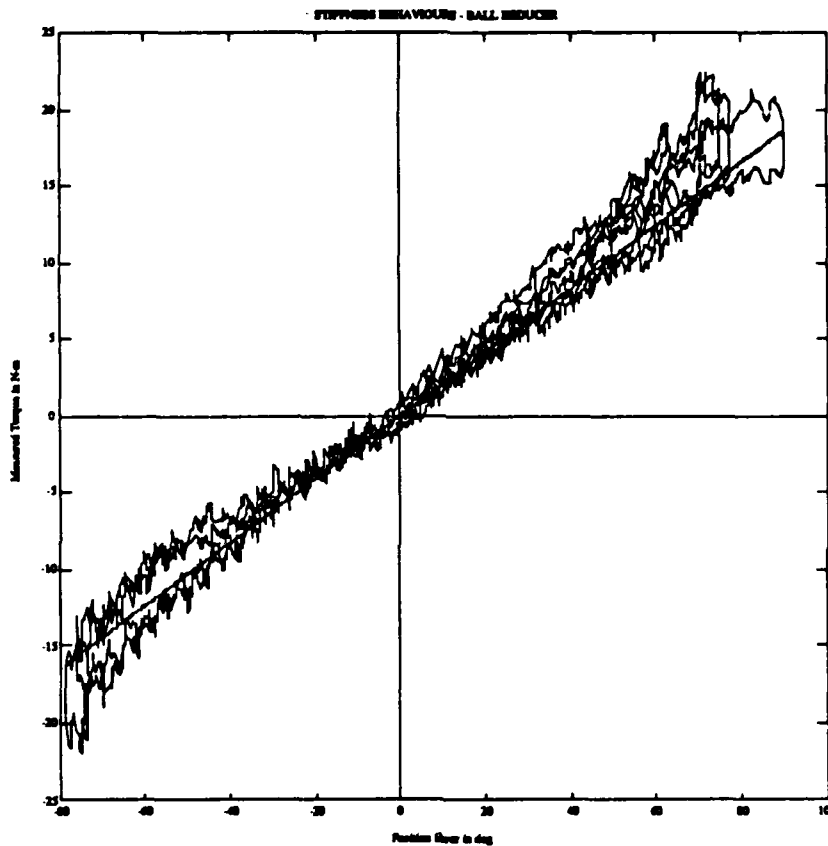


Figure 4.40 : Stiffness Fidelity for Ball Reducer as a function of transmission Preload.

The distinction between the two drive performances is not very visible from the plot above. But the ripple-torque present at increased levels of preload, is more than twice the level present for lowered preload levels. Another interesting phenomenon is the increase of frictional losses with increased torque-transmission (as with any device of rolling or sliding contact, where forces are transmitted perpendicular to the contact point/line). The torque-ripple magnitude obvious from both traces above is most certainly due to the nature of the drive (balls rolling in alternate grooves) coupled to the tolerances in machining such a device. If the preload on the disks is increased to the manufacturer's specified level, the

relative magnitude of the ripple would be superimposed on the pure friction and stiction losses, resulting in a hysteretic trace with high-frequency ripple.

The fidelity with which this transmission follows the desired stiffness is quite good (despite the apparent ripple). As a matter of fact it was among the best that was measured. No further data to prove stiffness fidelity, needs to be presented, since the plot above is a test for low stiffness fidelity, with the solid straight line representing the desired stiffness.

Efforts to compensate for the amount of coulomb friction present in the drive were meaningless due to the low level of frictional losses and the unmeasurable level of increase in frictional losses present at larger torque levels. Performing an impedance compensation scheme was equally fruitless, since the available bandwidth was not sufficient to get rid of the 'ripply' transmission behavior (see Figure 4.41).

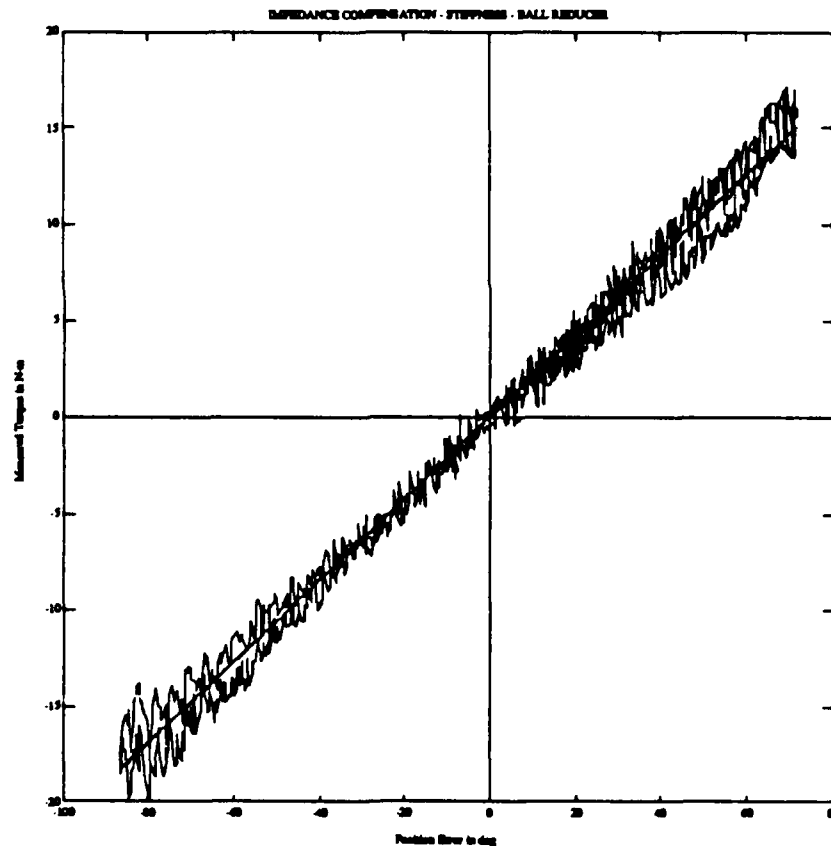


Figure 4.41 : Gain from impedance compensation scheme applied to ball reducer hampered by hardware constraints.

The trace clearly shows that compensation would be possible, but in the case of this transmission it may not necessarily mean an increase in fidelity, unless the bandwidth of the compensation scheme could be drastically increased.

The behavior encountered during the experimentation with high gain closed-loop systems with inherent backlash and/or areas of low stiffness (with or without any of these compensation schemes present), is very noteworthy. Like so many motor/actuator packages operating in the real world, many of them have a high update-rate local controller that has implemented on it high loop gain servos so as to achieve a high bandwidth controllable system. Most of these actuators have a varying degree of backlash inherent in their design and a varying transmission stiffness. Not only that, but they also have different levels of stiction/friction affecting their performance and limiting the type of tasks they can do. Many different implementations use friction compensation, of which the coulomb friction compensation scheme is its most simple example. The use of the impedance compensation scheme is simply a refinement in that it may be able to compensate for the transmissions' natural frictional behavior.

Both of these schemes were implemented on the ball reducer with a high loop gain and in the presence of substantial (and measurable) backlash. The resulting behaviors about the setpoint of the motor controller were very interesting to observe. In the case of the velocity compensation scheme, we would be able to excite a high-frequency low-amplitude limit-cycle (about the size of the zone of lost motion), while the impedance compensation scheme would break down all together and make the system unstable. The data presented in Figure 4.42 clearly shows how friction compensation creates a limit cycle (left plot), while impedance compensation excites the system and can cause instability (right plot) - here the motor-shaft was slowed down by increasing the bearing friction using ones hand. A similar effect can be obtained if excessively large amounts of electronic damping are introduced.

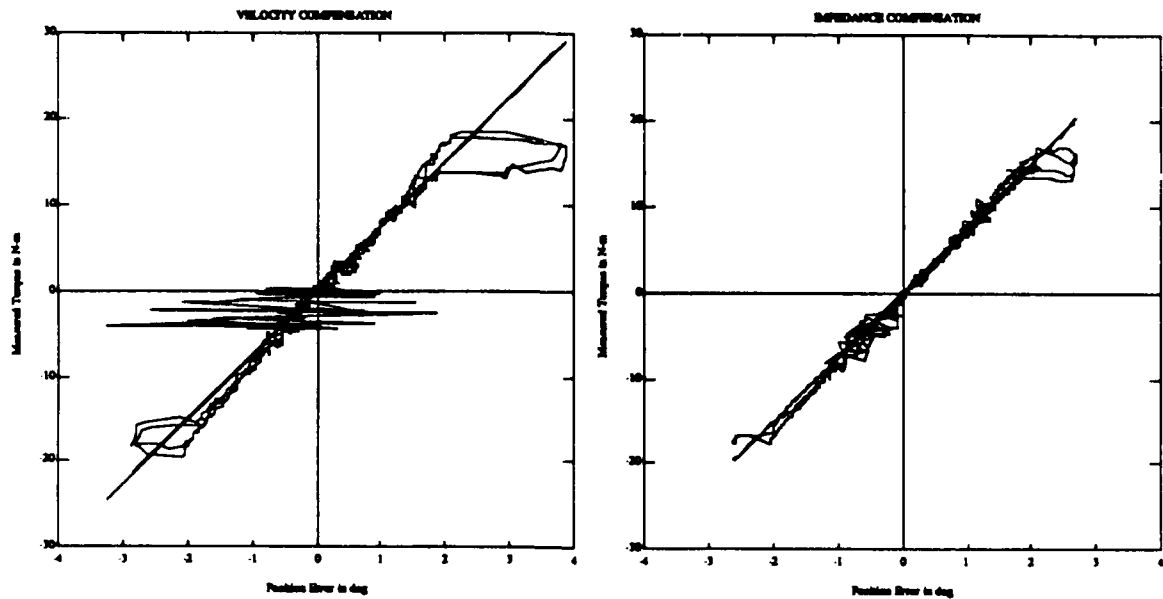


Figure 4.42 : Friction Compensation schemes excite (a) limit-cycle behavior in the case of coulomb-friction compensation (left plot) and (b) instability if impedance compensation is used (instability damped out by hand in right plot).

In the case of the coulomb-friction compensation, the limit-cycle (bounded instability) could only be avoided by increasing the torque to a level higher than that of the frictional feedforward torque (moving away from the setpoint), traversing the limit cycle area very fast, or by adding absurdly high amounts of electronic damping (this approach only reduced the amplitude of the limit cycle), or by drastically decreasing the size of the backlash to levels well below those that the controller could measure (a function of the position encoding sensor/scheme). The presence of any measurable amount of backlash coupled with the extremely low inertia present during motions inside this zone (purely the rotor and shaft but excluding reflected transmission- and load inertia), can cause a high gain position controller (despite electronic damping) to set up limit cycle behavior and possibly even cause instability in a discrete controller implementation. Integral controller gains are not really addressed here since they are not really part of an impedance controller due to their lack of physical equivalence, but they are bound to only add to the problem

When using the impedance compensation scheme, the instability was reduced only if the zero-setpoint zone was traversed fast enough, or excessive electronic damping was introduced, or the backlash zone was drastically reduced in size. Since we are closing a lower bandwidth loop around the transmission in this case, this scheme is not only more sensitive to sampling frequency, but results in instabilities right away. If the environment being contacted is fairly stiff, instabilities would be even harder to avoid (in this case it was the operator manually deflecting the output). Reducing the environment stiffness is not always in our hands (depends on the task) and adding excessive electronic damping is not really a viable solution at all times. The increase in compensation-loop bandwidth may be helpful, but it is the opinion of the author that instabilities may be avoided only at the price of setting up limit-cycle behavior, or excessively damped responses.

For the same transmission, the preload was increased (stepwise) in order to reduce the backlash zone, and indeed the limit cycles died away in amplitude until they disappeared completely (for the same high gain controller). The same was true for the impedance compensation scheme, where we went from downright instability to reduced limit-cycles and then to stable behavior.

However, the reasons for reducing limit-cycle behavior and stabilizing a system, are not only due to the reduction in backlash. As we saw earlier, a simple reduction of the backlash to 'zero', did not guarantee proper system behavior nor stability. The ball reducer was a fairly interesting transmission which exhibited a variable backlash zone together with a zone of variable stiffness. Like so many other drives (harmonic drive), the true transmission stiffness behavior could be represented by Figure 4.43 (even though shown as a linear relationship, all the transmissions tested here have more of a hysteretic stiffening behavior), which identifies two regions of different stiffness (which need not be omnidirectional) as a function of the applied torque:

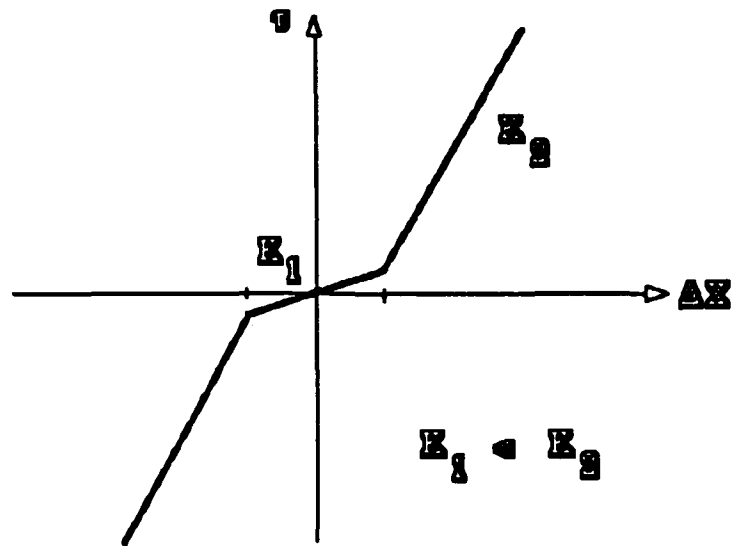


Figure 4.43 : Typical Transmission Stiffness Behavior includes 'soft-zone' around zero-load point and higher stiffness during torque transmission.

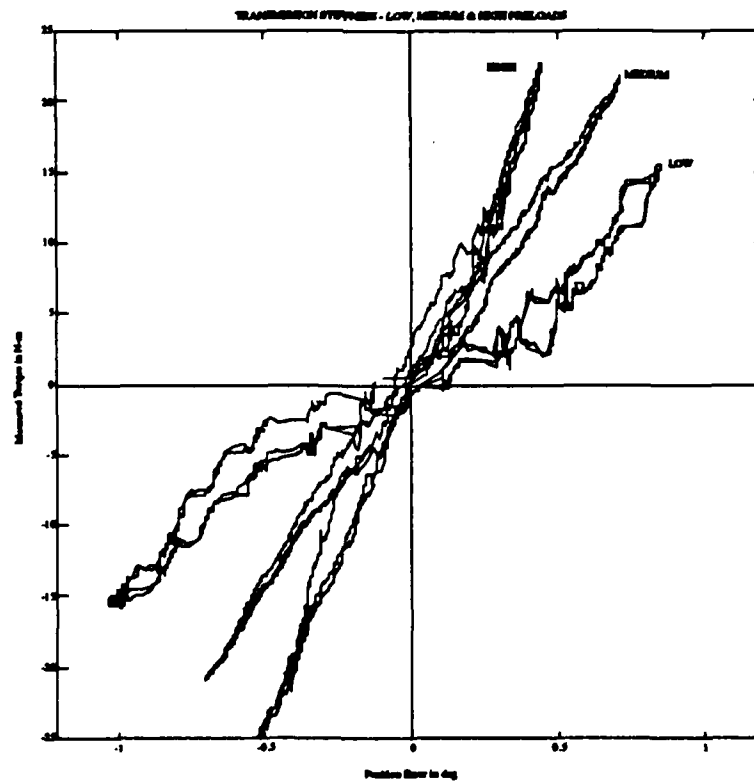


Figure 4.44 : Zones of varying stiffness as a function of preload in the ball reducer.

There is a region of lower stiffness around the 'no-load' point, which for a servo system represents its setpoint. The size of the 'soft'- or 'wind-up zone', the relative stiffness as well as the size of the inertia reflected onto the motor, have a dramatic effect on system behavior. The zone of reduced stiffness can be shrunk in the case of the ball reducer, by increasing the preload on the plates. In Figure 4.44 we have shown that there are indeed two zones of stiffness, and that their relative sizes are a function of transmission preload (low, medium and high).

The most jagged trace represents the transmission stiffness for a low value of preload. Notice that at about ± 0.5 degrees, the stiffness trace increases in slope abruptly. The two steeper traces for medium and high preload have a slope that is fairly constant throughout the displayed range and a change in transmission stiffness can no longer be detected. The maximum value of displayed 'Measured Torque' represents the saturation torque available from the motor at the output.

The price for a higher transmission preload lies in an increase in system stiction/friction. The next plot (Figure 4.45) analyzes the stiffness behavior for the ball reducer for a low and high degree of preload on the transmission. The difference is quite sizeable and the magnitude of the stiction is now comparable to that present in the cable reduction - and the ratio of reductions is 3 to 1! In other words the frictional losses in this transmission are high and are expected to be even higher in a 30:1 reduction. The large amount of torque-ripple in the high preload trace is also worth pointing out.

The fact that a load coupled through a low stiffness transmission to a high gain servo motor, with or without backlash present, can create limit-cycle behavior and even unstable behavior is nothing unexpected. This is demonstrated in the two separate data sets illustrated in figure 4.46. The plot on the left represents a stiffness fidelity test on the ball reducer under low preload (no backlash present) - the instability (limit-cycle) is evident. The plot on the right is the same test, but the preload on the ball reducer has been increased to reduce the zone of low transmission stiffness to undetectable levels - no instability can be seen nor was it possible to induce it.

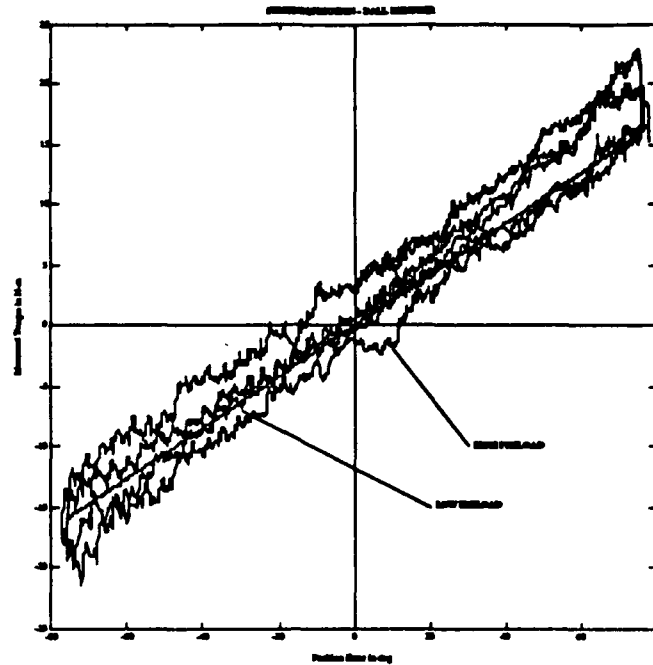


Figure 4.45 : Stiction/Friction and Torque-Ripple as a function of Transmission Preload in a Ball Reducer.

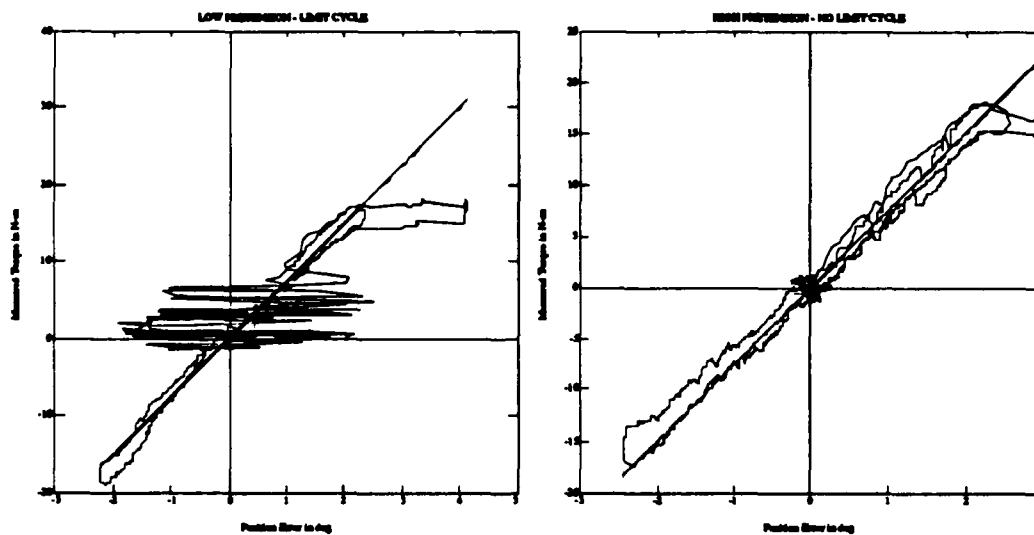


Figure 4.46 : Stability is a function of transmission preload in the case of the ball reducer - (a) limit cycles for low preload (left plot) and (b) stability for high preload (right plot).

It is interesting to note here is that a transmission's hardware characteristics will severely limit its dynamic behavior. Comparing the same limit-cycle behavior in the ball reducer to that in the cycloidal reducer, leads to yet another interesting conclusion. In order to achieve the same output behavior on the ball reducer [10:1] as on the cycloidal reducer [29:1], the motor-gains had to be increased by a factor of 8.41 $[(29/10)^2]$, which of course results in a much tighter controller bandwidth at the motor-end. But this does not imply that the size of the reduction is a factor, since this limit-cycle behavior was observed in both of them, for the same level of desired output stiffness. But smaller reduction ratios with soft-zones and/or backlash, will be more susceptible to instabilities with high-gain controllers.

Furthermore, the presence of increased levels of transmission friction can be stabilizing if all one has to deal with is a backlash zone and if the transmission is stiff, but the converse is not true. Proof for that comes from comparing the same high stiffness experiments run on the cycloidal reducer and the cable-pulley reducer (with or without any compensation schemes). Since the reductions are virtually identical [29:1 and 30:1], the controller gains are virtually identical. In other words we are implementing a stiffness controller that is 8.41 times higher than the largest stiffness tested before, since we are using the same gains for the cycloidal and cable reducer, as were used for the ball reducer. The cycloidal reducer has a fairly sizeable backlash zone (1°) and a higher frictional loss than the cable reduction but an otherwise higher transmission stiffness. The two plots below (Figure 4.47) show the cycloidal reducer developing a high amplitude limit-cycle about the backlash zone (on the left), while the cable reducer retains its high stiffness fidelity (on the right), along the solid line of $K = 68 \text{ N-m/deg}$, despite attempts to induce oscillatory behavior or even instability.

The test data for the cable reducer, shows no limit-cycles nor unstable behavior, while the cycloidal reducer experiences limit-cycle behavior (which would result in instabilities if the force transducer was included in a servo-loop for compensation purposes). All it took to excite the instability is a slight tap on the output shaft to deflect the input shaft and the oscillations would set in. The only successful attempts to damp this behavior required the operator to damp the shaft by hand or to introduce so much excessive electronic damping into the controller, that the system became extremely overdamped, to the point where the motor would start humming (high frequency oscillatory behavior - barely visible to the eye due to the resolution and discretization of the position/velocity encoding scheme and the associated high velocity gains).

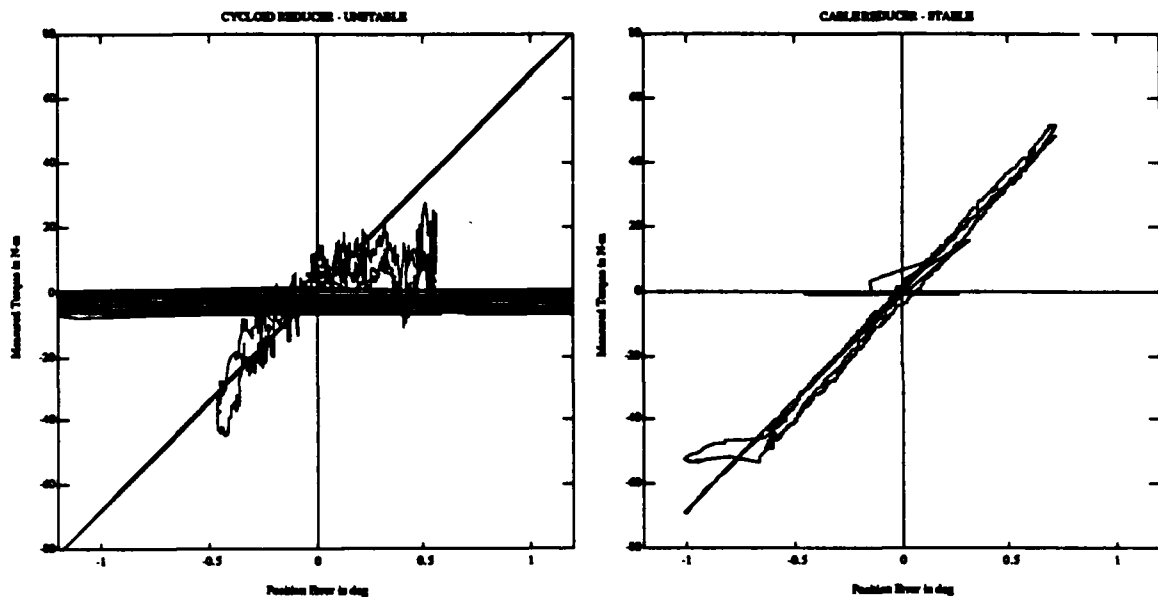


Figure 4.47 : Cycloidal Reducer experiences instability due to soft-zones and backlash, despite higher frictional damping (left plot), while cable reducer is stable at all times (right plot) due to absence of backlash and 'soft-zone'.

It is quite important to mention this behavior, since it addresses several questions that are raised in this chapter. The main question is that of transmission fidelity, and we have obviously encountered different levels of fidelity, that make some transmissions more attractive than others. The question was thus whether the desired behavior could be obtained by different levels of compensation. The answer to that question is that it is possible only for some transmissions, and then it may only be useful if certain hardware criteria can be met, which in turn means that some very important questions must be considered as early as in the design stage for not only the motor and transmission, but also the coupling of one to the other. Furthermore the presence of this behavior seems to be dependent on the controller gain implemented at the motor level (in the presence of backlash and or transmissions with a 'soft' wind-up zone). Most position-controlled systems today have a fixed gain (of course very high) motor-controller that receives setpoint updates based on decision making levels of varying complexity and are mostly not open-loop but closed loop and based on sensory feedback of all kinds. Friction compensation is one of

the most basic compensation schemes necessary in most industrial transmissions used on robots in the real world, and raises the question whether there is a subset of tasks, where operations are either not possible or can cause serious instabilities. Even if we decide to forego the attempt to increase the transmission fidelity via compensation, simple high-gain servos can not be expected to perform properly nor in a stable fashion at all times, if the transmission and the coupling are not properly designed. All these issues force one to be aware of what kinds of transmissions offer the best overall behavior, what are their respective characteristics (stiffness, backlash, ripple, stiction/friction), how do they reflect on the device's performance and what are the limitations in the task sense that are linked to these characteristics - these are the main questions this thesis seeks to find answers for.

Medium Model (30:1) - Backlash, Impedance Compensation, Torque-Ripple & Transmission Stiffness

This larger-sized unit was built specially for the force-control applications we were trying to implement. The disks and races for the cycloidal traces were specially hardened steel, while the balls and bearings (preloaded) were selected from a tighter tolerance selection. That made the unit more expensive, but it also performed much better than its smaller model. The preload of the unit was set at the factory, and was adjusted to guarantee the highest efficiency possible, without sacrificing stiffness and without incurring noticeable soft-zones nor any backlash.

The first and one of the more interesting experiments, to see how well the unit had been tuned, tested for the stiction/coulomb/viscous-friction behaviors present in this new design. Once again the unit was backdriven at the output, while output torques and (reflected input velocity measurements using the transmission ratio N) output velocities were measured. The test was performed many times, to get enough data for a good statistical representation, which barely needed any correction for false inertial loadings, thus guaranteeing good quasi-static data sets. The results are shown in Figure 4.48. The interesting point to note here, is that the unit was surprisingly backdriveable, with a(n) (average) coulomb-friction torque of $\pm 1.7/1.1$ N-m, and a maximum stiction torque around $\pm 3.0/2.5$ N-m. The viscous losses were one of the smallest recorded for any of the units tested ($\pm 0.017/0.0167$ N-m/deg/sec). These improvements stem from the lack of bearing- and shaft-seals (removed by request), as well as the use of a lower-viscosity grease to lubricate the balls and grooves.

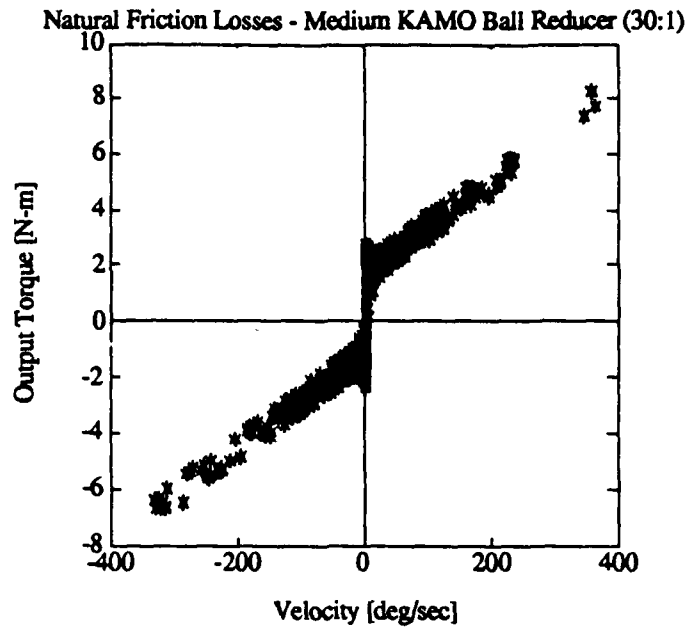


Figure 4.48 : Natural frictional losses in the new KAMO ball reducer, showing stiction-, coulomb-, and viscous-friction losses at the output.

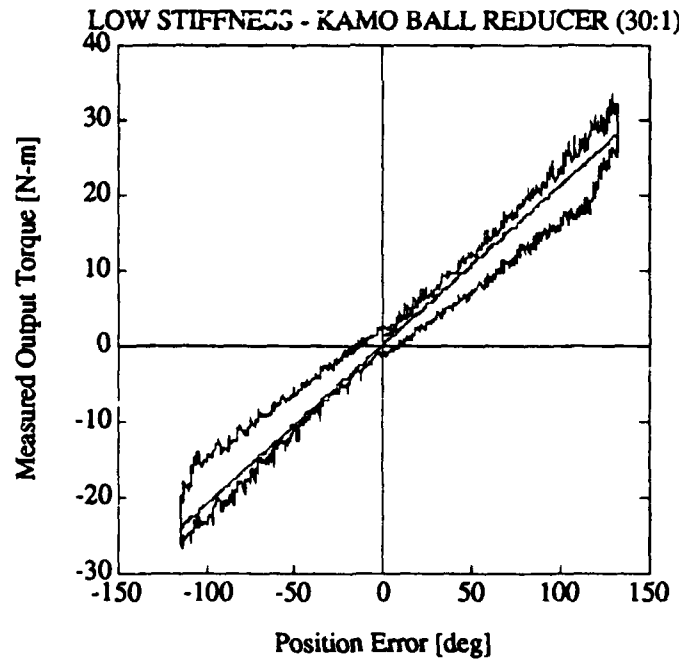


Figure 4.49 : Desired and actual stiffness behaviors for a low level (0.21 N-m/deg) of desired output stiffness, for the medium-size KAMO Ball reducer (30:1).

The stiction/friction ratio still hovers around the 2:1 level, which is an attribute that can not be avoided without reducing the preload on the unit and thus incurring large soft-zones which will reduce the stability of the unit.

Testing the impedance, or better, the stiffness fidelity of this transmission was another important comparison that needed to be done, in order to compare it to the smaller model, as well as all the other transmissions. First we performed a low stiffness experiment, which will show up the hysteretic effects of stiction/friction, as well as giving a good spatial correspondence of any ripple-torque or increased frictional losses during higher applied loads. The resulting data is shown in Figure 4.49, where the desired (straight-line according to Hooke's Law) and actual stiffness levels (hysteretic loop) are shown together. The hysteresis trace shows how well the unit follows the desired stiffness behavior when it is backdriven, with the hysteresis loop collapsing right around the zero-error position. Torque ripple has also been reduced, most certainly due to the tighter tolerances and better materials used in this particular unit. Yet it still represents a physical phenomenon that needs to be minimized in future designs, if this reducer is to be labelled a torque-multiplier. There is no real spatial nor load-dependent phenomenon that could be observed, except for the hysteretic energy loss due to friction.

The behaviors for medium and high levels of stiffness are also shown in Figure 4.50, to complete the fidelity study and illustrate the tendencies present at larger positional gains.

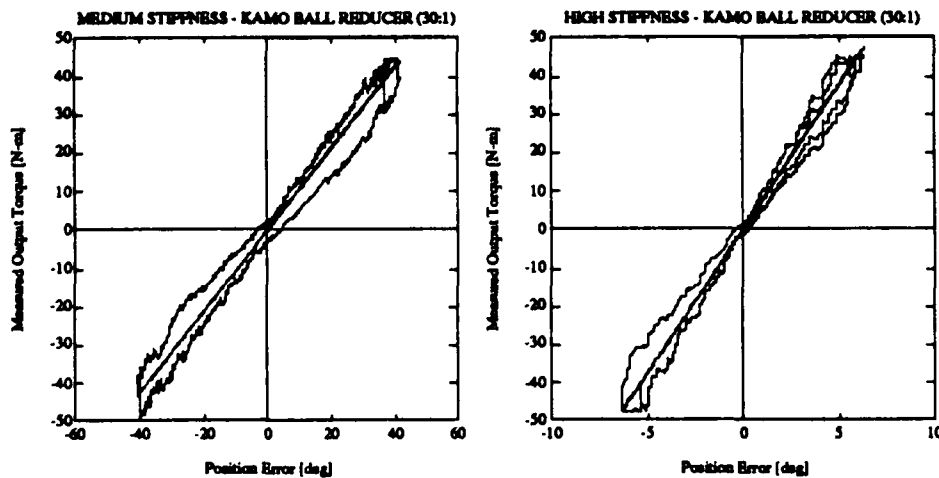


Figure 4.50 : Medium and high levels of desired stiffness and the corresponding hysteretic actual behaviors, for the KAMO Medium Ball reducer (30:1).

At a medium (1.1 N-m/deg) and high (7.1 N-m/deg) level of desired stiffness, both traces show a very high level of fidelity without a noticeable increase in ripple nor drastically increased levels of hysteretic loss. It seems as if the rolling torque transmission using balls instead of cams /gears and/or rollers is much less susceptible to improper load distribution and clearance removal. There is a good correlation between the slight bumps in the hysteretic curve, and the transitions of balls from the hypocycloid groove in one plate, to the epicycloid trace in the opposing plate. This proposed mechanism seems plausible yet requires more in-depth study. This slight undulation is much smaller than observed in the other unit, and attests to the fact that slight manufacturing problems still remain, but that the unit overall seems to outperform its smaller (mass-produced) cousin.

The last important test to undertake, is to see how the stiffness of the unit may be affected by the seemingly good results of all the previous tests. Remember that the manufacturer had to especially set the preload (under well controlled conditions), so as to obtain the increased levels of performance shown above. The price that usually has to be paid is in the form of reduced levels of stiffness. Figure 4.51 illustrates a two-step data acquisition procedure,

TRANSMISSION STIFFNESS - KAMO MEDIUM BALL REDUCER (30:1)

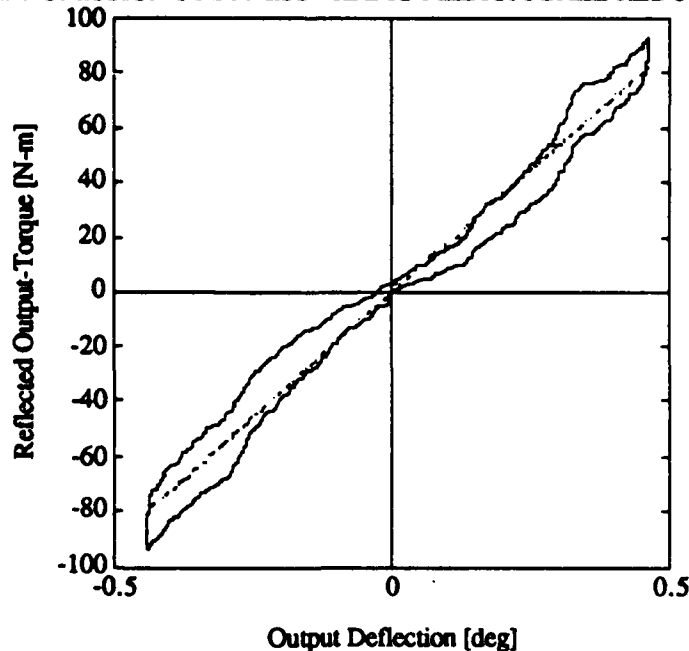


Figure 4.51 : Transmission stiffness data for the medium-size KAMO ball reducer transmission (30:1), showing two piece-wise data segments.

in which the output of the transmission was locked for each loading situation, separately. Notice how small the hysteretic losses are, attesting to the small levels of internal friction present. Furthermore notice how the stiffness behavior 'undulates' along the linearized average stiffness, indicating not a load-dependent, but a spatially dependent transmission stiffness behavior, with the motion of the output corresponding to exactly one lobe-motion per steel ball. In other words, the transmission stiffness is partly stiffening, and partly softening, depending on the spatial arrangement of its components. In its softest regions it demonstrates a 4000 N-m/deg stiffness, and about 8500 N-m/deg in its stiffest region. This behavior is quite interesting and was never observed for any of the other transmissions, and actually can represent a really tough controls problem, when a transmission has spatially (and not load-) dependent soft-zones. The lowest observed stiffness value is comparable to the cable-pulley reducer, and thus underscores the importance of transmission soft-zones which are load- and space dependent.

(e) DOJEN - CYCLOIDAL CAM REDUCER - A closer look

The DOJEN cycloidal cam reducer that was tested was a size 03, with a reduction of 33:1. It is one of the main players in the indexing and NC-machining market, and thus competes directly with SUMITOMO, HARMONIC DRIVE, REDEX, KAMO, as well as planetary gear-box manufacturers. The company claims zero backlash, and proves its claim by furnishing a stiffness-trace for each transmission. They are the only manufacture to provide real data in their literature, and make a clear distinction between backlash, wind-up and the lack of soft-zones which result in very linear low-hysteresis transmission stiffnesses.

The transmission is of the cycloidal type, using a single dual-faced epitrochoid cam which runs on a dual-bearing supported shaft and rolls past cantilevered needle-bearing supported pins. Compared to the SUMITOMO and REDEX units, torque is transmitted to the output via the epitrochoid profile (with a second set of fixed roller pins on the output flange), and not via milled holes in the epitrochoid cams, housing cantilevered sleeved pins. The short cantilevered studs at a greater radius reduce deflections and proper assembly allows for a reduction of the soft-zone and an overall homogeneous and fairly linear low hysteresis stiffness behavior.

Reductions are available in a wide variety, due to the fact that the reduction ratios are a function of the lobes/pins on the input housing/cam, as well as the pins/lobes on the output flange/cam. Most of their customer-base is in NC machining and indexing applications, as well as a cartesian-positioning robot built by Westinghouse.

Backdriveability

One of the main problems, but also attributes of these units, is that the relative efficiency, stiffness and backlash can be controlled during the assembly process. Most of the NC and indexing applications use drives where a premium is put on stiffness and zero backlash, while efficiency is sacrificed and only plays a role in motor-selection and duty/life-cycle of the system.

The unit tested in this thesis was optimized for efficiency and stiffness. During the assembly of the cantilevered needle-bearing supported pins, the tolerances were kept so as to achieve zero backlash and a minimum amount of dimensional preload to remove any lost-motion phenomena, and achieve a stiffness trace with no distinct zones of varying

stiffness. The transmission was tested for backdriveability and viscous losses in the low-to-medium torque range. The plot in Figure 4.52 below, illustrates how much torque was required to backdrive the unit at different speeds. It shows how close to linear the viscous losses are, and how stiction and friction are apparent in this unit.

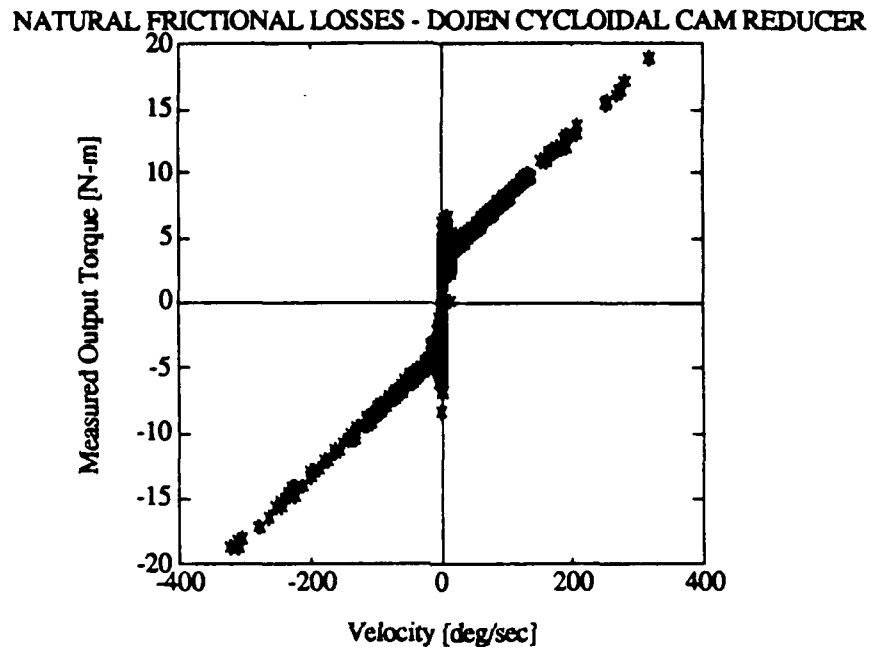


Figure 4.52 : Stiction/Friction and Viscous Damping Losses inherent in a DOJEN Cycloidal Cam Reducer.

Notice also how the stiction values vary for different directions of motion. The above test incorporates data taken over the entire positional spectrum of the unit's components, and thus shows off any spatially dependent stiction/friction characteristics - an important transmission characteristic. The above data set has only been corrected for acceleration-dependent torque-loads, but has not been filtered nor otherwise altered. The stiction values lie around $\pm 7/8$ N-m, while the coulomb-friction values are around ± 4 N-m. This data illustrates how for this unit the ratio of stiction to friction lies around 1.8 to 2.0. The spatial variation in stiction values accounts for this high variability in the friction index. The reasons are due to tolerances during machining and assembly. More clearer data can be used to underscore this behavior by studying the figures in the section on impedance fidelity.

Impedance Fidelity

This series of tests focussed mainly on the fidelity with which this transmission could reproduce pure stiffness behaviors. This test is important, because it shows how stiction/friction affects the stiffness-following properties at low levels of desired stiffness, while also highlighting the different behaviors as transmission torques vary over the entire load spectrum. Two data sets are presented next, illustrating all of the characteristics mentioned above.

The first data set illustrated in Figure 4.53, shows how well the transmission can replicate a desired level of low stiffness - in this case 0.21 N-m/deg at the output.

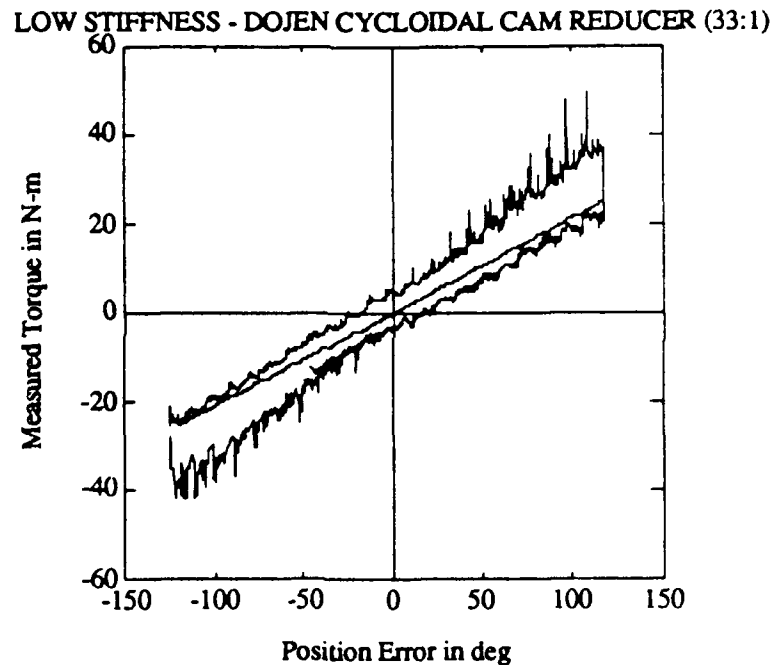


Figure 4.53 : Low Level of desired and actual stiffness for the DOJEN Cycloidal Cam reducer (33:1).

This test is very helpful, because it allows the unit to be moved through a large rotational envelope, thus showing off spatial dependencies of such variables as stiction/friction. Notice how there is very little increase in the hysteretical or coulomb - friction loss with increased torque transmission, which attests to very good load distribution and rolling contact. On the other hand notice the large spikes in measured output torque, while the unit is forward driven (in either direction). These spikes are most certainly due to lack of machining and assembly homogeneity. Furthermore, notice how due to the large range of deflection, the circular traces in the backdrive direction are a

testimony to the continuous circular rolling contact between successive sets of the cantilevered rollers (so called 'fishtailing'). Thus due to the manual assembly process and inherent tolerancing issues, the unit has spatially dependent dimensional preloads, giving rise to these traces.

The second data set illustrated in Figure 4.54, shows the unit's ability to faithfully follow levels of medium and high stiffness.

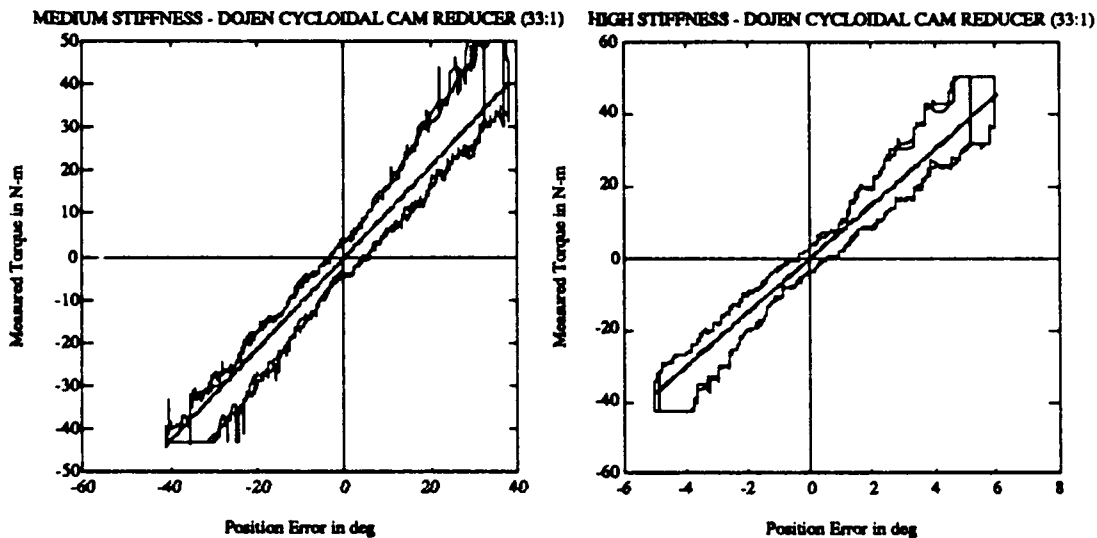


Figure 4.54 : Stiffness Fidelity for medium (1.1 N-m/deg) and high (7.2 N-m/deg) stiffness levels tested on the DOJEN cycloidal cam reducer (33:1).

The medium and high stiffness fidelity plots above illustrate the relative hysteretic loss present at higher levels of desired stiffness. Notice that even though the relative energy-losses may seem reduced compared to Figure 4.53, the efficiency of the unit is unchanged, with the hysteresis loop simply stretched due to the relative scales of the plot. Torque ripple is still very much present, with stepwise following underscoring the presence of stiction/friction transitions, as explained in the general data analysis section. The manufacturer is currently installing a new NC machining assembly, which will change the manufacture and assembly dramatically. Assembly inaccuracies will be removed, due to the ability to locate components with much improved tolerances. What effect that has on the homogeneity of the unit's response will have to be left to others to explore, as their new prototype was not ready when this document was written.

Transmission Stiffness

This unit is one of the ones for which the manufacturer supplies real and unadulterated stiffness data. Their claim is that this unit has zero backlash, and an undetectably small region of lost-motion, which gives the unit a fairly homogeneous and linear stiffness behavior. The unit we tested was designed and assembled especially to maximize efficiency while maintaining zero backlash and a minimum zone of lost-motion. The test performed here was to lock the output and increase the torque at the input, and plotting the applied torque vs. the measured displacement. Data was then scaled to show the effective output stiffness of the transmission (displacements).

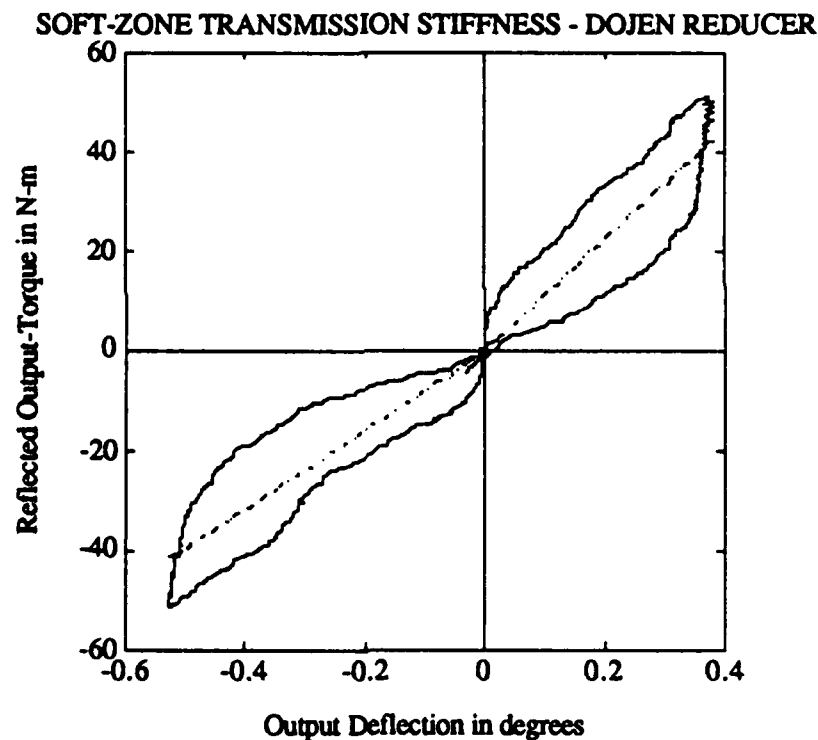


Figure 4.55 : Transmission Stiffness Trace for the DOJEN Cycloidal Cam Reducer.

Notice how the unit's hysteresis undulates in Figure 4.55, giving rise to zones of different stiffness. The reason why the hysteresis loop starts and ends at zero, is because the positive and negative responses were obtained in separate trials. Overall, the unit does display some soft-zone behavior which is introduced due to the trade-offs mentioned earlier. The unit's maximum stiffness of about 6300 N-m/rad, is about an order of magnitude lower than their maximum advertised values. Once again, this was to be

expected, since the amount of dimensional preloading was minimized to increase efficiency (by reducing interference fits and thus friction/stiction), and we are performing a forward-stiffness test. The manufacturer is currently working on setting up a new manufacturing facility that will enable them to increase their tolerances to 1/100000th of an inch, thereby being able to get as linear a transmission stiffness curve by removing the relatively tricky manual assembly process. Unfortunately, at the time of this report, such a unit was not yet available.

(f) REDEX - CYCLOIDAL GEAR REDUCER - A closer look

The geared cycloidal reducer made by REDEX in France, and dubbed the CORBAC (stands for Correctable Backlash), is similar in conceptual design to all the other cycloidal reducers, in that it uses the planetary/cycloidal method to generate large reductions in a compact volume. It differs in that its cycloidal disks do not have epitrochoid curves milled into them, but are rather simple involute-profile spur-gears. The rolling pins on the inner gear have been replaced by a set of split ring gears, which can be phased with respect to each other and thus serve to preload the two crown-gears and can remove backlash and other tolerance fits inside the unit. The proper adjustment of the relative phase is critical, since one could easily exert too much preload and hence reduce the efficiency and create excessive stiction/friction torques. The unit tested here was carefully tuned with a minimum of preload, which would achieve zero backlash but retain the high stiffness and backdriveability of the unit, according to the data that the manufacturer had supplied.

Backdriveability

In order to study this unit and compare it with all the other cycloidal-type units, we proceeded to run a simple backdriving-test at different speeds, to produce a frictional-torque vs. speed-curve which could yield information about the order and type of dissipative processes dominant in these units. The test data presented in Figure 4.56, was obtained for several runs, for different spatial locations of the output in order to get a statistically meaningful data set, which would capture all the spatial and temporal variations.

The levels of natural stiction and friction were measured to be at a maximum of $\pm 6/7$ N-m, with coulomb-friction values of around ± 2.5 N-m. The viscous losses are again very linear and about identical, at $\pm 0.029/0.0305$ N-m/deg/sec. It is important to mention that the stiction torque or maximum break-away torque was measured to be coincident with a certain arrangement of input/output shaft, thus indicating an excessive dimensional interference due to machining or assembly. The level of stiction was very noticeable at low- to stall-speeds, but the amount of vibration at higher speeds was very small.

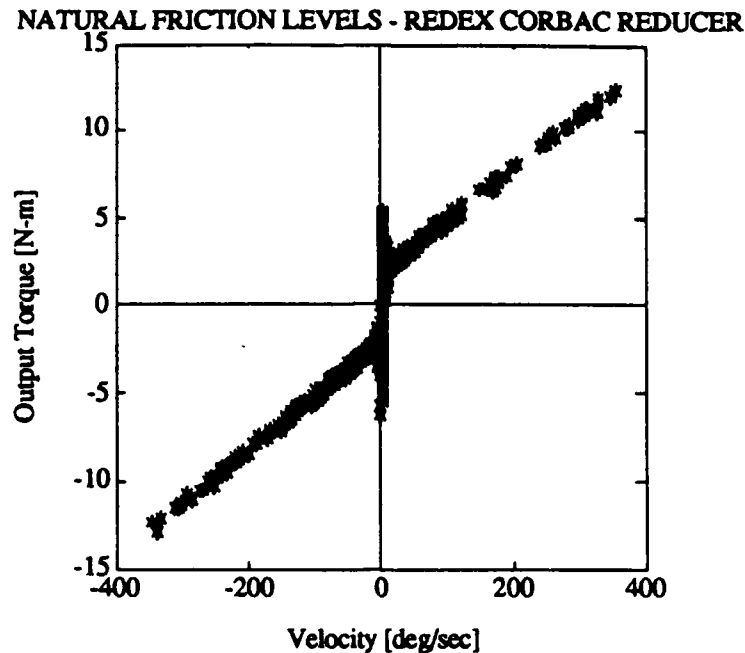


Figure 4.56 : Frictional Torques as a function of output velocity measured while backdriving the CORBAC reducer.

Such high values of stiction/friction are typical for geared mechanisms which are preloaded. If the preload on the crown gears and the inner gear is increased even further, the stiction/friction characteristics of the transmission will deteriorate. The above data set thus represents the optimal arrangement under which this drive should be operated.

Impedance Fidelity

The fact that this transmission consisted of cycloidal gears, made it an interesting case study for impedance fidelity tests. This unit represents a perfect study object for understanding phenomena of meshing teeth under various loading conditions, while incorporating a preload mechanism which would enable one to alter backlash, load-distribution, system efficiency and thus completely alter the natural system response. The fact that it is of the cycloidal type represents a good comparison with all the other transmission types studied in this thesis.

The impedance test was limited to studying the fidelity in following ideal spring behaviors. We have shown in Figure 4.57,

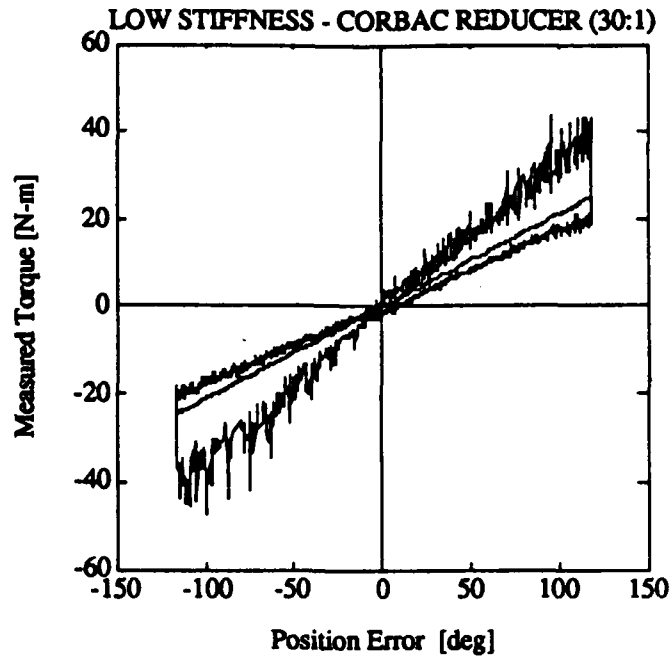


Figure 4.57 : Low level of desired output stiffness, showing the desired ideal stiffness behavior and the actual hysteretic behavior of the REDEX Corbac reducer.

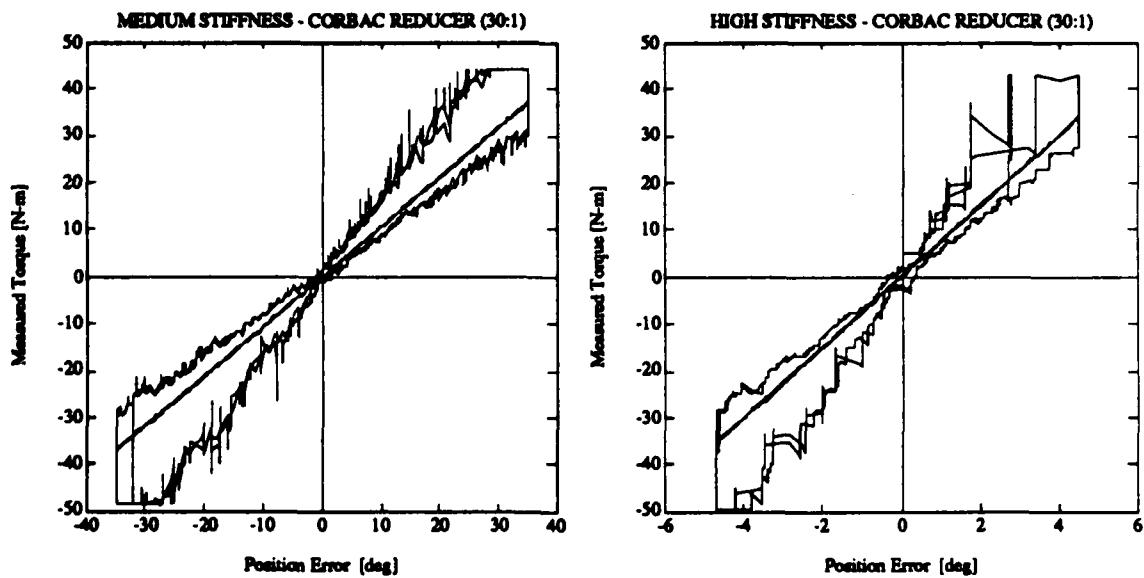


Figure 4.58 : Medium and high level of output stiffness for the REDEX Corbac reducer, showing both the desired and the actual levels of achieved stiffness behavior.

how a low level of desired output stiffness reveals the stiction/friction properties at zero load, as well as the effect of increased frictional losses at higher levels of transmitted torque, coupled to the presence of increased torque-ripple. From the plot above it is obvious that the unit can experience as much as 15 to 20% of torque-ripple magnitude at increased levels of torque-load. This phenomenon is very familiar in preloaded gear-trains, but is also indicative of improper tolerancing/assembly of this transmission. Notice that these spikes are only dominant when the unit is backdriven (direction of increased torque resistance, resulting in increased levels of hysteresis). The overall hysteresis also increases with increased loads (a flaring of the hysteresis loop with higher torques), while the stiffness following is improved for the situation when the output is forward driven (direction of motion and restoring torque sign coincide).

That these phenomena are also present at higher levels of stiffness, is apparent from the two plots in Figure 4.58, where we have shown stiffness fidelity for medium and high levels of desired output stiffness. Notice again how backdriving the unit still results in larger hysteresis than forward driving. The torque ripple is still present (at about 5 to 10%) but its frequency has been reduced due to the fact that the output of the unit traverses a much smaller envelope than for the case of low output stiffness (compare the ranges of the x-axis of Figure 4.57 and Figure 4.58). The horizontal portions of the high-torque traces are due to the saturation of the torque-sensor and are in no way representative of the motor nor transmission characteristics. Notice further that there are several traces for certain portions of the hysteresis trace, which coincide very well, attesting to the repeatability and spatial dependency of the ripple phenomena.

Transmission Stiffness

This type of cycloidal reducer has a very interesting stiffness behavior, due to the combination of preloaded meshing teeth and cantilevered pins in the cycloidal crown-gears. The trace of Figure 4.59, was obtained by locking the output shaft and ramping the input torque through plus and minus torque values while logging the input deflections. The positive and negative traces were obtained separately, which explains why the hysteresis goes to zero around the origin.

SOFT-ZONE TRANSMISSION STIFFNESS - REDEX CORBAC REDUCER

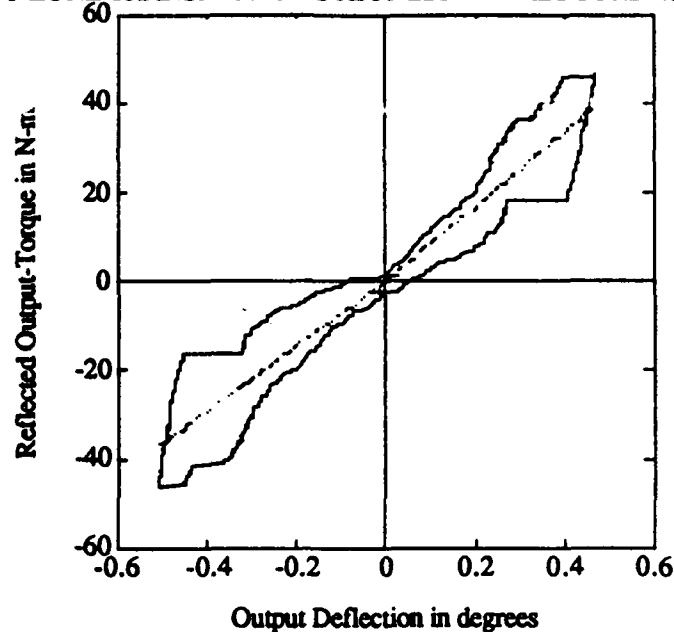


Figure 4.59 : Transmission stiffness and associated variability for the REDUX Corbac reducer (30:1).

The resulting stiffness behavior of this transmission can be seen to be one with a stiffening behavior, with a stiffness which lies around 6600 N-m/rad, which is one of the highest values obtained for any of the transmissions tested. Notice the large kinks in the hysteresis loop, which are present for loads in both directions, and implies a slippage of some kind within the transmission - a slippage which occurred at almost identical torque levels. The source for this behavior is most likely a frictional torque build-up during backdriving, which is then relieved, as the applied torque onto the unit is reduced. The presence of such slippage can have important closed-loop performance implications. The amplitude of the slip nor its physical location/origin within the transmission could be ascertained. More study in this area would certainly be beneficial.

(g) BRUSHLESS DC SENSORIMOTOR

This brief section is meant to illustrate some of the other interesting hardware issues concerning the type of brushless motors used in these experiments. There are many manufacturers of brushless motors toting their motors as the solution to many position-control problems. There are several issues that are important in choosing the most appropriate motor for one's application. Since in the field of robotics the control algorithms specify a desired torque to be applied at each joint, the motors are designed to deliver as linear a torque as possible. Below are a few of the points that should be considered when deciding on what motor to use for which application (We in no way claim that this is a complete list of factors to consider, nor is each section explored in every detail since that is better left for an appendix or other references). The fact that there are a lot of consultants out there, making a lot of money, advising customers as to which motor to buy, attests to the size and diversity in the motor and motor-controller market alone !!

Torque Linearity

Short of using a direct-drive motor, the issue of torque-linearity becomes more and more important as the fidelity of transmissions improves, since these inaccuracies in torque transmission can turn out to have an effect. Most commercially available motors have an analog current servo that is interfaced to the local motor-controller via a D/A converter whose output is proportional to the desired torque. Besides the resolution of this D/A converter and the nonlinearity of the attached analog circuitry (as analyzed by Asada), the design of the stator and rotor are critical in achieving a constant torque independent of any other variable (speed, position, current, etc.). The number of stator poles and their shape, the number of magnets and their orientation on the rotor, as well as the way the stator is wound, have an effect on the motor performance.

The spec. that was quoted to the manufacturer, SEIBERCO in our case, was that we wanted to be perfectly linear and allow no more than a $\pm 1\%$ (of maximum rated torque) torque-ripple at all times. The solution consisted of upping the number of stator poles (24 for us as compared to 4 for a MOOG brushless motor) as well as the number of magnets on the rotor (18 in our case). The increased number of magnets meant 9 electrical cycles, which forces the PWM frequency of the power-driver to be fairly high (70 to 80 kHz) - a careful digital design of the driver circuitry took care of that hurdle. The magnets were

made of samarium cobalt (strongly magnetic) and insured torque constancy over time (most commonly used magnetic material used today in brushless DC motors). The placement of these magnets was not just axially along the outer surface of the rotor, but at a slight (7°) angle to reduce the position-dependent torque-ripple, as one magnet transitions from one stator-pole to the next. The penalty is a slight decrease in overall motor-efficiency, but a price worth paying since it reduces the complexity of the stator-pole design as well as the necessary software compensation to account for higher harmonics in the torque-ripple. Data provided to us by the manufacturer, obtained from a rotary torque transducer, showed that the $\pm 1\%$ limits were obtained in the $\pm 1\%$ to $\pm 100\%$ torque range. Other important aspects were those of magnetic homogeneity not only from magnet to magnet, but also across the face of a single magnet, as well the concentricity of the rotor in order to obtain as constant and as small an air-gap as possible (a few thousands of an inch). All the above factors are worth considering when designing with the intent to use one of these motors as a pure torque-source. Implicit in this arrangement, barring any other external measurement, is the fact that the torque-constant and the torque-speed characteristics must be well characterized in order to make the jump from the electric domain into the mechanical domain.

Sensors

The inner workings of a brushless motors are such that the commutation is not done mechanically (like in a brush motor), but electronically. In order for the commutation to be successful, the controller must be aware of what the rotor's position is and at what speeds the rotor is turning. In addition, many motors differ in the type of sensors that are employed to obtain this information. There are basically three types of sensors currently being used to measure rotor position and velocity. They differ from each other in that they provide from coarse over medium to high resolution feedback.

The lowest resolution approach is via hall effect sensors. Physically the measurement has to be of a discrete nature, due to the size (they can be made fairly small) and the room available to place them near the rotor. Most motors are three-phase motors with four or less poles and thus require only a few number of hall effect sensors. They do require extra room for installation as well as support electronics (hall effect sensors have known characteristics that have to be compensated for - the most important one being temperature), but are fairly immune to electrical interference. Versions of this type of motor have been made for use in an oil bath and for high pressure (600 atm) environments

- they are used as the thruster motors for several deep diving submersibles as well as robots such as JASON.

A medium level of resolution can be obtained by what is called a *Sensorimotor*. The key to the position/velocity measurement technique is in the variable magnetic saturation levels in the stator teeth resulting from the proximity of the rotor magnets. This variation is sensed by monitoring the inductance of the sensor coils, which are excited with a 120 kHz square wave signal. With the appropriate location of the second sense-coil pair, sinusoidal and cosine signals may be obtained. Since we have eighteen magnets per rotor, we have eighteen sense cycles per revolution. The remaining 20 stator poles are used for the two phase windings, wound in pairs to accommodate the sense windings. Due to the nature of the physical measurement being taken, the accuracy is better than that for hall effect sensors. The signal requires some filtering due to the mutual inductance of the power- and sense-windings. The advantage of this approach is that it is extremely compact and can withstand the environment that we operate in (immersed in an oil-bath at 600 atm). The low level of discretization (also dependent on A/D resolution) coupled with a high bandwidth position-detection (integration) scheme, allows this motor to easily measure (and feed back to the user) position and velocity (and torque) without the introduction of any external sensor. The discretization inherent in such a position-detection scheme has an important meaning for position control for such a motor - this is discussed in the next section.

The highest resolution sensor is based on a similar principle to the *Sensorimotor*, except that it employs a high-resolution resolver which has to be rigidly coupled to the rotor (this is the principle behind all MOOG motors). Some motors even have another high-resolution position encoder coupled piggy-back on the rotor-shaft, to provide a separate means of position detection. Undoubtedly this measurement could represent a way of much finer control if coupled to the proper motor-design. The decision not to go with these motors is based on the fact that the external sensors necessary to run this unit can not stand up to the environment that we operate in. Furthermore, the main candidate's (MOOG) product has a very big and heavy support-electronics and driver setup that makes it extremely cumbersome and expensive (and thus impossible) to customize for our application (weight and form-factor).

The above discussion on the different types of sensing approaches in brushless DC motors, is solely meant as informational background to be considered during the initial selection process for a motor. It also sheds light on the abilities of what certain motors can, and can not do well.

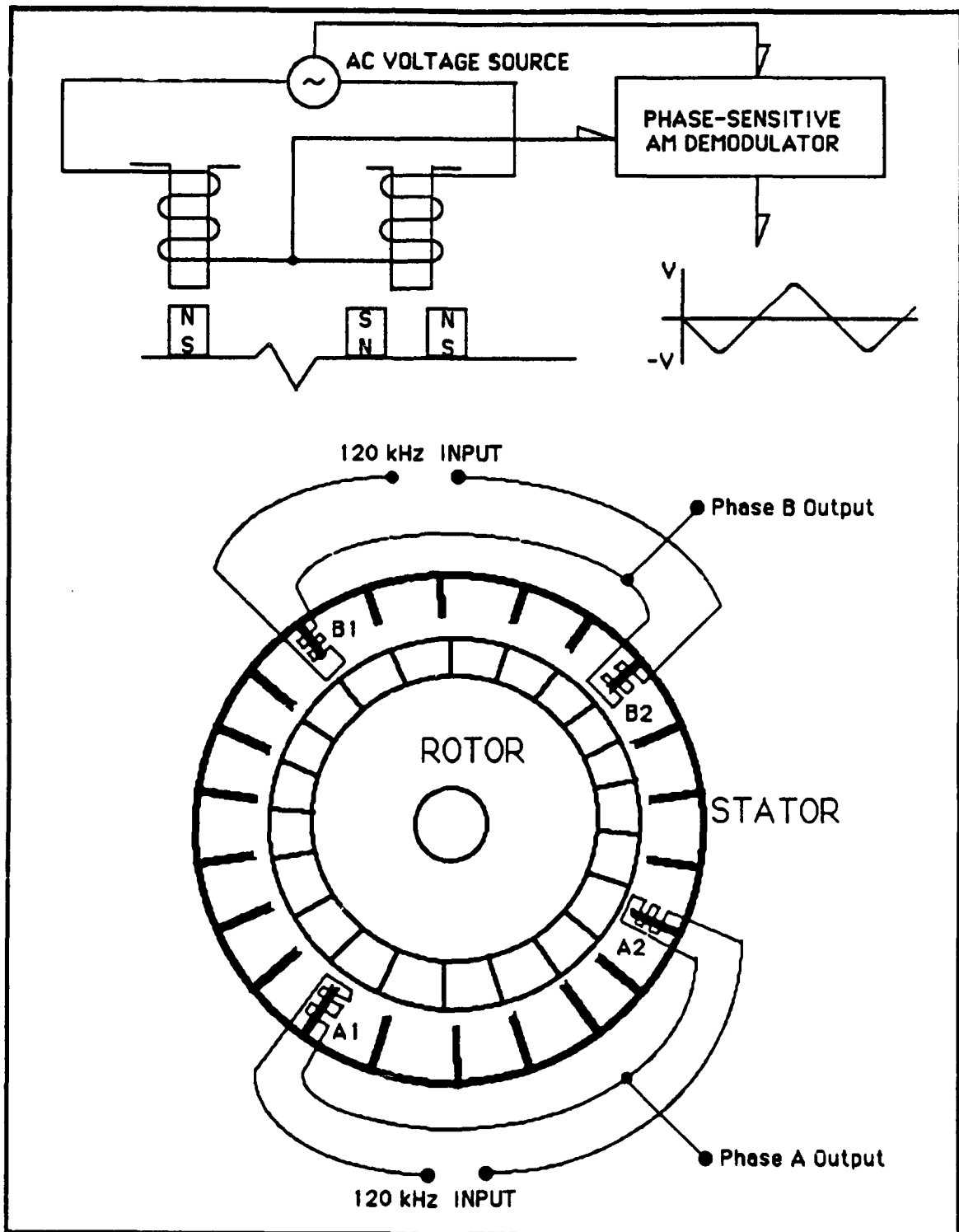


Figure 4.60 : SEIBERCO Sensorimotor arrangement, illustrating the mutual permeance principle and the location of sensor windings used for position- and velocity sensing.

Controller Structure and Implementation

This section briefly discusses some interesting low-level (yet real-world) control problems that had to be solved on the Sensorimotors from SEIBERCO used in the design and construction of DSL's underwater manipulator for JASON. The control structure that was to be used on the manipulator consisted of a vehicle-resident low-level computer that would act as the relay between the topside supervisory computer and the bottom-side motor controllers. The bottom-side controllers would implement a joint-servo on each motor (operating at 1000 Hz), while receiving their motor-gains and setpoints from the topside computer via the serial interface (topside loop runs at best at 20 Hz - limits of RS 422).

In order to get such high bandwidths on the motor-controller, the control algorithms themselves were written in assembler and employed raw motor position data in order to reduce scaling computations - all computations were done in integer arithmetic. The decision of what type of control structure to implement had to take into account the resolution of the position sensing scheme as well as the dynamic range of the desired joint behaviors. Since all desired motor behaviors are most easily described in continuous-time, a mapping scheme was required to map desired continuous-time gains to the discrete domain. The necessity to scale gains required deciding which controller structure would yield the largest dynamic range and the lowest level of discretization error once implemented in an integer-math approach. Given the fairly high controller sampling bandwidth, backwards difference mapping can be shown to meet all the previous requirements and be superior to Tustin's mapping, especially in terms of complexity.

Based on the above analysis, the motor manufacturer tailored the controller software to the necessary controller variables and the feedback it would need to provide to the supervisory computer. Notice that all these considerations were necessary due to the large difference between communication and controller bandwidths as well as computations in an integer environment. Work is currently in progress to install a LAN card in the bottom-side computer that would take advantage of the high-bandwidth (6km) fiber-optic cable between the robot and the surface ship. Once operational it will become a question of how powerful a topside machine is needed to perform the necessary computations. In general there should never be a communication bottle-neck like in our case, but rather a computational one which can be solved by introducing more and more powerful (supervisory) computers.

(4.4) CONCLUSIONS

(4.4.1) General Overview

The analysis approach used to test the six transmissions and the data presented in the previous sections can be summarized to reveal some interesting design-, control-, and task-guidelines. The main scope of this thesis centered around both, the general and more subtle design questions concerning motor- and transmission-design. One of the latest state-of-the-art brushless DC Sensorimotors was evaluated as part of the test procedure. Six different transmission types, (1) the WHOI Cable-Pulley Reducer, (2) H.D. Harmonic Drive, (3) SUMITOMO Cycloidal Disk Reducer, (4) KAMO Cycloidal Ball Reducer, (5) REDEX Corbac geared-cycloidal reducer, and (6) the DOJEN cycloidal cam reducer, were subjected to a series of experiments and their performance was evaluated. In the previous sections, general data trends and behaviors were presented, in addition to an in-depth look at the behavior of each separate transmission. Transmission fidelity was measured in terms of closed-loop controller parameters in this chapter. The controller parameters were chosen as those describing the impedance control algorithm. The fidelity with which these desired parameter values were achieved, in addition to task accomplishment, can be used as a performance metric for each transmission. We also established lumped numerical values for such phenomena as transmission stiffness, stiction, coulomb- and viscous friction. These parameters can be used as simple numerical comparators, as well as in models to try to describe transmission behavior.

The main hypothesis in the preceding analysis, is that these controller parameters represent a suitable set to measure system performance with, since they are the parameters that ultimately describe closed-loop performance. The controls engineer uses such terms as bandwidth, stiffness, damping, etc., to describe how well a system can perform a desired task. We have chosen to investigate those task scenarios where the interaction between the environment and the controlled system is substantial. This required the use of a controller structure that was known to be stable at all times given only minor restrictions on the types of environments encountered. Such terms as bandwidth and trajectory-following error are no longer applicable to this kind of task-setting. Instead terms such as endpoint-stiffness, -damping and -inertia can now be used to describe interactive behavior - so called endpoint-impedance behavior. These parameters alone do not immediately relate to the kinds of tasks that are achievable, but they can be used to measure the fidelity of a controlled

system. The ability to achieve a certain desired behavior can then be used to assess achievable task sets, based on the performance of a system accomplishing this task.

The topics that were addressed were concerned with system fidelity, as a function of factors that limit system performance. The transmissions analyzed are a representative set currently in use in most robotic applications. Many robotic systems employ transmissions in the robotic actuator packages and no clear performance evaluation of the relative merits of each transmission has been performed - especially the kind of analysis that would provide information as to system performance and stability during the actual execution of task scenarios. The 'nonlinear' characteristics that were encountered and studied are thus a representative set of real-life phenomena that control engineers have to deal with and designers should be trying to avoid/minimize. These characteristics were : (1) Backlash, (2) Transmission Stiffness, (3) Stiction, (4) Friction (coulomb and viscous) and (5) Torque Linearity. Another important component in a robotic actuator package that warrants our attention is the actual torque-source, the motor. We restricted ourselves to Brushless DC motors, since they are not only replacing brushed (AC or DC) motors and stepper motors (depending on the application requirements), but they are also a necessary choice for our application (underwater manipulator - oil-bath at 600 atm). Several factors critical to a proper motor design were discussed and motor characteristics that may impact system/task performance, such as (1) Torque Linearity and (2) Torque Ripple, were addressed and their effects quantified using the same method and criteria outlined above.

WHOI Cable/Pulley Reducer

Overall, it was quite evident from the data presented earlier, that cable/pulley reducers offer the most efficient transmission designs amongst those that we tested. This does not only imply the lowest levels of coulomb- and viscous-friction, but also stiction. The WHOI cable reducer had the lowest value for break-away stiction-torque at the output, making it the most backdriveable transmission in this study. Another important aspect of this cable transmission, was the very close agreement between stiction- and friction-torques, resulting in a ratio of stiction-to-friction of around 1.6. This ratio is important, since it points out that 60% of the stiction torque can not really be compensated for (open- or closed-loop), and can thus result in either inaccurate force control (by that amount), or possibly limit-cycle behavior if any kind of integral error scheme is used to reduce steady-state errors. The transmission stiffness of the unit was one of the smallest measured in these experiments, yet compared favorably with the soft-zones of other reducers. It is

important to note though, that the transmission exhibited this reduced stiffness value over the entire operating range, without any real softening-spring behavior, nor any wind-up zones. In other words, any controller designed based on this value, will not result in a possibly unstable system response due to reduced transmission stiffness regions. This has been shown in the previous chapter to be a very important stability guarantee.

KAMO Cycloidal Ball Reducer

The KAMO ball reducer was a completely novel transmission principle since it involved torque transmission via rolling steel balls. As one would expect, this unit came in a close second with respect to transmission efficiency. The unit also had appreciably low values for coulomb- and viscous friction losses. Its breakaway torque levels were about 50% higher than for the cable reducer, but with comparably low values for coulomb-losses. This of course implies that the ratio of stiction-to-friction torques is much higher, which lies around 2.1. In other words, the stiction torques are 100% larger than the coulomb torques, which implies a larger steady-state force-error, or a clear possibility of increased-amplitude limit-cycles. The stiffness of the unit did indeed exhibit a 100% stiffening behavior, with a soft-zone that had a stiffness comparable to that of the cable reducer. This soft-zone was present over about 10% of the full rated motor-torque, which is fairly substantial. If a controller is designed without modeling transmission compliance, the performance will be similar to that of the cable reducer over this torque-region. If one is to insure overall stability, the lowest stiffness value should be used for controller design. Such a restriction points out the importance of determining size and regions over which soft-zones are present and dominant in any transmission.

H.D. Harmonic Drive Reducer

The harmonic drive experiments revealed some of the more interesting results in this thesis. The overall efficiency claim was not found to be accurate, since the viscous losses were found to be rather high despite proper lubrication. The values for coulomb friction were found to be about 3 to 4 times higher than those for the cable reducer. Stiction values were found to be 4 to 5 times higher, resulting in a stiction-to-friction ratio of about 2.4. The unit exhibited a fair amount of ripple-torque, despite the proper alignment and lubrication. The unit does exhibit some wear after time, which does not necessarily result

in non-zero backlash, but instead increases the region of reduced stiffness. The cup-type drive that we analyzed had a much larger maximum stiffness than the cable reducer could achieve. On the other hand, it exhibited a very large soft-zone (over about 80% of the torque regime for the cable reducer) with a stiffness value below that of the cable reducer. In other words, this unit can not be expected to outperform the cable reducer, if we neglect to model transmission stiffness behaviors (and even if we do model it, better performance is not necessarily a given). A plausible mechanism for the reduced stiffness can be argued to be due to low radial stiffness levels (which are necessary), allowing the elliptical bearing to force the teeth on the flexspline into the teeth on the wavespline. After all the physical tolerances have been removed, we are left with the (axial) torsional rigidity of the cup itself. This phenomenon is responsible for the large amount of ripple-torque and the increased friction since we are no longer faced with rolling contact of involute tooth profiles. The unit's attribute of high torque-to-weight ratio is still unbeaten by any of its competitors. In a dynamic task setting where transmission stiffness becomes important though, the transmission stiffness and frictional behavior do not fair well compared to the cable- and ball reducers.

REDEX Geared Cycloidal Corbac Reducer

This cycloidal reducer was an interesting test case, since it allowed us to study the effects of backlash and friction due to the nature of its phase-adjustable gearing. This unit exhibited moderate viscous losses, placing it third in terms of efficiency amongst all the other transmissions. The same ranking is present when we look at stiction and friction torques. The unit was extremely backdriveable, with friction torques about a factor of two larger than for the cable reducer. Its stiction torques were highly spatially dependent, which resulted in a worst-case stiction-to-friction torque ratio of around 2.3. This transmission exhibited the largest transmission stiffness values of all the transmissions studied. It also exhibited a soft-zone which was fairly small, with a stiffness value well above that of the cable- and harmonic drive reducers. The weight and physical dimensions are fairly sizeable, which would limit its application to proximal links in a manipulator, and then only for robots above a certain size. Overall this unit was quite impressive, except for its high price-tag.

DOJEN Cycloidal Cam Reducer

This cycloidal reducer differs substantially from all the other cycloidal designs. The unit we tested was especially assembled for high efficiency and high stiffness. The efficiency levels were quite high, and rated fourth in the comparative scale. Its stiction and friction levels were also in the same ranking spot, with a resulting stiction-to-friction ratio of around 2.3. The unit was also fairly sizeable in terms of weight, with dimensions comparable to the SUMITOMO unit. There was some spatial dependency of the backdriving torque which was due to the assembly of the unit, and resulted in these high stiction-torque values. The manufacturer is moving to a new manufacturing process which will reduce these effects, with the ultimate goal to get rid of them. The stiffness of the unit was very close to that of the REDEX reducer, with an extremely small soft-zone (with higher stiffness levels than all the other reducers) and a very slight stiffening behavior. As promised by the manufacturer, the stiffness trace was very consistent and linear, except for a soft-zone which was found to be extremely small and then still quite stiff.

SUMITOMO Cycloidal Disk Reducer

This unit was especially designed for the robotic market. The only way that the manufacturer was able to reduce the backlash in these units to zero, was by a process termed dimensional preloading (oversized tolerance fits). The unit we tested had extremely large stiction- and coulomb friction torque values. They were about an order of magnitude larger than for the ball reducer. The relative size of the stiction-to-friction ratio lay around 2.5, but with a torque-deadband of as much as 19 N-m! The only way to use this unit, would be to size up the motor, to get any real dynamic range out of it. On the other hand, such large stiction and friction torques are bound to result in larger steady-state errors and larger limit-cycles than for all the other units tested. The stiffness of the unit was also extremely high, with a moderately sized soft-zone of increased stiffness (compared to cable- and ball reducers). The size and weight of the unit were also appreciable. We find this unit to be extremely unsuited for the newer generations of robots we should be trying to build. Any of the other units we tested outperformed it in just about any of the categories that we looked at. Despite the low cost of this unit, we would recommend a DOJEN or REDEX unit over a SUMITOMO unit any day.

(4.4.2) Detailed Conclusions

This section will address in turn those hardware factors identified as performance limiters and will refer to data that was presented in the previous sections. Performance will be described in terms of the previously mentioned impedance parameter fidelity criteria. Task scenarios employed in the laboratory setting, due to the need for reducing the number of variables in the analysis, will be expanded to tasks that could be performed in a more complex and realistic setting.

PERFORMANCE - (a) Transmission Stiction/Friction Characteristic

The results presented in Table 4.1, were gathered from all the transmissions tested. All the values represent statistical averages, due to the complexities involved in accurately determining each of the parameters of interest from the data sets presented earlier.

The different natural frictional losses in each transmission vary widely, and can be described surprisingly well with a simple stiction/friction model coupled to coulomb friction and viscous friction. Table 4.1 illustrates some of the more dramatic differences between several drives. The WHOI cable reducer and the KAMO ball reducer are fairly close, except that the cable reduction exhibits lower values for stiction/friction torques, with lower values for stiction-to-friction ratios, which reduces the possibility of limit-cycling during torque control with integral gains. The REDEX geared-cycloidal and the DOJEN cycloidal-cam reducers are fairly similar, except that the DOJEN unit exhibits a bit higher frictional losses, which make the unit a bit more inefficient. The REDEX Corbac reducer could have exhibited much higher efficiency values by removing the pretension between the crown- and inner gears. We did not want to reduce the stiffness of the unit, nor introduce any soft-zones nor backlash, so the pretension was optimized to achieve the highest stiffness possible without affecting the transmission stiffness nor introducing backlash.

	WHOI Cable Reducer (30:1)	KAMO Ball Reducer (30:1)	REDEX Corbac Reducer (30:1)	DOJEN Cam Reducer (33:1)	H.D. Harmonic Drive (60:1)	SUMITOMO Servo-Match Reducer (59:1)
Pos. Viscous Damping Coefficient [N-m/deg/sec]	0.0198	0.017	0.029	0.048	0.271	0.036
Max. Pos. Stiction Torque [N-m]	2.40	3.60	6.0	7.0	8.0	39.0
Max. Pos. Coulomb Friction [N-m]	1.38	1.70	2.5	3.5	5.0	19.1
Max. Neg. Coulomb Friction [N-m]	-1.32	-1.45	-2.5	-3.5	-5.5	-15.4
Max. Neg. Stiction Torque [N-m]	-2.20	-2.75	-7.0	-8.0	-12.0	-31.0
Neg. Viscous Damping Coefficient [N-m/deg/sec]	0.0127	0.0167	0.0305	0.047	0.210	0.022

Table 4.1 : Tabular representation of frictional losses in all the six transmission types tested.

The H.D. harmonic drive is clearly the transmission with the highest frictional losses of all those considered (10% of maximum rated output torque). On the other hand it also has a higher reduction ratio (60:1) as compared to the cable reducer (30:1). But even if we assume in the case of the cable reducer, that the entire stiction/friction forces are located at the input shaft, building an additional cable stage of 2:1 to increase the overall cable reduction, will not result in the increased level of stiction/friction that is present in the harmonic drive. The SUMITOMO cycloidal disk reducer shows again how inefficient it is and how astronomically high the stiction/frictional losses are, with high values for the ratio of stiction-to-friction. Using this transmission in medium to small robots is almost impossible, since it requires that the motor be sized according to the transmission, which comes with the smallest transmission ratio of 59:1 - a requirement which extremely limits

the universal applicability of this transmission to robot design. The SUMITOMO unit has a level of inefficiency which is only matched by such highly preloaded gear-trains (to reduce backlash) as used in some of the older PUMA robot models, which quote a figure of 30 to 40% of maximum motor-torque required to overcome stiction.

The WHOI cable reducer is employed as the actuator packages in the underwater manipulator built at our lab (DSL - Deep Submergence Laboratory). The frictional losses can be shown to be related to cable pre-tension (a useful and absolutely necessary element in insuring high performance and stability). Frictional losses between cable and pulley as well as in the pulley support-bearings, magnetic 'drag' (when stator is in place and deactivated due to induced magnetic torques - Lentz's Rule), and the presence of a rotary oil-seal on the output shaft (two concentric rings of highly-polished graphite and ceramic riding on top of each other), were determined to be the main performance limiting characteristics. The oil-seal on the output shaft contributes up to 50% of the total stiction forces (about 25% of the friction forces) measured at the output (figures provided by the manufacturer - CRANE SEALS Inc.). The presence of this seal is necessary due to the intended work environment of this manipulator. If any of the other transmissions was to be considered as a replacement candidate, these stiction/frictional seal losses would have to be added to the actual transmission losses presented in Table 4.1. The relative loss in dynamic range is small compared to the harmonic drive, since only about 2% of the maximum rated torque is lost to these parasitic phenomena. Otherwise, this transmission can conclusively be shown to have the highest dynamic range in impedance fidelity over the entire range of impedance behaviors that were tested.

The question of stiction and friction is not just a matter of a reduction in the dynamic range available from the actuator, but also has clear implications in terms of achieving middle- to low-end stiffnesses. As was shown earlier in the section on general data trends, the error in stiffness fidelity decreases with increasing levels of desired electronic stiffness^{#1}. The 'error band' (energy loss) is always defined by roughly twice the stiction forces and has a much more drastic effect on lower levels of desired electronic stiffness. Low contact stiffness with any type of environment is not possible without added sensors (even then performance and stability are not guaranteed), since the motor-reflected contact forces do not exceed the stiction force and thus place a hard limit on the low end of achievable stiffness. For an actuator of limited total travel range $\Delta\theta_{\max}$, with a known

^{#1} We refer here to electronic stiffness in order to distinguish it from transmission stiffness, which is a physical system characteristic

maximum stiction torque of τ_s , the absolute minimum level of achievable joint-stiffness K_{\min}^{θ} can be described as :

$$K_{\min}^{\theta} = \tau_s / \Delta\theta_{\max}$$

Many applications in the real world are not really concerned with this criteria, since they mostly deal with high-gain (-bandwidth) servo loops, which implement a high electronic stiffness, and thus have error margins that can be neglected. However, for contact tasks where delicate contact needs to be made and low contact forces must be accurately controlled via the motor (remember that the actuator and sensor are colocated in this case), this hard limit is present at all times. The stiffness that is apparent to the environment is much higher than the desired electronic stiffness and may make many tasks harder to achieve and possibly even unachievable. The kinds of tasks that may fall in this category will be part of the next set of research experiments. Employing some form of (filtered) integral control is an often attempted scheme to overcome steady-state errors in force-control (and position control), but has been shown to result in limit cycles. The effects of such a controller for each transmission, will be experimentally determined. This is an important experiment, as we want to understand the limitations placed on performance and stability in a closed-loop torque-controlled system, due to hardware characteristics present in the transmission.

Employing certain compensation schemes to reduce the limit from the stiction level to the difference between stiction (τ_s)- and coulomb-friction (τ_c) torques yields an expression where the basic relation is still the same, except that the numerator has been altered to reflect the effect of the compensation :

$$K_{\min}^{\theta} = |\tau_s - \tau_c| / \Delta\theta_{\max}$$

But the success of these compensation schemes is limited by several factors outlined earlier, which illustrate that compensation can only work up to a point and then only if fairly stringent hardware/software requirements can be met. Many times the inevitable conclusion is that the performance is severely limited by transmission stiction and friction levels, especially since most of the more successful implementations use an open-loop feedforward friction term, which is an underestimate of coulomb-plus-viscous friction, gathered from a previous off-line experiment. Time- and load-dependency of such parameters is a completely unaddressed issue so far, and adaptive algorithms have not yet

been shown to properly estimate such phenomena (and result in a stable closed-loop system).

The experimental realization that coulomb friction losses (and thus quite possibly also stiction losses) seem to depend on whether the output is being backdriven or whether the input is forward driving the output, as well as the type of transmission, is an important one. No further analysis on this behaviour will be given in this thesis, but it is very likely that this could be another reducer-dependent conditionally stable behaviour, especially in systems where friction compensation schemes are used. Overcompensation may inject undesirable energy into the system. Relying on the higher level of coulomb friction for increased stability can also be a mistake since reduced levels of friction are possibly present during tasks involving some level of forward-driving.

PERFORMANCE - (b) Transmission Backlash Characteristic

The only two transmissions that exhibited any kind of backlash (related to lost motion), were the industrial version of the SUMITOMO cycloidal reducer (29:1) and the small KAMO (10:1) ball reducer. The latter had a way of correcting backlash, which not only had an effect on stiction/friction levels present in the drive, but also resulted in a variation of transmission stiffness as a function of preload. The relative size of the backlash zones were all measured at the output, and were 0.8° for the cycloid reducer and 1.1° for the ball reducer. The backlash for the cycloidal reducer could not be changed, and as previously mentioned, a reduction in backlash could not be accomplished while retaining the same order of magnitude stiction/friction forces listed earlier (as quoted by the manufacturer). As shown in the data section for the ball reducer, the reduction of backlash (down to almost zero) could be accomplished by increasing the preload up to a level where backlash could no longer be measured, and, according to the manufacturer, is no larger than 10 arc-sec ($\approx 3 \times 10^{-3}$ deg).

The ability to change the amounts of backlash was an important experiment, since it validated some of the easily explained performance criteria resulting from deadband. This discussion is restricted to performance while the effect of backlash on stability is discussed further on in this section. We will limit ourselves here to the effect that backlash has on positioning accuracy. Since the level of achieved output stiffness is a direct relation between effort and integrated flow (torque and displacement in this case), the error induced by backlash again results in a hard lower limit on achievable stiffness. If the backlash in the transmission unit has the value ϕ , the error in stiffness following can be expressed as

the actual achieved stiffness K_a and the desired stiffness K_d (where θ is the sensor measurement of the current position error) :

$$K_a = K_d / [1 + \phi/\theta]$$

The relative error in stiffness is again reduced for larger errors in displacement and is more pronounced in systems where low values of position error are present (a good example would be a stiff position-tracking controller). Compensation for such offsets in the static sense could be performed by measuring relative displacements between motor-input and transmission-output. This is not too realistic a solution since we would require a sensor with high position resolution at the output (like a CANON optical shaft encoder) and we would have to decide when the transmission was in a 'static' state, so as not to excite any unmodelled transmission dynamics. Performing such tasks as surface/trace following while in contact with the environment can lead to a discrete error (which may or may not be acceptable), if backlash is present. Flipping a switch with different values of switch-detente, can be quite hard to do if backlash is not accommodated (commanding displacement until switch is flipped) and as an operator one needs some practice to be successful at this.

Notice though that beyond the offset in achievable endpoint impedance and uncertainty/discretization in attainable endpoint position, the relative importance of backlash in transmissions is most profoundly felt when it comes to insuring system stability while interacting with the environment. This issue is the more important conclusion to be drawn in this report, by relating the effect of transmission backlash on impedance behavior and system stability and will be treated in the stability section of the conclusions.

PERFORMANCE - (c) Transmission Stiffness Characteristic

Every transmission has a finite transmission stiffness, which has been shown to affect system performance and stability. Believing the figures the manufacturers publish is not a very reliable approach, since their experiments are sometimes flawed, measurement environments are ideal, and almost never is there real data presented. All brochures have only linear approximations or a single tabulated value. Furthermore, all manufacturers measure an output-transmission stiffness by locking the input and applying known torques to the output while measuring output deflection. Our experiments were done for input transmission stiffness, and revealed overall smaller levels of transmission stiffness.

Different transmission stiffness regions are present in almost every transmission that was tested. The physical reasons for such different behaviors can be found in improper dimensioning and load distribution, sloppy tolerancing and assembly, as well as bad material selection, undersized load-bearing members, etc.. The reasons differ for each transmission and were explained earlier in detail in each separate transmission-analysis section. We have re-compiled all the traces shown earlier for easier pictorial comparison. Figure 4.61 (a thru f) shows the different transmission stiffness behaviors:

Each separate transmission analysis has shown and explained the different stiffness traces that were generated, with the final results tabulated below in Table 4.2:

	WHOI Cable Reducer (30:1)	KAMO Ball Reducer (30:1)	REDEX Corbac Reducer (30:1)	DOJEN Cam Reducer (33:1)	H.D. Harmonic Drive (60:1)	SUMITOMO Servo-Match Reducer (59:1)
Measured Max. Stiffness [N-m/rad]	5,150	8,600	14,000	13,000	6,300	12,000
Measured Min. Stiffness [N-m/rad]	4,100	4,300	6,600	6,500	3,000	6,000
Published Max. Stiffness [N-m/rad]	-	19,000	35,000	14,600	10,200	26,000
Published Min. Stiffness [N-m/rad]	-	19,000	16,000	14,600	5,100	11,000

Table 4.2 : Measured and Published minimum and maximum transmission stiffness values for all the six transmissions tested.

These values were selected not only for the earlier performance and stability analysis, but will also be used for the theoretical/experimental torque-control stability analysis performed in the next chapter. One of the important things to notice before delving into a more detailed study of this data, is that the harmonic drive has a fairly low level of minimum stiffness - even lower than the cable reducer.

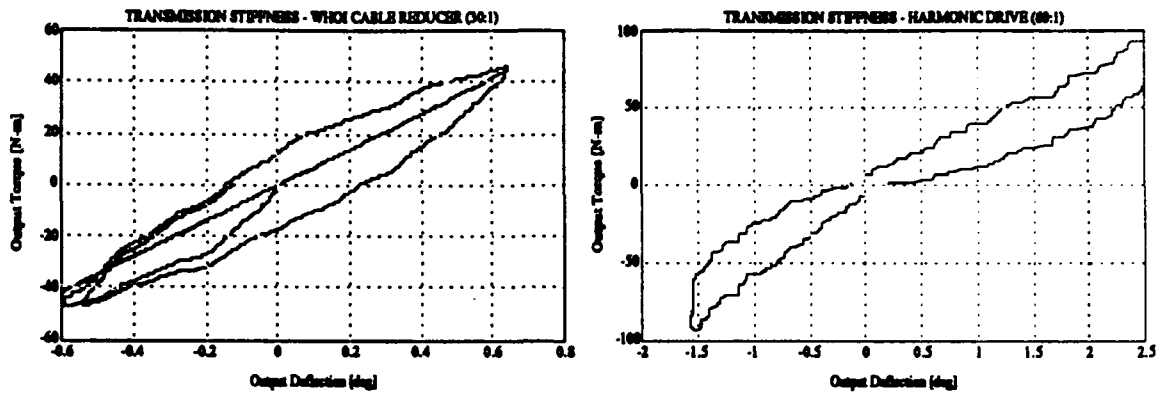


Figure 4.61 (a, b) : Transmission Stiffness Traces for (a) the WHOI Cable/Pulley Reducer (30:1), and (b) the H.D. Harmonic Drive Cup Reducer (60:1).

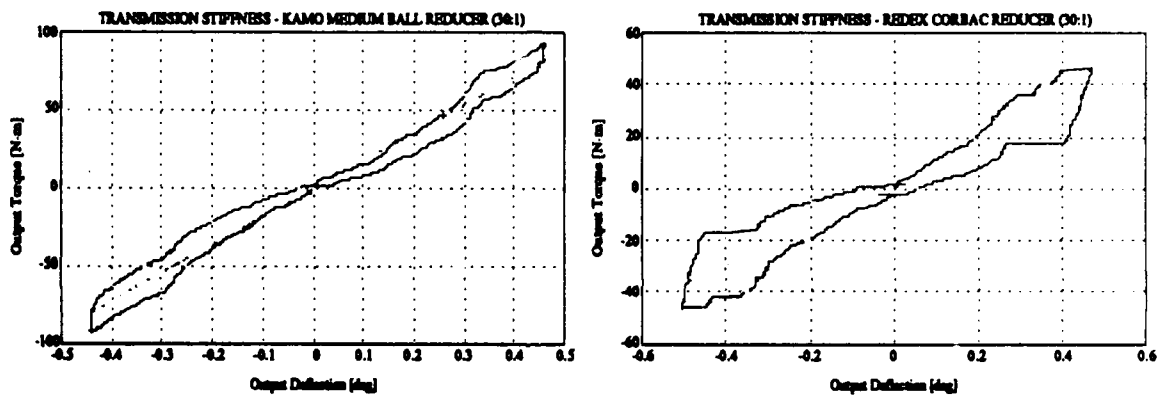


Figure 4.61 (c, d) : Transmission Stiffness Traces for (c) the KAMO Cycloidal Ball Reducer (30:1), and (d) the REDEX Corbac Geared Cycloidal Reducer (30:1).

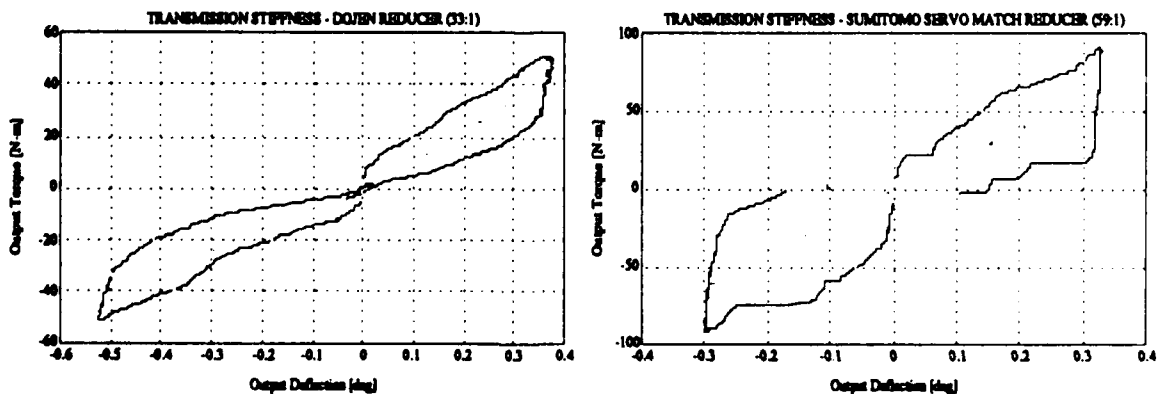


Figure 4.10 (e, f) : Transmission Stiffness Traces for (e) the DOJEN Cycloidal Cam Reducer (33:1), and (f) the SUMITOMO Cycloidal Disk Reducer (59:1).

If one goes through the product literature, one can see that the lowest value of published stiffness is present over a large range of transmitted torques, before the stiffness jumps sharply (by about a factor of 5 to 10). In other words, this drive does not exhibit any stiffening behavior unless properly loaded.

This implies further, that trying to apply light to medium torques at the transmission output will have to be severely limited in frequency, if one is not to excite the first resonant mode due to the soft-zone in the harmonic drive. The cable reducer exhibits only a slight stiffening trend, but it retains its consistent stiffness levels over the entire range of torques that our motors can produce. Thus the usual argument of lack-of-stiffness in cable reducers is only partially true, and may in many cases or different tasks, when compared to a harmonic drive at least, can be completely misleading.

The above data illustrates some of the advantages certain drives have in terms of stiffness, while others may prove to be good alternate candidates for a fairly wide array of tasks. Comparing the harmonic drive and cable reducers in terms of torque-to weight ratio is still an important distinction. The usual stiffness argument seems to no longer hold true though. We have illustrated this point not only in the previous sections in this chapter, but also in the next chapter, where we will close a torque loop around these motor/transmission/load setups, while attempting to perform stable contact-force control.

Most transmissions are designed to be as stiff as possible. This is achieved by proper design and material selection of load-carrying elements inside the transmission. Since there is relative motion in all transmissions, everybody tries to build transmissions which involve pure rolling contact on the faces where loads are transmitted perpendicular to the contact point/line/surface. Often the design of a transmission which attempts to reduce backlash, while ensuring rolling contact, results in a transmission where the actual stiffness is not constant, but varies as a function of the applied torque/force. Such is the case in most of the reducers tested in this analysis. In the case of the harmonic drive, the area of reduced stiffness around the no-load point (called 'soft-zone') is fairly large, and the associated stiffness is two to three times smaller than the stiffness for higher loads. The same phenomenon is present in the REDEX, SUMITOMO, and KAMO designs.

The first ball reducer that was tested, clearly exhibited a soft-zone which could only be controlled through further pretensioning. The increase in friction made this approach unfeasible though. The second (30:1) custom-design fared much better, with an improved stiffness trace, with stiffnesses comparable to all the other transmissions. The REDEX CORBAC geared-cycloidal reducer, the SUMITOMO servo-match cycloidal reducer, and the DOJEN cycloidal cam reducer, all exhibited the highest stiffnesses measured. The SUMITOMO unit can be found to have three distinct zones of increasing stiffness, and the

REDEX reducer has two such regions. Both units transmit loads to cantilever sleeved-pins, and are thus subject to such cantilever-bending stiffness losses, as the loads are continuously borne by all pins. The DOJEN unit is a bit different, since it uses very short cam-following studs, which results in much lower levels of deflection, and implies an even stiffness trace, which has no real appreciable soft-zones, compared to the other transmissions.

The cable reduction has a slight stiffening behavior which can only be observed at high torque levels. It has one of the lower stiffness figures in the above table, but also the smallest amount of stiffening of any of the units. Low stiffness is not inherently bad for stability nor performance, as long as such a stiffness can be guaranteed to be present at all times. Thus the dismissal of a cable reduction in favor of a harmonic drive, is not always the correct decision, since the closed-loop gains necessary for stable control for the harmonic drive have to be chosen based on the lowest level of transmission stiffness. Comparing the two values of relative minimum stiffness, the harmonic drive does not really outperform the cable reducer, especially since the soft-zone in the harmonic drive is present over $\pm 20\%$ of the full rated torque load of the drive (which turns out to be about 60% of our motor's saturation torque level!!). The choice between these two reducers has to be based on the type of fidelity one requires to achieve in a certain task, and if large values of MTBF and reliability are crucial.

One can conclude that a system with a lower internal stiffness than the desired electronic stiffness, will have a behavior that is dominated by the reciprocal sum of these two stiffnesses. If the electronic stiffness greatly exceeds the hardware stiffness, the measured behavior will be characterized by the physical characteristics of the transmission stiffness. In other words we can never achieve a stiffness larger than the inherent transmission stiffness. This argument has a lot of meaning in a static task environment, but also dominates the performance and stability characteristics of a system's dynamic behavior. The dynamic task analysis for all the above transmissions will be presented in the experiments outlined in the Chapter 5.

PERFORMANCE - (d) Ripple-Torque Characteristic (Motor and Transmission)

Most of the individual sections for each transmission analyzed, comprise an analysis of torque-ripple (defined here as the maximum absolute value of torque-variation as a function of output position). Torque-ripple can be generated by imperfect motor/rotor design and improper motor-commutation compensation, but it can also originate in the

transmission itself. As was shown previously, the ball reducer and harmonic drive are the two transmissions with the largest transmission-induced torque-ripple. Compensation for these inaccuracies is extremely hard to accomplish. Cable reducers have almost no torque ripple, which is also true for cycloidal reducers (when components are machined to tight tolerances). The ripple present there was comparable to motor detente-torque levels.

The phenomena of stiction and friction are responsible for the presence of torque-ripple. The expected values are usually given by motor manufacturers as a percentage (usually 2 to 5%) of the maximum rated torque. In our test set-up, the theoretical motor-induced torque-ripple was compensated so as to lie below the $\pm 1\%$ threshold, which meant a ripple of ± 0.4 N-m for the cable reduction and cycloidal reducer (was present in the hysteretic traces), ± 0.9 N-m for the harmonic drive (below stiction/forces and thus undetected), and ± 0.2 N-m in the case of the ball reducer (also undetected due to dominant transmission ripple).

Motor-induced torque ripple can result in a severe digression of actual stiffness behavior from desired behavior. Tasks where this is an important criteria include attempts to follow a surface while maintaining a (possibly constant) desired interface force. The speed at which the surface is followed has a direct relation to the frequency of the ripple (since it depends on the spatial rotation frequency of rotor/transmission-components). Compensation via measurement of interface force may be useless, unless it can be carried out at the same bandwidth as the motor-commutation cycle (about 100 μ secs for our motor) to result in any appreciable benefit at all. Such a task did exist and resulted in the need for meticulous motor/transmission knowledge about ripple behavior. The task was to roll down a thin-walled stainless-steel tube containing a light-carrying optic fiber, to a thickness where the fiber would be firmly held but not pinched by the surrounding walls. Extrusion through a die proved too complicated and a cold-rolling process was decided upon where motors controlled the applied forces on the tubing through rollers as the stainless tube is pulled through several stages of 8 radially symmetric rollers to reduce the I.D. of the tube down to slightly less than the O.D. of the optical fiber. Any excessive torque-ripple in this scheme would result in kinks and undulations on the tube's surface and lead to pinching of the fiber (even excessive compression of the fiber was undesirable), which results in loss of strength of the optical signal measurable in dB at both ends of the fiber. Assistance in selection and analysis of the proper motor and transmission was given to the company by the author, based on the test results from several of the transmissions analyzed above. This represents just one of the real-life tasks that could be properly analyzed, resulting in criteria that could be matched to data from this analysis, while successfully implementing an important application.

PERFORMANCE - (e) Sensor Characteristics (Type & Placement for Control)

The entire set of experiments was performed using no more sensors than were provided by the manufacturer of the motor and the output torque sensor manufacturer (JR³). The motor uses sense windings that relate mutual inductance (very coarse explanation) in the sensor windings to rotational speeds. Proper location of two phase windings will yield cosine and sine waves which can be used for speed and direction of motion information. Since this information is required to commutate the windings, and position is calculated via high-speed sampling, the motor could provide to its own controller and to the user, information about position, velocity and torque (from analog current loop) for use in any kind of supervisory control scheme.

Inherent in this scheme is a certain level of discretization in terms of positional accuracy (2304 counts per motor revolution or ± 9.4 arc-min of input motion) and velocity resolution (1.8×10^{-4} rad/sec). The figure given for position-resolution is fairly good compared to conventional external encoders, while the velocity resolution figure of 0.01 deg/sec is more in the medium resolution range (higher resolution tachometers/resolvers do exist and are used in other brushless motors, but require them to be attached to the rotor). The relatively coarse velocity signal results in roughened damped behavior, especially at high damping gain levels (due to inherent noise/discretization levels).

The location of the sensors used for control has been shown to be very important in several papers/theses published in the last few years, as well as in Chapter 3. The so-called question of co-located and non-co-located sensing and actuation became an important issue due to the simplified models of transmissions used when designing a controller. Most of the controllers resulted in high-bandwidth control action which excited several of the unmodelled modes or nonlinearities in the transmission and caused poor system performance and instability. As shown earlier, even the location of the control-sensors at the input, while in the presence of such nonlinearities as backlash and low transmission stiffness, resulted in highly undesirable behavior. If a sensor located at the output was used to close a compensation loop around the entire motor/transmission assembly, only limited success was achieved (due to hardware limits), and sometimes the system was destabilized, as in the case of impedance compensation of high gain controlled nonlinear transmission systems (elaborated on in a later part in this section). This whole area of research is dealt with experimentally in Chapter 5.

STABILITY - (a) Limit-Cycle Behavior

During the test of the different transmissions, the goal was to achieve the same output behaviors (stiffness and damping) irrespective of the transmission being tested. Thus for smaller transmission ratios, the motor-gains had to be subsequently increased, while for higher ratios, smaller gains were sufficient. It was observed that during the testing of certain transmissions, a limit-cycle behavior (low-amplitude, high-frequency) would develop around the setpoint or no-load point of the motor/transmission. The reason for the limit-cycle was due mainly to the presence of backlash at the transmission input as well as relatively low transmission stiffness.

The zone of lost motion, or backlash, represents a range of motion in which the dynamic properties of the motor/transmission/load system are changed to that of purely the rotor and the motor-shaft. That means that the gains that were designed based on a dynamic model of the motor/transmission/load dynamics, result in a much different dynamic behavior once acting purely on the motor and motor-shaft system.

In the figure below (Figure 4.62), we have shown a linear representation of the motor/transmission/load dynamics while interacting with the environment.

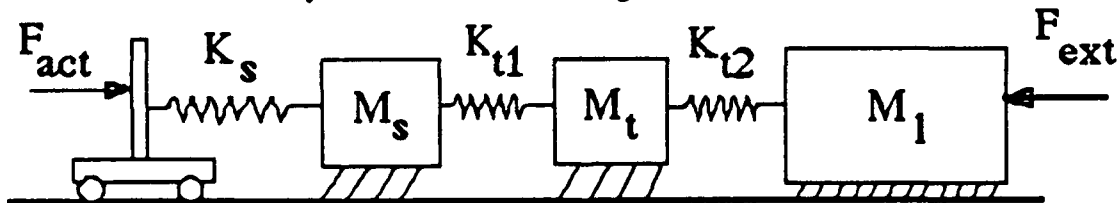


Figure 4.62 : Representation of Linear 1 DOF Motor/Transmission/Load Dynamic System for controller-gain design purposes.

The motor provides a force F_{act} which is normally opposed at the output by the environment force F_{ext} . The forces are transmitted by the shaft (with stiffness K_s and inertia M_s) and through the transmission (with distributed stiffnesses $1/K_{t1} + 1/K_{t2} = 1/K_t$ and inertia M_t) to drive the load (inertia M_l). The gains based on this dynamic system are chosen so as to cause the output to have a certain desired behavior. If the transmission input has a zone of backlash, the motor gains will be acting on a reduced dynamic system as shown below (Figure 4.63), while the motor-shaft is in that region,

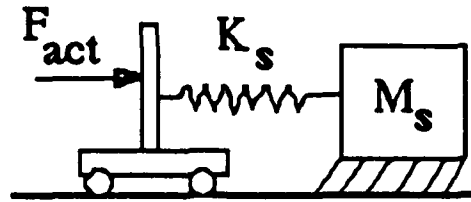


Figure 4.63 : Reduced Dynamic System during transitions through the backlash zone.

and will result in a system with a much higher bandwidth than the design called for, since the load parameters have been reduced from the inertia $M_s + M_t + M_l$ to purely M_s . We also lose some of the stabilizing effects of friction present in the transmission.

In a purely linear sense, the root-locus plot of the two systems (where we assume to have a pure load and an actuator for control design purposes - in order to show the open-loop poles as drawn) is a transition between the two root loci pairs shown in Figure 4.64 below.

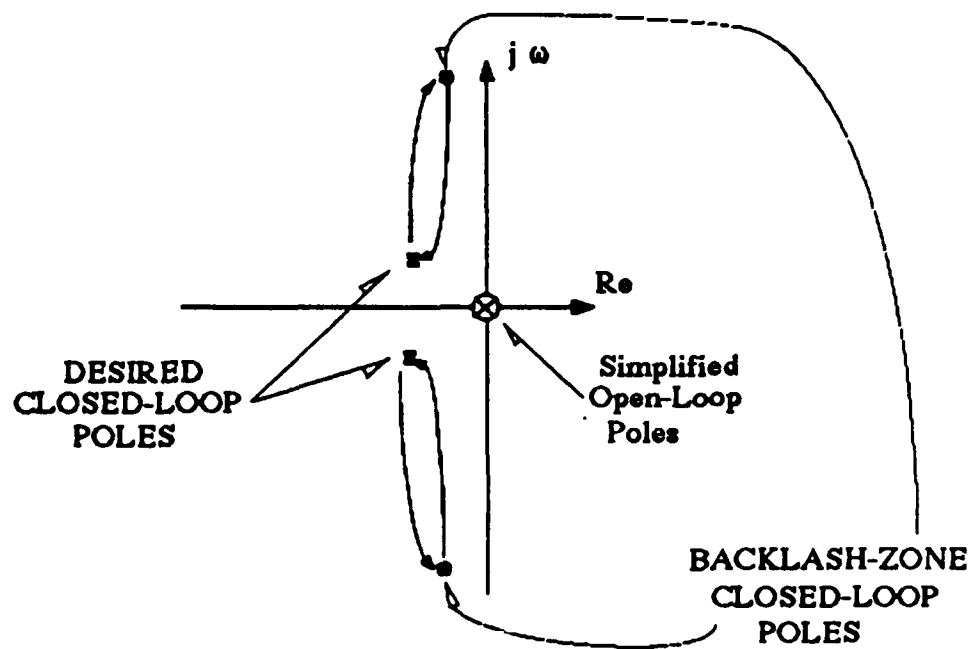


Figure 4.64 : Root-Locus representing the dynamic behavior for different dynamic systems and the transition between the two.

The new effective bandwidth (the term bandwidth here is justified, since the system is theoretically able to achieve any position inside the backlash zone and can thus be thought of as a dynamic system capable of being positioned anywhere inside that zone) for the reduced dynamic system can be expressed in terms of ω_n^* ,

$$\omega_n^* = \omega_n \sqrt{1 + \frac{M_L + M_T}{M_s}},$$

where ω_n is the bandwidth designed for the entire dynamic system. The transition between these two dynamic regimes, coupled with a discrete implementation of the control law can result in limit cycles that have been described in the chapter regarding the ball reducer.

The limit-cycle could be reduced in amplitude but not avoided, in the case of the commercial ball reducer, by adding inordinate amounts of electronic damping, or increasing the preload so as to get rid of the backlash or holding the motor-shaft with one hand. Any attempt to damp the system by hand via the output was completely fruitless. The motor would start humming due to the high-frequency damping torque that is directly related to the velocity-sensor accuracy and resolution (more about that in the earlier section on sensors) when the necessary electronic damping was used. In an operational scenario, the requirement for system damping limits the usefulness of such a transmission.

Another way to reduce the limit-cycle, was to load the transmission via the output by causing motor-torques that surpass those that result from the backlash zone and the desired stiffness. In other words, the torque that would be generated by the stiffness controller for a high value of stiffness, acting over the size of the backlash-zone ($\tau_b = K_d * \phi$), was the torque necessary to insure borderline system stability. Once the positional error signal resulted in a torque below this value, just the slightest disturbance (slightly tapping output or input of the transmission) would result in the immediate occurrence of limit-cycles. The experiment that was performed was to load up the transmission to maximum torque and then reduce the applied torque to the above value (while tapping the output shaft lightly) to the point where instability would set in. This was done in both directions with similar results - that is the reason why the stiffness following plots seen in the ball reducer section do indeed show stable behavior under higher loads.

The above behavior was observed not only in the ball reducer but also in the commercial version of the cycloidal reducer (29:1). That comes as no surprise, since they both have a backlash zone. One of the most obvious solutions would be to obtain a higher gear ratio for the ball reducer, so as to be able to reduce the motor gains substantially. This is an interesting way of specifying what kinds of behaviors a certain transmission with a given ratio will be able to reproduce if any backlash is present, and still do so in a stable manner.

The commercial cycloidal reducer (29:1) was also controlled with numerically the same gains as the ball reducer (since the transmission ratios vary by about a factor of 8.4, the gains were now that much larger resulting in 3 times the bandwidth), and sure enough, the limit-cycle behavior would immediately return. The fact that this limit-cycle was not due to too high a gain and was to be expected with any transmission type was demonstrated by using the same numerical gain values on the cable reducer and attempting the same kind of task whilst attempting to destabilize the system. The experiment was successful in that no amount of disturbance was able to result in detectable limit-cycling. The cause for that can be easily found in the absence of backlash in the cable reducer. A possible difference in transmission damping was unlikely to be responsible either, since the cycloidal reducer has a higher amount of stiction/friction and viscous losses than the cable reducer. The two transmissions (cable and cycloidal) having almost identical transmission ratios, can thus be said to have different upper levels of achievable impedance (stiffness), yielding very different figures for dynamic range, which favor the cable reducer.

In addition to backlash, the ball reducer also experienced another behavior which can be explained in terms of linear dynamics. As one can see from the transmission stiffness data of the ball reducer as a function of transmission preload, there were 2 different zones of stiffness (which the harmonic drive also has, except that the area of reduced stiffness is much smaller and the stiffness value itself is much larger). The area around the no-load point (setpoint for the controller) exhibits a 'soft-zone' in which the transmission stiffness is drastically reduced. During the experimental phase where we incrementally increased the preload in the ball reducer, we were able to reduce the backlash to virtually zero, but the limit-cycle persisted with a continually decreasing amplitude. Once the preload exceeded a certain value (which could not be measured), the limit-cycles were completely absent. The importance in this behavior can be explained via Figure 4.62, which shows the entire discretely modelled system dynamics. The assumption that transmission stiffness is very high when designing a controller must be carefully checked, since the relative size of the electronic stiffness and the transmission stiffness K_t , coupled to the transmission and load inertia (M_t and M_l) can result in oscillatory behavior, as evidenced in our experiment. The presence of increased friction as the preload was increased could not have been the cause for the following reasons : (1) unusually high electronic damping (beyond the coulomb friction present in the ball reducer) was necessary to avoid limit-cycles and (2) the stiction/friction levels in the ball reducer under high preloads (for which the behavior was stable), was of the same magnitude as that measured in the cable reducer, which showed no sign of any instabilities.

Since the motor-controller implementation in our experiment was of a fixed-gain nature, our findings regarding the transmission stiffness could not be incorporated into a real-time controller model. No compensation could be attempted and thus the upper limit on achievable stiffness was once again not simply a function of actuator sensing and actuation, but rather due to a hardware characteristic in the transmission itself. Limit cycle behavior represents a metastable state, since once the system makes contact with an environment of large stiffness, the resulting behavior yields undesirable performances and possibly even instability. This could be easily shown by running the output into a stiff surface (the stiffer the surface the more violent the contact bouncing) or by losing contact with a surface (the stickier the surface, the easier it was to induce limit-cycling which prevailed once contact was lost with the surface).

COMPENSATION SCHEMES - (a) Software Compensation

Many papers and theses deal with the idea of compensating for inherent system dynamics. Yet few reports have successfully dealt with the compensation of some of the more nonlinear characteristics of a motor/transmission system. Such nonlinearities as stiffness could possibly be modelled by linear techniques (not only transmissions with varying stiffness but also the vibrational modes of flexible manipulator structures - a very necessary undertaking as the lack of 'good' control of the space-shuttle's robot arm showed all too clearly) and successfully used in improving transmission models for control purposes, resulting in improved system behavior (more about that in Chapter 5).

Models for system backlash are by their own nature nonlinear and represent a characteristic that is very hard to compensate for. The only real solution is to reduce the inherent transmission backlash by careful hardware design. The presence or absence of backlash is almost always related to another physical phenomenon - that of stiction and friction. The most common high-precision gear-reducers used in robotics have precision-ground gears that are forced to mesh by preloading the gears upon assembly. The preload insures metal-to-metal contact at all times, but also increases the rolling and sliding friction (undoubtedly present despite the involute tooth profiles). The use of preloading transmission components is also used in the ball reducer (adjustable by the user) and the cycloidal reducer (done during assembly). The harmonic drive achieves the same goal by not only slightly preloading the meshed teeth, but also by insuring that there are at least 2 teeth contacting their opposite teeth at all times. The absence of backlash in harmonic drives and their 'low' value of stiction/friction as compared to other geared reducers, has

made this transmission the prime candidate for many space applications. An important yet unmentioned aspect is that of temperature-induced friction. In preloaded assemblies, as the elements heat up due to continuous use, the material expands, possibly further increasing the preload, which can drastically change the stiction/friction characteristics of any transmission.

Compensation schemes for stiction and friction have been used for a long time in several important applications. Models for compensation range from dithering (high-frequency low amplitude torque disturbance), simple coulomb- and viscous-friction compensation (implemented in digital controllers with the accuracy purely dependent on the quality of the scheme and sensor used), to nonlinear compensation that attempted to understand and compensate for the transition between stiction and friction. Dithering has proven to be quite successful in purely trajectory following devices and is used on many robotic systems out on the factory floors today. On the other hand it has encountered serious problems when used during interactive tasks. If a force-sensor was used to relay interface forces back to the control computer or the user, the force/torque information was corrupted by the small scale accelerations of the system that would be registered as inertial forces on the sensor. The only way to compensate for that was to severely filter the force information (resulting in loss of valuable information) or turn off the dithering during contact (not a good solution either). Direct friction compensation using a feedforward coulomb- and viscous-friction term is standard in most controlled systems today, where precision (position) or fidelity (force accuracy) is required. These compensation schemes are very device- and time-dependent, since they usually involve an off-line SYSID to determine the best parameters for the frictional models, which are then stored as feedforward terms for compensation during operation. Estimating these parameters on line, while performing a variety of tasks, is very complicated and has not been performed successfully to the author's knowledge.

The attempt to understand and compensate for stiction and the transition to coulomb friction has recently been attempted with the Stanford arm [Armstrong (1988)]. A destabilizing negative friction behavior during this transition has been postulated (and also proven to be destabilizing even in the presence of a simple PD controller using tools similar to SIDF techniques [Tustin (1960)]), and data has been presented to show that the compensation approach offers some advantages. Once again the identification and open-loop compensation approach explained earlier is used. The inherent nature of these (usually Least-Squares) curve-fit approaches will always result in some residual error that can not be compensated for. Unfortunately the author did not present a comparative analysis between a simple coulomb-viscous compensation and the much more complex

approach explored in his analysis (the relative improvement may not warrant this effort, since the low-velocity region is quickly traversed in the tasks that were performed in that study). Furthermore the author mentioned having to be careful with the maximum value for stiction compensation, because even the slightest amount of over-compensation could result in reduced performance and increased stability problems. The compensation technique also has difficulty operating in a near-zero range where it assumes that stiction is present, since the sign of the compensation torque must be chosen correctly. Furthermore, the state of the system is indeterminate at that point because there is no motion information nor knowledge of breakaway direction available (this can be extremely hard to implement on a multi-link device like a robot-arm with several serial links present). In the Stanford report, a very delicate task was attempted and completed (insertion of bus wire into a slightly larger ID hole) using a force-dithering scheme. The reason for its success can be seen in the use of finger-mounted force sensors (mounting strain gauges on the fingers of the manipulator end effector) which reduces the inaccuracies due to inertial, gravity and coriolis force readings (gauges can be tuned to be much more sensitive), as well as the handling of a very low mass device (in this case the bus wire) which also reduces the inertia between the sensor and the environment. Further information on tasks with heavier interaction and/or heavier tools are not provided and are seen by this author to be the real test for such a compensation scheme.

Overall, the compensation schemes used today are quite simple and offer some benefit in performance. The difference between the actual values of stiction and friction is a physical characteristic of big importance. No compensation scheme to date can account for this phenomenon, which points out the importance of proper hardware design to not only reduce the relative size of friction, but also to minimize the difference between stiction and coulomb-friction (main reason for designing transmissions with rolling elements to transmit torque, since rolling friction \ll sliding friction).

COMPENSATION SCHEMES - (b) Hardware Compensation

The attempt to optimize characteristics such as transmission stiffness, ripple, backlash and stiction/friction has to start during the basic design phase of the transmission itself. Minimizing backlash by pre-tensioning or pre-loading the torque-transmitting members not only reduces backlash to negligible levels, but it also increases the stiction/friction level. Since backlash is a considerable concern in system stability, insuring stability is the first step necessary. Stiction and friction are known to be of a conditionally

stabilizing nature and usually result in reduced system performance. The transition between stiction and friction can result in severe limit-cycles if certain controller structures are used. Many compensation techniques can be used, but their residual effects will still limit system performance. There are a lot of transmissions on the market where the trade-off between backlash/stability and friction/performance has to be made if the unit is to be of any use. Cable reducers do not have this problem. Their usefulness is mostly governed by lowered system stiffness and friction levels, as well as component fatigue life. Research is proceeding in this field and some day we may be able to build purer transmissions that have longer life expectancies.

Simply dimensionally preloading a transmission is not necessarily advantageous, as was proven by the SUMITOMO unit. The large increase in stiction and friction can result not only in excessively oversized motors, but also heavier and larger robotic designs. Designing a controller around such a stick-slip system to perform torque control is bound to run into trouble. The approach taken by DOJEN to set the dimensional preload during assembly is a very useful one, since it allows for a trade-off between efficiency and stiffness (as well as backlash). The design of a transmission where the load-bearing members are always in full contact with their opposing members, is one of the most crucial design rules. That this is the case for the cable reducer, is clear due to the lack of any variable transmission-stiffness zones. The ball reducer was able to meet this requirement quite well. In the case of the harmonic drive we indeed had full contact at all times, but we were limited by a second lower frequency resonant mode, which is essential to the workings of this transmission. Other transmissions where loads would only be evenly borne once the initial load-bearing members had sustained some deflection, exhibited variable transmission stiffness zones. Insuring rolling contact at the load-transmitting interfaces was shown to result in the lowest levels of stiction and friction. Geared mechanisms with ideally involute tooth profiles can not always compete, due to material flexibility, machining tolerances, and dimensional preloading. All in all, these are some of the more important areas that require careful design. If a transmission is being evaluated, these criteria need to be considered and the experiments run in this chapter should provide additional information in order to judge transmission candidates.

(4.5) SUGGESTIONS AND MOTIVATIONS FOR FURTHER EXPERIMENTS

In order to make the concluding arguments more meaningful, further experiments that will lend a better sense of reality to the experiments performed earlier need to be performed, in order to highlight the bond between task behavior and impedance fidelity - the only missing link in making this transmission fidelity analysis approach more practical and useful.

The selected task will be a 1 DOF output force-control task, where a torque sensor at the output of each transmission will be used to close a torque-loop around some of the transmissions studied. The task itself will consist of an output lever-arm resting on different environment profiles, while maintaining a certain desired contact force. The environment profiles can be made of different materials with different compliance and different severity in profile gradients. The test setup and data analysis will form part of Chapter 5.

The experimental apparatus will include the previously discussed transmission types in this 1 DOF task setting, as well as the cable-driven manipulator. The analyzed task will be chosen to represent settings in which system/task performance and system stability are important issues. Designing a meaningful task for a 1 DOF system is not trivial. The reason for analyzing 1 DOF systems was to reduce the number of variables present in multi-degree-of-freedom systems to a known and controllable set, thus making it possible to isolate motor/transmission behaviors and create fair and equal experiments to judge hardware by.

Careful selection of profiles, controllers, lubrication, and other hardware characteristics, will shed light on what hardware/software characteristics/approaches yield stable and acceptable performance levels, while at the same time classifying each of the transmissions being tested as suitable or unsuitable for certain force/torque-control tasks.

CHAPTER 5

(5) FORCE CONTROL TRANSMISSION EXPERIMENTS

In this chapter we will analyze the experimentally determined performance and stability regions for the tested transmissions. We will then determine how these experimental stability and performance regimes compare to the theoretically determined boundaries. Using a 1 DOF torque control task we will attempt to fit the linear/nonlinear lumped parameter models with the previously determined parameters, to two of the transmissions we studied (cable reducer & harmonic drive). Furthermore we will determine the overall performance of all the transmissions for a distinct set of task scenarios. Different controller structures will be studied, and their effects on improving performance in the presence of different levels of hard nonlinearities.

The choice of a 1 DOF force control task was governed by the need to reduce the number of variables affecting system performance and stability, since we were mainly concerned with transmission dynamics. The use of a multi-degree-of-freedom manipulator to perform a tractable force-control task, was not considered, due to the number of extra variables present which would not add more information to this study, but would rather complicate the analysis and possibly even alter results and mask tendencies and behaviors.

On the other hand, there are not too many 1 DOF force-control tasks, which could be considered to be a representative set of real life tasks. The choice of designing a surface-contact/following task represents a compromise between a realistic 1 DOF task and experimental complexity. If the actual layout of the environment profile, to be followed with different levels of desired force, is chosen properly, the task can be structured to introduce fairly complex environment contact scenarios. Simple triangular up-and-down ramps can test contact maintenance. Steps in the environment cross-section test the ability to lose and regain contact while maintaining desired performance and overall system stability. The tests performed here simply involve unidirectional contact, since the output of the transmission is free to lose contact with the environment. Most of the experiments to be presented deal with such unidirectional contact, with contact acquisition and maintaining contact with different time-varying contact force levels. Such tasks are quite basic, yet turned out to reveal a lot of information which could be termed conclusive with respect to comparing transmission performance and stability.

(5.1) Experimental Setup

The experimental setup is basically analogous to the one used for the performance data gathered for each transmission. The drawing in Figure 5.1 illustrates the main components used in this experiment.

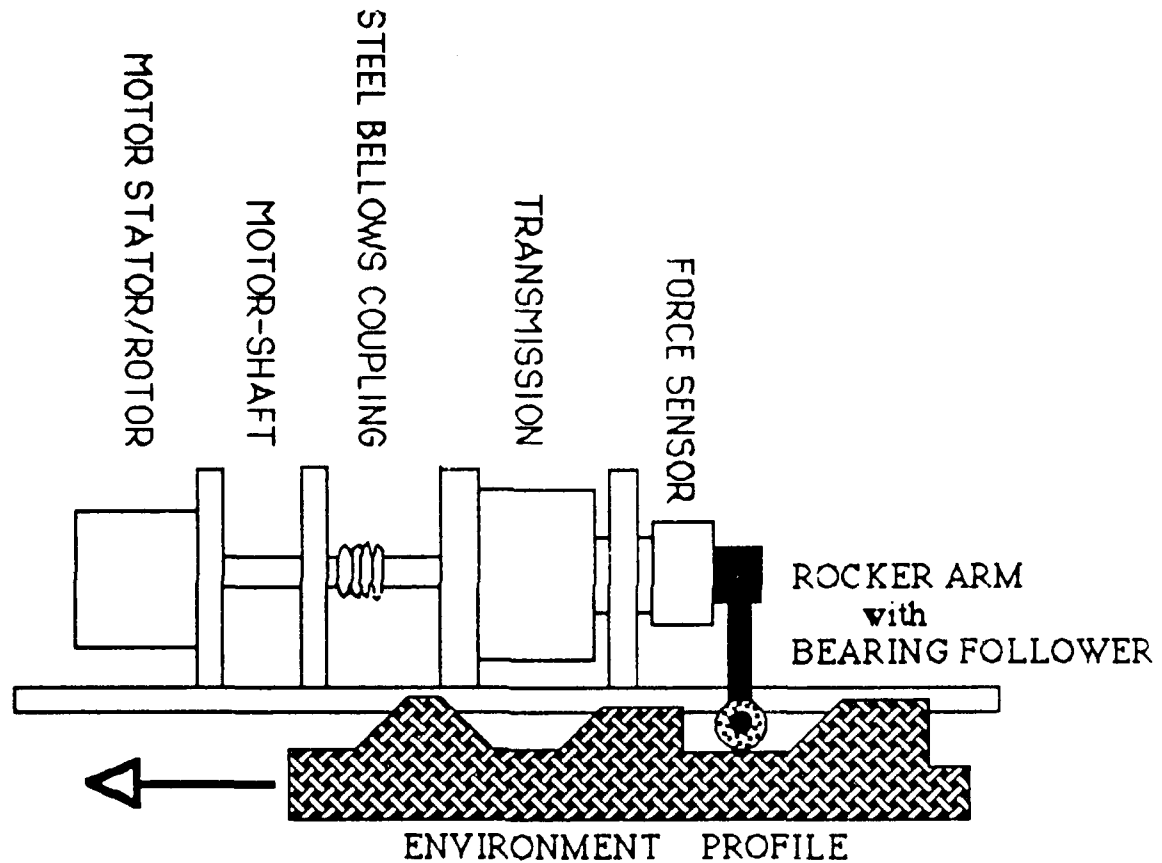


Figure 5.1a : Experimental Force/Torque Control Test Setup.

The motor is coupled to the transmission via a rotor/shaft/steel-bellows assembly. The coupling bellows is chosen to correct for any misalignments and offsets between motor-shaft and transmission input. The steel bellows was selected based on the criteria that it be at least two orders of magnitude stiffer than any of the transmissions tested. This procedure was seen to be the most important component selection process for the entire experimental setup. The steel-bellows from SERVOMETER were selected just for that reason, despite their high price. The face-plates, between which any of the transmissions are connected and centered, are concentrically located and support the input and output shaft/flanges, in order to reduce cantilever loads on the transmission assembly itself. The force sensor is attached to the output shaft/flange, and measures the forces and moments

applied to the transmission. A very stiff cross-beam with an attached bearing riding at the end of a long peg, form the rocker-arm arrangement, which will ride on the surface of the environment profiles.

As the environment profiles are pushed backed and forth inside the laterally mounted channel guide, the bearing attached to the rocker-arm will ride up and down the desired profiles. The outer bearing race is of concave cross-section and thus contacts the profile surface at a single point/line. The controllers will be structured so as to give a constant desired contact force, which will be taken to be the vector sum of forces applied to the surface at a local normal vector. Thus despite the fact that the moment arm changes between the contact point and the rotational axis as the rocker arm moves up and down an inclined surface, positional information as well as measured force-components, can always be used to resolve the local normal force.

The environment profiles were built of two distinct materials in order to simulate two different environments. First we used polyurethane whose durometer would classify it as a medium-hard material which deforms under impact. The second set of profiles were made from LEXAN, a bullet-proof synthetic material which is extremely hard yet does a good ability of absorbing impact without any plastic deformation. The latter was used in all the experiments unless otherwise stated.

The experimental procedure was to run several open-loop and closed-loop experiments in order to characterize the different transmission performances. The variables that were logged in the open-loop runs were simply the input motor-position and -velocity as well as the commanded motor torque (in terms of measured armature current) and the output torque (measured via the JR³ force/torque sensor). The open-loop experiments simply involved commanding a desired input torque with different waveforms, frequencies and amplitudes, while measuring the output torque. The closed-loop experiments involved a set of different digital controllers that would use the desired and measured output torque to generate current commands to the motor. Other variables such as input velocity, force rate, and integral force error were used to generate a wide combination of standard torque control algorithms.

Pictures in Figures 5.1b and 5.1c, depict the setups for the cable reducer experiments, and all the other transmissions. Shown in Figure 5.1b is the harmonic drive coupled to the motor, the torque sensor and the environment profile via the bearing-follower and the rocker arm. Figure 5.1c shows a similar arrangement for a single joint of the cable transmission.



Figure 5.1b : Experimental Setup for most transmissions. Shown here is the harmonic drive coupled to the motor, the torque sensor, contacting the environment profile with the bearing-follower & the rocker arm.

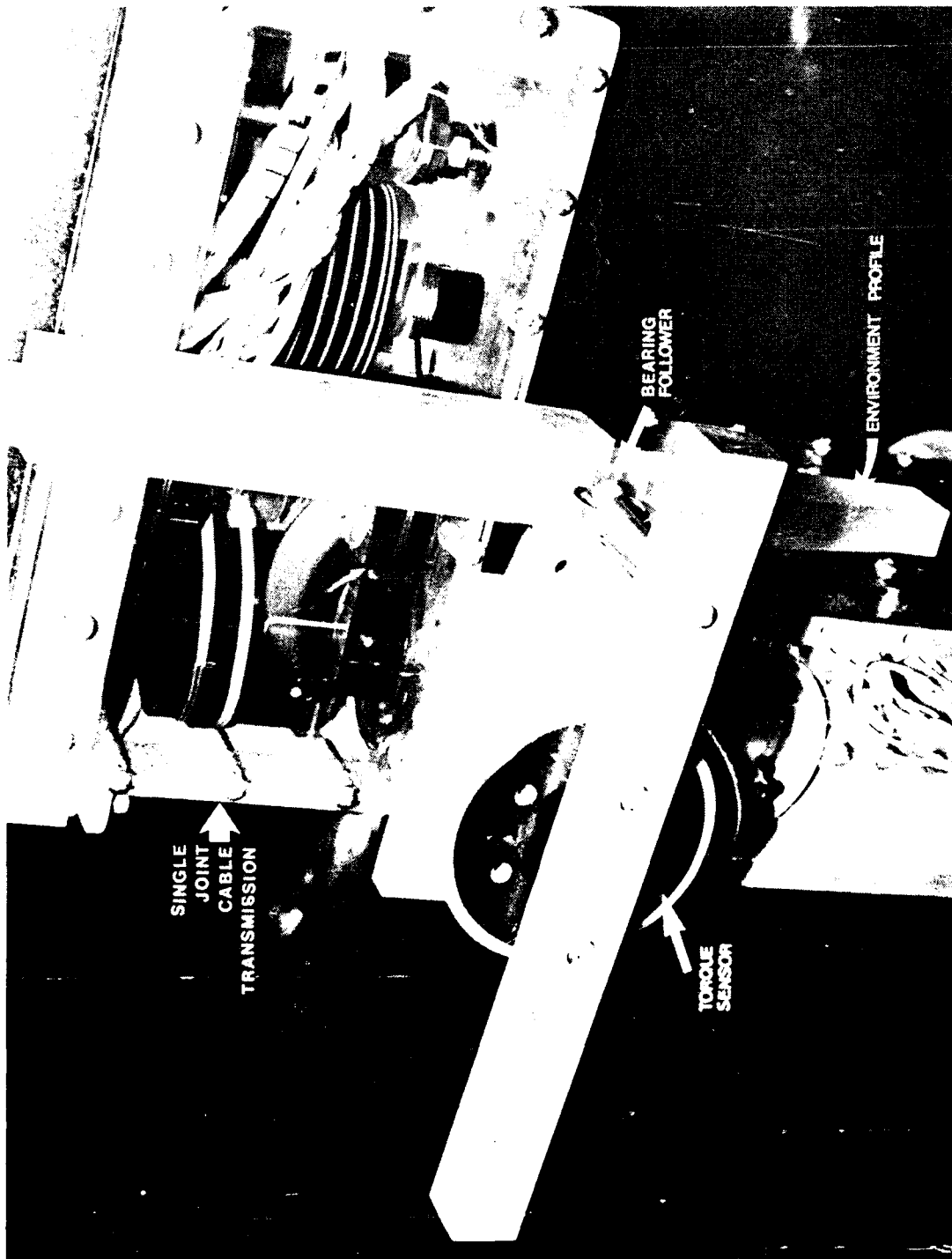


Figure 5.1c : Experimental Setup for cable reducer. Shown here is the housing of the next joint coupled to the torque sensor, contacting the environment profile with the bearing-follower & the rocker arm

(5.2) Experimental performance and stability analysis of force-controlled actuator/transmission/load systems

The open- and closed-loop experiments outlined in this section are also intended to provide numeric evidence for some of the theoretical developments of Chapter 3. Furthermore, the descriptors identified in chapter 4 (stiction, friction, viscous friction, stiffness, inertia) will be used in a nonlinear simulation to attempt to reproduce time responses. The goal will be to see how applicable the chosen model structures are, but also how accurate the numeric descriptors are in describing transmission behavior. The procedure will be to present the experimental data first, and to then compare experimental and simulated/theoretical results.

(5.2.1) Hardware-Setup Experiments

The test-stand setup requires that two separate experiments be run first, in order to establish some of the ground facts we will be using in the next sections. First we will have to look at the torque linearity of the motor itself, by plotting commanded torque vs. measured torque. The measurement was taken by attaching a lever arm of known length to the motor shaft, and letting it rest in single-point contact on the face of the force sensor (which was moved next to the motor). By recalibrating this particular set of strain gauges, the gains can be changed in order to achieve the desired resolution, since the maximum torque output of the motor is no bigger than 2 N-m. The experiments were performed with the motor-shaft unable to move, and with the lever arm resting on a compliant surface on the sensor, so that relative motion was possible. The latter of the two tests was done to simulate the change in position of the rotor for compliant transmissions. The commanded torque was computed based on the knowledge of the motor's torque constant and the desired armature current - the profile was chosen to be a ramp up and ramp down, with enough samples to achieve steady-state at each level of commanded torque.

Shown in Figures 5.2 and 5.3, we see the linearity of the torque command vs. the measured torque to be quite good. The two traces disagree most notably near the maximum torque level, and we do have a slight indication of a small torque deadband. The case of the moving rotor shows itself to have a slight yet repetitive variation in torque, which when plotted vs. rotor position and analyzed via an FFT, reveals the first torque harmonic of the motor, measured to lie around 60 to 65 Hz (the theoretical value based on a finite-element

method is supposed to be at 70 Hz). The agreement overall is quite good though, with errors no larger than 1 to 2% (RMS values) of maximum torque. This result then allows one to plot in the subsequent plots, the desired torque levels as being almost identical to the actual applied torque. This is an important distinction, since it negates the need for a separate (mechanical) measurement of torque, or any other fancy computations to determine the mechanical domain equivalence. Notice also that for the 30:1 and the 60:1 reducers, the applied input torque for commanded levels of 5-to-20 N-m and 10-to-40 N-m lies in the region of 0.15-to-0.67 N-m at the motor end. In that region, the motor torque linearity is extremely good, which lends even more weight to the assumption that commanded torque is almost identical to actual torque.

The second experiment performed to test the experimental setup was made in order to rule out effects on the data by the steel bellows and the torque motor itself. The coupling bellows (from SERVOMETER) itself was selected based on its static properties. Its stiffness was at least two orders of magnitude larger than the highest stiffness measured for any of the tested reducers. Yet these static properties did not guarantee a certain dynamic performance. The known 'knotting-up' of these couplings was reduced by reducing the length of the bellows section. The overall bellows length then governs the upper limits on the angular- and parallel misalignment allowed for each setup. In Chapter 7, one of the appendices goes into more detail about the tolerances and alignment issues that were considered during the design stage of the test stand. Overall though, the parallel misalignment was no worse than 50% of its rated 5/1000 of an inch dimension, and the maximum angular misalignment that we measured in our setup (0.1 deg or 0.00175 rad) did not exceed its 0.5 deg rating. Note that both numbers quoted above are worst case!

We chose to perform an experiment, where a torque wrench with a (more or less calibrated) readout like the ones used to tighten head gaskets on car engines, was attached directly to the input of the reducer, and two different frequency torque signals (of about the same amplitude) were applied to the input of the transmission. The experiment was performed by hand, and the frequency and amplitude had to be eyeballed using several visual aids. The application of the input torque was performed as smooth as was humanly possible. The input was a signal resulting in about 10 to 20 N-m amplitude at the output, and a frequency of around 1 Hz and 0.3 to 0.25 Hz. The selected transmission was the harmonic drive, since it had the most interesting behavior to sinusoidal inputs (see Figure 5.4 and 5.5).

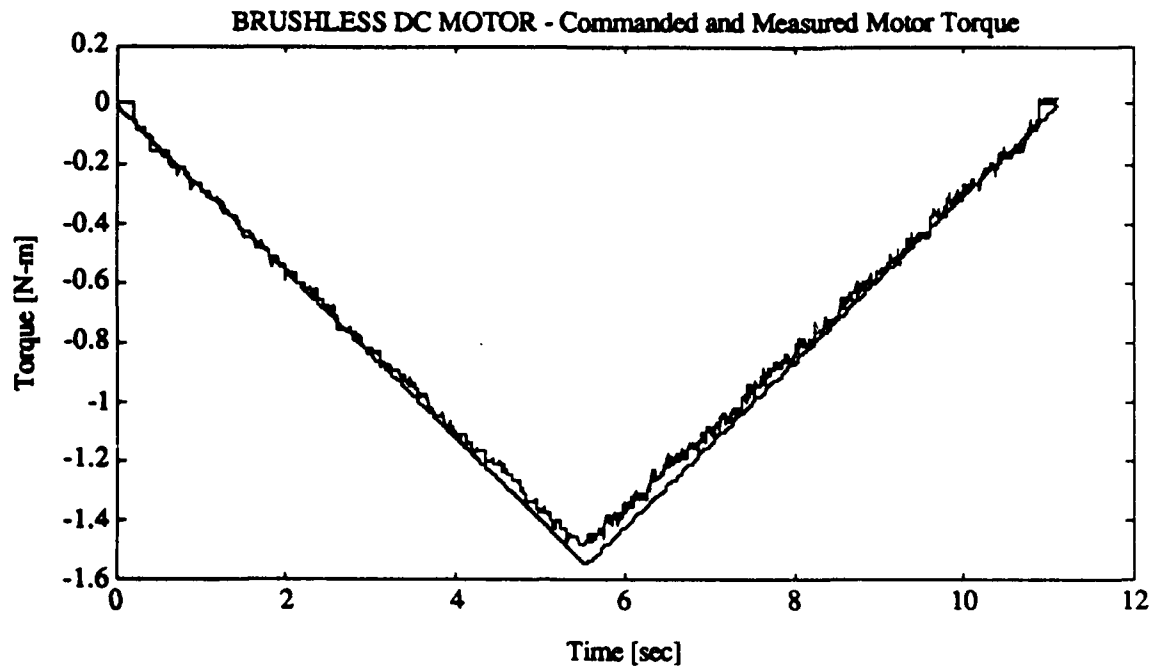


Figure 5.2 : Experimental Torque Linearity of Brushless DC Motor - Measured vs. Commanded Motor Torque with the rotor locked.

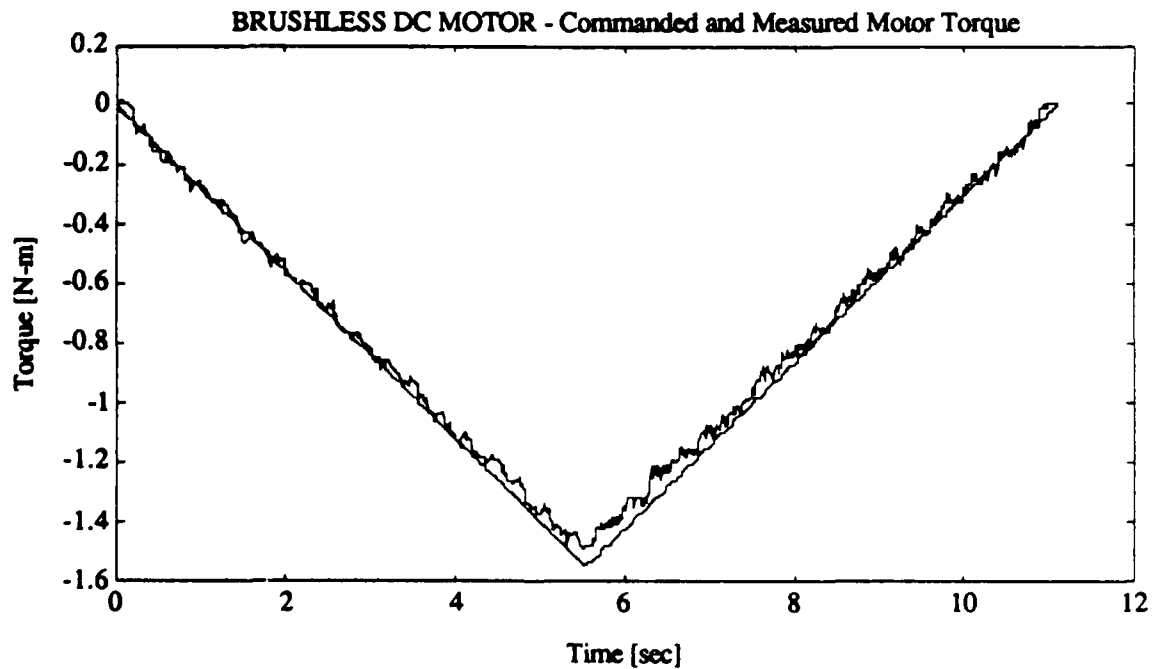


Figure 5.3 : Experimental Torque Linearity of Brushless DC Motor - Measured vs. Commanded Motor Torque with the rotor free to move over a limited range.

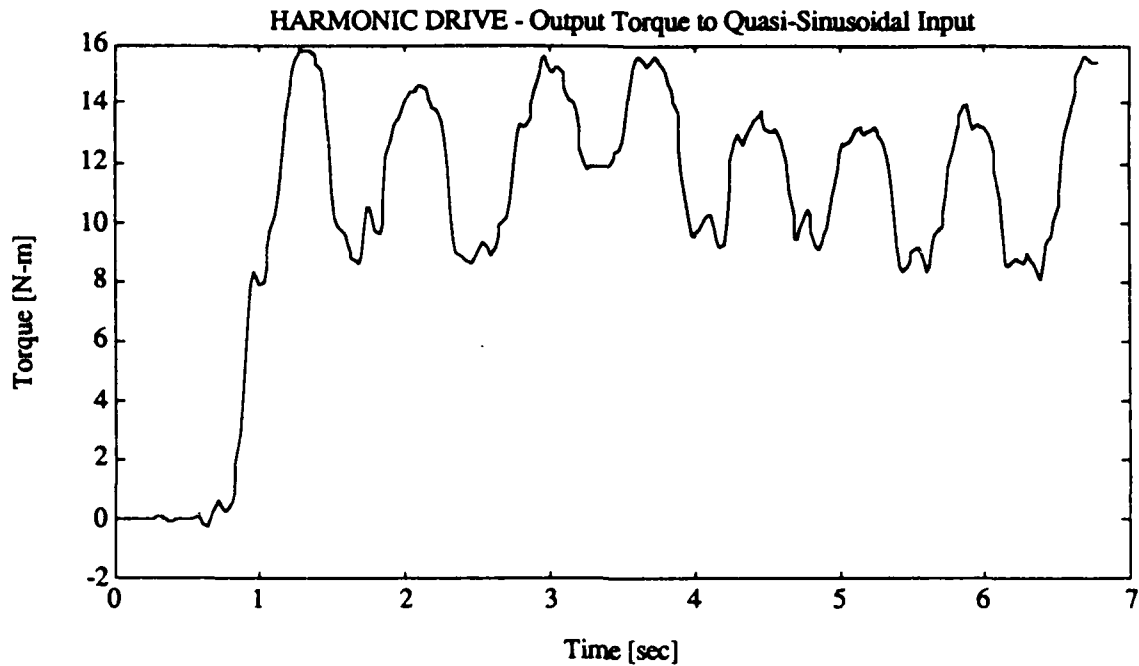


Figure 5.4 : Open-Loop Torque Input to the Harmonic Drive Reducer with a simple torque wrench - high frequency input signal.

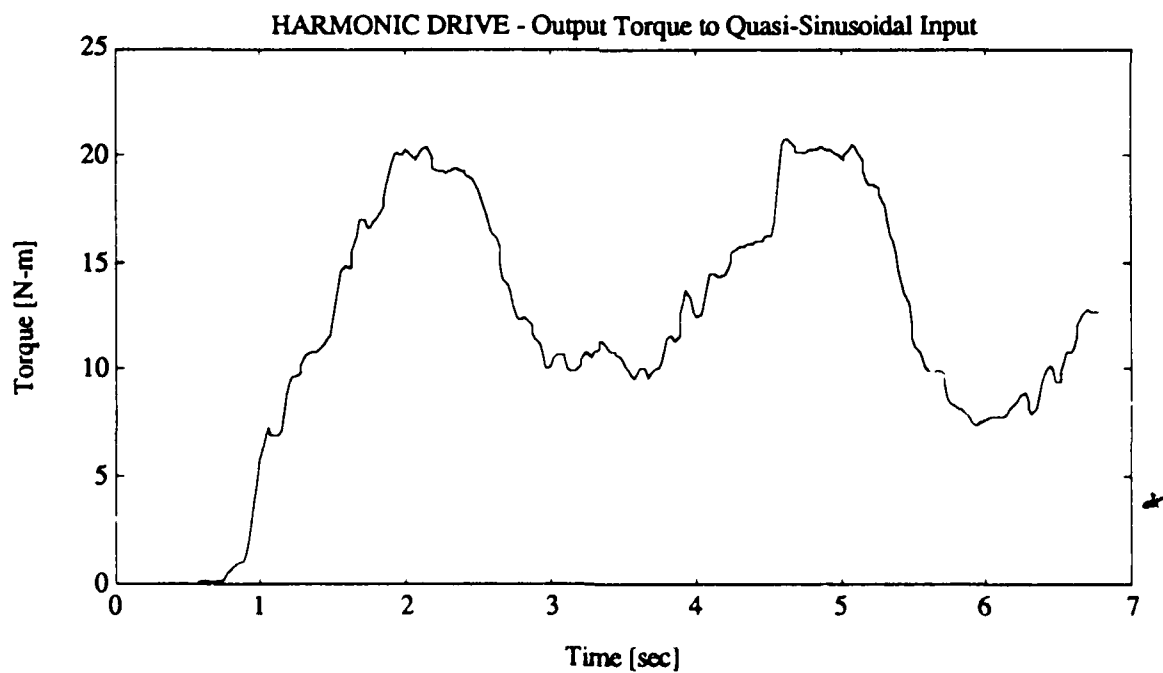


Figure 5.5 : Open-Loop Torque Input to the Harmonic Drive Reducer with a simple torque wrench - low frequency input signal.

The 1 Hz input signal results in output torques that show the resonance or stick-slip peaks at the low torque end, as well as at the high torque end (see Figure 5.4). The stick-slip behavior and the associated 'ringing' in the transmission is apparent even more if we look at the 0.25 to 0.33 Hz input signal of Figure 5.5. The peaks and resonances at the low torque end are quite apparent, as the input torque increases. The observed trends here show that we will certainly expect to see such behavior in the experiments yet to come. But we will know with a very high degree of certainty that such behaviors are not due to the steel bellows resonating/vibrating, nor to the presence of some motor nonlinearity that may cause torque variations resulting in fictitious torque readings.

(5.2.2) Open Loop Experiments

Open-loop torque experiments are extremely useful in determining the performance of each transmission as a torque multiplier. The differences in performance can become quite apparent depending on the type of input waveform, amplitude and frequency that is chosen. This set of experiments will use different kinds of commanded torque profiles in order to uncover the different behaviors. The offsets of the wave forms were selected in order to result in breakaway out of the stiction band upon startup, while the relative amplitude or magnitude of the signal is selected to lie outside the stiction band for all the reducers. This setup will thus allow a fair comparison of relative torque-following fidelity, since stiction and friction are theoretically overcome. Even then, the experimental results will show a large inter-transmission discrepancy. In order to account for the difference in transmission ratio between the harmonic drive and the rest of the transmissions, we have selected the input to the harmonic drive to be analogous to the other reducers. In other words, the motor delivers the same amount of torque as with the other reducers, resulting in amplitudes and offsets that are thus twice as large (due to the difference in 30:1 and 60:1 reductions).

Square Wave Input:

Using a square-wave in commanded torque would seem to be the most appropriate waveform, since it theoretically contains an infinite frequency band, and would thus certainly excite any transmission dynamics. The output-amplitudes were chosen to lie between 5 and 10 N-m and 5 to 20 N-m for the 30:1 reducers, and 10 to 20 N-m and 10 to 40 N-m for the harmonic drive (60:1). This convention is due to the difference in transmission ratio, and allows us to input equal torque levels at the motor-end. The frequency was chosen to be 1 Hz, in order to let the responses settle for all the transmissions.

Shown in Figure 5.6 are the responses to both of these waveforms, for the WHOI cable reducer:

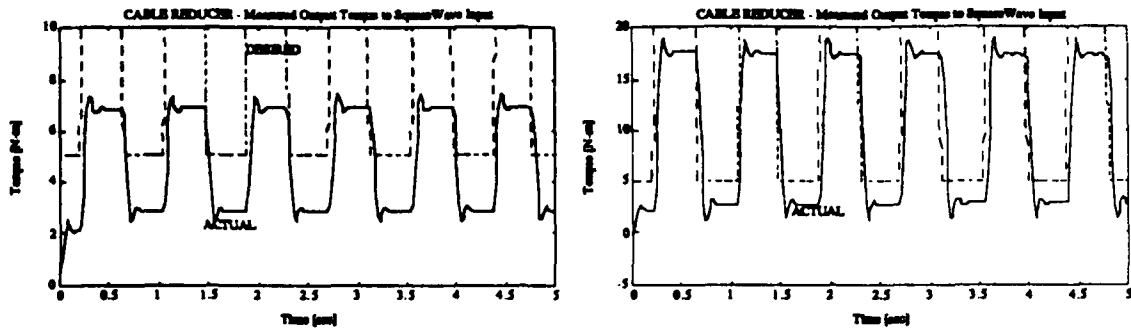


Figure 5.6: Measured Output Torque to Square-Wave Input at 1 Hz and 5-to-10 and 5-to-20 N-m amplitudes for the WHOI cable reducer.

Notice that in the case of the cable reducer, the magnitudes do not match perfectly, since we expect stiction and friction to offset the two data sets. The difference between actual and desired waveforms reaches steady-state values that are in very good agreement with the stiction and friction values that were measured earlier (2 to 3 N-m).

The harmonic drive exhibits similar behavior, with offsets that are also in good agreement with the static descriptors measured earlier. Figure 5.7 shows the time responses to square-wave inputs at 1 Hz, but at double the amplitude, in order to account for the discrepancy in reduction ratios (equalizes motor input-torques).

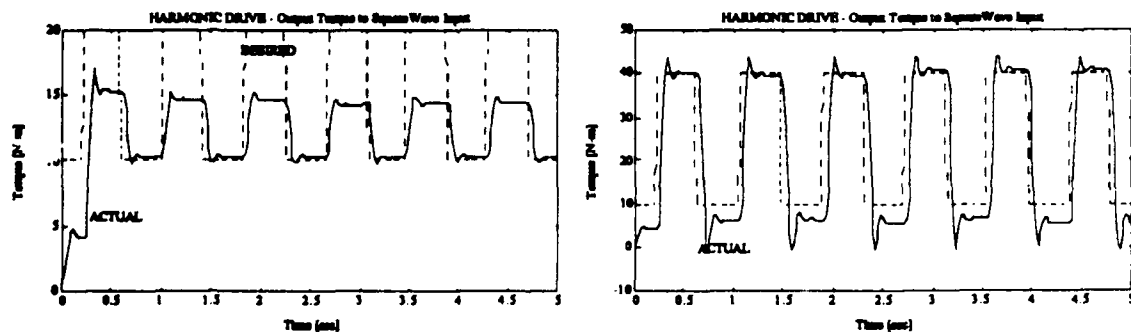


Figure 5.7: Measured Output Torque to Square-Wave Input at 1 Hz and 10-to-20 and 10-to-40 N-m amplitudes for the HARMONIC DRIVE reducer.

Notice how the harmonic drive has increased stiction values resulting in larger torque errors at low amplitude torques. The fact that the response seems to settle to the desired 10 N-m level in the left plot can be explained by realizing that the stiction value for this drive can reach as high as 10 N-m. The response also does not settle out in the right plot, where the overshoot over the 40 N-m level seems to monotonically increase.

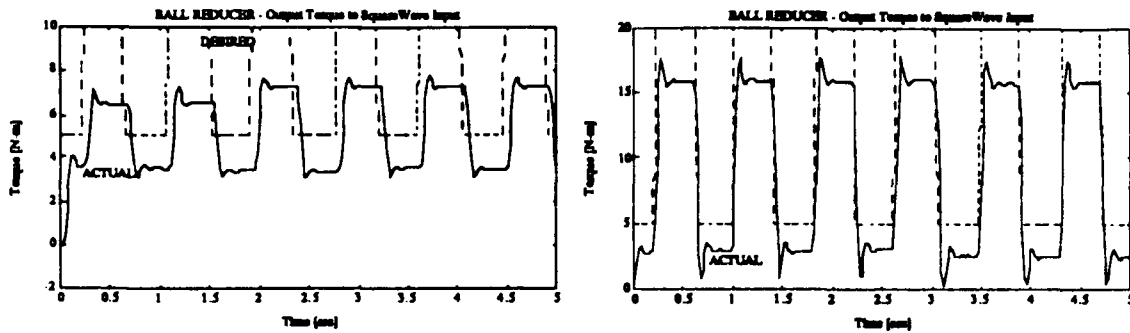


Figure 5.8: Measured Output Torque to Square-Wave Input at 1 Hz and 5-to-10 and 5-to-20 N-m amplitudes for the KAMO ball reducer.

Another interesting behavior is also exhibited by the KAMO ball reducer. Using the same input waveform as for the cable reducer, Figure 5.8 shows its open-loop response. Notice that in the small amplitude case, the response takes a while to ramp up to the desired value. This phenomenon was fairly repeatable and is thus presented here, with the possible explanation that this effect is dependent on the spatial location of the steel balls that transmit the torque. The difference in the stiction and coulomb friction values can also be seen to lie around 2 to 5 N-m, which lies in the range of values that were measured for this reducer.

The DOJEN cycloidal cam reducer exhibits another completely different phenomenon (see Figure 5.9), where for the small level of desired step amplitudes, the measured output torque actually decreases in time, implying that stiction and friction are highly dependent on the mode of operation (time- and wear-dependent stiction/friction but on a very fast time-scale compared to component-wear time-scales).

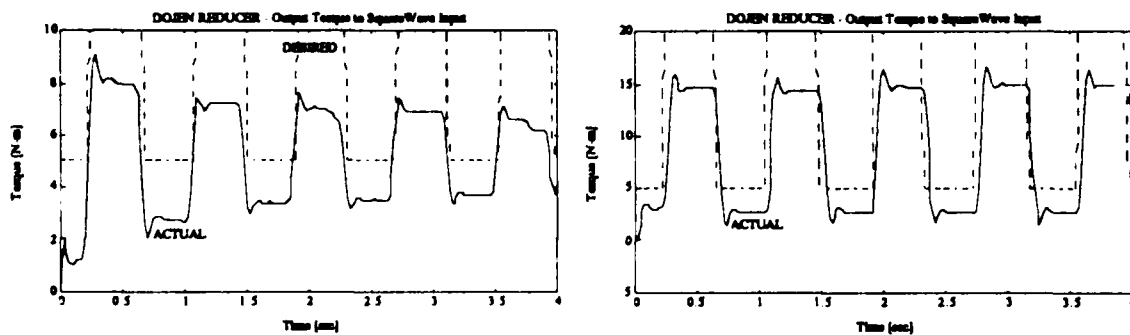


Figure 5.9: Measured Output Torque to Square-Wave Input at 1 Hz and 5-to-10 and 5-to-20 N-m amplitudes for the DOJEN cycloidal cam reducer.

Even though it is hard to tell from the first plot, the overall stiction values are quite different and seem to converge to the +2.5 and -5 N-m values. These values are obvious

from the second plot, where the response of the reducer is quite consistent and settles faster into a steady state.

The REDEX Corbac reducer also exhibits interesting behavior which is present in most of the reducers that we studied. In the small amplitude run (see Figure 5.10), we can see that the reducer exhibits fairly consistent stiction/friction offsets which lie around 2 to 3.5 N-m. On the other hand, at larger levels of transmitted torque, the values are different. The torque offsets due to friction/stiction are now clearly load dependent, since the low-end offset of around 2 to 3 N-m has grown to around 6 N-m at four times the desired torque. Such behavior seems to support the claim that stiction/friction and efficiency are highly dependent on the amount of torque-load that a transmission carries. This behavior was visible earlier in the stiffness fidelity experiments, evidenced by the 'flaring out' of the hysteresis envelope (see Chapter 4).

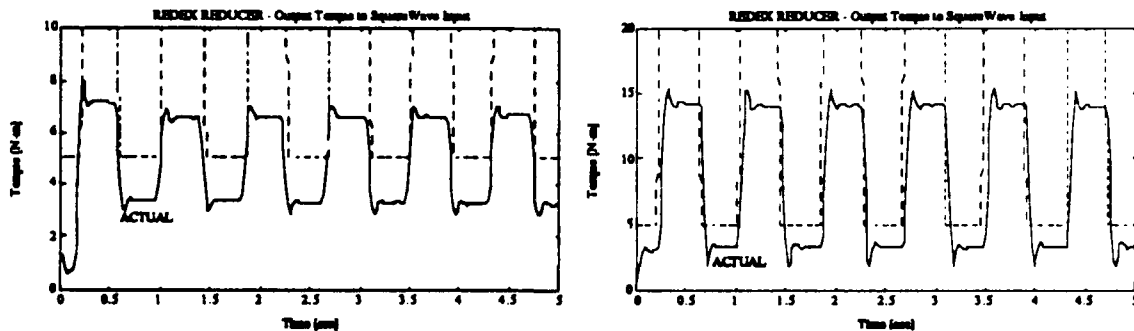


Figure 5.10: Measured Output Torque to Square-Wave Input at 1 Hz and 5-to-10 and 5-to-20 N-m amplitudes for the REDEX Corbac reducer.

In general we could say that this type of waveform at different magnitudes, does a good job of illustrating the rough values of frictional losses in the transmission, while also pointing out load- and time-dependent stiction and friction characteristics which are different from transmission to transmission.

Sine Wave Input:

A sine wave in commanded armature current has the ability to show off different time-dependent phenomena better than a step response. Even though its frequency content is limited, it can really tax the torque-following ability of a reducer, by constantly exciting the stick-slip transition behavior. This phenomenon results in some completely different behaviors for the reducers that we studied. The DC offsets are going to be different from

the square wave experiment, but most of all we will be able to show how stiction/friction, as well as internal transmission dynamics can be brought out by slowly varying sinusoidal commanded input currents.

The WHOI cable reducer was subjected to 1 Hz and 0.25 Hz 5-to-10 N-m and 5-to-20 N-m pure sinusoidal input current waveform, while we were logging the output torque with the force sensor, as shown in Figure 5.11. It is important to note at this moment that all subsequently presented data sets should be compared with this set. The reason is that we have a very taxing set of inputs applied to the most backdriveable reducer, which we expect to result in the cleanest data set to be collected in this chapter. That this is indeed the case can be seen from Figure 5.11 and other figures to follow.

The difference in behaviors between the two frequencies is quite apparent. At moderately high frequencies (1 Hz), the response is quite consistent and homogeneous, with offsets that are in between 1 and 2.5 N-m, which is well within the measured data presented earlier. On the other hand, at low amplitude and reduced frequency, the stick-slip behavior in the transmission is accentuated, leading to a response as seen in the bottom left plot of Figure 5.11. There is not only a clearly visible stick-slip behavior, but also the possible excitation of an internal resonant mode (data on the upswing from 5 N-m shows a rather consistent resonant vibration which dies out quickly). A simple FFT analysis of the data has revealed that there is a noticeable frequency peak at around 20 to 25 Hz, which is close to the predicted first resonant mode of the transmission, theoretically determined to lie around 32 Hz [DiPietro (1988)]. The stick-slip and resonance are much less noticeable in the low frequency high-amplitude experiment (yet still present). The data becomes much smoother with much lower frequency components than in the low-amplitude case.

Similar experimental conditions for the harmonic drive reveal a very different behavior than observed for the cable reducer (see Figure 5.12). Even at moderate frequencies (1 Hz), the harmonic drive does not follow the desired waveform very well. The fact remains that the amplitude of the control signal is larger than the stiction band of the reducer, but depending on where the reducer 'gets stuck' during the experiment, the waveforms differ and in no way approach a sinusoidal shape. The problem is somewhat alleviated when the magnitude of the input signal is doubled, with the resulting output torque showing a more sinusoidal-like behavior, but with 'clipped' upper peaks, and friction offsets ranging from 5 to 10 N-m, which fall well within the numeric range measured in Chapter 4.

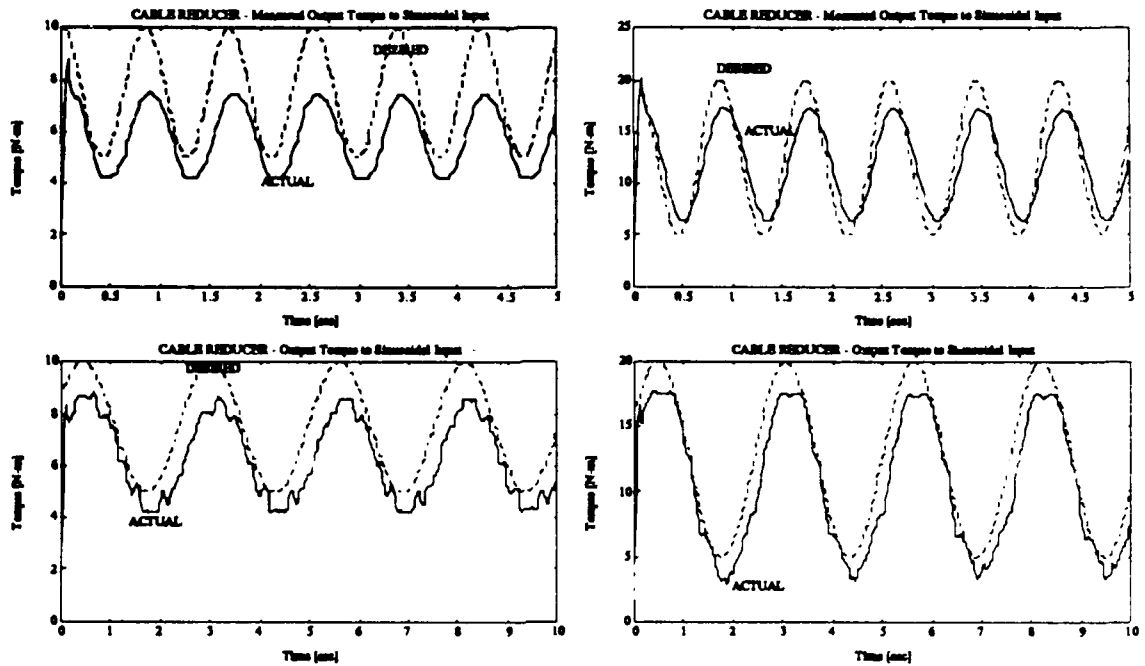


Figure 5.11: Measured Output Torque to Sine-Wave Inputs at 1 and 0.25 Hz with 5-to-10 and 5-to-20 N-m amplitudes for the WHOI cable reducer.

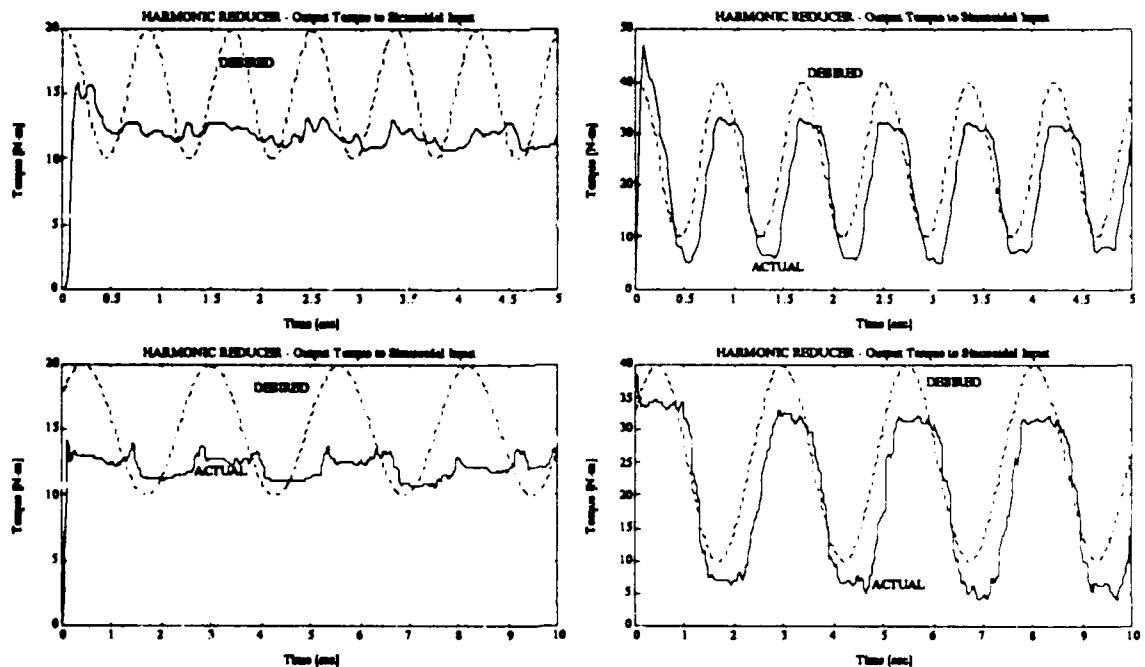


Figure 5.12: Measured Output Torque to Sine-Wave Inputs at 1 and 0.25 Hz with 10-to-20 and 10-to-40 N-m amplitudes for the HARMONIC DRIVE reducer.

Reducing the frequency of the input signal clearly illustrates the stick-slip phenomenon and its dependence on input amplitudes. At increased amplitudes, the output torque begins to look more pyramid-like, with clearly identifiable stick-slip behaviors. There are oscillatory peaks during the peaks and valleys of the commanded input current, whose spatial spacing correlates well to the inter-tooth spacing of the harmonic drive. This phenomenon is also well known, since the teeth do not roll on top of each other despite their involute profiles, but they wedge into each other, especially due to the radial and axial deformation of the wave-spline.

The response of the KAMO ball reducer to similar inputs is shown in Figure 5.13:

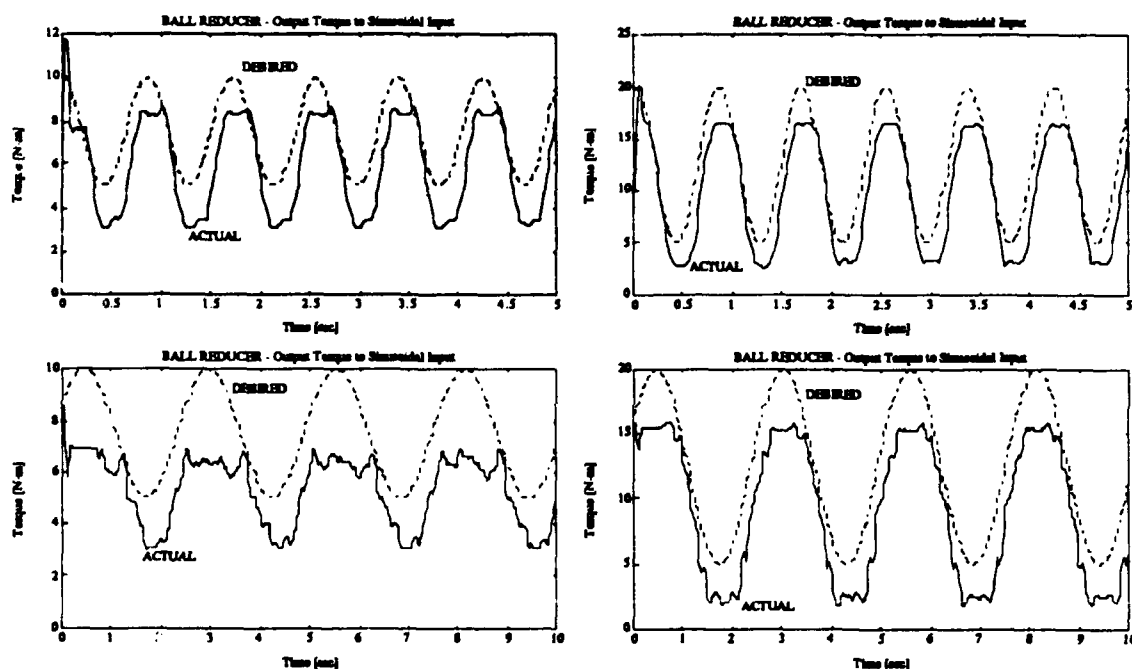


Figure 5.13: Measured Output Torque to Sine-Wave Inputs at 1 and 0.25 Hz with 5-to-10 and 5-to-20 N-m amplitudes for the KAMO ball reducer.

Once again the response at moderate frequencies can be termed to be quite sinusoidal, except for the amplitude- and phase modulation. There are a set of repetitive peaks and valleys that occur at high torques, which are very hard to explain geometrically, since the physical configuration of the internal torque-transmitting members is quite complex. Thus unlike with the harmonic drive, the correlation between peaks and valleys and the relative position of the reducer input is not quite as obvious. One may argue rather effectively that this could be due to the increased hertzian contact stresses of the balls running in their grooves and transitioning from one groove profile in one plate to the profile in the opposing plate, but no real concrete proof for this can be given without running another specific

experiment (very complicated experiment and beyond the scope of this thesis). Yet the ripple-torque phenomenon discovered earlier can be seen to filter into the data here.

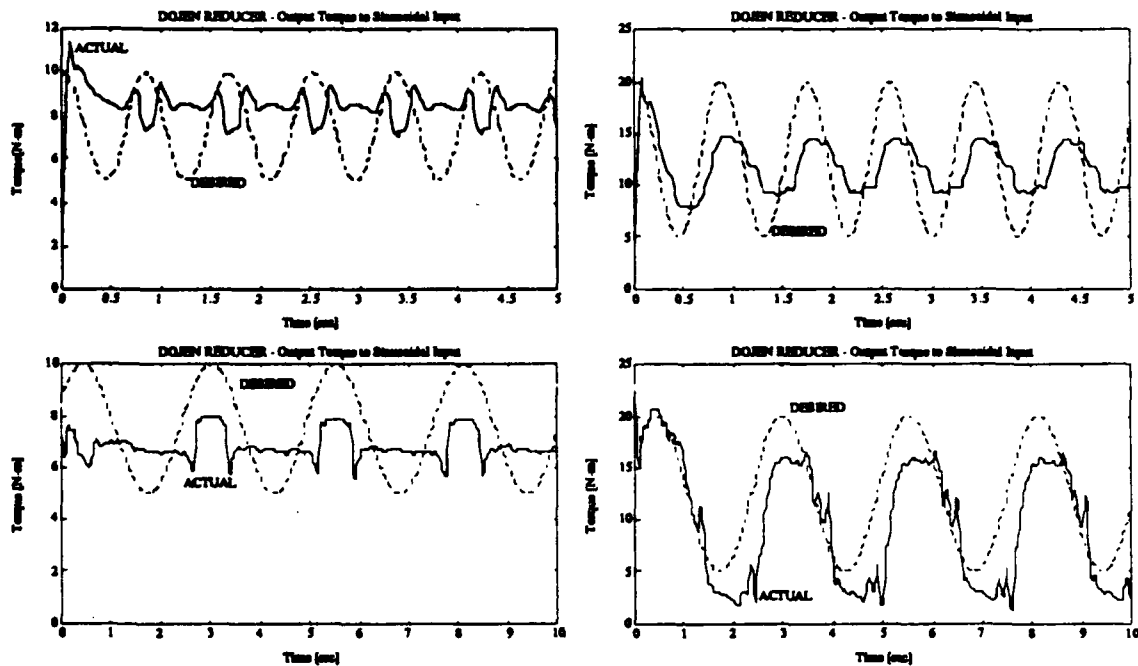


Figure 5.14: Measured Output Torque to Sine-Wave Inputs at 1 and 0.25 Hz with 5-to-10 and 5-to-20 N-m amplitudes for the DOJEN cycloidal cam reducer.

The data in Figure 5.14 shows the response of the DOJEN cycloidal cam reducer to the selected set of input torques. Notice how qualitatively different the responses are, depending on the frequency and amplitude of the input. The upper left plot seems to show that the transmission is able to store energy internally and then release it so that the torque signal not only has a high DC component, but the variation can be as much as 180 degrees out of phase with the commanded torque. This sudden release seems to indicate that the stiction/friction characteristics are highly variable with the amount of transmitted torque. Increasing the input amplitude at the same frequency results in better following with a seemingly uniform 5 N-m stiction/friction band. A reduction in input frequency at the same amplitudes is able to illustrate the stick-slip phenomenon even better. The sudden release is always accompanied with a reduction in measured output torque, before the transmission sticks again. If a larger input amplitude is selected, the stick-slip phenomenon can be seen to excite internal structural dynamics of the transmission. This phenomenon is most obvious in the bottom right plot of Figure 5.14. We have these oscillations upon reduction of torque, as well as upon increase in torque, which are both situations when the onset of stick-slip is most pronounced and energy stored would be most likely to be released.

Plots in Figure 5.15 illustrate the behavior of the REDEX Corbac reducer to the analogous set of inputs. Clipping of the output torque wave form due to stiction and friction is again more obvious at the lower input frequencies (no surprise there). The inability of the reducer to reproduce the sinusoidal input waveform is obvious at moderate and low frequencies.

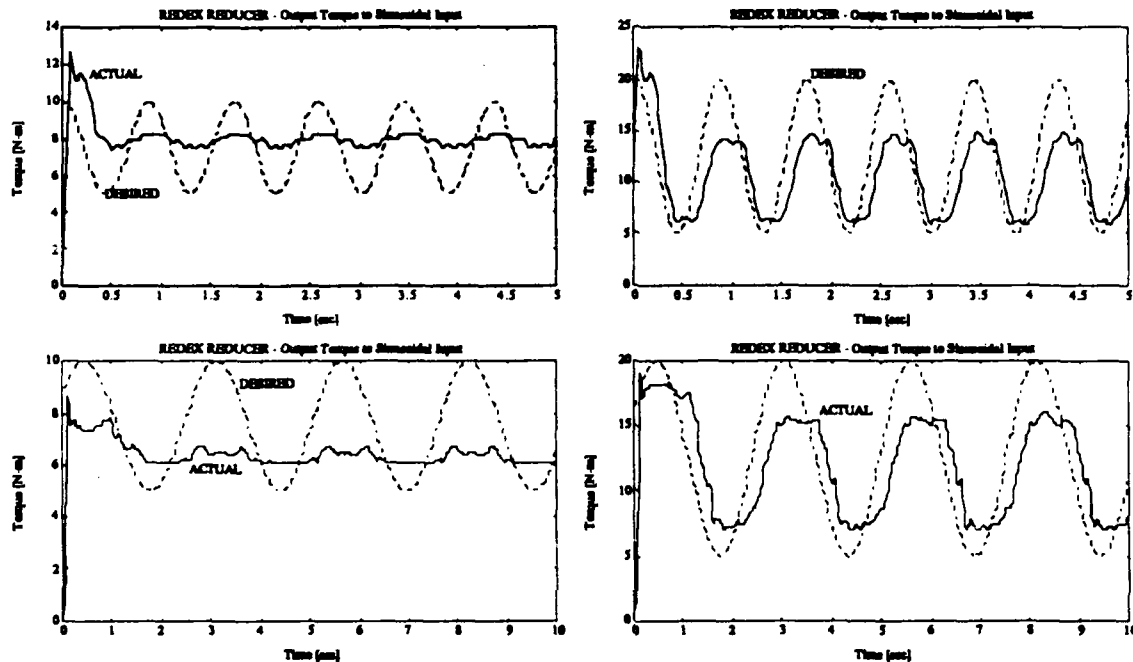


Figure 5.15: Measured Output Torque to Sine-Wave Inputs at 1 and 0.25 Hz with 5-to-10 and 5-to-20 N-m amplitudes for the REDEX Corbac reducer.

Despite the fact that the amplitude of the input signal is above the stiction band, the reducer's output comes to 'rest' at a position where the relative changes in input torque have no real effect since they lie within the stiction band. This problem is reduced for increased amplitude input torques, but even there stick-slip is present. This reducer shows no lowly damped oscillations during stick-slip, as did some of the previous reducers. The recurring double-bump visible in the lower left plot of Figure 5.15 could not be matched to meshing gear teeth in the reducer - its occurrence is sustained and periodic over a longer time period than shown here.

Concluding this section, we can say that the ability of a reducer to follow a low-frequency signal with amplitudes comparable to its relative stiction band is a very good open-loop performance qualifier. Such phenomena as stick-slip and internal vibrations and damped oscillations can be best observed with this type of experiment, due to the enlarged time-scales and the high-frequencies that are injected during stick-slip and breakaway,

which will excite internal oscillations that can then be measured. The periodic occurrence of torque-ripple need not only be plotted against time, but also against the spatial orientation of the the reducer components. Only in the case of the harmonic drive was this match possible, since the reducer is simple and single-stage. Other reducers are less straightforward and thus such a claim would be hard to substantiate without further experiments especially focussed on measuring these phenomena.

Simulation & Experiment: WHOI Cable Reducer

This section will deal with the question of how well the simple set of measured transmission descriptors (friction, stiffness, inertias) can reproduce the measured data under similar operating conditions. This required using the same input torque waveform in a nonlinear simulation of the dynamic system, which included stiction, coulomb friction, viscous damping, and inertias as lumped parameters. The parameters for these simulation parameters were taken as the measured data from Chapter 4, and the simulated and experimental responses were then compared. Compared below are the results for the WHOI cable reducer and the HARMONIC DRIVE reducer. The reason for only comparing the data sets for these two reducers will become apparent as we proceed, and will be dealt with in more detail at the end of this section.

Since we know that the transmissions exhibit highly variable responses depending on input waveform, -frequency and -magnitude, we have shown in the next few plots the model fidelity for all the previously shown experimental situations. The first set of experimental conditions that we explored was that of the square wave input at 1 Hz with 5-to-10 N-m and 5-to-20 N-m amplitudes for the cable reducer (see Figure 5.16). Notice that the desired waveforms are not shown in order to avoid cluttering the plot.

The responses agree quite well in steady-state, except for the initial transient response. The difference between the simulated and experimental data sets is small enough, so that the simple change of some of the simulation parameters (negative coulomb friction and stiction), could easily account for the discrepancy. Similarly a change in positive coulomb friction and stiction for the larger amplitude scenario (by about 1 N-m) can also match the two responses quite well. These changes in parameters are well within the measurement values taken for this transmission.

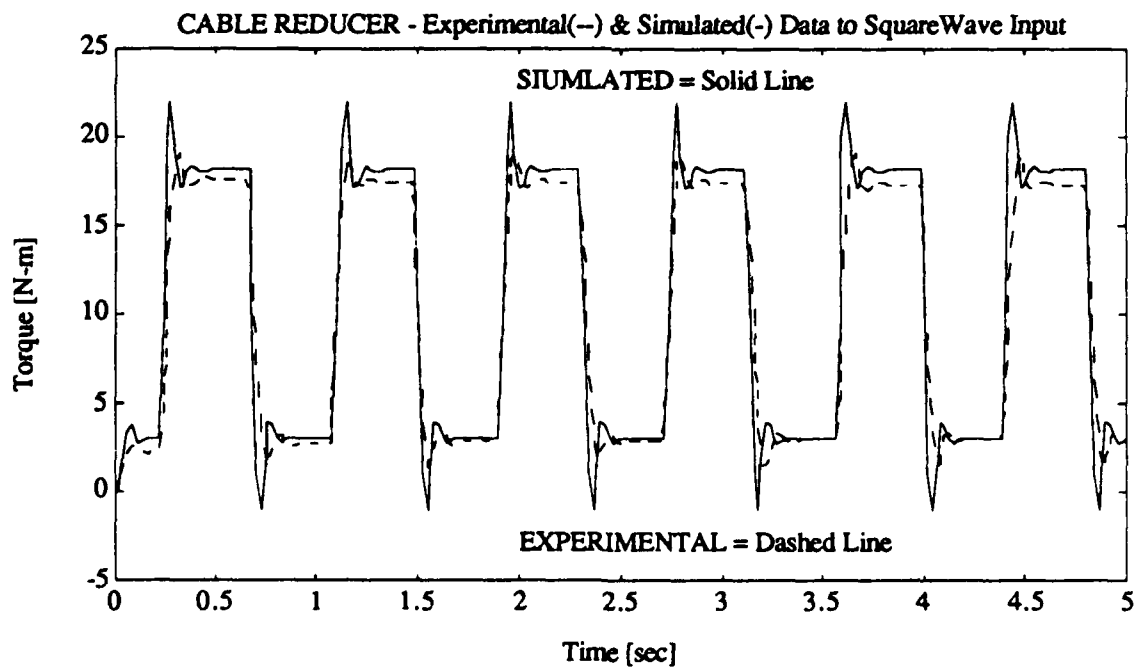
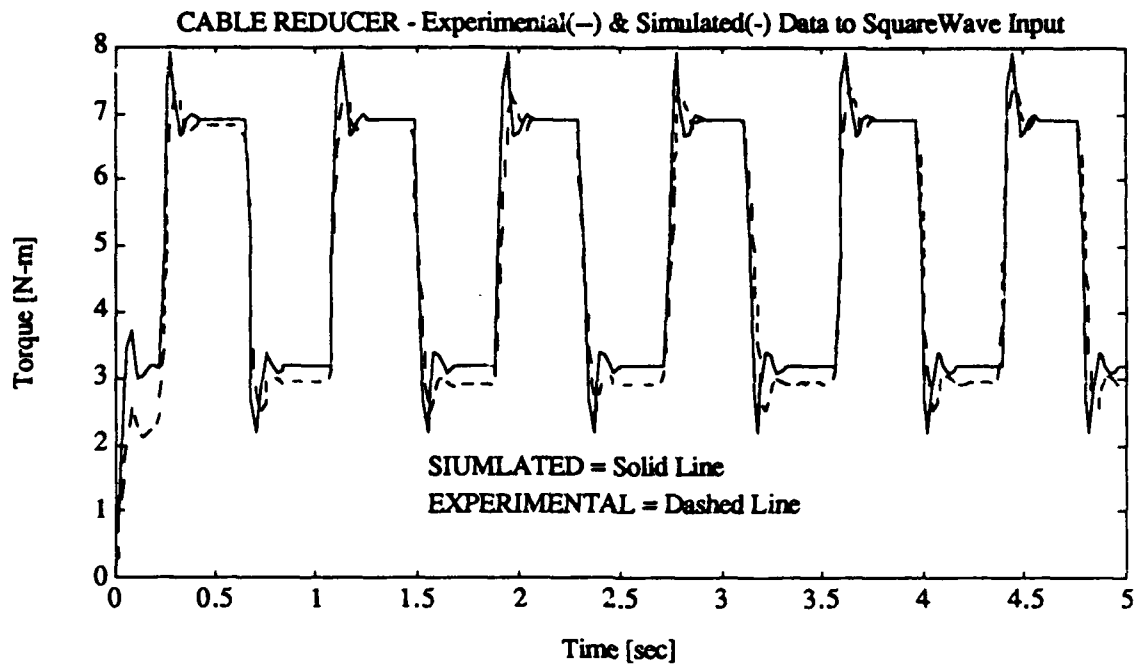


Figure 5.16: Measured Output Torque to Square-Wave Inputs at 1 Hz with 5-to-10 and 5-to-20 N-m amplitudes for the WHOI cable reducer.

The important thing to realize here, is that a seemingly small change in simulation parameters would seem to indicate that the basic structure of the model is correct and that better estimates of the static system descriptors is all that is required. That this is not entirely true can be proven with the next experiment, where the inputs are sinusoids of different frequencies and amplitudes.

The use of sinusoidal inputs was necessary to see how well the simple nonlinear model will match the experimental data. In Figure 5.17 we show two plots corresponding to the same input frequency but different amplitudes - both at 1 Hz. The difference between actual and simulated data is fairly small, even though the errors are more pronounced in the small amplitude case, where the simulation predicts a larger phase-lag. Thus the break-away is not perfectly well modelled, but the discrepancies are not serious at all, which still suggests that the simple nonlinear model may not be perfect but can do an adequate job overall (at least so far).

This simple nonlinear model though breaks down rather rapidly, when the frequency of the input signal is reduced. This can be observed in Figure 5.18, where the same conditions are present as before, except that the input signal frequency was dropped from 1 Hz to 0.25 Hz. Since we would expect this experiment to really tax the ability of the model to properly represent simple stick-slip phenomena, we can not be too surprised when we compare the simulated and experimental data sets. The match between the two data sets is far from ideal, especially in the low torque experiment (5-to-10 N-m). As the input amplitude increases, so does the match between the two data sets.

This last experiment points out the weakness of this simple lumped- and fixed-parameter nonlinear model. It is capable of predicting high-frequency, high-amplitude input-signal scenarios, but begins to break down as the input amplitude and frequency are reduced. The discrepancy between simulated and experimental data can not be corrected by simply tuning the values of the simulation parameters (fixed in each simulation run), and thus points to the inaccuracy of the lumped-parameter nonlinearities represented by the static descriptors of a transmission. The stiction/friction phenomenon can thus not be seen as a 'static' description, but must be measured and modelled more as a dynamic phenomenon dependent on more parameters than just transmitted torque. Mostly spatial relationships of friction characteristics are important, but they are extremely hard to measure, certainly highly variable amongst transmissions of the same type, as well as dependent on usage time (wear-and-tear) of the transmission. The lumped nonlinear model is not appropriate for such scenarios, underscoring the need for better stick-slip models with either more 'friction-nodes' or of a more continuous nature (infinite number of stiction/friction nodes).

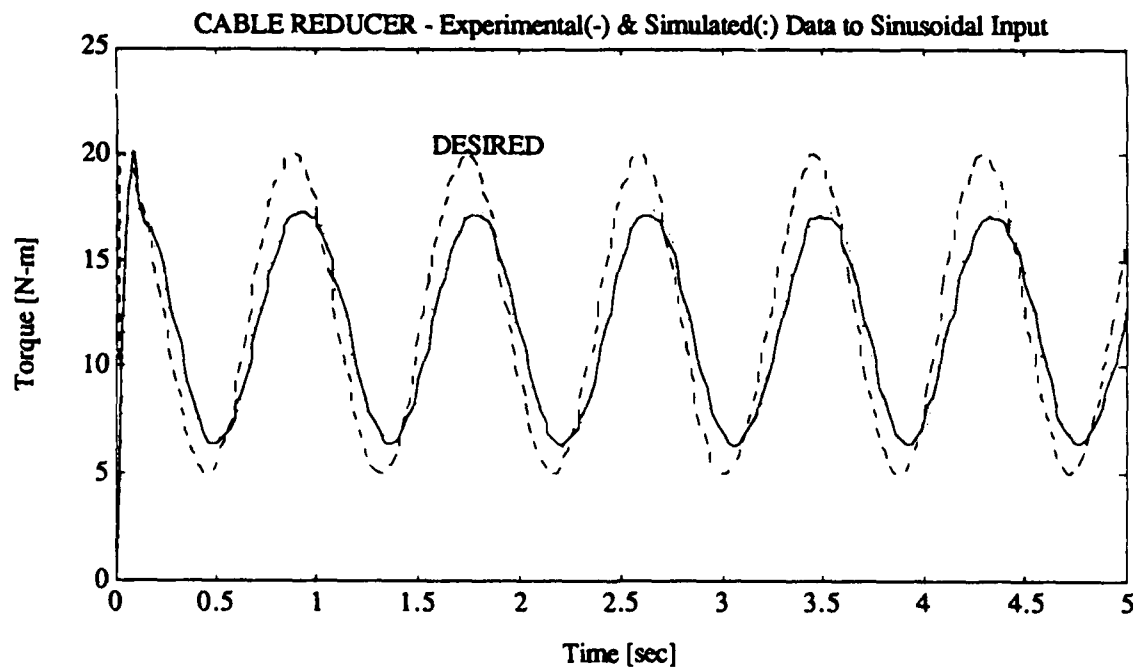
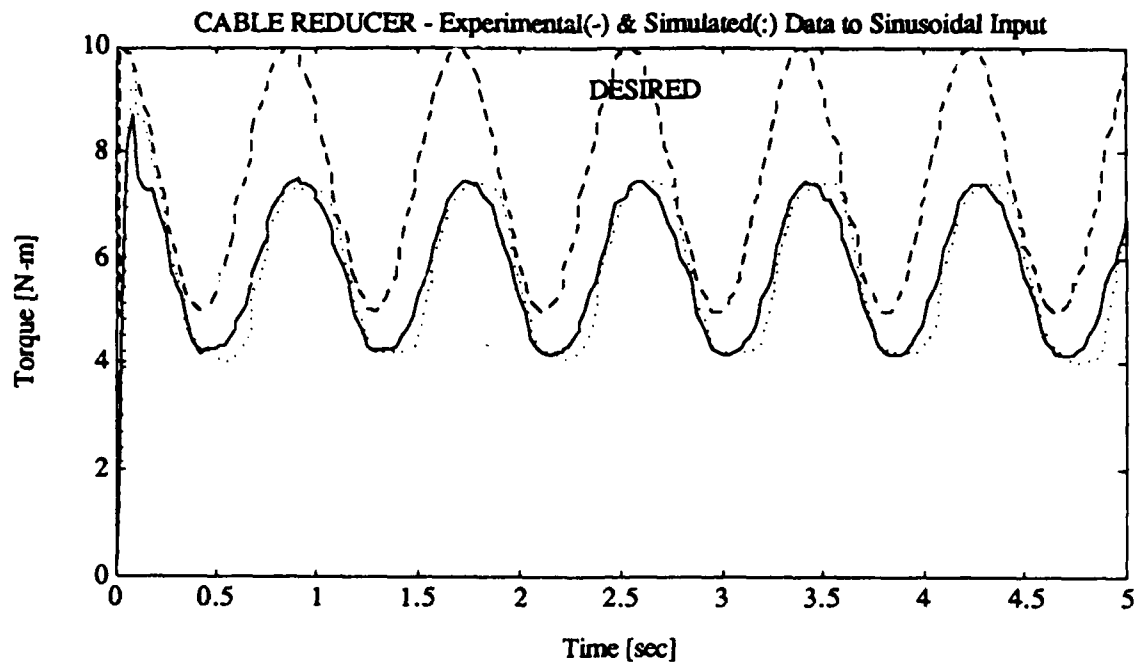


Figure 5.17: Measured Output Torque to Sine-Wave Inputs at 1 Hz with 5-to-10 and 5-to-20 N-m amplitudes for the WHOI cable reducer.

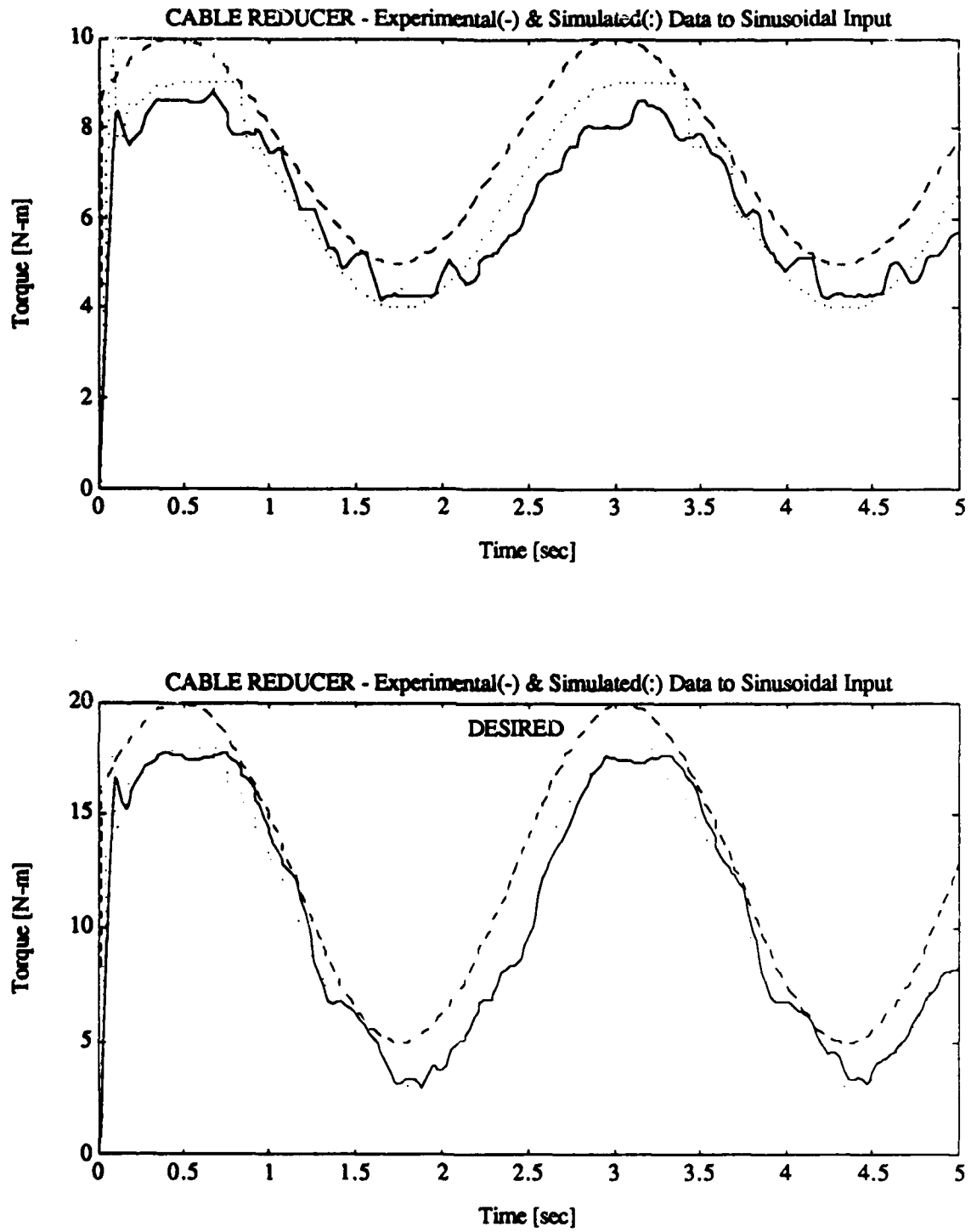


Figure 5.18: Measured Output Torque to Sine-Wave Inputs at 0.25 Hz with 5-to-10 and 5-to-20 N-m amplitudes for the WHOI cable reducer.

Simulation & Experiment: HARMONIC DRIVE Reducer

Since the sinusoidal inputs seem to be the most taxing on the model structure, revealing any discrepancy due to modeling errors in the numerical values of the static descriptors as well as the model structure itself, we will limit the experiments to this type of input. The trends that were obvious from the cable reducer are also evident in these data sets.

Figure 5.19 illustrates the response of the transmission to a 1 Hz sinusoidal input signal of two different amplitudes. The response for the high-amplitude case (5-to-40 N-m) is in general quite repeatable, yet the agreement between simulated and experimental data breaks down at the lower and higher torque limits. Neither the sloping descent at high torques, nor the excessive undershoot are well predicted. Even though the response of the reducer at the low torque end seems to settle to within the relative amplitudes of the simulation, the simulation fails to properly predict the low-speed portions of the response. In the case of reduced input amplitudes, the simulation completely fails to predict the highly oscillatory stick-slip behavior. Even though relative DC values are close, the AC components due to variations in the static descriptors can not be properly predicted by this model.

By reducing the input frequency to 0.25 Hz, as shown in Figure 5.20, the details of model inaccuracy can be clearly seen. The model again has a hard time predicting lower-amplitude responses, by completely mispredicting stick-slip behavior in the transmission. The problem is somewhat alleviated at higher amplitudes, but the change in stiction/friction, obvious from the flattening in the experimental data, is a phenomenon that creates disagreements in the two data sets at high and low levels of torque - situations of low or zero relative motion between components inside the transmission.

Overall the same conclusions can be drawn here, as were drawn for the cable reducer, only that the disagreements between simulated and experimental data are even larger. The model structure itself should not simply comprise constant-value lumped nonlinear stiction/friction phenomena, but should consist of a rather more distributed, variable parameter model. On the other hand, these variations are extremely hard to model and thus predict, making compensation very empirical and thus unreliable.

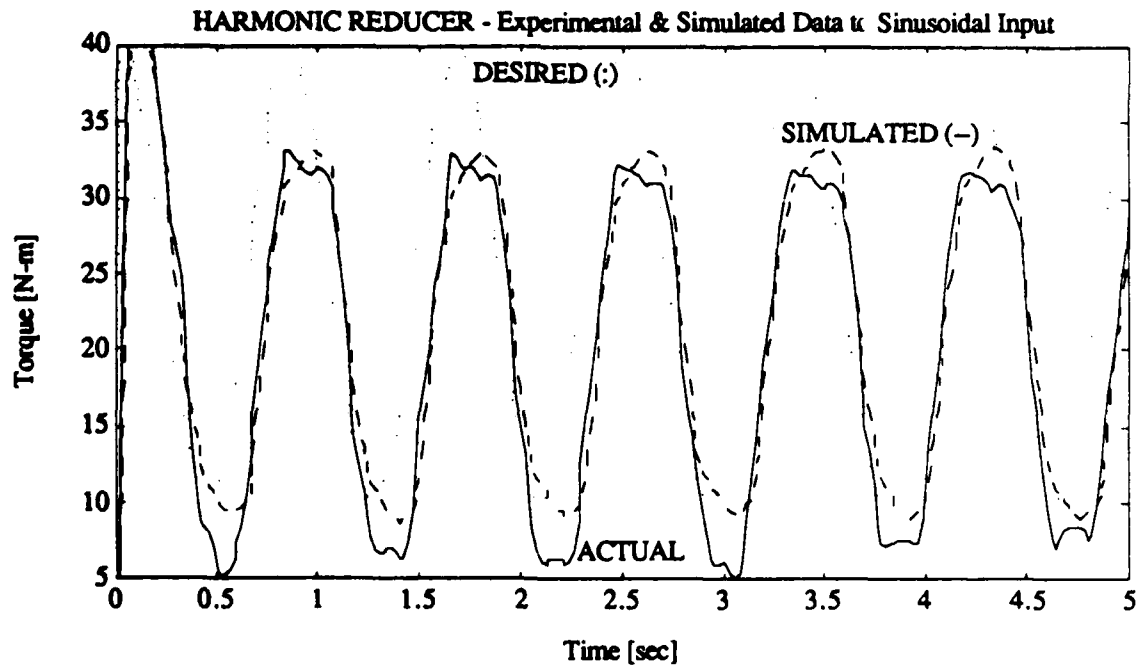
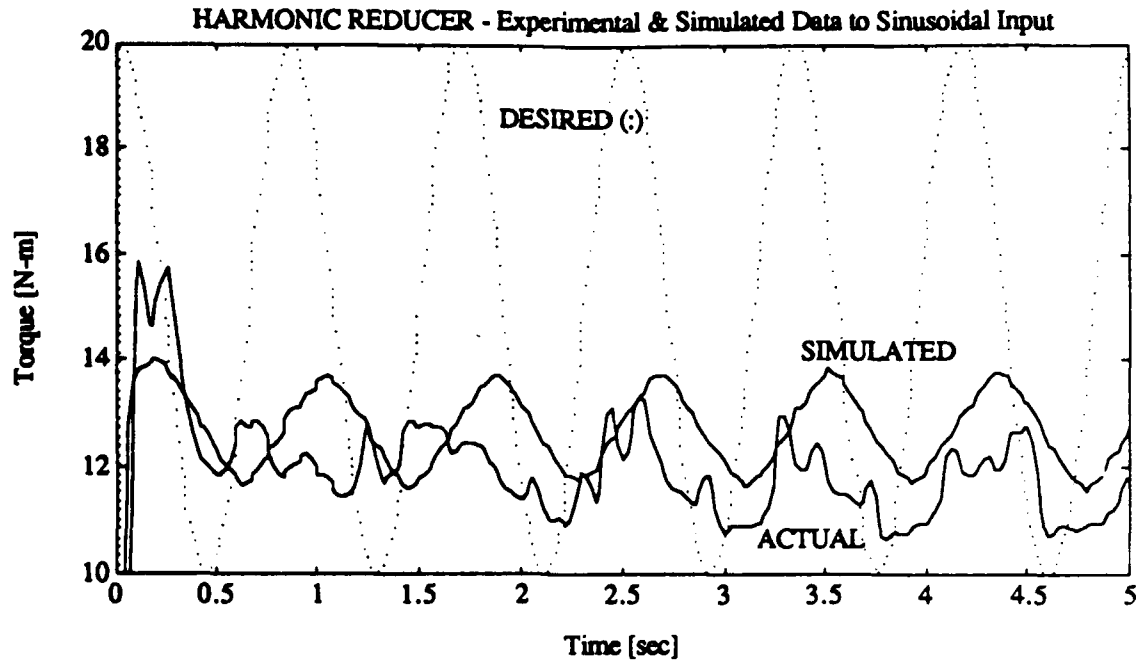


Figure 5.19: Measured Output Torque to Sine-Wave Inputs at 1.0 Hz with 10-to-20 and 10-to-10 N-m amplitudes for the HARMONIC DRIVE reducer.

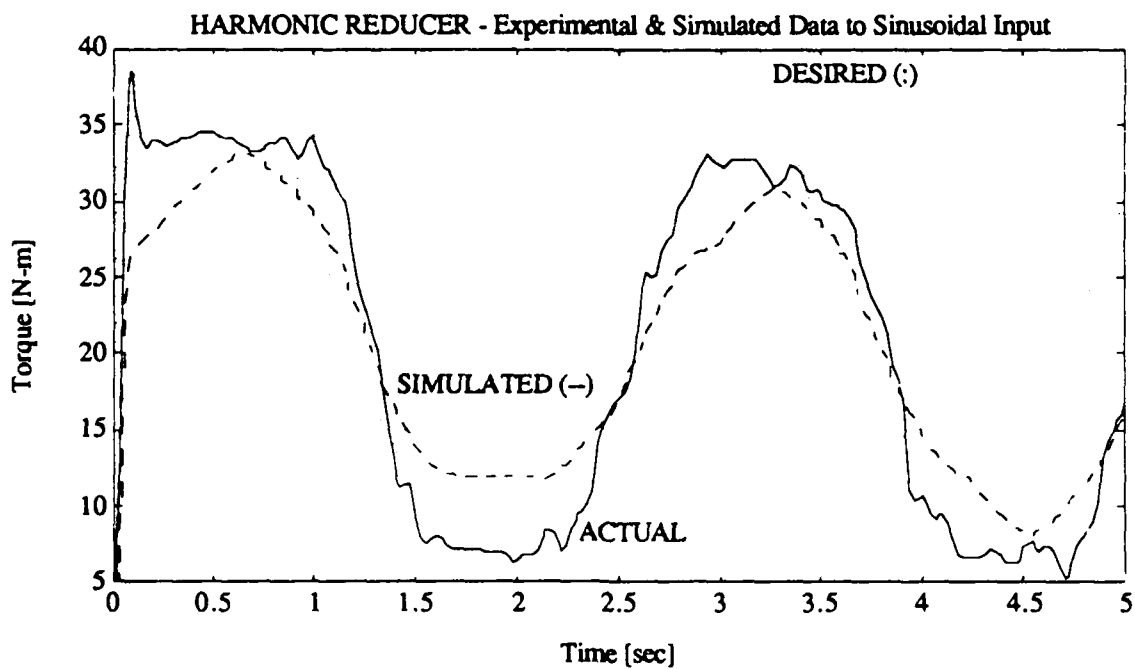
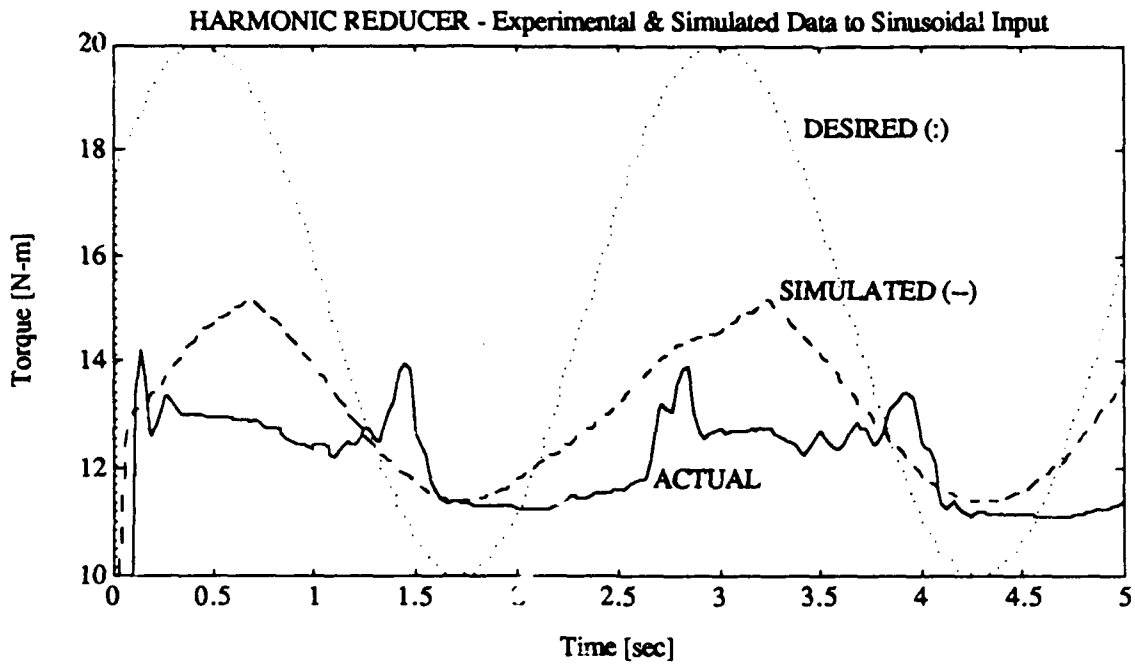


Figure 5.20: Measured Output Torque to Sine-Wave Inputs at 0.25 Hz with 10-to-20 and 10-to-10 N-m amplitudes for the HARMONIC DRIVE reducer.

Simulation & Experiment: Remaining Reducers

The two previous data sets illustrate very clearly the benefits and shortcomings of simple lumped nonlinear models. The ability of such models to accurately predict observed behavior is highly dependent on the type of transmission and the input amplitudes and frequencies. The responses of the other transmissions to similar inputs was presented earlier, which illustrates how different and nonlinear these behaviors can be. Looking at the responses of the DOJEN and REDEX reducers for instance, the simulation will utterly fail to predict the behaviors at low amplitudes and frequencies, while doing an acceptable job for higher frequency and amplitude scenarios (especially the square wave inputs).

Instead of going into the fine points for each reducer, we will simply state that the trends will not be very different from those found for the WHOI cable reducer and the HARMONIC DRIVE reducer. It is again evident that we need to formulate more sophisticated models of distributed- and variable-parameter stiction-friction behaviors, as well as any internal oscillatory modes which may have been neglected in the two-mass lumped-parameter model. Adding spatially-dependent and load-dependent stiction/friction characteristics into such a model does not markedly improve the fidelity between simulated and experimental response. Choosing the proper functional relationship between these parameters is at best guess work, unless these relationships could be properly motivated and validated via some conclusive set of additional experiments. Another complicating factor is that these phenomena are most certainly variable in time, as the transmission experiences component wear and tear.

(5.2.3) Closed-Loop Experiments

This section will deal with the performance and stability margins of transmissions in closed-loop torque/force control tasks. The control scenario is as explained at the beginning of this chapter, where the motor-torque is based on a control law that tries to generate torques in order to match the desired output torque with that measured by the force sensor at the output. The type of input is chosen to almost always be a square wave of different amplitude, since such an input makes it easy to excite transmission-internal system dynamics, and observe performance in terms of frequency, damping ratio, settling- and rise-times, etc..

Closed-loop data is presented for the case of the harmonic drive and the cable reducer. The reason lies in the physical attributes of these two reducers. They both have almost identical input inertias which makes a controller comparison much more meaningful and realistic. Other reducers have input inertias that are much larger (factor of 5 to 10), and thus a performance comparison would not really be very fair nor meaningful. Both of these reducers exhibit the more peculiar transmission stiffness behaviors measured for all the reducers. Such a condition allows this analysis to make conclusions which will be valid over a comparable set of similar operating ranges.

The fact that the output inertias between the harmonic drive and the cable reducer are somewhat different is an issue that was resolved as follows. Theory predicts that the effects of output inertia for a system in hard surface contact are minimal for the operating range we are in. Furthermore a few simple experiments were performed, where the output inertia was drastically increased through the addition of lead weights at the output. No appreciable change in performance nor stability tendencies was observed, and thus the two experimental setups were considered to be as best a dynamic match as was possible within our experimental capabilities.

PD - Torque Controller:

The most simple controller (beyond a simple proportional controller) is the PD controller providing proportional force-error correction and force-rate damping. The simple controller structure is:

$$\tau_m = K_p(\tau_d - \tau_f) - K_d \frac{d}{dt} \tau_f \quad (\text{Eqn. 5.1})$$

The desired torque τ_d , and the measured torque τ_f , are both used in conjunction with the proportional gain K_p , and the derivative gain K_d . The force-rate is computed based on a digital differentiation scheme, which introduced a fair amount of noise that had to be low-pass filtered out. This fact alone limited the usefulness of this type of controller, but at low gain levels for K_d , the trends were still very informative. At higher levels of K_d , the low-pass filtering had to be so severe, that the damping control action became meaningless and even destabilizing - thus the choice of only using a small subset of the achievable damping gains K_d as reliable data sets.

In Figures 5.21 we have shown the responses for the WHOI cable reducer and the HARMONIC DRIVE reducer to a square-wave input of comparable amplitude (remember the difference in reduction ratio of 60:1 and 30:1), with a purely proportional controller. The frequencies of the two different square waves was selected in order to make the measurement of resonance frequency as easy as possible. The proportional gain was tuned so as to barely result in a stable system. You can see in both plots, that the responses are very lightly damped, which places them right on the edge of stability. The respectively stable gains for the cable and harmonic reducer were 1.3 and 0.95. One can also see that the differences in the closed-loop instability frequency is about a factor of 2. While the closed-loop resonance for the cable reducer lies around 4 to 5 Hz, the harmonic drive exhibits a closed-loop resonance at 2 to 3 Hz.

It is important at this point to notice the difference in maximum achievable (stable) closed-loop frequency, since the difference can be modelled and predicted as a difference due to the transmission stiffness measured for both of these transmissions. This limit is thus strictly imposed by the hardware characteristics of the transmission itself. The addition of force-rate damping should be able to achieve small increases in this bandwidth, as predicted by theory (at the expense of reduced damping though). We were unfortunately only able to implement low levels of force-rate damping due to the hardware limitations we were living with. The difference in performance was not really measurable.

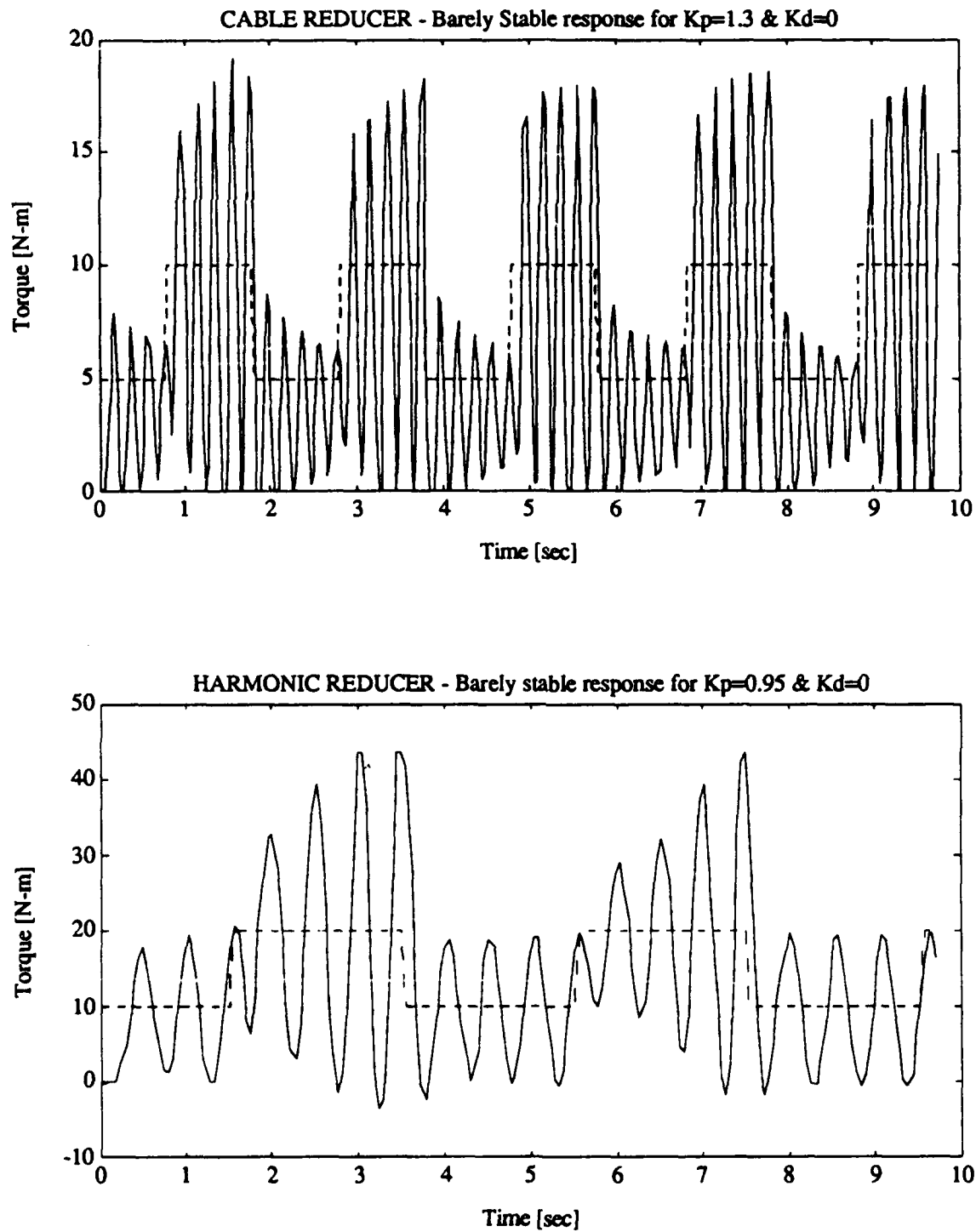


Figure 5.21: Closed-Loop Resonance Frequencies at maximum proportional force-error gain K_p , for the HARMONIC DRIVE and the WHOI cable reducers.

In Figures 5.22 and 5.23, we have shown the stability margins and instability frequencies that we should theoretically achieve for the WHOI cable reducer and the HARMONIC DRIVE reducer, as well as the experimental data points we collected (shown as large dots). Notice that the agreement between theory and experiment is no better than about 20% in the case of the stability margins associated with controller gains, but the agreement is much better (5 to 10%), when it comes to predicting the frequency at instability. The discrepancy at increased levels of electronic force-damping increases and points out even further the implementation problems which reduced our ability to faithfully implement such a controller.

Notice that the ability of the linear model, using the measured values for the dynamic system parameters, is able to accurately predict stable frequencies to within 10%, while the errors are a bit larger (up to 20%), when it comes to predicting gains at the stability margin. Such models can thus be helpful to determine the system performance levels in terms of ultimate achievable bandwidth. The theoretical gains necessary for a certain performance are harder to predict accurately, since the real system is clearly not linear. Furthermore, at the edge of the stability margin, we have fairly large motions, which tend to minimize the effects of such static descriptors as stiction/coulomb-friction (which we saw earlier do not predict performance well for low-amplitude, low-frequency signals), and put more emphasis on the stiffness of the transmission as well as its viscous damping coefficient and inertias. If properly parameterized, a simple linear model can do a fairly competent job of predicting system stability margins and bandwidth performance.

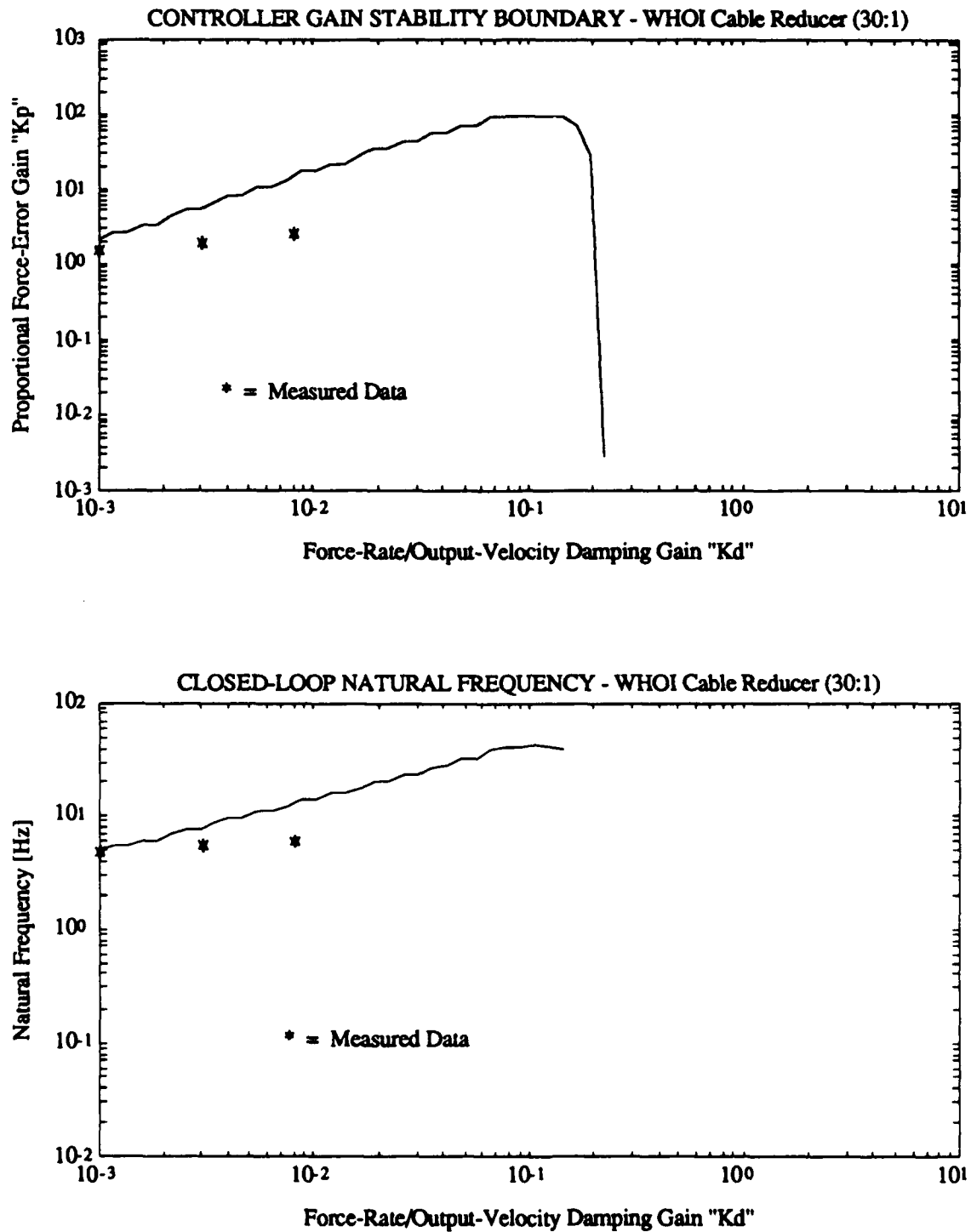


Figure 5.22: Theoretical Closed-Loop Stability Margin, associated gains and bandwidth, with experimental data points, for the WHOI cable reducer.

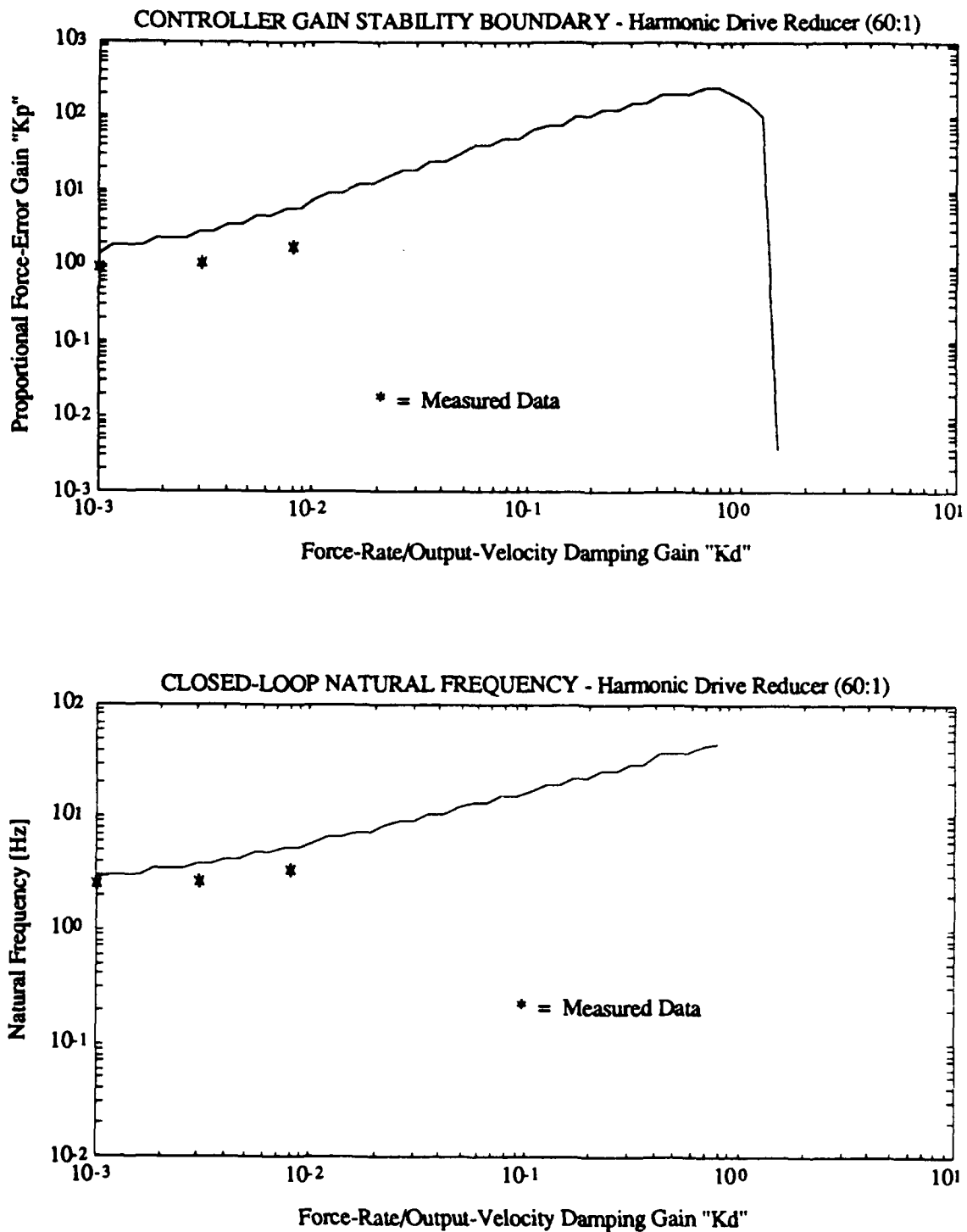


Figure 5.23: Theoretical Closed-Loop Stability Margin, associated gains and bandwidth, with experimental data points, for the HARMONIC DRIVE reducer.

PD - Torque/Input-Velocity Controller:

Another common controller is the PD controller providing proportional force-error correction and damping based on a measurement of input-velocity. Such a controller is most helpful, since it provides the ability to dampen out the proximal mode, which represents the lowest resonant mode and is responsible for the dominant stability properties of the system. The simple controller structure is:

$$\tau_m = K_p(\tau_d - \tau_f) - K_d \frac{d}{dt} \theta_1 \quad (\text{Eqn. 5.2})$$

where $d\theta_1/dt$ is measured at the motor-end. The experimental data showing the effectiveness of input-velocity damping is clearly shown in Figure 5.24, where we have added enough electronic damping to the system which was barely stable with $K_p=0.95$ ($K_d=0$), to result in a damped response with better than a 0.707 damping ratio. Using the same set of gains (see Figure 5.25), we performed a contact acquisition task, where the transmission/sensor output was not in contact with the environment, but gained contact after a few seconds, with very much reduced transients and faster settling times. This same task would not have been possible (in a stable fashion), if electronic input-velocity damping had not been used. Due to the increased damping levels of the proximal vibratory mode, we can increase the value of the proportional force-error gain by 100%, before the system starts to go unstable again. These two responses can be seen in Figure 5.26. The differences in bandwidth right before instability are very small, indicating what linear theory also predicts: input-velocity damping can increase the performance of the closed-loop system, but the eventual bandwidth at the stability margin varies very little, and is solely due to the hardware characteristics of the transmission. The root-locus of the motor/transmission/load/sensor system is shown in Figure 5.27, and clearly illustrates a few important points. In an ideal system, the open-loop poles of the proximal vibratory mode, are fixed at a location from which they can only be moved via closed-loop input velocity damping feedback. The effect is to (ideally) increase the damping ratio at a constant frequency, signified by the migration of the closed-loop poles around the origin along a radius equal to the natural frequency of the pole-pair. For a proportional controller, increases in proportional gain K_p , will have to be larger and larger, before the root-locus reaches the $j\omega$ -axis. The crossing-point of the $j\omega$ -axis will not vary much, since the asymptotes will not have moved much, because the distal vibratory mode is much higher in frequency (due to the larger stiffness of the force/torque sensor), and thus dominates the location of the asymptote intersection along the real axis.

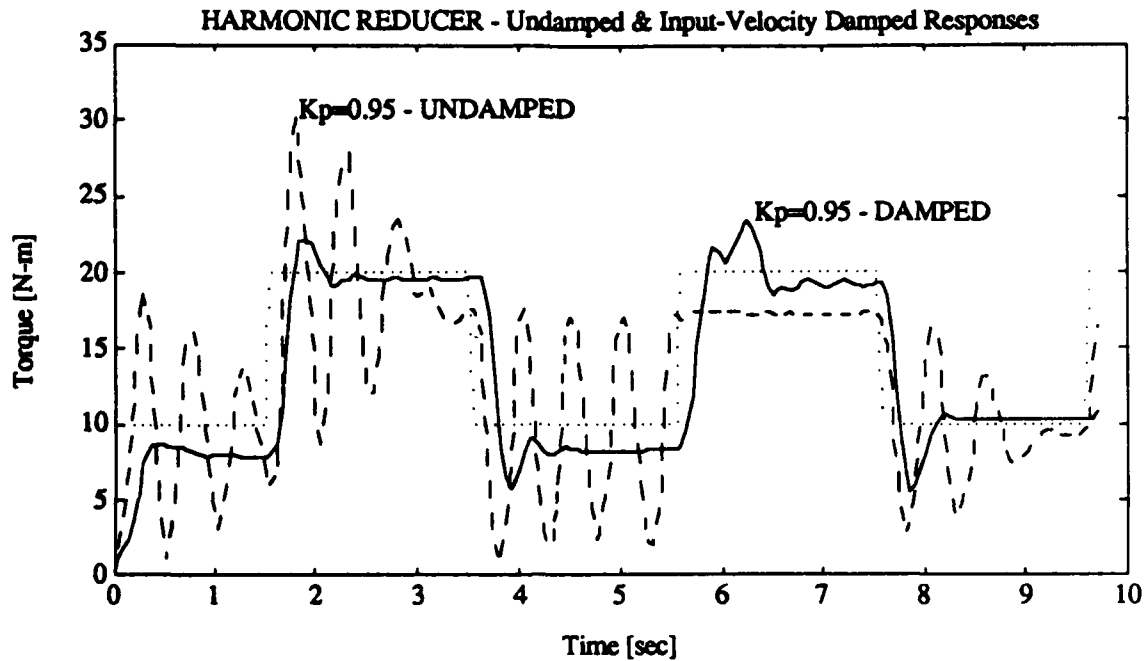


Figure 5.24: Response to Square Wave Input for max. K_p gain ($K_p=0.95$) without and with input-velocity damping for the HARMONIC DRIVE reducer - in contact with surface.

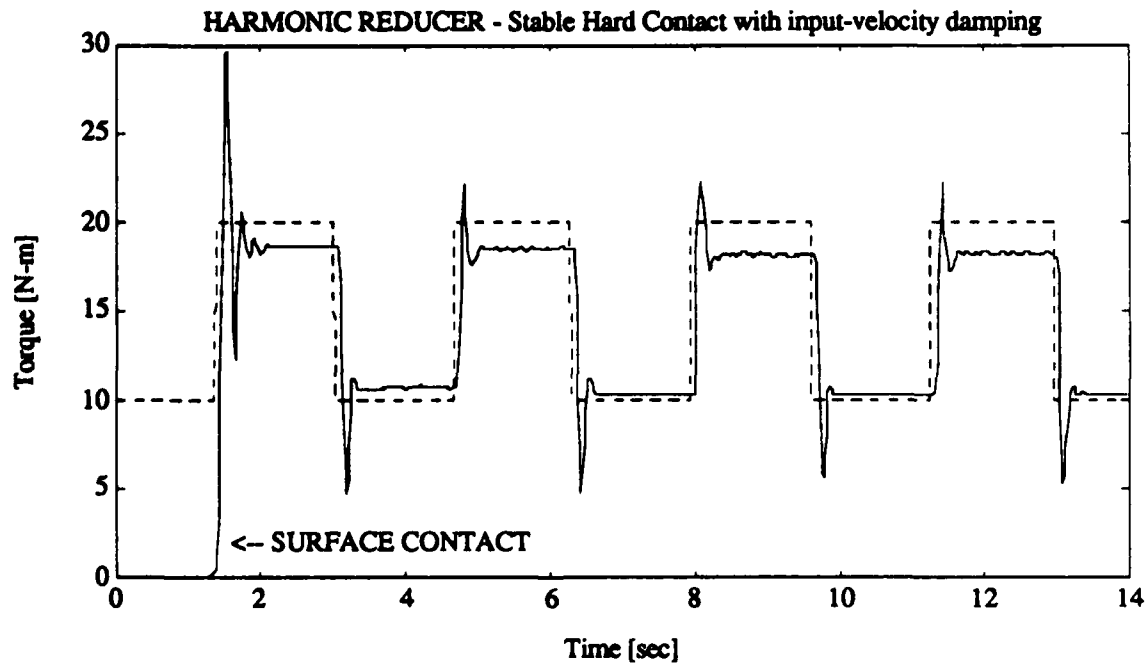


Figure 5.25: Response to Square Wave Input for max. K_p gain ($K_p=0.95$) with input-velocity damping with acquisition of surface contact for the HARMONIC DRIVE reducer.

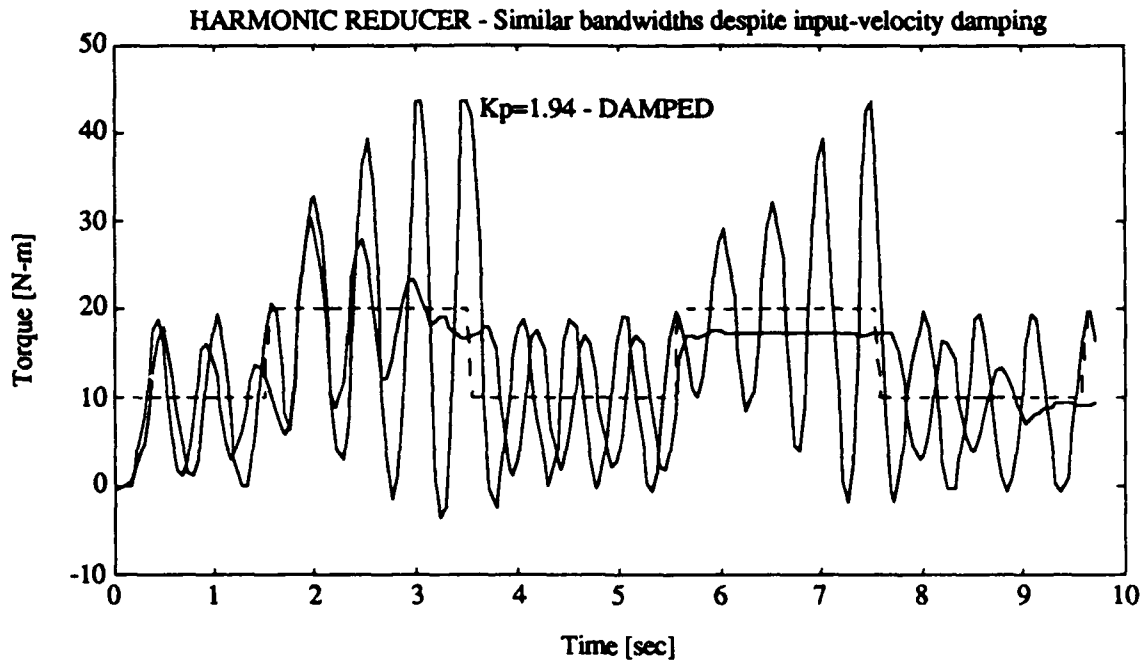


Figure 5.26: Response to Square Wave Input for max. K_p gain ($K_p=0.95$) without damping, and ($K_p=1.94$) with input-velocity damping illustrating similar bandwidths for the HARMONIC DRIVE reducer.

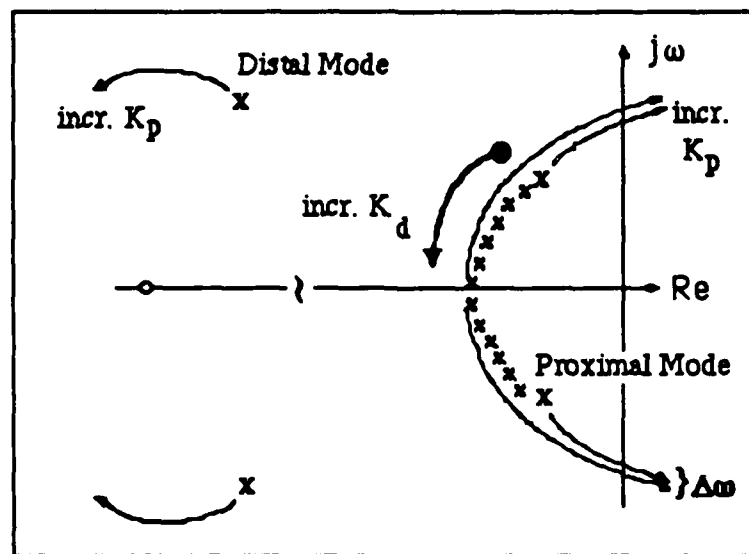


Figure 5.27: Root-Locus for Input-Velocity damping, illustrating the increase in performance due to increased damping of the proximal mode (with increasing K_d), and the negligible change in bandwidth ($\Delta\omega$) at the edge of the stability margin.

We have so far only shown data for the harmonic drive reducer, since the above trends were not measured in the case of the cable reducer. Shown in Figure 5.28, are the closed-loop responses for purely proportional gain $K_p=1.3$ ($K_d=0$), and with added input-velocity damping. It is clear that the effect of damping is not as drastic as expected. The selected value for the electronic viscous damping coefficient was limited by the fact that the input velocities were much smaller than for the harmonic drive due to the larger stiffness of the cable reducer, resulting in much smaller damping torques which were highly dominated by velocity-sensor resolution and torque resolution. This fact alone accounts for the seemingly poor increase in performance. The value for the added viscous damping coefficient had to be kept below a certain value, due to the resolution/noise levels of the velocity sensor. Any higher gains resulted in a violent high-frequency low-amplitude oscillation of the motor-shaft and the entire transmission.

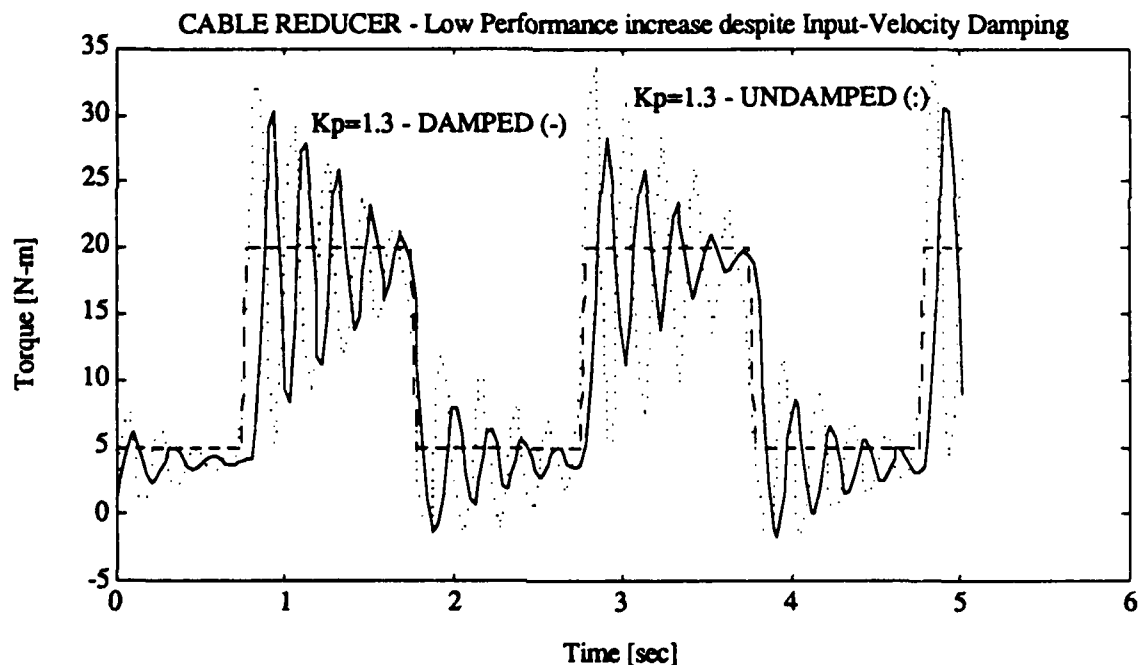


Figure 5.28: Lack of performance increase with added Input-Velocity damping due to sensor-hardware limitations (resolution) in the case of the WHOI cable reducer.

The type of motor that we used (*Sensorimotor*) has a medium resolution velocity sensor based on mutual inductance of sensor windings in the armature. It is of better quality than a hall-effect sensor, yet not as desirable as a separate resolver which is attached to the motor shaft and can have a much higher pole-count than the motor-stator itself. This

fact places a hard upper limit on the implementation of large viscous-damping behaviors for such systems. Resolution and noise-levels in the sensor (and actuator) played a big role in determining the maximum achievable viscous-damping behavior that was possible with the cable reducer.

Thus despite the fact that the harmonic drive's performance could be increased by adding electronic damping, the clear difference in system performance is still apparent in the bandwidth that both systems can achieve. Adding extra damping did allow one to increase proportional gain levels, but had almost no effect on increasing system bandwidths. The cable reducer, hampered by hardware constraints, would thus still be a suitable choice for higher frequency tasks, even with reduced levels of proportional gain, necessary to achieve a certain performance. A better velocity sensor arrangement would most certainly cure this limitation, but due to the environment this transmission has to operate in (mineral oil at up to 600 atm), the most obvious solutions are not trivial to implement.

Pa - Torque/Low-Pass Controller:

Many successful torque control applications have used the advantages that low-pass filtering can deliver for a non-rigid transmission link. It is generally known, that introducing a first-order lag filter into the feedforward path of a rigid-body system under torque control, will result in an unstable system (see Eppinger, 1988). On the other hand, the introduction of a first-order lag into a system with finite stiffness, has a completely different effect.

If we inspect the plots of Figure 5.29, we can see that for the cable reducer, a proportional gain value of $K_p=1.3$, which used to be an unstable gain, can result in a stable behavior, as long as the value of the filter constant is chosen to be smaller than $a=100$ rad/sec. The top plot is shown for a value of $a=20$ rad/sec. A similar plot can be generated for a pure PI controller, that used to be right at the edge of the stability region. The values of $K_p=1.0$ and $K_i=5.0$, would normally result in an oscillatory system which can again be controlled with a low-pass filter to remain stable and with a more damped response ($a=95$ rad/sec). The settling-time or 'bandwidth' is of course now reduced, which is the cost of increasing the stability margin of such a torque-controlled system. The increase in settling-time is clearly dominated by the first-order dynamics. The extent to which the first-order time-constant affects the 'bandwidth' of the system can be seen by observing the difference in settling-times between the two plots of Figure 5.29, where values of $a=20$ rad/sec and $a=95$ rad/sec were used.

As shown in Figure 5.30, the addition of such a first-order filter into the feedforward path of a pure PD torque-controller or a P-torque & D-input velocity controller, has a predictable effect on the stability margin of the system. If we decrease the value of the time-constant of the filter ('a' goes to Inf.), the effect of the lag filter will become more and more negligible, until the response asymptotically approaches that of the pure PD-controller. Yet for a certain gain K_p , which may otherwise be unstable, a value of 'a' can be found that will stabilize the system. The performance will suffer, since the dominant dynamics will be those of the first-order filter, but at least the system will be stable. Such a behavior makes it clear that one can tune such a system in order to obtain stability. The meaning of such behavior in the root-locus sense, can be found in the different graduations of the root locus. This change in locus-graduation implies that for smaller and smaller values of 'a', the proportional gain can be gradually increased before instability sets in.

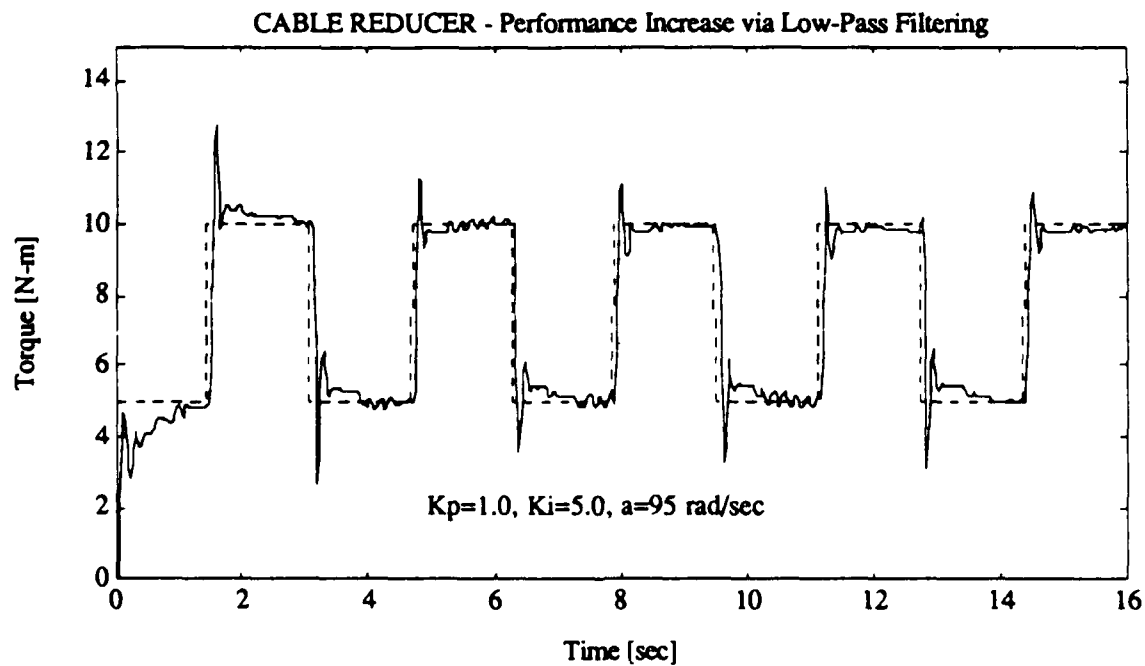
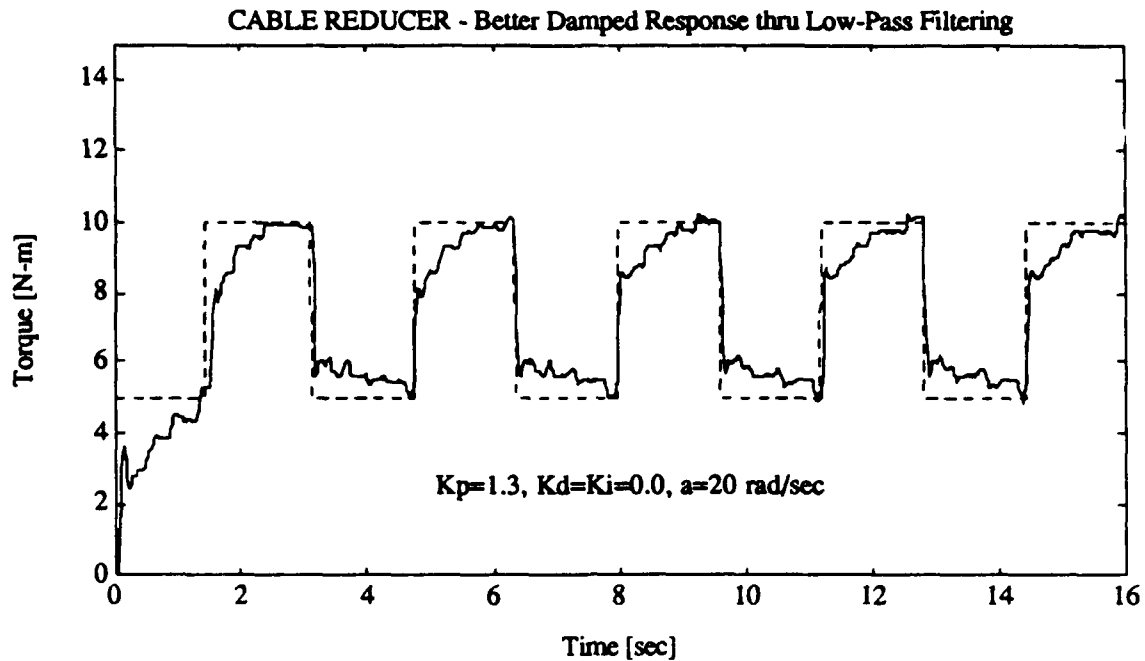


Figure 5.29: Time Responses to a Square Wave Input in desired output torque for (i) a purely proportional controller ($K_p=1.3$) with low-pass filtering ($a=20 \text{ rad/sec}$), and (ii) a PI-controller ($K_p=1.0, K_i=5.0$) with low-pass filtering ($a=95 \text{ rad/sec}$) implemented on the WHOI cable reducer.

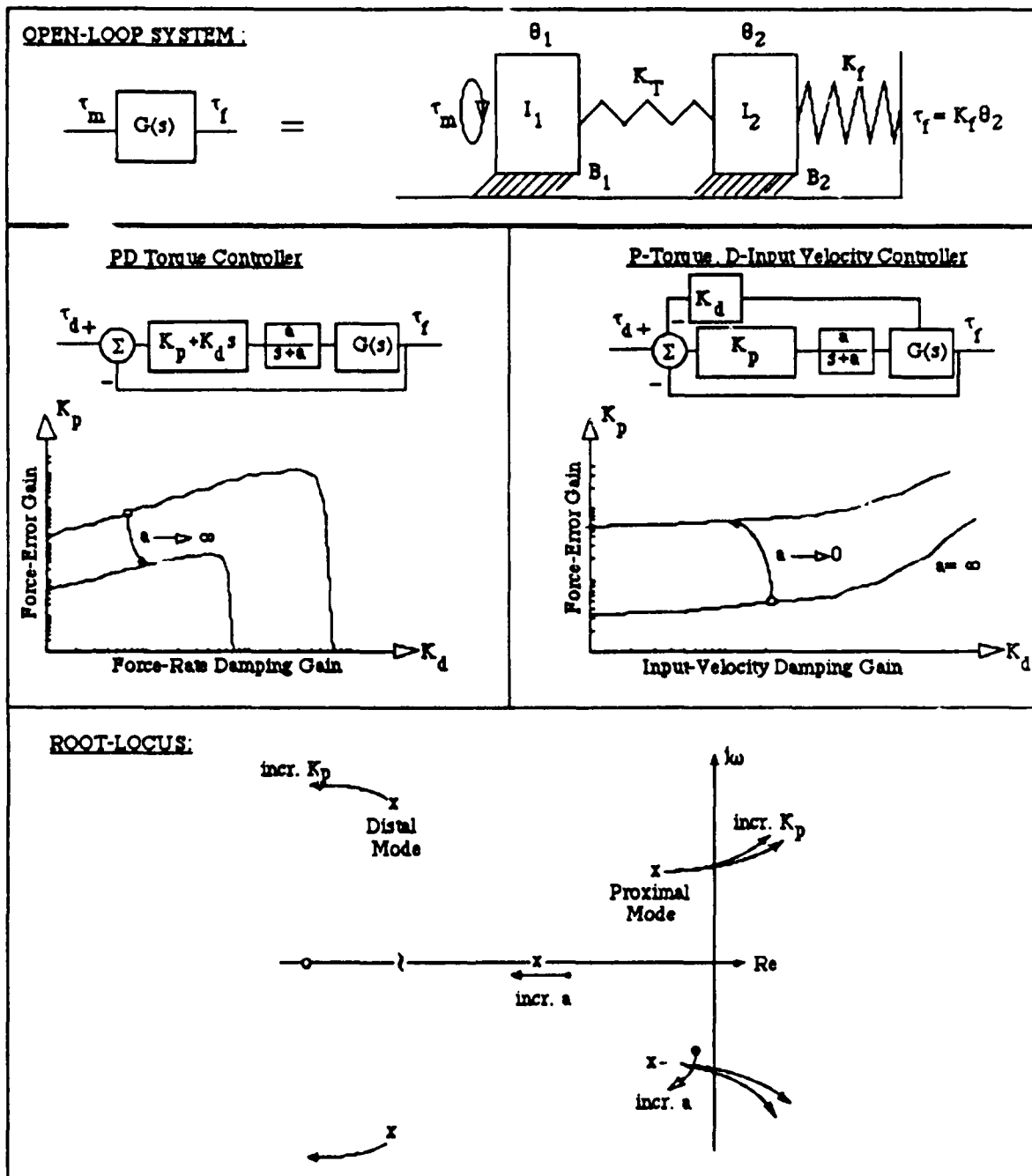


Figure 5.30: Block Diagram of a First-order Lag Filter introduced into the feedforward path of a single-compliance transmission model in hard surface contact, together with PD torque controller and P-Torque & D-Input Velocity Controller Stability Margins.

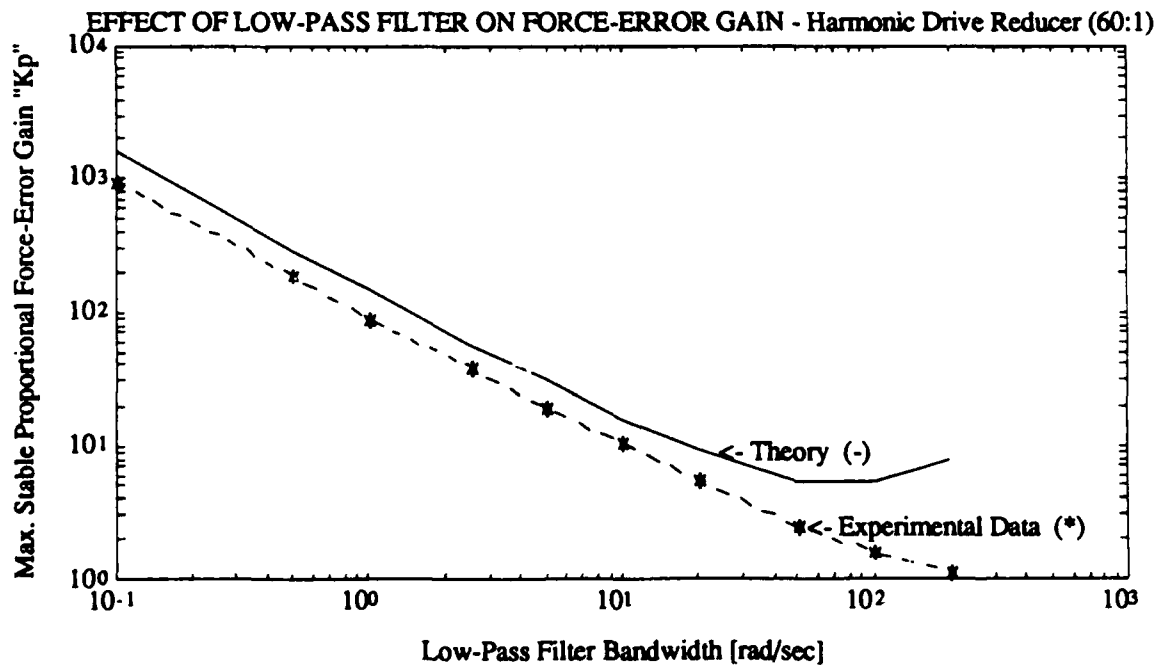
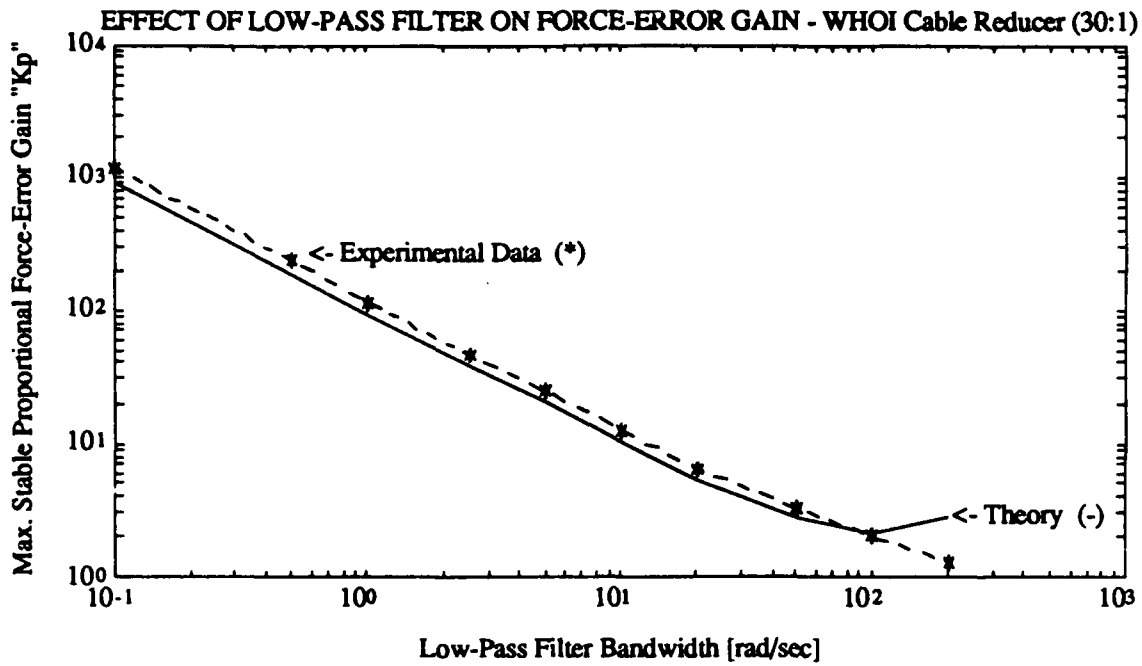


Figure 5.31: Proportional Gains K_p at the edge of the Stability Margin vs. the first-order filter constant 'a', for the WHOI cable reducer and the HARMONIC DRIVE reducer.

The increase in proportional gain as a function of filter constant 'a', is shown in Figure 5.31. We have plotted the theoretically predicted values of K_p at instability (vs. 'a') as well as the experimentally measured values, for the WHOI cable reducer and the HARMONIC DRIVE reducer. Notice that the trends are identical, with an actual error of around 10 to 15%. Another interesting aspect worth mentioning, is that the frequency at the edge of the stability margin is always less than if no first-order filter was used. The difference overall is not very drastic, but it points out that filtering will allow increased proportional gains K_p (and thus decrease steady-state error) as well as reducing oscillatory behavior for a wide range of K_p , but in no way can the bandwidth of the system be increased. The upper limit of the bandwidth will always be that of the unfiltered closed-loop system.

PI - Torque Controller:

In pure torque control, a very common control method to reduce steady-state errors, is to employ an integral control term in the control algorithm, as shown in Eqn. 5.3:

$$\tau_m = K_p(\tau_d - \tau_f) + K_i \int (\tau_d - \tau_f) dt \quad (\text{Eqn. 5.3})$$

The introduction of an integral controller term increases the oscillatory behavior of the system in the transient phase, and can result in limit-cycle behavior, whose severity depends on the value of the gain K_i and the relative size of stiction and coulomb friction in the drive. This type of experiment is thus very useful in illustrating the relative effects of stiction/friction in the different transmissions being studied. As we have discovered from earlier experiments, the most challenging task is that of a low-frequency sinusoidal torque signal to be followed. We have run the test with a 2 rad/sec (0.32 Hz) sinusoid with 5 to 10N-m amplitude for the 30:1 reducers, and 10 to 20 N-m for the 60:1 reducer.

The control gains were selected in order to make this comparison meaningful. The proportional gain K_p for each reducer was tuned so as to achieve a 0.7 damping ratio (remember that most drives have about a 0.8 to 0.9 open-loop damping ratio), and then K_i was increased until step responses yielded at worst a 0.5 damping ratio. Since the attempt here is not to illustrate system bandwidth with a tuned controller, but the effects of stiction and friction on a low-frequency torque signal, such a choice of common desired performance amongst transmissions, represents a meaningful experimental setup.

The response for the HARMONIC DRIVE and WHOI cable reducers are both shown in one plot - Figure 5.32. Remember that we had measured larger values of stiction and friction for the harmonic drive, which when coupled to this type of controller, should result in offsets, as well as accentuating the stick-slip behaviors of this drive. Notice the enlarged spikes at large amplitude and the step-wise transition between minimum and maximum amplitude, which are behaviors that were present in the open-loop experiment, but are now accentuated with this controller. The WHOI cable reducer also experiences stick-slip, but the relative amplitudes are much smaller due to the reduced values of stiction and friction, as well as the smaller ratio of stiction-to-coulomb friction, compared to the harmonic reducer.

The DOJEN and KAMO reducers' responses are shown in Figure 5.33. Notice the large stick-slip transitions in the ball reducer (most probably due to the interaction of the integral controller action and the ripple-torque phenomenon), and the somewhat 'calmer' response of the DOJEN cycloidal cam reducer.

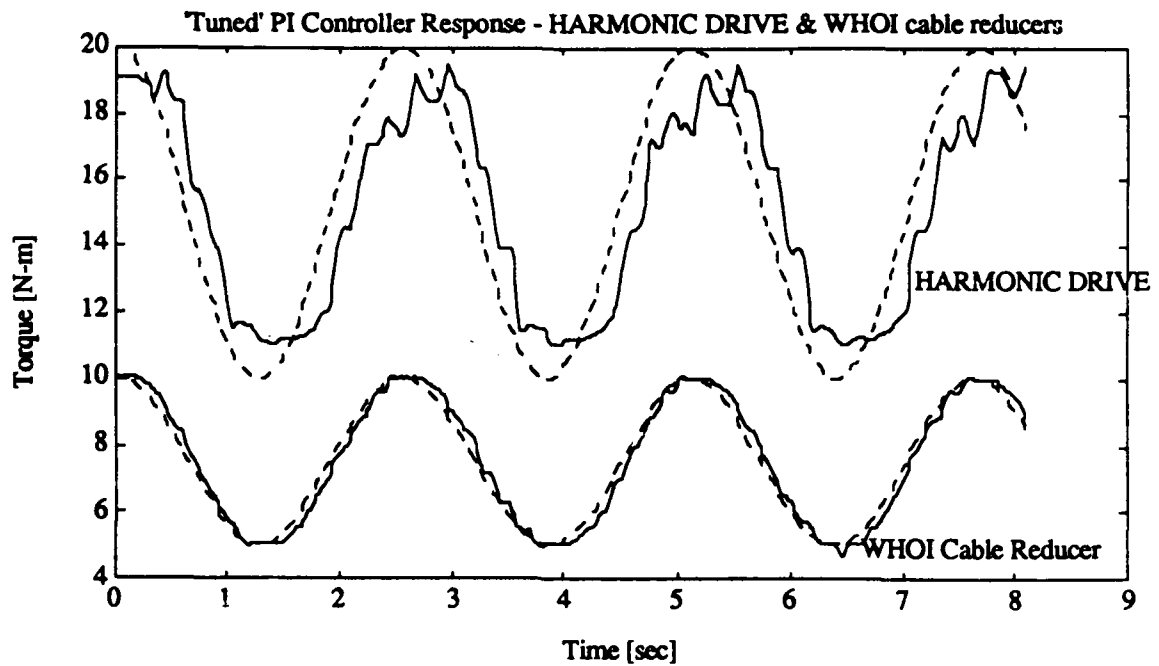


Figure 5.32: Response of WHOI cable reducer and HARMONIC DRIVE reducer to a desired sinusoidal output torque (5 to 10 and 10 to 20 N-m), both running with similarly 'tuned' PI controllers.

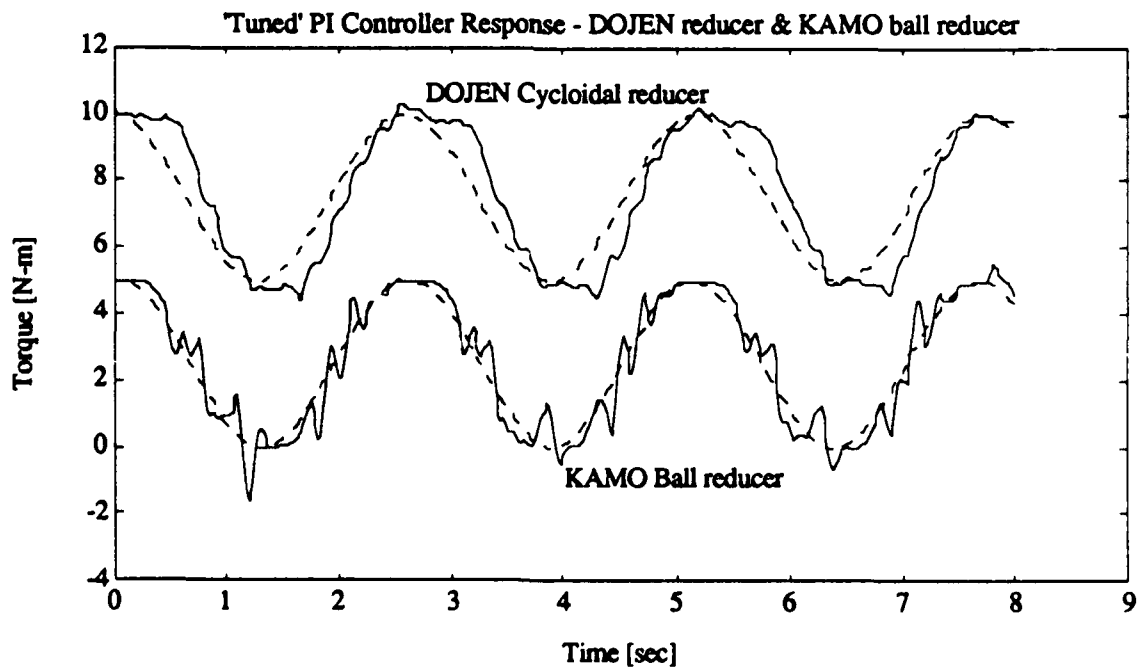


Figure 5.33: Response of DOJEN Cycloidal cam reducer and KAMO Ball reducer to a desired sinusoidal output torque (5 to 10 N-m), both running with similarly 'tuned' PI controllers - KAMO trace has been offset by -5N-m to show both traces on a single plot with similar scales.

It also experiences some stick-slip and phase offsets, yet the relative size and distribution of stiction and friction phenomena seems smaller than in the ball reducer. We would almost expect this behavior, since we had measured a ripple-torque phenomena for the ball reducer, which was highly torque dependent with a high-frequency spatial distribution. A simple cure would be to reduce the integral gain level, but it would result in larger steady-state errors and more phase lag, which would not make this a fair comparison against all the other reducers.

Another important comparison relating to the different dynamic responses, can be made by looking at the data of Figure 5.34. We have used the WHOI cable reducer and the HARMONIC DRIVE reducer to make an important statement about input-dependent stability and uniformity of response. We have used a PI controller here, whose relative gains are not crucial, since we want to make a comparison for each reducer's behavior at different torque levels. The response to the square-wave input to the cable reducer is shown to have a characteristic frequency of about 4 to 5 Hz, with a slightly underdamped response, which is very similar at the different torque levels that we command. The response to a similar input (of different frequency) by the harmonic reducer tells a different story. The PI-gains were purposefully tuned in order to illustrate that a well behaved response need not be achieved at different commanded torque levels. A controller tuned to result in good performance at the higher torque levels, can easily result in barely stable behavior at lower torques. Thus a stable controller would have to be tuned for the lower-torque end in order to remain stable at higher torques. The difference in response between the two levels is not necessarily attributed to a stiffening transmission (no real data to show stiffening in that region, nor is a difference in frequency of oscillation apparent), but rather to a higher frictional loss in the transmission (most probably coulomb losses). We know from earlier gathered data that the viscous losses do not vary much at these different torque levels, but that stiction and friction can almost double. This physical phenomenon, which has a high-frequency spatial dependency as well, could account for these markedly different responses.

Despite the fact that these systems are highly nonlinear and thus closed-loop responses will vary depending on the controller structures and their associated gains, this experiment aids in understanding the pitfalls of empirical gain tuning. Tuning gains for high amplitudes in the harmonic drive results in a desirable response, which can not be guaranteed for lower amplitude inputs. The cable reducer on the other hand exhibits similar behaviors (the gains are detuned on purpose to accentuate the response homogeneity) at different amplitudes, further accentuating the difference in the degree of nonlinearity between these two reducers.

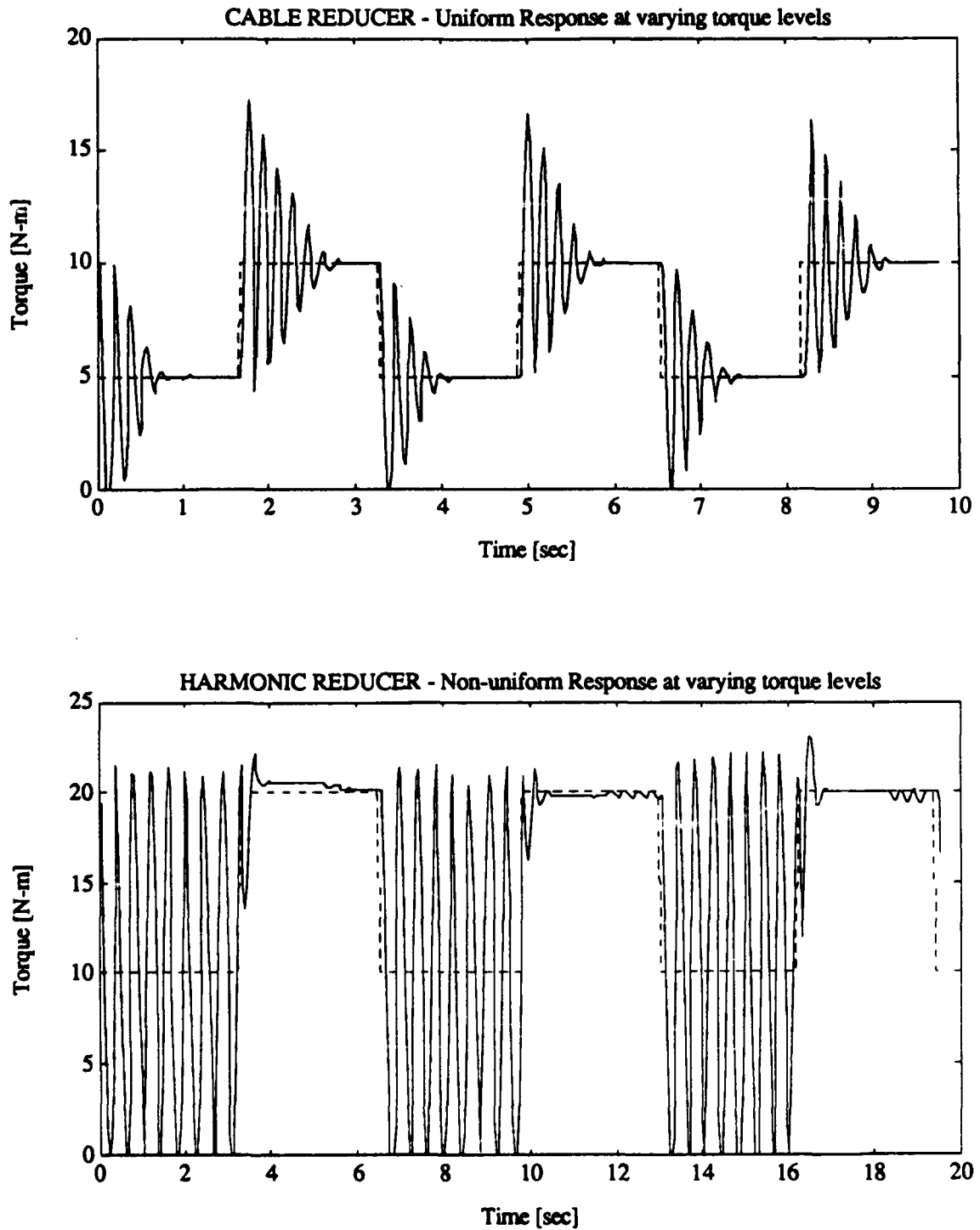


Figure 5.34: Response of WHOI Cable reducer and HARMONIC DRIVE reducer to square wave input running under PI controllers, to illustrate torque-dependent stability and performance issues.

(5.3) Summary and Conclusions

The 1 DOF task chosen for these experiments was certainly very well suited to analyzing transmission behavior since it minimized the number of variables that can affect the reliability of the measured data. The hardware setup needed to be properly tested as well, since the presence of any nonlinearities of the motor and the coupling between transmission and motor should not affect the measurement data. The torque linearity of the DC motor was shown to be well within a 1% error band, which is not enough to affect the experimental data we present here. Such linearity values are probably the best found in any commercially available DC brushless motor. The selection of the stiff coupling was also shown to have no real effect on the data gathered. Its stiffness was 1.5 to 2 orders of magnitude higher than the transmission stiffnesses we were measuring. Its dynamic effects were shown to be negligible via a simple 'manual' experiment. The importance of a proper experimental setup was very important, and the individual components needed to be shown to have little or no effect on the measured data.

The open-loop experiments revealed some very interesting results that affect transmission models. Square-wave inputs proved to be of high enough frequency content, such that coulomb and stiction values measured earlier were consistent and repeatable in the experiments run for all the reducers. They also revealed that certain reducers have torque-dependent offsets due to varying stiction/coulomb friction. The data gathered for sinusoidal inputs was even more conclusive in proving that the differences in stiction and friction are highly reducer-dependent, and that very good agreement with the static parameters measured earlier can be observed (such signals reduce the inertial under/overshoots in measured torque-readings). The selection of input amplitude was crucial for certain reducers, since only amplitudes guaranteeing break-away would result in any kind of decent signal-following. But the selection of amplitudes to result in initial break away was not the only important variable, as the reducer may settle at a torque level, where incremental torque changes do not result in much change in output torque. Hence overall signal amplitude is also important. This problem is accentuated for reducers with increasing levels of stiction and friction. The use of low-frequency sinusoidal input torques (at the same amplitudes as before), revealed the large discrepancies in performance that certain reducers experience when the reducer is constantly experiencing stick-slip behavior. The difference in performance can be shown to be related to the difference in relative stiction and friction values and their relative spatial distribution.

The attempt to use the measured static (stiction/friction) and dynamic (stiffness, inertias, viscous friction) system descriptors to simulate system responses to identical input sequences, resulted in interesting conclusions about model reliability and input signals. For input signals above a certain frequency (with square-wave inputs having ideally infinite frequency content and sinusoids above a certain frequency) and amplitude, the model response can match the experimental data very well. Any errors can readily be accounted for by variation of parameters that are well within the respective measurement 'errors', mainly for stiction and friction parameters. Yet for input signals of reduced frequency and/or amplitude, when the stick-slip behavior is constantly being excited, the experimental and simulated data show considerable disagreement. The disagreement does not manifest itself in the DC signal components (which could be accounted for by slight changes in parameter values within the measurement error), but rather in the AC signal component. Such discrepancies clearly illustrate the problems of using a fixed-parameter nonlinear lumped model to predict system response.

It became clear from the measured data, that stiction- and friction parameters were highly sensitive to transmitted loads and spatial location of reducer components. Such behavior can not be replicated with the lumped fixed-parameter nonlinear models we proposed, illustrating the inaccuracies of such lumped-parameter modeling techniques. A solution would certainly be to attempt to match a more accurate distributed- and variable-parameter stiction/friction model to the measured data. On the other hand, measuring the different distributed parameter values is less than trivial, and would require very complex measurement setups. The usefulness of such a measurement could also be questioned as to how valid such parameters are over the life-time of a transmission, as component-wear and -tear play a bigger and bigger role in the performance of a reducer. The operation of a reducer at non-zero speeds over prolonged periods of time can accentuate thermal dependencies of stiction and friction properties, due to thermal expansion of transmission components. Another argument for better models was obvious from some of the data, where evidence was clearly indicating some sort of reducer-internal energy storage and release mechanism which resulted in oscillatory output torque readings. In one instance, such oscillations could be shown to lie close to the first (predicted) oscillatory mode of the transmission. Another reducer revealed the likely presence of energy storage in the cantilever-beam arrangement of its main torque-transmitting members (cam followers in this case). Other reducers showed a very good correlation between measured torque-spikes and the location of meshing/contacting torque-transmitting elements - in this case gear-teeth. Such signals were measured to be of high-frequency spatial distribution with considerable amplitude modulation (see the HARMONIC DRIVE and REDEX reducers).

The closed-loop torque experiments revealed how system performance is ultimately linked to the open-loop transmission behavior as well as certain implementation issues. The use of PD torque/velocity-damping algorithms was shown to be very advantageous in increasing system performance by damping the oscillations of the proximal vibratory mode (the mode that results in instabilities and is the lowest-frequency resonant mode of the actuator/transmission/load/sensor arrangement). On the other hand, such an algorithm's success is tied to the relative resolution of the employed input-velocity sensors (and motor-torque resolution), as well as the relative compliance of a transmission. The stiffer the transmission, the less effective electronic input-velocity damping will be for a system with fixed-resolution sensors and actuators. High-speed contact acquisition tasks were shown to very much benefit from such damping techniques, as they reduce impact forces and damp out oscillatory tendencies.

The use of a standard PD torque controller (force error and force-rate), was shown to have severe implementation constraints, since force-rate is hard to measure without introducing excessive noise levels. Filtering was not much help as the introduced phase lag can destabilize the system even further. The dynamic model structures proposed and analyzed earlier, were shown to be quite accurate predictors of system bandwidth along the stability margin of the system (5 to 15% max. error), while the predicted gains at the stability margin could also be predicted, but not with as much accuracy (about 20% error). Using simple linear Root-Locus and Routh-Hurwitz techniques we showed that the ultimate bandwidth of such a system is governed by the characteristics of the transmission itself (inertia distribution, compliance). The use of a controller can improve performance, yet the bandwidth of the system is ultimately governed by the system's open-loop characteristics (first resonant mode termed proximal mode due to inertia distribution and transmission compliance). The implications are that the ultimate shape or trace of the root-locus can be modelled very closely, yet the graduation along the trace (closed-loop roots for a given gain) can not be predicted as accurately. This restriction does not minimize the usefulness of such an analysis, as it points out the limitations that hardware characteristics impose on ultimate system bandwidth, which no controller analyzed in this thesis can circumvent.

It is important to point out here that the use of a properly parameterized linear model can be a good predictor of bandwidths at instability over a fixed operational range for a given transmission. Since a true dynamic comparison can only be drawn between the HARMONIC DRIVE and WHOI cable reducers (due to matched input inertias), the operational range was picked as the range of mutually achievable maximum torque transmission. Such a constraint is not too restrictive, as it points out that certain reducers

may be more suited for certain kinds of tasks, than other transmissions. Thus a question as 'Which reducer is the best?' can not be answered conclusively, until we know what kinds of tasks and applications the designer/user has in mind.

Standard controller designs involving low-pass filtering in the feedforward path were also shown to have beneficial performance implications, yet the ultimate bandwidth of the unfiltered system can not be surpassed. Transients can be reduced and oscillations damped out, but in the limit as the first-order dynamics become infinitely fast, the system response approaches that of an unfiltered system. The simple rule that such an approach will extend the stability margin of a system by allowing larger gain values was also shown theoretically, by using the Routh-Hurwitz and Root-Locus arguments (different graduations of the root-locus traces for the proximal vibratory mode) - be it a proportional low-pass or a proportional-integral controller design.

The most common controller that is used to overcome the large discrepancies in open-loop torque following is a controller containing an integral term. The important point illustrated with the previous experiments, is that the addition of such an integral term to reduce steady-state errors results in performance levels that are again dependent on the open-loop response of the transmission itself. The most dramatic proof can be given by attempting to follow a low-frequency (sinusoidal) desired output-torque signal with different transmissions that are equally 'tuned'. The term 'equally tuned' is important, since we have to make a comparison based on similar experimental conditions. Tuning a proportional and integral controller to have similar damping ratios for step responses (irrespective of their natural frequencies) is a good compromise, especially if the performance that we are measuring is not based on a dynamic or bandwidth comparison. The experiments were laid out such that a low-frequency desired output torque signal (which was chosen to lie well below any of the achievable bandwidths of all transmissions) was to be followed by each transmission with its own set of PI-gains. Not only the absolute values of stiction and friction were shown to be important in the ability to follow the desired signal, but also the relative difference between stiction and friction, as well as spatial- and load dependencies of stiction and friction. This experiment illustrated that it is important for a transmission to have as constant a stiction/coulomb friction behavior with respect to time, spatial orientation and transmitted load, but that the relative magnitudes of these frictional losses observed in open-loop experiments has a direct implication on the closed-loop system performance (severity of stick-slip behavior, phase lag, etc.).

CHAPTER 6

(6) CONCLUSIONS AND SUGGESTIONS FOR FURTHER RESEARCH

(6.1) Conclusions

The experimental and theoretical analysis of robotic transmissions undertaken in this thesis has limited itself to a variety of commercially available and innovative transmission types. The use of zero backlash, highly backdriveable transmissions was a pre-condition imposed on the selection process, since we were analyzing their respective fidelity as pure torque multipliers for use in force/torque control tasks. This analysis does not cover transmissions types such as direct-drive (does not really involve a 'transmission' anyway), pneumatic and hydraulic, nor friction-drives. These transmissions represent a subset that would be worth exploring, but were beyond the scope of this thesis, due to the complexity in designing and building a prototype, and since such finished designs are not really available commercially.

The need to characterize transmission behavior by a set of models which could be described by the smallest set of descriptors, became obvious from the lack of understanding present in the current body of robotic literature. The necessity of representing a transmission with a compliant element is a well known fact, as it is one of the only ways to understand bandwidth limitations present in current applications of force/torque control. Understanding and modeling transmission behavior is important, since the dynamics introduced by the transmission into the feedforward loop of a force control loop dominate the closed-loop response (as well as open-loop) of the overall system. By understanding and measuring the basic physical processes governing such transmission performance, we can make direct conclusions as to the design of better transmissions, how to better control them, and how to predict ultimate performance beforehand.

Measuring such system descriptors as transmission compliance, stiction, coulomb friction and viscous friction, we were able to generate an extended set of comparative descriptors that can be very useful in the design and selection of an actuator system. This set of descriptors clearly extends the currently available data set available from manufacturers, and guarantees a common set of experiments which generate true comparative data. The experiments were also able to pin-point and numerically characterize certain behaviors such as torque-ripple and load-dependent efficiencies - all measurements that are not available from a manufacturer's data sheet. This approach assumed that we

could lump all the transmission behaviors into single numerical descriptors, which for a rough comparative table is very useful, but will also be shown to result in meaningful conclusions about transmission models and performance analysis and prediction.

The measurement of transmission stiffness brought to light the fact that most reducers contain so-called soft-zones, which are regions at low levels of transmitted torque where the loads are not equally shared by all the supposed load-carrying members, resulting in load-dependent zones of reduced stiffness. As the transmitted torques (loads) increase, all the load is borne equally by internal members, and the reducer experiences a stiffening response. Manufacturers mostly publish these higher values, or are very inaccurate about the compliant behavior at low loads (far and above the stiction and friction levels). On the other hand other manufacturers provide real data showing a lack of soft-zones, which was achieved by 'dimensional pre-loading' which forces all the load-carrying members into contact even at zero loads - similar to preloading meshed gear-teeth.

All manufacturers measure their reducer's transmission stiffness at the output. By locking the input and applying torque to the output and measuring output deflection, they are able to generate torque-vs.-deflection curves. The measurements taken in this analysis were all taken from the input-side, by locking the output, and applying torque to the input and measuring the input-deflections. This choice for measurement was experimentally motivated, as the available hardware made such a measurement possible. The setups required to perform the output stiffness measurement on all the tested transmissions, would have been very complicated and presents technical challenges that could represent a completely separate experimental study. The numerical values measured with the latter technique were somewhat lower than the published data, clearly illustrating that quoting a stiffness value or showing stiffness data needs to be prefaced with an explanation of how the data was gathered. The data sets that we gathered were nonetheless useful, as they revealed that for instance the cable reducer does not experience any soft-zones, and can thus be fairly well represented by a single constant transmission stiffness value. In comparison with the harmonic reducer, whose soft-zone stiffness was present over more than 20% of its load rating, the stiffness value was shown to be higher and thus represents a viable alternative to harmonic reducers over this region of torque-loads. This is an important conclusion, as it emphasizes that certain reducers may not be ultimately as stiff as others, but that the absence of soft-zones makes them better performers over a region where their own (constant) stiffness values are larger than the other reducer's soft-zone stiffness values. Thus the selection of a 'stiff' reducer has to also include a description of the type of application, since for instance cables could outperform harmonic reducers over a certain torque range.

Measurement of the more static transmission descriptors such as stiction and friction (coulomb and viscous) was also done at the output. This was accomplished by backdriving the output and measuring applied output torques, while the speed was measured at the input. This type of measurement for stiction and coulomb friction turned out to be very accurate, since a measurement of the forward-characteristics (stiction/coulomb-friction) did not reveal any real differences. Using the backwards measurement was more accurate, as we had much better torque resolution from the torque-sensor mounted at the output. Coulomb friction was shown to also depend on whether the output was being forward- or backdriven. The degree of variability was dependent on the type of transmission being analyzed. Measurement of the viscous damping coefficient was also more reliable if performed at the output, due to torque-resolution and the absence of speed-dependent torque inputs (represented by the speed-torque curve of any motor).

The experimental data clearly illustrates the differences in backdriveability for each reducer. Not only the absolute values for stiction and coulomb friction were important, but also the relative values for the ratio of stiction-to-coulomb friction. This ratio was shown to be an important indicator of system performance, since stick-slip behavior is related to the relative amount of stiction and coulomb losses present in a reducer. Any input-torque sequence (open-loop or closed-loop), which induces the stick-slip behavior, clearly illustrates the performance differences between the different reducers. Real transmission efficiencies can also be deduced from the measurement of the viscous losses in the transmission. The measured values indicate that the reducers are not quite as efficient as the optimistic data published by the respective manufacturers. Notice further, that we replaced any highly viscous lubricants in tested units, with a common low-viscosity mineral oil in order to get an objective efficiency comparison. Such changes in lubrication were well within the allowed specs recommended by the manufacturer, and improved the overall characteristics of a transmission. Many times the replacement of a certain lubricant had a large effect on not only the efficiency, but also the stiction and coulomb-friction characteristics of the reducer. In one instance, the heavy grease-packing (together with shaft- and bearing-seals) in a cycloidal reducer from SUMITOMO, actually masked the presence of a large backlash-zone (10 degrees at the input). The stability and performance guarantees drastically changed once the lubricant was exchanged for a lower viscosity one. The effects of seals (shaft- or bearing-) was mostly obvious in the WHOI cable reducer, since it incorporates a shaft-seal to contain pressure-compensation oil. The stiction and coulomb-friction introduced by the seal accounted for 50% of the reducer's frictional losses, while the rest were mostly due to rolling losses in the loaded bearings (due to radial loads from pretensioning of the cabled stages).

Since we wanted to use these measured parameters to determine how well we could model transmission performance, we needed to evaluate the fidelity between experimental data and theoretically predicted data, performance and stability. Based on previous papers and theses, we were aware that a finite-compliance transmission can result in unstable force control behavior with most of the standard controllers used to date. Given the measured parameters for system inertias, compliance and viscous damping coefficients, one can assemble a simple linear model in order to try to analyze the performance and stability of the closed-loop system. This approach makes it possible to analyze the effects of most of the more common linear torque-control algorithms used today. For the controller structures that we analyzed in this thesis, we were able to predict to within 5 to 15%, the closed-loop frequency at the stability margin of the system. In other words the frequency at which the root-locus crosses the $j\omega$ -axis and the system goes unstable. The ability to predict the stability margin in terms of controller gains can only be accomplished with a 20% error margin. This implies that the overall trace or shape of the root-locus is predictable, but that the graduations along the root-locus are not as accurate as one would hope for. The prediction of system bandwidth at the edge of the instability margin is nonetheless important as it highlights the limitations of many controllers in attempting to raise the bandwidth above levels imposed by the system hardware characteristics. These bandwidth and gain estimates are only valid for a certain operating range in terms of transmitted torque.

The performance and stability comparison centers mainly around the WHOI cable reducer and the HARMONIC DRIVE reducer. A comparison of their relative stiffness traces shows that up to 50 N-m of transmitted torque, both transmission compliances can be represented by different slopes of a fixed value. This comparison is based on the operational range of the cable reducer, which is meant to illustrate that certain reducers can outperform others in certain operational regimes for which they were designed. The difference in transmission stiffness is mirrored in the frequency content of the closed-loop system response. By matching respective input inertias, and observing a factor of 2 difference in reducer compliance, the overall difference in bandwidth was measured (and predicted) to be about a factor of 1.5 to 2. The WHOI cable reducer achieved a closed-loop torque-control bandwidth of 4 to 5 Hz, while the HARMONIC DRIVE reducer approached levels of 2 to 3 Hz.

The controllers that we analyzed were all linear and included a PD-controller (proportional in torque-error with input velocity damping, and proportional in torque-error and torque-rate), a Pa-controller (proportional in torque-error with low-pass filtering), and a PI-controller (proportional and integral in torque-error). Using root-locus and Routh-

Hurwitz analyses, we were able to show that any of these controllers were only able to improve system performance in terms of settling-time, damped response and steady-state errors, but in no way were they able to extend the system bandwidth significantly over the open-loop characteristics of the transmission itself. In the case of the pure PD torque-controller, the addition of torque-rate damping increases the phase margin of the closed-loop system, yet the response becomes less and less damped, eventually resulting in system instability. Experimentally this theoretical prediction was hard to measure (except for the gains and bandwidths at 'zero' damping gain). The problem was due to the determination of force-rate itself, without introducing excessive noise levels nor phase-lag. Both of these criteria could only be met for small levels of force-rate damping. Larger gain values magnified the noise-levels in the digitally differentiated force measurements. Filtering the force-rate measurements only worsened the situation, as the introduced phase-lag accelerated the onset of system instability.

The switch to a proportional torque-error controller with added input-velocity damping was successful in damping out the highly oscillatory proximal vibrational mode for a fixed proportional gain. The system was thus 'stabilizable', yet the frequency content remained unchanged. Increasing the proportional gain for a fixed damping gain resulted in unstable behavior at nearly the same frequency, as in a system where no damping is used. This behavior could also be explained via Root-Locus and Routh-Hurwitz arguments. It was interesting to note that the success of this technique was highly dependent on transmission- and other hardware characteristics. Applying this technique to the cable reducer had limited success, as the stiffness was much higher than for the harmonic reducer. The relative difference in input-velocities was large enough, that the resolution of the velocity sensor (built into the motor) as well as the motor's torque resolution were unable to accurately deliver the desired torque damping. Increasing the electronic damping coefficient worsened the situation as it amplified the sensor noise and discretization levels, resulting in high frequency oscillations of the motor-shaft. Such implementation issues are important to consider as they have an effect on how well we can control the performance of a given transmission system. Especially if we want to build stiffer transmissions, damping techniques will be governed more and more by sensor and motor characteristics.

Low-pass filtering the torque commands to the motor, the input to the filter being from a purely proportional controller, again resulted in performance increases by reducing overly oscillatory behavior. Ultimately though, the maximum bandwidth that could be achieved was limited by a system with a purely proportional controller, which is itself limited by the open-loop characteristics of the transmission itself. The larger the low-pass filter time-constant, the smaller the oscillatory behavior, the larger the stability margin and

the smaller the achievable system bandwidth. Increasing the proportional gain for a given filter-constant resulted in a response with comparable bandwidths as in a scenario without any filtering at all. These experimental results are completely consistent with the predicted behaviors determined with simple linear analysis/modeling techniques.

The use of a PI controller was very helpful in illustrating the performance difference between different reducers for low-frequency and -amplitude desired torque levels. This controller was not used to obtain a comparative bandwidth measure, but rather a steady-state response comparison. Since it is well known that such a controller structure continuously excites the stick-slip behavior causing limit-cycling, the absolute and relative values of stiction and coulomb friction clearly affected the fidelity with which the measured output torque signal followed the desired torque signal. The experimentally proven conclusion is that a reducer with low absolute friction levels, and a small ratio of stiction-to-coulomb friction, will have the least oscillatory and stick-slip behavior and thus the highest command following fidelity of all reducers, given a comparable set of controller gains. The gains for the separate transmissions were selected so as to achieve equal damping ratios to step inputs. The proportional gain was tuned to $\zeta=0.7$, with added integral gain to reduce ζ to no less than $\zeta=0.5$. Such a convention for the selection of controller gains represents a fair experimental comparison for all the reducers, despite the fact that input-inertias were quite different.

The use of a PI controller structure was thus helpful in pointing out performance differences related to the lumped-parameter values of stiction and coulomb friction, determined in earlier experiments. The attempt to use these lumped, static, system descriptors in a nonlinear model to simulate responses to input sequences and then compare them to the actual measured data, resulted in some interesting conclusions. In operational scenarios, where stick-slip behavior was not dominating the response, because speeds were large enough such that viscous losses were dominant, the agreement between simulated and experimental data was quite good. There were small errors which easily fell within the experimental measurement-error band, and thus validates not only the parametric reliability of the lumped descriptors, but also the model structure itself. This further substantiates the good agreement between theory and experiment for predicting stability margins and related bandwidths. The highly oscillatory behavior and its bandwidth at the edge of the stability margin focus mostly on the more dynamic aspects of the model : system damping, transmission stiffness and inertia distribution. The use of a correctly parametrized model can thus yield important information for such operational regimes. On the other hand, if we try to match simulated and experimental responses to low-frequency, low-amplitude signals, the agreement between theory and experiment begins to worsen and

deteriorates rapidly, depending on the reducer we are looking at. It was interesting to notice that the DC components of the simulated and measured data agreed quite well, but substantial disagreement was found in the AC-component. This lead to the conclusion, that for these types of input or desired torque signals (low frequency and amplitude), a lumped-parameter nonlinear model is not accurate enough in predicting system behavior. The constant excitation of stick-slip brings out the spatial- and load-dependencies of stiction and friction, exciting lowly-damped internal oscillatory modes, underscoring the inaccuracies between reality and such a simplified model structure.

Another important result worth mentioning, is that the type of open-loop torque input signal or closed-loop desired torque-signal is important in determining system performance. Using step-inputs or square-wave torque signals above certain amplitudes, would lead one to believe that transmissions are indeed systems whose behavior can be captured with a few linear and nonlinear elements. The fact that they are indeed nonlinear, and that there are different 'system structures', can be shown by reducing the amplitude and/or the frequency of the torque command. This amplitude and frequency dependency (as well as other relations such as spatial location and torque-levels), illustrates the inability of such simplified nonlinear models to fully capture the true behavior when it is governed by stiction and coulomb friction characteristics of the transmission itself. A reducer that has fairly uniform characteristics, such as directional stiction/friction- and constant stiffness-characteristics (such as the cable reducer), was shown to experience consistent and torque-amplitude independent closed-loop behavior. Such a statement becomes less accurate, when the amplitude of the signal is reduced to levels approaching the stiction/friction torques of a transmission, or when the frequency of the torque command is reduced to the point where the stiction/friction induced stick-slip behavior dominates the open- or closed-loop system behavior.

----- o -----

Many of the theoretical sections and experimental data sets in this thesis point to conclusions about the benefits that could be reaped by properly designing a transmission, which would qualify more and more as a torque multiplier and less as a strict speed reducer. Every transmission is a speed reducer, but the efficiency and stiction/friction characteristics are the main descriptors necessary to grade them as torque multipliers. It is obvious that we need as stiff a transmission as is physically possible. The first natural mode of the transmission should be well damped, so that if is not colocated at the input, it becomes harder to excite. If the transmission is built in discrete stages, each discrete

inertia/compliance stage should also be well damped, and the relative distribution of discrete stiffness stages should be arranged such that a certain ratio between successive reflected stiffnesses can be maintained. If there is a resonant mode with a low bandwidth, it should be ideally located at the motor-end, where electronic damping can be used to stabilize the system. Such a scheme of stabilizing the lowest resonant mode (proximal mode) at the input-end, will only be successful if sensors and motors with appropriate resolution and low noise levels (measurement-noise and torque-ripple) are used. The proper selection of a lubricant can have a large impact on system damping and the levels of static system descriptors (stiction, coulomb friction) as well as viscous losses. The presence of backlash and its impact on stability margins can also be affected by the proper selection and placement of highly viscous lubricants. Reducing the absolute and relative values of reducer-internal stiction and coulomb friction is crucial in determining open- and closed-loop system performance. Thus stiffening a transmission by 'dimensional preloading', is not a desirable alternative, as it amplifies such static (and dynamic) losses, and also accentuates the presence of assembly-errors and errors in machining and component tolerancing. The increased spatial- and load-dependency of such parameters reduces performance within the stiction-band, which is now larger than if other methods than preloading were used.

Continuous load-distribution is important and is best accomplished by elements in constant rolling contact. Some arrangements for continuous rolling contact suffer more from increased contact stresses at increased loads than do others. The effects are visible through increased ripple torque and load-dependent frictional characteristics. For all reducers, except the cable reducer, the transmission characteristics dominated the motor-induced nonlinearities (ripple). The dominant frictional characteristics could mostly be traced to positional dependencies of transmission components (rollers, teeth, cam-lobes, etc.). Dimensional preloading was shown to introduce severe frictional nonlinearities, further accentuating tolerances in machining and errors in assembly for individual load-bearing transmission components.

The selection of input-parameters such as inertia, have a drastic effect on shaping the response of the proximal mode, since the dominant resonant (proximal) mode depends not only on transmission stiffness, but also inertia distribution. It was shown that a low value for input inertia is desirable, as it increases the open-loop bandwidth of the dominant vibratory system resonance. For hard contact tasks, stability and performance could be shown to be much less dependent on values for output inertia. Depending on the controller structure used, a minimum in system stability and performance could be theoretically predicted for the case of matched input and output inertias ($I_1 = I_2/N^2$).

The distribution of stiction and coulomb friction within a reducer is a physical phenomenon worth understanding. If we have the freedom to place such devices as shaft- or bearing seals, locating them at the 'high-speed' end (namely the input) would seem best, since non-zero speeds reduce the effects of stiction. But if on the other hand, a reducer is stiff enough or the task slow enough, that non-zero speeds are less common at the input, the seals should best be placed at the output stage. Furthermore, such seal-friction would increase the deadband of the motor-torque, which is much reduced if placed at the output. The effects of input-stiction reflected to the output is also worse than a fixed value of stiction present at the output, due to the fixed value for seal friction, and the transmission ratio N being much bigger than unity.

(6.2) Suggestions for further research

It seems useful to be able to understand, and conclusively measure, the difference in transmission stiffnesses that are obtained in a forward-stiffness (locking the output and torquing at the input-end while measuring input deflections) measurement vs. a backwards- or output-stiffness measurement (locking the input and torquing at the output side while measuring output deflections), which is the common measurement mode for most manufacturers. The latter yields larger stiffness values than the former. Such effects are important to understand, as they could be used to account for further aspects of nonlinear closed-loop transmission behavior. Setting up a directionally dependent stiffness model would be quite a challenge but may yield an added nonlinear behavior of importance in understanding performance and stability properties of torque control tasks. Further study is needed in proposing better models for the discrete distribution, spatial dependency and load-modulated presence of stiction and transmission stiffness. We were able to measure the presence of ripple torque which had a high correlation to the spatial position of a reducer's components (input shaft for example), but the quantitative study requires a more sophisticated experimental setup.

The implication on system stability for coulomb variability in forward- vs. backdriven task scenarios needs to be explored. We have seen for different reducers that (mainly) coulomb losses depend on whether the output is backdriven against an opposing torque (supplied by the motor), or whether the output is forward driven by the motor against a certain resisting output torque. This phenomenon can maybe be shown to introduce a further level of nonlinearity into the stability analysis of real actuator systems. It may also be helpful in improving model fidelity and thus improve any type of

compensation scheme. The fact that this behavior is transmission dependent would make it a fairly empirical and limited study, but would not take away from its importance.

The study of transmission-specific zero-velocity stick-slip behaviors was found to be the most challenging aspect of characterizing a transmission. Such behavior needs to be characterized especially for different types of rolling contacts (gear heads, spheres under 4-point contact, cables wrapped on bearing-supported drums, etc.). Such experiments should be performed under different loads (applied torques) and at different speeds. The experimental setup required for an objective comparison would be quite involved, yet not impossible. The functional relationship to wear-and-tear of a transmission's components would be hard to predict yet easier to measure (if time permits). Modelling the low-amplitude low-frequency response of transmissions, in the absence of any transmission-internal sensors, could certainly result in better open- and closed-loop control. Getting a more realistic representation of the discrete nature of stiction distribution would be a first step. The extent to which model details would be necessary, depends on the type of reducer and task accuracy required.

The extension of this 1 DOF analysis into multiple DOFs is an important yet far from trivial area of study. Such a step, similar to the better understanding of the discrete distribution of stiction and oscillatory modes, requires that the response of individual elements (robot joints for instance) in a system be well characterized. If we can reasonably well approximate such behaviors with simple enough models, we should be able to better compensate for nonlinearities that reduce system performance or stability margins in more complex systems.

In the absence of proper sensors and lack of actuators, we may benefit from an electronically controllable (or fixed parameter) passive damping element. Such ideas as eddy-current dampers are a step in that direction, except that miniaturization and efficiency at low speeds would be technical hurdles that need to be overcome. The ability to damp out rotary oscillations in such a way, would be the most effective way to damp unwanted and uncontrollable oscillations.

The tasks selected for the 1 DOF setup in our experiments could be increased. Forcing continuous hard contact by locking the output to 'ground' would be a task in which the directional properties of a transmission could be tested. At the no-load point, when the transmission input torque transitions to the opposite sign, we expect more nonlinear behaviors which could cause undesirable performance and reduce stability margins. Experimental data gathered from such experiments may be useful in establishing yet another model structure which modulates parameter values (and model structure) based on the sign of the loading situation. Transitions through the region of zero load would

yield a wealth of information about the directional properties of a transmission. We know that this point is important, since we were able to measure directional dependencies in most of the reducers analyzed in this thesis.

Theoretical predictions of reduced stability margin and performance were theoretically shown to exist in systems with matched input- and output-inertias. Thus the practice of impedance matching for hard contact tasks would seem to reduce system performance and stability, which is exactly opposite to the effect shown for positioning applications (Pasch & Seering). Using the inequality of Chapter 3, and the formulation for the natural frequencies presented in the Appendix, more theoretical analyses should be performed to further explore this issue. Despite the fact that this is a purely linear analysis, it may benefit the design of a system, for those operational scenarios where linear models were shown to be fairly accurate stability and performance predictors.

CHAPTER 7**(7) APPENDICES****(7.1) Manufacturer Listing**

- (1) WHOI Cable Reducer
Woods Hole Oceanographic Institution
c/o Dr. Dana Yoerger
DSL - Blake 109
Woods Hole, MA 025434
(508) 548-1400
- (2) KAMO SEIKO Co., Ltd.
Represented by :
Carlisle Johnson Inc.
c/o Don Kenneth\
52 Main St.
Manchester, CT 06040
(203) 643-1531
- (?) REDEX Corbac
Represented by:
Andantex Inc.
c/o Bob Van Nostrand
1705 Valley Road, Wanamassa
Ocean Township, NJ 07712
(201) 493-2812
- (4) DOJEN Lenze
c/o Eric Stucker
4c Henshaw St.
Woburn, MA 01801
(617) 935-6835
- (5) HARMONIC DRIVE
c/o Mark Gould
51 Armory St.
Wakefield, MA 01880
(617) 245-7802
- (6) SUMITOMO
Dealer Rep. : DELTA ELECTRIC, c/o Jim Rapoza (508) 997-0582
Factory Rep.: c/o Page Cohen (603) 934-3301
Factory Inquiry Dept. : (800) 541-5830 or (804) 485-3355

OTHER TRANSMISSION MANUFACTURERS OF INTEREST

(7) TELJIN SEIKI

Represented by:

NIMAC America
c/o Mr. T. Kita
500 Marathon Pkway N.W.
Arbor Business Park
Lawrenceville, GA 30246
(404) 339-3510

(8) TRANSMISSION RESEARCH Inc. - NASTECH Inc., Division

c/o Bill Anderson
Cleveland, OH
(216) 231-1391

(7.2) Natural System Resonance

For the system depicted in Figure 7.1, we can determine the open-loop resonant modes for the uncontrolled transmission-load-sensor system.

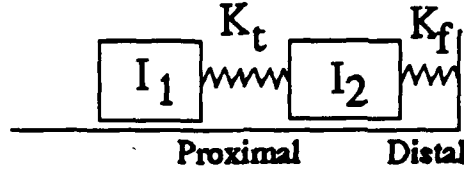


Figure 7.1 : Open-Loop Transmission-Load-Sensor System.

Using the principles of conservative systems, we can express the energy content of this system at all times, to be equal to :

$$E = \frac{1}{2} \dot{x}^T \underline{M} \dot{x} + \frac{1}{2} x^T \underline{K} x \quad (\text{Eqn. 7.1})$$

The values for the inertia and stiffness tensors can be shown to be:

$$\underline{M} = \begin{bmatrix} I_1 & 0 \\ 0 & I_2 \end{bmatrix}, \quad \text{and} \quad \underline{K} = \begin{bmatrix} K_t & -K_t \\ -K_t & K_t + K_f \end{bmatrix} \quad (\text{Eqn. 7.2})$$

This simplification then allows us to determine the resonant modes as the solution to:

$$|\underline{M}\omega^2 - \underline{K}| = 0 \quad (\text{Eqn. 7.3})$$

The roots of the determinant of $|\underline{M}\omega^2 - \underline{K}|$, can then easily be shown to be:

$$\omega_{1,2} = \sqrt{\frac{K_t(I_1 + I_2) + K_f I_1}{2I_1 I_2}} \left\{ 1 \pm \sqrt{1 - \frac{4K_t K_f I_1 I_2}{[K_t(I_1 + I_2) + K_f I_1]^2}} \right\} \quad (\text{Eqn. 7.4})$$

This solution differs from the resonant mode of an unconstrained dynamic system, which can easily be shown to be (by setting K_f equal to zero),

$$\omega = \sqrt{K_t \frac{I_1 + I_2}{I_1 I_2}} \quad (\text{Eqn. 7.5})$$

which is a result used by Asada & Lim (1985) to motivate the location of their torque sensor in the strain-gauge torque-servo design for their direct-drive robot (where I_1 represented the motor inertia, and I_2 the link- and load inertias downstream of the compliant strain-gauge sensor arrangement).

(7.3) Experimental Setup - Tolerances and Alignment

The experimental test stand was carefully designed to minimize alignment problems between the different transmissions mounted to the assembly. Here we briefly explain the sources of machining and assembly tolerances, and generate a list of numerical values which represent the cumulative radial and angular misalignments present in the test stand.

The motor and rotor-shaft assembly was carefully arranged and the runout and misalignment measured. This assembly was never touched again during any of the experiments we performed. The output-end of the shaft was coupled to a steel bellows coupling, which itself introduced additional radial misalignment. The total distance spanned between the output of the motor shaft, and the input to the transmission, represents a worst-case parallel (radial) misalignment, which was kept to minimum.

The flanges or face plates for each transmission were fit into milled slots which had a negligible degree of angular misalignment with respect to the motor flanges. The radial misalignment was minimized by carefully bored bolt holes which had a known amount of misalignment. The concentricity and alignment of the different transmission housings on their respective flanges introduced an additional amount of misalignment, which was also known a priori. The assumption that there is a negligible degree of misalignment between the housings of the transmissions and their input shafts, was supported by the tolerances quoted by every single manufacturer.

Below is a list of sources and degrees of radial (parallel) and angular misalignments present between the motor and the input to each transmission. The cumulative values represent the required specifications for the 'stiff' bellows coupling required between motor and transmission.

Location <u> </u>	Radial Misalignment <u>in 1/1000th of an inch</u>	Angular Misalignment <u>in degrees</u>
Motor Shaft Output	0.45	0.01
Coupling Bellows Output	0.05	0.05
Transmission Input	0.50	0.01
Transmission Adapter	1.00	0.05
	-----	-----
Cumulative Tolerances & Alignment Specs	2.05	0.12

CHAPTER 8

(8) THESIS BIBLIOGRAPHY

- Abelow, A.V., "Dynamic Equation Set for a simplified simulation of the Space Shuttle Remote Manipulator System", Charles Stark Draper Laboratory Technical Report, no. R-258, 1980
- An, C.H., Hollerbach, J.M., "Dynamic Stability Issues in Force Control of Manipulators", IEEE Proc of 1987 Conf. on Robotics and Automation, April 1987
- An, C.H., Hollerbach, J.M., "Kinematic Stability Issues in Force Control of Manipulators", IEEE Proc of 1987 Conf. on Robotics and Automation, April 1987
- An, C.H., Atkeson, C.G., Hollerbach, J.M., "Estimation of Internal Parameters of Rigid Body Links of Manipulators", AI-Lab. Memo, MIT 887, Feb. 1986
- Andeen, G.B., Kornbluh, R., "Design of Compliance in Robotics", IEEE Proc of 1988 Conf. on Robotics and Automation, v.1, pp.276-281
- Anderson, R.J., Spong, M.W., "Hybrid Impedance Control of Robotic Manipulators", IEEE Proc of 1987 Conf. on Robotics and Automation, April 1987
- Andrews, J.R., "Impedance Control as a Framework for Implementing Obstacle Avoidance in a Manipulator", S.M. Thesis, Department of Mechanical Engineering, MIT Feb. 1983
- Andrews, R.J., "Doulou Systems: Design and Construction of a Manipulator and Controller for Research in Impedance Control", S.B. Thesis, Dept. of Mech. Eng., MIT, June 1981
- Andrews, J.R. & Hogan, N., "Impedance Control as a Framework for Implementing Obstacle Avoidance in a Manipulator" pp. 243-251 in: Control of Manufacturing Processes and Robotic Systems, Eds. Hardt, D.E. and Book, W.J., American Society of Mechanical Engineers, New York, 1983
- Armstrong, B.S.R., Khatib, O., Burdick, J., "The explicit dynamic model and inertial parameters of the PUMA 560", IEEE International Conference on Robotics and Automation, pp. 510-518, April 1986
- Armstrong, B.S.R., "Control of Machines with n-Linear, Low-Velocity Friction: A Dimensional Analysis", Proc of 1st Int. Symposium on Experimental Robotics, Montreal, Quebec, June 1989
- Armstrong, B.S.R., "Friction : Experimental Determination, Modelling and Compensation", IEEE Proc of 1988 Conf. on Robotics and Automation, v.3, pp.1422-1427
- Arnold, F., "Understanding and ranking motion control figures of merit", Motion control Magazine, vol.5, no.6, November/December 1989

- Asada, H., Ogawa, K., "On the Dynamic Analysis of a Manipulator and its End-Effector interacting with the Environment", IEEE Proc of 1987 Conf. on Robotics and Automation, April 1987
- Asada, H., Goldfine, N., "Optimal Compliance Design for Grinding Robot Tool Holders", Proceedings IEEE Conference on Automatic Control, 1985, pp.316-322
- Asada, H., Goldfine, N., "Process Analysis and Compliance Design for Grinding with Robot s", In Donath, M. and Leu, M. (editors), *Robotics and Manufacturing Automation* ASME Winter Annual Meeting, November 1985, vol. PED-15, pp.79-88
- Asada, H. "A Geometrical Representation of Manipulator Dynamics and its Application to Arm Design", Journal of Dyn. Syst., Meas. and Control, Sept. 1983, vol.105, pp.131-135
- Asada, H., Youcef-Toumi, K., "Analysis and Design of Semi-Direct-Drive Robot Arms", Proc. of the 1983 American Control Conference, San Francisco, pp.757-764
- Asada, H., Youcef-Toumi, K., "Analysis and Design of Semi-Direct-Drive Robot Arms", Proc. of the 1983 American Control Conference, San Francisco, pp.757-764
- Asada, H., Youcef-Toumi, K., "Development of a Direct-Drive Arm using High-Torque Brushless Motors", Proceedings of the 1st Symposium of Robotics Research, August 1983
- Asada, H., Youcef-Toumi, K., Ramires, R., "Design of MIT Direct-Drive Arm", International Symposium on Design and Synthesis, Tokyo, Japan, 1984
- Asada, H., Youcef-Toumi, K., Lim, S.K., "Joint-Torque Measurement of a Direct-Drive Arm", 23rd Conf. on Decision and Control, Las Vegas, Dec. 1984
- Asada, H., Asari, Y., "The direct teaching of tool manipulation skills via the impedance identification of human motions", Proc. IEEE Conf. on Robotics & Automation, pp.1269-1274, 1988
- Asada, H., Yang, B.H., "Skill acquisition from human experts through pattern processing of teaching data", Proc. IEEE Conf. on Robotics & Automation, pp.1302-1307, 1988
- Asada, H., Kakumoto, Y., "The dynamic RCC hand for high-speed assembly", Proc. IEEE Conf. on Robotics & Automation, pp.120-125, 1988
- Asada, H., Lim, S.K., "Design of Joint Torque Sensors and Torque Feedback Control for Direct-Drive Arms", In Donath, M. and Leu, M. (editors), *Robotics and Manufacturing Automation* ASME Winter Annual Meeting, November 1985, vol. PED-15, pp.277-284
- Asada, H., Izumi, H., "Direct teaching and automatic program generation for the hybrid control of robot manipulators", Proc. IEEE Conf. on Robotics & Automation, pp.1401-1406, 1987

- Asada, H., Ogawa, K., "On the dynamic analysis of a manipulator and its end effector interacting with the environment", Proc. IEEE Conf. on Robotics & Automation, pp.751-756, 1987
- Asada, H., West, H., "Design and analysis of braced manipulators for improved stiffness", Proc. 3rd Int. Symposium on Robotics Research, October 1985
- Atkeson, C.G., Hollerbach, J.H., "Kinematic Feature of Unrestrained Arm Movements", AI-Lab. Memo, MIT 790, July 1984
- Austin, E., Fong, C., "Teleoperated Position Control of a PUMA Robot", JPL-Lab. Memo
- Aylor, J.H., Ramey, R.L., Cook, G., "Design and application of a microprocessor PID predictor controller", IEEE Trans. Ind. Conf. Inst., Vol.27, No.3, pp.133-137, Aug. 1980
- Baillieul, J., "Kinematic Programming Alternatives for Redundant Manipulators", Proceedings of the 1985 IEEE Conf. on Automatic Control, pp.722-728
- Bejczy, A.K., "Robot Arm Dynamics and Control", Cal. Inst. of Techn., J.P.L. Memo TM33-669, Feb. 1974
- Bejczy, A.K., Salisbury Jr., J.K., "Controlling Remote Manipulators Through Kinesthetic Coupling", Computers in Mechanical Engineering, July 1983, pp.48-60
- Bejczy, A.K., Salisbury Jr., J.K., "Kinesthetic Coupling between Operator and Remote Manipulator", ASME Int. Computer Technology Conf., 1980
- Book, W.J., "Characterization of strength and stiffness constraints on manipulator control", *Theory and Practice of Robots and manipulators*, 1976
- Book, W.J., Lee, S., Sangveraphunsiri, V., "The bracing strategy for robot operation", *Theory and Practice of Robots and Manipulators*, June 1984
- Brady, M., "Artificial Intelligence and Robotics", AI-Lab. Memo, MIT 756, Feb. 1984
- Brock, D., Chiu, S., "Environment Perception of an articulated robot hand using contact sensors", In Donath, M. and Leu, M. (editors), *Robotics and Manufacturing Automation* ASME Winter Annual Meeting, November 1985, vol. PED-15, pp. 89-96
- Brooks, R., "Solving the Find-Path Problem by representing Free Space as generalized Cones", AI-Lab. Memo, MIT 674, May 1982
- Brooks, R., Lozano-Perez, T., "A Subdivision Algorithm in Configuration Space for Findpath with Rotation", AI-Lab. Memo, MIT 684, Dec 1982
- Brooks, R., "Planning Collision-Free Motions for pick and place operations", AI-Lab. Memo, MIT 725, May 1983
- Brooks, T.L., "Telerobot Response Requirements - A Position Paper on Control Response Requirements for the FTS Telerobot", STX Robotics, 400 Forbes Blvd., Lanham, MD 20706, Report No. STX/ROB/90-03, March 1990

- Book, W.J., "Recursive Lagrangian Dynamics of Flexible Manipulator Arms", International Journal of Robotics Research, 1984, vol.3, no.3, pp.87-101
- Buckley, S.J., "Planning and Teaching Compliant Motion Strategies", MIT AI-Lab. Technical Report 936, January 1987
- Cai, C., Roth, B., "On the Spatial Motion of a Rigid Body with Point Contact", IEEE Proc of 1987 Conf. on Robotics and Automation, April 1987
- Cannon, R.H., Rosenthal, D.E., "Experiments in Control of Flexible Structures with noncolocated sensors and actuators", International Journal of Robotics Research, Fall 1984, vol.3, no.3, pp. 62-75
- Cannon, R.H., Schmitz, E., "Initial experiments on the end-point control of a flexible one-link robot", AIAA Journal of Guidance and Control, September-October 1984, vol.7, no.5, pp.546-553
- Cannudas, C., Astrom, K.J., Braun, K., "Adaptive Friction Compensation in DC Motor Drives", IEEE Proc of 1986 Conf. on Robotics and Automation, v.3, pp.1556-1561
- Chang, P., "A closed-form solution for inverse Kinematics of Robot Manipulator with Redundancy", AI-Lab. Memo, MIT 854, March 1986
- Chapel, J.M., Lawrence, D.A., "Stability Analysis for Alternative Force Control Schemes as applied to Remote Space Teleoperation", 10th Annual AAS Guidance & Control Conference, Keystone Colorado, 1987
- Chiang, W.W., "Endpoint position control of a flexible manipulator with a quick wrist", Ph.D. Thesis, Dept. of Aeronautics and Astronautics, Stanford Univ., 1985
- Colgate, J.E., "The control of dynamically interacting systems", Ph.D. Thesis, Mech. Engineering Dept., MIT, 1988
- Cotter, S.L., "Nonlinear Feedback Control of Manipulator Endpoint Impedance", S.M. Thesis, Department of Mechanical Engineering, MIT, Sept. 1982
- Craig, J.J., *Introduction to Robotics : Mechanics and Control*, Addison Wesley, Reading, MA, 1986
- Cutkosky, M.R., Wright, P.K., "Position Sensing Wrists for industrial manipulators", 12th Int. Symposium on Industrial Robots, 1982
- Dahl, P.R., "Measurement of Solid Friction Parameters of Ball Bearings", Proc. of 6th Annual Symposium on Incremental Motion, Control Systems and Devices, U. of Illinois, pp.49-60
- Daniel, J.D., Krogh, B.H., Friedman, M.B., "Kinematics and Open-Loop Control of an Inertial-Based Mobile Platform", Proceedings of the 1985 IEEE Conf. on Automatic Control, pp.346-351

- DeFazio, T.L., "Feedback in Robotics for Assembly and Manufacturing", Charles Stark Draper Laboratory Technical Report, no.R-1450, 1981
- DiPietro, D., "Development of an active compliant underwater manipulator", M.S. Thesis in Mechanical Engineering, Massachusetts Institute of Technology, December 1988
- Donald, B., "Hypothesizing Channels through Free Space in solving the Find-Path problem", AI-Lab. Memo, MIT 736, June 1983
- Donald, B., "Motion Planning with six degrees of freedom", AI-Lab. Technical Report 791, May 1984
- Donald, B.R., "On Motion Planning with Six Degrees of Freedom: Solving the Intersection Problems in Configuration Space", Proceedings of the 1985 IEEE Conf. on Automatic Control, pp.536-541
- Donaldson, D.D., Leonedes, C.T., "A model reference parameter tracking technique for adaptive control systems: Part I - The principles of adaptation & Part II - Stability Analysis by the second method of Lyapunov", IEEE Trans. on Applications and Industry, Vol.82, No.68, pp.241-262, Sept. 1963
- Drake, S.H., "Using Compliance in Lieu of Sensory Feedback for Automatic Assembly", Sc. D. Thesis, Dept. of Mech. Eng., MIT, Sept. 1977
- Dubowsky, S., Des Forges, D.T., "The Application of Model Referenced adaptive control to robotic manipulators", ASME Journal of Dynamic Systems, Measurement and Control 101: 193-200, 1979
- Dubowsky, S., Zia, V., "A Virtual Manipulator Model for Space Robotic Systems", Proc. of NASA Workshop on Space Telerobotics, Jan. 20-22, 1987, JPL, CALTECH, Pasadena, CA
- Dwyer, T.A.W. III, Fadali, M.S., Ning, C., Lee, G.K.F., "Manipulator Maneuvering by Feedback Linearization with Saturating Inputs", IEEE International Conf. on Robotics and Automation, pp.947-953, March 1985
- Egeland, O., "Cartesian Control of a Hydraulic Redundant Manipulator", IEEE Proc of 1987 Conf. on Robotics and Automation, April 1987
- Eppinger, S.D., Seering, W.P., "On Dynamic Models of Robot Force Control", IEEE Proc. of 1986 Conf. on Robotics and Automation, v.1, pp.29-34 or also in MIT AI Lab Memo AIM-910
- Eppinger, S.D., Seering, W.P., "Understanding Bandwidth Limitations in Robot Force Control", IEEE Proc of 1987 Conf. on Robotics and Automation, April 1987 or also in MIT AI Lab Memo AIM-948
- Eppinger, S.D., Seering, W.P., "Modeling Robot Flexibility for Endpoint Force Control", IEEE Proc of 1988 Conf. on Robotics and Automation, April 1988 or also in MIT AI Lab Memo AIM-1946
- Eppinger, S.D., Seering, W.P., "An introduction to dynamic models for robot force control", IEEE Control Systems Magazine, vol.7, no.2, pp. 48-52, April 1987

- Fasse,E.D., "Stability Robustness of Impedance Controlled Manipulators coupled to Passive Environments", M.S. Thesis, MIT, Mech. Eng.'g, June 1987
- Fasse,E.D., Hogan,N., "A Lyapunov-based approach to designing manipulator controllers robust to interaction with dynamic environments", *Decision and Control*, Monthly Publication, pp.115-124, March 1989
- Faye,I.C., "An Impedance Controlled Manipulandum for Human Movement Studies", M.S. Thesis, MIT, Mech. Eng.'g, June 1986
- Fearing, R.S., "Simplified Grasping and Manipulation with Dexterous Robot Hands", AI-Lab. Memo, MIT 809, Nov. 1984
- Fernandez,B.R., "Control of Multivariable Nonlinear Systems", *Int. Journal of Control*, Sept. 1986
- Ferrell, W.R., "Delayed Force Feedback", *Human Factors*, Oct. 1966, pp.449-455
- Ferrell, W.R., Sheridan, T.B., "Supervisory Control of Remote Manipulation", *IEEE Spectrum*, Oct. 1967, pp.81-88
- Freund,E., "Fast Nonlinear Control with arbitrary pole-placement for Industrial Robots and Manipulators", *Int. Journal of Robotics Research*, Vol. 1, No. 1, Spring 1982, pp. 65-78
- Gavrilovic,M.M.,Maric,M.R., "New Development in Synergistic Rate Control of Manipulators", *Proc. of the First CISM-IFTOMM Symposium on Theory and Practice of Robots & Manipulators*, Sept. 1973, Udine, Italy
- Gevarter, W.B., "Basic Relations for Control of flexible vehicles", *AIAA Journal*, April 1970, vol.8, no.4, pp.666-672
- Gilbert,E.G.,Johnson,D.W., "Distance Functions and their Application to Robot Path Planning in the Presence of Obstacles", *Center for Robotics and Integrated Manufacturing*, Univ. of Michigan, Ann Arbor, Sep. 1984
- Giraud, A., "Generalized Active Compliance for Part Mating with Assembly Robots", *Int. Symposium on Robotics Research*, pp.949-960
- Goertz, R.C., "Fundamentals of General Purpose Manipulators", *Nucleonics*, November 1952, vol.10, pp.36-42
- Gougoussis,A., Donath,M., "Coulomb Friction Joint and Drive Effects in Robot Mechanisms", *Proc. 1987 IEEE Int. Conf. on Robotics & Automation*, pp.828-836
- Gougoussis,A., Donath,M., "Coulomb Friction Effects on the Dynamics of Bearings and Transmissions in Precision Robot Mechanisms", *Proc. of the 1988 IEEE Int. Conf. on Robotics & Automation*, v.3, pp.1440-1446
- Good, M.C., Sweet, L.M., Strobel, K.L., "Dynamic Models for control system design of integrated robot and drive systems", *ASME Journal of Dynamic Systems, Measurement and Control*, March 1985, vol.107, pp.53-59

- Goor, R.M., "A New Approach to Robot Control", Int. Symposium on Robotics Research, pp.387-389
- Handlykken, M., Turner, T., "Control System Analysis and Synthesis for a Six-Degree-of-Freedom Force-Reflecting Hand Controller", IEEE Conf. on Decision & Control, 1980
- Hannaford, B., Andersen, R., "Experimental and Simulation Studies on Hard Contact in Force Reflecting Teleoperation", September 1987
- Hannaford, B., "Testing and Analysis of JPL-OMV Smart Hand", Interoffice Memo JPL-Lab, February 1987
- Hanselmann, H., Moritz, W., "High bandwidth control of the head-positioning mechanism in a winchester disk drive", IEEE Control Systems Magazine, vol.7, no.5, pp.15-19, October 1987
- Hashimoto, H., Slotine, J.J.E., Xu, J.X., Harashima, F., "Practical Design of VSS Controller using Balance Condition", IEEE Proc of 1987 Conf. on Robotics and Automation, April 1987
- Hastings, G.G., Book, W.J., "Experiments in optimal control of a flexible arm", American Control Conference, 1985, pp. 728-729
- Hennessey, M.P., Priebe, J.A., Huang, P.C., Grommes, R.J., "Design of a lightweight robotic arm and controller", 1987 IEEE Conf. on Robotics and Control, pp.779-785
- Hillis, D., "Dynamics of Manipulators with less than One Degree of Freedom", AI-Lab. Working Paper 241, MIT, Jan. 1983
- Hogan, N. "Adaptive Stiffness Control in Human Movement", pp. 53-54 in: 1979 Advances in Bioengineering, Ed. Wells, M.K., American Society of Mechanical Engineers, New York, 1979
- Hogan, N., "Impedance Control: An approach to manipulation", Proc. 1984 American Control Conference, San Diego, CA, pp.304-313, June 6-8, 1984
- Hogan, N., "Mechanical Impedance Control in Assistive Devices and Manipulators", Proceedings of the Joint Automatic Control Conferences, Vol.1, San Francisco, Aug. 1982
- Hogan, N., "Control and Coordination of voluntary Arm Movement", Proc. 1982 Automatic Control Conference 1, pp. 552-558, 1982a
- Hogan, N., "An Organising Principle for a class of Movements", Journal of Neurosciences 4, pp. 2745-2754, 1984
- Hogan, N., "The Mechanics of Multi-Joint Posture Control", Biological Cybernetics, 52, pp.315-331, Springer Verlag, 1985
- Hogan, N., "Some Computational Problems simplified by Impedance Control", Proc. 1984 ASME Conf. Comput. Eng. 1, pp. 203-209, 1984

- Hogan, N., "Impedance Control of a Robotic Manipulator", Presented at the Winter Annual Meeting of the American Society of Mechanical Engineers, Washington, D.C., 1981
- Hogan, N., "Adaptive Control of Mechanical Impedance by Coactivation of Antagonist Muscles", in: IEEE Transactions on Automatic Control, Vol.AC-29, No. 8, Aug. 1984, pp. 681-690
- Hogan, N., "Programmable Impedance Control of Industrial Manipulators", Proceedings of the Conference on CAD/CAM in Mechanical Engineering, MIT, Mar. 1982
- Hogan, N., "Impedance Control Applied to Automated Deburring", Adaptive and Learning Systems, Ed. by Kumpati S. Navendra, Plenum, 1986
- Hogan, N. & Cotter, S.L., "Cartesian Impedance Control of a Nonlinear Manipulator", pp.121-128 in: Robotics Research and Advanced Applications, Ed. Book, W.J., American Society of Mechanical Engineers, New York 1982
- Hogan, N., "Stable Execution of Contact Tasks using Impedance Control", IEEE Proc of 1987 Conf. on Robotics and Automation, April 1987
- Hogan, N., "Impedance Control of industrial robots", IRobotics and computer-integrated manufacturing, vol.1, no.1, pp.97-113, 1984
- Hollars, M.G., Cannon, R.H., "Initial experiments on the end-point control of a two-link manipulator with flexible tendons", ASME Winter Annual Meeting, November 1985
- Hollerbach, J.M., Atkeson, C.G., "Characterization of Joint interpolated Arm Movements", AI-Lab. Memo, MIT 854, June 1985
- Hollerbach, J.M., "A Recursive Formulation of Lagrangian Manipulator Dynamics", IEEE Transactions on Systems, Man and Cybernetics, Vol.10, 1980, pp.730-736
- Hollerbach, J.H., "Dynamic Scaling of Manipulator Trajectories", AI-Lab. Memo, MIT, Jan. 1983
- Hollerbach, J.H., Suh, K.C., "Redundancy Resolution of Manipulators through torque optimization", AI-Lab. Memo, MIT 882, Jan. 1986
- Hollerbach, J.H., Sahar, G., "Wrist-Partitioned Inverse Kinematic Acceleration and Manipulator Dynamics", AI-Lab. Memo, MIT 717, April 1983
- Hollerbach, J.M., "Computers, Brains, and the control of Movement", AI-Lab. Memo, MIT 686, June 1982
- Hollerbach, J.M., Flash, T., "Dynamic Interactions between Limb Segments during Planar Arm Movement", AI-Lab. Memo, MIT 635, Nov. 1981
- Hollerbach, J.M., "Workshop on the Design and Control of Dexterous Hands", AI-Lab. Memo, MIT 661, April 1982
- Hollerbach, J.M., "A Recursive Lagrangian Formulation of Manipulator Dynamics and a comparative study of Dynamics Formulation Complexity", AI-Lab. Memo, MIT 533, June 1979

- Horn,B.K.P., Raibert,M.H., "Configuration Space Control", AI-Lab. Memo, MIT 458, Dec. 1977
- Horn,B.K.P., Hirokawa,K., Vazirani,V.V., "Dynamics of a three degree of freedom kinematic chain", AI-Lab. Memo, MIT 478, Oct. 1979
- Humphreys,D.E., Watkinson,K.W., "Hydrodynamic Stability and Control Analyses of the UNH-EAVE Autonomous Underwater Vehicle", ARAP-Lab. Tech.Memo No. 82-2, Jan. 1982
- Humphreys,D.E., "Development of the Equations of Motion and Transfer Functions for Underwater Vehicles", NCSL Report No. 286-76, July 1976
- Inoue,H., "Force Feedback in precise Assembly Tasks", MIT AI Memo# 308, Aug. 1974
- Ishida,T., "Force Control in Coordination of Manipulator in fine Motions", Fifth International Conference on Artificial Intelligence, 1977
- Itkis,U., "Control Systems of Variable Structure", Halstead Press 1977
- Jacobsen, S.C., et al, "The UTAH/MIT dexterous hand: Work in Progress", Int. Journal of Robotics Research, vol.3, no.4, 1984
- Kahn,M.E,Roth,B., "The Near-Minimum time control of open-loop articulated kinematic chains", ASME Journ. of Dynamic Syst., Meas. & Control, pp. 164-172, Sept 1971
- Kahng,J.,Amirouche,F.M.L., "Impact Force Analysis in Mechanical Hand Design", IEEE Proc of 1987 Conf. on Robotics and Automation, April 1987
- Karlen,J.P., Thompson Jr.,J.M., Farrell,J.D., "Design and Control of Modular Kinematically-Redundant Manipulators", 2nd AIAA/NASA/USAF Symposium on Automation, Robotics and Advanced Computing for the National Space Program, March 9-11, 1987/Arlington, VA
- De Keyser,R.M.C., Van Cauwenberghe,A.R., "Self-Tuning Prediction and Control", Int. J. of Systems Science, Vol.14,No.2,pp.147-168, 1983
- Kazerooni,H., Sheridan,T.B., Hogan,N.J., "Wide Bandwidth Positioning Systems for Space and Underwater Systems", 4th Int. Submersible Tech. Conf., UNH, Durham, NH, June 1985
- Kazerooni,H., "A Robust Design Method for Impedance Control of Constrained Dynamic Systems", MIT Sea Grant 85-35TN, Feb. 1985
- Kazerooni,H., Sheridan,T.B., "Computer Simulation and Control of Underwater Vehicles", MIT Sea Grant 82-19, Oct. 1982
- Kazerooni,H., Houpt, P.K., Sheridan,T.B., "The fundamental concepts of robust compliant motion for robot manipulators", IEEE Int. Conference on Robotics and Automation, April 1986, pp.418-427
- Kazerooni,H., Houpt, P.K., Sheridan,T.B., "Design Method for robust compliant motion for robot manipulators", American Control Conference, June 1986, pp.1897-1906

- Kazerooni,H., "Robust, Non-Linear Impedance Control for Robot Manipulators", IEEE Proc of 1987 Conf. on Robotics and Automation, April 1987
- Kazerooni,H., Guo,J., "Direct-Drive, Active Compliance End-Effector", IEEE Proc of 1987 Conf. on Robotics and Automation, April 1987
- Kazerooni,H., "Direct-Drive, Active Compliant End-Effector (Active RCC)", IEEE Journal of Robotics and Automation, June 1988, vol.4, no.3, pp. 324-333
- Kazerooni,H., "Automated Roboting Deburring using Electronic Compliance; Impedance Control", IEEE Proc of 1987 Conf. on Robotics and Automation, April 1987
- Kazerooni,H., Bausch, J.J, Kramer, B.M., "Automated Deburring by robot manipulators", American Control Conference, June 1986, pp. 1749-1755
- Kelly,R., Carelli,R., Amestegui,M., Ortega,R., "On adaptive impedance control of robot manipulators", IEEE Proc of 1989 Conf. on Robotics and Automation, pp.572-577
- Khalil,W., Liegois,A., "The dynamics of a class of electrically-actuated and cable-driven manipulators", Dynamics of Multi-body Systems, Springer Verlag 1978, pp.120-132
- Khatib,O.,LE Maitre,J.F., "Dynamic Control of Manipulators operating in a complex Environment", Third Symposium on Theory and Practice of Robots and Manipulators, Udine, Italy, 1978, pp.267-282
- Khatib,O., "Dynamic Control of manipulators in operational spaces", Proc. 6th World Congress on Theory of Machines and Mechanisms, pp.1128-1131, 1983
- Khatib,O., "Real-Time Obstacle Avoidance for Manipulators and Robots", Proceedings of the 1985 IEEE Conf. on Automatic Control, pp.500-505
- Khatib,O., Burdick,J., "Motion and Force Control of Manipulators", Proceedings of the 1986 IEEE Conf. on Robotics and Automation, v.2, pp.1381-1386
- Khosla,P.K., Kanada,T., "Parameter Identification of Robot Arms", Proceedings of the 1985 IEEE Conf. on Decision and Control, pp.1754-1760
- Kishimoto,O., Kuboh,K., Itiaka,H., Honma,T., "Experimental Study of the Hydrodynamic Properties of the Unmanned Submersible", Nav. Eng. Journal, Vol.92, pp.25-35, Feb.
- Kissel,G.J., Hegg, D.R., "Stability enhancement for control of flexible space structures", IEEE Control Systems Magazine, June 1986
- Kleidon,M.A., "Modeling & Performance of a Pneumatic/Hydraulic Actuator with tunable mechanical impedance", S.M. Thesis, Dept. of Mech. Eng., MIT, Sept. 1984
- Kondoh,T., Yamamoto,H., Okuda,H., Youcef-Toumi,K., "Practical Issues in the Design and Control of Direct-Drive Robots", ASME Journal of Machine Theory, 1986
- Kosuge,K., Furuta,K., "Kinematic and Dynamic Analysis of Robot Arm", Proceedings of the 1985 IEEE Conf. on Automatic Control, pp.1039-1044

- Kubo,T., Anwar,G., Tomizuka,M., "Application of Nonlinear Friction Compensation to Robot Arm Control", Proc. of the 1986 IEEE International Conference of Robotics and Automation, v.2, pp.722-727
- Kunze,H.-B., Jacobash,A.H.K., "Control Algorithms for Stiffening an Elastic Industrial Robot", IEEE Journal of Robotics and Automation, v.RA-1, no.2, pp.71-78, June 1985
- Landau,I.D., "A Survey of model reference adaptive techniques - Theory & Applications", Automatica, Vol.10, pp.353-379, 1974
- Lawrence,D.A., "Actuator Limitations on achievable Manipulator Impedance", Proc. of the 1989 Conf. on Robotics and Automation, pp.560-565
- Lawrence,D.A., "Impedance Control Stability Properties in Common Implementations", Proc. of the 1988 Conf. on Robotics and Automation, Philadelphia, April 1988, pp.1185-1191
- Lawrence,D.A., Stoughton,R.M., "Position-Based Impedance Control: Achieving Stability in Practice", 1987 AIAA Conf. on Guidance, Navigation & Control
- Lee,C.S.G., "Robot Arm Kinematics, Dynamics & Control", Computer, Vol.15, No.12, pp.62-80, Dec.1982
- Lee,S., Bekey,G., Bejczy,A.K., "Computer Control of Space-Borne Teleoperators with Sensory Feedback", Proceedings of the 1985 IEEE Conf. on Automatic Control, pp.205-214
- Levin,M.D., "Design and Control of a Closed-Loop Brushless Torque Actuator", S.M. Thesis in Mech. Eng'g, Massachusetts Institute of Technology, May 1990.
- Lewis,R.A., "Practical Manipulator Software", Proc. of IEEE Milwaukee Symp. on Automatic Computation & Control, Milwaukee, Wis., pp.17-19, 1976
- Lewis,D.J., Lipscombe,J.M., Thomasson,P.G., "The Simulation of Remotely Operated Underwater Vehicles",
- Lim,K.H., "Control of a Tendon Arm", AI-Lab. Memo, MIT 617, Feb.1981
- Lin,S.K., "Coordinate Transformation with Euler Parameters as a Quaternion - An Alternative Approach to Kinematics and Dynamics of Manipulators", IEEE Proc of 1987 Conf. on Robotics and Automation, April 1987
- Lyung,L., "Recursive Techniques for Identifying Dynamic Systems", AI-Lab. Memo, MIT 617, Feb.1981
- Longman,R.W., Lindberg,R.E., Zedd,M.F., "Satellite-Mounted Robot Manipulators - New Kinematics and Reaction Moment Compensation", Int. Journal of Robotics Research, Vol.6, No.3, Fall 1987
- Lozano-Perez, T., "Automatic Planning of Manipulator Transfer Movements", IEEE Transactions on Systems, Man and Cybernetics, SMC-11, pp. 681-698, 1981

- Lozano-Perez, T., Mason, M.T., Taylor, R., "Automatic Synthesis of Fine-Motion Strategies for Robots", AI-Lab. Memo, MIT 759, Dec. 1983
- Lozano-Perez, T., "Spatial Planning: A Configuration Space Approach", AI-Lab. Memo, MIT 605, December 1980
- Lozano-Perez, T., "Automatic Planning of Manipulator Transfer Movements", AI-Lab. Memo, MIT 606, Dec. 1980
- Luh, J.Y.S., Fisher, W.D., Paul, R.P.C., "Joint Torque Control by a Direct Feedback for Industrial Robots", IEEE Transactions on Automatic Control, v.AC-28, pp.153-161, 1983
- Luh, J.Y.S., Walker, M.W., & Paul, R.P.C., "On-line Computational Scheme for Mechanical Manipulators", ASME Journal of Dynamic Systems, Measurement and Control, Vol.102, pp.69-76, June 1980
- Luh, J.Y.S., Gu, Y.L., "Some Results on Industrial Robots with Redundancy using Dual-Number Transformation", 1984 American Control Conf., June 8 1984, San Diego
- Luh, J.Y.S., Gu, Y.L., "Industrial Robots with seven joints", 1985 IEEE American Control Conf.
- Luh, J.Y.S., Walker, M.W., Paul, R.P.C., "Resolved Acceleration Control of Mechanical Manipulators", IEEE Transactions on Automatic Control, Vol.AC-25, 1980, pp. 468-474
- Maloof, R.H., Forrester, N.C., Albrecht, C.E., "A Brushless Propulsion System for the Research Submersible Alvin", WHOI MEMO, 1986
- Maples, J.A., Becker, J.J., "Experiments in force control of robotic manipulators", IEEE Int. Conference on Robotics and Automation, April 1986, pp. 6995-702
- Markiewicz, B.R., "Analysis of the computed Torque Drive Method & Comparison with conventional Position Servo for a Computer Controlled Manipulator", Tech. Memo 33-601, J.P.L., Pasadena, CA, March 15, 1973
- Mason, M.T., "Compliance and Force Control for Computer Controlled Manipulators", IEEE Transactions on Systems, Man and Cybernetics, Vol. SMC-11, No.6, 1981
- Mason, M.T., "Compliance and Force Control for Computer Controlled Manipulators", AI-Lab. Technical Report 515, April 1979
- Mason, M.T., "Manipulator Grasping and Pushing Operations", AI-Lab. Technical Report 690, June 1982
- McClamroch, N.H., Wang, D., "Feedback Stabilization and tracking of constrained robots", IEEE Transactions on automatic control, May 1988, pp. 1690-1695
- Merlet, J-P., "C-Surface applied to the Design of an Hybrid Force-Position Robot Controller", IEEE Proc of 1987 Conf. on Robotics and Automation, April 1987
- Merritt, L.V., "The space station rotary joint motor controller", MOTION Control Magazine, vol.6, no.1, January/February 1990

- Milliken, L.G., "Multivariable Control of an Underwater Vehicle", Engineer's and Master's Thesis, MIT, May 1984
- Morris, H.M., "Robotic Control Systems: More than simply collections of servo loops", Control Engineering, May 1984
- Moore, S.R., "Part Referenced Manipulation: Applications for a Drilling Operation", MS Thesis in Mech. Eng'g., MIT, May 1983
- Morasso, P., "Spatial Control of Arm Movements", Exp. Brain Res.: pp. 223-227, 1981
- Nakamura, Y., Hanafusa, H., "Task Priority based Redundancy Control of Robot Manipulators", Int. Symposium on Robotics Research, pp.156-161
- Nevins, J.L., Whitney, D.E., "Computer-Controlled Assembly", Scientific American, February 1978, vol. 238, no.2
- Newman, W.S., Hogan, N., "High Speed Robot Control and Obstacle Avoidance using Dynamic Potential Functions", IEEE Proc of 1987 Conf. on Robotics and Automation, April 1987
- Niemeyer, G., Slotine, J.-J.E., "Computational Algorithms for adaptive compliant motion", IEEE Conf. on Robotics & Automation, pp.566-571, 1989
- Olsen, H.B., Bekey, G.A., "Identification of Robot Dynamics", IEEE 1986 Int. Conf. on Robotics and Automation, v.2, pp.1004-1010
- Orin, D.E., Oh, S.Y., "Control of force distribution in robotic mechanisms containing closed kinematic chains", Journal of Dyn. Syst. & Meas. Control, Vol.103, pp.134-141, June 1981
- Ortega, R., Spong, M., "Adaptive Motion Control of rigid robots: A tutorial", Proc. of the 27th Conf. on Decision & Control, pp.1575-1584, Austin, TX, Dec. 1988
- Ohwovoriole, M.S., Hill, T.H., Roth, B., "On the Theory of Single and Multiple Insertions in Industrial Assemblies", Proc. of the 10th Int. Conf. on Industrial Robots and 5th Conf. on Industrial Robot Technology, Milan, Italy
- Ogata, K., "Modern Control Engineering", Prentice Hall, Englewood Cliffs, NJ, 1970
- Pasch, K., Seering, W.P., "On the Drive Systems for high Performance Machines", ASME Journal of Mechanisms, Transmissions and Automation in Design, Vol.106, No.1, March 1983, pp.102-108
- Paul, R.P., "Robot Manipulators : Mathematics, Programming, and Control", MIT Press, 1981
- Paul, R.P., "Modeling, Trajectory Calculation and Servoing of a computer controlled arm", Stanford AI Project, Memo #177, Mar. 1973
- Paul, R.P., Robot Manipulators: Mathematics, Programming and Control, MIT Press, Cambridge, Mass. 1981

- Paul,R.P.C., & Shimano, B., "Compliance and Control", Proceedings of the Joint Automatic Control Conference, 1976, pp. 694-699
- Paul,R.P., Zhang,H., "Robot Motion Trajectory Specification and Generation", Int. Symposium on Robotics Research, pp.187-194@>(.)
- Paul,R.P., "Problems and Research Issues associated with the Hybrid Control of Force and Displacement", IEEE Proc of 1987 Conf. on Robotics and Automation, April 1987
- Person,E., "Brushless DC Motors in High Performance Servo Systems", Electro-Craft Cooperation, Hopkins, Minnesota, 1989 ed.
- Pfeiffer, F., Gebler, B., "A multi-stage approach to the dynamics and control of flexible robots", IEEE Int. Conference on Robotics and automation, April 1988, pp.2-8
- Pierre,D.A., "Steady State Error conditions for use in the design of look-ahead digital control systems", IEEE Trans. Con.,Vol.27,No.4,Aug. 1982
- Pierre,D.A,Uhlich,P.E., "Look-ahead control algorithms for computer control of machine tools", Proc. Joint Automatic Contr. Conf., Charlottesville,VA,June 1981
- Piller, G., "A compact six-degree-of-freedom sensor for assembly robots", Proc. of the 12th Int. Symposium on Industrial robots, 6th Int. conference on industrial robot technology, IFS Publications, Bedford, England, 1982, pp.121-129
- Plank, G., Hirzinger, G., "Controlling a robot's motion speed by a force-torque sensor for deburring problems", In Hardt, D. (editor), *Information control problems in manufacturing technology*, 4th IFAC/IFIP Symposium, 1982, pp.97-102
- Poggio,T., Rosser,B.L., "The Computational Problem of Motor Control", AI-Lab. Memo, MIT 687, May 1983
- Rabinowicz,E., "A study of the Stic-Slip Process", publ. in Friction and Wear, ed. by Robert Davies, Elsevier Pub. Co., N.Y., 1959
- Raibert, M.H., & Craig, J.J., "Hybrid Position/Force Control of Manipulators", ASME Journal of Dynamic Systems, Measurement and Control, Vol. 102, June 1981, pp. 126-133
- Raibert, M.H., & Horn, B.K.P., "Manipulator Control Using the Configuration Space Method", Industrial Robot, Vol. 5, June 1978, pp. 69-73
- Rajan,V.T., Burrige,R.,Schwartz,J.T., "Dynamics of a Rigid Body in Frictional Contact with Rigid Walls", IEEE Proc of 1987 Conf. on Robotics and Automation, April 1987
- Rajan,V.T., "Minimum Time Trajectory Planning", IEEE Proc of 1985 Conf. on Robotics and Automation, April 1985
- Raju,G.J., "An Experimental Master-Slave Manipulator System to study the Feasibility of Operator Adjustable Impedance in Remote Manipulation", Man-Machine Systems Lab., Internal Memo Ref. No.86-1

- Renaud, M., Zabala-Turralde, J., "Robot Manipulator Control", Proc. 9th Int. Symp. on Industrial Robots, Washington, pp.463-475, March 1979
- Roberts, R.K., Paul, R.P., Hillberry, B.M., "The Effect of Wrist Force Sensor Stiffness on the Control of Robot Manipulators", Proceedings of the 1985 IEEE Conf. on Automatic Control, pp.269-274
- Roderick, M.D., "Discrete Control of a robot arm", Stanford AI Project, Memo #287, Aug. 1976
- Ryzin Van, J.C., "Wind Tunnel Hydrodynamic Testing of a Large Submersible Vehicle Model", 9th Annual Offshore Techn. Conf., May 2-5 1977
- Salisbury, J.K., Craig, J.J., "Articulated Hands: Kinematic and Force Control Issues", Int. Journal of Robotics Research, Vol.1, pp.4-17, Spring 1982
- Salisbury, J.K., "Active Stiffness Control of a Manipulator in Cartesian Coordinates", IEEE Conference on Decision and Control, New Mexico, 1980
- Salisbury, J.K., "Design and Control of an articulated hand", 1st Int. Symposium on Design and Synthesis, Tokyo, July 1984
- Salisbury, J.K., Abramowitz, J.D., "Design and Control of a Redundant Mechanism for small motion", Proceedings of the 1985 IEEE Int. Conference on Robotics & Automation, St. Louis, Mo., March 1985
- Salisbury, J.K., Townsend, W., Eberman, B., DiPietro, D., "Preliminary Design of a Whole-Arm Manipulation System (WAMS)", Proceedings of the 1988 IEEE Int. Conference on Robotics & Automation
- Salisbury, J.K., Roth, B., "Kinematic and Force Analysis of Articulated Mechanical Hands", ASME Journal of Mechanical Design, September 1982
- Salisbury, J.K., "Whole-Arm manipulation", 4th Int. Symposium on robotics research, Santa Cruz, CA, August 1987
- Schempf, H., "Combined Vehicle/Manipulator Controller Structures", DSL Lab. Internal Memo, Aug. 1987
- Schiehlen, W.O., "Computer Generation of Equations of Motion", NATO ASI Series Vol.F9, pp.183-215
- Seeger, G.H., Paul, R.P., "Optimizing Robot Motion along a Predefined Path", IEEE 1985, pp.765-770
- Seering, W.P., Eppinger, S.D., "The dynamics of robot force control", IFToMM Seventh World Congress on the theory of machines and mechanisms, September 1987
- Seitz, W.E., "Sensorimotor Systems", Electronic MOTORtechnics Magazine, vol.1, no.2, January 1990

- Shamma, J., "Analysis and Design of Gain Scheduled Control Systems", Ph.D. Thesis, MIT, Laboratory for Information and Decision Systems, Cambridge, MA, May 1988
- Shamma, J., Athans, M., "Stability and Robustness of Slowly Time-Varying Linear Systems", IEEE Decision and Control Conference, CA, December, 1987
- Sharon, A., "Enhancement of robot accuracy using a macro/micro manipulator system", M.S. Thesis, Mech. Engineering Dept., MIT, 1983
- Sharon, A., Hogan, N., Hardt, D.E., "High Bandwidth Force Regulation and Inertia Reduction using a Macro/Micro Manipulator System", IEEE Conf. on Robotics & Automation, 1988
- Sharon, A., Hogan, N., Hardt, D.E., "Controller Design in the Physical Domain (Application to robotic impedance control)", IEEE Conf. on Robotics & Automation, pp.552-559, 1989
- Sharon, A., Hardt, D., "Enhancement of Robot Accuracy Using Endpoint Feedback and a Macro-Micro Manipulator System", IEEE Proc. of the American Control Conference 1984
- Sheridan T.B., Ferrell, W.R., "Man Machine Systems: Information, Control and Decision Models of Human Performance", Massachusetts, MIT Press, 1974
- Sheridan T.B., et al, "Supervisory Control, Mental Models and Decision Aids", Man-Machine-Systems-Lab, MIT, July 1986
- Sheridan T.B., "Telerobotics", 10th IFAC Congress on Automatic Control, 27-31 July 1987, Munich, West G.
- Sheridan T.B., "Supervisory Control", Handbook of Human Factors/Ergonomics, Wiley, NY, 1986
- Sherley, D.E., "Control System Design for the Advanced Unmanned Search System Vehicle", Naval Research Lab. Report
- Shimano, B., "The Kinematic Design and Force Control of Computer Controlled Manipulators", Stanford AI Lab. Memo 313, March 1973
- Silver, W.M., "On the representation of angular velocity and its effect on the efficiency of Manipulator Dynamics Computation", AI-Lab. Memo, MIT 622, March 1981
- Simunovic, S.N., "Force Information in Assembly Processes", Proc. of the 5th Int. Symposium on Industrial Robots, Chicago, Illinois, pp.415-431
- Slotine, J.J.E., "Tracking Control of Nonlinear Systems using Sliding Surfaces", Ph.D. Thesis, MIT AeroAstro Department, May 1983
- Slotine, J.J.E., Asada, H., "Robot Analysis and Control", Wiley, NY, Dec 1985
- Slotine, J.J.E., Yoerger, D., "A Rule-Based Inverse Kinematic Algorithm for Redundant Manipulators", Int. Journal Robotics and Automation, 1(4), 1986

- Slotine, J.J.E., "Putting Physics in control - The example of robotics", IEEE Control Systems Magazine, 1988
- Slotine, J.J.E., Li, W., "On the Adaptive Control of Robot Manipulators", Nonlinear Systems Laboratory, MIT, June 1986
- Slotine, J.J.E., Li, W., "Adaptive Manipulator Control - A Case Study", Nonlinear Systems Laboratory, MIT, June 1986
- Slotine, J.J.E., Li, W., "Theoretical Issues in Adaptive Manipulator Control", Nonlinear Systems Laboratory, MIT, June 1986
- Slotine, J.J.E., Hedrick, J.K., Misawa, E.A., "On Sliding Observers for Nonlinear Systems", Nonlinear Systems Laboratory, MIT, June 1986
- Slotine, J.J.E., Coetsee, J.A., "Adaptive Sliding Controller Synthesis for Nonlinear Systems", Nonlinear Systems Lab., MIT, Sept. 1985
- Slotine, J.J.E., "Robustness Issues in Robot Control", IEEE Int. Conf. on Robotics and Automation, St. Louis 1985
- Slotine, J.J.E., "Sliding Controller Design for Nonlinear Systems", IEEE Int. Journal of Control, Vol.40, No.2, pp.421-434
- Slotine, J.J.E., Hong, S., "Two-Time Scale Sliding Control of Manipulators with Flexible Joints", 1986 American Control Conference, Seattle WA
- Slotine, J.J.E., Spong, M.W., "Robust Control with Bounded Input Torques", Int. Journal of Robotic Systems 2(4), 1984
- Slotine, J.J.E., Li, W., "Adaptive Strategies in Constrained Manipulation", IEEE Proc of 1987 Conf. on Robotics and Automation, April 1987
- Smith, J.M., *Mathematical Modelling and Digital Simulation for Engineers and Scientists* - Chapter 6: Nonlinear System Simulation, J.Wiley & Sons, New York, 1977
- Stanisic, M.M., Pennock, G.R., "A Non-Degenerate Orientation Solution of a Four-Jointed Wrist", IEEE 1985
- Streiff, G., Auchapt, P., Vertut, J., "Association of Remote Dexterity and Remote Lifting for Maintenance in Fuel Reprocessing Industry", Robotics and Remote Handling in Hostile Environments, Gatlinburg VA, 1984
- Stepien, T.M., Sweet, L.M., Good, M.C., Tomizuka, M., "Control of Tool/Workpiece contact force with application to robotic deburring", IEEE Int. Conference on robotics and automation, March 1985
- Sweet, L.M., Good, M.C., "Redefinition of the robot motion-control problem", IEEE Control Systems Magazine, August 1985, pp.18-25

- Takegaki, M. & Arimoto, S., "A New Feedback Method for Dynamic Control of Manipulators", *Journal of Dynamic Systems, Measurement and Control*, Trans. SME, Vol. 102, June 1981, pp. 119-125
- Tal, J., "Motion Control by Microprocessors", GALIL Motion Control Memo
- Tal, J., "What Limits the performance of servo systems?", *MOTION Control Magazine*, vol.5, no.6, November/December 1989
- Tal, J., "Current vs. Voltage amplifiers - the better choice", *MOTION Control Magazine*, vol., no.1, January/February 1990
- Thomas, M., Yuan-Chou, H.C., Tesar, D., "Optimal Actuator Stiffness Distribution for Robotic Manipulators based on Local Dynamic Criteria", *Proceedings of the 1985 IEEE Conf. on Automatic Control*, pp.275-281
- Tilley, S.W., Cannon, R.H., Kraft, R., "End point force control of a very flexible manipulator with a fast end-effector", *ASME Winter Annual Winter Meeting*, December 1986
- Townsend, W.T., Salisbury, K.J.Jr., "The Effect of Coulomb Friction and Stiction on Force Control", *IEEE Int. Conf. on Robotics and Automation*, Raleigh, NC, April 1987
- Townsend, W.T., Salisbury, K.J., "The Efficiency Limit of Belt and Cable-Drives", *ASME Journal of Mechanisms, Transmissions and Automation in Design*, Vol. 110, No.3, September 1988, pp.303-307
- Townsend, W.T., Salisbury, K.J., "Mechanical Bandwidth as a guideline to High-Performance Manipulator Design", Draft Copy rec'd. 10/31/89
- Townsend, W.T., "The effect of transmission design on the performance of force-controlled manipulators", *Doctoral Thesis*, Massachusetts Institute of Technology, April 1988, also as MIT AI Lab. Technical Report no. AIM-1054
- Tustin, A., "The effects of backlash and of speed-dependent friction on the stability of closed-cycle control systems", *IEE Journal*, v.94, Part 2A:143-151, 1947
- Uicker, J.J.Jr., "Dynamic Force Analysis of Spatial Linkages", *ASME Journal of Applied Mechanics*, June 1967
- Ulrich, N., "Mechanical Design Optimization of Robot Manipulator Performance", Ph.D. Thesis in Mechanical Engineering, September 1990, U. of Pennsylvania.
- Utkin, V.I., "Variable Structure Systems with Sliding Modes", *IEEE Transactions on Automatic Control*, Vol. AC-22, No.2, April 1977
- Utkin, V.I., "Equations of the Slipping Regime in Discontinuous Systems", *Translated from Automatika* No.12, pp.42-54, Dec. 1971
- Vafa, Z., Dubowsky, S., "On the Dynamics of Manipulators in Space", *IEEE Conf. on Robotics and Automation*, March 30- Apr. 3, 1987, Raleigh, NC

- Vafa, Z., Dubowsky, S., "Kinematic and Dynamic Models of Manipulators for Use in Space: The Concept of the Virtual Manipulator", Proc. of the Seventh World Congress on the Theory of Machines and Mechanisms, Sevilla, Spain, Sept. 17-22, 1987
- Van Brussel, H., Simmons, J., "The adaptable compliance concept and its use for automatic assembly by active force feedback accommodations", 9th Int. Symposium on Industrial Robots, Washington, D.C., 1979
- Vertut, J., "Advances in Computer Aided Teleoperation Systems (CATS) in the Frame of the French Advanced Robotics and Automation (ARA) Project", 1983 ICAR, Tokyo, Japan
- Vertut, J., Espiau, B.G.A., "Advances in a Computer Aided Bilateral Manipulator System", Topical Meeting : Robotics and Remote Handling in Hostile Environments, Gatlingburg VA, 1984
- Vertut, J., Marchal, P., "MA-23 M Contained Servomanipulator with Television Cameras on PICA and PLAIDE Telescopic Supports with Computerized Integrated Control", ANS Proc. of 28th Conf. RSTD, 1980
- Vertut, J., Marchal, P., Germond, J.C., "Protection, Transfer, and Maintenance of the MA-23 Bilateral Manipulator", Proc. of 26th Conf. on Remote Systems Technology, 1978
- Vertut, J., Espiau, B.G.A., Coiffet, P., "Human Factor Aspects of Computer Enhanced Teleoperation", ANS - 1983 Annual Meeting, Detroit, USA
- Vertut, J., Liegeois, A., "General Design Criteria for manipulators", Mechanism and Machine Theory, Vol.16, pp65-70, Pergamon Press
- Vidyasagar, M., "On the Stabilization of Nonlinear Systems Using State Detection", IEEE Transactions on Automatic Control Vol.AC-25, No.3, June 1980
- Vranish, J.M., Mitchell, E.E., Demoyer, R., "Magnetoelastic force feedback sensors for robots and machine tools", Proc. of 12th Int. Symposium on Industrial robots & 6th Int. Conference on industrial robots, IFS Publications, Bedford, England, 1982, pp.131-142
- Wada, M., Kuba, Y., Tuchiko, T., Hari, H., Misukoa, S., "Development of a Human-Type Manipulator using a High-Performance Control Cable for Robots", J. Rob. Mech., Vol. 1 [42-46], 1989
- Wada, M., Hari, H., "Development of a High-Performance Control Cable for Robots", Robot, No.66, pp.90-95 (in Japanese), 1989
- Walrath, C.D., "Adaptive Bearing Friction Compensation based on recent Knowledge of Dynamic Friction", Automatica, v.20(6), pp.717-727, 1984
- Wang, Y., Mason, M.T., "Modeling Impact Dynamics for Robotic Operations", IEEE Proc of 1987 Conf. on Robotics and Automation, April 1987

- Wang,S.,Will,P., "Sensors for Computer Controlled Assembly", The Industrial Robot, March 1978
- Wang,C.-C., "The optimal design of robot drive system - actuator gains", 1987 IEEE Conf. on Robotics and Automation, pp.816-821
- Wang,C.-C., "The optimal design of robot drive system - gear ratios and actuator impedances", 1986 IEEE Conf. on Robotics and Automation, v.1, pp.67-74
- Waters, C.W., "Mechanical Arm Control", AI-Lab. Memo, MIT 549, Oct. 1979
- West,H., Asada,H., "A Method for the Control of Robot Arms Constrained by Contact with the Environment", IEEE Conf. on Robotics and Automation, St. Louis, March 1985
- Weiping,Li, Slotine,J.J E., "Parameter Estimation Strategies for Robotic Applications", Unpublished as of 9/10/87
- Whitney,D.E., "The Mathematics of Coordinated Control of Prosthetic Arms and Manipulators",ASME Journal of Dynamic Systems, Measurements and Control, Dec.1972, pp.303-309
- Whitney, D.E., "Resolved Motion Rate Control of Manipulators and Human Prostheses",IEEE Transactions on Man-Machine Systems,Vol.NMS-10,No.2,June 1969, pp.47-53
- Whitney, D.E., "Force Feedback Control of Manipulator Fine Motions", ASME Journal of Dynamic Systems, Measurement and Control, June 1971, pp. 91-97
- Whitney, D.E., "Historical Perspective and State of the Art in Robot Force Control", Proceedings of the 1985 IEEE Conf. on Automatic Control, pp.262-268
- Whitney, D.E., "Quasi-Static Analysis of Compliantly supported rigid bodies", ASME J. of Dynamic Systems, Meas. & Control, V.104, No.1, pp65-77, 1982
- Whitney,D.E., Rourke,J.M., "Mechanical Behaviour &Design Equations for Elastomer Shear Pad RCCs", ASME J. of Dynamic Systems, Meas. & Control, V.108, No.3, pp223-232, Sept. '86
- Whitney,D.E., Nevins,J.L., "What is the Remote Center Compliance (RCC) and what can it do?", Proceedings of the 9th Int. Symposium on Industrial Robots, Washington, D.C., pp.135-152, Summer 1979
- Williams,R.J., Seireg,A., "Interactive Modeling and Analysis of Open or Closed Loop Dynamic Systems with Redundant Actuators", Journal of Mechanical Design Vol.101, pp.407-416, 1979
- Williams,S.J., Glover,K., "Robotic Dynamic Control Instabilities", Int. J. of Robotics and Automation, 2(2), 1987
- Wlassich,John J., "Nonlinear Force Feedback Impedance Control", S.M. Thesis, Dept. of Mech. Eng., Mit, Feb. 1986

- Wu, C.H., Paul, R.L., "Manipulator Compliance based on joint torque control", IEEE Conference on Decision and Control, Albuquerque, N.Mexico, Dec. 1980
- Yabuta, T., Chona, A., "Stability of force-control servomechanism for a manipulator", 9th IASTED Int. Symposium on Robotics and Automation, Santa Barbara, CA, May 1987
- Yastrebov, V.S., Stefanov, G.A., "Underwater Robot/Manipulator Development", MTS Journal Vol.12, No.1, 1985
- Yoerger, D., Sheridan, T.B., "Supervisory Control of the JASON Vehicle Manipulator System", DSL Lab. Proposal, Sept. 1985
- Yoerger, D., "Man-Machine Interface and Control Schemes for the JASON Program", DSL
- Yoerger, D., Newman, J.B., "Demonstration of Supervisory Control for ROVs and Manipulators", ROV 1986 IEEE/MTS
- Yoerger, D., Newman, J.B., "JASON: An Integrated Approach to ROV and Control System Design", ROV 1986 IEEE/MTS
- Yoerger, D., Slotine J.-J.E., "Robust Trajectory Control of Underwater Vehicles", IEEE J. Oceanic Eng. Vol. OE10, No.4, Oct. 1985
- Yoerger, D., Slotine J.-J.E., "Robust and Adaptive Trajectory Control of Autonomous Underwater Vehicles", 25th Conf. on Decision and Control, Dec. 10-12, 1986
- Yoerger, D., Slotine J.-J.E., "Supervisory Control System for the JASON ROV", IEEE J. Oceanic Eng., 1986
- Yoerger, D., Van Alt, C.J., Bowen, A.D., Newman, J.B., "Design of Underwater Vehicles for High Performance Control", IEEE J. Oceanic Eng., 1986
- Yoerger, D., Slotine J.-J.E., "Supervisory Control Architecture for Underwater Teleoperation", Int. J. of Robotics and Automation, 1987
- Yoerger, D., Slotine J.-J.E., "Task-Resolved Motion Control of Vehicle-Manipulator Systems", Int. J. of Robotics and Automation 2(1), 1987
- Yoerger, D., DiPietro, D., Schempf, H., "Design and evaluation of an actively compliant underwater manipulator", Proc. of the ROV'90 Conf., Vancouver, CANADA, 1990.
- Yoshikawa, T., "Dynamic Manipulability of Robot Manipulators", Proceedings of the 1985 IEEE Conf. on Automatic Control, pp.1033-1038
- Yoshikawa, T., "Analysis and Control of Robot Manipulators with Redundancy", Int. Symposium on Robotics Research, pp.735-747
- Yoshikawa, T., "Manipulability and Redundancy Control of Robotic Mechanisms", IEEE 1985, pp.1004-1009

- Yoshikawa, T., Sugie, T., Tanaka, M., "Dynamic Hybrid Position/Force Control of Robot Manipulators - Controller Design and Experiment", IEEE Proc of 1987 Conf. on Robotics and Automation, April 1987
- Youcef-Toumi, K., Asada, H., "The Design of Open-Loop Manipulator Arms with Decoupled and Configuration-Invariant Inertia Tensors", IEEE Int. Conf. on Robotics and Automation, April 1987
- Youcef-Toumi, K., Asada, H., "The Design of arm linkages with decoupled and configuration-invariant inertia tensors: Part I: Open kinematic chains with serial drive mechanisms; Part II : Actuator relocation and mass redistribution", In Donath, M. and Leu, M. (editors), *Robotics and manufacturing automation*, ASME Winter annual meeting, November 1985, vol. PED-15, pp.145-152, pp. 153-161
- Youcef-Toumi, K., Asada, H., "Dynamic Decoupling and Control of a Direct Drive Manipulator", IEEE Int. Conf. on Decision and Control, Dec. 1985
- Youcef-Toumi, K., Li, D., "Force Control of Direct-Drive Manipulators for Surface Following", IEEE Proc of 1987 Conf. on Robotics and Automation, April 1987
- Youcef-Toumi, K., Nagano, H., "Drive Systems of Robot Manipulators", Draft of Internal Memo of the Laboratory for Manufacturing and Productivity, April 1986
- Young, K.K.D., "Controller Design for a Manipulator Using Theory of Variable Structure Systems", IEEE Transactions on Systems, Man and Cybernetics, Vol.SMC-8, No.2, Feb. 1978

DOCUMENT LIBRARY

January 17, 1990

Distribution List for Technical Report Exchange

Attn: Stella Sanchez-Wade
Documents Section
Scripps Institution of Oceanography
Library, Mail Code C-075C
La Jolla, CA 92093

Hancock Library of Biology &
Oceanography
Alan Hancock Laboratory
University of Southern California
University Park
Los Angeles, CA 90089-0371

Gifts & Exchanges
Library
Bedford Institute of Oceanography
P.O. Box 1006
Dartmouth, NS, B2Y 4A2, CANADA

Office of the International
Ice Patrol
c/o Coast Guard R & D Center
Avery Point
Groton, CT 06340

NOAA/EDIS Miami Library Center
4301 Rickenbacker Causeway
Miami, FL 33149

Library
Skidaway Institute of Oceanography
P.O. Box 13687
Savannah, GA 31416

Institute of Geophysics
University of Hawaii
Library Room 252
2525 Correa Road
Honolulu, HI 96822

Marine Resources Information Center
Building E38-320
MIT
Cambridge, MA 02139

Library
Lamont-Doherty Geological
Observatory
Columbia University
Palisades, NY 10964

Library
Serials Department
Oregon State University
Corvallis, OR 97331

Pell Marine Science Library
University of Rhode Island
Narragansett Bay Campus
Narragansett, RI 02882

Working Collection
Texas A&M University
Dept. of Oceanography
College Station, TX 77843

Library
Virginia Institute of Marine Science
Gloucester Point, VA 23062

Fisheries-Oceanography Library
151 Oceanography Teaching Bldg.
University of Washington
Seattle, WA 98195

Library
R.S.M.A.S.
University of Miami
4600 Rickenbacker Causeway
Miami, FL 33149

Maury Oceanographic Library
Naval Oceanographic Office
Bay St. Louis
NSTL, MS 39522-5001

Marine Sciences Collection
Mayaguez Campus Library
University of Puerto Rico
Mayaguez, Puerto Rico 00708

Library
Institute of Oceanographic Sciences
Deacon Laboratory
Wormley, Godalming
Surrey GU8 5UB
UNITED KINGDOM

The Librarian
CSIRO Marine Laboratories
G.P.O. Box 1538
Hobart, Tasmania
AUSTRALIA 7001

Library
Proudman Oceanographic Laboratory
Bidston Observatory
Birkenhead
Merseyside L43 7 RA
UNITED KINGDOM

REPORT DOCUMENTATION PAGE	1. REPORT NO. WHOI-90-43	2.	3. Recipient's Accession No.
4. Title and Subtitle Comparative Design, Modeling, and Control Analysis of Robotic Transmissions			5. Report Date August 1990
7. Author(s) Hagen Schempf			8. Performing Organization Rept. No. WHOI-90-43
9. Performing Organization Name and Address The Woods Hole Oceanographic Institution Woods Hole, Massachusetts 02543, and The Massachusetts Institute of Technology Cambridge, Massachusetts 02139			10. Project/Task/Work Unit No.
			11. Contract(C) or Grant(G) No. (C) N00014-86-C-0038 (G) N00014-88-K-2022
12. Sponsoring Organization Name and Address The Office of Naval Research and the Ocean Industries Program			13. Type of Report & Period Covered Ph.D. Thesis
			14.
15. Supplementary Notes This thesis should be cited as: Hagen Schempf, 1990. Comparative Design, Modeling and Control Analysis of Robotic Transmissions. Ph.D. Thesis, MIT/WHOI, WHOI-90-43.			
16. Abstract (Limit: 200 words) Transmission dynamics are shown to dominate the stability and performance of impedance-and torque controlled rotary electro-mechanical systems where sensor and actuator are noncolocated. The experimental part of the analysis focuses on planetary, cycloidal, harmonic and cable reducers. Simple transmission models are proposed to model such effects as (1) transmission stiffness, (2) soft-zones and wind-up, (3) backlash and lost motion, and (4) stiction, friction and viscous losses. These models are experimentally verified using six different transmission types most commonly used in robot designs. Simple lumped-parameter linear/nonlinear models are shown to predict stability margins and bandwidths fairly closely. Simple nonlinear lumped-and fixed-parameter models were unable to properly predict responses when the torque signals were of low-frequency and amplitude, underscoring the complexity in modeling the transmission-internal stick-slip phenomena. Transmission soft-zones are proven to reduce the stability margins of colocated impedance controlled and noncolocated torque-servoed electro-mechanical systems. None of the standard controller structures explored here could noticeably increase the system bandwidth of the closed-loop system, without reducing the overall system performance. System damping, whether active or passive, as well as low-pass filtering motor-controller signals, are shown to dramatically increase stability without having any effect on increasing system bandwidth.			
17. Document Analysis a. Descriptors 1. robot 2. transmission 3. dynamics b. Identifiers/Open-Ended Terms c. COSATI Field/Group			
18. Availability Statement Approved for publication; distribution unlimited.		19. Security Class (This Report) UNCLASSIFIED	21. No. of Pages 363
		20. Security Class (This Page)	22. Price